สารออกฤทธิ์ทางชีวภาพจากองค์ประกอบที่ได้จากเปลือกมังคุด *Garcinia mangostana* L.

นางสาวอรพิน จันทรศรีวงศ์

วิทยานิพนธ์นี้เป็นส่วนหนึ่งของการศึกษาตามหลักสูตรปริญญาวิทยาศาสตรดุษฎีบัณฑิต
สาขาวิชาเคมี   ภาควิชาเคมี
คณะวิทยาศาสตร์ จุฬาลงกรณ์มหาวิทยาลัย
ปีการศึกษา 2553

BIOACTIVE COMPOUNDS BASED ON CONSTITUENTS FROM PERICARP OF MANGOSTEEN *Garcinia mangostana* L.

Miss Oraphin Chantarasriwong

ศูนย์วิทยทรัพยากร
จุฬาลงกรณ์มหาวิทยาลัย

A Thesis Submitted in Partial Fulfillment of the Requirements
for the Degree of Doctor of Philosophy Program in Chemistry
Department of Chemistry
Faculty of Science
Chulalongkorn University
Academic Year 2010

Thesis Title   Bioactive Compounds Based on Constituents from Pericarp of Mangosteen *Garcinia mangostana* L.

By   Miss Oraphin Chantarasriwong

Field of Study   Chemistry

Thesis Advisor   Assistant Professor Warinthorn Chavasiri, Ph.D.

Thesis Co-Advisor   Professor Emmanuel A. Theodorakis, Ph.D.

Accepted by the Faculty of Science, Chulalongkorn University in Partial Fulfillment of the Requirements for the Doctoral Degree
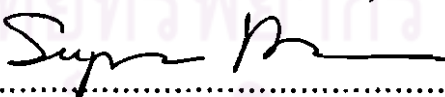
....Dean of the Faculty of Science

(Professor Supot Hannongbua, Dr. rer. nat.)

THESIS COMMITTEE

.... Chairman

(Associate Professor Sirirat Kokpol, Ph.D.)

.... Thesis Advisor

(Assistant Professor Warinthorn Chavasiri, Ph.D.)

.... Thesis Co-Advisor

(Professor Emmanuel A. Theodorakis, Ph.D.)

.... Examiner

(Associate Professor Supason Wanichwecharungruang, Ph.D.)

.... Examiner

(Assistant Professor Chamnan Patarapanich, Ph.D.)

.... External Examiner

(Professor Somsak Ruchirawat, Ph.D.)

อรพิน จันทรศรีวงศ์ : สารออกฤทธิ์ทางชีวภาพจากองค์ประกอบที่ได้จากเปลือกมังคุด Garcinia mangostana L. (BIOACTIVE COMPOUNDS BASED ON CONSTITUENTS FROM PERICARP OF MANGOSTEEN Garcinia mangostana L.) อ.ที่ปรึกษาวิทยานิพนธ์หลัก: ผศ.ดร.วรินทร ชวศิริ, อ.ที่ปรึกษาวิทยานิพนธ์ร่วม: PROF. Emmanuel A. Theodorakis, Ph.D., 280 หน้า.

ได้ทดสอบฤทธิ์ยับยั้งแบคทีเรียของ α-mangostin (1) และอนุพันธ์ที่สังเคราะห์ขึ้นต่อเชื้อ Staphylococcus aureus และเชื้อดื้อยาเมทิซิลลิน และประเมินค่าเพื่อหาความสัมพันธ์ระหว่าง โครงสร้างและฤทธิ์ทางชีวภาพ สาร M3 มีประสิทธิภาพในการต้านเชื้อ S. aureus เท่ากับสาร 1 ด้วยค่า MIC 0.78 μg/mL และฤทธิ์ฆ่าแบคทีเรียมากกว่าสาร 1 สองเท่า ด้วยค่า MBC 1.56 μg/mL การดัดแปลง หมู่ไฮครอกซีลตำแหน่งคาร์บอนที่สามและหกทำให้ฤทธิ์ยับยั้งแบคทีเรียลดลง นอกจากนี้ สาร 1 และ อนุพันธ์ที่สังเคราะห์ขึ้นไม่แสดงฤทธิ์ยับยั้ง Candida albicans ในการทดสอบฤทธิ์ยับยั้งการกินของ ปลวก, สาร 1 ยับยั้งการกินของปลวกอย่างสมบูรณ์ ด้วยค่า %FI 97.8 และ 85.0 ที่ 100 และ 50 μg/disk ตามลำดับ การแทนที่หมู่ไฮครอกซีที่ตำแหน่งคาร์บอนสามและหกทำให้ฤทธิ์ยับยั้งการกินของปลวกลดลง การศึกษาความสัมพันธ์ระหว่างโครงสร้างและฤทธิ์ทางชีวภาพชี้ให้เห็นว่าหมู่ไฮครอกซีตำแหน่งคาร์บอน ที่สามและหกและสายโซ่พรีนิลมีความสำคัญต่อการออกฤทธิ์ยับยั้งแบคทีเรียและการกินของปลวก ฤทธิ์ที่เหมาะสมขึ้นกับความสมดุลของส่วนไฮโดรฟิลิกและไฮโดรโฟบิกของโมเลกุล

ได้ประเมินฤทธิ์ทางเภสัชวิทยาของอนุพันธ์ที่มีโครงสร้างอย่างง่ายของ gambogic acid (77) พบว่าปฏิกิริยาพรีนิลเลชันแบบกลับที่เร่งปฏิกิริยาด้วย Pd(0) ตามด้วยปฏิกิริยา Claisen/Diels-Alder แบบ แคสเคดเป็นวิธีที่เร็วและมีประสิทธิภาพต่อการสังเคราะห์อนุพันธ์เคจ ได้ศึกษาความสัมพันธ์ระหว่าง โครงสร้างและฤทธิ์ทางชีวภาพของสารประกอบเหล่านี้ในเซลล์มะเร็งเม็ดเลือดขาวชนิดโปรมัยอีลอยศ์ที่ ดื้อยาแอนเดียรไมซิน (HL-60/ADR) โครงสร้างเล็กที่สุดที่แสดงฤทธิ์ทางชีวภาพได้แก่ วง ABC ที่สมบูรณ์ ซึ่งประกอบไปด้วยโครงสร้างเคจบนวง C คือ cluvenone (196) แสดงฤทธิ์ความเป็นพิษโดยการ เหนี่ยวนำให้เซลล์ตายแบบแอโพบโทซิสดีเทียบเท่ากับสาร 77 นอกจากนี้ สาร 196 แสดงฤทธิ์ความเป็น พิษต่อเซลล์มะเร็งเม็ดเลือดขาวลิมโฟไซต์เฉียบพลันชนิดบี (IC$_{50}$ 1.1 μM) มากกว่าเซลล์เม็ดเลือดขาวปกติ ชนิดไมโนนิวเคลียร์ (IC$_{50}$ 5.2 μM) ประมาณห้าเท่า

ภาควิชา ___เคมี___ ลายมือชื่อนิสิต ___อรพิน จันทรศรีวงศ์___

สาขาวิชา ___เคมี___ ลายมือชื่อ อ.ที่ปรึกษาวิทยานิพนธ์หลัก _____

ปีการศึกษา ___2553___ ลายมือชื่อ อ.ที่ปรึกษาวิทยานิพนธ์ร่วม _____

4973862623   : MAJOR CHEMISTRY

KEYWORDS: MANGOSTEEN / MANGOSTIN / GARCINIA PLANTS / CAGED XANTHONE / GAMBOGIC ACID

ORAPHIN CHANTARASRIWONG: BIOACTIVE COMPOUNDS BASED ON CONSTITUENTS FROM PERICARP OF MANGOSTEEN *Garcinia mangostana* L. THESIS ADVISOR: ASST. PROF. WARINTHORN CHAVASIRI, Ph.D., THESIS CO-ADVISOR: PROF. EMMANUEL A. THEODORAKIS, Ph.D., 280 pp.

Antibacterial activities of α-mangostin (1) and its synthetic derivatives against *Staphylococcus aureus* and methicillin-resistant *S. aureus* were conducted and evaluated for the structure-activity relationships (SAR). M3 was as effective as 1 against *S. aureus* with the MIC value of 0.78 μg/mL, and exhibited twice more bactericidal than 1 with the MBC value of 1.56 μg/mL. The derivatization of hydroxyl groups at C3 and C6 rendered antibacterial activities. In addition, 1 and its synthetic derivatives did not show activity against *Candida albicans*. In termite antifeedant assay, 1 completely inhibited termite feeding with the %FI of 97.8 and 85.0 at a dose of 100 and 50 μg/disk, respectively. Substitution of hydroxyl groups at C3 and C6 decreased antifeedant activities. SAR studies suggested that the hydroxyl groups at C3 and C6 and the prenyl chains at C2 and C8 may be important for antibacterial and antifeedant activity. The optimal activity was found to depend on a balance of the hydrophilic and hydrophobic portions of molecule.

The simplified analogues of gambogic acid (77) and their pharmacological evaluations have been explored. The Pd(0)-catalyzed reverse prenylation of catechols, followed by the Claisen/Diels-Alder reaction cascade provided rapid and efficient access to various caged analogues. SAR studies of these compounds were evaluated in a multi-drug resistant promyelocytic leukemia cell line, HL-60/ADR (Adriamycin). The minimum bioactive motif of such compounds was represented by the intact ABC ring containing the C-ring caged structure. Cluvenone (196) exhibited a comparable cytotoxicity by inducing apoptosis to 77. In addition, 196 was almost 5-fold more toxic to primary B-cell acute lymphoblastic leukemia (IC_{50} 1.1 μM) than peripheral blood mononuclear cells from normal donors (IC_{50} 5.2 μM).

Department:	Chemistry	Student's Signature _Oraphin Chantarasriwong_
Field of Study:	Chemistry	Advisor's Signature _Warinthorn Chavasiri_
Academic Year:	2010	Co-advisor's Signature _E. Theodorakis_

ACKNOWLEDGEMENTS

CONTENTS

LIST OF TABLES

Tables   **Pages**

LIST OF FIGURES

Figures   **Pages**

Figures   **Pages**

Figures   **Pages**

Figures **Pages**

Figures   **Pages**

LIST OF SCHEMES

Schemes **Pages**

Schemes   **Pages**

Schemes   **Pages**

LIST OF ABBREVIATIONS

Å	angstroms
ADR	adriamycin-resistant
AlCl$_3$	aluminum chloride
anh.	anhydrous
aq.	aqueous
BBr$_3$	boron tribromide
Bn	benzyl
Bu	n-butyl
br s	broad singlet (NMR)
calcd	calculated
conc.	concentrated
CH$_2$Cl$_2$	dichloromethane
ClCOCOCl	oxayl chloride
d	doublet (NMR)
DBU	1,8-diazabicyclo[5.4.0]undec-7-ene
DCC	1,3-dicyclohexylcarbodiimide
dd	doublet of doublet (NMR)
DDQ	2,3-dichloro-5,6-dicyano-1,4-benzoquinone
DIBAL-H	diisobutylaluminum hydride
DIPEA	N,N-diisopropylethylamine
DMAP	4-(N,N-dimethylamino)pyridine
DMF	N,N-dimethylformamide
DMSO	dimethylsulfoxide
EC$_{50}$	effective concentration 50 %
EDC	N-ethyl-N'-(3-dimethylaminopropyl)carbodiimide
equiv.	equivalent (s)
Et	ethyl
EtOH	ethanol
g	gram (s)
FAB	fast atom bombardment

FT	fourier transform
Δ	heat
h	hour (s)
HATU	2-(1*H*-7-azabenzotriazol-1-yl)-1,1,3,3-tetramethyl uranium hexafluorophosphate
HEL	human embryonic lung fibroblasts
HeLa	henrietta lacks cervical cancer
HMDS	hexamethyldisilazane
HRMS	high resolution mass spectra
Hz	hertz
IC$_{50}$	inhibition concentration 50 %
IR	infrared
J	coupling constant (NMR)
m	multiplet (NMR)
m-CPBA	*m*-chloroperoxybenzoic acid
Me	methyl
MEMCl	2-methoxyethoxymethyl chloride
MeOH	methanol
m.p.	melting point
μg	microgram
min	minute (s)
mL	milliliter (s)
mmol	millimole (s)
MOM	methoxymethyl
N	normal
Na$_2$CO$_3$	sodium carbonate
NaClO$_2$	sodium chlorite
NADP$^+$	Nicotinamide adenine dinucleotide phosphate
ND	yield not determined
nm	nanometer
NMR	nuclear magnetic resonance
OsO$_4$	osmium tetroxide

°C	degree of Celsius
p	pentet
PCC	pyridinium chlorochromate
Pd	palladium
Ph	phenyl
ppm	part per million
PPTS	pyridinium p-toluenesulfonate
q	quartet (NMR)
quant	quantitative
R_f	retardation factor
RSM	recovered stating material
rt	room temperature
s	singlet (NMR)
SEM	[2-(trimethylsilyl)ethoxy]methyl
SeO$_2$	selenium dioxide
t	triplet (NMR)
t	tert
TBAF	tetrabutylammonium fluoride
t-BuOOH	tert-butyl hydroperoxide
TBS	$tert$-butyldimethylsilyl
THF	tetrahydrofuran
TFA	trifluoroacetic acid
TFAA	trifluoroacetic anhydride
TLC	thin layer chromatograph
UV	ultraviolet
W	watt
%	percent
α	alpha
β	beta
γ	gramma
δ	chemical shift

CHAPTER I

INTRODUCTION

The tropical trees and shrubs of the *Garcinia* species are mostly found in lowland rainforests of Southeast Asia, and are widely known for their pigments and as folk medicines [1]. Phytochemically, they are recognized as a rich source of xanthone natural products with high pharmaceutical potential [2-4]. Chemically, xanthones (9*H*-xanthen-9-ones) are a class of heterocylic compounds with dibenzo-γ-pyrone framework (Figure 1.1). Biosynthetically, xanthones are presumed to derive from a common benzophenone intermediate of a mixed shikimate (ring A)-acetate (ring C) pathway.
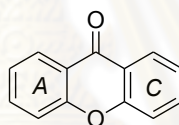
Figure 1.1 Representation of xanthone nucleus

Natural occurring xanthones, secondary metabolites, are found in a select number of rain forest plants, but nowhere are they found in more abundant than in the pericarp, or the rind of *Garcinia mangostana* Linn. *G. mangostana* is commonly called as a mangosteen and has been used as a traditional medicine for its anti-inflammatory properties as well as the treatment of skin infections and wounds for many centuries [5-6]. The phytochemistry study led to the isolation of α-mangostin found as a major compound in various parts of mangosteen [7]. α-Mangostin has been confirmed to show a variety of potent biological activities such as anti-inflammatory [8], antimicrobial [9] and antiproliferative activities [2]. As aforementioned facts, α-mangostin is an interesting target of opportunities for the discovery in chemistry and biology, leading to obtain a new drug and enhance the useful knowledge from the structure-activity relationship (SAR) study.

Caged xanthones are another compound which possesses an abundance of biologically active and unusually structural features. The chemical structure of these compounds is highlighted by the fusion of a unique 4-oxa-tricyclo[4.3.1.0^{3,7}]decan-2-one scaffold onto a common xanthone motif. Many caged natural xanthones are isolated from the plants in several *Garcinia* species *e.g.*, *G. bracteata* [10], *G. gaudichaudii* [11], *G. Morella* [12], *G. scortechinii* [13], and *G. hanburyi* [14]. Compounds of this type interestingly exhibited cytotoxic properties in several mammalian cancer cell lines [15], antitumor [16], anti-HIV-1 [17], and antibacterial activities [18]. The SAR studies of gambogic acid, a caged xanthone isolated from *G. hanburyi*, and related natural compounds have been reported that the unusual caged structure played an essential role in cytotoxic activities [19]. For these aforementioned reasons, the simplified caged xanthones have increased the interest in the synthesis to optimize the minimum pharmacophore of the caged *Garcinia* xanthones for the exploration of the new potent drug.

1.1 The Objective of This Research

This research was divided into two parts:

1. SAR of *α*-mangostin and its analogues

    - To isolate *α*-mangostin from the pericarp of *G. mangostana*

    - To synthesize the analogues of *α*-mangostin

    - To evaluate the antibacterial activity against *Staphylococcus aureus* ATCC 25923 and methicillin-resistant *S. aureus* (MRSA) and to analyze the SAR of *α*-mangostin and its analogues

    - To determine the anticandidal activity against *Candida albicans* of *α*-mangostin and its analogues

    - To evaluate the termite antifeedant activity and to analyze the SAR of *α*-mangostin and its analogues

2. Synthesis and pharmacological evaluation of caged *Garcinia* xanthones

    - To synthesize the simplified caged analogues through two key reactions: Pd(0) catalyzed reverse prenylation and Claisen/Diels-Alder rearrangement

- To explore the novel method for one-step introduction of di-allyoxy units using Pd(0) catalyst

- To investigate the cell proliferation and to analyze the SAR of caged *Garcinia* natural products and synthetic analogues against promyelocytic leukemia cell lines (HL-60) and multidrug-resistant promyelocytic leukemia (HL-60/ADR) cell lines

- To evaluate the antibacterial activity and to analyze the SAR of synthetic caged compounds against the community-associated MRSA strain TCH1516

- To explore the mechanism of cluvenone in the inhibition of HL-60/ADR cell growth whether involve inducing apoptosis

CHAPTER II

STRCTURE-ACTIVITY RELATIONSHIP OF α-MANGOSTIN AND ITS ANALOGUES

2.1   Introduction

Mangosteen, *Garcinia mangostana* Linn. (Guttiferae), -not just the inner flesh, but the whole fruit- represents the single greatest supply of beneficial xanthones. Research has revealed the mangosteen as the source of more than 40 distinct xanthones [3, 20] and ongoing science is finding new benefits of these xanthones every day.

The fruits of *G. mangostana* have been used as a traditional medicine [5-6] in Southeast Asia for the treatment of diarrhea, inflammation, and ulcers. Several preliminary screening showed that the crude extracts of mangosteen pericarps possessed antiproliferative [2], antibacterial [3], antioxidative, cytoprotective [4], antityrosinase [21] activities and apoptotic effects against human breast cancer SKBR3 cells [2]. In the United States, mangosteen products are now widely available and are highly popular because of their perceived role in enhancing human health. Mangosteen fruit juice has become a major botanical dietary supplement, and was ranked as one of the top-selling „botanicals‟ on the market since 2005. Nowadays, the extracts from mangosteen are used to apply to cosmetic uses such as soaps, creams, and washes in Thailand. It is claimed that mangosteen-made products are exactly the conditions encountered in acne-prone skin [22].

Studies from different laboratories have shown that α-mangostin (**1**) is a major secondary metabolite found in various parts of the mangosteen [7]. It consists of two isoprenyl units at C2 and C8, and three hydroxy groups at C1, C3 and C6, all of which connect to a xanthone backbone (Figure 2.1).
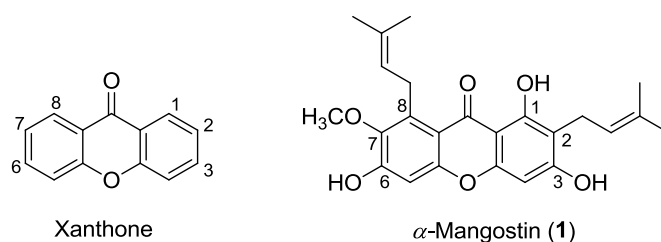
Figure 2.1 Xanthone backbone and α-mangostin (**1**)

α-Mangostin (**1**) has been extensively confirmed their biological activities for a competitive antagonism of the histamine H1 receptor [23], anti-inflammatory activities [8], inhibition of oxidative damage by human low-density lipoproteins (LDL) [24], antimicrobial activity against many microorganisms and weak antioxidant activity [23].

Due to being a major component in the pericarps of mangosteen and exhibiting potent biological activities, the structure of α-mangostin (**1**) was thus attractive in the modification to obtain an idea drug for medicine and useful information in chemical reaction.

2.1.1 Botanical Characteristics of *Garcinia mangostana* Linn. [25]

Scientific Name: *Garcinia mangostana* Linn.

Family Name: Guttiferae

Common Name: Mangosteen

Origin: India, Myanmar, Malaysia, Philippines, Sri Lanka and Thailand

The fruits of *G. mangostana* (Figure 2.2) are often called the "Queen of Fruits" and have been well-known as Mung Kun in Thai. The botanical characteristics of this plant can be described as follows:

Trees: 7-8 m high with dense heavy profusely bunched crown

Bark: dark-brown and rather hard with the yellowish inner bark

Leaves: leathey with the dark-brown timber

Flowers: 5 centimeters in diameter, 4-parted, bisexual, and borne singly or in pairs at the ends of the branchlets

Seeds: large, flattened- and embedded in snowy-white or pinkish delicious pulp, which is botanically called the aril

Figure 2.2 Fruit hulls of *Garcinia mangostana* Linn.

2.1.2 Preliminary Biological Activities and Literature Review on the Extracts from *Garcinia mangostana* Linn.

Due to the fact that the mangosteen fruits have been used as a traditional medicine for many years, this lets many scientists increase an interest in the extensively biological evaluations of their extracts such as antimicrobial, antioxidant, antifeedant, and anticancer activities.

Antimicrobial activity

The extracts of *G. mangostana* have been exhibited strong antimicrobial activities for many years. Gritsanapan and Chulasiri [26] found that the water extract of pericarps showed good activity to inhibit *Streptococcus faecalis* and *Vibrio cholerae* growth. Chomnawang and co-workers [3] evaluated in 2005 the antimicrobial activity of diverse Thai medicinal plants against acne-inducing bacteria using disc diffusion and broth dilution methods. The same minimum inhibitory concentration (MIC) values of *G. mangostana* in *Propionibacterium acnes* and *Staphylococcus epidermidis* were reported to be 0.039 mg/mL, and the minimum bactericidal concentration (MBC) for those bacterial species were 0.039 and 0.156 mg/mL, respectively. Studies on inflammation in terms of free radical scavenging and cytokine reducing properties were investigated in 2007 [3]. The ethanolic extract

showed the most potent activity against *Propionibacterium acnes* with an IC_{50} value of 6.13 μg/mL. In addition, this extract reduced both reactive oxygen species (ROS) production and the tumor necrosis factor-alpha (TNF-α) production with the highest inhibitory ratio at 77±1.28 and 94.59% (at 50 μg/mL of extract used), respectively. Antibacterial activity of the ethanolic extract against methicillin-resistant *S. aureus* (MRSA) was reported by Voravuthikunchai and Kitpipit [27] in 2005. The MIC and MBC values for that stain were reported around 0.05-0.4 and 0.1-0.4 mg/mL, respectively. Tadtong and co-workers [21] recently reported in 2009 the antibacterial activity of the extract from the pericarps to inhibit the pathogenic bacteria growth in the oral cavity, *Streptococcus mutans* DMST18777, *Porphyromonas gingivalis* DMST2136, and *Streptococcus pyogenes* DMST17020. This crude extract exhibited good activity against those three stains tested with the MIC value of 0.01 mg/mL. The related activity on *S. aureus* ATCC 25923 was examined, and its MIC was found to be 0.1 mg/mL. In addition to antifungal activities, the ethanolic, acetone, and methanolic extracts showed a moderate activity against three species of tinea: *Trichophyton rudrum*, *Trichophyton mentagrophyte*, and *Microsporum gypseum* [28].

Antioxidant activity

The methanolic extract of fruits was investigated by Kosem and co-workers [4] in 2007 for antioxidant and cytoprotective activities. The results indicated that its extract possessed reducing power as well as Fe^{2+} chelating activity. In addition, it revealed potent radical scavengers against hydroxyl and superoxide radicals and enhanced the cell survival by decreasing the oxidative damage in ECV304 endothelial cells after H_2O_2 exposure. In the 2,2-diphenyl-1-picrylhydrazyl radical (DPPH) assay, the ethanolic extract showed very good antioxidant activity with 50% inhibition of free radicals at a concentration of 6.13 μg/mL [3].

Antifeedant activity

The ethanolic extracts from the pericarps were subjected to control brown planthopper, *Nilaparvata lugens* Stal., (BPH) growth by Bullanpoti and co-workers [29] in 2006. The crude extract containing mangostin (**1**) *ca*. 2.96% w/w was trailed

by the topical sprayer method. This extract showed the toxicity in terms of LC_{50} *ca.* 1.39, 2.26, 5.44, 4.49, 4.03, and 3.84% w/v at 24 h exposure when using the 1st, 2nd, 3rd, 4th and 5th nymph, and adult BPH, respectively tested.

Anticancer activity

The effect of mangosteen extracts (100, 70 and 40% EtOH-H_2O) on histamine release and prostaglandin E2 synthesis was evaluated. Among them, 40% EtOH-H_2O extract showed potent inhibitory activities of both histamine release and prostaglandin E2 synthesis [30]. In addition, the methanolic extract from the pericarps displayed a dose-dependent inhibition of cell proliferation against human breast cancer (SKBR3) cell lines with ED_{50} of 9.25±0.64 μg/mL [2].

2.1.3 Chemical Constituents and Literature Reviews on *Garcinia mangostana* Linn.

A great variety of traditional medicine uses of *G. mangostana* and their preliminarily biological activities have guided the isolation and structural elucidation of chemical constituents from different parts of this plant. Schmid first reported [31] in 1855 the isolation of α-mangostin (**1**) from the pericarps of *G. mangostana*. Another richest sources were disclosed from the bark and dried sap containing α-mangostin (**1**) in 30-50% yield [32]. Although many scientists had proposed the molecular formulas and substituent connection of α-mangostin (**1**) since 1850s, the exact structure was successfully deduced by Yates and Stout [33] in 1958 as represented in Figure 2.3. Several different laboratories have confirmed the identities of α-mangostin (**1**) using many types of the spectroscopic methods [7, 34-36] such as ^{1}H, ^{13}C NMR and UV, and its X-ray structure was finally explored by Gales and Damas [37].

Besides α-mangostin (**1**), other chemical constituents of *G. mangostana* have been extensively isolated and are summarized in Table 2.1 and the structures of isolated xanthones are shown in Figure 2.3.

Table 2.1 Chemical constituents of *Garcinia mangostana* Linn.

Compound	Plant part	Reference
α-mangostin (**1**)	pericarp	[8, 33, 35, 38-40]
	bark	[33]
	latex	[33]
	aril	[35]
	young fruit	[41]
	green fruit	[42]
	stem bark	[43]
	root bark	[44-45]
	fruit	[46]
β-mangostin (**2**)	pericarp	[35]
	green fruit	[42]
	root bark	[44-45]
	stem bark	[43]
	leave	[47]
	root bark	[44-45]
γ-mangostin (**3**)	pericarp	[35]
	root bark	[44-45]
	fruit	[8, 39-40]
2,8-bis-(*γ,γ*-dimethylallyl)-1,3,7-trihydroxyxanthone (**4**)	aril	[35]
2-(*γ,γ*-dimethylallyl)-1,7-dihydroxy-3-methoxyxanthone (**5**)	aril	[35]

Table 2.1 (*Continued*)

Compound	Plant part	Reference
1-isomangostin (**6**)	pericarp	[35]
3-isomangostin (**7**)	pericarp	[35]
1-isomangostin hydrate (**8**)	pericarp	[35]
3-isomangostin hydrate (**9**)	pericarp	[35]
(5,9-dihydroxy-8-methoxy-2,2-dimethyl-7-(3-methylbut-2-enyl)-2*H*,6*H*-pyrano-[3,2-b]-xanthene-6-one) (**10**)	fruit	[48]
	stem bark	[43]
calabaxanthone (**11**)	aril	[35]
demethylcalabaxanthone (**12**)	aril	[35]
1,3,5-trioxygenated xanthone (**13**)	fruit	[49]
1,3,7-Trioxygenated xanthone (**14**)	fruit	[49]
1,6-dihydroxy-3,7-dimethoxy-2-(3-methylbut-2-enyl)-xanthone (**15**)	stem bark	[43]
gartanin (**16**)	pericarp	[35, 39]
	leave	[47]
8-deoxygartanin (**17**)	fruit	[39]
garcinone A (**18**)	fruit	[50]
garcinone B (**19**)	green fruit	[42, 50]
garcinone C (**20**)	fruit	[50]
garcinone D (**21**)	stem bark	[43, 45]
	root bark	[44]
garcinone E (**22**)	fruit	[39]
garcimangosone A (**23**)	fruit	[51-52]
garcimangosone B (**24**)	pericarp	[51-53]
garcimangosone C (**25**)	pericarp	[51-52]

Table 2.1 (*Continued*)

Compound	Plant part	Reference
garciniafuran (**26**)	heartwood	[54]
garcimangosxanthone A (**27**)	pericarp	[55]
garcimangosxanthone B (**28**)	pericarp	[55]
garcimangosxanthone C (**29**)	pericarp	[55]
BR-xanthone A (**30**)	pericarp	[56]
BR-xanthone B (**31**)	pericarp	[56]
mangosharin (**32**)	stem bark	[43]
mangostanol (**33**)	fruit	[39]
	stem bark	[43, 45]
	root bark	[44]
	green fruit	[42]
mangostanin (**34**)	fruit	[46]
6-deoxy-7-demethylmangostanin (**35**)	fruit	[46]
6-*O*-methylmangostanin (**36**)	not stated	[52]
mangostenol (**37**)	green fruit	[42]
mangostenone A (**38**)	green fruit	[42]
mangostenone B (**39**)	green fruit	[42]
mangostenone C (**40**)	fruit	[41]
mangostenone D (**41**)	young fruit	[41]
mangostenone E (**42**)	young fruit	[41]
mangostinone (**43**)	green fruit	[42]
smeathxanthone A (**44**)	pericarp	[53]
mangoxanthone (**45**)	heartwood	[57]
cudraxanthone G (**46**)	pericarp	[53]

Table 2.1 (*Continued*)

Compound	Plant part	Reference
8-hydroxycudraxanthone (**47**)	pericarp	[53]
1,3,6,7-tetrahydroxyxanthone (**48**)	heart wood	[58]
dulxanthone D (**49**)	heartwood	[57]
1,3,6,7-tetrahydroxy-2,8-(3-methyl-2-butenyl) xanthone (**50**)	pericarp	[40]
1,3,7-trihydroxy-2,8-di-(3-methylbut-2-enyl)xanthone (**51**)	fruit	[46]
1,5-dihydroxy-2-(3-methylbut-2-enyl)-3-methoxy-xanthone (**52**)	pericarp	[59]
1,5,8-trihydroxy-3-methoxy-2-(3-methylbut-2-enyl) xanthone (**53**)	leave	[34, 47, 58]
1,6-dihydroxy-3-methoxy-2[3-methyl-2-butenyl] xanthone (**54**)	leave	[47, 58]
1,6-dihydroxy-3,7-dimethoxy-2-(3-methylbut-2-enyl)-xanthone (**55**)	heartwood	[43, 52, 54]
1,7-dihydroxy-2-(3-methylbut-2-enyl)-3-methoxy-xanthone (**56**)	pericarp	[52, 59-61]
1,5-dihydroxy-2-isopentyl-3-methoxy xanthone (**57**)	pericarp	[58]
1,7-dihydroxy-2-isopentyl-3-methoxy xanthone (**58**)	pericarp	[58]
1,3-dihydroxy-2-(2-hydroxy-3-methylbut-3-enyl)-6,7-dimethoxy-8-(3-methylbut-2-enyl)-xanthone (**59**)	heartwood	[52, 54]
1,6-dihydroxy-2-(2-hydroxy-3-methylbut-3-enyl)-3,7-dimethoxy-8-(3-methylbut-2-enyl)-xanthone (**60**)	heartwood	[52, 54]
1-hydroxy-2-(2-hydroxy-3-methylbut-3-enyl)-3,6,7-trimethoxy-8-(3-methylbut-2-enyl)-xanthone (**61**)	heartwood	[52, 54]
1,6-dihydroxy-3,7-dimethoxy-2-(3-methylbut-2-enyl)-8-(2-oxo-3-methylbut-3-enyl)-xanthone (**62**)	heartwood	[52, 54]
1,6-dihydroxy-8-(2-hydroxy-3-methylbut-3-enyl)-3,7-dimethoxy-2-(3-methylbut-2-enyl)-xanthone (**63**)	heartwood	[52, 54]

Table 2.1 (*Continued*)

Compound	Plant part	Reference
1-hydroxy-8-(2-hydroxy-3-methylbut-3-enyl)-3,6,7-trimethoxy-2-(3-methylbut-2-enyl)-xanthone (**64**)	heartwood	[52, 54]
(16*E*)-1,6-dihydroxy-8-(3-hydroxy-3-methylbut-1-enyl)-3,7-dimethoxy-2-(3-methylbut-2-enyl)-xanthone (**65**)	heartwood	[52, 54]
(16*E*)-1-hydroxy-8-(3-hydroxy-3-methylbut-1-enyl)-3,6,7-trimethoxy-2-(3-methylbut-2-enyl)-xanthone (**66**)	heartwood	[52, 54]
1,2-dihydro-1,8,10-trihydroxy-2-(2-hydroxypropan-2-yl)-9-(3-methylbut-2-enyl) furo[3,2-a] xanthen-11-one (**67**)	fruit	[46]
1,3,5-trihydroxy-13,13-dimethyl-2H-pyran[7,6-b]xanthen-9-one (**68**)	heartwood	[57]
1,3,7-trihydroxy-2-methoxyxanthone (**69**)	heartwood	[57]
trapezifolixanthone (**70**)	green fruit	[42]
thwaitesixanthone (**71**)	fruit	[41]
tovophyllin A (**72**)	pericarp	[53]
tovophyllin B (**73**)	green fruit	[42]
	pericarp	[52]
2,7-di-(3-methylbut-2-enyl)-1,3,8-trihydroxy-4-methyl-xanthone (**74**)	fruit	[62]
2,8-di-(3-methylbut-2-enyl.-7-carboxy-1,3-dihydroxyxanthone (**75**)	fruit	[62]
2,8-dihydroxy-6-methoxy-5-(3-methylbut-2-enyl)-xanthone (**76**)	stem	[45]

1: R^1 =H, R^2 = OH, R^3 = CH$_3$
2: R^1 = CH$_3$, R^2 = OH, R^3 = CH$_3$
3: R^1 =H, R^2 = OH, R^3 = H
4: R^1 =H, R^2 = H, R^3 = H

5

6: 1-isomangostin

7: 3-isomangostin

8: 1-isomangostin hydrate

9: 3-isomangostin hydrate

10: R^1 = OH, R^2 = CH$_3$
11: R^1 = H, R^2 = CH$_3$
12: R^1 = H, R^2 = H

13: R^1 = OH, R^2 = H, R^3 = H
14: R^1 = H, R^2 = H, R^3 = OH
15: R^1 = H, R^2 = OH, R^3 = OCH$_3$

16: R^1 = OH: gartanin
17: R^1 = H: 8-deoxygartanin

18: garcinone A

19: garcinone B

20: R^1 = H: garcinone C
21: R^1 = CH$_3$: garcinone D

22: garcinone E

23: garcimangosone A

24: garcimangosone B

Figure 2.3 Chemical constituents of *Garcinia mangostana* Linn.
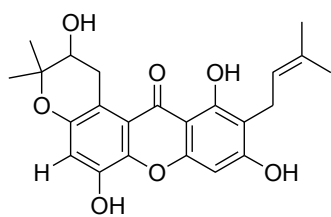
25: garcimangosone C
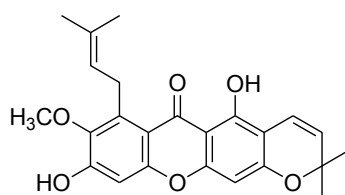
26: garciniafuran
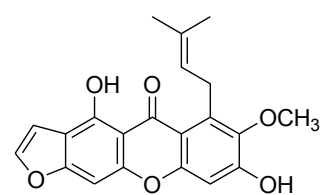
27: garcimangosxanthone A
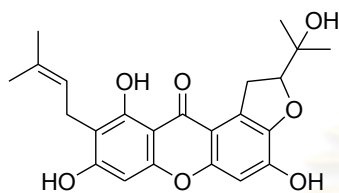
28: garcimangosxanthone B
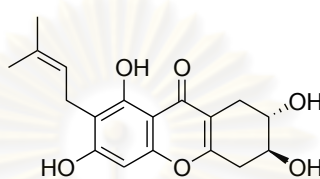
29: garcimangosxanthone C
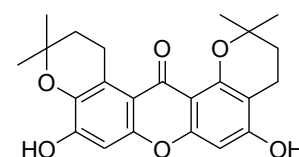
30: BR-xanthone B
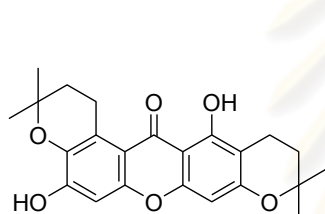
31: BR-xanthone A
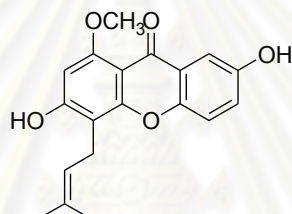
32: mangosharin
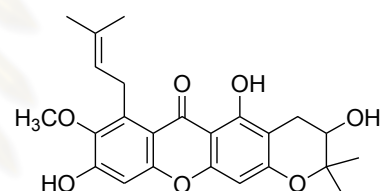
33: mangostanol
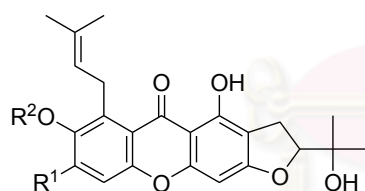
34: R^1 = OH, R^2 = CH$_3$: mangostanin
35: R^1 = H, R^2 = H
36: R^1 = OCH$_3$, R^2 = CH$_3$
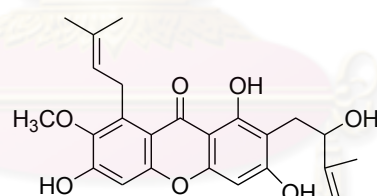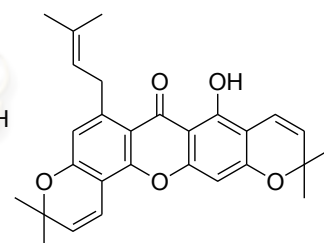
37: mangostenol
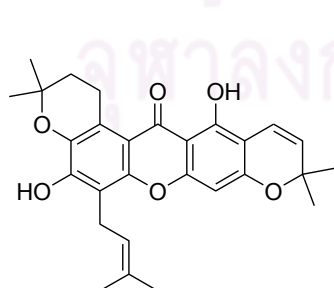
38: mangostenone A
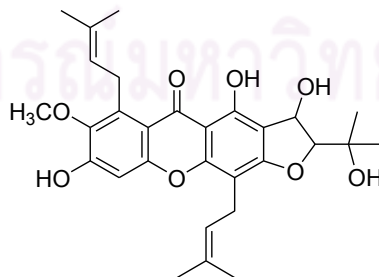
39: mangostenone B

40: mangostenone C
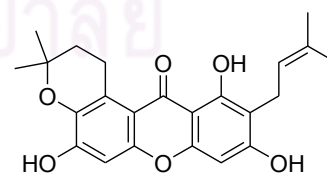
41: mangostenone D

Figure 2.3 (*Continued*)

42: mangostenone E

43: R^1 = H, R^2 = H: mangostinone
44: R^1 = H, R^2 = OH: smeathxanthone A

45: mangoxanthone

46: R^1 = CH$_3$: cudraxanthone G
47: R^1 = H

48

49: R^1 = OH, R^2 = CH$_3$: dulxanthone D
50: R^1 = OH, R^2 = H
51: R^1 = H, R^2 = H

52: R^1 = H,
53: R^1 = OH

54: R^1 = OH, R^2 = H
55: R^1 = OH, R^2 = OCH$_3$
56: R^1 = H, R^2 = OH

57: R^1 = OH, R^2 = H
58: R^1 = H, R^2 = OH

59: R^1 = H, R^2 = CH$_3$
60: R^1 = CH$_3$, R^2 = H
61: R^1 = CH$_3$, R^2 = CH$_3$

62: R^1 = H, X = O
63: R^1 = H, X = H, OH
64: R^1 = CH$_3$, X = H, OH

65: R^1 = H,
66: R^1 = CH$_3$

67

68

69

Figure 2.3 (*Continued*)

70: trapezifolixanthone   **71:** thwaitesixanthone   **72:** tovophyllin A

73: tovophyllin B   **74**   **75**

76

Figure 2.3 (*Continued*)

2.1.4 Literature Review on Biological Activities of α-Mangostin

There are significant numbers of reports on the biological activity of α-mangostin (**1**) against a verity of microorganisms.

Antibacterial activity

Mahabusarakam and co-workers [9] addressed in 1986 the isolation of α-mangostin (**1**) and related components from the fruits of *G. mangostana*. α-Mangostin (**1**) was tested for its antibacterial activity against *S. aureus* both normal (ATCC 25923) and penicillin-resistant strains using the broth dilution method and using methicillin as a comparison. α-Mangostin (**1**) exhibited the best activity against

normal *S. aureus* with the MIC value of 15.6 μg/mL among all the isolated compounds tested. An additional study on penicillin-resistant strains showed that the MIC of α-mangostin (**1**) was found to be in the range of 1.56-12.5 μg/mL.

Due to the highest activity of mangosteen extract against *S. aureus* NIHJ 209p found, the antibacterial activity of α-mangostin (**1**) against methicillin-resistant *S. aureus* (MRSA) was examined by Linuma and co-workers in 1996 [63]. It suggested that α-mangostin (**1**) have the potent activity with the MIC value of 0.31-1.25 μg/mL, which was more active than the antibiotic vancomycin (3.13-6.25 μg/mL). In 2005, Sakagami and co-workers [64] isolated α-mangostin (**1**) from the stem bark of *G.mangostana* and tested their antibacterial and synergism effects. α-Mangostin (**1**) itself displayed the MIC values of 6.25 and 6.25-12.5 μg/mL against vancomycin resistant *Enterococci* (VRE) and MRSA, respectiviely. Similar activities were found on the synergism between α-mangostin (**1**) and commercially available gentamicin or vancomycin hydrochloride. In addition, α-mangostin (**1**) exhibited good activity against *Mycobacterium tuberculosis* with the MIC value of 6.25 μg/mL [61].

Qualitative antimicrobial studies in 2006 showed that α-mangostin (**1**) was inactive against Gram-negative *Vibrio anguillarum* (ATCC 19264), but displayed moderate activity against Gram-positive bacteria *S. aureus* (ATCC 6538) with a diameter of inhibition zone of 16 mm which was twice less active than the reference oxacillin [65].

Antifungal activity

α-Mangostin (**1**) showed no activity against *Candida tropicalis* (ATCC 66029) [65], *Candida albicans* and *Cryptococcus neoformans*, and exhibited moderate activities against *Trichophyton mentagrophytes* and *Microsporun gypseum* [9].

Gopalakrishnan and co-workers [66] reported in 1997 the antifungal evaluation of α-mangostin (**1**) against three phytopathogenic fungi: *Fusarium*

oxysporum f.sp. *vasinfectum*, *Alternaria tenuis*, and *Dreschlera oryzae*. At the concentration of 1000 ppm, α-mangostin (**1**) exhibited 66.7, 39.7 and 23.3% inhibitions on the growth of *Fusarium oxysporum* f.sp. *vasinfectum*, *Alternaria tenuis*, and *Dreschlera oryzae*, respectively.

Recently, Kaomongkolgit and co-workers [67] evaluated in 2009 the antifungal activity of α-mangostin (**1**) against *Candida albicans*, the most important microorganism implicated in oral candidiasis, using broth dilution method. α-Mangostin (**1**) was effective against *Candida albicans* with the MIC and MFC values of 1,000 and 2,000 μg/mL, respectively, which was more active than both Clotrimazole and Nystatin. Related to the toxicity study, α-mangostin (**1**) was not toxic to human gingival fibroblast at 4,000 μg/mL for 480 min.

Antiplasmodium activity

α-Mangostin (**1**) was found to be moderately active against two strains of *Plasmodium falciparum*: F32 (chloroquine-sensitive) and FcM29 (chloroquine resistant) [65].

Antioxidant activity

In various antioxidant assays, α-mangostin (**1**) exhibited the moderate antioxidant capability. Its scavenging effect on the DPPH, superoxide anion, and hydroxy radicals was 53.5, 72.9, and 49.4%, respectively at 20 μg/mL. Similar result was found on the inhibition of linoleic acid peroxidation (62.4% at 40 μg/mL) [40]. In addition, α-mangostin (**1**) seemed to be a free radical scavenger to protect the low density lipoprotein (LDL) from oxidative damage [24].

Six xanthones from the pericarps of mangosteen were investigated to inhibit the human leukemia (HL-60) cell lines growth. Among them, α-mangostin (**1**) displayed the best activity in the complete inhibition at 10 μM through the induction of apoptosis [60]. α-Mangostin (**1**) was suggested to induce Ca(2+)-ATPase-dependent apoptosis *via* mitochondrial pathway in PC12 rat pheochromocytoma cells with the EC_{50} value of 4 μM [68]. The cytotoxicity of xanthones isolated from the

young fruit of *G. mangostana* was examined. Among all tested compounds, α-mangostin (**1**) exhibited the most efficient activity against both breast cancer (BC-1) cell lines with the IC_{50} value of 0.92 μg/mL and epidermoid carcinoma of the mouth (KB) cell lines with an IC_{50} value of 2.08 μg/mL [41]. In vitro cytotoxicity study indicated that α-mangostin (**1**) exhibited high inhibitory effect on the growth of human colon cancer DLD-1 cells with the IC_{50} of 7.5±0.3μM [69]. It was also suggested that α-mangostin (**1**) have antiproliferative effects against human colon cancer DLD-1 cells by inducing cell-cycle arrest and apoptosis [70], but weak cytotoxicity (IC_{50} 79.2 μg/mL) against human melanoma cells (A375) [65]. Studies on CEM-SS cell line, γ-Mangostin (**3**) displayed the most cytotoxicity with a very low IC_{50} value of 4.7 μg/mL, while α-mangostin (**1**), mangostanol (**33**), and garcinone D (**21**) showed significant activities with IC_{50} values of 5.5, 9.6, and 3.2 μg/mL, respectively [45].

Anti-inflammatory activity

α-Mangostin (**1**) could be used as an anti-inflammatory agent. It inhibited nitric oxide (NO) and PGE_2 production from lipopolysaccharide LPS-stimulated RAW 264.7 cells, showing the IC_{50} values of 12.4 and 11.08 μM, respectively. The effects of this compound on the induction of iNOS and COX enzyme expression were also tested. α-Mangostin (**1**) reduced the induction of inducible nitric oxide synthase (iNOS) at 3-5 μM, but not cyclooxygenase 2 (COX-2) [8].

Antifeedant activity

α-Mangostin (**1**) was identified as a mosquito sterol carrier protein-2 inhibitor *via* high throughput insecticide screening [71]. This compound was tested for its larvicidal activity against third instar larvae of six mosquito species, and the median lethal concentration values range from 0.84 to 2.90 ppm. The residual larvicidal activity of α-mangostin (**1**) was examined under semifield conditions and revealed that the tested compound was photolytic with a half-life of 53 min in water under full sunlight exposure. The effect of α-mangostin (**1**) on activities of major detoxification enzymes such as P450, glutathione *S*-transferase, and esterase was investigated.

α-Mangostin (**1**) significantly elevated activities of P450 and glutathione *S*-transferase in larvae, whereas it suppressed esterase activity. Toxicity of *α*-mangostin (**1**) against young rats was studied, and there was no detectable adverse effect at dosages as high as 80 mg/kg.

2.1.5 Literature Review on Structure-Activity Relationship of *α*-Mangostin and Related Compounds

A wide variety of reports have been addressed for the structure-activity relationships (SAR) of *α*-mangostin (**1**) and its synthetic derivatives.
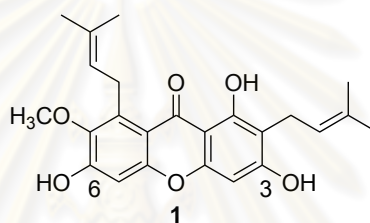
In 1997, Gopalakrishnan and co-workers [66] evaluated the antifungal activity of several xanthones isolated from the fruits of *G. mangostana* and some derivatives of *α*-mangostin (**1**) against three phytopathogenic fungi, *Fusarium oxysporum* f.sp. *vasinfectum*, *Alternaria tenuis*, and *Dreschlera oryzae*. The natural xanthones: *α*-mangostin (**1**), *γ*-mangostin (**3**) and gartanin (**16**) showed good inhibitory activity against the three fungi. The alkylation of C3 and C6 hydroxyls with isopropyl, allyl and acetyl groups reduced the inhibitory activity drastically.

In 1998, Lu and co-workers [72] examined the inhibition of eukaryote protein kinases and of a cyclic nucleotide-binding phosphatase by a series of prenylated xanthones. The prenylated xanthones examined were mostly derivatives of *α*-mangostin (**1**) in which the 3- and 6-hydroxyl groups were variously substituted, or derivatives of 3-isomangostin (**7**) in which the 6-hydroxyl was substituted or the prenyl side chain was modified.

In 2000, Mahabusarakam and co-workers [73] reported that structure modification of mangostin can provide a very profound effect on inhibitory oxidation activity of LDL, low density lipoprotein. Derivatization of the C3 and C6 hydroxyl groups with either methyl, acetate, propane diol or nitrite substantially reduced

antioxidant activity. In contrast, derivatization of the C3 and C6 with aminoethyl derivatives enhanced antioxidant activity, which may be related to changes in solubility. Cyclization of the prenyl chains displayed little influence on antioxidant activity.

In 2003, Suksamrarn and co-workers [61] reported that α-mangostin (**1**), β-mangostin (**2**) and garcinone B (**19**) exhibited strong inhibitory effect against *Mycobacterium tuberculosis* with MIC value of 6.25 μg/mL. Tri- and tetra-oxygenated xanthones with di-isoprenyl units or with a isoprenyl unit and a modified isoprenyl groups are essential for high activities.

In 2006, Mahabusarakam and co-workers [74] investigated α-mangostin (**1**) and a series of synthetic derivatives for their *in vitro* antiplasmodial activity against *Plasmodium falciparum*. α-Mangostin (**1**) itself showed moderate activity, but prenylated xanthones containing alkylamino groups exhibited potent antiplasmodial activity.

Recently, Ha and co-workers [75] synthesized mono- and di-alkylated α-mangostin derivatives and evaluated the cytotoxicity against DLD-1 (human colon cancer cells) cell lines using the MTT assay. The SAR study indicated that α-mangostin (**1**) exhibited the strongest activity with the 87.1 and 96.7 % inhibition of cell proliferation after 48 h and 72 h of exposure of the tested compound to cell lines, respectively. After 48 h, the mono-*O*-alkylated derivative (37% inhibition) showed more active than di-*O*-alkylated compound (4.4% inhibition). From these results, it was proposed that the activity depended on the number of free hydroxyl groups.

2.2 Experimental

2.2.1 Instruments and Equipment

Thin layer chromatography (TLC) was performed on aluminum sheets precoated with silica gel (Merck Kieselgel 60 PF$_{254}$). Column chromatography was carried out on silica gel (Merck Kieselgel 60, 70-230 mesh).

The ^{1}H and ^{13}C NMR spectra were performed in deuterated chloroform (CDCl$_3$) with tetramethylsilane (TMS) as an internal reference on the Varian nuclear magnetic resonance spectrometer, model Mercury plus 400 NMR spectrometer which operated at 399.84 MHz for ^{1}H and 100.54 MHz for ^{13}C nuclei. The chemical shifts (δ) are assigned by comparison with residue solvent protons.

2.2.2 Chemicals

All solvents used in this research were purified prior to use by standard methodology. The reagents used for synthesis were purchased from Fluka chemical company or otherwise stated and were used without further purification.

2.2.3   Isolation of α-Mangostin (1) from *Garcinia mangostana* Linn.

2.2.3.1 Plant Material

The pericarps of *G. mangostana* were collected in May 2007 from commercially available markets in Bangkok, Thailand.

2.2.3.2 Isolation and Extraction

Dried and ground pericarps (2.40 kg) were macerated in EtOAc. After 3 days, the mixture was filtered, and the residue was re-extracted three more times with EtOAc. The combined filtrate was concentrated under reduced pressure to yield the EtOAc crude extract in 27% w/w (0.64 kg). The EtOAc crude extract was then crystallized using hexane and EtOAc to give 1% (23.0 g) of α-mangostin (1) from the pericarp.
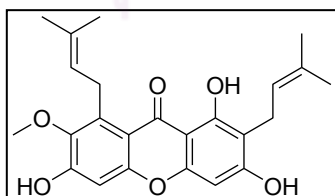
α-mangostin (1): light yellow solid (1%); R_f = 0.23 (33% EtOAc-hexane); ^{1}H NMR (400 MHz, CDCl$_3$) δ 13.77 (s, 1H), 6.82 (s, 1H), 6.35 (s, 1H), 6.29 (s, 1H), 6.21 (s, 1H), 5.31-5.25 (m, 2H), 4.09 (d, J = 6.0 Hz, 2H), 3.80 (s, 3H), 3.45 (d, J = 7.0 Hz, 2H), 1.84 (s, 3H), 1.83 (s, 3H), 1.77 (s, 3H), 1.69 (s, 3H); ^{13}C NMR (100 MHz, CDCl$_3$) δ 182.0, 161.5, 160.5, 155.7, 155.0, 154.5, 142.5, 137.0,

135.5, 132.1, 123.1, 121.5, 112.1, 108.6, 103.6, 101.6, 93.3, 62.0, 26.5, 25.8, 25.8, 21.4, 18.2, 17.9; HRMS calc. for $C_{24}H_{26}O_6$ (M + Na)$^+$ 433.1622, found 433.1625.

2.2.4 General Procedure for the Synthesis of Ester Analogues of α-Mangostin (M1-M11 and D1-D11)

From acid chloride

To a stirred solution of α-mangostin (**1**) (0.41 g, 1 mmol) and 4-picoline (3 mL, 3 mmol) in CH_2Cl_2 (3 mL) was added selected acylating agent (3 mmol) at room temperature. Then, the reaction mixture was allowed to heat at refluxing CH_2Cl_2. After 3 h, the reaction was allowed to warm at room temperature and was then diluted with CH_2Cl_2. The organic layer was extracted with 1 N HCl and saturated aq. NaHCO$_3$, respectively, dried over anh. Na$_2$SO$_4$ and evaporated *in vacuo*. The mixture was separated with silica gel column chromatography eluting with appropriate hexane/EtOAc system to achieve the desired esters.
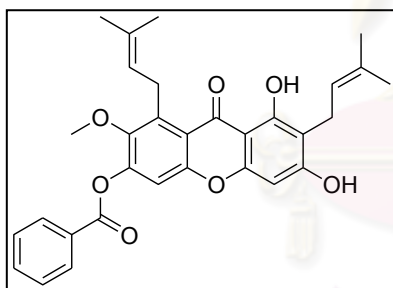
6-Mono-O-benzoyl mangostin (M1): Yellow needle (30%); R_f = 0.42 (33% EtOAc-hexane); ^{1}H NMR (CDCl$_3$) δ 13.59 (s, 1H), 8.25 (d, J = 7.4 Hz, 2H), 7.70 (t, J = 7.5 Hz, 1H), 7.57 (t, J = 7.8 Hz, 2H), 7.23 (s, 1H), 6.30 (s, 1H), 6.28 (s, 1H), 5.29-5.24 (m, 2H), 4.17 (d, J = 6.1 Hz, 2H), 3.77 (s, 3H), 3.46 (d, J = 7.0 Hz, 2H), 1.85 (s, 3H), 1.83 (s, 3H), 1.77 (s, 3H), 1.69 (s, 3H); ^{13}C NMR (100 MHz, CDCl$_3$) δ (ppm) 182.1, 164.1, 162.1, 160.7, 155.0, 153.9, 149.1, 146.7, 139.0, 135.8, 134.2, 132.2, 130.4, 128.8, 122.9, 121.3, 116.9, 110.6, 108.7, 103.9, 93.4, 61.9, 26.5, 25.9 (2C), 21.5, 18.2, 17.9.

3,6-Di-O-benzoyl mangostin (D1): Yellow needle (42%); R_f = 0.63 (33% EtOAc-hexane); ^{1}H NMR (CDCl$_3$) δ 13.44 (s, 1H), 8.17-7.43 (m, 10H), 7.21 (s, 1H), 6.70 (s, 1H), 5.20-5.10 (m, 2H), 4.11 (d, J = 6.1 Hz, 2H), 3.72 (s, 3H), 3.32 (d, J = 6.8 Hz, 2H), 1.78 (s, 3H), 1.64 (s, 3H),

1.53 (s, 6H); ^{13}C NMR (100 MHz, CDCl$_3$) δ 182.9, 164.2, 163.9, 161.0, 155.3, 154.1, 153.8, 149.7, 146.9, 139.1, 134.2, 133.9, 132.4, 130.4, 130.3, 128.9, 128.8, 128.7, 128.5, 122.7, 121.4, 116.8, 116.5, 110.8, 107.2, 100.6, 61.9, 26.5, 25.9, 25.7, 22.4, 18.3, 17.8.
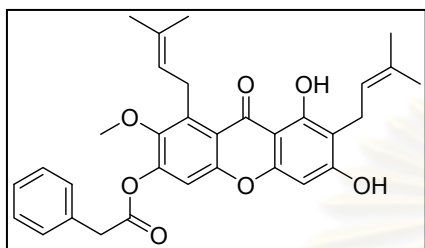
6-Mono-O-phenylacetyl mangostin (M2): Yellow needle (25%); R_f = 0.43 (33% EtOAc-hexane); ^{1}H NMR (CDCl$_3$) δ 13.57 (s, 1H), 7.43-7.34 (m, 5H), 7.07 (s, 1H), 6.28 (s, 1H), 6.19 (s, 1H), 5.28 (t, *J* = 5.4 Hz, 1H), 5.18 (t, *J* = 5.4 Hz, 1H), 4.10 (d, *J* = 5.7 Hz, 2H), 3.93 (s, 2H), 3.48 (s, 3H), 3.47-3.45 (m, 2H), 1.84 (s, 3H), 1.80 (s, 3H), 1.77 (s, 3H), 1.66 (s, 3H); ^{13}C NMR (100 MHz, CDCl$_3$) δ 181.8, 169.4, 161.8, 160.6, 154.7, 153.7, 148.7, 146.3, 139.1, 132.7, 132.0, 129.5, 128.9, 127.7, 123.0, 121.6, 117.0, 110.2, 103.6, 93.1, 61.6, 41.4, 26.4, 25.8, 21.4, 18.2, 17.9.
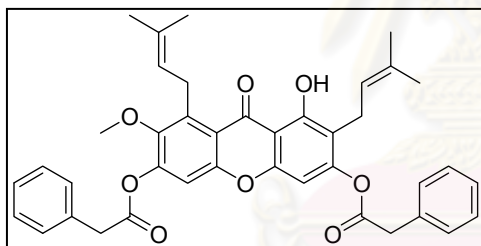
3,6-Di-O-phenylacetyl mangostin (D2): Yellow needle (33%); R_f = 0.63 (33% EtOAc-hexane); ^{1}H NMR (CDCl$_3$) δ 13.42 (s, 1H), 7.42-7.33 (m, 10H), 7.09 (s, 1H), 6.60 (s, 1H), 5.17-5.04 (m, 2H), 4.09 (d, *J* = 5.9 Hz, 2H), 3.94 (s, 2H), 3.91 (s, 2H), 3.47 (s, 3H), 3.24 (d, *J* = 6.6 Hz, 2H), 1.82 (s, 3H), 1.74 (s, 3H), 1.68 (s, 3H), 1.67 (s, 3H); ^{13}C NMR (100 MHz, CDCl$_3$) δ 182.8, 169.1, 168.6, 160.9, 154.8, 154.0, 153.6, 149.5, 146.7, 139.1, 132.9, 132.7, 132.4, 132.3, 129.5, 129.4, 128.9, 128.8, 127.6 (2C), 122.6, 121.3, 116.8, 116.3, 110.5, 107.1, 100.2, 61.6, 41.4 (2C), 26.4, 25.9, 25.7, 22.2, 18.2, 17.9.
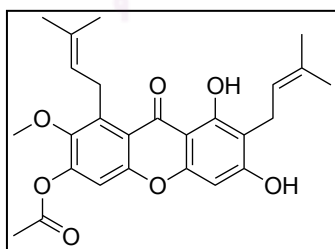
6-Mono-O-acetyl mangostin (M3): light yellow solid (22%); R_f = 0.33 (33% EtOAc-hexane); ^{1}H NMR (400 MHz, CDCl$_3$) δ 13.55 (s, 1H), 7.08 (s, 1H), 6.35 (s, 1H), 6.25 (s, 1H), 5.30-5.20 (m, 2H), 4.13 (d, *J* = 6.1 Hz, 2H), 3.76 (s, 3H), 3.44 (d, *J* = 7.0 Hz, 2H), 2.39 (s, 3H), 1.84 (s, 3H), 1.83 (s, 3H), 1.76 (s, 3H), 1.68 (s, 3H); ^{13}C NMR (100 MHz, CDCl$_3$) δ 182.3, 168.0, 162.3, 160.9, 155.2, 154.1, 149.0, 146.7, 139.2, 135.9, 132.4, 123.1, 121.6,

117.2, 110.6, 109.0, 104.0, 93.6, 61.9, 26.7, 26.1, 21.7, 21.2, 18.4, 18.2; HRMS calc. for $C_{26}H_{28}O_7$ $(M + Na)^+$ 475.1727, found 475.1729.
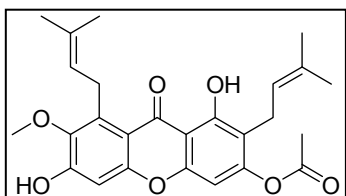
*3-Mono-O-acetyl mangostin (**M3a**)*: light yellow solid (10%); R_f = 0.33 (33% EtOAc-hexane); ^{1}H NMR (400 MHz, CDCl$_3$) δ 13.63 (s, 1H), 6.83 (s, 1H), 6.60 (s, 1H), 6.39 (s, 1H), 5.23-5.14 (m, 2H), 4.07 (d, J = 6.1 Hz, 2H), 3.80 (s, 3H), 3.31 (d, J = 6.9 Hz, 2H), 2.34 (s, 3H)1.83 (s, 3H), 1.77 (s, 3H), 1.69 (s, 6H). ^{13}C NMR (100 MHz, CDCl$_3$) δ 182.5, 168.6, 161.0, 156.0, 156.0, 155.1, 154.4, 153.6, 137.3, 132.3, 132.2, 132.1, 122.9, 121.5, 116.0, 107.0, 101.6, 100.2, 62.1, 26.6, 25.8, 25.7, 22.3, 21.0, 18.2, 17.8.
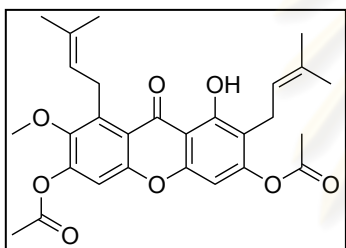
*3,6-Di-O-acetyl mangostin (**D3**)*: light yellow solid (48%); R_f = 0.45 (33% EtOAc-hexane); ^{1}H NMR (400 MHz, CDCl$_3$) δ 13.42 (s, 1H), 67.13 (s, 1H), 6.64 (s, 1H), 5.19-5.14 (m, 2H), 4.13 (d, J = 6.2 Hz, 2H), 3.78 (s, 3H), 3.32 (d, J = 6.9 Hz, 2H), 2.39 (s, 3H), 2.34 (s, 3H), 1.83 (s, 3H), 1.78 (s, 3H), 1.69 (s, 6H); ^{13}C NMR (100 MHz, CDCl$_3$) δ 182.8, 168.4, 168.0, 161.0, 154.8, 154.0, 153.7, 149.4, 146.7, 139.1, 132.3, 132.2, 122.6, 121.3, 116.8, 116.2, 110.6, 107.1, 100.3, 61.7, 26.4, 25.8, 25.7, 22.3, 21.0, 20.9, 18.2, 17.8; HRMS calc. for $C_{28}H_{30}O_8$ $(M + Na)^+$ 517.1833, found 517.1830.

From carboxylic acid

According to the method reported by Chantarasriwong and co-workers [76], the ester analogues using a carboxylic acid as a starting material could be prepared by two-step process as follows:

Step 1: PPh$_3$ (0.52 g, 2 mmol) in CH$_2$Cl$_2$ (3 mL) was added to a mixture of selected carboxylic acid (1 mmol) and Cl$_3$CCONH$_2$ (0.32 g, 2 mmol) in CH$_2$Cl$_2$ (3 mL) at reflux temperature. The mixture was stirred for approximately 1 h.

Step 2: A mixture of α-mangostin (**1**) (0.41 g, 1 mmol) and 4-picoline (0.3 mL, 3 mmol) was added to the above mixture. The reaction was continued

stirring for another 3 h or followed by TLC at reflux temperature. When the reaction was completed, the organic layer was extracted with 1N HCl and saturated aq. $NaHCO_3$, respectively, dried over anh. Na_2SO_4 and evaporated *in vacuo*. The mixture was separated with silica gel column chromatography eluting with appropriate hexane-EtOAc system to achieve the desired esters.
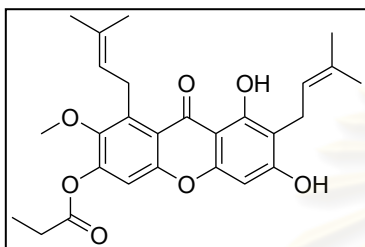
6-Mono-O-propinoyl mangostin (M4): light yellow solid (35%); R_f = 0.29 (25% EtOAc-hexane); ^{1}H NMR (400 MHz, $CDCl_3$) δ 7.08 (s, 1H), 6.34 (s, 1H), 6.20 (s, 1H), 5.30-5.21 (m, 2H), 4.12 (d, J = 6.0 Hz, 2H), 3.75 (s, 3H), 3.43 (d, J = 6.9 Hz, 2H), 2.70 (q, J = 15.1, 7.6 Hz, 2H), 1.83 (s, 6H), 1.76 (s, 3H), 1.68 (s, 3H), 1.33 (t, J = 15.1 Hz, 3H); ^{13}C NMR (100 MHz, $CDCl_3$) δ 182.3, 172.2, 162.2, 160.9, 155.2, 154.1, 149.1, 146.7, 139.2, 135.6, 132.3, 123.2, 121.6, 117.1, 110.6, 109.1, 104.0, 93.5, 61.9, 27.9, 26.6, 26.1, 21.7, 18.4, 18.1, 9.2; HRMS calc. for $C_{27}H_{30}O_7$ $(M + Na)^+$ 489.1884, found 489.1882.
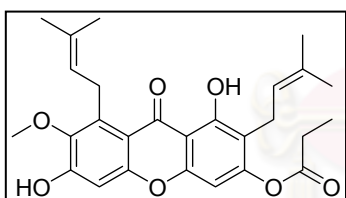
3-Mono-O-propinoyl mangostin (M4a): light yellow solid (5%); R_f = 0.29 (25% EtOAc-hexane); ^{1}H NMR (400 MHz, $CDCl_3$) δ 13.62 (s, 1H), 6.83 (s, 1H), 6.61 (s, 1H), 6.35 (s, 1H), 5.24-5.13 (m, 2H), 4.08 (d, J = 5.8 Hz, 2H), 3.81 (s, 3H), 3.30 (d, J = 6.6 Hz, 2H), 2.63 (q, J = 15.1, 7.5 Hz, 2H), 1.83 (s, 3H), 1.76 (s, 3H), 1.69 (s, 3H), 1.68 (s, 3H), 1.30 (t, J = 7.6 Hz, 3H).
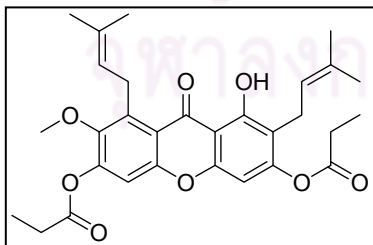
3,6-Di-O-propinoyl mangostin (D4): light yellow solid (13%); R_f = 0.56 (25% EtOAc-hexane); ^{1}H NMR (400 MHz, $CDCl_3$) δ 7.13 (s, 1H), 6.64 (s, 1H), 5.21-5.13 (m, 2H), 4.13 (d, J = 6.1 Hz, 2H), 3.77 (s, 3H), 3.31 (d, J = 6.8 Hz, 2H), 2.69 (q, J = 15.1, 7.6 Hz, 2H), 2.64 (q, J = 15.1, 7.6 Hz, 2H), 1.83 (s, 3H), 1.77 (s, 3H), 1.69 (s, 6H), 1.32 (t, J = 7.6 Hz, 3H), 1.29 (t, J = 7.5 Hz, 3H); ^{13}C NMR (100 MHz, $CDCl_3$) δ 183.1, 172.2, 171.8, 161.2, 155.2, 154.3, 153.9, 149.8, 146.9, 139.3, 132.5, 132.5, 122.9,

121.6, 117.0, 116.5, 110.8, 107.3, 100.5, 61.9, 28.0, 27.9, 26.7, 26.1, 26.0, 22.5, 18.4, 18.1, 9.2; HRMS calc. for $C_{30}H_{34}O_8$ $(M + Na)^+$ 545.2146, found 545.2147.
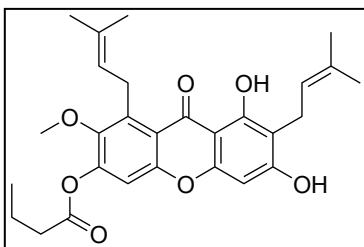
6-Mono-O-butanoyl mangostin (M5): light yellow solid (38%); R_f = 0.42 (33% EtOAc-hexane); ^{1}H NMR (400 MHz, $CDCl_3$) δ 13.54 (s, 1H), 7.07 (s, 1H), 6.32 (s, 1H), 6.22 (s, 1H), 5.28 (t, J = 6.6 Hz, 1H), 5.21 (t, J = 6.2 Hz, 1H), 4.13 (d, J = 6.1 Hz, 2H), 3.75 (s, 3H), 3.43 (d, J = 7.0 Hz, 2H), 2.64 (t, J = 7.3 Hz, 2H), 1.85-1.83 (m, 8H), 1.76 (s, 3H), 1.68 (s, 3H), 1.03 (t, J = 7.4 Hz, 3H); ^{13}C NMR (100 MHz, $CDCl_3$) δ 182.0, 171.1, 162.0, 160.7, 155.0, 153.8, 148.9, 146.5, 138.9, 135.4, 132.0, 123.0, 121.4, 116.8, 110.4, 108.8, 103.8, 93.3, 61.6, 36.1, 26.4, 25.8, 21.4, 18.4, 18.2, 17.9, 13.6; HRMS calc. for $C_{28}H_{32}O_7$ $(M + Na)^+$ 503.2040, found 503.2039.
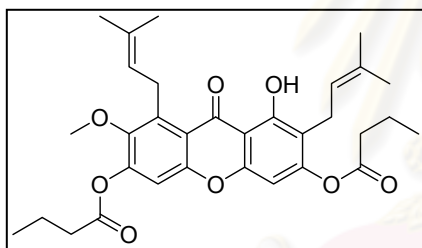
3,6-Di-O-butanoyl mangostin (D5): light yellow solid (21%); R_f = 0.51 (33% EtOAc-hexane); ^{1}H NMR (400 MHz, $CDCl_3$) δ 7.12 (s, 1H), 6.63 (s, 1H), 5.02-5.15 (m, 2H), 4.13 (d, J = 6.1 Hz, 2H), 3.76 (s, 3H), 3.31 (d, J = 6.7 Hz, 2H), 2.64 (t, J = 7.3 Hz, 2H), 2.58 (t, J = 7.4 Hz, 2H), 1.83-1.77 (m, 7H), 1.77 (s, 3H), 1.69 (s, 6H), 1.10-1.05 (m, 6H); ^{13}C NMR (100 MHz, $CDCl_3$) δ 183.1, 171.4, 170.9, 161.2, 155.2, 154.3, 153.9, 149.7, 147.0, 139.3, 132.5, 122.9, 121.6, 117.0, 116.5, 110.8, 107.3, 100.5, 61.9, 36.4, 36.3, 26.7, 26.1, 25.9, 22.5, 18.6, 18.4, 18.1, 13.9; HRMS calc. for $C_{32}H_{38}O_8$ $(M + Na)^+$ 573.2459, found 573.2460.
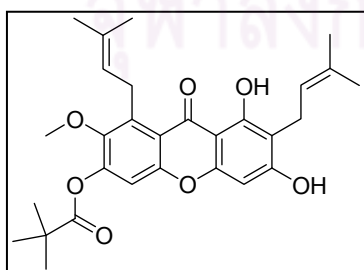
6-Mono-O-pivalyl mangostin (M6): light yellow solid (24%); R_f = 0.42 (33% EtOAc-hexane); ^{1}H NMR (400 MHz, $CDCl_3$) δ 13.58 (s, 1H), 7.05 (s, 1H), 6.29 (s, 1H), 6.26 (s, 1H), 5.21 (t, J = 6.8 Hz, 1H), 5.27 (t, J = 6.8 Hz, 1H), 4.13 (d, J = 6.2 Hz, 2H), 3.74 (s, 3H), 3.45 (d, J = 7.0 Hz, 2H), 1.84 (s, 3H), 1.83 (s, 3H), 1.77 (s, 3H), 1.68 (s, 3H), 1.42 (s, 9H).
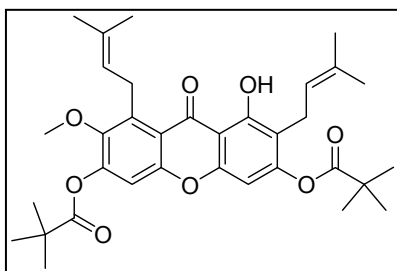
*3,6-di-O-pivalyl mangostin (**D6**)*: light yellow solid (5%); R_f = 0.51 (33% EtOAc-hexane); ^{1}H NMR (400 MHz, CDCl$_3$) δ 13.44 (s, 1H), 7.07 (s, 1H), 6.58 (s, 1H), 5.20 (t, J = 6.4 Hz, 1H), 5.12 (t, J = 6.6 Hz, 1H), 4.13 (d, J = 6.1 Hz, 2H), 3.75 (s, 3H), 3.30 (d, J = 6.5 Hz, 2H), 1.83 (s, 3H), 1.77 (s, 3H), 1.69 (s, 3H), 1.68 (s, 3H), 1.42 (s, 9H), 1.39 (s, 9H); ^{13}C NMR (100 MHz, CDCl$_3$) δ 182.9, 176.1, 175.7, 161.0, 155.3, 154.1, 153.7, 150.0, 146.9, 139.1, 132.5, 132.3, 122.8, 121.4, 116.7, 116.4, 110.6, 107.0, 100.0, 61.9, 39.4, 27.1, 26.4, 25.8, 25.7, 22.1, 18.2, 18.0.
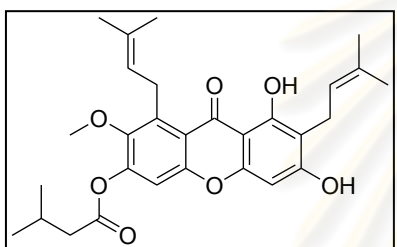
*6-Mono-O-3-methylbutanoyl mangostin (**M7**)*: light yellow solid (15%); R_f = 0.42 (33% EtOAc-hexane); ^{1}H NMR (400 MHz, CDCl$_3$) δ 13.59 (s, 1H), 7.08 (s, 1H), 6.28 (s, 1H), 6.26 (s, 1H), 5.30-5.20 (m, 2H), 4.14 (d, J = 6.0 Hz, 2H), 3.75 (s, 3H), 3.46 (d, J = 7.1 Hz, 2H), 2.52 (d, J = 7.2 Hz, 2H), 2.32-2.25 (m, 1H), 1.84 (s, 3H), 1.83 (s, 3H), 1.77 (s, 3H), 1.68 (s, 3H), 1.09 (d, J = 6.6 Hz, 6H); ^{13}C NMR (100 MHz, CDCl$_3$) δ 181.9, 170.8, 161.9, 160.6, 154.8, 153.8, 148.7, 146.5, 139.0, 134.8, 132.0, 123.0, 121.5, 116.9, 110.4, 109.1, 103.7, 93.1, 61.7, 43.2, 26.4, 25.8, 25.8, 22.4, 21.4, 18.2, 17.9.
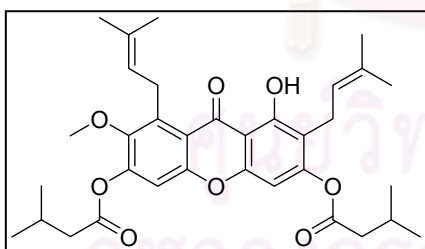
*3,6-Di-O-3-methylbutanoyl mangostin (**D7**)*: light yellow solid (31%); R_f = 0.51 (33% EtOAc-hexane); ^{1}H NMR (400 MHz, CDCl$_3$) δ 13.43 (s, 1H), 7.09 (s, 1H), 6.61 (s, 1H), 5.20 (t, J = 6.2 Hz, 1H), 5.14 (t, J = 6.8 Hz, 1H), 4.13 (d, J = 6.1 Hz, 2H), 3.76 (s, 3H), 3.30 (d, J = 6.8 Hz, 2H), 2.52 (d, J = 7.1 Hz, 2H), 2.48 (d, J = 7.1 Hz, 2H), 2.32-2.23 (m, 2H), 1.84 (s, 3H), 1.77 (s, 3H), 1.69 (s, 3H), 1.68 (s, 3H), 1.09 (d, J = 6.6 Hz, 6H), 1.08 (d, J = 6.6 Hz, 6H); ^{13}C NMR (100 MHz, CDCl$_3$) δ 182.8, 170.6, 170.1, 161.0, 154.9, 154.0, 153.6, 149.5, 146.8, 139.0, 132.3, 132.2, 122.7, 121.4, 116.7, 116.2, 110.6, 107.0, 100.3, 61.7, 43.2, 43.1, 26.5, 25.9, 25.8, 25.7, 25.7, 22.4, 22.4, 22.3, 18.2, 17.9.
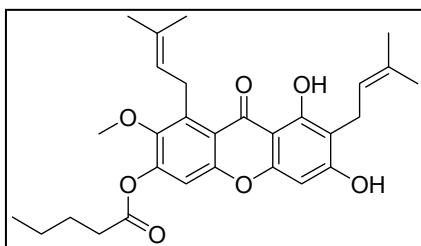
6-Mono-O-pentanoyl mangostin (M8): light yellow solid (16%); R_f = 0.52 (25% EtOAc-hexane); ^{1}H NMR (400 MHz, CDCl$_3$) δ 13.58 (s, 1H), 7.08 (s, 1H), 6.26 (s, 1H), 5.30-5.20 (m, 2H), 4.13 (d, *J* = 5.9 Hz, 2H), 3.75 (s, 3H), 3.45 (d, *J* = 6.9 Hz, 2H), 2.66 (t, *J* = 7.4 Hz, 2H), 1.84-1.83 (m, 8H), 1.77 (s, 3H), 1.68 (s, 3H), 1.49-1.47 (m, 2H), 1.00 (t, *J* = 7.3 Hz, 3H); ^{13}C NMR (100 MHz, CDCl$_3$) δ 181.7, 172.0, 161.7, 160.6, 154.5, 153.8, 148.7, 146.4, 139.0, 134.2, 132.0, 123.0, 121.7, 116.9, 110.3, 109.4, 103.5, 93.0, 61.7, 34.0, 26.8, 26.4, 25.8, 22.2, 21.4, 18.2, 17.9, 13.7.
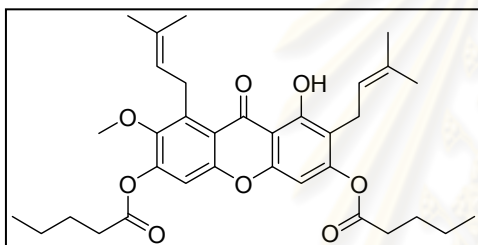
3,6-Di-O-pentanoyl mangostin (D8): light yellow solid (4%); R_f = 0.63 (25% EtOAc-hexane); ^{1}H NMR (400 MHz, CDCl$_3$) δ 13.42 (s, 1H), 7.10 (s, 1H), 6.62 (s, 1H), 5.21-5.12 (m, 2H), 4.12 (d, *J* = 6.2 Hz, 2H), 3.76 (s, 3H), 3.30 (d, *J* = 6.7 Hz, 2H), 2.65 (t, *J* = 7.4 Hz, 2H), 2.60 (t, *J* = 7.4 Hz, 2H), 1.83-1.68 (m, 10H), 1.68 (s, 6H), 1.47 (p, *J* = 15.0, 7.5 Hz, 4H), 1.01-0.96 (m, 6H); ^{13}C NMR (100 MHz, CDCl$_3$) δ 182.8, 171.4, 170.9, 160.9, 154.9, 154.0, 153.6, 149.5, 146.7, 146.2, 139.0, 132.3, 122.7, 121.4, 116.7, 116.2, 110.6, 107.0, 100.3, 61.7, 34.0, 34.0, 29.7, 29.6, 26.8, 26.4, 25.8, 25.7, 22.3, 22.2, 18.2, 17.9, 13.7.
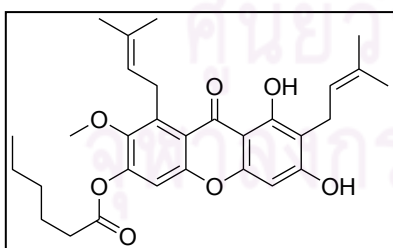
6-Mono-O-hexanoyl mangostin (M9): light yellow solid (16%); R_f = 0.37 (25% EtOAc-hexane); ^{1}H NMR (400 MHz, CDCl$_3$) δ 13.59 (s, 1H), 7.08 (s, 1H), 6.27 (s, 1H), 6.22 (s, 1H), 5.30-5.20 (m, 2H), 4.14 (d, *J* = 5.9 Hz, 2H), 3.75 (s, 3H), 3.45 (d, *J* = 7.1 Hz, 2H), 2.64 (t, *J* = 7.5 Hz, 2H), 1.84-1.83 (m, 8H), 1.77 (s, 3H), 1.68 (s, 3H), 1.43-1.40 (m, 4H), 0.94 (t, *J* = 6.8 Hz, 3H); ^{13}C NMR (100 MHz, CDCl$_3$) δ 182.2, 171.2, 162.1, 160.7, 155.1, 153.9, 149.0, 146.6, 138.9, 135.7, 132.1, 123.0, 121.4, 116.9, 110.5, 108.8, 103.9, 93.4, 61.7, 34.3, 31.2, 26.5, 25.9, 24.5, 22.3, 21.5, 18.2, 17.9, 13.9.
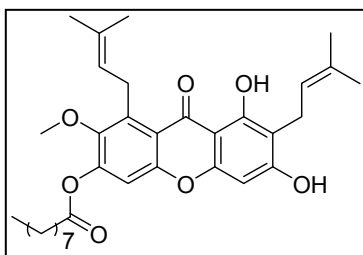
6-Mono-O-nanoyl mangostin (M10): light yellow solid (14%); R_f = 0.56 (33% EtOAc-hexane); ^{1}H NMR (400 MHz, CDCl$_3$) δ 13.58 (s, 1H), 7.08 (s, 1H), 6.26 (s, 1H), 6.21 (s, 1H), 5.30 (t, J = 5.9 Hz, 1H), 5.21 (t, J = 6.2 Hz, 1H), 4.14 (d, J = 6.1 Hz, 2H), 3.75 (s, 3H), 3.45 (d, J = 6.8 Hz, 2H), 2.64 (t, J = 7.4 Hz, 2H), 1.84-1.83 (m, 8H), 1.77 (s, 3H), 1.68 (s, 3H), 1.34-1.30 (m, 10H), 0.90 (t, J = 6.9 Hz, 3H); ^{13}C NMR (100 MHz, CDCl$_3$) δ 181.9, 171.7, 161.9, 160.6, 154.7, 153.8, 148.8, 146.4, 138.9, 134.6, 132.0, 123.0, 121.6, 116.8, 110.4, 109.2, 103.6, 93.1, 61.7, 34.3, 31.8, 29.2, 29.1, 29.1, 26.4, 25.8, 24.8, 22.6, 21.4, 18.2, 17.9, 14.1.
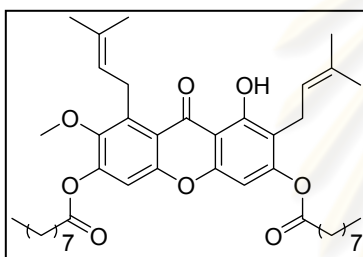
3,6-Di-O-nanoyl mangostin (D10): yellow solid (15%); R_f = 0.77 (33% EtOAc-hexane); ^{1}H NMR (400 MHz, CDCl$_3$) δ13.43 (s, 1H), 7.11 (s, 1H), 6.62 (s, 1H), 5.19-5.12 (m, 2H), 4.13 (d, J = 5.9 Hz, 2H), 3.76 (s, 3H), 3.30 (d, J = 6.6 Hz, 2H), 2.64 (t, J = 7.5 Hz, 2H), 1.83 (s, 3H), 1.77 (s, 3H), 1.83-1.77 (m, 4H), 1.68 (s, 6H), 1.42-1.25 (m, 20H), 0.89-0.87 (m, 6H); ^{13}C NMR (100 MHz, CDCl$_3$) δ 182.9, 171.4, 170.9, 161.0, 154.9, 154.1, 153.7, 149.5, 146.7, 139.0, 132.3, 122.7, 121.4, 116.7, 116.2, 110.6, 110.0, 107.0, 100.3, 61.7, 34.3 (2C), 31.8, 29.2 (2C), 29.1 (3C), 26.5, 25.8, 25.7, 24.8 (2C), 22.6, 22.3, 18.2, 17.9, 14.1.
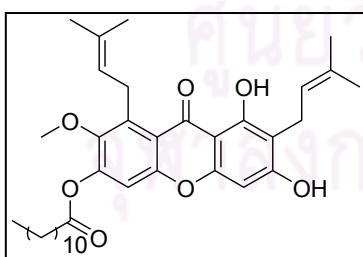
6-Mono-O-lauryl mangostin (M11): light yellow solid (34%); R_f = 0.44 (25% EtOAc-hexane); ^{1}H NMR (400 MHz, CDCl$_3$) δ 13.54 (s, 1H), 7.07 (s, 1H), 6.34 (s, 1H), 6.20 (s, 1H), 5.29-5.19 (m, 2H), 4.12 (d, J = 5.8 Hz, 2H), 3.75 (s, 3H), 3.43 (d, J = 6.8 Hz, 2H), 2.65 (t, J = 7.4 Hz, 2H), 1.83-1.75 (m, 8H), 1.76 (s, 3H), 1.68 (s, 3H), 1.28-1.27 (m, 16H), 0.88 (t, J = 6.6 Hz, 3H); ^{13}C NMR (100 MHz, CDCl$_3$) δ 182.0, 171.4, 162.0, 160.6, 154.9, 153.8, 148.9, 146.5, 138.9, 135.5, 132.1, 122.9, 121.4, 116.8, 110.4, 108.8, 103.8, 93.3, 61.7, 34.3, 31.9, 29.6, 29.4, 29.3, 29.3, 29.1, 26.4, 25.8, 24.8, 22.7, 21.4, 18.2, 17.9, 14.1.
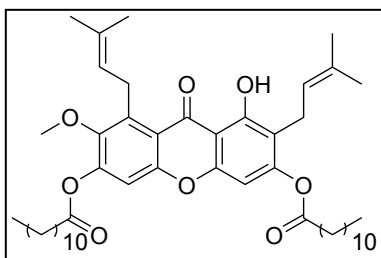
3,6-Di-O-lauryl mangostin (D11): yellow solid (16%); R_f = 0.74 (25% EtOAc-hexane); ^{1}H NMR (400 MHz, CDCl$_3$) δ 13.43 (s, 1H), 7.11 (s, 1H), 6.62 (s, 1H), 5.20-5.12 (m, 2H), 4.12 (d, *J* = 5.2 Hz, 2H), 3.75 (s, 3H), 3.30 (d, *J* = 6.7 Hz, 2H), 2.65 (t, *J* = 7.4 Hz, 2H), 2.58 (t, *J* = 7.6 Hz, 2H), 1.83 (s, 3H), 1.77 (s, 3H), 1.83-1.77 (m, 4H), 1.68 (s, 6H), 1.43-1.27 (m, 32H), 0.89-0.86 (m, 6H); ^{13}C NMR (100 MHz, CDCl$_3$) δ 182.9, 171.3, 170.9, 161.0, 155.0, 154.1, 153.7, 149.6, 146.8, 139.1, 132.3, 122.7, 121.4, 116.8, 116.3, 110.6, 107.1, 100.3, 61.7, 34.8, 34.4, 34.3, 31.9, 29.7, 29.6, 29.4, 29.3, 29.2, 29.1, 26.5, 25.8, 25.7, 25.1, 24.9, 24.8, 22.7, 22.3, 21.9, 18.2, 17.9, 14.1.

2.2.5 Preparation of Triethylene Glycol Monomethyl Bromide [77]

To a stirred solution of triethylene glycol monomethyl ether (1.56 mL, 10 mmol) in CH$_2$Cl$_2$ (10 mL) was added CBr$_4$ (4.9 g, 15 mmol). The solution of PPh$_3$ (3.9 g, 15 mmol) in CH$_2$Cl$_2$ was slowly added to the reaction mixture at 0 °C. The reaction mixture was then allowed to stir at room temperature. After 4 h, the reaction mixture was concentrated under reduced pressure and the crude material was purified by column chromatography (Silica, 33% EtOAc-hexane) to give triethylene glycol monomethyl bromide in 97% (2.20 g).

Triethylene glycol monomethyl bromide: colorless oil (97%); R_f = 0.42 (50% EtOAc-hexane); ^{1}H NMR (400 MHz, CDCl$_3$) δ 3.81 (t, *J* = 6.3 Hz, 2H), 3.68-3.64 (m, 6H), 3.57-3.54 (m, 2H), 3.47 (t, *J* = 6.3 Hz, 2H), 3.38 (s, 3H); ^{13}C NMR (100 MHz, CDCl$_3$) δ 71.9, 71.2, 70.6 (2C), 70.5, 60.4, 59.0.

2.2.6 General Procedure for the Synthesis of Ether Analogues of α-Mangostin [66]

To a stirred solution of α-mangostin (**1**) (0.41 g, 1 mmol) in acetone (10 mL) was added K$_2$CO$_3$ (0.14 g, 1 mmol) followed by the selected alkyl halide (3 mmol). After 3 h of continued stirring at reflux temperature, the reaction mixture was concentrated under reduced pressure. Water (10 mL) was then added to the reaction mixture. The reaction mixture was partitioned between EtOAc (2 × 25 mL) and water

(25 mL). The combined organic layers were dried over anh. NaSO$_4$, filtered, and concentrated by rotary evaporation. The crude material was purified by column chromatography (silica, EtOAc-hexane) to give the desired ether analogues.
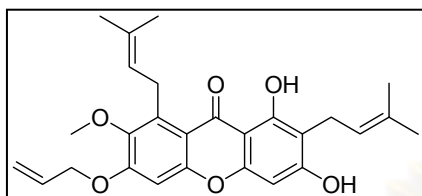
6-Mono-O-allyl mangostin (M12): yellow sold (33%); R_f = 0.36 (25% EtOAc-hexane); ^{1}H NMR (400 MHz, CDCl$_3$) δ 13.80 (s, 1H), 6.67 (s, 1H), 6.23 (s, 1H), 6.12-6.04 (m, 1H), 5.48 (d, J = 17.2 Hz, 1H), 5.36 (d, J = 10.6 Hz, 1H), 5.30-5.23 (m, 2H), 4.64 (d, J = 5.1 Hz, 1H), 4.12 (d, J = 7.0 Hz, 2H), 3.81 (s, 3H), 3.42 (d, J = 7.0 Hz, 2H), 1.85 (s, 3H), 1.83 (s, 3H), 1.75 (s, 3H), 1.68 (s, 3H); ^{13}C NMR (100 MHz, CDCl$_3$) δ 182.0, 161.4, 160.5, 156.9, 155.2, 154.9, 144.0, 137.3, 134.8, 131.9, 131.7, 123.2, 121.7, 118.4, 111.9, 108.8, 103.6, 99.2, 93.0, 69.4, 60.8, 26.2, 25.9, 25.8, 21.4, 18.2, 17.9.
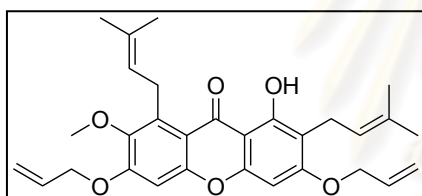
3,6-Di-O-allyl mangostin (D12): yellow solid (29%); R_f = 0.62 (25% EtOAc-hexane); ^{1}H NMR (400 MHz, CDCl$_3$) δ 13.48 (s, 1H), 6.70 (s, 1H), 6.27 (s, 1H), 6.12-6.02 (m, 2H), 5.45 (d, J = 17.4 Hz, 1H), 5.49 (d, J = 17.4 Hz, 1H), 5.38 (d, J = 10.6 Hz, 1H), 5.31 (d, J = 10.6 Hz, 1H), 5.23-5.25 (m, 2H), 4.66 (d, J = 5.2 Hz, 1H), 4.61 (d, J = 5.0 Hz, 1H), 4.13 (d, J = 6.3 Hz, 2H), 3.82 (s, 3H), 3.38 (d, J = 7.1 Hz, 2H), 1.85 (s, 3H), 1.80 (s, 3H), 1.68 (s, 6H); ^{13}C NMR (100 MHz, CDCl$_3$) δ 182.0, 162.2, 159.9, 156.8, 155.1, 155.0, 144.1, 137.3, 132.5, 132.0, 131.7, 131.5, 123.2, 122.3, 118.4, 117.7, 112.1, 111.7, 104.0, 99.2, 89.6, 69.4, 69.0, 60.8, 26.2, 25.9, 25.8, 21.5, 18.2, 17.9.
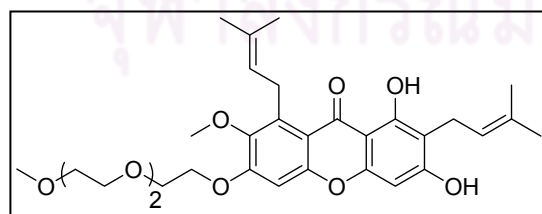
6-Mono-O-triethylene glycol monomethyl mangostin (M13): yellow solid (15%); R_f = 0.14 (50% EtOAc-hexane); ^{1}H NMR (400 MHz, CDCl$_3$) δ 13.66 (s, 1H), 7.58 (s, 1H), 6.54 (s, 1H), 6.19 (s, 1H), 5.28 (t, J = 6.5 Hz, 1H), 5.17 (t, J = 6.3 Hz, 1H), 4.14 (t, J = 4.2 Hz, 2H), 4.01 (d, J = 6.1 Hz, 2H), 3.90 (t, J = 4.5 Hz, 2H), 3.76 (s, 3H), 3.76-3.70 (m, 2H), 3.70-3.65 (m, 4H), 3.55 (t, J = 4.1 Hz, 2H), 3.39-3.37 (m, 2H), 3.35 (s, 3H), 1.80 (s, 6H), 1.70 (s, 3H), 1.64 (s, 3H).

2.2.7 Synthesis of Ether Analogues M14 and M15

To a stirred solution of α-mangostin (**1**) (0.41 g, 1 mmol) in acetone (10 mL) was added K_2CO_3 (0.14 g, 1 mmol) followed by the selected epichlorohydrin (0.23 mL, 3 mmol). After 3 h of continued stirring at reflux temperature, the reaction mixture was concentrated under reduced pressure. Water (10 mL) was then added to the reaction mixture. The reaction mixture was partitioned between EtOAc (2 × 25 mL) and water (25 mL). The combined organic layers were dried over anh. Na_2SO_4, filtered, and concentrated by rotary evaporation. The crude material was purified by column chromatography (silica, 50% EtOAc-hexane) to give the desired ethers **M14** and **M15**.
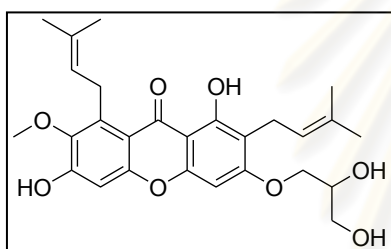
*3-Mono-O-(2,3-dihydroxy propyl) mangostin (**M14**)*: yellow solid (3%); R_f = 0.12 (50% EtOAc-hexane); ^{1}H NMR (400 MHz, CDCl$_3$) δ 13.49 (s, 1H), 6.82 (s, 1H), 6.28 (s, 1H), 5.26-5.23 (m, 1H), 5.16-5.12 (m, 1H), 5.11-5.08 (m, 1H), 4.66 (t, J = 8.5 Hz, 1H), 4.57 (dd, J = 8.6, 6.0 Hz, 1H), 4.35 (dd, J = 10.6, 4.0 Hz, 1H), 4.22 (dd, J = 10.6, 4.0 Hz, 1H), 4.08 (d, J = 6.0 Hz, 2H), 3.81 (s, 3H), 3.33 (d, J = 6.7 Hz, 2H), 1.83 (s, 3H), 1.78 (s, 3H), 1.69 (s, 3H), 1.68 (s, 3H); ^{13}C NMR (100 MHz, CDCl$_3$) δ 181.9, 161.0, 160.1, 155.5, 154.9, 154.8, 142.8, 137.1, 132.2, 132.1, 123.0, 121.9, 112.1, 111.7, 104.3, 101.6, 89.3, 73.8, 67.0, 66.0, 61.9, 26.5, 25.8, 25.7, 21.3, 18.2, 17.8.
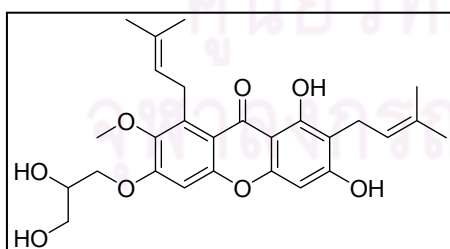
*6-Mono-O-(2,3-dihydroxy propyl) monomethyl mangostin (**M15**)*: yellow solid (11%); R_f = 0.12 (50% EtOAc-hexane); ^{1}H NMR (400 MHz, CDCl$_3$) δ 13.62 (s, 1H), 6.54 (s, 1H), 6.16 (s, 1H), 5.27-5.24 (m, 1H), 5.20-5.18 (m, 1H), 5.15-5.12 (m, 1H), 4.71-4.62 (m, 2H), 4.31 (dd, J = 10.7, 2.8 Hz, 1H), 4.14 (dd, J = 10.1, 3.0 Hz, 1H), 4.05 (d, J = 7.2 Hz, 2H), 3.74 (s, 3H), 3.39 (d, J = 6.9 Hz, 2H), 1.82 (s, 6H), 1.74 (s, 3H), 1.68 (s, 3H); ^{13}C NMR (100 MHz, CDCl$_3$) δ 181.8, 161.7, 160.4, 155.8, 154.7, 154.7, 154.6, 143.8, 137.9, 134.9, 132.0, 122.9, 121.5, 112.7, 109.1, 103.5, 99.2, 93.1, 73.8, 67.6, 65.9, 61.1, 26.2, 25.9, 25.8, 21.4, 18.2, 17.9.

2.2.8 Acid-Catalyzed Cyclization of α-Mangostin [66]

α-Mangostin (**1**) (2 g, 4.8 mmol) and *p*-toluenesulfonic acid (0.20 g, 1.14 mmol) were dissolved in dried benzene (140 mL). The reaction mixture was heated with a Dean-Stark apparatus. After 5 h, the solvent was removed by rotary evaporator and the residue was extracted with CH_2Cl_2. The organic layer was washed with H_2O and the combined organic layers were dried over anh. Na_2SO_4, filtered, and concentrated under reduced pressure. The crude material was purified by column chromatography (silica, 20% EtOAc-hexane) to give 3-isomangosin (**7**) in 66% (1.32 g) and BR-xanthone A (**30**) in 4% (80 mg).
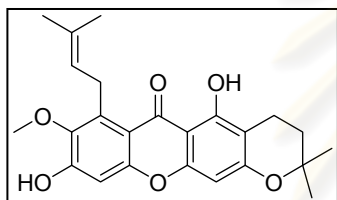
3-Isomangostin (7): yellow solid (66%); R_f = 0.47 (50% EtOAc-hexane); ^{1}H NMR (400 MHz, CDCl3) δ 13.71 (s, 1H), 6.82 (s, 1H), 6.28 (s, 1H), 6.23 (s, 1H), 5.28 (t, J = 6.2 Hz, 1H), 4.10 (d, J = 6.2 Hz, 2H), 3.80 (s, 3H), 2.72 (t, J = 6.8 Hz, 2H), 1.87-1.83 (m, 2H), 1.83 (s, 3H) 1.69 (s, 3H), 1.36 (s, 6H); ^{13}C NMR (100 MHz, CDCl3) δ 181.9, 160.6, 160.4, 155.7, 154.6, 154.5, 142.4, 136.9, 132.0, 123.3, 112.0, 109.9, 103.7, 101.7, 94.0, 76.0, 61.9, 31.8, 26.7, 26.5, 25.9, 18.2, 16.1.
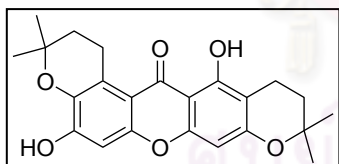
BR-Xanthone A (30): yellow solid (33%); R_f = 0.63 (50% EtOAc-hexane); ^{1}H NMR (400 MHz, CDCl3) δ 13.72 (s, 1H), 6.78 (s, 1H), 6.38 (s, 1H), 6.23 (s, 1H), 3.50 (t, J = 6.8 Hz, 2H), 2.71 (t, J = 6.7 Hz, 2H), 1.88 (t, J = 6.7 Hz, 2H), 1.83 (t, J = 6.7 Hz, 2H), 1.38 (s, 6H), 1.37 (s, 6H); ^{13}C NMR (100 MHz, CDCl3) δ 182.6, 160.5, 160.4, 154.9, 153.2, 151.5, 137.7, 121.3, 111.2, 103.5, 103.0, 100.5, 94.0, 75.9, 75.5, 32.9, 31.9, 26.7, 26.5, 22.3, 16.1.

2.2.9   Synthesis of 3-Isomangostin Analogues I1-I5

The synthesis of esters analogues **I1-I5** was carried out by using the general procedure as described in section 2.2.4. In this experiment, 2 h was used for step II.
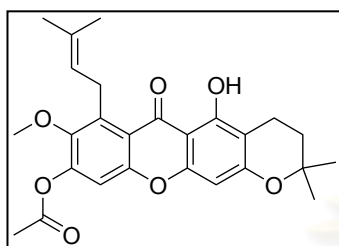
6-O-Acetyl-3-isomangostin (I1): light yellow solid; R_f = 0.55 (15% EtOAc-hexane); ^{1}H NMR (400 MHz, CDCl$_3$) δ 13.54 (s, 1H), 7.09 (s, 1H), 6.24 (s, 1H), 5.22 (t, J = 6.3 Hz, 1H), 4.15 (d, J = 6.0 Hz, 2H), 3.76 (s, 3H), 2.72   (t, J = 6.6 Hz, 2H), 2.38 (s, 3H)1.87-1.83 (m, 5H), 1.68 (s, 3H), 1.37 (s, 6H); ^{13}C NMR (100 MHz, CDCl$_3$) δ 182.1, 168.2, 161.2, 160.7, 154.7, 153.9, 148.7, 146.3, 138.8, 132.1, 123.0, 116.9, 110.5, 104.0, 103.1, 94.1, 61.6, 31.8, 26.7, 26.4, 25.9, 20.9, 18.2, 16.1.
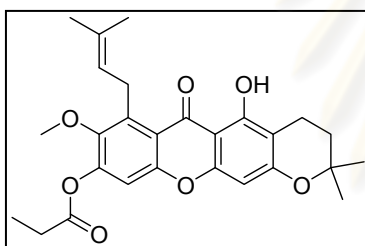
6-O-Propanoyl-3-isomangostin (I2): light yellow solid; R_f = 0.55 (15% EtOAc-hexane); ^{1}H NMR (400 MHz, CDCl$_3$) δ 13.54 (s, 1H), 7.08 (s, 1H), 6.24 (s, 1H), 5.23 (m, 1H), 4.14 (d, J = 5.2 Hz, 2H), 3.74 (s, 3H), 2.73-2.67 (m, 4H), 1.87-1.83 (m, 5H), 1.68 (s, 3H), 1.37 (s, 6H), 1.32 (t, J = 7.4 Hz, 3H); ^{13}C NMR (100 MHz, CDCl$_3$) δ 182.1, 171.7, 161.2, 160.7, 154.7, 153.9, 148.9, 146.3, 138.7, 132.0, 123.0, 116.8, 110.5, 103.9, 103.1, 94.1, 61.6, 31.8, 27.6, 26.7, 26.4, 25.9, 18.2, 16.1, 9.0.
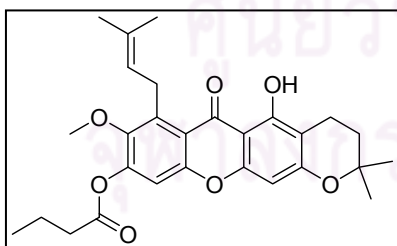
6-O-Butynoyl-3-isomangostin (I3): light yellow solid; R_f = 0.57 (15% EtOAc-hexane); ^{1}H NMR (400 MHz, CDCl$_3$) δ 13.55 (s, 1H), 7.08 (s, 1H), 6.24 (s, 1H), 5.23 (t, J = 5.7 Hz, 1H), 4.15 (d, J = 6.0 Hz, 2H), 3.75 (s, 3H), 2.72 (t, J = 6.7 Hz, 2H), 2.63 (t, J = 7.3 Hz, 2H), 1.87-1.83 (m, 7H), 1.68 (s, 3H), 1.37 (s, 6H), 1.08 (t, J = 7.4 Hz, 3H); ^{13}C NMR (100 MHz, CDCl$_3$) δ 182.1, 170.9, 161.2, 160.7, 154.7, 154.0, 148.9, 146.4, 138.7, 132.0, 123.0, 116.8, 110.5, 103.9, 103.1, 94.1, 61.6, 36.1, 31.8, 26.7, 26.4, 25.9, 18.4, 18.2, 16.1, 13.6.
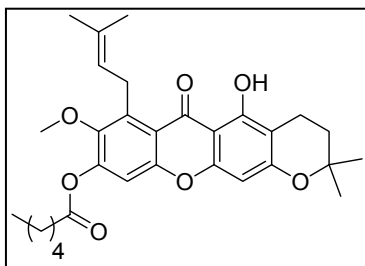
6-O-Hexanoyl-3-isomangostin (I4): light yellow solid; R_f = 0.58 (15% EtOAc-hexane); ^{1}H NMR (400 MHz, CDCl₃): δ 13.55 (s, 1H), 7.08 (s, 1H), 6.24 (s, 1H), 5.23 (t, J = 5.4 Hz, 1H), 4.14 (d, J = 6.0 Hz, 2H), 3.74 (s, 3H), 2.72 (t, J = 6.6 Hz, 2H), 2.64 (t, J = 7.3 Hz, 2H), 1.84-1.83 (m, 7H), 1.68 (s, 3H), 1.39-1.38 (m, 4H), 1.37 (s, 6H), 0.95 (t, J = 6.9 Hz, 3H); ^{13}C NMR (100 MHz, CDCl₃) δ 182.1, 171.1, 161.2, 160.7, 154.7, 153.9, 148.9, 146.4, 138.7, 132.0, 123.0, 116.8, 110.5, 103.9, 103.1, 94.1, 61.6, 34.2, 31.8, 31.2, 26.7, 26.4, 25.9, 24.5, 22.3, 18.2, 16.1, 13.9.
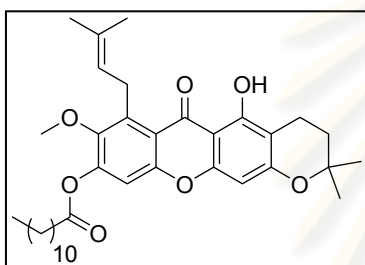
6-O-Lauryl-3-isomangostin (I5): light yellow solid; R_f = 0.70 (20% EtOAc-hexane); ^{1}H NMR (400 MHz, CDCl₃) δ 13.55 (s, 1H), 7.08 (s, 1H), 6.23 (s, 1H), 5.23-5.22 (m, 1H), 4.14 (d, J = 6.0 Hz, 2H), 3.74 (s, 3H), 2.72 (t, J = 6.7 Hz, 2H), 2.64 (t, J = 7.5 Hz, 2H), 1.87-1.77 (m, 7H), 1.68 (s, 3H), 1.37 (s, 6H), 1.37-1.27 (m, 16H), 0.89 (t, J = 6.0 Hz, 3H); ^{13}C NMR (100 MHz, CDCl₃) δ 182.1, 171.0, 161.2, 160.7, 154.7, 153.9, 148.9, 146.4, 138.7, 132.0, 123.1, 116.7, 110.5, 103.9, 103.1, 94.1, 61.6, 34.2, 31.9, 31.8, 29.6, 29.4, 29.3, 29.3, 29.1, 26.7, 26.4, 25.9, 24.8, 22.7, 18.2, 16.1, 14.1.

2.2.10 Bioassays

2.2.10.1 Antibacterial Assay

Disc diffusion method

The test bacteria used in this study were two Gram-positive bacteria, *Staphylococcus aureus* ATCC 25923 and *S. aureus* ATCC 43300 (MRSA), and four Gram-negative bacteria, *Escherichia coli* ATCC 25922, extended-spectrum β-lactamase-producing *E. coli* (ESBL), *Pseudomonas aeruginosa* ATCC 27853 and *Ps. aeruginosa* (multidrug resistance). This experiment was performed using disc diffusion method [78]. The test bacteria were grown on Mueller Hinton agar at 37 °C for 24 h. The cultures were adjusted with sterile saline solution (0.85%) to obtain turbidity by comparison with a 0.5 MacFarland turbidity standard (1.0×10^8 CFU/mL).

A 100 μL of 10^8 cells/mL of suspension of the test bacteria was spread on the Mueller Hinton agar. Filter paper discs (6 mm in diameter) were impregnated with 10 μL of each tested compound and placed on the agar surface. Discs impregnated with suitable solvent were used as negative controls. Discs with Chloramphenicol were used as a positive control. These plates were incubated at 37 $^{\circ}$C for 24 h. The antibacterial activity of tested compounds was determined by the presence of the inhibition zones compared to the controls. All experiments were performed in triplicate.

Broth microdilution method

The minimum inhibitory concentration (MIC) value was determined by the broth microdilution method, according to the Clinical and Laboratory Standards Institue protocol [79]. Each test compound was individually dissolved in polyethylene glycol M.W. 400 (PEG400) to give a concentration of 1 mg/mL, and 40 μL of test solution was added to 20 μL of Mueller Hinton broth (MHB) in a 96-well microtiter plate. Serial doubling dilutions of test compounds were prepared in a 96-well microtiter plate in the range 200 to 0.2 μg/mL in each well at 100 μL final volume. These were inoculated with 20 μL of a day old culture of bateria, prepared in 0.85% of normal saline by comparison with a 0.5 MacFarland turbidity standard (10^8 CFU/mL). After incubation of the cultures at 37 °C for 24 h, the MIC was recorded as the lowest concentration at which no growth was observed. Then, the minimum bactericidal concentration (MBC) was evaluated by reinoculating on agar plate with 10 μL of each culture medium from the microplates. The MBC is defined as the lowest concentration in μg/mL of test compound that results in more than 99.9% killing of the bacteria tested. Chloramphenicol was used as a positive control in parallel experiments. All experiments were carried out in triplicate.

2.2.10.2 Anticandidal Assay

The determination of MIC and minimum candicidal concentrations (MCC) for anticandidal activity was similar to that for antibacterial activity described in 2.2.10.1. In this experiment, the pathogenic yeast like fungi *Candida albicans* was tested as a

stain and Sabouraud dextrose broth (SDB) was used as media. Amphotericin B was served as a positive control in parallel experiments.

2.2.10.3 Termite Antifeedant Assay

Insect rearing

The Subterranean termite (*Reticulitermes speratus*) was collected from a pine forest near the Enju coast (Wakayama Pref. Japan, N35°53" 15". E135°07" 51") in 2004, brought to Kinki university (Japan) and maintained by feeding with pieces of pine wood in a controlled environment at 26.5 °C.

Dual choice type antifeedant test [80]

Filter paper disks (Toyo filter paper, No. 1; 6 mm in diameter) were used for the antifeedant assay. Two disks were treated with an appropriate amount of test compounds as an acetone solution and another two disks were treated with only acetone as a control. The treated disks were placed on a petri dish (5 cm in diameter) with moistened vermiculite (ca. 2 mm thick). Four paper disks were set alternating positions in the same petri dish. After complete removal of the solvent, twenty *R. speratus* workers from the same colony were then released into the dish and maintained for 2 weeks in darkness at 27 °C with occasional spaying with water to avoid dryness. Partially consumed filter paper disks were taped onto paper, photocopied and confirmed to contain no errors, then converted to digital data files with a digital scanner. Digital data analysis was performed on a PC using the Scion Image program. For each experiment, the data file of an intact disk was measured and compared to that of a treated disk. To measure the activity of test compounds, the antifeedant index (AFI) was adopted as AFI = % of treated disks consumed / (% of control disks consumed) x 100. Then, the FI index was used to indicate the feeding inhibitory as FI (%) = (50-AFI) x 2. The termite antifeedant activity was converted from AFI to a corresponding 0-100% feeding inhibition range.

2.3   Results and Discussion

2.3.1   Isolation of α-Mangostin (1) from *Garcinia mangostana* Linn.
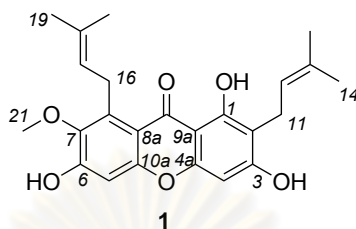
The extraction of *G. mangostana* pericarps with EtOAc led to the isolation of α-mangostin (**1**). α-Mangostin (**1**) as a light yellow amorphous and its molecular ion of *m/z* (M+Na)$^+$ 433.1625 was in agreement with the molecular formula $C_{24}H_{26}O_6$. The ^{1}H NMR spectrum (Figure 2.4) of **1** showed a singlet signal of chelated phenolic hydroxy group (OH-1) at δ_H 13.77 and two singlet signals of remaining phenolic hydroxy groups at δ_H 6.35 (OH-6), and 6.21 (OH-3). The two singlet signals at δ_H 6.82 (ArH-5) and 6.29 (ArH-4) were assigned for two aromatic protons. A multiplet signal of two olefinic protons on C12 and C17 was observed at δ_H 5.31-5.25. The two doublet signals at δ_H 4.09 (J = 6.0 Hz, H-16) and 3.45 (J = 7.0 Hz, H-11) were ascribed to four protons belonging to a prenyl unit. A singlet signal of methoxy group (OCH$_3$-7) at δ_H 3.80 and four singlet signals of four methyl groups at δ_H 1.84-1.69 (H-20, H-19, H-15, H-14) were observed.

The ^{13}C NMR spectrum (Figure 2.5) showed resonances for all twenty-four carbons belonging to the molecule of α-mangostin (**1**). A characteristic carbonyl carbon signal of xanthone at δ_C 182.0, six oxygenated aromatic at δ_C 161.5 (C-3), 160.5 (C-1), 155.7 (C-6), 155.0 (C-4a), 154.5 (C-10a) and 142.5 (C-7), and ten sp2 carbon signals at δ_C 137.0 (C-8), 135.5 (C-13), 132.1 (C-18), 123.1 (C-17), 121.5 (C-12), 112.1 (C-8a), 108.6 (C-2), 103.6 (C-9a), 101.6 (C-5) and 93.3 (C-4) were observed. The methoxy carbon at δ_C 62.0 and two methylene carbons adjacent to aromatic ring at δ_C 26.5 (C-16) and 21.4 (C-11) were detected. Four methyl carbons at δ_C 25.8-17.9 (C-15, C-20, C-14 and C-19) were exhibited. All aforementioned data of α-mangostin (**1**) was corresponding to the previous works [9, 35].
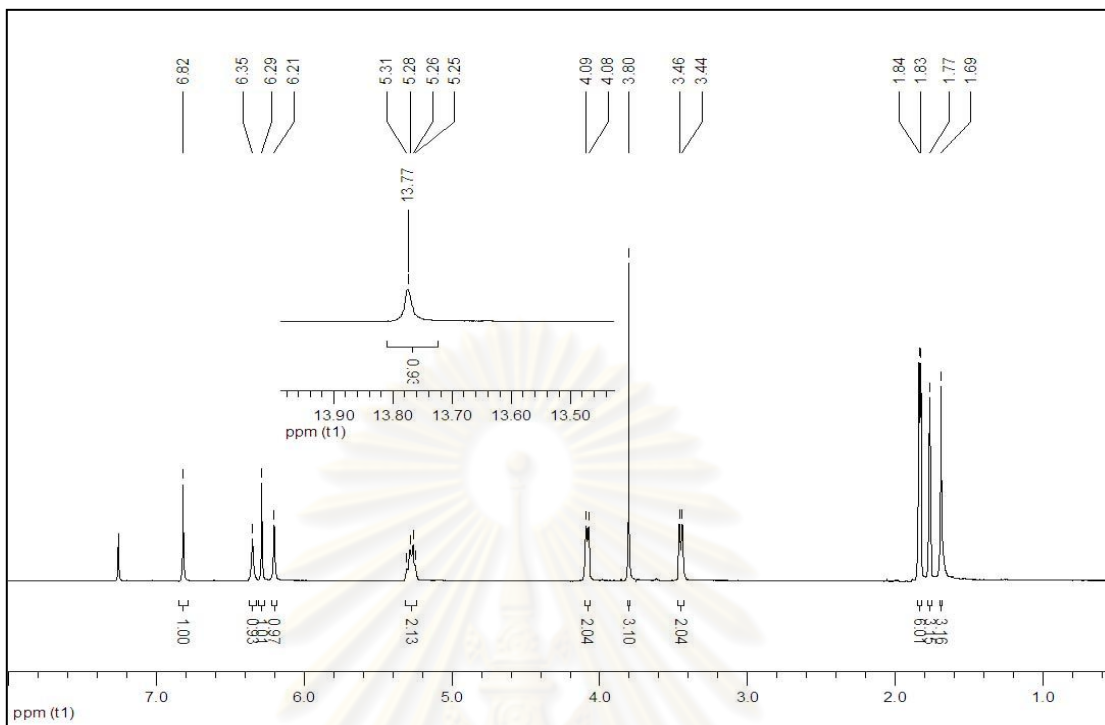
Figure 2.4 The ^{1}H NMR spectrum (CDCl$_3$, 400 MHz) of compound **1**
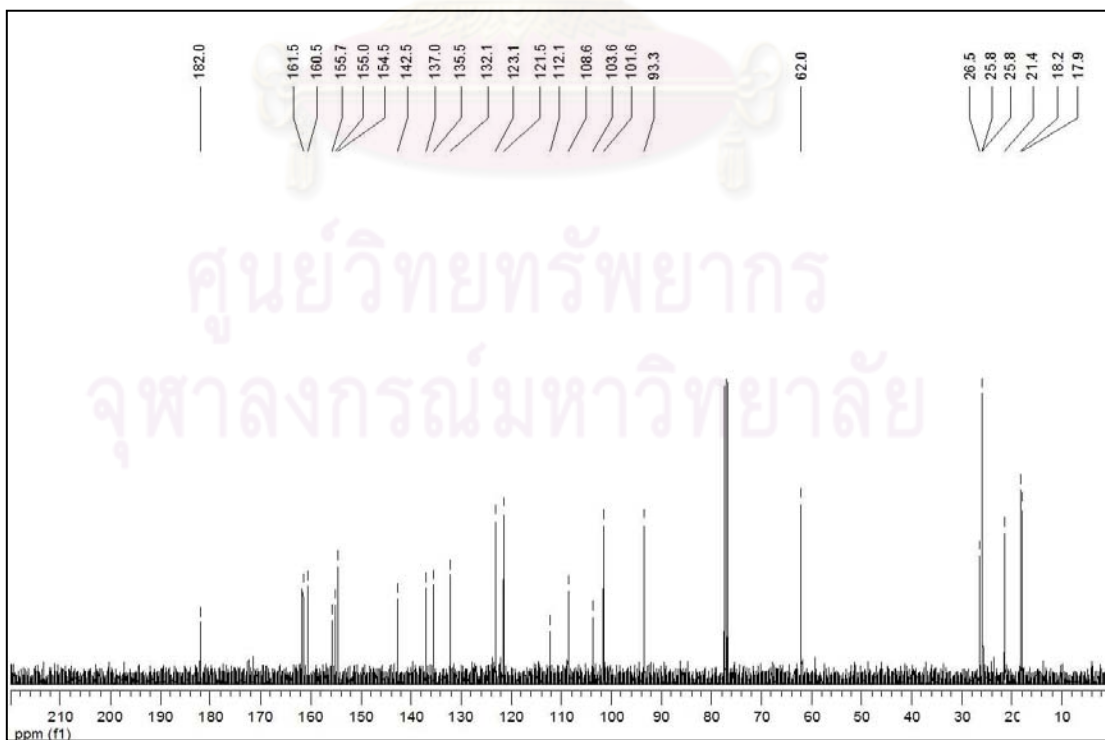
Figure 2.5 The ^{13}C NMR spectrum (CDCl$_3$, 100 MHz) of compound **1**

2.3.2 Synthesis of α-Mangostin Analogues

According to the literature reviews, α-mangostin (**1**), a major component in *G. mangostana*, possesses a variety of biological activities. These facts provided α-mangostin (**1**) as a fascinated molecule leading to its structural modification and biologically active evaluation. Considering the functional groups of α-mangostin (**1**), a hydroxyl group at C3 and C6 and a prenyl unit substituted on C2 and C8 could be modified to provide the analogues of α-mangostin (**1**).

2.3.2.1 Synthesis of Ester Analogues

Ester derivatives of α-mangostin (**1**) were synthesized by the use of either acid chlorides or carboxylic acids as a staring material and the results are demonstrated in Tables 2.2 and 2.3.

Table 2.2 Synthesis of ester analogues of α-mangostin (**1**) from acid chlorides

Entry	Acylating agent	6-Mono-*O*-acylated		3,6-Di-*O*-acylated	
		Compound	%Isolated yield	Compound	%Isolated yield
1		M1	30	D1	42
2		M2	25	D2	33
3		M3	22 (10)[a]	D3	48

[a] The corresponding 3-mono-*O*-acetyl adduct (**M3a**)

From Table 2.2, benzoyl chloride smoothly reacted with α-mangostin (**1**) providing 6-mono-*O*- benzoyl product (**M1**) and 3,6-di-*O*-benzoyl product (**D1**) in 30 and 42% yields, respectively (entry 1). Phenylacetic acid could be used to react with α-mangostin (**1**) to give the corresponding 6-mono-*O*-phenylacetyl (**M2**) and 3,6-di-*O*-phenylacetyl (**D2**) products in 25 and 33% yields, respectively under the same reaction condition (entry 2). In addition, using acetic acid, the reaction can perform to give 6-mono (**M3**) and 3-mono-*O*-acetyl (**M3a**) compounds in 22 and 10% yield, respectively, together with 3,6-di-*O*-acetyl product (**D3**) in 48% yield (entry 3). Comparison of the structure of carboxylic acid employed with their % yield of products suggested that the %yield of 3,6-di-*O*-acylated compounds **D1-D3** significantly increased when using carboxylic acids consisting of less sterically hindered substituents. The structures of synthesized compounds **M1-M3** and **D1-D3** were characterized by ^{1}H and ^{13}C NMR spectroscopic methods.

The ^{1}H NMR spectrum of 6-mono-*O*-benzoyl mangostin (**M1**) (Figure 2.6) revealed the signals for a chelated hydroxyl proton at δ_H 13.59 (OH-1), an aromatic proton at δ_H 6.28 (H-3), a hydroxyl proton at δ_H 6.30 (OH-3), two olefinic protons at δ_H 5.29-5.24 (H-17 and H-21), two methylene protons at δ_H 4.17 (d, J = 6.1 Hz, H-16) and 3.46 (d, J = 7.0 Hz, H-11), three protons of methoxy group at δ_H 3.77, and twelve methyl protons at δ_H 1.85-1.69 (H-20, H-19, H-15, H-14). Comparison of this spectrum with that of **1** found that the singlet signal of H5 shifted to downfield showing at δ_H 7.23, indicating that OH group at C6 was substituted. Five aromatic protons of benzoyl group were inferred from the presence of signals at δ_H 8.25 (d, J = 7.4 Hz, 2H), 7.70 (t, J = 7.5 Hz, 1H) and 7.57 (t, J = 7.8 Hz, 2H). The ^{13}C NMR spectrum (Figure 2.7) presented the characteristic carbonyl carbon signals of xanthone and ester at δ_C 182.1 and 164.1, respectively. The peaks at δ_C 162.1, 160.7, 155.0, 153.9, 149.1 (C-6) and 146.7 indicated the presence of six oxygenated aromatic carbons. The chemical shifts at 139.0-93.4 were observed from the presence of six aromatic carbons of benzoyl unit and ten sp2 carbons of mangostin core. The signals of a methoxy carbon at δ_C 61.9, two methylene carbons at δ_C 26.5 and 21.5, and four methyl carbons at δ_C 25.9 (2C), 18.2 and 17.9 were detected.

Additionally, the HMBC experiment was performed and the HMBC correlation of this compound is shown below.
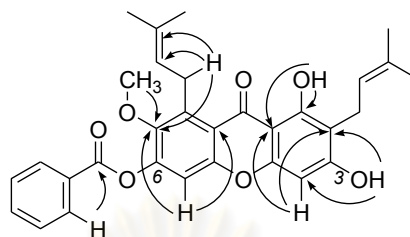
It was manifested the correlations between OH-1 (13.59) and C-1 (δ 160.7), C-9a (δ 103.9) and C-2 (δ 108.7), between OH-3 (δ 6.30) and C-3 (δ 162.1), C-2 (δ 108.7) and C-4 (δ 93.4), between H-4 (δ 6.28) and C-4a (δ 155.0), C-2 (δ 108.7) and C-9a (δ 103.9), between H-5 (δ 7.23) and C-7 (δ 146.7), C-6 (δ 149.1) and C-8a (116.9), between OCH$_3$-7 (δ 3.77) and C-7 (δ 146.7), and between H-16 (4.17) and C-7 (δ 146.7), C-17 (δ 122.9) and C-18 (δ 132.2). All aforementioned NMR data truly affirmed the linkage of benzoyl group to C6.

The ^{1}H NMR spectrum of 3,6-di-*O*-benzoyl mangostin (**D1**) (Figure 2.8) showed the characteristic signals of mangostin core at δ_H 13.44 (s), 5.20-5.10 (m, H-12 and H-17), 4.11 (d, *J* = 6.1 Hz, H-16), 3.72 (s, OCH$_3$-7), 3.32 (d, *J* = 6.8 Hz, H-11) and 1.78-1.53 (s, 3H each, H-14, H-15, H-19 and H-20). Comparison of the ^{1}H NMR spectrum of this compound with that of α-mangostin (**1**) indicated the downfield shift of singlet signals from 6.29 to 6.70 and 6.82 to 7.21 referred to aromatic protons H4 and H5, respectively. These finding indicated that both of the OH-3 and OH-6 hydroxyl groups were completely changed to ester groups. The signals of ten aromatic protons belonged to two benzoyl moieties were also detected. The ^{13}C NMR spectrum (Figure 2.9) presented the peaks at δ_C 182.9, 164.2 and 163.9 ascribed for a carbonyl carbon of xanthone, ester on C6 and ester on C3, respectively. The six peaks at δ_C 161.0-146.9 could be designated for six oxygenated carbons. The signals at δ_C 139.1-107.2 were detected, indicating to the presence of twelve aromatic carbons of a benzoyl group and ten sp2 carbons of mangostin motif. In addition, the downfield shift of C4 signal was observed at δ_C 100.6. The peak at δ_C 61.9 was resonated from the presence of methoxy group. The six peaks of four methyl carbons and two methylene carbons of a prenyl unit were presented at δ_C 26.5-17.8.

The ^{1}H NMR spectrum of 6-mono-*O*-phenyl acetyl mangostin (**M2**) (Figure 2.10) showed the signals of mangostin core as follows: at δ_H 13.57 referred to a chelated OH proton; at δ_H 7.07 and 6.28 referred to two aromatic protons; at δ_H 6.19 referred to a OH proton at C3; at δ_H 5.28-5.18 referred to two olefinic protons at C12 and C17; at δ_H 4.10 and 3.46 referred to two methylene protons of prenyl unit; at δ_H 3.48 referred to a methoxy proton; and at δ_H 1.84-1.66 referred to twelve methyl protons. In addition, the presence of a multiplet signal at δ_H 7.43-7.34 and a singlet signal at δ_H 3.93 could be assigned for seven protons of phenyl acetyl group. The ^{13}C NMR spectrum (Figure 2.11) presented the characteristic peak of carbonyl carbon of xanthone and ester at δ_C 181.8 and 169.4, respectively. Six peaks at δ_C 161.8-146.3 could be designed for six oxygenated aromatic carbons. The chemical shifts at 139.1-93.1 were observed from the presence of six aromatic carbons of phenyl unit and ten sp2 carbons of mangostin core. The signals of methoxy carbon at δ_C 61.6, three methylene carbons at δ_C 41.4, 26.4 and 21.4, and four methyl carbons at δ_C 25.8 (2C), 18.2 and 17.9 were detected.

The ^{1}H NMR spectrum of 3,6-di-*O*-phenyl acetyl mangostin (**D2**) (Figure 2.12) displayed the singlet signal of chelated hydroxyl proton at δ_H 13.42. Two multiplet signals at δ_H 7.60-7.20 assigned for ten aromatic protons of phenyl group and δ_H 5.17-5.04 belonged to four methylene protons of prenyl unit were detected. Two double signals at δ_H 4.09 and 3.24 were observed from the presence of two olefinic protons of prenyl unit. Two doublet signals at δ_H 3.94 and 3.91 ascribed for two ester-connected methylene protons and three singlet signals at δ_H 1.82-1.67 assigned to twelve methyl protons were detected. The ^{13}C NMR spectrum (Figure 2.13) presented the characteristic carbonyl carbon signals of xanthone and two esters at δ_C 182.8 and 169.1 and 168.6, respectively. Six peaks at δ_C 160.9-146.7 could be designated for six oxygenated aromatic carbons. The signals at δ_C 139.1-100.2 were belonged to twelve aromatic carbons of phenyl unit and ten sp2 carbons of mangostin core. The signals of a methoxy carbon at δ_C 61.6, two ester-connected methylene carbons at δ_C 41.4, other two methylene carbons at δ_C 26.4 and 22.2, four methyl carbons at δ_C 25.9 (2C), 18.2 and 17.9 were detected.

The ^{1}H NMR spectrum of 6-mono-*O*-acetyl mangostin (**M3**) (Figure 2.14) was similar to that of *α*-mangostin (**1**), except the singlet signal of H5 was shifted to δ_H 7.08, indicating that OH group at C6 was substituted. In addition, it showed the singlet signal at δ_H 2.39, belonging to three methyl protons of acetyl group. The ^{13}C NMR spectrum (Figure 2.15) confirmed the presence of carbonyl carbon for xanthone and ester from the presence of two peaks at δ_C 182.3 and 168.0, respectively. The signals of six oxygenated aromatic carbons were observed at δ_C 162.3-146.7. The peaks of the other sp2 carbons and methoxy carbon were revealed at δ_C 139.2-93.6 and 61.9, respectively. The signals of two methylene carbons connected to double bond, one methyl carbon connected to carbonyl group and four methyl carbons of prenyl group were detected at δ_C 26.7-18.2.

The ^{1}H NMR spectrum of 3-mono-*O*-acetyl mangostin (**M3a**) (Figure 2.16) showed three singlet signals at δ_H 6.83, 6.39 and 3.80 belonging to the signal of protons ArH-5, OH-6 and OCH$_3$-7. The signals at δ_H 1.83-1.69 were belonged to four methyl groups. The singlet signal of ArH-4 was shifted to downfield showing at δ_H 6.60. This indicated that the acetate group was connected to C3. A multiplet signal at δ_H 5.23-5.14 and two doublet signals at δ_H 4.07 and 3.31 assigned to two olefinic and four methylene protons of a prenyl unit, respectively. A singlet signal at δ_H 2.34 was belonged to three methyl protons of acetate group. The ^{13}C NMR spectrum (Figure 2.17) presented the carbonyl carbon signals of xanthone and ester at δ_C 182.5 and 168.6, respectively. The signals of six oxygenated aromatic carbons were detected at δ_C 161.0-153.6. The peaks of the other sp2 carbons and methoxy carbon were observed at δ_C 137.3-100.2 and 62.1, respectively. The signals of two methylene carbons connected to double bond, one methyl carbon connected to carbonyl group and four methyl carbons of prenyl group were detected at δ_C 26.6-17.8.

The ^{1}H NMR spectrum of 3,6-di-*O*-acetyl mangostin (**D3**) (Figure 2.18) showed the characteristic signals of mangostin core at δ_H 13.44 (s), 5.19-5.14 (m, H-12 and H-17), 4.13 (d, $J = 6.2$ Hz, H-16), 3.78 (s, 7-OCH$_3$), 3.32 (d, $J = 6.9$ Hz, H-11) and 1.83-1.69 (s, 3H each, H-14, H-15, H-19 and H-20). Comparision of this spectrum with that of *α*-mangostin (**1**) indicated the downfield shift of aromatic signals from δ_H 6.29 to 6.70 (H-4) and 6.82 to 7.21 (H-5). This finding indicated that

both of the hydroxyl groups at C3 and C6 were completely converted to ester groups. The ^{13}C NMR spectrum (Figure 2.19) presented the peaks at δ_C 182.9, 168.4 and 168.0 ascribed for a carbonyl carbon of xanthone, ester connected to C6 and C3, respectively. The peaks at δ_C 161.0-146.7 and 139.1-100.3 could be designated for six oxygenated and ten sp2 carbons, respectively. In addition, the downfield shift of C4 signal was observed at δ_C 100.3. The peak of methoxy carbon was detected at δ_C 61.7. The peaks of two methylene carbons (δ 26.4 and 22.3), four methyl carbons of prenyl unit (δ 25.8, 25.7, 18.2 and 17.8) and two methyl carbons of acetate group (δ 21.0 and 20.9) were observed.

Figure 2.6 The ^{1}H NMR spectrum (CDCl$_3$, 400 MHz) of compound **M1**
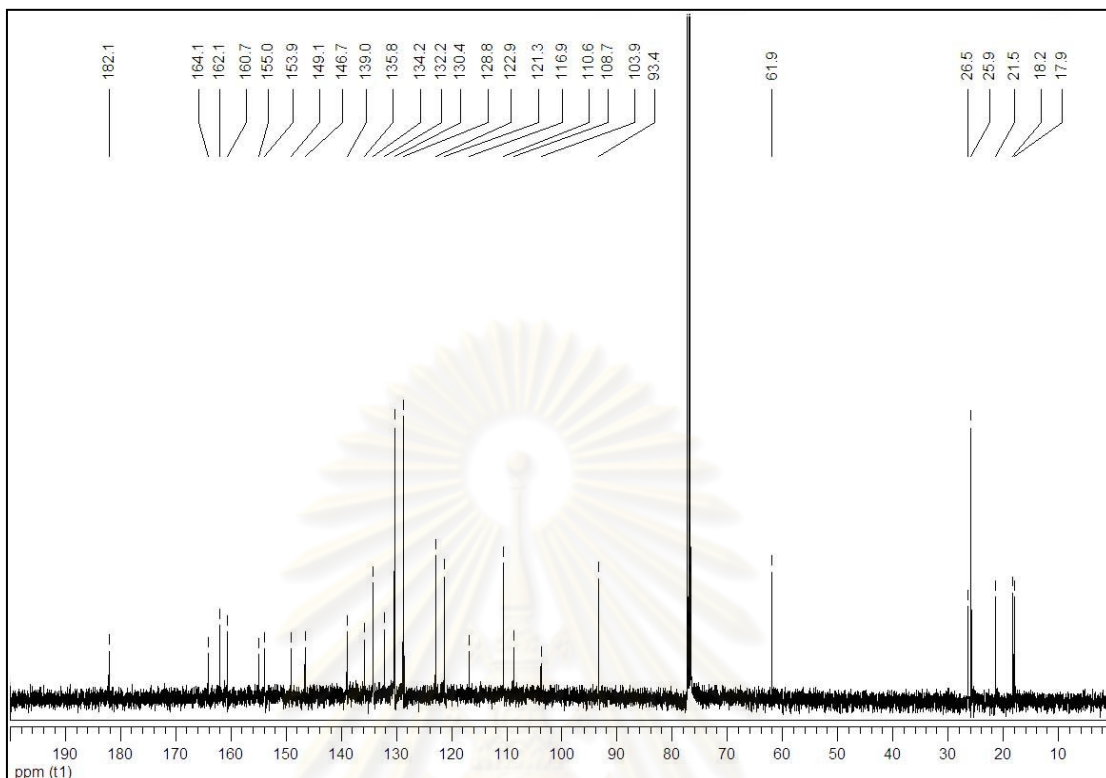
Figure 2.7 The ^{13}C NMR spectrum (CDCl$_3$, 100 MHz) of compound **M1**

Figure 2.8 The ^{1}H NMR spectrum (CDCl$_3$, 400 MHz) of compound **D1**

Figure 2.9 The ^{13}C NMR spectrum (CDCl$_3$, 100 MHz) of compound **D1**

Figure 2.10 The ^{1}H NMR spectrum (CDCl$_3$, 400 MHz) of compound **M2**

Figure 2.11 The ^{13}C NMR spectrum (CDCl$_3$, 100 MHz) of compound **M2**

Figure 2.12 The ^{1}H NMR spectrum (CDCl$_3$, 400 MHz) of compound **D2**

Figure 2.13 The ^{13}C NMR spectrum (CDCl$_3$, 100 MHz) of compound **D2**

Figure 2.14 The ^{1}H NMR spectrum (CDCl$_3$, 400 MHz) of compound **M3**

Figure 2.15 The ^{13}C NMR spectrum (CDCl$_3$, 100 MHz) of compound **M3**

Figure 2.16 The ^{1}H NMR spectrum (CDCl$_3$, 400 MHz) of compound **M3a**

Figure 2.17 The ^{13}C NMR spectrum (CDCl$_3$, 100 MHz) of compound **M3a**

Figure 2.18 The ^{1}H NMR spectrum (CDCl$_3$, 400 MHz) of compound **D3**
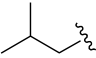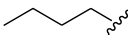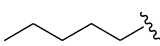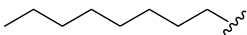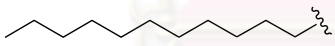
Figure 2.19 The ^{13}C NMR spectrum (CDCl$_3$, 100 MHz) of compound **D3**

ศูนย์วิทยทรัพยากร
จุฬาลงกรณ์มหาวิทยาลัย

Table 2.3 Synthesis of ester analogues of α-mangostin (**1**) from carboxylic acids

Entry	R	6-Mono-*O*-acylated product		3,6-Di-*O*-acylated product	
		Compound	%Isolated yield	Compound	%Isolated yield
1		**M4**	35 (5)[a]	**D4**	13
2		**M5**	38	**D5**	21
3		**M6**	24	**D6**	5
4		**M7**	15 (2)[a]	**D7**	31
5		**M8**	16 (4)[a]	**D8**	4
6		**M9**	16 (13)[a]	**D9**	3
7		**M10**	14 (10)[a]	**D10**	15
8		**M11**	34 (8)[a]	**D11**	16

[a] NMR yield of the corresponding 3-mono-*O*-acylated product

As presented in Table 2.3, all ester analogues were synthesized from carboxylic acids using the procedure described in 2.2.4. Eight aliphatic carboxylic acids were selected to couple with a combined reaction of PPh_3 and Cl_3CCONH_2 in refluxing CH_2Cl_2 for 1 h to generate the corresponding acid chlorides as an intermediate in the first step. Then, α-mangostin (**1**) was added to the reaction mixture in the presence of 4-picoline, and the reaction was stirred in refluxing CH_2Cl_2 for another 3 h to give the desired esters **M4-M11** and **D4-D11**.

The reaction of propinoic acid can perform to give the corresponding 6-mono-*O*-propinoyl adduct (**M4**) and 3,6-di-*O*-propinoyl adduct (**D4**) in 35 and 13% isolated yields, respectively (entry 1). Under this condition, 3-mono-*O*-propinoyl mangostin could be observed as a minor product in 5% ^{1}H NMR yield. Using butanoic acid and

its structurally different isomers: pivalic acid and 3-methylbutanoic acid, the corresponding 6-mono-*O*-acylated adducts **M5**, **M6**, and **M7** were isolated in 38, 24 and 15% yields, respectively, together with the corresponding 3,6-di-*O*-acylated adducts **D5**, **D6**, and **D7** in 21, 5 and 31% yields, respectively (entries 2-4). In the case of 3-methylbutanoic acid, 3-mono-*O*-3-methylbutanoyl mangostin could be determined in 2% ^{1}H NMR yield (entry 4). For the reaction of pentanoic acid, hexanoic acid, nanoic acid and lauric acid, their corresponding 6-mono-*O*-acylated adducts **M8**, **M9**, **M10** and **M11** could be isolated in 16, 16, 14 and 34% yields, respectively, along with their 3,6-di-*O*-acylated adducts **D8**, **D9**, **D10** and **D11** in 4, 3, 15 and 16% yields, respectively (entries 5-8). In addition, the hydroxyl group at C3 could react with the acid chlorides giving the corresponding 3-mono-*O*-acylated adducts in 4, 13, 10 and 8% ^{1}H NMR yields, respectively (entries 5-8). According to the results obtained, the %yield of the desired esters was low. This may be speculated that the conversion of aliphatic carboxylic acids to their acid chlorides did not completely proceed in the first step. Also, the steric hindrances of methoxy group or prenyl unit substituted on a xanthone backbone seemed to reduce the nucleophilicity of hydroxyl groups at C3 and C6. However, the yield of ester analogues of *α*-mangostin (**1**) would be improved in case that it could exhibit potent activity after biological activity studies.

All structures of ester analogues were well confirmed by ^{1}H and ^{13}C NMR spectroscopies. The ^{1}H and ^{13}C NMR spectra of those compounds were similar to those of mono- or di-*O*-acetyl mangostin (**M3** or **D3**) compared to the signals of mangostin core. Therefore, the additional signals of substituents on C3 and C6 would be discussed as below.

The ^{1}H NMR spectrum of 6-mono-*O*-propinoyl mangostin (**M4**) (Figure 2.20) showed a quartet at δ_H 2.70 (J = 15.1, 7.6 Hz) a triplet signal at δ_H 1.33 (J = 15.1 Hz), appropriated for propinoate group. The ^{13}C NMR spectrum (Figure 2.21) presented an ester carbonyl peak at δ_C 172.2. In addition, two peaks at δ_C 27.9 and 9.2, indicating the presence of methylene and methyl carbons, respectively of propionate group were detected.

The ^{1}H NMR spectrum of 3-mono-O-propinoyl mangostin (**M4a**) (Figure 2.22) displayed a quartet at δ_H 2.63 (J = 15.1, 7.6 Hz) and a triplet at δ_H 1.30 (J = 7.6 Hz) suggested to a proton of propionate group.

The ^{1}H NMR spectrum of 3,6-di-O-propinoyl mangostin (**D4**) (Figure 2.23) contained two quartet (δ 2.69 and 2.64, J = 15.1, 7.6 Hz) and two triplet (δ 1.32, J = 7.6 Hz and 1.29, J = 7.5 Hz) signals. The ^{13}C NMR spectrum (Figure 2.24) presented two ester carbonyl peaks at δ_C 172.2 and 171.8 together with four peaks at δ_C 28.0, 27.9 and 9.2 (2C), belonging to four aliphatic carbons of propionate group.

The ^{1}H NMR spectrum of 6-mono-O-butanoyl mangostin (**M5**) (Figure 2.25) presented a quartet at δ_H 2.64 (J = 7.3 Hz), a multiplet at δ_H 1.85 and a triplet at δ_H 1.03 (J = 7.4 Hz) assigned to two methylene protons connected to a carbonyl group, the remaining of methylene proton and three methyl protons, respectively for butyrate group. The ^{13}C NMR spectrum (Figure 2.26) revealed four signals of butyrate unit as follows: an ester carbon at δ_C171.1; two methylene carbons at δ_C 36.1 and 17.9; and methyl carbon at δ_C 13.6. In addition, the HMBC experiment was performed to confirm the presence of the ester linkage between C6 and butanoate group. It showed the correlations between OH-1 (δ 13.59) and C-1 (δ 160.7), C-9a (δ 103.8) and C-2 (δ 108.8), between OH-3 (δ 6.32) and C-3 (δ 162.0), C-2 (δ 108.8) and C-4 (δ 93.3), between H-4 (δ 6.22) and C-4a (δ 155.0), C-3 (δ 162.0) and C-2 (δ 108.8), between H-5 (δ 7.07) and C-10a (δ δ 153.8), C-7 (δ 146.5), C-6 (δ 148.9) and C-8a (δ 116.8), between OCH$_3$-7 (δ 3.75) and C-7 (δ 146.5), between H-11 (δ 3.43) and C-3 (δ 162.0), C-1 (δ 160.7), C-12 (δ 121.4) and C-2 (δ 108.8) and between H-16 (δ 4.13) and C-7 (δ 146.5), C-17 (δ 123.0) and C-18 (δ 132.0).

The ^{1}H NMR spectrum of 3,6-di-O-butanoyl mangostin (**D5**) (Figure 2.27) exhibited two triplet signals at δ_H 2.64 (t J = 7.3 Hz) and 2.58 (t, J = 7.4 Hz) belonged to four methylene protons on a carbon connected to a carbonyl group. In addition, two multiplet signals at δ_H 1.83-1.70 and 1.10-1.05 were ascribed to four methylene and six methyl protons of butanoyl group. The ^{13}C NMR spectrum (Figure 2.28) displayed two ester carbonyl peaks at δ_C 171.4 and 170.9. Two peaks at δ_C 36.4 and 36.1 were

assigned to two ester-attached methylene carbons. The four peaks at δ_C 18.1-13.9 could be designated for the remaining aliphatic carbons of butyrate group.

The ^{1}H NMR spectrum of 6-mono-*O*-pivalyl mangostin (**M6**) (Figure 2.29) showed a singlet signal at δ_H 1.42 with nine protons integration assigned to three methyl groups substituted on a quaternary carbon.

The ^{1}H NMR spectrum of 3,6-di-*O*-pivalyl mangostin (**D6**) (Figure 2.30) exhibited two singlet signals at δ_H 1.42 and 1.39, inferred to eighteen methyl protons of pivalate group. The ^{13}C NMR spectrum (Figure 2.31) displayed two ester carbonyl peaks at δ_C 176.1 and 175.7. The signals of quaternary carbon at δ_C 39.4 and six identical methyl carbons at δ_C 27.1 were observed in addition.

The ^{1}H NMR spectrum of 6-mono-*O*-3-methylbutanoyl mangostin (**M7**) (Figure 2.32) showed a doublet at δ_H 2.52 ($J = 7.2$ Hz) and a multiplet at δ_H 2.32-2.25 belonging to two methylene protons on an ester-connected carbon and a proton on a carbon connecting to two methyl groups. A doublet signal at δ_H 1.09 ($J = 6.6$ Hz) was due to six methyl protons of 3-methylbutanoyl group. The ^{13}C NMR spectrum (Figure 2.33) contained a peak at δ_C 170.8, belonged to an ester carbonyl carbon. A peak at δ_C 43.2 was assigned to an ester-connected methylene carbon. The presences of CH carbon and two methyl carbons of 3-methylbutanoyl group were observed at δ_C 25.8-22.4.

The ^{1}H NMR spectrum of 3,6-di-*O*-3-methylbutanoyl mangostin (**D7**) (Figure 2.34) displayed two doublet signals at δ_H 2.52 and 2.48 ($J = 7.1$ Hz) and a multiplet at δ_H 2.32-2.25, suggested for four methylene protons connected to a carbonyl group and two CH protons attached to two methyl groups, respectively. Two doublet signals at δ_H 1.09 ($J = 6.6$ Hz) and 1.08 ($J = 6.3$ Hz) were ascribed to twelve methyl protons of 3-methylbutanoyl group. The ^{13}C NMR spectrum (Figure 2.35) contained a characteristic ester carbonyl peak at δ_C 170.6 and 170.1. Two peaks at δ_C 43.2 and 43.1 were assigned to two ester-connected methylene carbons. The two peaks at δ_C 25.7 and 22.4 were belonged to two identical CH carbons and four identical methyl carbons, respectively.

The ^{1}H NMR spectrum of 6-mono-O-pentanoyl mangostin (**M8**) (Figure 2.36) presented a triplet at δ_H 2.66 (J = 7.4 Hz), two multiplets at δ_H 1.84-1.83 and 1.49-1.47, and a triplet at δ_H 1.00 (J = 7.3 Hz) assigned to two methylene protons connected to a carbonyl group, other four methylene protons and three methyl protons, respectively of pentanoate group. The ^{13}C NMR spectrum (Figure 2.37) revealed the characteristic signal of ester carbonyl carbon at δ_C 172.0. The peak at δ_C 34.0 indicated the methylene carbon connecting to carbonyl group was observed. The peaks at δ_C 26.8 and 22.2 could be assigned for two methylene carbons of pentanoate group. The peak at δ_C 13.7 appropriated for a methyl carbon was also detected.

The ^{1}H NMR spectrum of 3,6-di-O-pentanoyl mangostin (**D8**) (Figure 2.38) showed two triplets at δ_H 2.56 and 2.60 (J = 7.4 Hz), three multiplets at δ_H 1.84-1.70, 1.51-1.43 and 1.01-0.96 indicated to four methylene protons connected to a carbonyl group, other eight methylene protons and six methyl protons, respectively. The ^{13}C NMR spectrum (Figure 2.39) exhibited two ester peaks at δ_C 171.4 and 170.9. The peaks at δ_C 34.0 were belonged to two methylene carbons connected to a carbonyl group. The four peaks at δ_C 29.7, 26.9, 22.3 and 22.2 were detected from the presence of four methylene carbons of pentanoate group. The peak at δ_C 13.7 was due to two identical methyl carbons.

The ^{1}H NMR spectrum of 6-mono-O-hexanoyl mangostin (**M9**) (Figure 2.40) presented the signals of hexanoate group as follows: a triplet at δ_H 2.64 (J = 7.5 Hz) appropriated for two methylene protons connected to a carbonyl group; two multiplet at δ_H 1.84-1.83 and 1.43-1.40 ascribed to six methylene protons; and a triplet at δ_H 0.94 (J = 6.8 Hz) indicated three methyl protons. The ^{13}C NMR spectrum (Figure 2.41) contained an ester carbonyl peak at δ_C 171.2. A signal at δ_C 34.3 was assigned to ester-connected methylene carbon. The three peaks at δ_C 31.2, 24.5 and 22.3 were observed from the presence of three methylene carbons of hexanoate group. The peak at δ_C 13.9 was belonged to a methyl carbon.

The ^{1}H NMR spectrum of 6-mono-O-nanoyl mangostin (**M10**) (Figure 2.42) presented a triplet at δ_H 2.64 (J = 7.4 Hz), two multiplets at δ_H 1.84-1.83 and 1.34-1.30, and a triplet at δ_H 0.90 (J = 6.9 Hz) assigned to two methylene protons

connected to a carbonyl group, twelve methylene protons and three methyl protons, respectively. The ^{13}C NMR spectrum (Figure 2.43) contained a peak at δ_C 171.7 of ester carbonyl carbon and 34.3 of methylene carbon adjacent to a carbonyl group. The peaks at δ_C 31.8-29.1, 24.8 and 22.6 could be designated for six methylene carbons. The peak at δ_C 14.1 was assigned to a methyl carbon.

The ^{1}H NMR spectrum of 3,6-di-*O*-nanoyl mangostin (**D10**) (Figure 2.44) showed two triplets at δ_H 2.64 (*J* = 7.4 Hz) and 2.59 (*J* = 7.4 Hz), three multiplets at δ_H 1.83-1.77, 1.42-1.25 and 0.89-0.87 indicated to four methylene protons connected to a carbonyl group, other twenty methylene protons and six methyl protons, respectively. The ^{13}C NMR spectrum (Figure 2.45) exhibited two ester carbonyl peaks at δ_C 171.4 and 170.9. Two identical peaks at δ_C 34.3 were displayed from the presence of a methylene carbon adjacent to a carbonyl group. The presence of twelve methylene carbons of nanoate group was inferred from the detection of peaks at δ_C 31.8-29.1, 24.8 and 22.6. The two methyl peaks were observed at δ_C 14.1.

The ^{1}H NMR spectrum of 6-mono-*O*-lauryl mangostin (**M11**) (Figure 2.46) presented a triplet at δ_H 2.65 (*J* = 7.4 Hz), two multiplets at δ_H 1.84-1.83 and 1.40-1.27, and a triplet at δ_H 0.88 (*J* = 6.6 Hz) assigned to two methylene protons connected to an ester carbonyl group, eighteen methylene protons and three methyl protons, respectively. The ^{13}C NMR spectrum (Figure 2.47) contained a peak at δ_C 171.4 and 34.3 indicated ester carbonyl and ester-attached methylene carbons, respectively. The peaks at δ_C 31.9-29.1, 24.8 and 22.7 were belonged to eight methylene carbons of laurate group. The peak at δ_C 14.1 appropriated for a methyl carbon was also detected.

The ^{1}H NMR spectrum of 3,6-di-*O*-lauryl mangostin (**D11**) (Figure 2.48) showed two triplets at δ_H 2.65 (*J* = 7.4 Hz) and 2.58 (*J* = 7.6 Hz), three multiplets at δ_H 1.84-1.77, 1.43-1.27 and 0.89-0.86 indicated to four methylene protons connected to a carbonyl group, other thirty-two methylene protons and six methyl protons, respectively. The ^{13}C NMR spectrum (Figure 2.49) exhibited two ester carbonyl peaks at δ_C 171.3 and 170.9. Two peaks at δ_C 34.8 and 34.4 indicated each methylene carbon next to ester bond. The eight peaks at δ_C 34.3-29.1 and 25.1-22.3 could be designed

for sixteen methylene carbons of laurate group. The peak at δ_C 14.1 appropriated for two methyl carbons was also detected.
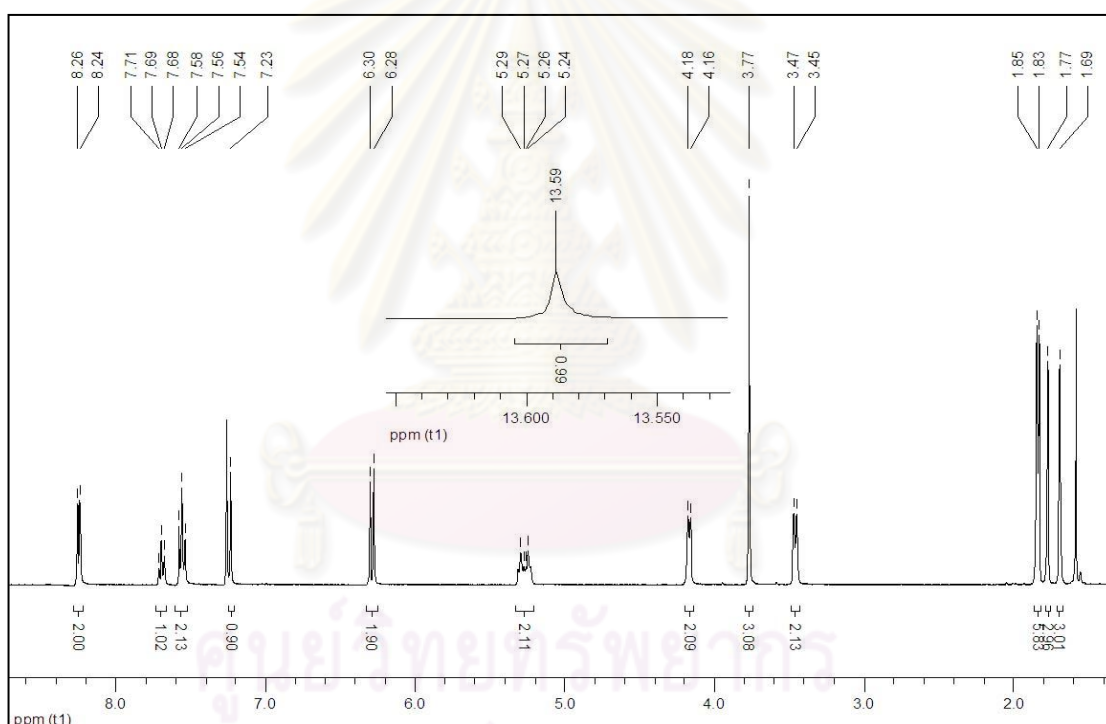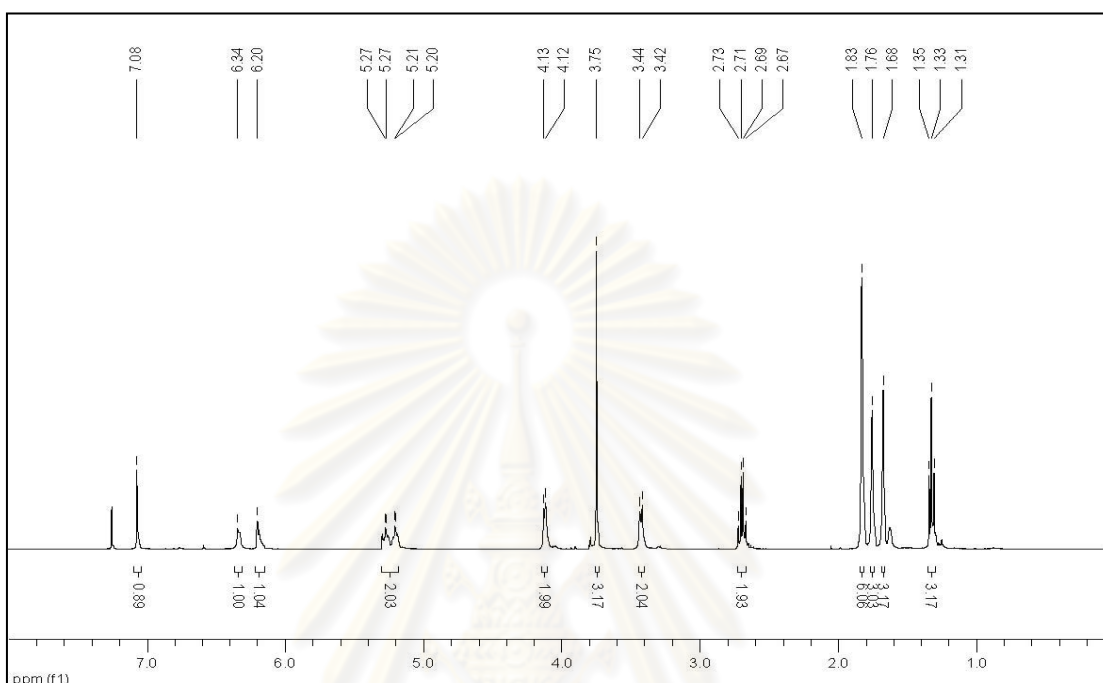

Figure 2.20 The ^{1}H NMR spectrum (CDCl$_3$, 400 MHz) of compound **M4**
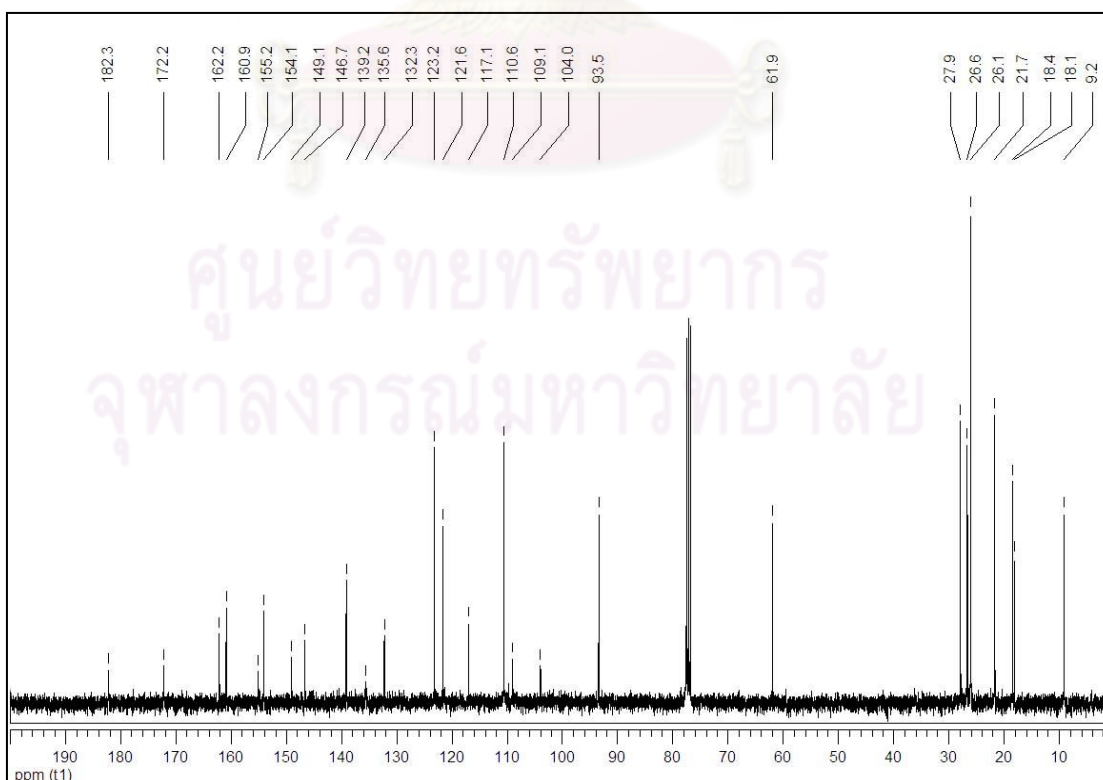
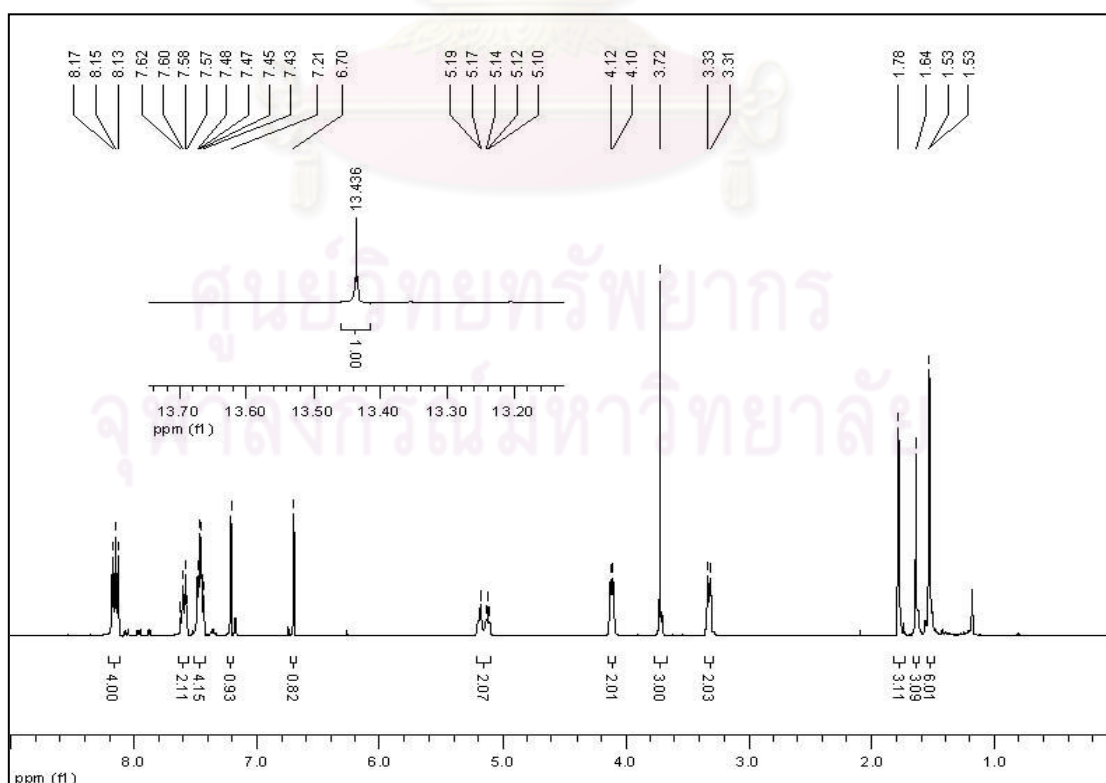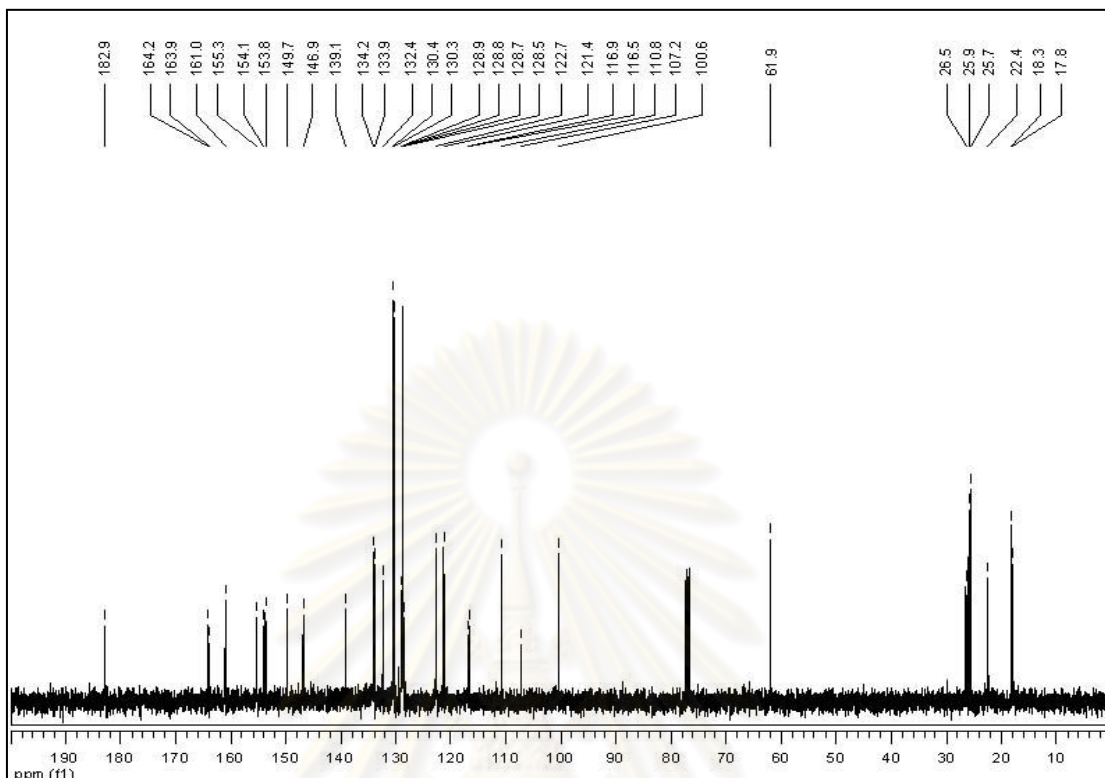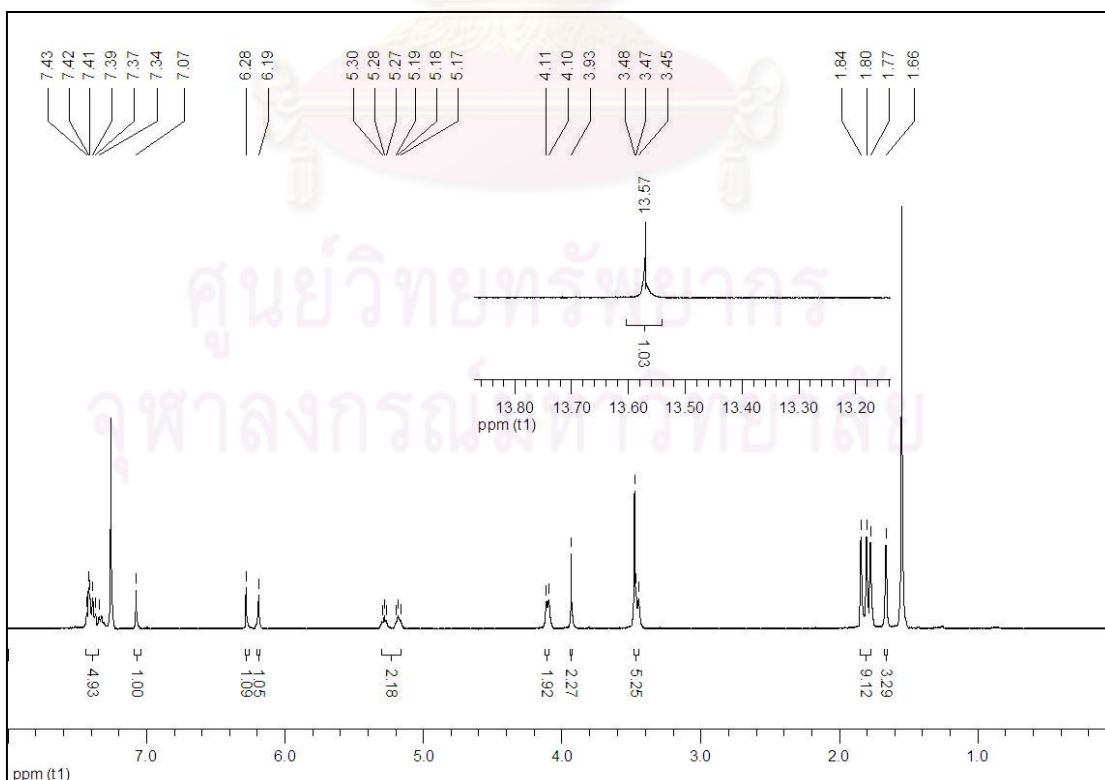**Figure 2.21** The ^{13}C NMR spectrum (CDCl$_3$, 100 MHz) of compound **M4**
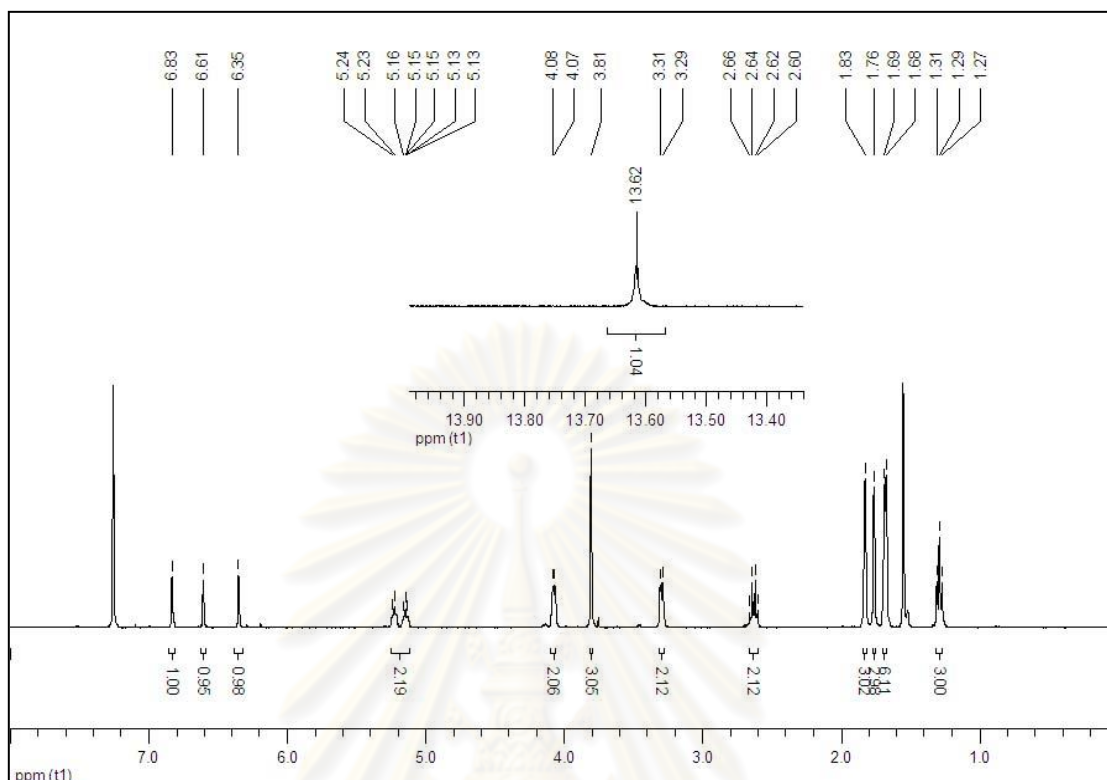
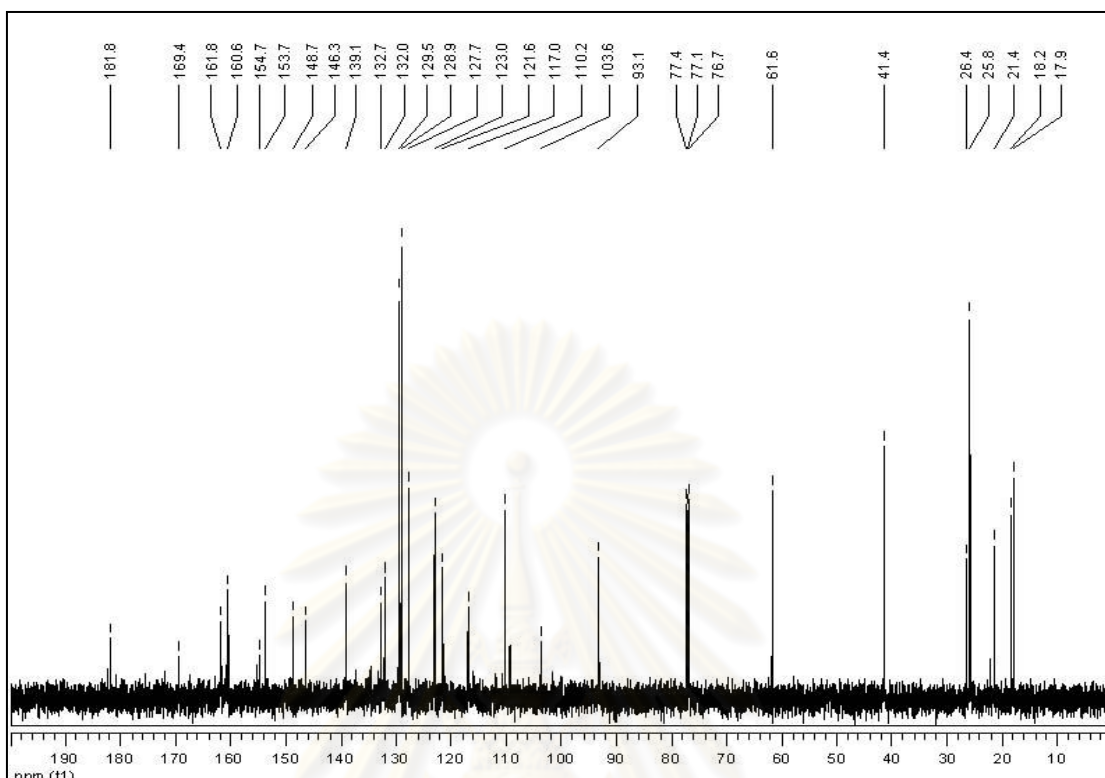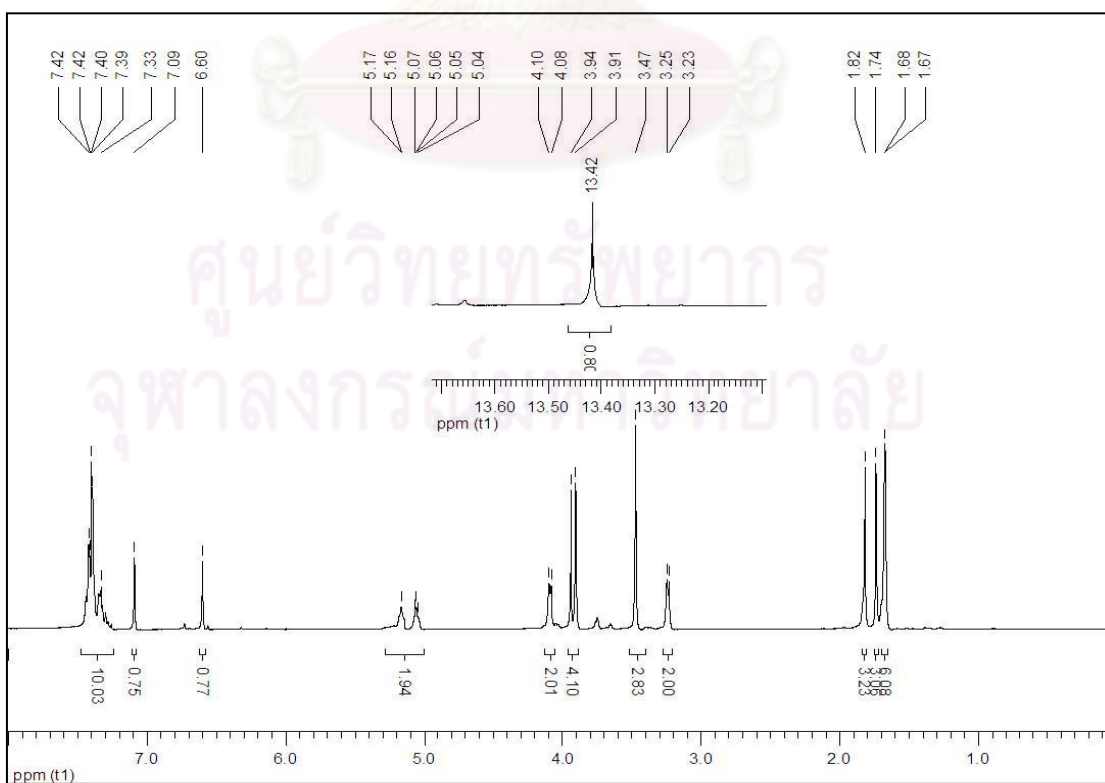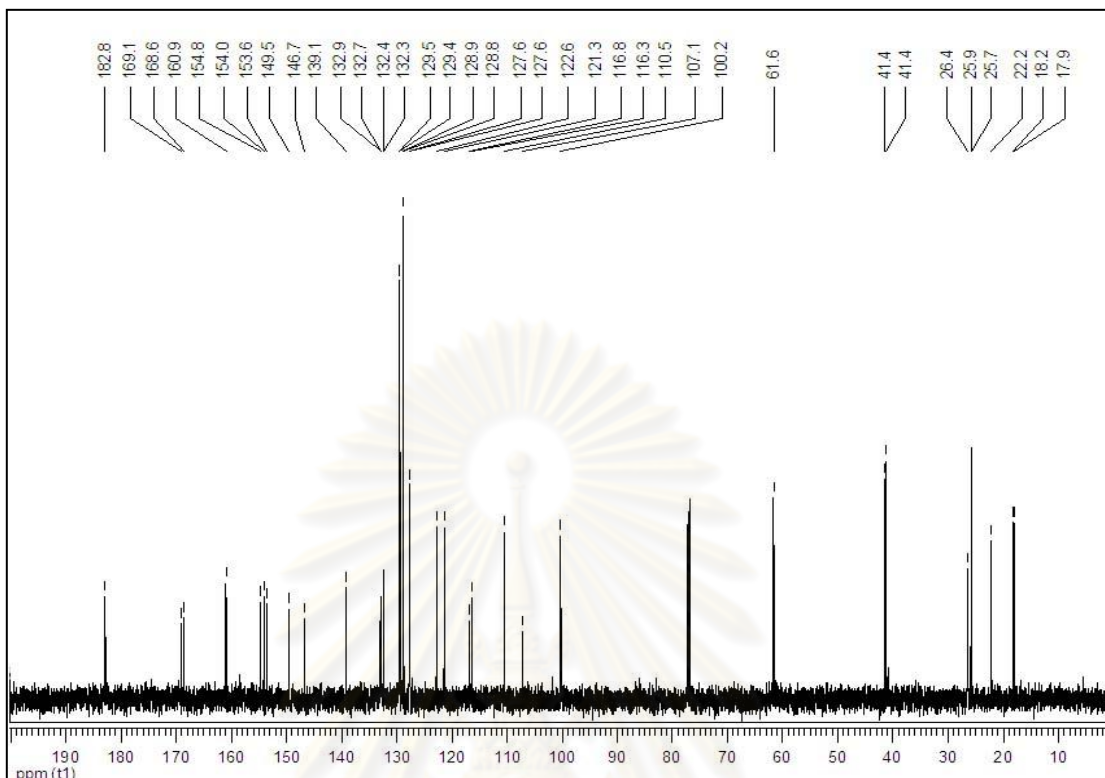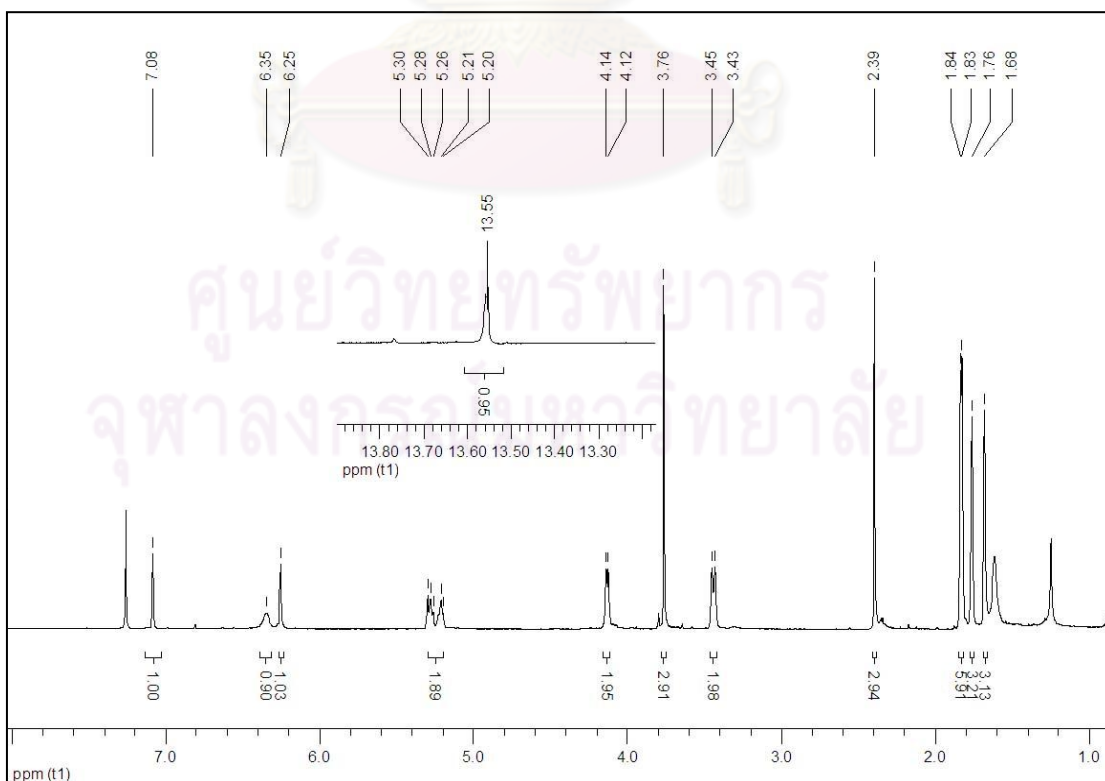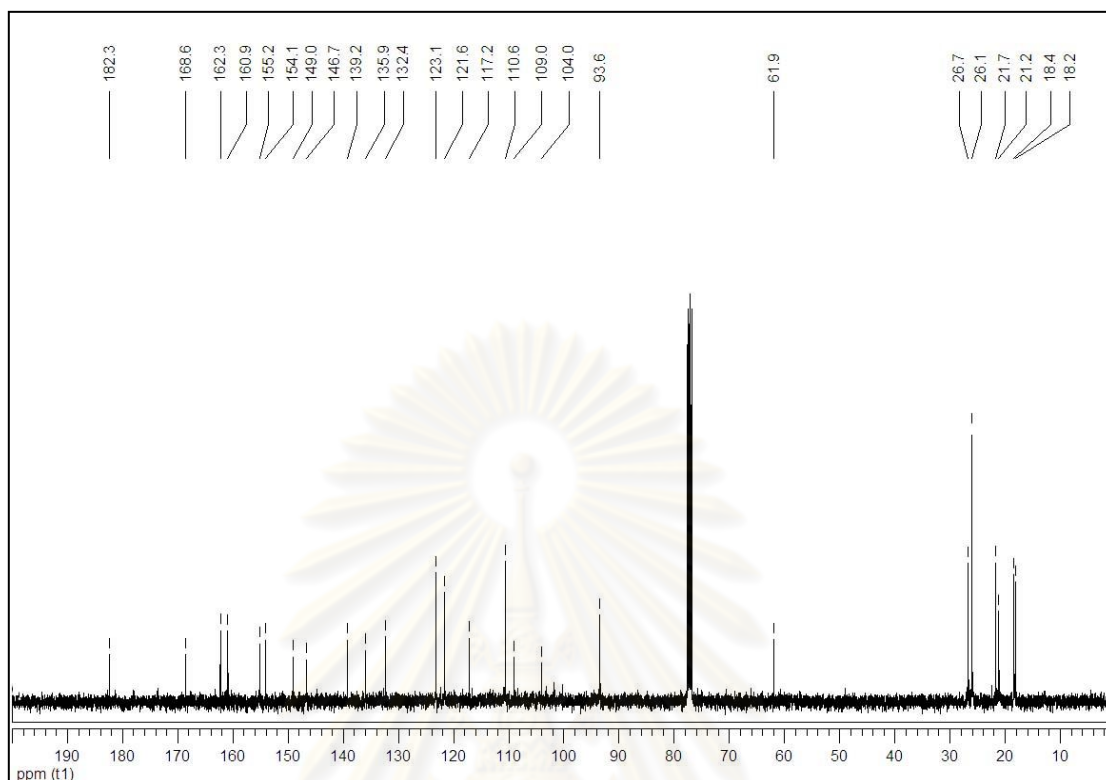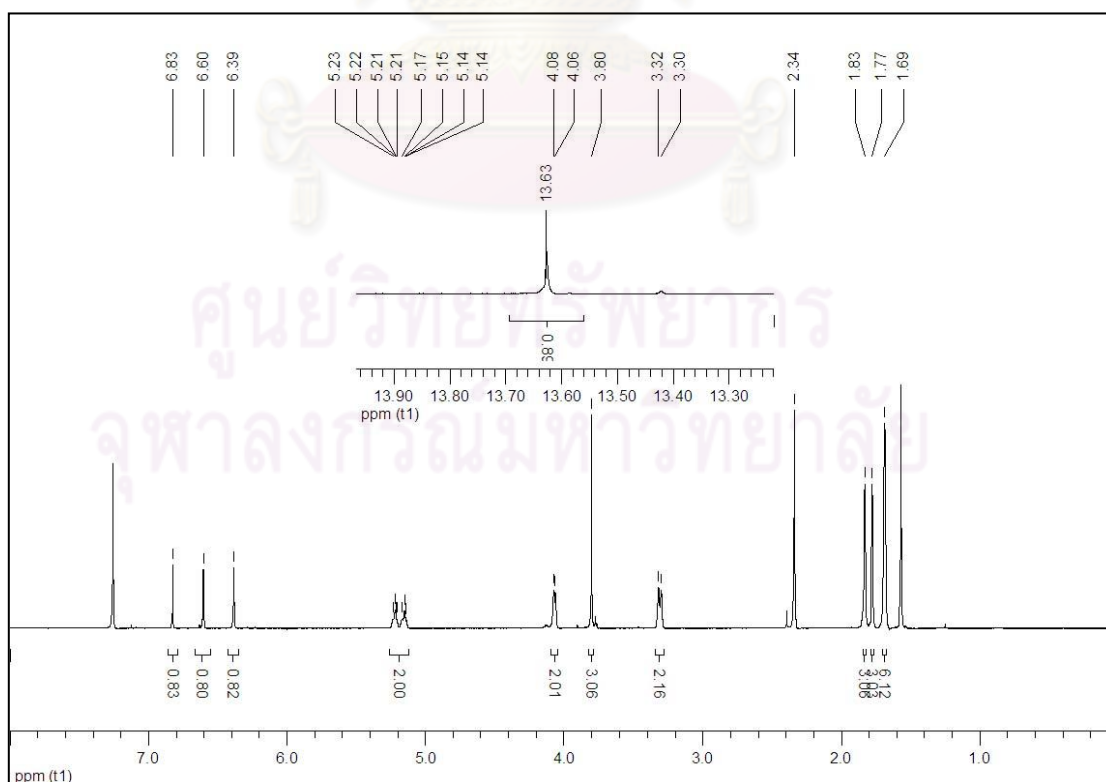**Figure 2.22** The ^{1}H NMR spectrum (CDCl$_3$, 400 MHz) of compound **M4a**
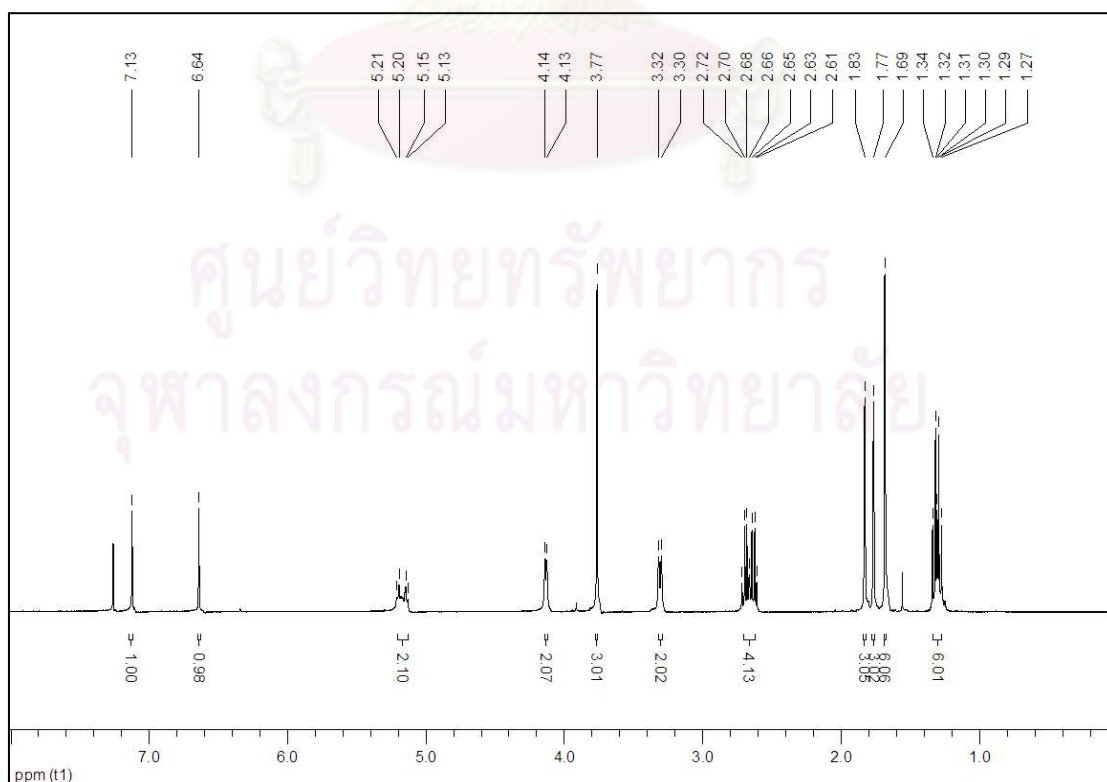
Figure 2.23 The ^{1}H NMR spectrum (CDCl$_3$, 400 MHz) of compound **D4**
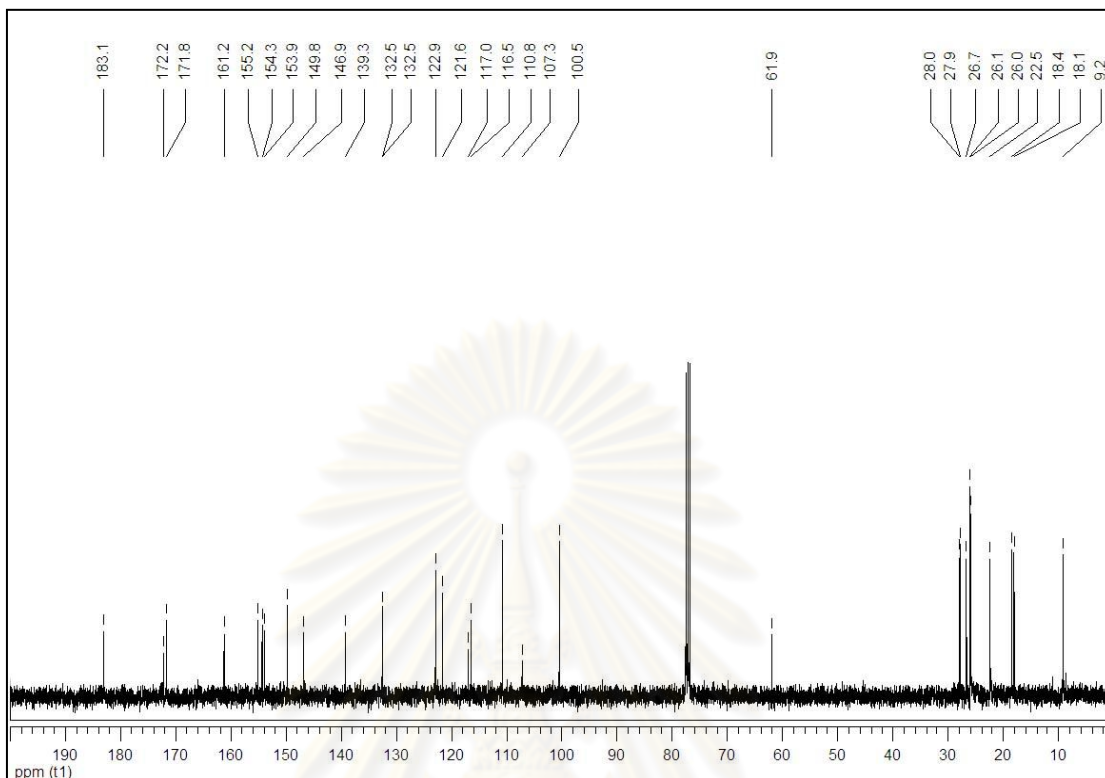
Figure 2.24 The ^{13}C NMR spectrum (CDCl$_3$, 100 MHz) of compound **D4**
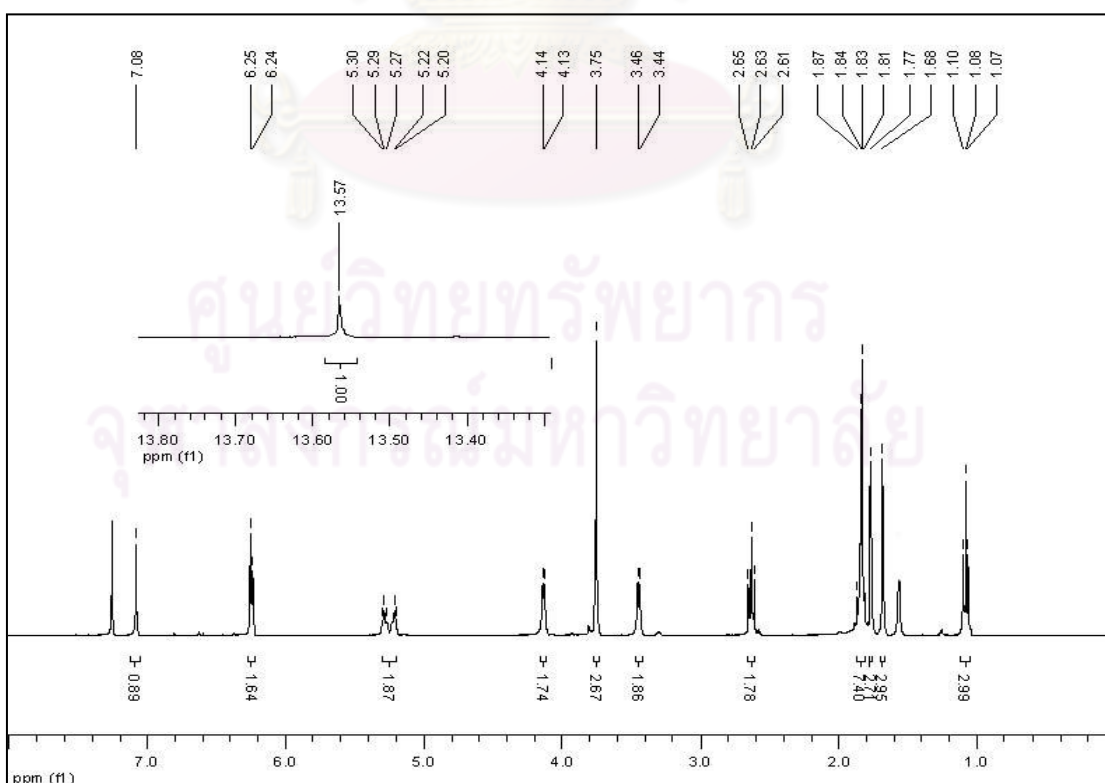
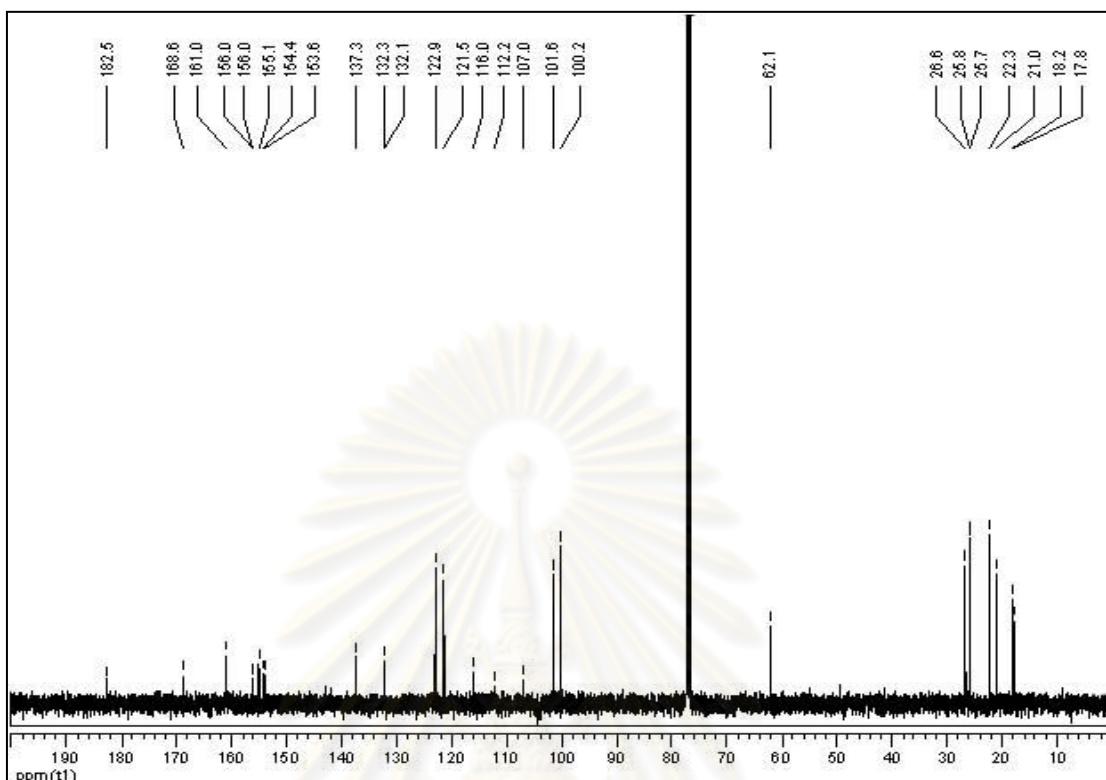**Figure 2.25** The ^{1}H NMR spectrum (CDCl$_3$, 400 MHz) of compound **M5**
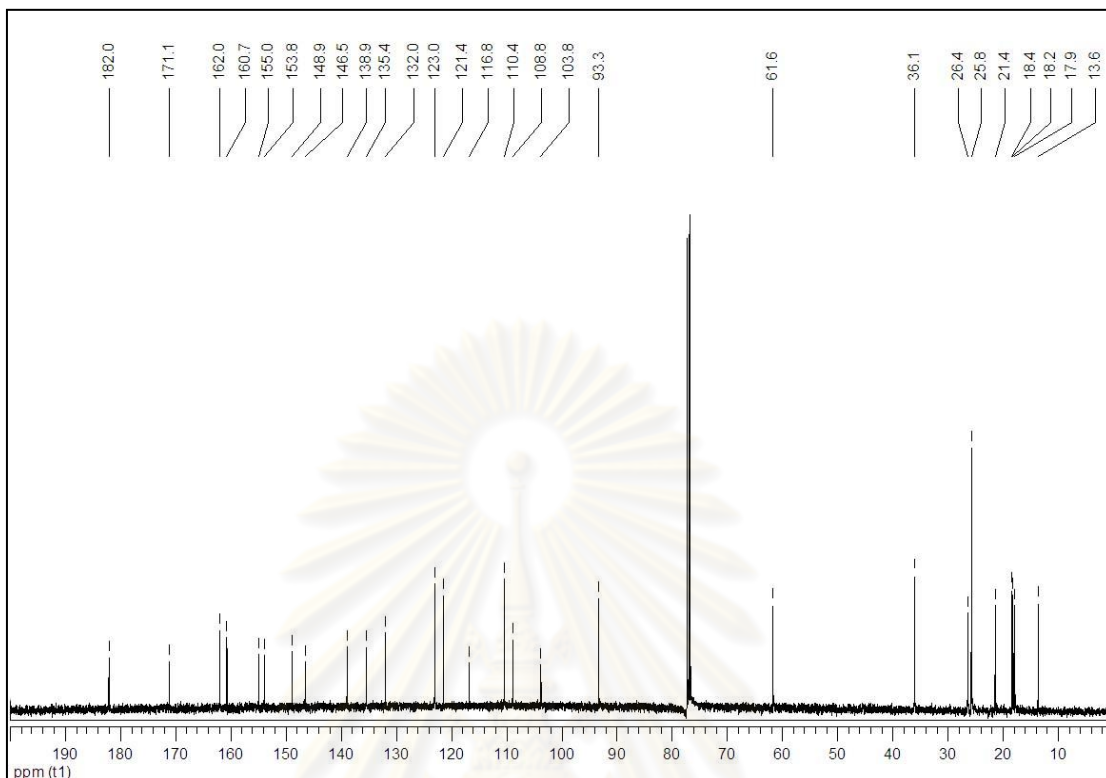
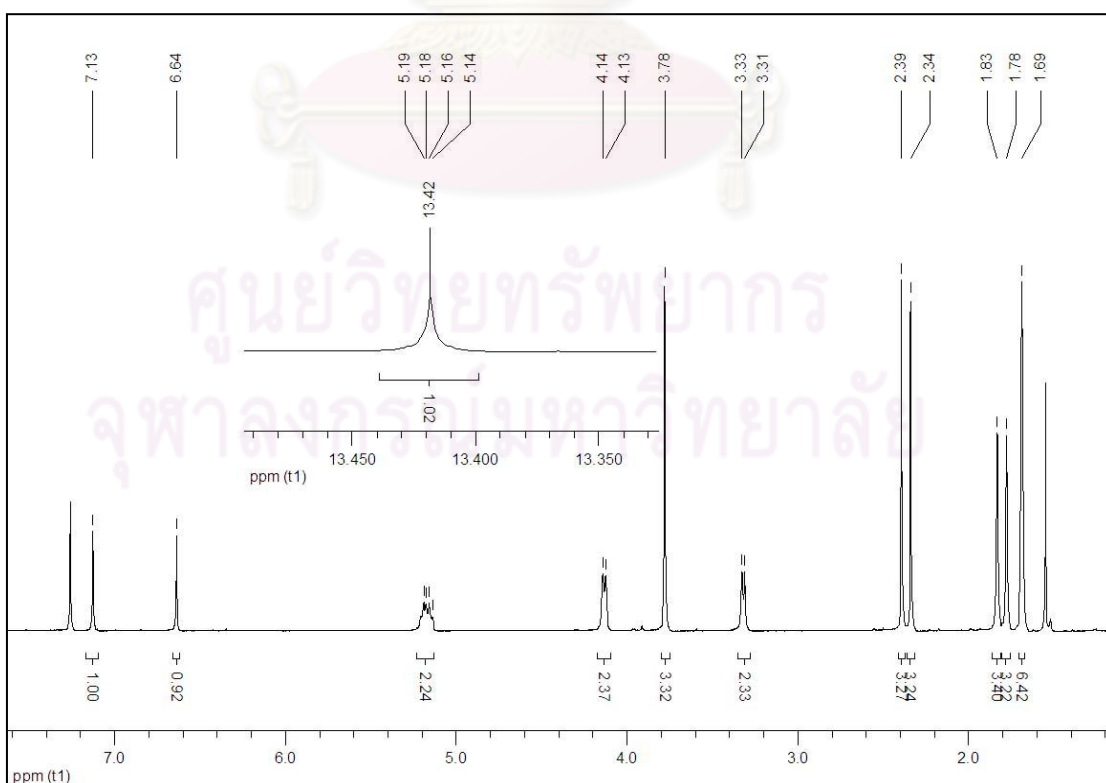**Figure 2.26** The ^{13}C NMR spectrum (CDCl$_3$, 100 MHz) of compound **M5**
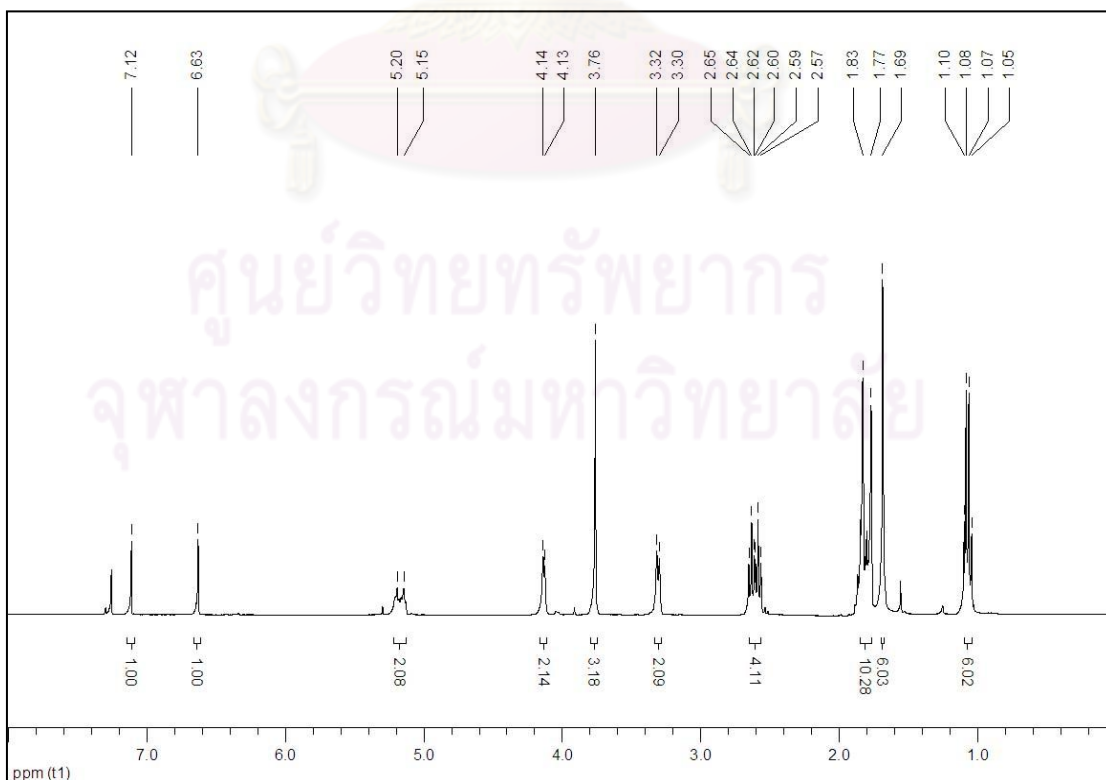
Figure 2.27 The ^{1}H NMR spectrum (CDCl$_3$, 400 MHz) of compound **D5**
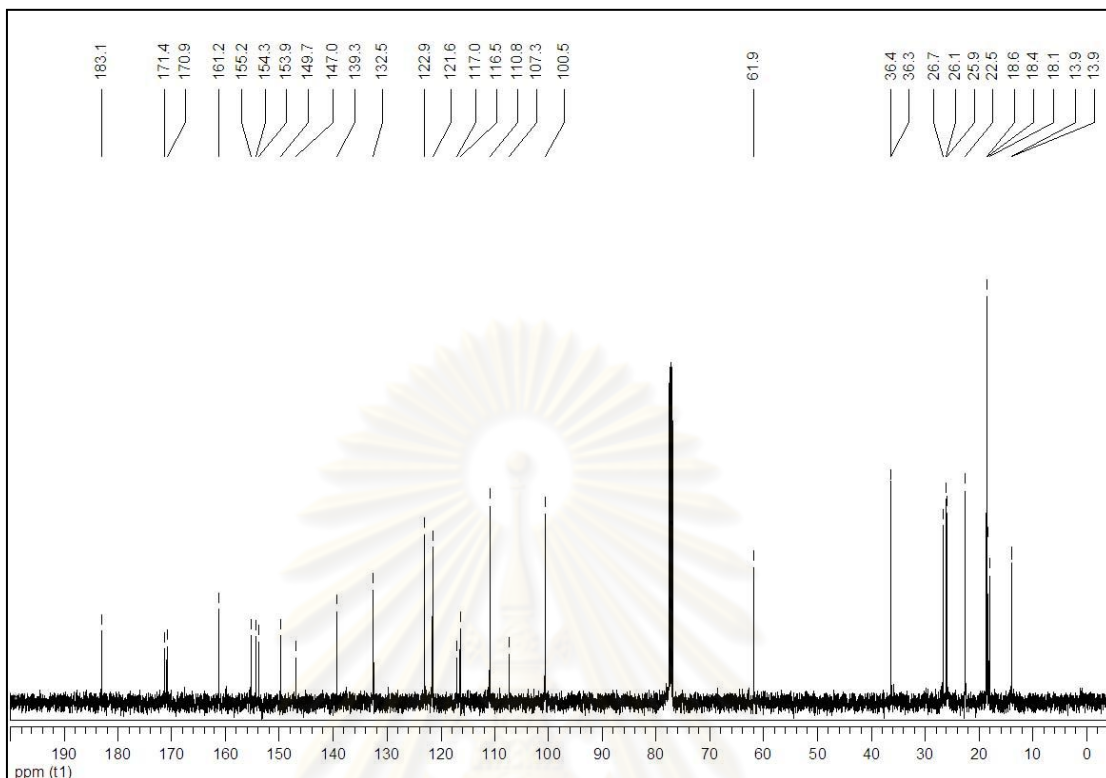
Figure 2.28 The ^{13}C NMR spectrum (CDCl$_3$, 100 MHz) of compound **D5**
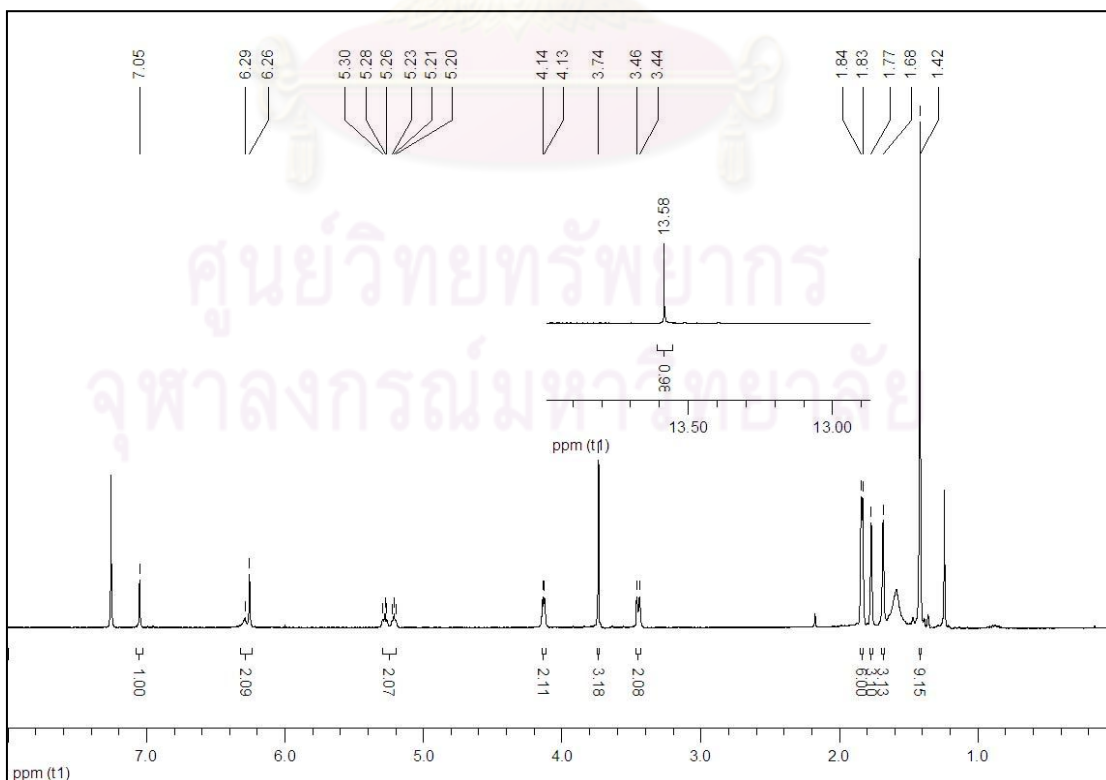
Figure 2.29 The ^{1}H NMR spectrum (CDCl$_3$, 400 MHz) of compound **M6**
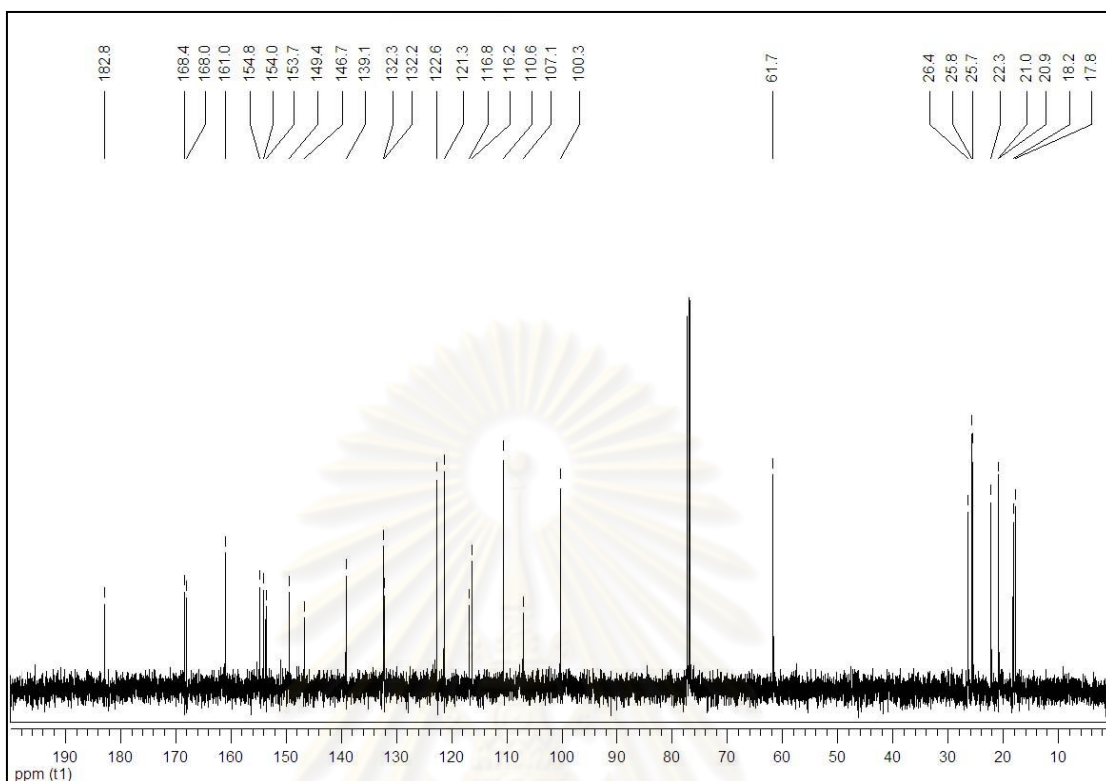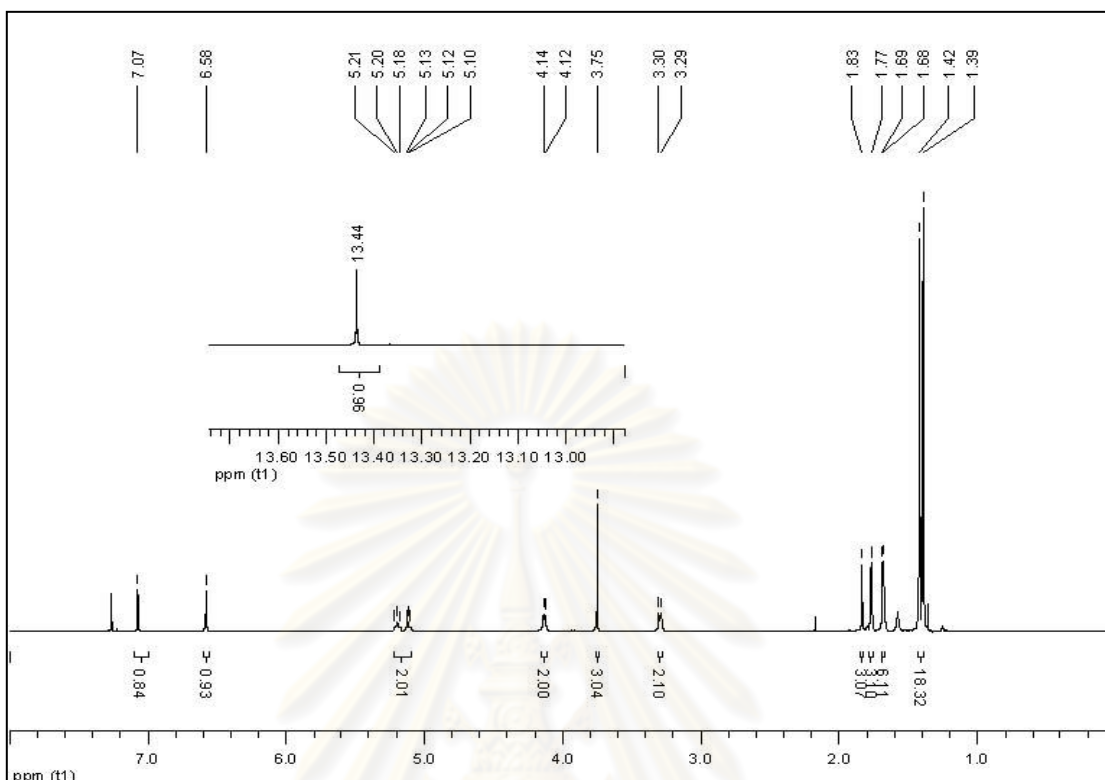
Figure 2.30 The ^{1}H NMR spectrum (CDCl$_3$, 400 MHz) of compound **D6**
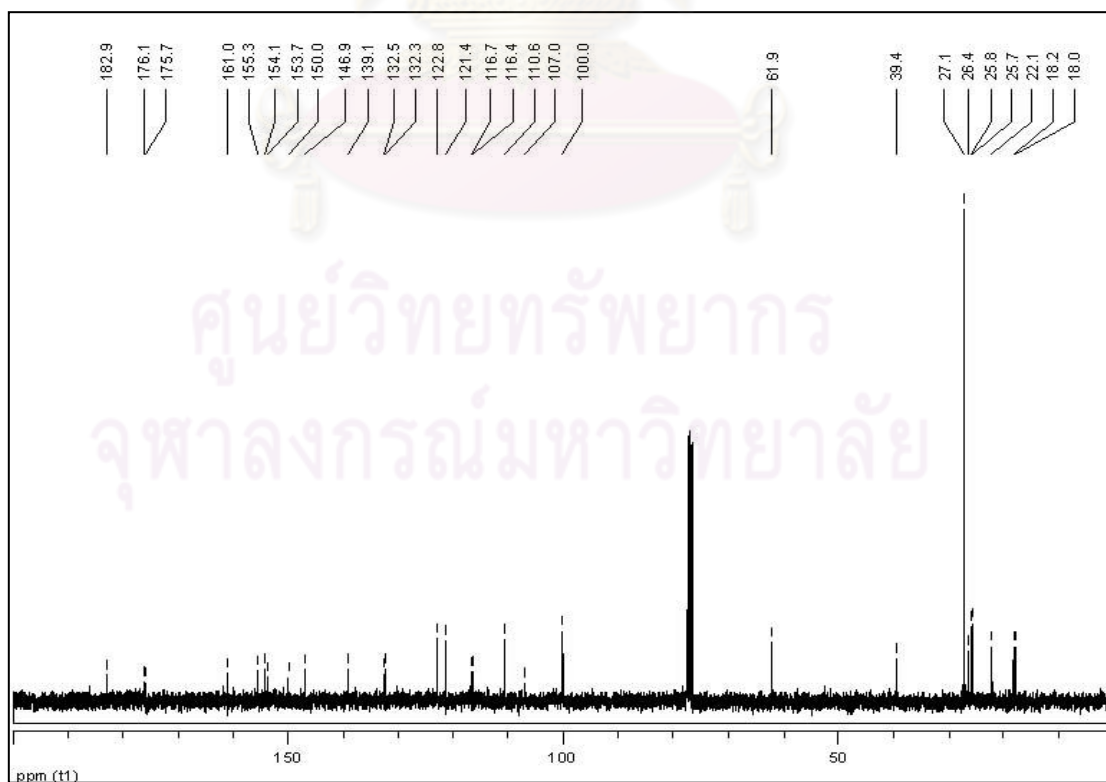
Figure 2.31 The ^{13}C NMR spectrum (CDCl$_3$, 100 MHz) of compound **D6**
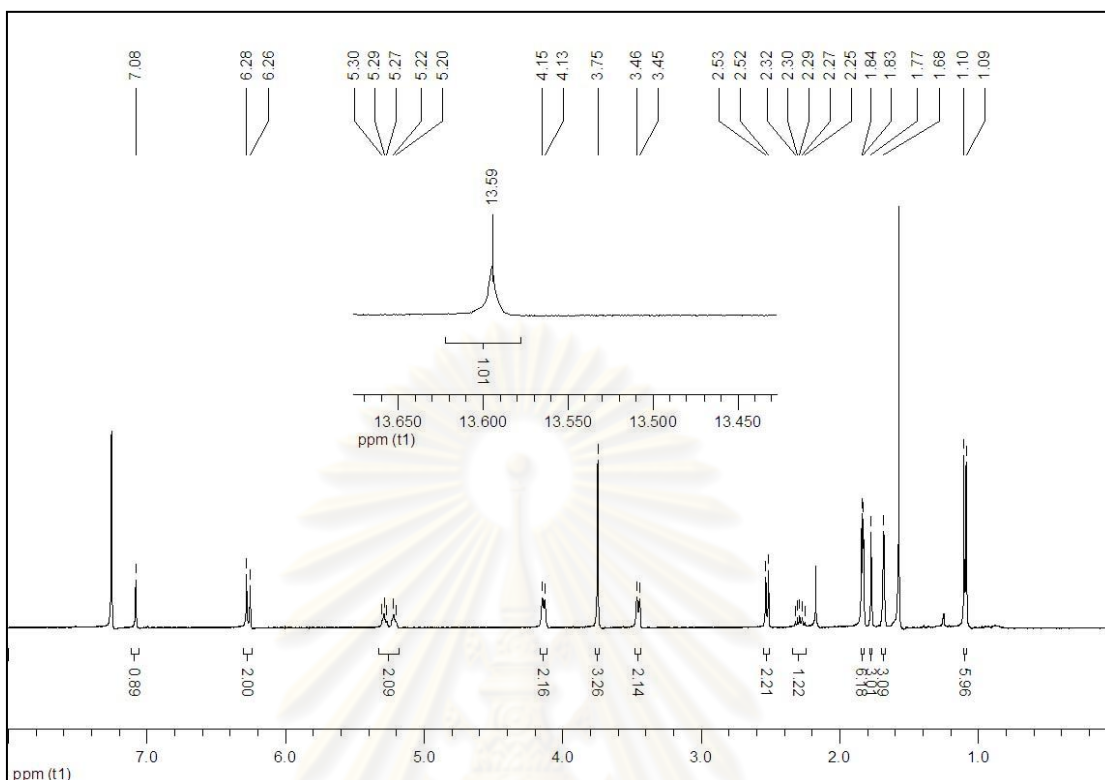
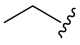**Figure 2.32** The ^{1}H NMR spectrum (CDCl$_3$, 400 MHz) of compound **M7**
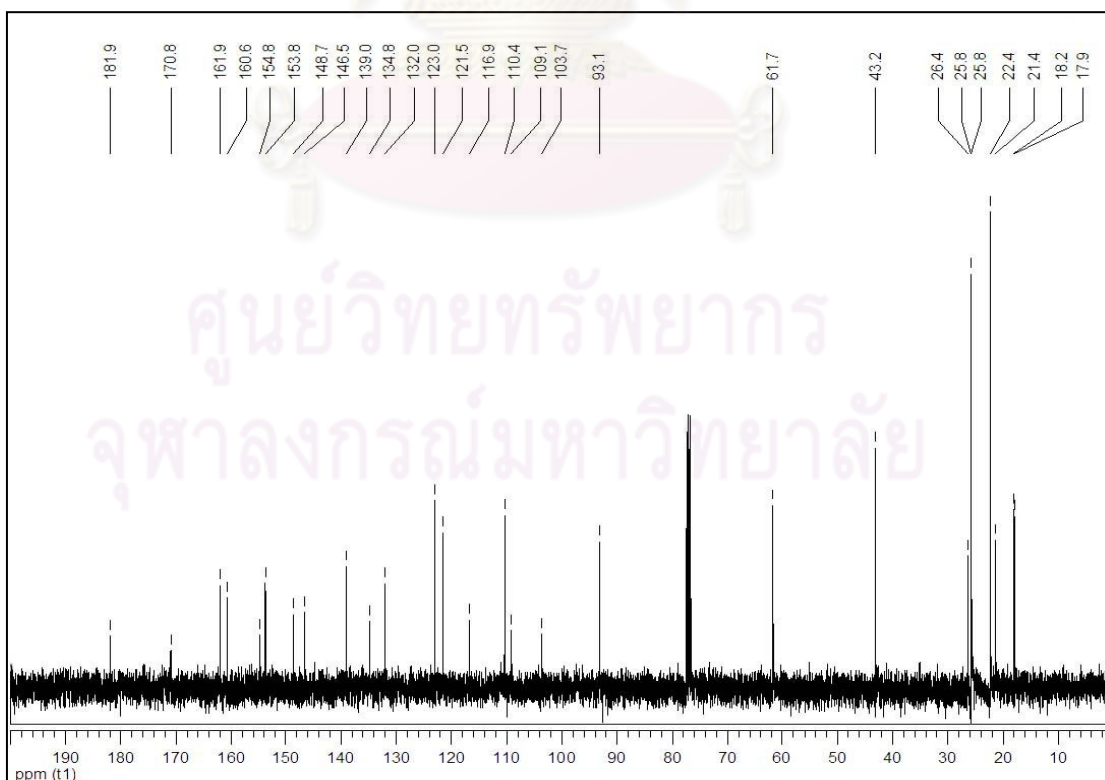
Figure 2.33 The ^{13}C NMR spectrum (CDCl$_3$, 100 MHz) of compound **M7**

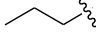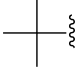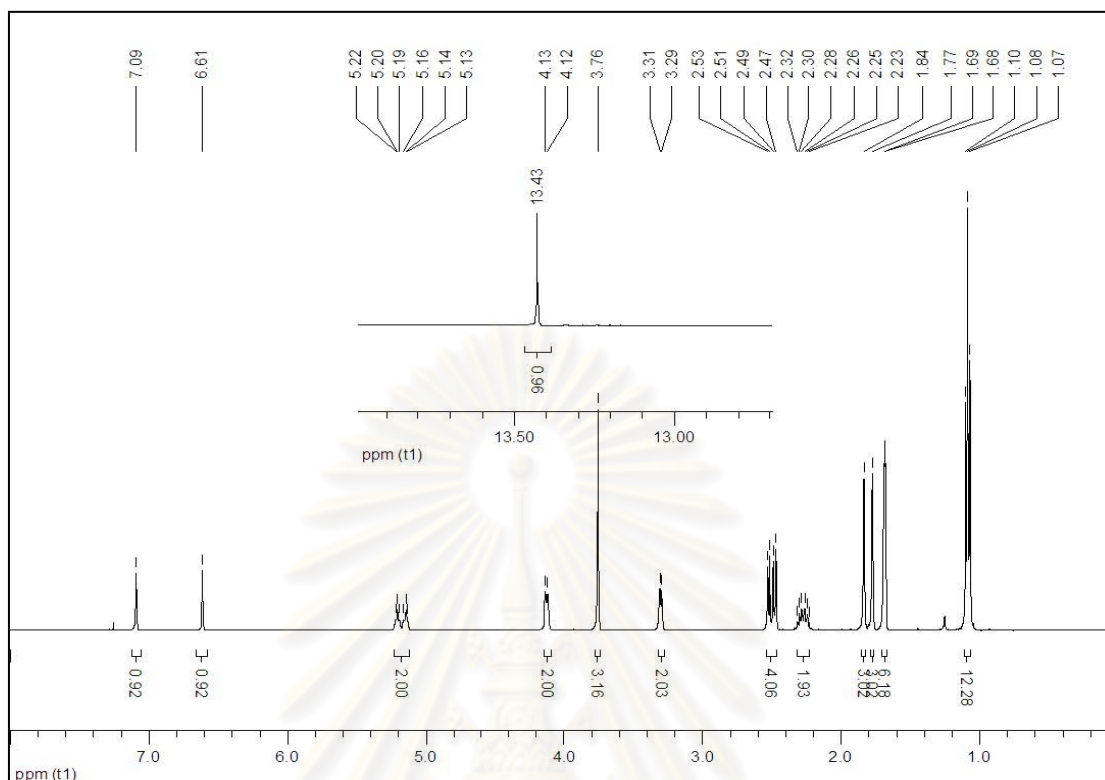**Figure 2.34** The ^{1}H NMR spectrum (CDCl$_3$, 400 MHz) of compound **D7**
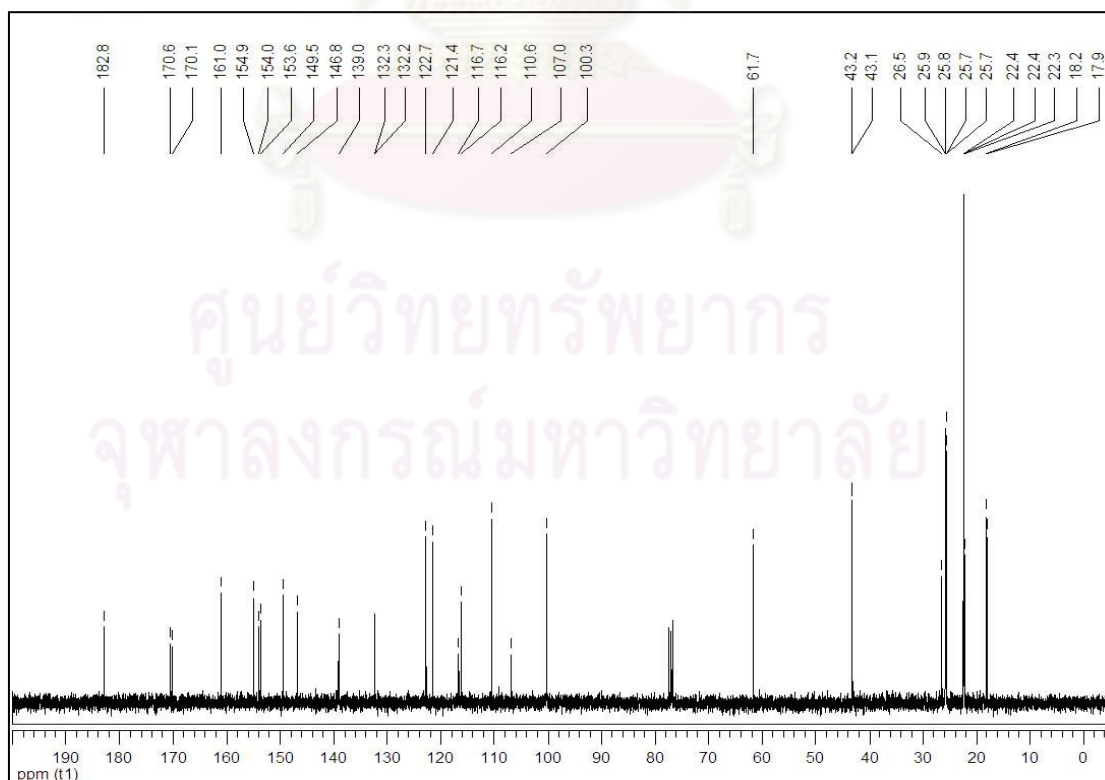
Figure 2.35 The ^{13}C NMR spectrum (CDCl$_3$, 100 MHz) of compound **D7**
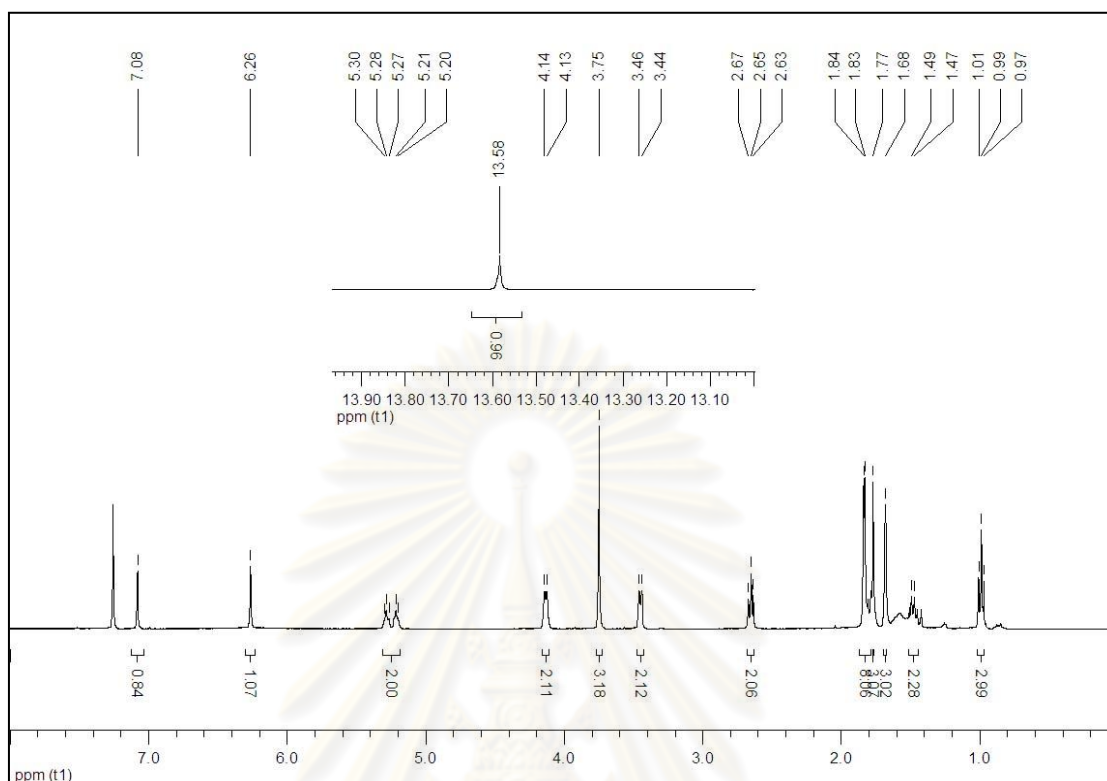
Figure 3.36 The ^{1}H NMR spectrum (CDCl$_3$, 400 MHz) of compound **M8**
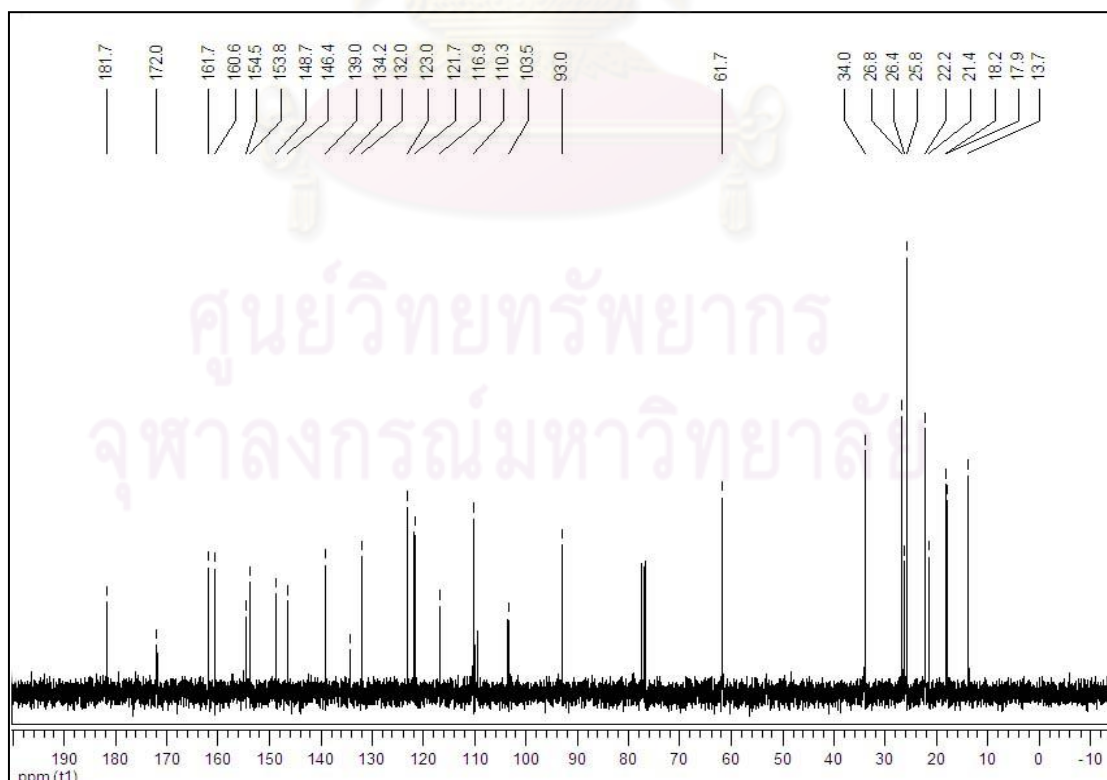
Figure 2.37 The ^{13}C NMR spectrum (CDCl$_3$, 100 MHz) of compound **M8**
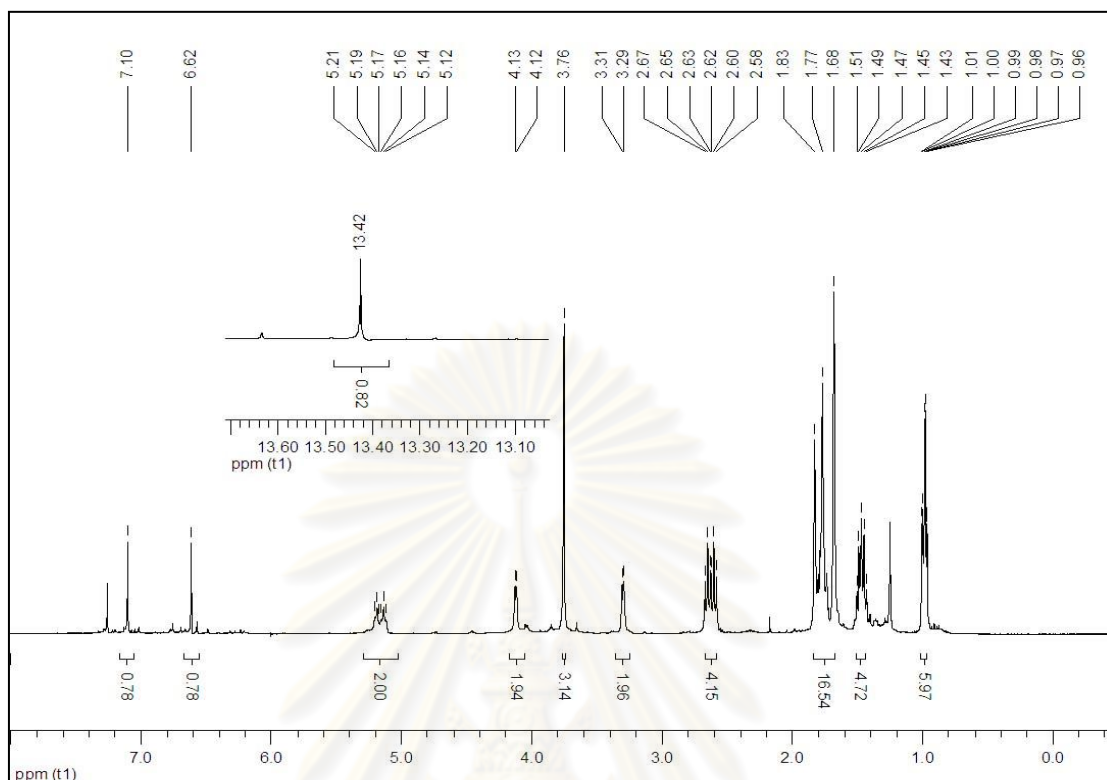
Figure 2.38 The ^{1}H NMR spectrum (CDCl$_3$, 400 MHz) of compound **D8**
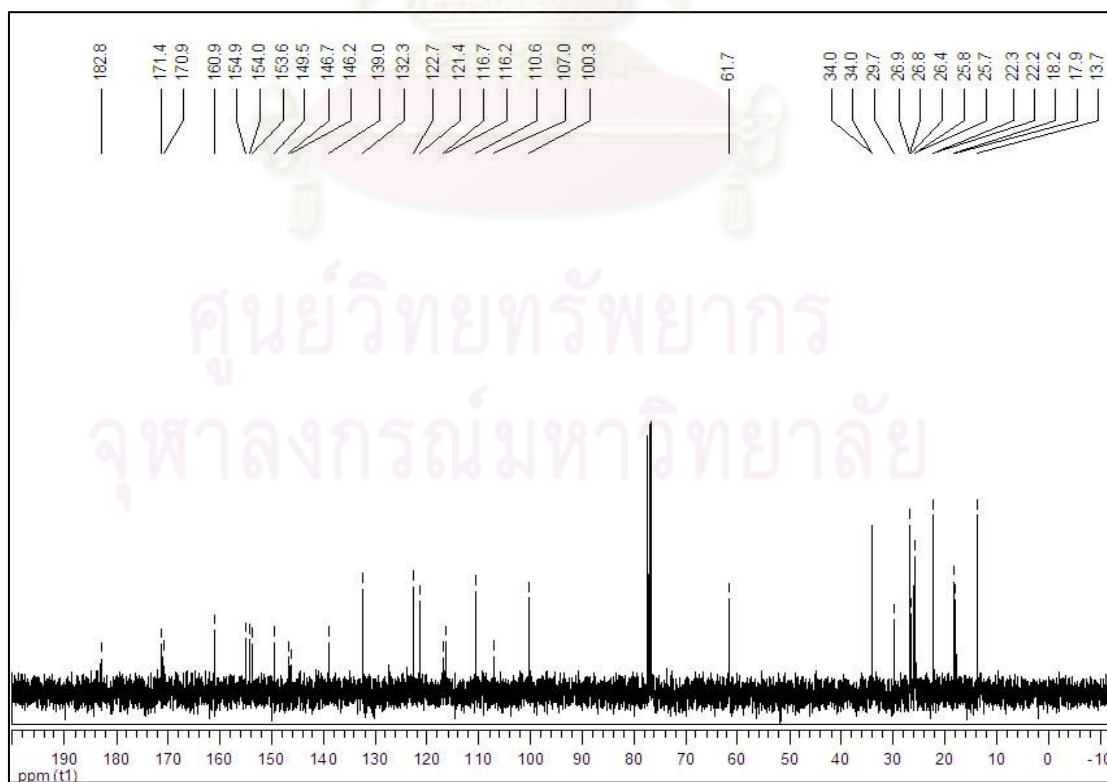
Figure 2.39 The ^{13}C NMR spectrum (CDCl$_3$, 100 MHz) of compound **D8**
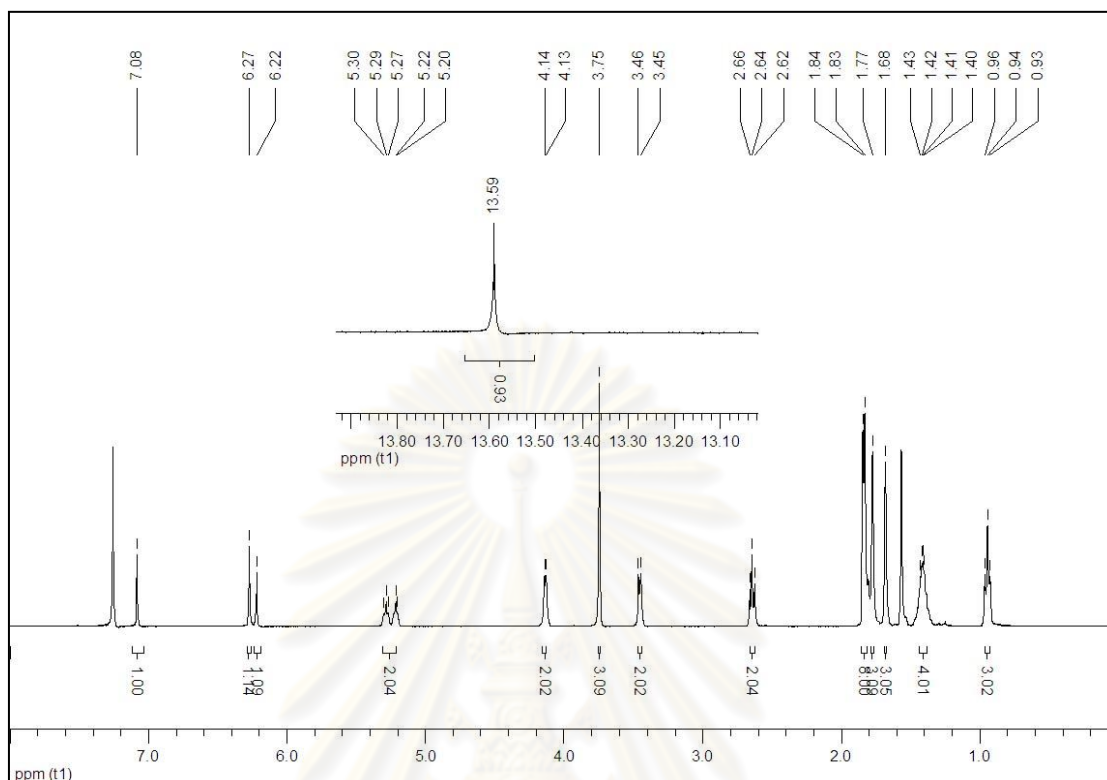
Figure 2.40 The ^{1}H NMR spectrum (CDCl$_3$, 400 MHz) of compound **M9**
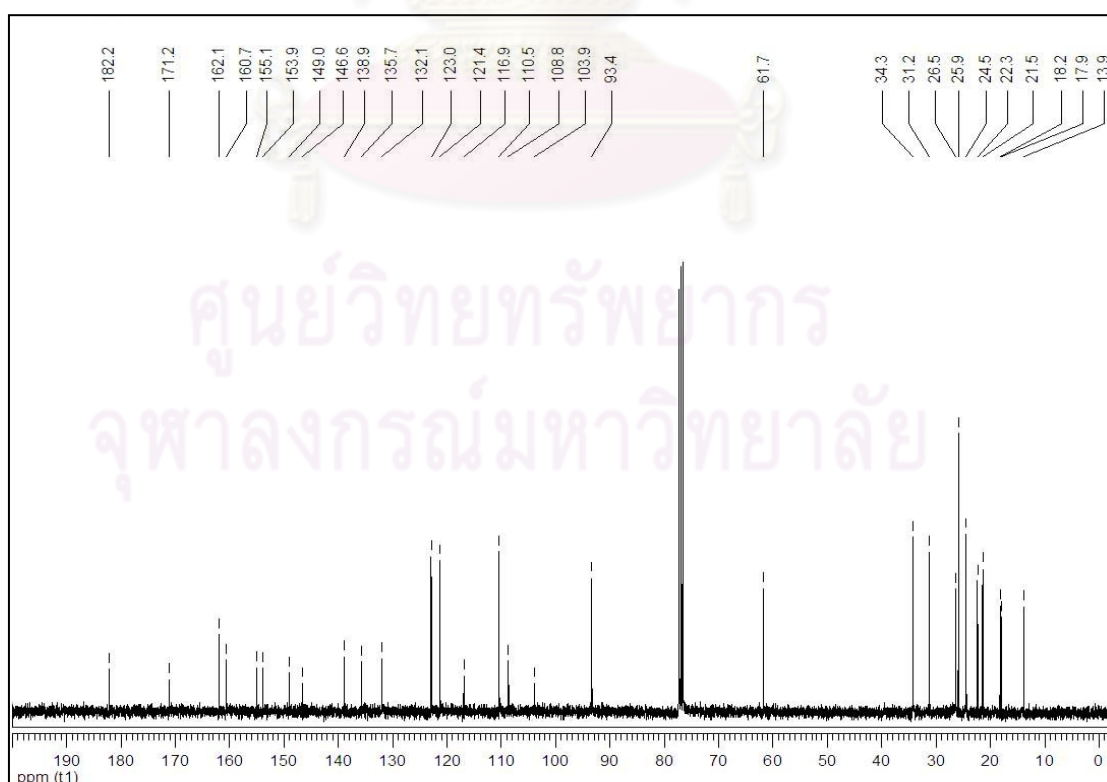
Figure 2.41 The ^{13}C NMR spectrum (CDCl$_3$, 100 MHz) of compound **M9**
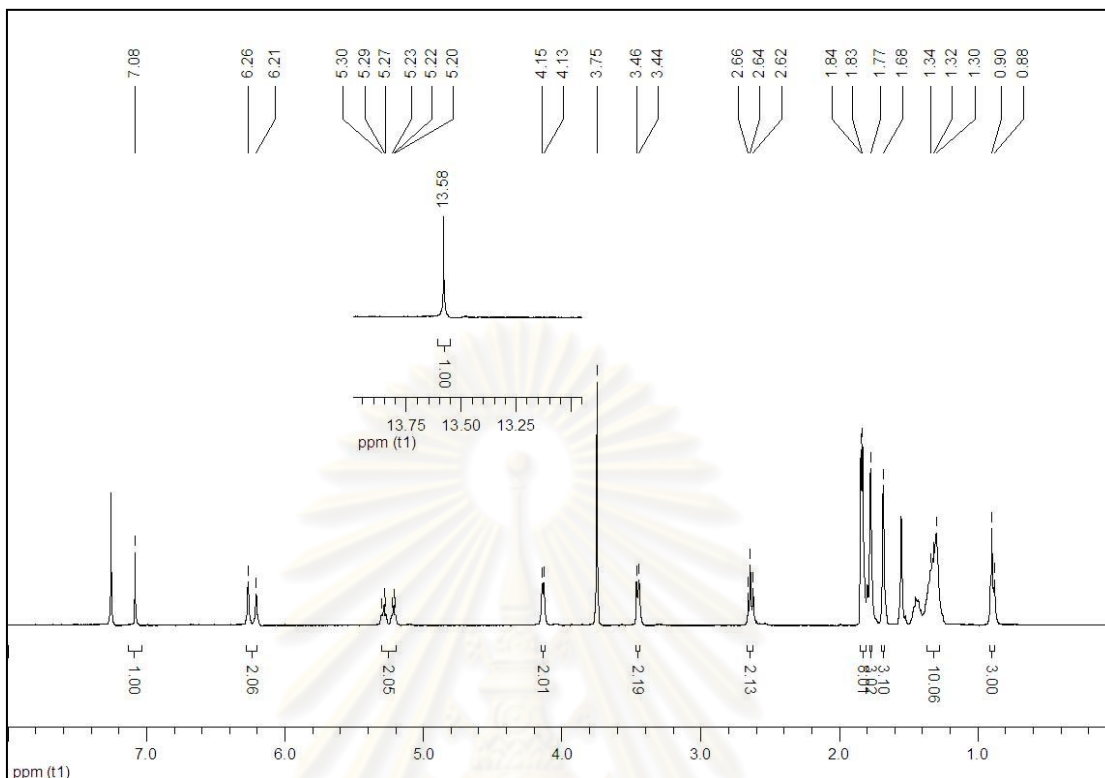
Figure 2.42 The ^{1}H NMR spectrum (CDCl$_3$, 400 MHz) of compound **M10**
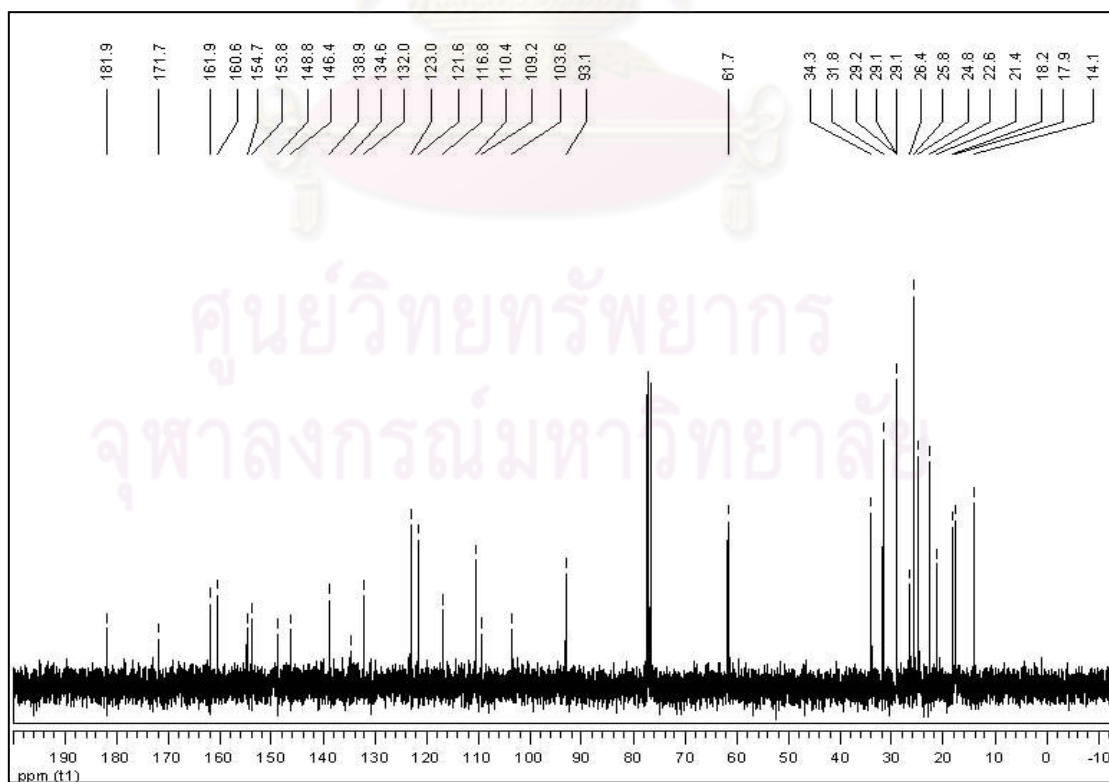
Figure 2.43 The ^{13}C NMR spectrum (CDCl$_3$, 100 MHz) of compound **M10**
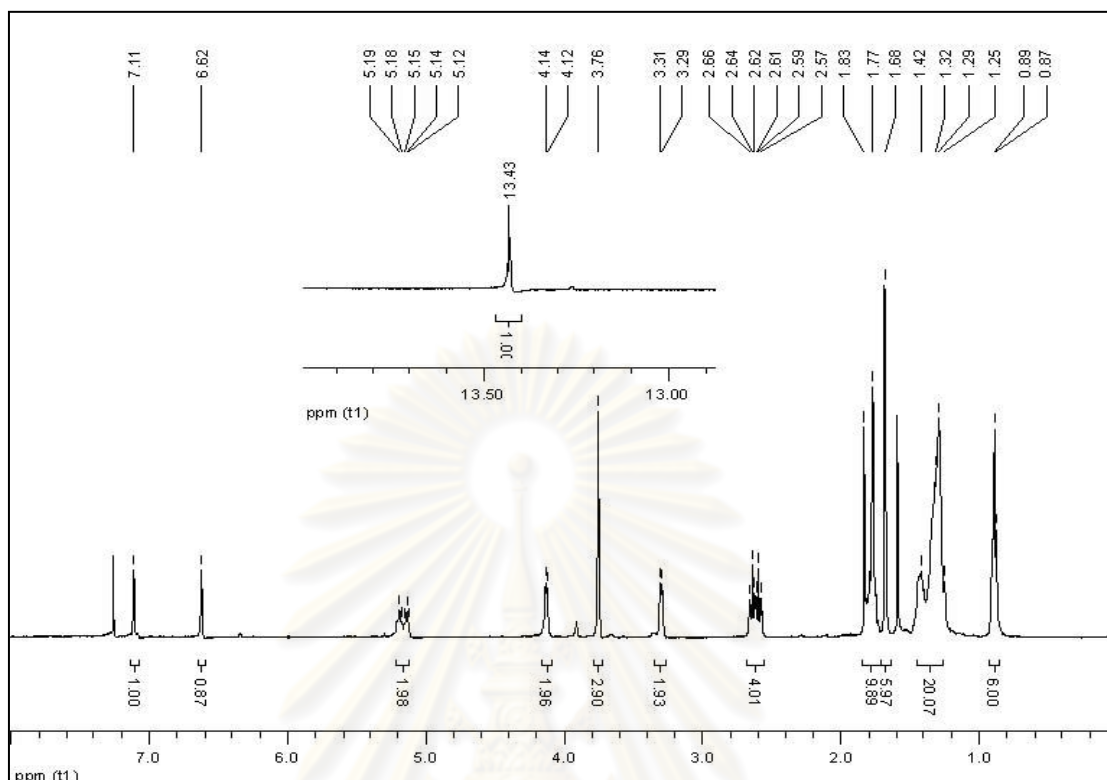
Figure 2.44 The ^{1}H NMR spectrum (CDCl$_3$, 400 MHz) of compound **D10**
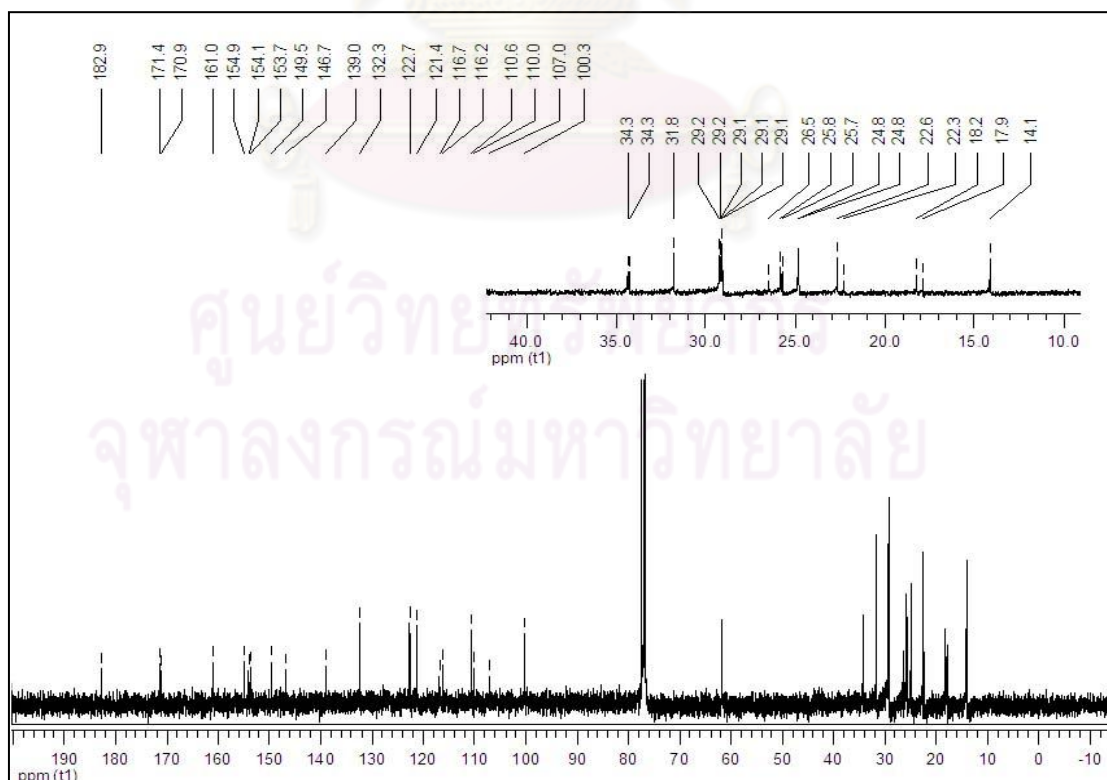
Figure 2.45 The ^{13}C NMR spectrum (CDCl$_3$, 100 MHz) of compound **D10**
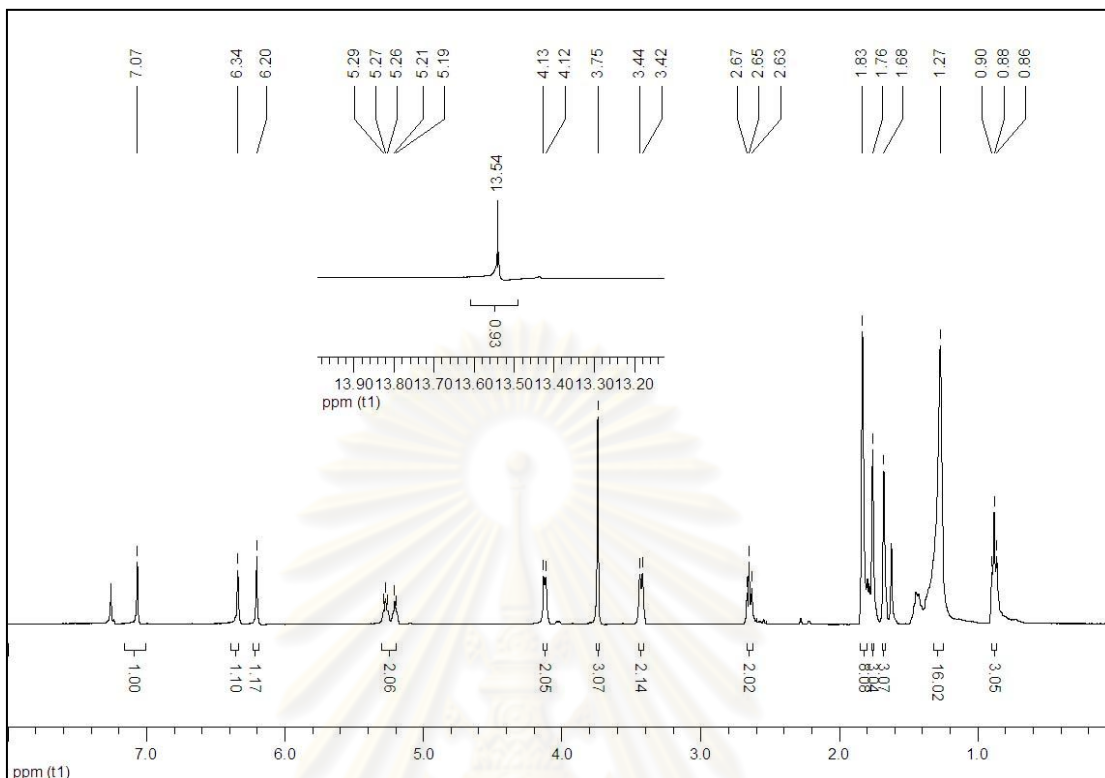
Figure 2.46 The ^{1}H NMR spectrum (CDCl$_3$, 400 MHz) of compound **M11**
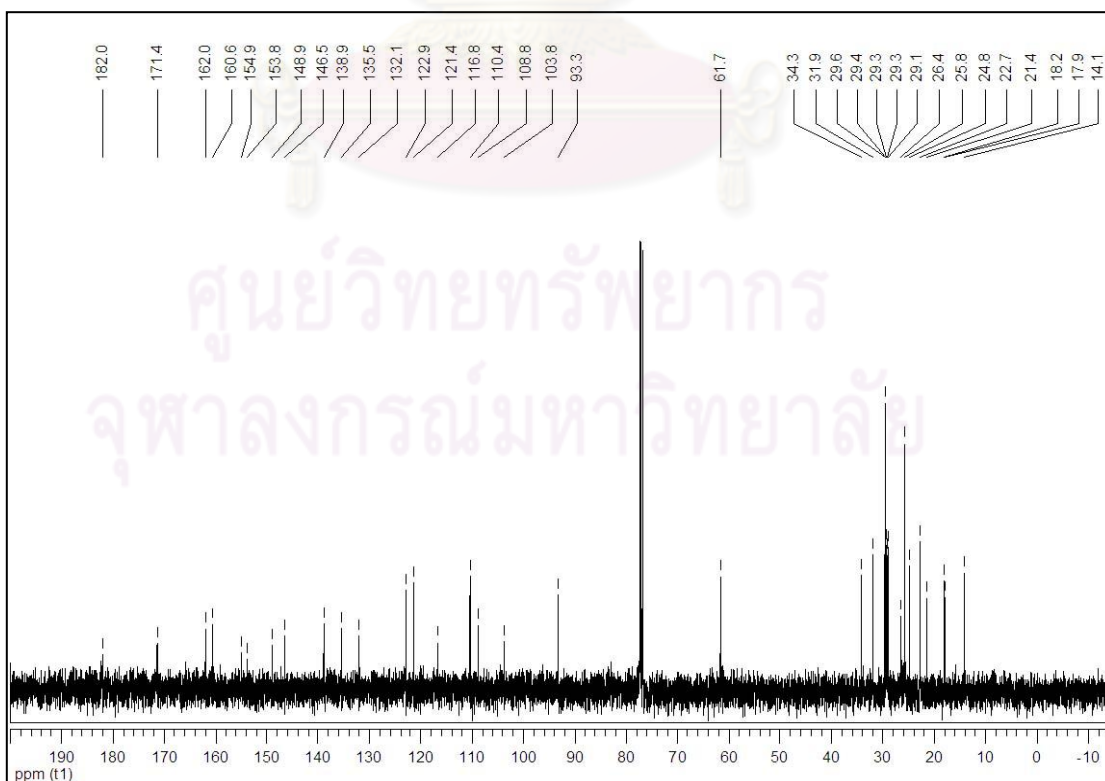
Figure 2.47 The ^{13}C NMR spectrum (CDCl$_3$, 100 MHz) of compound **M11**
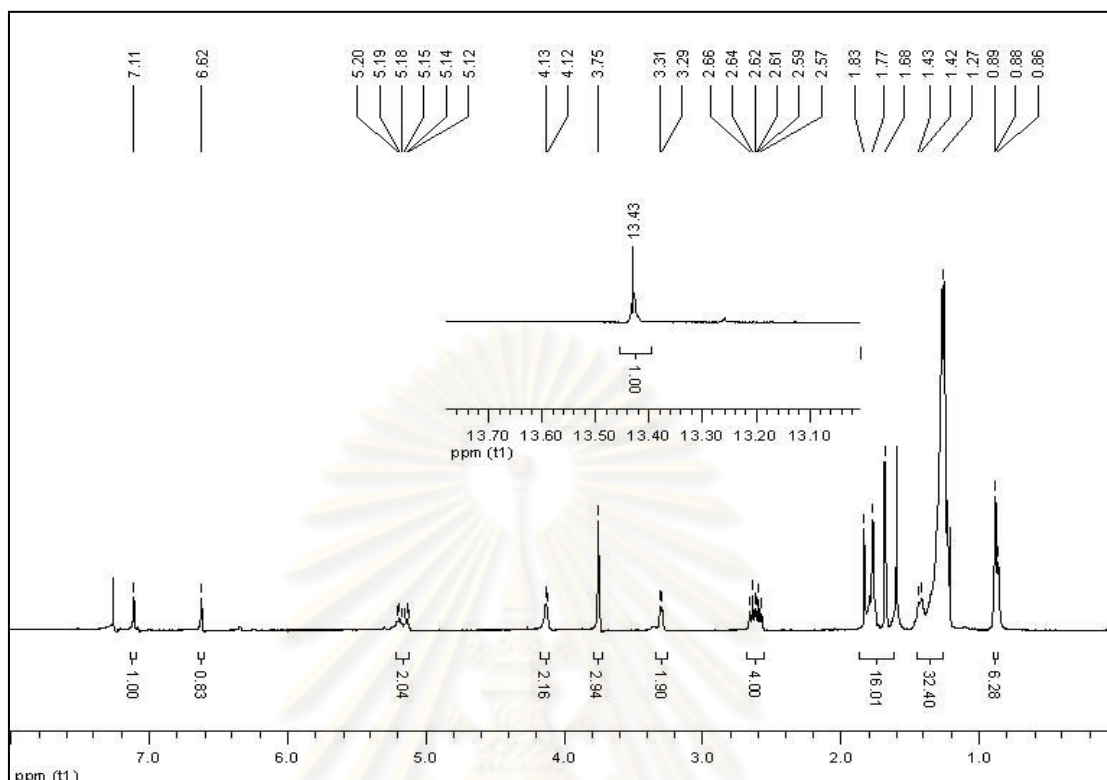
Figure 2.48 The ^{1}H NMR spectrum (CDCl$_3$, 400 MHz) of compound **D11**
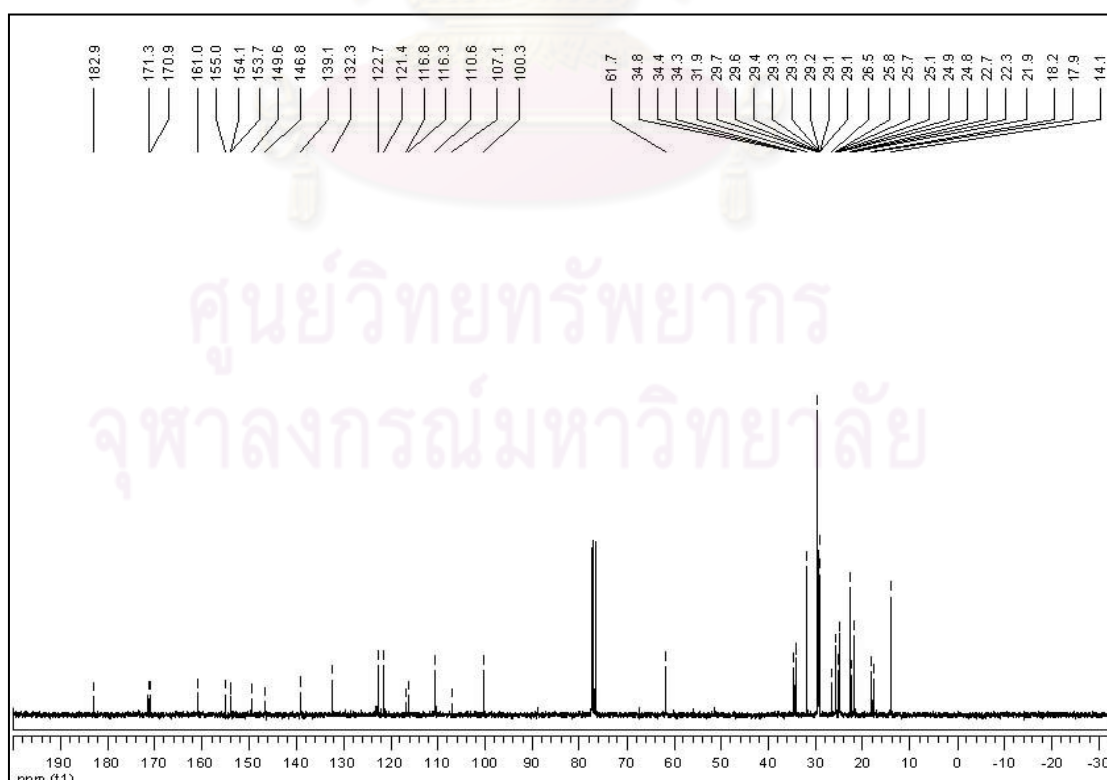
Figure 2.49 The ^{13}C NMR spectrum (CDCl$_3$, 100 MHz) of compound **D11**

2.3.2.2 Acid-Catalyzed Cyclization of α-Mangostin (1)

To investigate whether the prenyl units substituted on C2 and C8 of α-mangostin (1) were necessary for the bioactivity, an acid-catalyzed cyclization of α-mangostin (1) was carried out to give a pale yellow solid of 3-isomangostin (7) as a major product in 66% yield together with a yellow solid of BR-xanthone A (30) in 4% yield (Scheme 2.1).
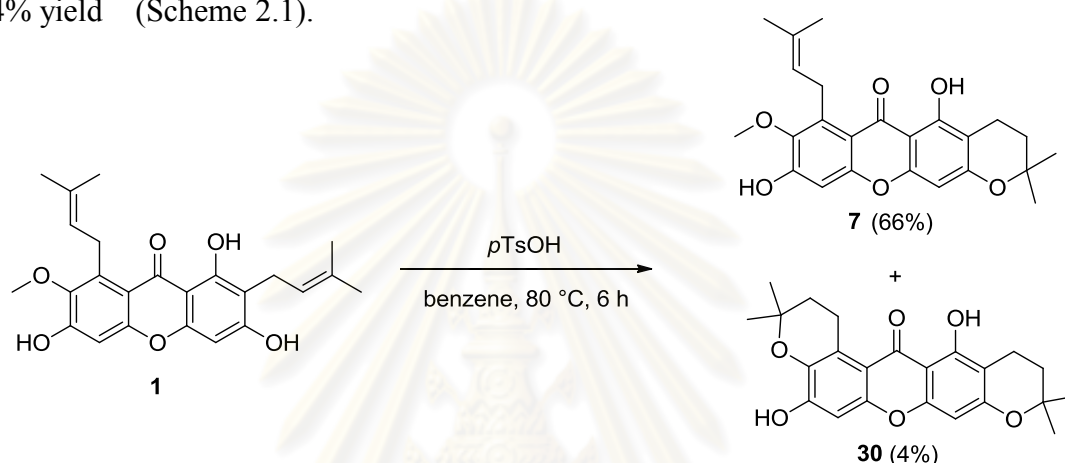
Scheme 2.1 Acid-catalyzed cyclization of α-mangostin (1)

3-Isomangostin (7) was subjected to the electron impact mass spectrum (EI-MS) analysis. The molecular ion peak was observed at m/z 412.174 (M+H)$^{+}$, defined as $C_{24}H_{26}O_6$. The structure of this compound was also confirmed by ^{1}H and ^{13}C NMR techniques as well as BR-xanthone A (30).

The ^{1}H NMR spectrum of 3-isomangostin (7) (Figure 2.50) showed the characteristic chemical shift of chelated hydroxyl proton (OH-1) at 13.71. Compared this spectrum with the ^{1}H NMR spectrum of α-mangostin (1), it was found that a singlet signal of H4 aromatic proton was shifted from 6.29 to 6.23, and the triplet signal at δ_H 5.30 inferred to H12 olefinic proton of α-mangostin (1) was disappeared. The chemical shift of H5 aromatic proton for this compound was the same value as that of α-mangostin (1) (δ 6.82). A broad singlet at δ_H 6.28, a triplet at δ_H 5.28 ($J = 6.2$ Hz) and a doublet at δ_H 4.10 ($J = 6.2$ Hz) were referred to OH-6, H17 olefinic proton and H16 methylene proton, respectively. In addition, two new signals at δ_H 2.72 (t, $J = 6.8$ Hz) and 1.87-1.83 (m) were assigned to methylene protons H11 and H12, respectively. These findings indicated that the reaction proceeded through the

cyclization of a hydroxyl group on C3 into C13 of prenyl unit. The remaining signals could be observed at δ_H 1.83-1.38, indicating four methyl groups. The ^{13}C NMR spectrum (Figure 2.51) exhibited the characteristic peak of xanthone carbonyl carbon at δ_C 181.9. The peaks at δ_C 160.6-142.4 were assigned to six oxygenated aromatic carbons. Two peaks of C13 and C12 were shifted from δ_C 135.5 to 76.0 and from δ_C 121.5 to 31.8, respectively compared to the ^{13}C NMR spectrum of α-mangostin (**1**). In addition, the signals of other eight sp2, methoxy, another methylene, and four methyl carbons were observed at δ_C 136.9-94.0, 61.9, 26.5 and 26.7-16.1, respectively.

Comparison of the ^{1}H NMR spectrum of BR-xanthone A (**30**) (Figure 2.52) with that of α-mangostin (**1**) indicated the same signal of a chelated hydroxyl proton (OH-1) was presented at δ_H 13.72, and aromatic protons H5 and H4 were shifted at δ_H 6.78 and 6.38, respectively. Four new triplet signals at δ_H 3.50 (t, J = 6.8 Hz), 2.71 (t, J = 6.7 Hz) 1.88 (t, J = 6.7 Hz) and 1.83 (t, J = 6.7 Hz) were belonged to methylene protons H16, H11, H12 and H17, respectively. Two singlet signals at δ_H 1.38 and 1.37 were observed with each six protons integration, belonging to four methyl groups. The ^{13}C NMR spectrum (Figure 2.53) exhibited a characteristic xanthone carbonyl carbon signal at δ_C 182.6. Six peaks at δ_C 160.5-137.7 were assigned to six oxygenated aromatic carbons. The peaks at δ_C 121.3-94.0 were belonged to six aromatic carbons. Two peaks at δ_C 75.9 and 75.5 could be designated for oxygenated aliphatic carbon. Other peaks at δ_C 32.9-16.1 were ascribed for two methylene and four methyl carbons.

Figure 2.50 The ^{1}H NMR spectrum (CDCl$_3$, 400 MHz) of compound **7**

Figure 2.51 The ^{13}C NMR spectrum (CDCl$_3$, 100 MHz) of compound **7**

Figure 2.52 The ^{1}H NMR spectrum (CDCl$_3$, 400 MHz) of compound **30**

Figure 2.53 The ^{13}C NMR spectrum (CDCl$_3$, 100 MHz) of compound **30**

2.3.2.3 Synthesis of 3-Isomangostin Analogues I1-I5

To confirm the importance of prenyl unit and hydroxyl group of α-mangostin (**1**), 3-isomangostin (**7**) was converted into its ester analogues from six aliphatic carboxylic acids using the developed method described in 2.2.4 and the results are presented in Table 2.4.

Table 2.4 Synthesis of 3-isomangostin analogues

Entry	Compound	R	%Isolated yield
1	I1		98
2	I2		94
3	I3		92
4	I4		82
5	I5		quant

As shown in Table 2.4, 6-*O*-acteyl 3-isomangostin (**I1**) could be synthesized in near quantitative yield (98%, entry 1). In the case of propinoic acid, butanoic acid, hexanoic acid and lauric acid, increasing the carbon chain length of carboxylic acids did not affect the yield of the desired esters; the reaction still provided the products **I2-I6** in excellent yield (entries 2-6). These results indicated that this developed method using PPh$_3$/Cl$_3$CCONH$_2$ was efficient to convert long chain carboxylic acids to their acid chlorides as a reactive intermediate.

The structures of 3-isomangostin analogues **I1-I5** were fully confirmed by ^{1}H and ^{13}C NMR. The ^{1}H NMR spectrum of 6-*O*-acetyl 3-isomangostin (**I1**) (Figure 2.54) showed the same pattern of signals when comparing with that of 3-isomangostin (**7**), except the chemical shift of H5 being shifted from 6.82 to 7.09. That indicated

that the hydroxyl group at C6 was truly substituted by acetyl group. In addition, a new singlet signal of a methyl of acetyl group was observed at δ_H 2.38. The ^{13}C NMR spectrum (Figure 2.55) was similar to that of **7**, but two additional peaks of ester carbonyl and ester-attached methyl carbons at δ_C 168.2 and 20.9, respectively were observed in addition.

For the other 3-isomangostin analogues, the ^1H and ^{13}C NMR spectra of which were similar to those of 6-*O*-acetyl 3-isomangostin (**I1**) in case of the signals for 3-isomangostin core. From these observations, only a part of substituents on C6 would be discussed below.

The ^1H NMR spectrum of 6-*O*-propinoyl 3-isomangostin (**I2**) (Figure 2.56) showed a multiplet signal at δ_H 2.73-2.67 and triplet signal at δ_H 1.32 (J = 7.4 Hz), appropriated for propinoate group. The ^{13}C NMR spectrum (Figure 2.57) revealed a signal of ester carbonyl carbon at δ_C 171.7. In addition, two peaks at δ_C 27.6 and 9.0 indicated the presence of methylene and methyl carbons, respectively of propionate group were detected.

The ^1H NMR spectrum of 6-*O*-butanoyl 3-isomangostin (**I3**) (Figure 2.58) presented a quartet at δ_H 2.63 (J = 7.3 Hz), a multiplet at δ_H 1.87-1.83 and a triplet at δ_H 1.08 (J = 7.4 Hz) assigned to two methylene protons connected to a carbonyl group, the remaining of methylene proton and three methyl protons, respectively of butyrate group. The ^{13}C NMR spectrum (Figure 2.59) contained four signals for an ester carbon at δ_C170.9. The signals at δ_C 36.1, 18.4 and 13.6 could be designated for methylene and methyl carbons of butyrate unit.

The ^1H NMR spectrum of 6-*O*-hexanoyl 3-isomangostin (**I4**) (Figure 2.60) exhibited the signals of hexanoate group as follows: a triplet at δ_H 2.64 (J = 7.4 Hz) appropriated for two methylene protons connected to a carbonyl group; two multiplets at δ_H 1.83-1.82 and 1.40-1.36 ascribed to six methylene protons; and a triplet at δ_H 0.95 (J = 6.9 Hz) indicated three methyl protons. The ^{13}C NMR spectrum (Figure 2.61) contained an ester carbonyl signal at δ_C 171.0. Two peaks at δ_C 34.2 and three peaks at δ_C 31.2, 24.5 and 22.3 were belonged to an ester-attached methylene carbon

and other three methylene carbons, respectively of hexanoate group. The peak at δ_C 13.9 was belonged to a methyl carbon.

The ^{1}H NMR spectrum of 6-O-lauryl 3-isomangostin (**I5**) (Figure 2.62) showed a triplet at δ_H 2.64 (J = 7.5 Hz), two multiplets at δ_H 1.87-1.77 and 1.37-1.27, and a triplet at δ_H 0.89 (J = 6.0 Hz) assigned to two methylene protons connected to a carbonyl group, eighteen methylene protons and three methyl protons, respectively of laurate group. The ^{13}C NMR spectrum (Figure 2.63) displayed a peak at δ_C 171.0 and 34.2 indicating an ester carbonyl carbon and a methylene carbon next to ester bond, respectively. The signals at δ_C 31.9, 26.9-29.1, 24.8 and 22.7 were belonged to eight methylene carbons of laurate group. The peak at δ_C 14.1 appropriated for a methyl carbon was also detected.
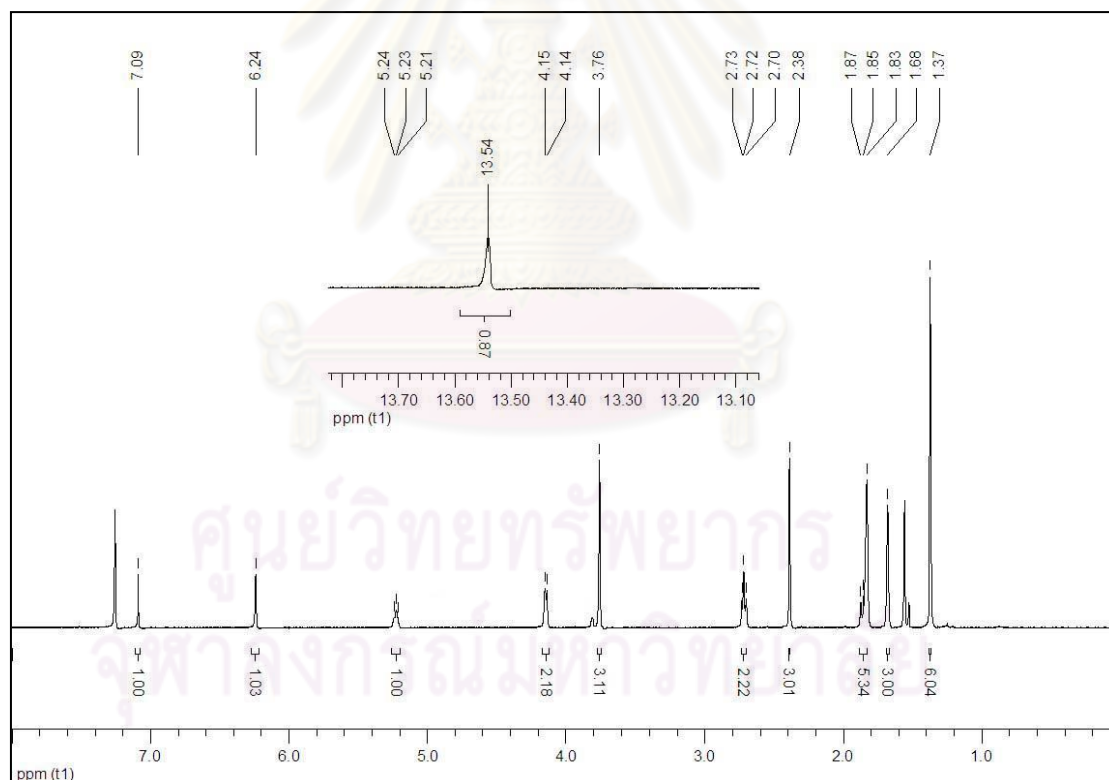
Figure 2.54 The ^{1}H NMR spectrum (CDCl$_3$, 400 MHz) of compound **I1**
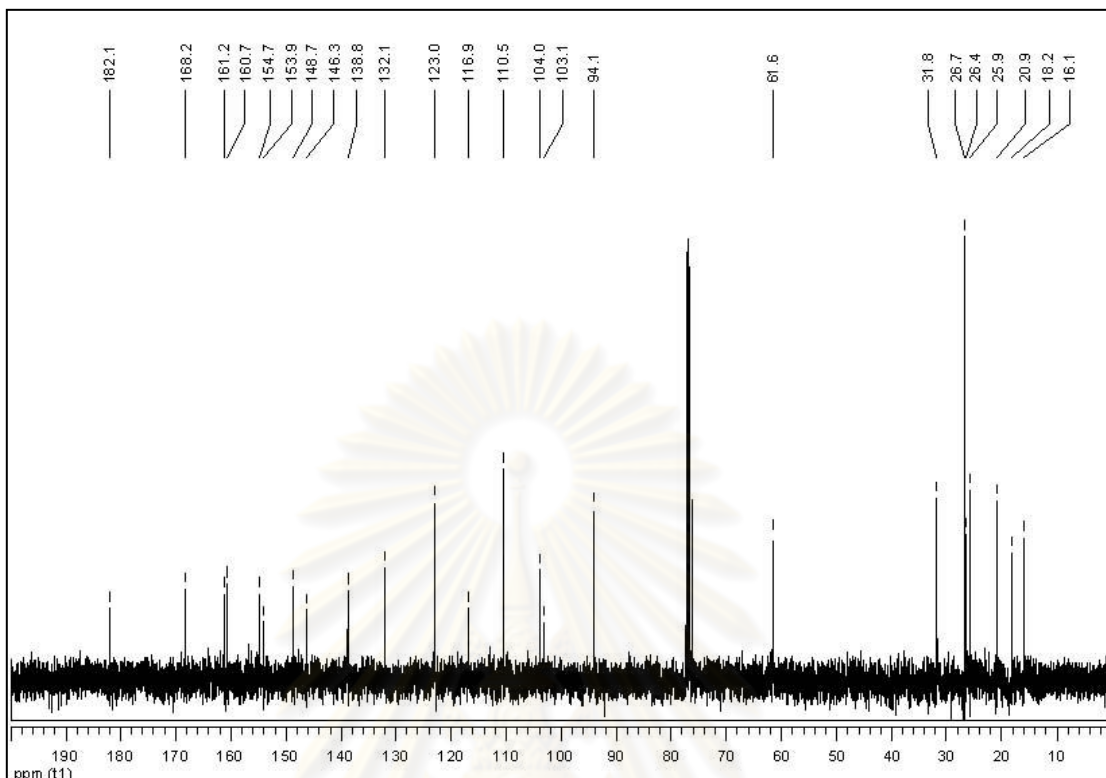
Figure 2.55 The ^{13}C NMR spectrum (CDCl$_3$, 100 MHz) of compound **I1**
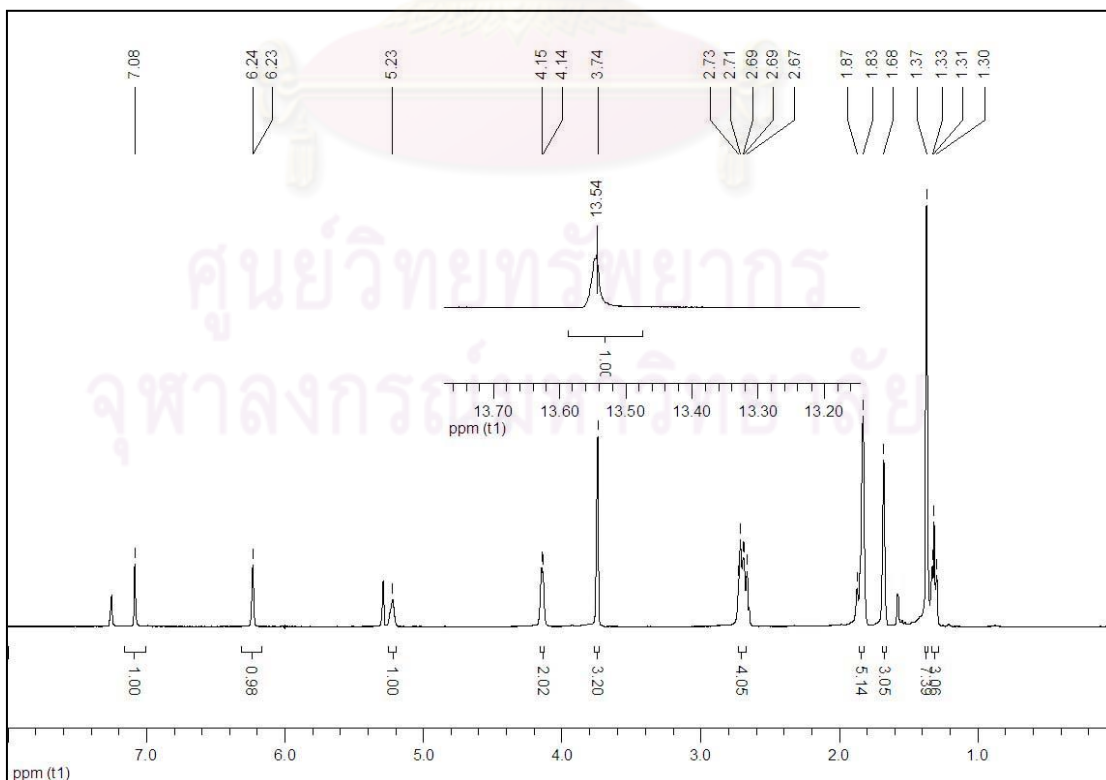
Figure 2.56 The ^{1}H NMR spectrum (CDCl$_3$, 400 MHz) of compound **I2**
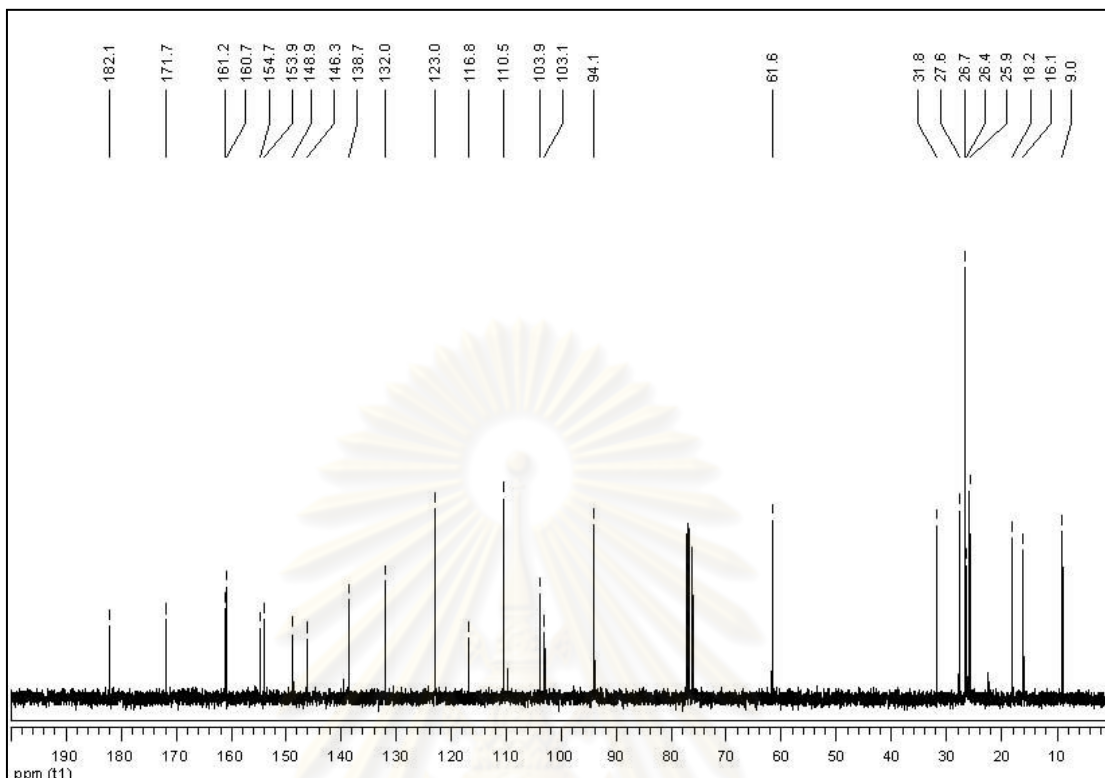
Figure 2.57 The ^{13}C NMR spectrum (CDCl$_3$, 100 MHz) of compound **I2**
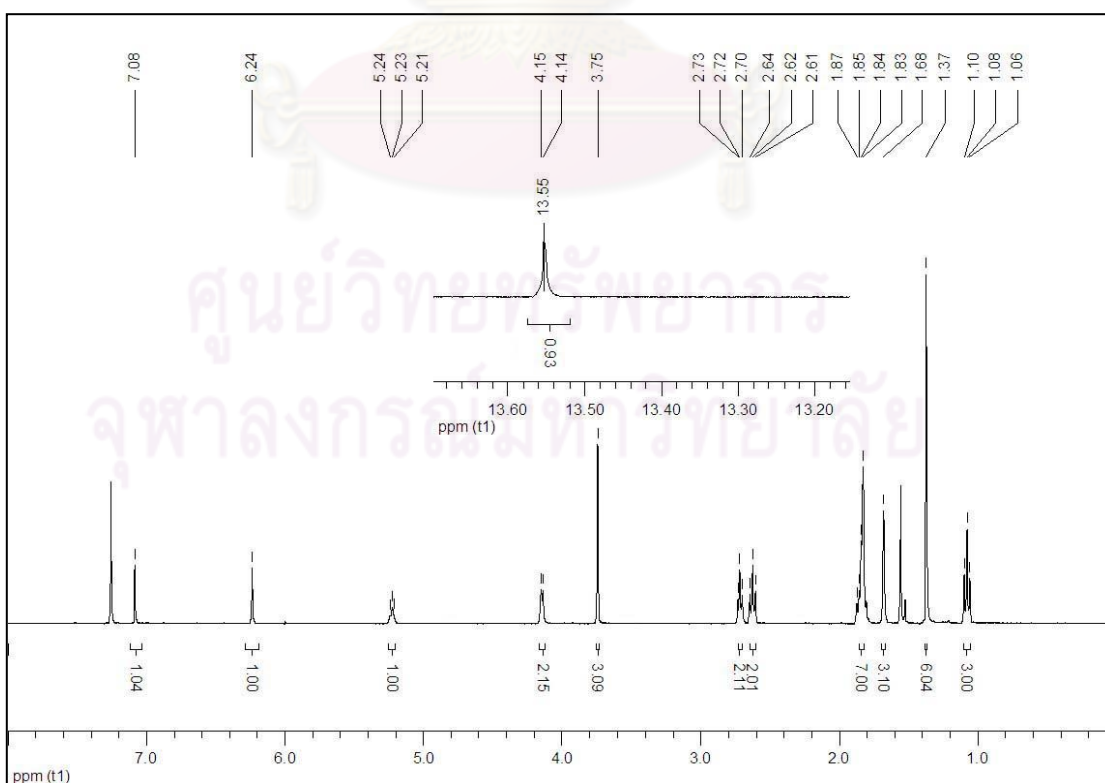
Figure 2.58 The ^{1}H NMR spectrum (CDCl$_3$, 400 MHz) of compound **I3**
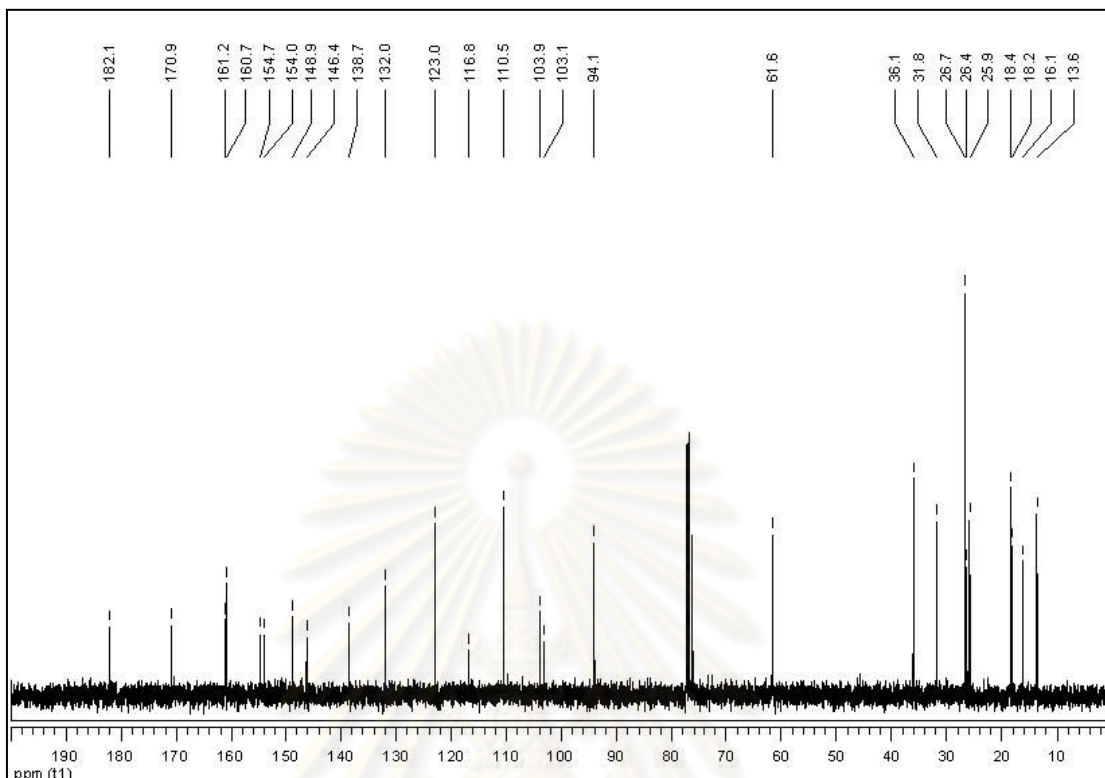
Figure 2.59 The ^{13}C NMR spectrum (CDCl$_3$, 100 MHz) of compound **I3**
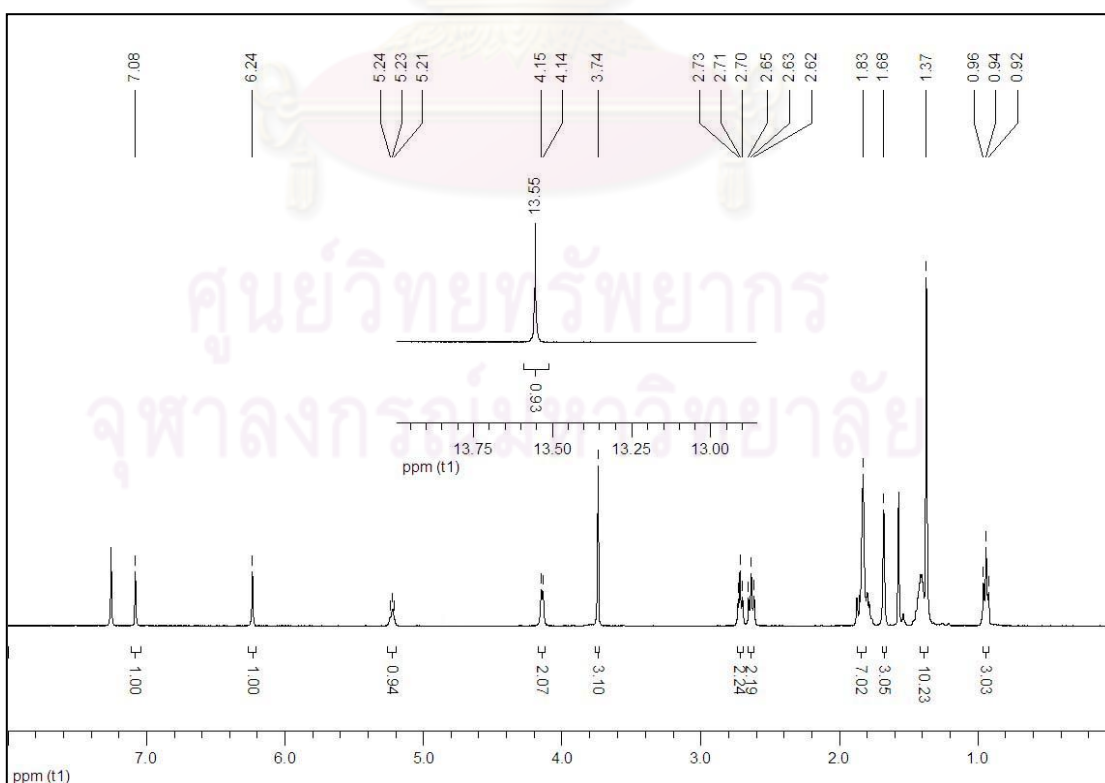
Figure 2.60 The ^{1}H NMR spectrum (CDCl$_3$, 400 MHz) of compound **I4**
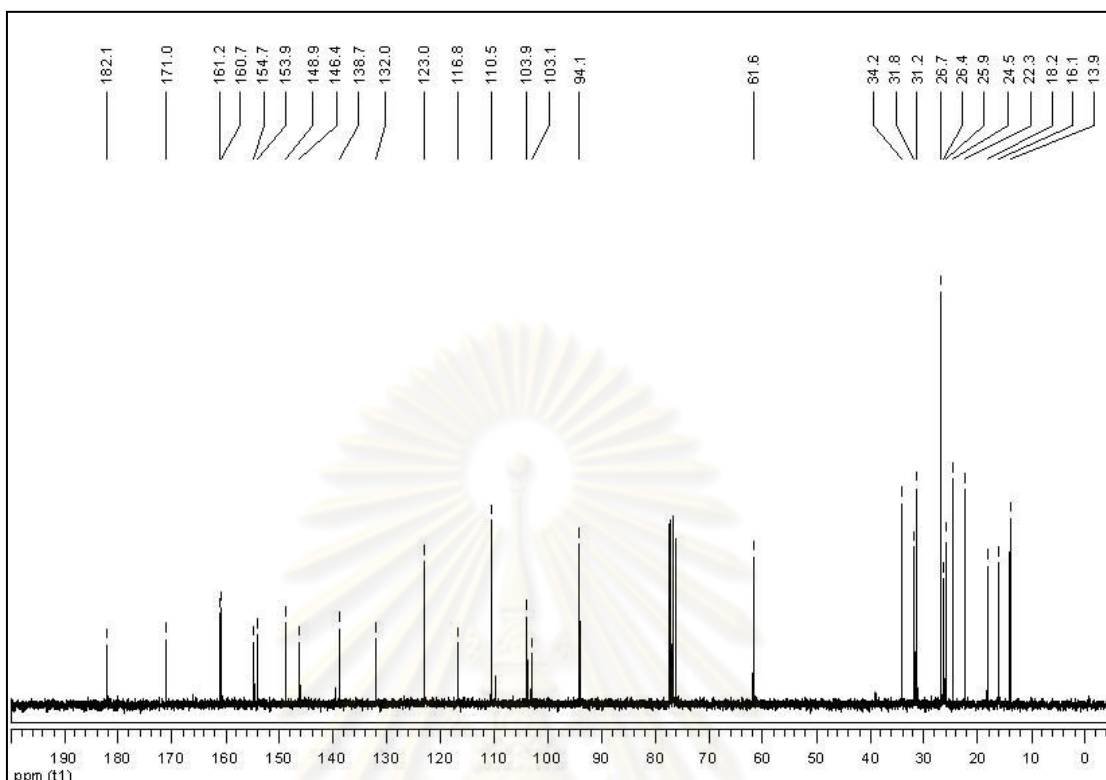
Figure 2.61 The ^{13}C NMR spectrum (CDCl$_3$, 100 MHz) of compound **I4**
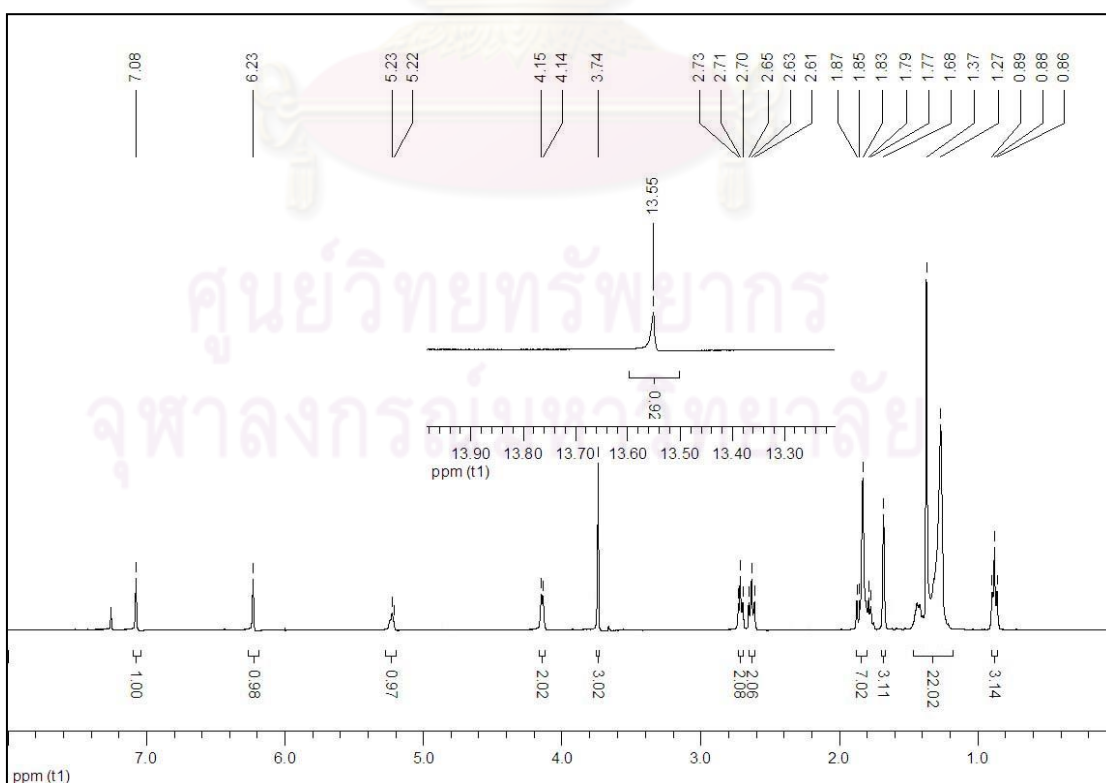
Figure 2.62 The ^{1}H NMR spectrum (CDCl$_3$, 400 MHz) of compound **I5**
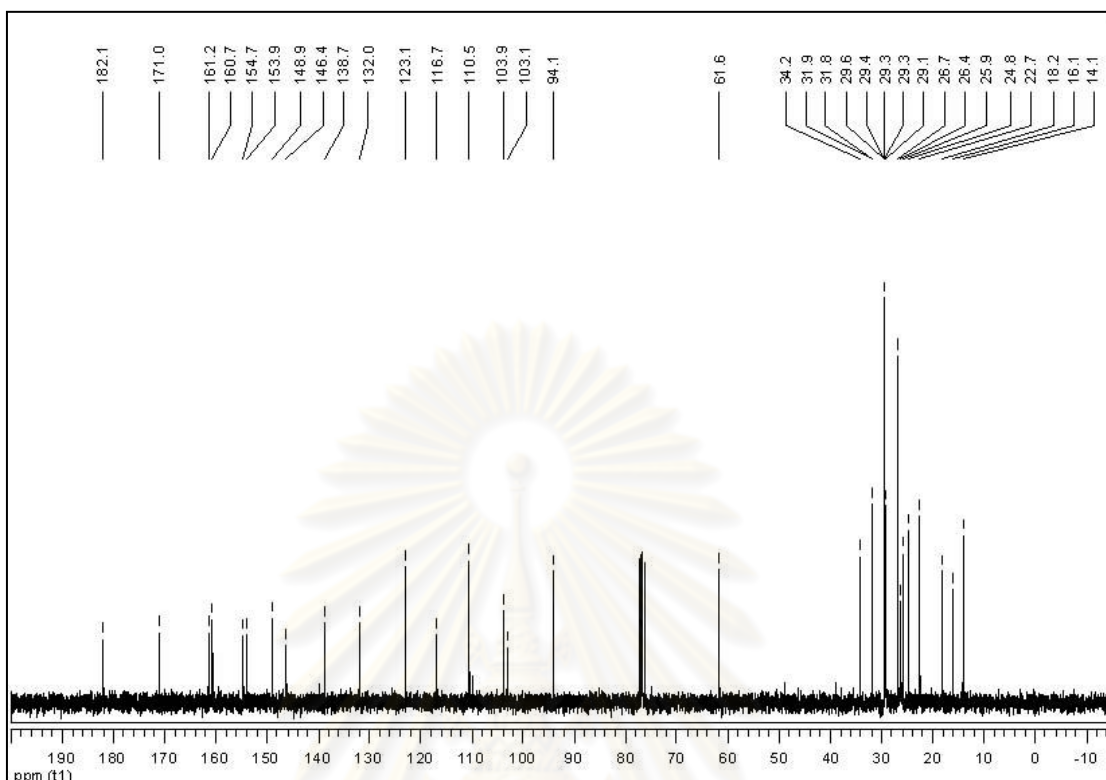
Figure 2.63 The ^{13}C NMR spectrum (CDCl3, 100 MHz) of compound **I5**

2.3.2.4 Synthesis of Ether Analogues of *α*-Mangostin (1)

The synthesis of ether analogues was performed using the method displayed in 2.2.6 and 2.2.7 and the results are presented in Table 2.5.

Table 2.5 Synthesis of ether analogues

Entry	Alkylating agent	6-Mono-*O*-alkylated product		3,6-Di-*O*-alkylated product	
		Compound	%Isolated yield	Compound	%Isolated yield
1		**M12**	33	**D12**	29
2		**M13**	14	-	ND
3		-	ND	-	ND
4[a]		**M14**[b]	3	-	ND
		M15[c]	11		

[a] DMF, 65-70 °C and 3 h were used.
[b] 3-mono-*O*-(2,3-dihydroxypropyl) mangostin
[c] 6-mono-*O*-(2,3-dihydroxypropyl) mangostin
ND: Not detected

The *O*-alkylation of *α*-mangostin (**1**) and allyl iodide in acetone in the presence of K_2CO_3 yielded 6-mono-*O*-allyl mangostin (**M12**) in 33% yield together with 3,6-di-*O*-allyl mangostin (**D12**) in 29% yield (entry 1). To prepare the analogues with highly soluble in water, triethylene glycol monomethyl bromide was used. The corresponding 6-mono-*O*-alkyl mangostin (**M13**) having a higher polarity than *α*-mangostin (**1**) was obtained in 14% yield (entry 2). In the case of epichlorohydrin, the reaction did not proceed to give the desired product when using acetone as a solvent (entry 3). Under this condition, it was found that the reaction mixture was not

homogenous; therefore, DMF was employed. Unfortunately, no desired product was formed, but 3- and 6-mono-O-(2,3-dihydroxypropyl) mangostins (**M14** and **M15**) were isolated in 3 and 11% yields, respectively instead (entry 3).

All structures of synthesized compounds were characterized by ^{1}H and ^{13}C NMR spectroscopic methods.

The ^{1}H NMR spectrum of 6-mono-O-allyl mangostin (**M12**) (Figure 2.64) revealed signals for a chelated hydroxyl proton at δ_H 13.80 (OH-1), an aromatic proton at δ_H 6.23 (H-3), two olefinic protons at δ_H 5.36-5.23 (H-17 and H-21), two methylene protons at δ_H 4.12 (d, J = 5.1 Hz, H-16) and 3.42 (d, J = 7.0 Hz, H-11), three protons of methoxy group at δ_H 3.81, and twelve methyl protons at δ_H 1.85-1.68 (H-20, H-19, H-15 and H-14). Comparison of this spectrum with that of α-mangostin (**1**) found that the singlet signal of H5 shifted to upfield showing at δ_H 6.67, indicating that OH group at C6 was transformed into ether group. A multiplet signal at δ_H 6.12-6.04 and three doublet signals at δ_H 5.48 (d, J = 17.2 Hz), 5.36 (d, J = 10.6 Hz) and 4.64 (d, J = 5.1 Hz) were observed from the presence of five protons of a prenyl unit next to ether bond. The ^{13}C NMR spectrum (Figure 2.65) presented a characteristic peak of xanthone carbonyl carbon at δ_C 182.0. The peaks at δ_C 161.4-144.0 were referred to six oxygenated aromatic carbons. The chemical shifts of eight sp2 carbons of mangostin core and two sp2 carbons of prenyl unit connected to ether bond were observed at 137.3-103.6. Compared to the ^{13}C NMR spectrum of α-mangostin (**1**), the signal of C5 was shifted from δ_C 101.6 to 99.2, indicating that the substituent at C6 was changed from hydroxyl to ether group. The peak of C4 did not significantly shift (δ 93.0) compared to that of α-mangostin (**1**). The signals of an oxygen-attached methylene carbon at δ_C 69.4, a methoxy carbon at δ_C 60.8, other methylene carbons at δ_C 26.2 and 21.4, and four methyl carbons at δ_C 25.9, 25.8, 18.2 and 17.9 were detected.

The ^{1}H NMR spectrum of 3,6-di-O-allyl mangostin (**D12**) (Figure 2.66) showed signals for a chelated hydroxyl proton at δ_H 13.48 (OH-1), two aromatic proton at δ_H 6.70 (H-5) and 6.27 (H-3), two olefinic protons at δ_H 5.26-5.25 (H-17 and H-21), two methylene protons at δ_H 4.13 (d, J = 6.3 Hz, H-16) and 3.38 (d, J = 7.1 Hz,

H-11), three methoxy protons at δ_H 3.82, and twelve methyl protons at δ_H 1.85-1.68 (H-20, H-19, H-15, H-14). A multiplet signal at δ_H 6.12-6.02 and five doublet signals at δ_H 5.45 (d, J = 17.4 Hz), 5.49(d, J = 17.4 Hz), 5.38 (d, J = 10.6 Hz), 5.31 (d, J = 10.6 Hz), 4.66 (d, J = 5.2 Hz) and 4.61 (d, J = 5.0 Hz) could be assigned for ten protons for a prenyl unit adjacent to ether bond. The ^{13}C NMR spectrum (Figure 2.67) presented a characteristic peak of xanthone carbonyl carbon at δ_C 182.0. The six peaks at δ_C 162.2-144.2 indicated the presence of six oxygenated aromatic carbons. The chemical shifts at 137.8-104.0 were ascribed for eight sp2 carbons of mangostin core together with four sp2 carbons of oxygenated prenyl unit. Compared to the ^{13}C NMR spectrum of α-mangostin (**1**), the C4 and C5 signals were shifted from δ_C 93.3 to 89.6 and from δ_C 101.6 to 99.2, respectively, indicating that the substituents at C3 and C6 were changed from a hydroxyl to an ether group. The signals of two oxygenated methylene carbons at δ_C 69.4 and 69.0, a methoxy carbon at δ_C 60.8, other methylene carbons at δ_C 26.2 and 21.4, and four methyl carbons at δ_C 25.9, 25.8, 18.2 and 17.9 were detected.

The ^{1}H NMR spectrum of 6-mono-O-triethylene glycol mono methyl mangostin (**M13**) (Figure 2.68) showed a singlet signal of chelated phenolic hydroxy group (OH-1) at δ_H 13.66. The two singlet signals at δ_H 6.54 (ArH-5) and 6.19 (ArH-4) were assigned for two aromatic protons. Two triplet signals of each two olefinic protons on C-12 and C-17 was observed at δ_H 5.28 (J = 6.5 Hz) and 5.17 (J = 6.3 Hz). The signals at δ_H 4.14-3.35 were ascribed to twelve oxygenated methylene protons, four methylene protons on a carbon connected to aromatic ring, and six methoxy protons. Four singlet signals of four methyl groups at δ_H 1.80-1.64 (H-20, H-19, H-15, H-14) were observed. The ^{13}C NMR spectrum (Figure 2.69) presented a characteristic peak of xanthone carbonyl carbon at δ_C 181.8. The six peaks at δ_C 161.5-143.7 indicated the presence of six oxygenated aromatic carbons. The eight peaks at δ_C 137.1-103.4 were assigned for eight sp2 carbons. Compared to the ^{13}C NMR spectrum of α-mangostin (**1**), the signal of C5 was shifted from δ_C 101.6 to 98.8, indicating that the substituent at C6 was changed from a hydroxyl to an ether group. The peak of C4 appeared at the same position (δ 92.9) compared to that of α-mangostin (**1**). The six peaks at δ_C 71.8-67.9 and two peaks at δ_C 60.8 and 58.9 could be designated for six

oxygenated methylene and two methoxy carbons, respectively. Other two methylene carbons at δ_C 26.1 and 21.4 and four methyl carbons at δ_C 25.9, 25.8, 18.1 and 17.9 were detected.

The ^{1}H NMR spectrum of 3-mono-O-(2,3-dihydroxypropyl) mangostin (**M14**) (Figure 2.70) displayed a singlet of chelated phenolic hydroxyl proton at δ_H 13.49. The chemical shifts of aromatic protons H5 and H4 appeared at 6.82 and 6.28, respectively. Two multiplet signals of each olefinic proton at δ_H 5.26-5.23 and 5.16-5.12 were observed. The signals at δ_H 5.11-5.08 (m, 1H), 4.66 (t, J = 8.5 Hz, 1H), 4.57 (dd, J = 8.6, 6.0 Hz), 4.35 (dd, J = 10.6, 4.0 Hz), and 4.22 (dd, J = 10.6, 4.0 Hz, 1H) could be ascribed for five protons for 2,3-dihydroxypropyl group. Two doublet signals at δ_H 4.08 (d, J = 6.0 Hz) and 3.33 (d, J = 6.7 Hz) belonged to four methylene protons of a prenyl group. Four singlet signals were detected at δ_H 3.81 and 1.83-1.68 assigned to three methoxy protons and twelve methyl protons, respectively. The ^{13}C NMR spectrum (Figure 2.71) presented a characteristic peak of xanthone carbonyl carbon at δ_C 181.9. The six peaks at δ_C 161.0 -142.8 indicated the presence of six oxygenated aromatic carbons. The chemical shifts at 137.1-101.6 could be designated for nine sp2 carbons of mangostin core. Compared to the ^{13}C NMR spectrum of α-mangostin (**1**) indicated the upfield shift of C4 signal at δ_C 89.3, confirmed that the hydroxyl group at C3 of α-mangostin (**1**) was converted to an ether group. The peaks at δ_C 73.8, 67.0 and 66.0 could be designated for three oxygenated sp3 carbons of 2,3-dihydroxylpropyl group. The peaks of a methoxy carbon at δ_C 61.9, two methylene carbons of a prenyl unit at δ_C 26.5 and 21.3, and four methyl carbons at δ_C 25.8-17.8 were also detected.

The ^{1}H NMR spectrum of 6-mono-O-(2,3-dihydroxypropyl) mangostin (**M15**) (Figure 2.72) displayed a singlet of chelated hydroxyl proton at δ_H 13.62. The chemical shift of aromatic protons H5 was shifted from 6.82 to 6.54 compared to the ^{1}H NMR spectrum of α-mangostin (**1**), indicating that a hydroxyl group at C6 of α-mangostin (**1**) was substituted to give ether functionality. A singlet of aromatic proton H4 at δ_H 6.18 and two multiplet signals of two olefinic protons at δ_H 5.27-5.24 and 5.20-5.18 were observed. The signals at δ_H 5.15-5.12 (m, 1H), 4.71-4.62 (m, 2H), 4.31 (dd, J = 10.7, 2.8 Hz, 1H) and 4.14 (dd, J = 10.1, 3.0 Hz) could be designated for

2,3-dihydroxypropyl group. Two doublet signals at 4.05 (d, J = 7.2 Hz) and 3.39 (d, J = 6.9 Hz) belonged to four methylene protons of a prenyl group. Four singlet signals were detected at δ_H 3.74 and 1.82-1.68 assigned to three methoxy and twelve methyl protons, respectively. The ^{13}C NMR spectrum (Figure 2.73) presented a characteristic peak of xanthone carbonyl carbon at δ_C 181.8. The six peaks at δ_C 161.7-143.8 were referred to six oxygenated aromatic carbons. The chemical shifts at 137.9-103.5 could be designated for eight sp2 carbons of mangostin core. Compared to the ^{13}C NMR spectrum of α-mangostin (**1**) indicated the upfield shift of C5 signal showing at δ_C 99.2 while the C4 signal still showed at the same position (δ 93.1). These confirmed that the hydroxyl group at C6 of α-mangostin (**1**) was changed to an ether group. The three peaks at δ_C 73.8, 67.6 and 65.9 could be designed for three carbons of 2,3-dihydroxylpropyl group. The peak of a methoxy carbon at δ_C 61.1, two methylene carbons of a prenyl unit at δ_C 26.2 and 21.4, and four methyl carbons at δ_C 25.9 (2C), 18.2 and 17.9 were also detected.
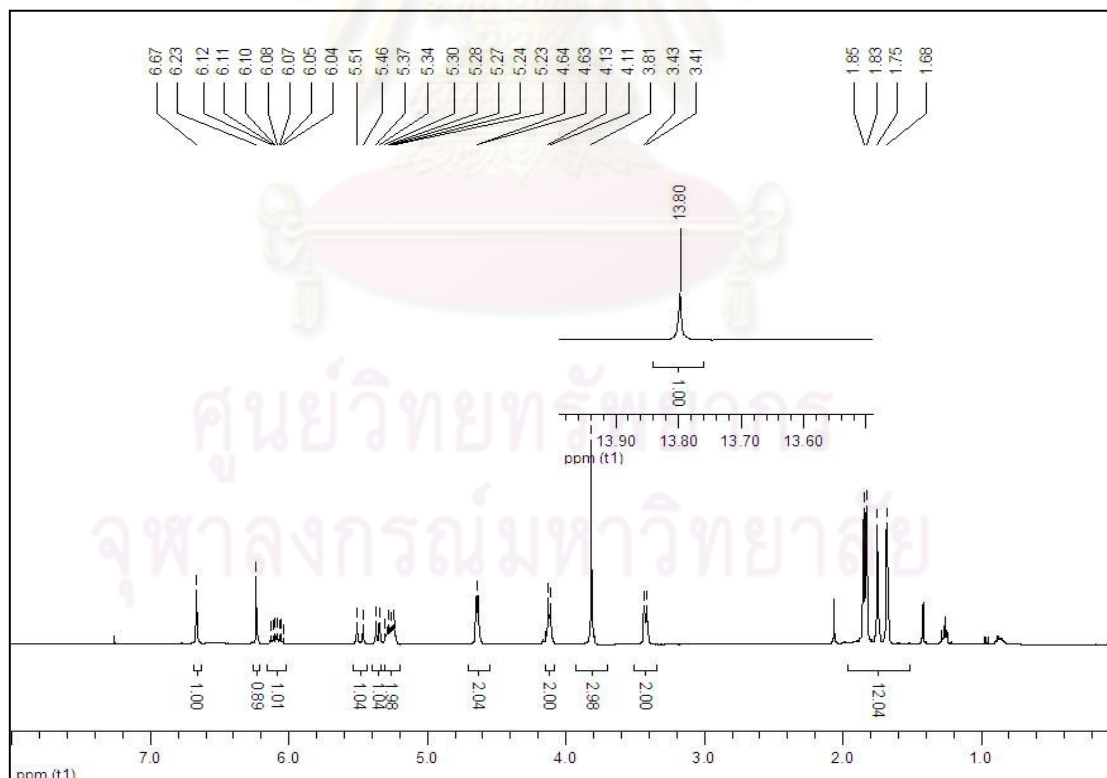
Figure 2.64 The ^{1}H NMR spectrum (CDCl$_3$, 400 MHz) of compound **M12**
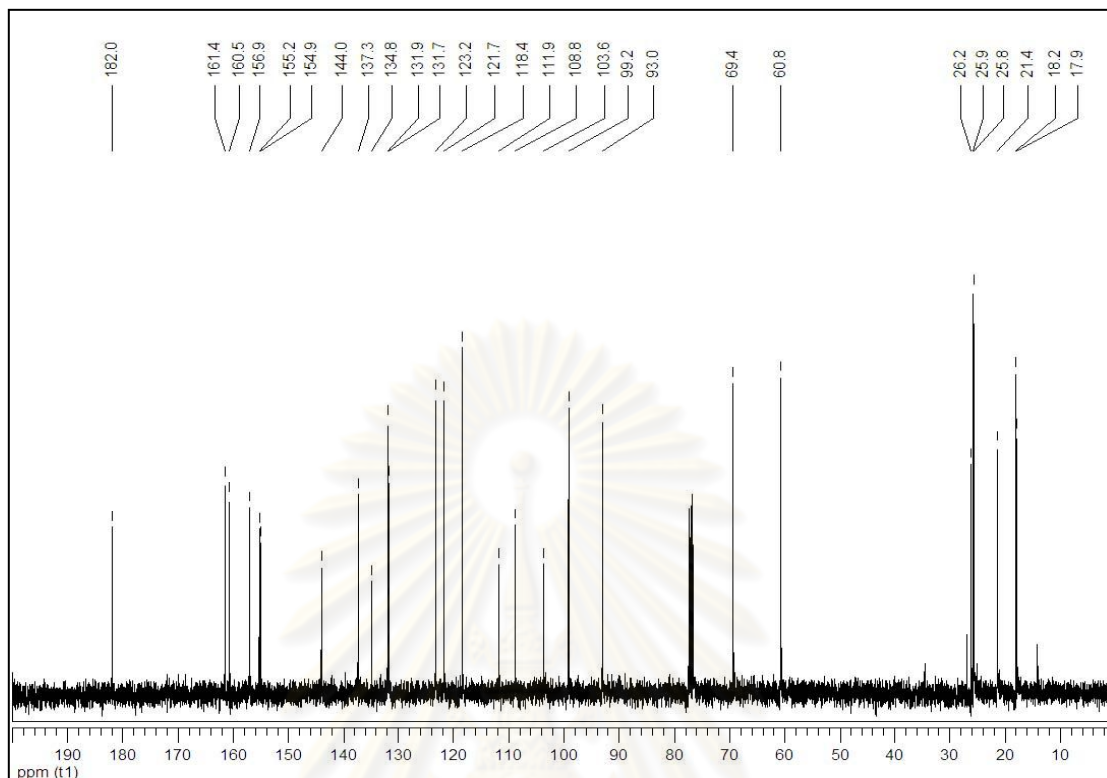
Figure 2.65 The ^{13}C NMR spectrum (CDCl$_3$, 100 MHz) of compound **M12**
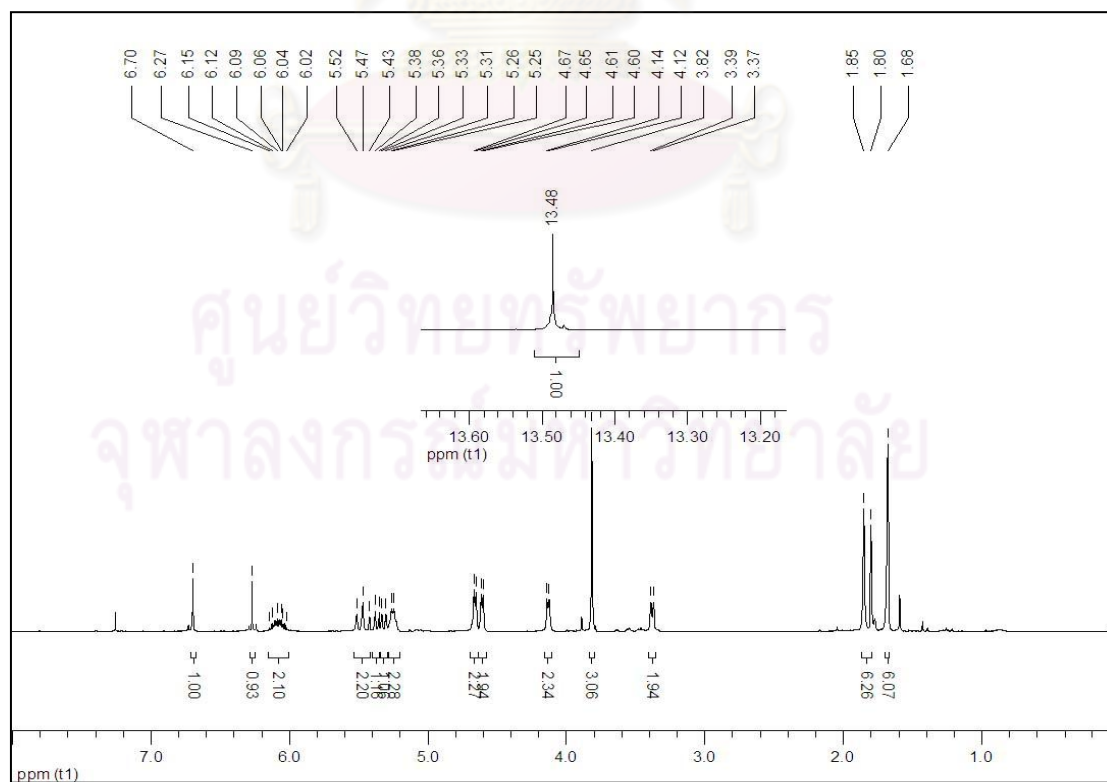
Figure 2.66 The ^{1}H NMR spectrum (CDCl$_3$, 400 MHz) of compound **D12**
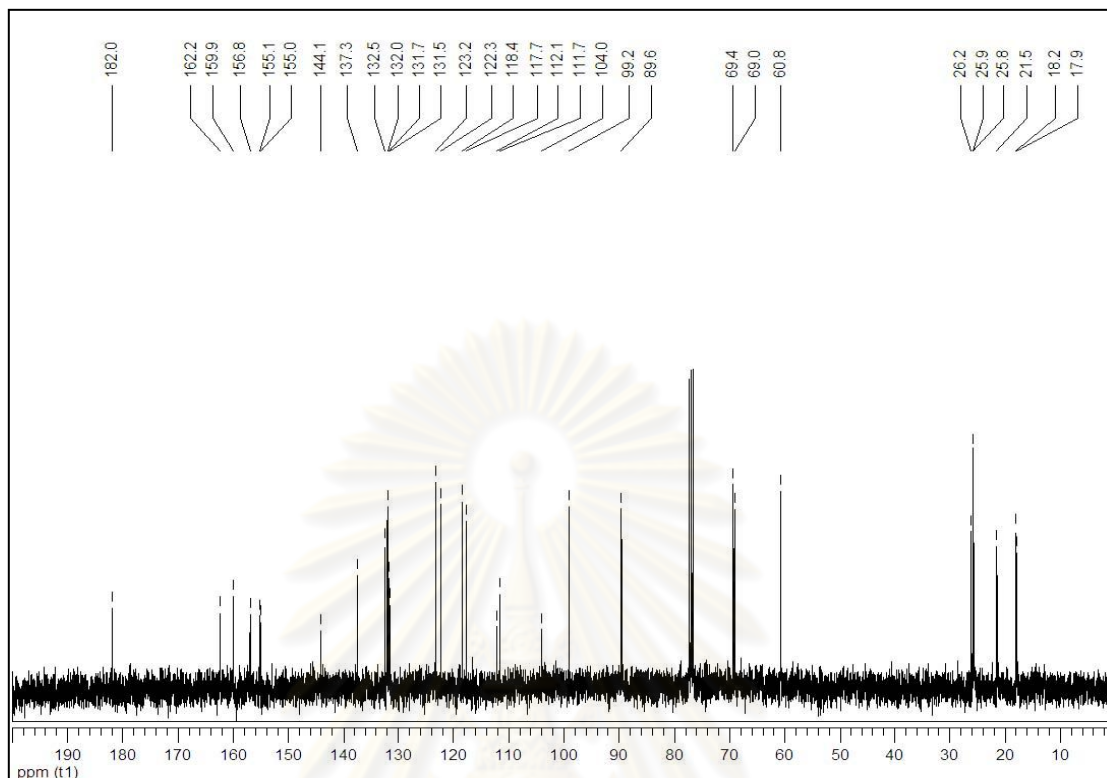
Figure 2.67 The ^{13}C NMR spectrum (CDCl$_3$, 100 MHz) of compound **D12**
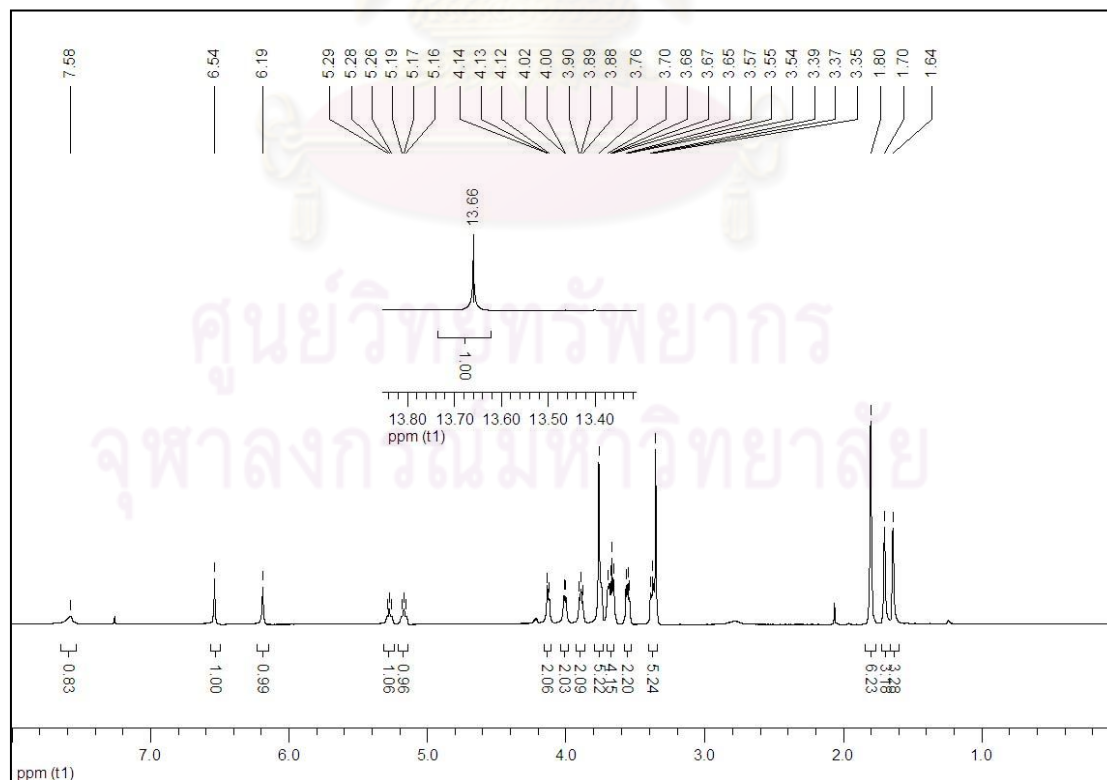
Figure 2.68 The ^{1}H NMR spectrum (CDCl$_3$, 400 MHz) of compound **M13**
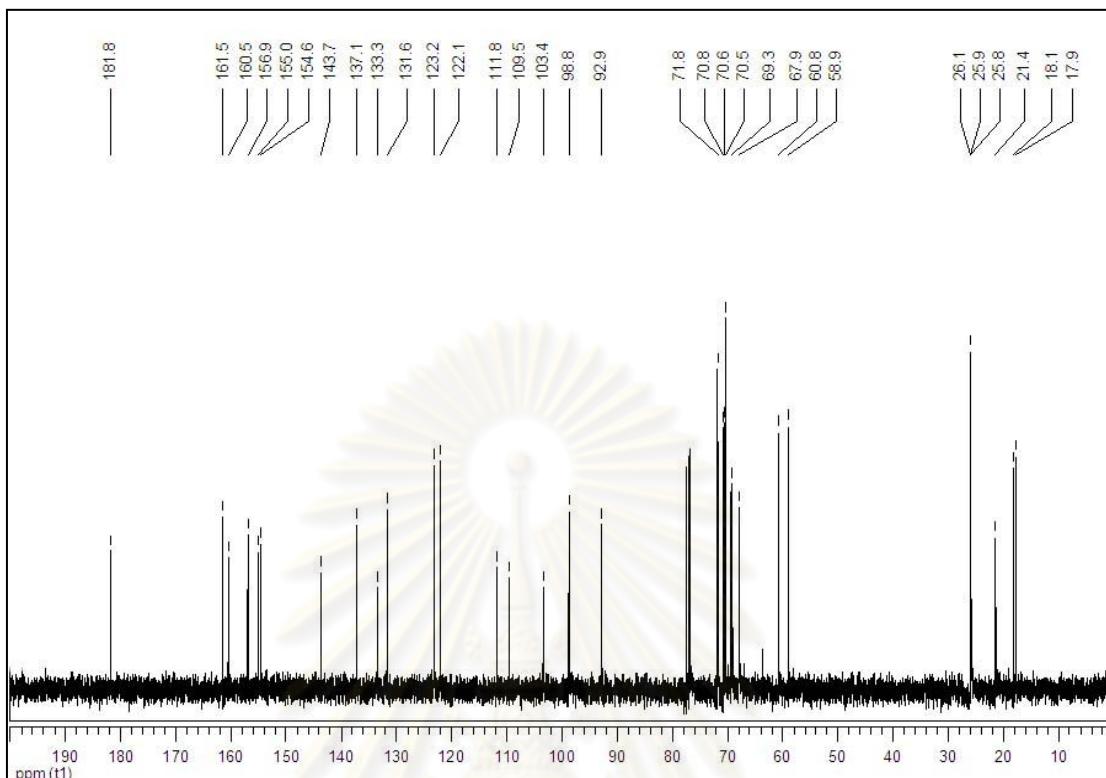
Figure 2.69 The ^{13}C NMR spectrum (CDCl$_3$, 100 MHz) of compound **M13**
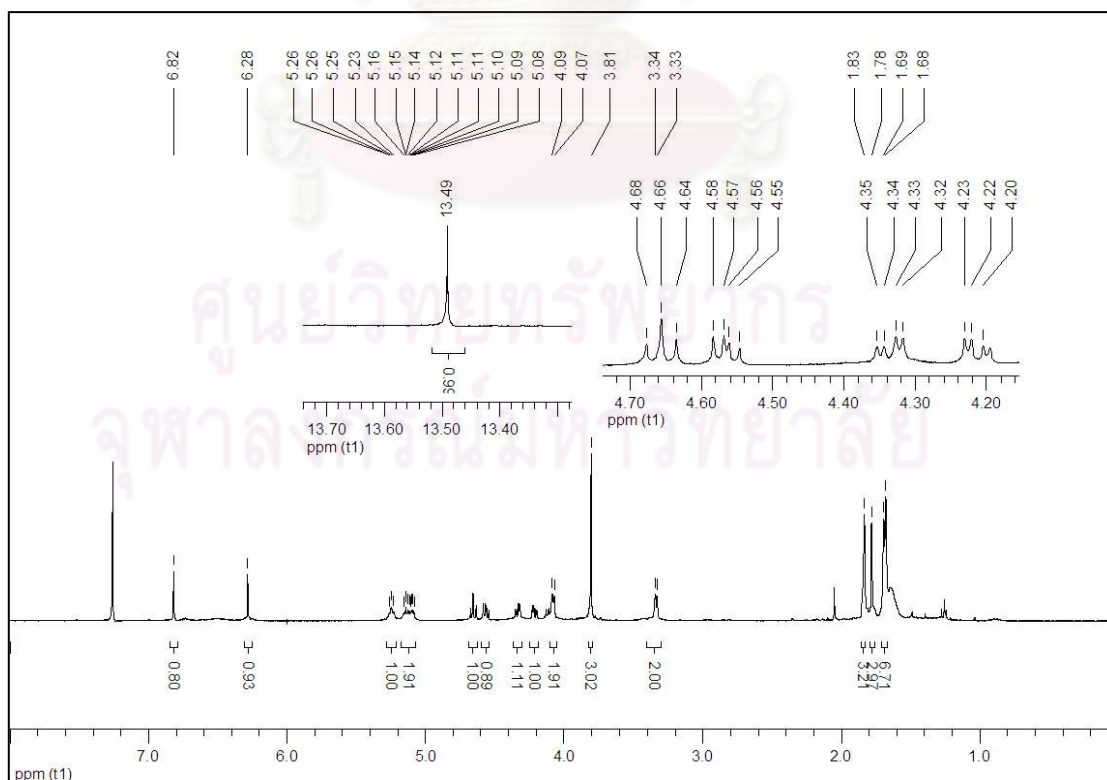
Figure 2.70 The ^{1}H NMR spectrum (CDCl$_3$, 400 MHz) of compound **M14**
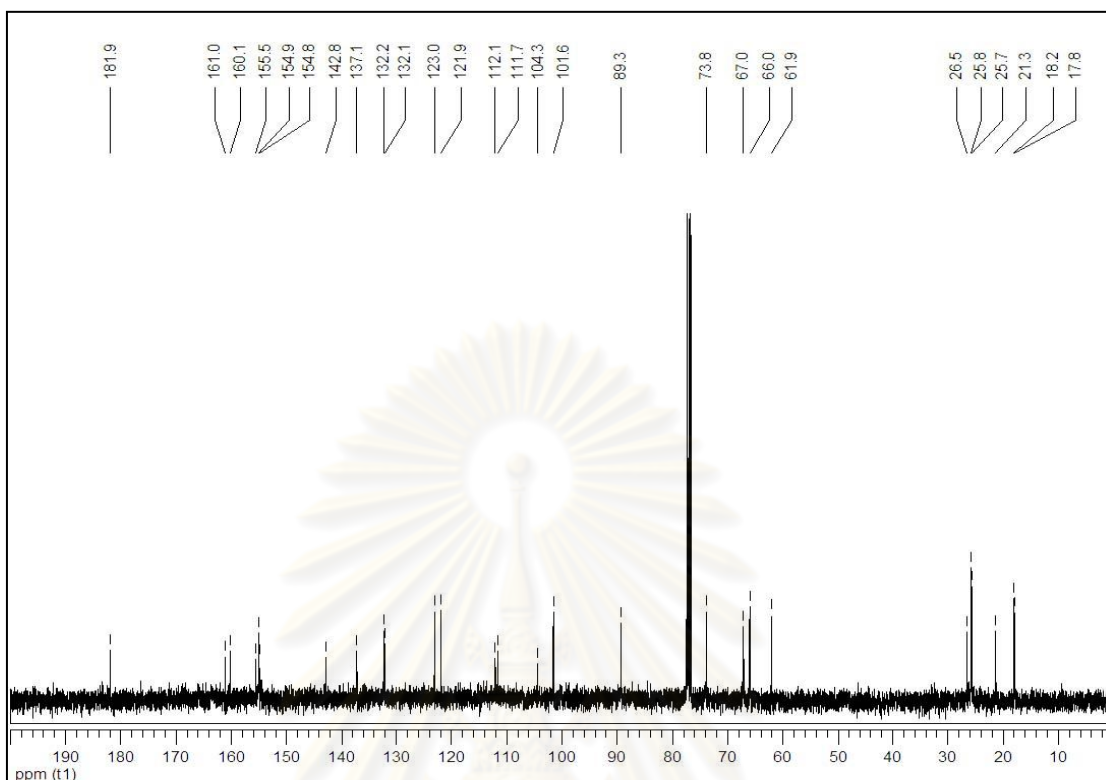
Figure 2.71 The ^{13}C NMR spectrum (CDCl$_3$, 100 MHz) of compound **M14**
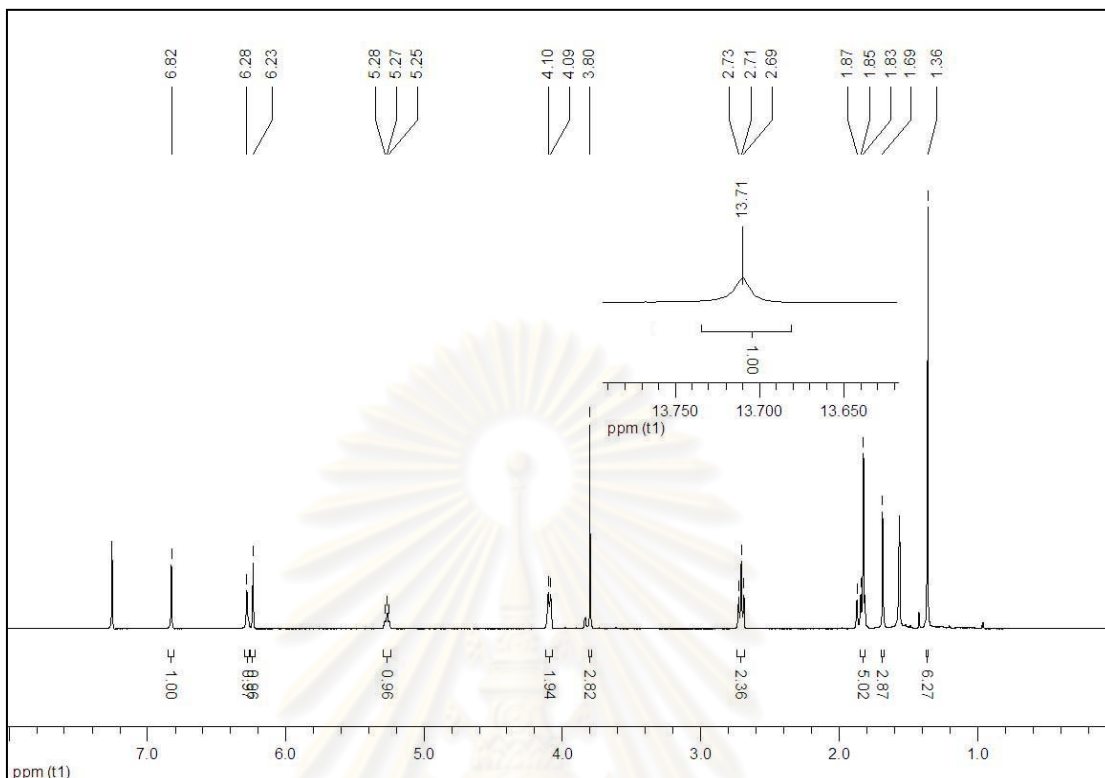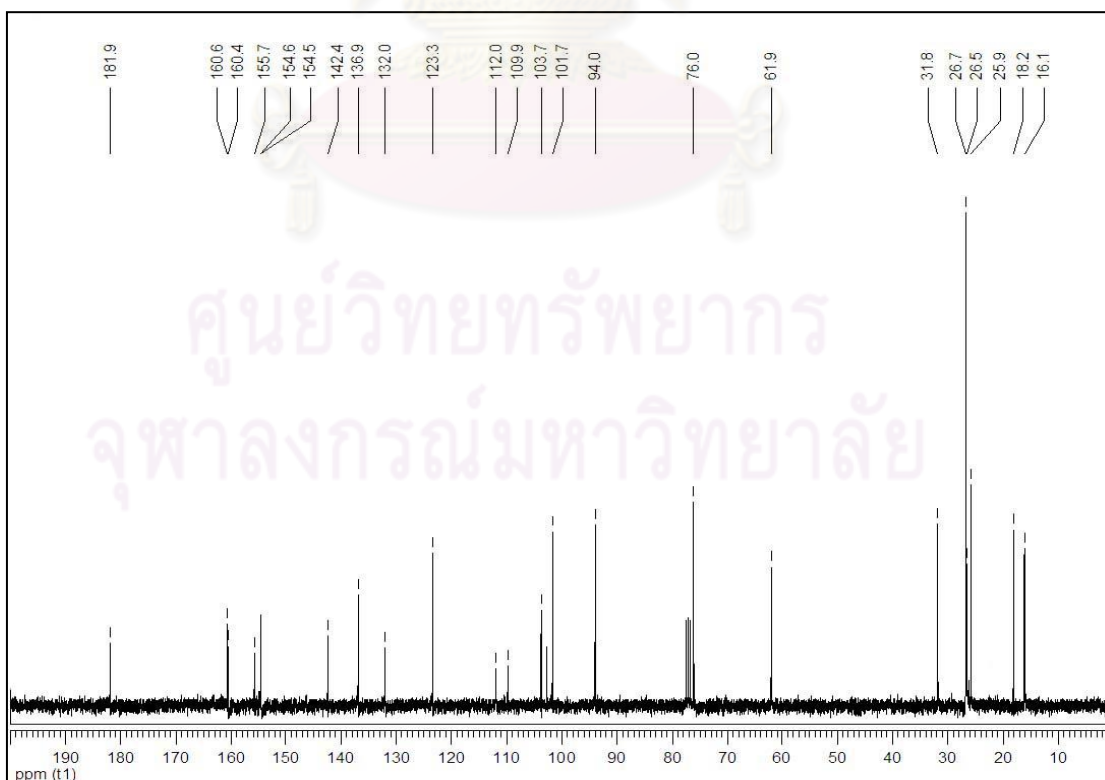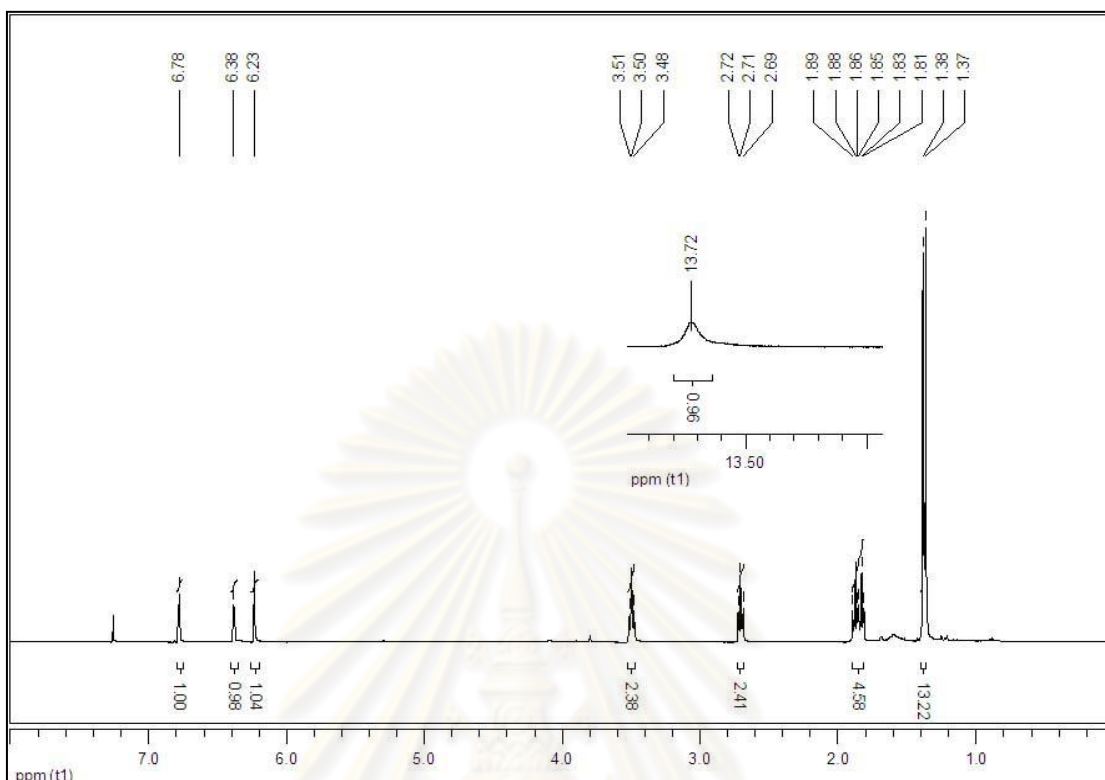

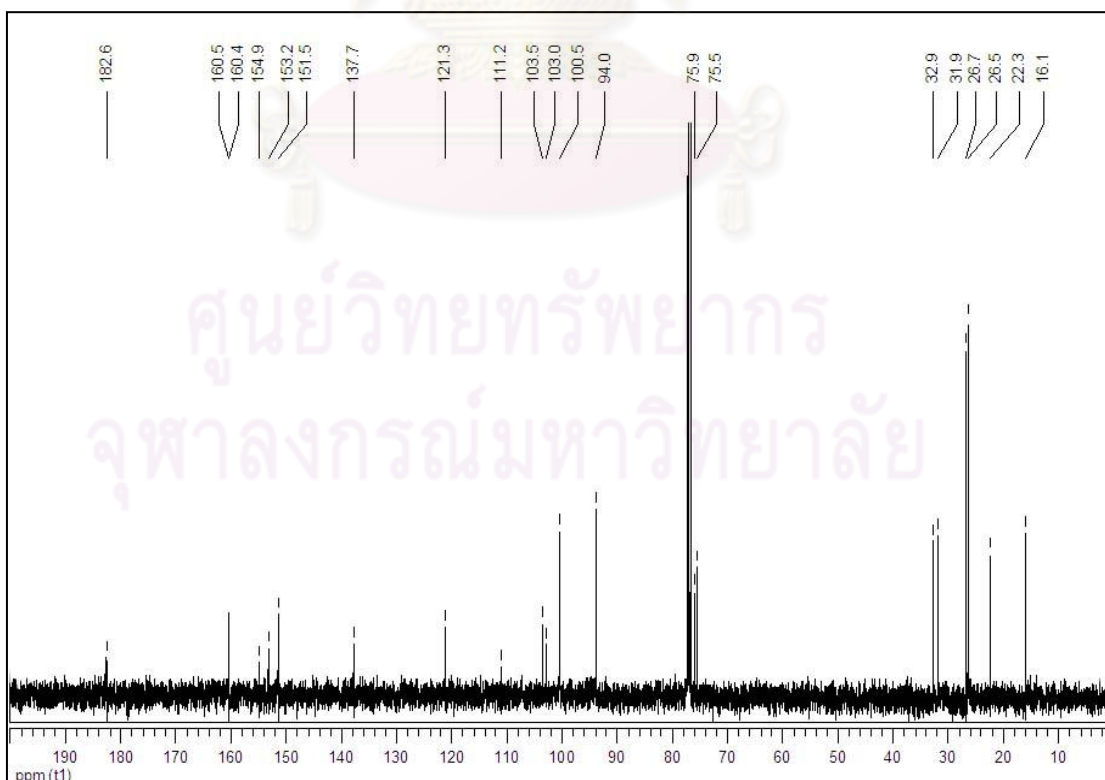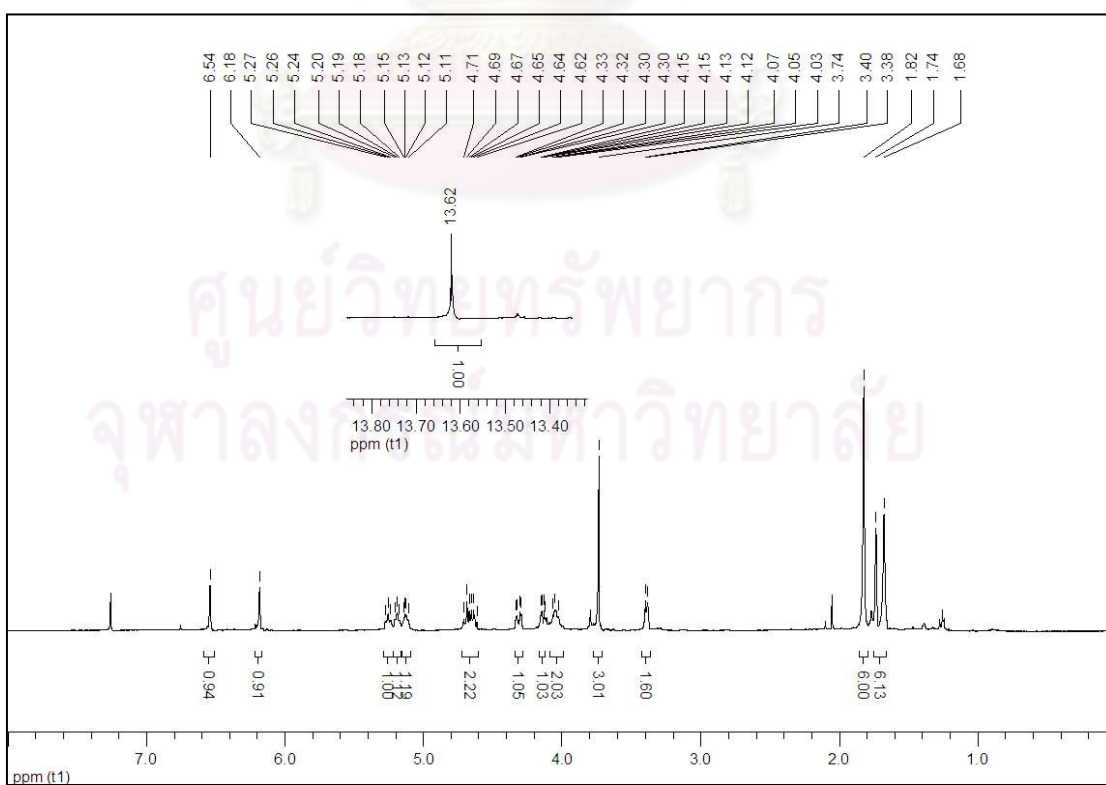**Figure 2.72** The ^{1}H NMR spectrum (CDCl$_3$, 400 MHz) of compound **M15**
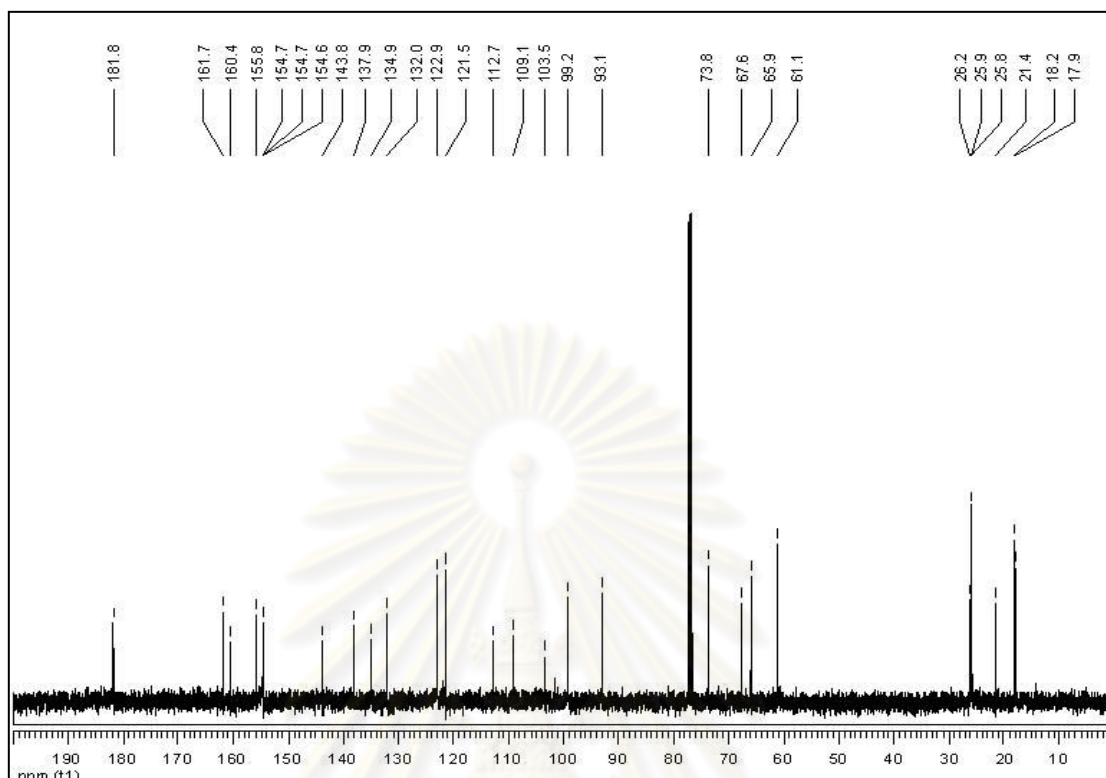
Figure 2.73 The ^{13}C NMR spectrum (CDCl$_3$, 100 MHz) of compound **M15**

2.3.3 Biological Activity Study of *α*-Mangostin (1) and Its Analogues

As aforementioned discussion, the analogues of *α*-mangostin (**1**) were synthesized to evaluate their biological activities and to investigate the SAR. The antibacterial, anticandidal and antifeedant activities were examined and their protocols were described in 2.2.10.

2.3.3.1 Antibacterial Activity

2.3.3.1.1 Preliminary Study on Antibacterial Activity of *α*-Mangostin (1)

α-Mangostin (**1**) was screened for its antibacterial activity against two Gram-positive bacteria: *S. aureus* ATCC 25923 and *S. aureus* ATCC 43300 (MRSA) and four Gram-negative bacteria: *E. coli* ATCC 25922, *E. coli* ESBL, *Ps. aeruginosa* ATCC 27853 and *Ps. aeruginosa* (multidrug resistance). The preliminarily antibacterial activiy of *α*-mangostin (**1**) was performed by disc diffusion method described in 2.2.10.1. After incubation of the cultures at 37 °C for 24 h, the inhibition

zone was observed and designated as a positive result. The results are concluded as presented in Table 2.6.

Table 2.6 Preliminary study on antibacterial activity of α-mangostin (**1**)

Bacteria	Results
S. aureus ATCC 25923	+
S. aureus ATCC 43300 (MRSA)	+
E. coli ATCC 25922	-
E. coli ESBL	-
Ps. aeruginosa ATCC 27853	-
Ps. aeruginosa (multidrug resistance)	-

Positive (+): Inhibition zone was detected.
Negative (-): No inhibition zone was detected.

A preliminary screening on α-mangostin (**1**) showed the antibacterial activity against two Gram-positive bacteria: *S. aureus* ATCC 25923 and *S. aureus* ATCC 43300 (MRSA), while it displayed no activity against any Gram-negative bacteria. Therefore, *S. aureus* ATCC 25923 and *S. aureus* ATCC 43300 (MRSA) were then used as an organism to evaluate the minimum inhibitory concentration (MIC) and bactericidal concentration (MBC) of α-mangostin (**1**) and its analogues.

2.3.3.1.2 Determination of Minimum Inhibitory Concentration (MIC) and Minimum Bactericidal Concentration (MBC)

The MIC of α-mangostin (**1**) and its twenty-six analogues against *S. aureus* ATCC 25923 was determined by the broth microdilution method described in 2.2.10.1. Final concentration was ranged from 200, 100, 50, 25, 12.5, 6.25, 3.13, 1.56, 0.78, 0.39 to 0.20 μg/mL. Chloramphenicol was employed as an antibiotic. After incubation of the cultures at 37 °C for 24 h, the MIC was recorded as the lowest concentration at which no growth was observed. The MBC was subsequently tested and the results are displayed in 2.7.

Table 2.7 Antibacterial activity of α-mangostin (**1**) and its analogues against
S. aureus ATCC 25923
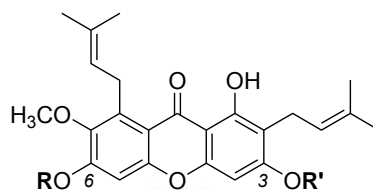
Entry	Compound	R	R'	S. aureus ATCC 25923 MIC (μg/ml)	MBC (μg/ml)
1	**1**	H	H	0.78	1.56
2	**M1**	PhCO	H	>200	-
3	**M2**	$PhCH_2CO$	H	50	50
4	**M3**	CH_3CO	H	0.78	0.78
5	**M3a**	H	CH_3CO	>200	-
6	**M4**	CH_3CH_2CO	H	6.25	12.5
7	**M5**	$CH_3(CH_2)_2CO$	H	>200	-
8	**M6**	—|—CO	H	>200	-
9	**M7**	⋋CO	H	>200	-
10	**M8**	$CH_3(CH_2)_3CO$	H	>200	-
11	**M9**	$CH_3(CH_2)_4CO$	H	>200	-
12	**M10**	$CH_3(CH_2)_7CO$	H	>200	-
13	**M11**	$CH_3(CH_2)_{10}CO$	H	>200	-
14	**M12**	$CH_2=CHCH_2$	H	>200	-
15	**D5**	$CH_3(CH_2)_2CO$	$CH_3(CH_2)_2CO$	>200	-
16	**D12**	$CH_2=CHCH_2$	$CH_2=CHCH_2$	>200	-
17[a]	Chloramphenicol			6.25	12.5

[a] Antibiotic

α-Mangostin (**1**) was active with the MIC and MBC values of 0.78 and 1.56 μg/mL, respectively (entry 1). A series of α-mangostin derivatives were synthesized and then tested to investigate the SAR. The hydroxyl groups at C3 and C6 were modified to give either mono ether or ester derivatives. In the case of hydroxyl group at C6 was only substituted; ester **M1** and ether **M12** derivatives were inactive (entries

2 and 14), whereas ester **M2** exhibited moderate activity with the MIC value of 50 μg/mL (entry 3). It was worth pointing out that the hydroxyl group at C6 might be important to inhibit the growth of *S. aureus*. In addition, an extra methylene group adjacent to ester functionality of **M2** seemed to affect the bioactivity. These results have increased the interest of varying the hydrophobic chain length of carboxylic acid part. Notably, the activity was not significantly increased for every additional methylene group. Acetate **M3** (entry 4) was found to be the same potent antibacterial activity with the MIC value of 0.78 μg/mL as α-mangostin (**1**). Propinoate **M4** exhibited was 6 times less active than both α-mangostin (**1**) and **M3** with the MIC value of 6.25 μg/mL (entry 6). Considering the MBC of α-mangostin (**1**), **M3** and **M4**, only **M3** exhibited significantly higher activity, 2-fold, over α-mangostin (**1**) with the MBC value of 0.78 μg/mL (entries 1, 4 and 6). In contrast, butanoate **M5**, pivalate **M6**, 3-isobutanoate **M7** Pentanoate **M8**, Hexanoate **M9**, nanoate **M10**, and laurate **M11** (entries 7-13) exhibited no antibacterial activity with their MIC values up to 200 μg/mL. According to the MIC values of those tested compounds, increasing the length of hydrophobic alkyl chain to C6 of α-mangostin (**1**) could affect the bioactivity.

To confirm the significance of hydroxyl group, **D5** and **D12**, both hydroxyl groups at C3 and C6 were substituted, were tested. Such compounds were not bactericidal with the MIC values up to 200 μg/mL (entries 15 and 16). In addition to the antibacterial investigation of compound **M3a**, this compound was inactive with the MIC value up to 200 μg/mL (entry 5). These findings strongly suggested that the hydroxyl groups at C3 and C6 were necessary for bioactivity.

To investigate the importance of a prenyl unit connected to C2 and C8 for activity, 3-isomangostin (**7**) and BR-xanthone A (**30**), prepared from acid catalyzed of α-mangostin (**1**), were examined. The results are shown in Table 2.8.

Table 2.8 Antibacterial activity of 3-isomangostin (**7**) and its analogues and BR-xanthone A (**30**) against *S. aureus* ATCC 25923

| Entry | Compound | R | *S. aureus* ATCC 25923 | |
			MIC (μg/ml)	MBC (μg/ml)
1	**7**	H	25	50
2	**I1**	CH_3CO	>200	-
3	**I2**	CH_3CH_2CO	>200	-
4	**I3**	$CH_3(CH_2)_2CO$	>200	-
5	**I4**	$CH_3(CH_2)_4CO$	>200	-
6	**I5**	$CH_3(CH_2)_7CO$	>200	-
7	**30**		>200	-
8[a]	Chloramphenicol		6.25	12.5

[a] Antibiotic

3-Isomangostin (**7**) was found to be active for antibacterial activity with the MIC and MBC values of 25 and 50 μg/mL, respectively (entry 1), but less active than **1**. **I1-I5** and **30** (entries 2-7) were synthesized and tested to confirm the above hypothesis. Such compounds did not show any activity with the MIC values up to 200 μg/mL. This was clearly indicated that two prenyl units were important for antibacterial activity against *S. aureus* ATCC 25923.

According to the results displayed in Tables 2.6-2.8, the antibacterial activity decreased when the hydrophobicity of tested compounds increased. Therefore, the antibacterial activity of analogues with higher hydrophilicity than α-mangostin (**1**) against *S. aureus* should be considered. Their results are presented in Table 2.9.

Table 2.9 Antibacterial activity of α-mangostin analogues with high polarity against *S. aureus* ATCC 25923

Entry	Compound	R¹	R²	S. aureus ATCC 25923	
				MIC (μg/mL)	MBC (μg/mL)
1	**M13**		H	>200	-
2	**M14**	H		>200	-
3	**M15**		H	>200	-
4ᵃ	Chloramphenicol			6.25	12.5

ᵃ Antibiotic
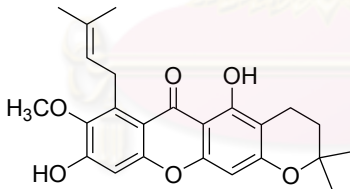
As the results presented in Table 2.9, all synthetic compounds **M24**-**M26** did not show antibacterial activity against *S. aureus* ATCC 25923. It was pointed out that the analogues with more hydrophilic group than α-mangostin (**1**) could not improve the bioactivity.

Owing to the potent antibacterial activity of α-mangostin (**1**) and three analogues **M3**, **M4** and 3-isomangostin (**7**) against *S. aureus* ATCC 25923, their antibacterial activities against MRSA ATCC 43300 were extended to evaluate. In addition, α-mangostin (**1**) and 3-isomangostin (**7**) were tested against the community-

associated MRSA strain TCH1516 (USA300 strain of CA-MRSA), performed by Dr. M. Hensler at Nizet Laboratory, Department of Pediatrics, UCSD School of Medicine. All of the results are shown in Table 2.10.

Table 2.10 Antibacterial activity of α-mangostin (**1**), **M3**, **M4** and 3-*iso*mangostin (**7**) against methicillin-resistance *S. aureus* (MRSA) ATCC 43300 and MRSA TCH1516
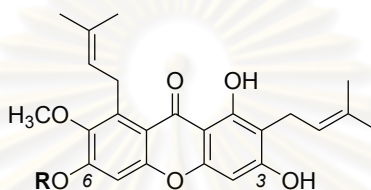
| Entry | Code | R | MRSA ATCC 43300 | | MRSA TCH 1516 |
			MIC (μg/ml)	MBC (μg/ml)	MIC (μg/ml)
1	**1**	H	0.78	1.56	5.1
2	**M3**	CH_3CO	3.13	50	-
3	**M4**	CH_3CH_2CO	100	200	-
4	**7**		25	50	5.1
5[a]		Chloramphenicol	12.5	50	-

[a] Antibiotic

From the results presented in Table 2.10, among tested compounds against MRSA ATCC 43300, α-mangostin (**1**) displayed the most antibacterial activity with the MIC and MBC values of 0.78 and 1.56 μg/mL, respectively (entry 1). **M3** was active with the MIC and MBC values of 3.13 and 50 μg/mL, respectively (entry 2), but still less active than α-mangostin (**1**). In the case of **M4**, it showed no good activity with the MIC and MIC values of 100 and 200 μg/mL, respectively (entry 3). In addition, 3-isomangostin (**7**) exhibited moderate activity with the MIC and MBC values of 25 and 50 μg/mL, respectively (entry 4). In the case of antibacterial activity

against MRSA TCH1516, α-mangostin (**1**) and 3-isomangostin (**7**) showed good activity at the same MIC value of 5.1 μg/mL (entries 1 and 4). Compared to the antibacterial activity of these compounds against *S. aureus* ATCC 25923 and MRSA ATCC 43300, it was found that their activities to inhibit MRSA ATCC 43300 growth were less than those to inhibit *S. aureus* ATCC 25923 growth.

2.3.3.1.3 Structure-Antibacterial Relationship (SAR) Study

As the antibacterial results of α-mangostin (**1**) and its analogues described in 2.3.3.1.2, α-mangostin (**1**) could not be modified to give a more active compound. However, some SAR of α-mangostin (**1**) could be suggested herein.

Noticeably, natural-occurring α-mangostin (**1**) exhibited the most antibacterial activity against both normal *S. aureus* and metthicilin-resistant *S. aureus* (MRSA), which pointed out that α-mangostin (**1**) possessed the best structure for those stains. In addition, the hydroxyl groups at C3 and C6 and the prenyl chains substituted on C2 and C8 of α-mangostin (**1**) played an essential role for the bioactivity. It has been proposed that the maximum activity depends on a balance between hydrophilic hydroxyl group and hydrophobic alkyl chain of test molecule [81-82]. The hydrophilic head, hydroxyl group, can bind with an intermolecular hydrogen bond like a „hook‟ attaching itself to the hydrophilic portion of the membrane of bacterial cells, and then the hydrophobic tail portion, alkyl chain, of the molecule is able to enter into the membrane lipid bilayer resulting in happening of disorder in the fluid bilayer of the membrane. This hypothesis can be used to explain why α-mangostin (**1**) exhibits the best antibacterial activity among all compounds tested, and why increasing the hydrophobic alkyl chain to the structure of α-mangostin (**1**) destroys its activity. To consider the structure of α-mangostin (**1**), there are at least three hydrophilic hydroxyl groups and two hydrophobic prenyl chains. α-mangostin (**1**) could enter the membrane with the polar hydroxyl group oriented into the aqueous phase by hydrogen bonding and prenyl chain aligned into the lipid phase by dispersion forces. When either hydrophobic chain length or hydrophilic group of α-mangostin analogues is more than that of **1**, the dispersion force becomes greater

than the hydrogen bonding force and *vice versa*, resulting in the balance is destroyed and the activity disappears.

2.3.3.2 Anticandidal Activity

As the literature review, α-mangostin (**1**) showed the anticandidal activity against *Candida albicans* ATCC 90028 with the MIC and minimum candicidal concentration (MCC) values of 1,000 and 2,000 μg/mL, respectively [67]. It has been increased the interest in the evaluation of α-mangostin (**1**) and its analogues against yeast with the expectation that some analogues could be more active than α-mangostin (**1**). The anticandidal activity of test compounds against *C. albicans* was tested by the broth microdilution method in Sabouraud dextrose broth described in 2.2.10.2. Two-fold diluted test concentration was ranged from 2000 to 2.0 μg/mL. After incubation of the cultures at 25 °C for 24 h, the MIC was recorded as the lowest concentration at which no growth was observed. The MCC was subsequently tested and the results are presented in Table 2.11.

Table 2.11 Anticandidal activity of *α*-mangostin (**1**) and its analogues against *C. albicans*

Entry	Compound	R	R'	C. albicans	
				MIC (μg/ml)	MCC (μg/ml)
1	**1**	H	H	>2000	-
2	**M3**	CH_3	H	>2000	-
3	**M3a**	H	CH_3	>2000	-
4	**M4**	CH_3CH_2CO	H	>2000	-
5	**M5**	$CH_3(CH_2)_2CO$	H	>2000	-
6	**M9**	$CH_3(CH_2)_4CO$	H	>2000	-
7	**M10**	$CH_3(CH_2)_7CO$	H	>2000	-
8	**M13**		H	>2000	-
9	**M14**	H		>2000	-
10	**M15**		H	>2000	-
11	**7**			>2000	-
12	**30**			>2000	-
13[a]	Amphotericin B				

[a] Antibiotic

As the results showed in Table 2.11, α-mangostin (**1**) did not show any activity against *C. albicans* with the MIC value up to 2000 μg/mL. Attempt to the structural modification of α-mangostin (**1**) met with failure**,** all test analogues exhibited no activity with the MIC value up to 2000 μg/mL.

2.3.3.3 Termite Antifeedant Activity

α-Mangostin (**1**) and its twelve analogues were evaluated their antifeedant activities against wood-feeding termite: *Reticulitermes speratus*.

R. speratus (Figure 2.76) commonly lives in Japanese forests and feeds on rotten wood.

Figure 2.74 *Reticulitermes speratus* workers

The antifeedant activity of tested compounds against *R. speratus* was kindly performed by Professor M. Morimoto at Kinki University, Japan. A choice paper disk bioassay was used and its protocol was described in 2.2.10.3. To measure the activity of each test compound, the antifeedant index (AFI) was used and AFI can be calculated from the equation (**1**).

$$\text{The antifeedant index (AFT)} = \%T / (\%T + \%C) \times 100 \qquad (\mathbf{1})$$

%T is consumption of treated disk   %C is consumption of control disk

Then, the AFI value was converted to the feeding inhibition (FI) by using the equation (**2**) to a corresponding 0 to 100% inhibition range.

The feeding inhibition (FI) = (50 x AFI) x 2   **(2)**

An FI value under 50% when treated at 100μg/disk is indicative as inactive in this study. The results are displayed in Table 2.12.

Table 2.12 Termite antifeedant activity of α-mangostin (**1**) and its analogues against

        R. speratus
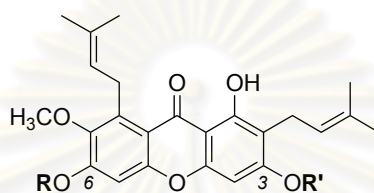
Entry	Compound	R	R'	FI (%) (100 μg/disk)
1	**1**	H	H	97.8 (85.0)[a]
2	**M1**	PhCO	H	Inactive
3	**D1**	PhCO	PhCO	Inactive
4	**M2**	PhCH$_2$CO	H	Inactive
5	**D2**	PhCH$_2$CO	PhCH$_2$CO	Inactive
6	**M12**	CH$_2$=CHCH$_2$	H	Inactive
7	**D12**	CH$_2$=CHCH$_2$	CH$_2$=CHCH$_2$	Inactive
8	**D3**	CH$_3$CO	CH$_3$CO	Inactive
9	**D4**	CH$_3$CH$_2$CO	CH$_3$CH$_2$CO	74.2
10	**M5**	CH$_3$(CH$_2$)$_2$CO	H	75.7
11	**D5**	CH$_3$(CH$_2$)$_2$CO	CH$_3$(CH$_2$)$_2$CO	80.8
12	**M10**	CH$_3$(CH$_2$)$_7$CO	H	Inactive
13	**7**	3-isomagostin		95.1 (56.0)[a]

[a] 50 μg/disk was tested.
Inactive, FI<50% (100 μg/disk)

From the results shown in Table 2.12, α-mangostin (**1**) completely inhibited termite feeding with the %FI value of 97.8 at a dose of 100 μg/disk (entry 1). In addition, α-mangostin (**1**) still showed good termicidal activity with the %FI value of 85.0 at a dose of 50 μg/disk (entry 1). In contrast, **M1**, **M2** and **M12**, hydroxyl group at C6 was substituted, were inactive (entries 2, 4 and 6). No activity was observed for 3,6-di-substitued products **D1**, **D2**, **D12** and **D3** (entries 3, 5, 7 and 8). Interestingly, 3.6-di-*O*-propinoyl mangostin (**D4**) exhibited good activity with the %FI value of 74.2 (entry 9). For 6-mono and 3,6-di-*O*-butanoyl mangostins (**M5** and **D5**), both compounds exhibited potent activity with the %FI values of 75.7 and 80.8, respectively (entries 10 and 11). On the other hand, the activity disappeared when increasing the carbon chain length of C6-connected substituent to a nanoate group (entry 12). Using 3-isomagostin (**7**), it displayed potent and moderate activities with %FI values of 95.1 and 56.0 at a dose of 100 and 50 μg/disk, respectively (entry 13).

2.3.3.3.1 Structure-Antifeedant Activity Relationship Study

The SAR suggested that the hydrophilic hydroxyl groups at C3 and C6 seemed to display an essential role for bioactivity. For example, the activity of **M1** and **M12**, and **D1** and **D12** disappeared in case that hydroxyl groups at C6 or both of C3 and C6 were converted to less hydrophilic groups such as esters or ethers. In contrast, the prenyl unit adjacent to C2 seemed to be less necessary than the hydroxyl group for bioactivity. All findings were similar to the SAR studies on antibacterial activity, indicated that the optimal activity depended on the balance between hydrophilic hydroxyl group and hydrophobic alkyl chain of α-mangostin (**1**) [81].

CHAPTER III

SYNTHESIS AND PHARMACOLOGICAL EVALUATION OF CAGED *GARCINIA* XANTHONES

3.1 Introduction

Extracts from the *Garcinia* family of tropical trees have led to the isolation of a variety of natural products referred to as the caged *Garcinia* xanthones, which contain a unique structural motif and promising biological activities. Several *Garcinia* species *e.g.*, *G. bracteata*, *G. gaudichaudii*, *G. hanburyi*, *G. Morella* and *G. scortechinii* have been distributed in nature; nonetheless, only two of which are found in Thailand: *G. hanburyi* and *G. morella*. To simplify the structure of caged motif presented in caged *Garcinia* xanthones, it could be defined as an unusual 4-oxa-tricyclo[4.3.1.0^{3,7}]dec-8-en-2-one (caged) scaffold [83-84] which is derived from the conversion of the C-aromatic ring of the xanthone backbone as demonstrated in Figure 3.1.

Gerneral motif of
the caged xantones
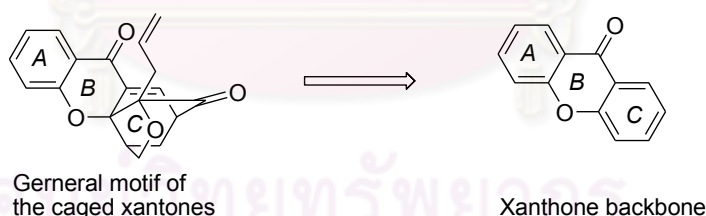
Xanthone backbone

Figure 3.1 Representative general motif of caged xanthones from xanthone backbone

3.1.1 Literature Review on Phytochemistry of Caged *Garcinia* Xanthones

Gambogic acid (**77**) appeared to be the first dominant example of the caged scaffold due to its noticeable biological activities. It could be isolated as a major component from the gamboge resin (gold resin) of *G. hanburyi* trees. These trees have been locally named as "RongThong", and mainly exist in Songkhla and Chantaburi provinces of Thailand. In 1934, it was initially isolated as monoacetyl derivative [85], and the structure and absolute stereochemistry were unambiguously determined in

2001 *via* an X-ray of its pyridine salt [86-87]. Related investigations from the seeds and the resin of *G. morella* led in 1937 to the isolation of morellin (**79**) [88]. In 1963 the *p*-bromobenzenesulfonyl ester of morellin was prepared and its constitution was determined by X-ray crystallography [89]. The crystal structures of gambogic acid (**77**) and morellin (**79**) were defined a new class of natural products that are collectively referred to as caged *Garcinia* xanthones.

The caged motif of xanthones is further customized *via* substitutions on the aromatic ring (ring A) and peripheral oxidations to produce a variety of structural subfamilies representative members of which are shown in Figure 3.2.

This is exemplified by the structure of forbesione (**83**), a natural product isolated from *G. forbesii* [90] *and G. hanburyi* [91-92]. For example, prenylation at the C5 center of forbesione (**83**) (gambogic acid numbering) gives access to the gaudichaudione scaffold [93-96], represented by deoxygaudichaudione (**85**) [97]. Oxidation at the C29 could then lead to gaudichaudione A (**86**) and gaudichaudiic acid G (**87**) [93]. Alternatively, prenylation of forbesione (**83**) at C5, followed by cyclization with the pendant phenol gives access to the morellin scaffold [12, 98-101] represented by desoxymorellin (**81**) [17, 102-103]. Progressive oxidations at the C30 of desoxymorellin (**81**) produce morellinol (**80**), morellin (**79**) and morellic acid (**82**) [18]. Compounds arising from isomerization around the C27-C28 double bond of morellins have also been isolated. Thus, morellin (**79**), having the *cis* configuration about the C27–C28 double bond, is known to isomerize to the *trans* isomer, isomorellin (**88**) [104]. Similar observations have been reported for gambogic acid (**77**) [14].

Geranylation at the C5 of forbesione (**83**) forms desoxygambogenin (**84**) and, after formation of the pyran ring, produces gambogin (**78**) [105]. Further oxidation at C29 leads to gambogic acid (**77**) [91]. Isolated from *G. bracteata,* the bractatin subfamily (**89**, **90**, **91**) [10, 106] serves as an example of forbesione-type natural products that contain a reverse prenyl group at C17. Interestingly, 6-*O*-methylneobractatin (**91**) is the only natural product known to contain a modified caged structure, referred to as the neo motif [10, 106].

77: R= CO₂H: gambogic acid
78: R= CH₃: gambogin

79: R = CHO: morellin
80: R = CH₂OH: morellinol
81: R = CH₃: desoxymorellin
82: R = CO₂H: morellic acid

83: R = H: forbesione
84: R = geranyl: desoxygambogenin

85: R = CH₃: desoxygaudichaudione A
86: R = CHO: gaudichaudione A

87: gaudichaudiic acid G

88: isomorellin

89: R = H: bractatin
90: R = Me: 1-O-methylbractatin

91: 6-O-methylneobractatin

92: hanburin

93: cantleyanone A

94: R = CH₃: scortechinone A
95: R = CO₂H: scortechinone B

96: R = H: conchichinone C
97: R = OH: conchichinone D

Figure 3.2 Representative structures of natural products from *Garcinia* and related plants containing the caged xanthone motif. To facilitate structural comparison, the carbon numbering of gambogic acid has been used for all compounds in this chapter.

The C11 is another diversity point. For example, hanburin (**92**) [105] is a C11 prenylated product of forbesione (**83**), while cantleyanone A (**93**) [15] and scortechinones A (**94**) [13, 107-108] and B (**95**) [109] contain a methoxy group at that position. This motif has also been identified in cochinchinones C (**96**) and D (**97**), two natural products isolated from the roots of *Cratoxylum cochinchinense* [110].

In addition, there are a number of *Garcinia* natural products possessing a rearranged caged xanthone motif (Figure 3.3). For instance, in lateriflorone (**98**) [111], the caged motif is attached to an unprecedented spiroxalactone core, likely a product of an oxidative rearrangement of the central xanthone ring. Similar rearrangements at the C ring may account for gaudispirolactone (**99**) [11, 112]. Gambogoic acid (**100**) [97, 113], dihydroisomorellin (**101**) [17] and isomoreollin (**102**) [114-115] are a few representative examples of caged xanthones with a modified C9-C10 double bond.

98: lateriflorone

99: gaudispirolactone

100: gambogoic acid

101: R = H: dihydroisomorellin
102: R = OEt: isomoreollin
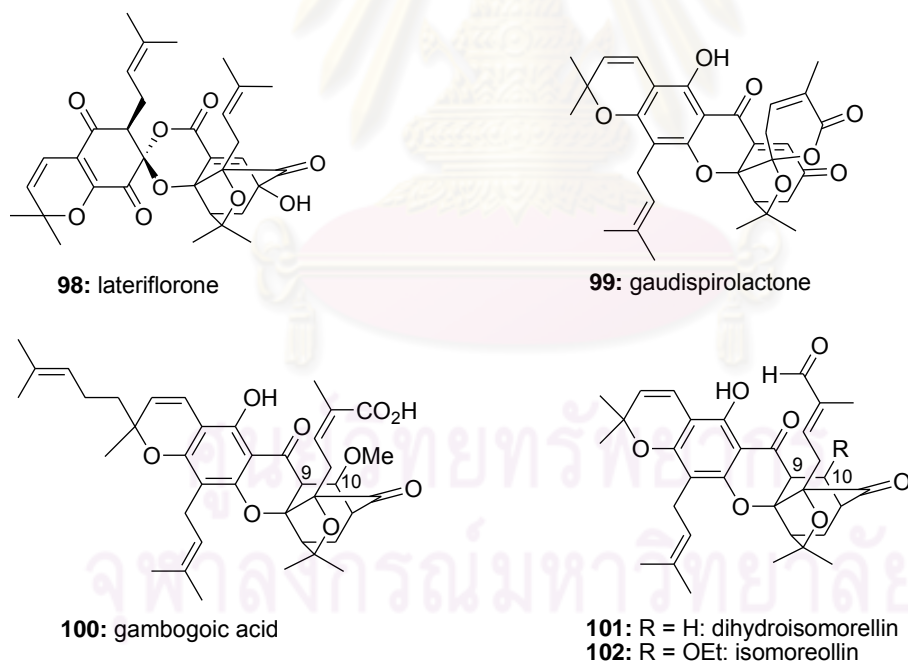
Figure 3.3 Representative structures of natural products containing a rearranged caged xanthone motif

It should be noted that the chemical structures shown in Figures 3.2 and 3.3 do not define the absolute stereochemistry of the caged motif. This is because the vast majority of the caged *Garcinia* xanthones have been characterized by NMR methods

and thus their absolute stereochemistry remains undetermined. It has been suggested that these natural products exist as racemic mixtures and their enantiomeric composition can be enriched by repeated crystallizations [10, 106]. For instance, chiral HPLC analysis of bractatin (**89**) showed that this compound existed as a 6:4 mixture of two enantiomers, the ratio of which varied with different crystallizations [10, 106]. Moreover, gambogic acid (**77**) occurs in nature as a mixture of epimers at the C2 that can be separated by modern chromatographic and analytical techniques [116-117]. The optical rotation recorded for the C2-*R* epimer is $[\alpha]^{20}_D = -578$ (c= 0.201, CHCl$_3$) while that recorded for the C2-*S* epimer, also referred to as epigambogic acid, is $[\alpha]^{20}_D = -486$ (c= 0.197, CHCl$_3$) [118]. More recently, a combination of these techniques has been used for the identification of new bioactive xanthones from *Garcinia* plants [119-120].

3.1.2 Literature Review on Biogenesis Studies

Biosynthetically, the xanthone backbone of the caged *Garcinia* natural products is presumed to derive from common benzophenone intermediates of a mixed shikimate-acetate pathway [121-122]. Whereas xanthones produced in fungi have been shown to be wholly acetate-derived [123], those found in higher plants exhibit oxygenation patterns that originate from a combination of the acetate (ring A) and shikimate (ring C) pathways. This proposed biogenetic scenario is illustrated with the synthesis of maclurin (**107**) and tetrahydroxy xanthone **108** (Scheme 3.1) [124]. An aldol-type condensation of phosphoenolpyruvate (PEP) and D-erythrose 4-phosphate leads to shikimic acid (**103**) that after oxidation, dehydration and enolization forms protocatechuic acid (**104**). Reaction of **104** with coenzyme A (HSCoA) produces activated ester **105** that can then react with three units of malonyl-coenzyme A (malonyl-CoA) to produce intermediate **106**. An intramolecular Claisen condensation followed by enolization leads to benzophenones such as maclurin (**107**). Depending upon the benzophenone produced, this may be a branch point in the biogenesis of other benzophenone-type natural products. It is generally accepted that the formation of xanthones such as 1,3,5,6-tetrahydroxyxanthone occurs by means of phenolic coupling of maclurin (**107**) [125-126].
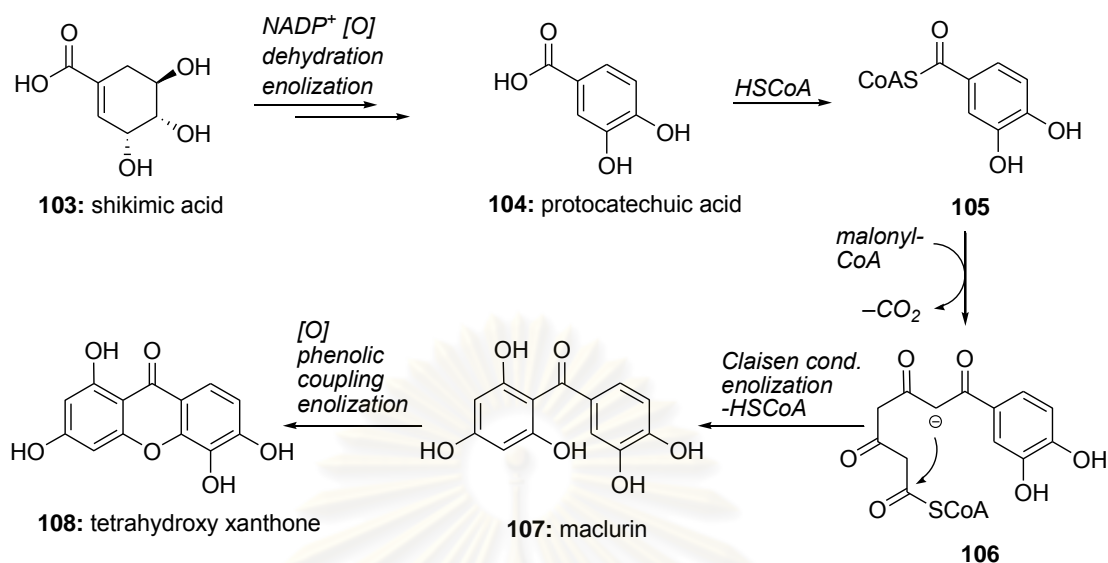
Scheme 3.1 Proposed biosynthesis of benzophenones and xanthones in higher plants

Different hypotheses have been proposed for the biosynthetic conversion of xanthones, such as **108**, to the unusual motif of the caged *Garcinia* xanthones. The first hypothesis departed from prenylation of a xanthone, such as **109**, at C11 and C13 to produce compound **110** (Scheme 3.2) [127]. Oxidation at the C13 would then introduce the essential tertiary alcohol, while reduction of the C10-C11 double bond would form compound **111** that can assume the geometry required for cyclization (structure **112**). Nucleophilic attack by the C13 tertiary alcohol on the pendant prenyl group was then presumed to initiate the cyclization cascade leading to caged **113**. The complete caged system **114** could then be formed by oxidation between carbons C9 and C10. The biosynthetic scenarios that followed were variations of this hypothesis that simply reduced the number of oxidations and reductions [12, 83, 98-101]. Unfortunately, both the molecular geometry and the reactivity required for the cascade of nucleophilic attacks from **111** to **113** would make this hypothesis implausible.
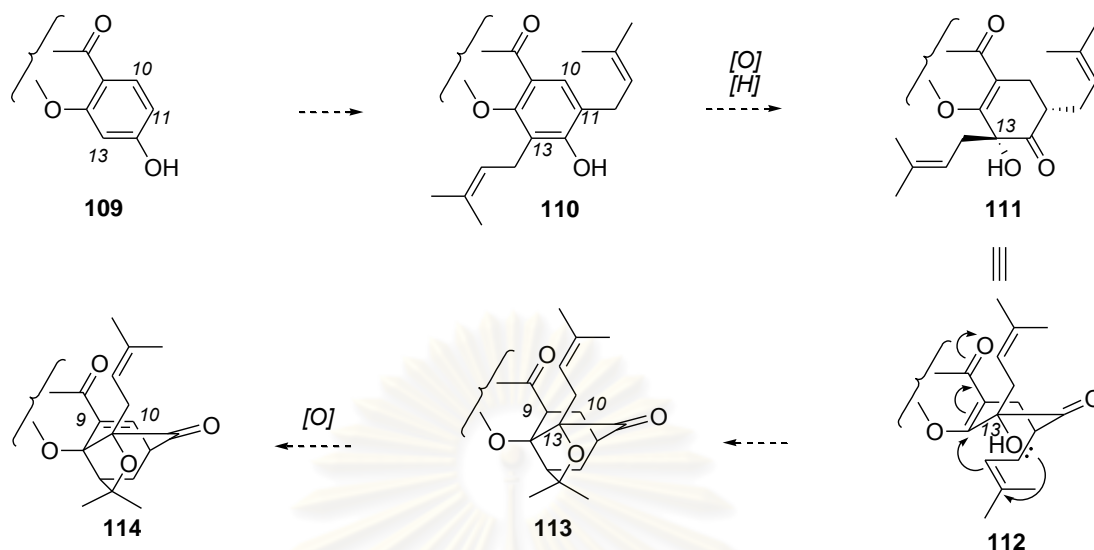
Scheme 3.2 Proposed biosynthesis of the caged xanthone motif *via* a cascade of
nucleophilic attacks

A more realistic biosynthetic scenario emerged from the pioneering work of
Quillinan and Scheinmann [128]. Isoprenylation of tetrahydroxyxanthone **108** with
four isoprene units can lead to desoxymorellin and related metabolites. The caged
motif of these compounds can thus be formed *via* a Claisen rearrangement followed
by a Diels-Alder reaction on the intermediate dienone. This scenario is highlighted in
Scheme 3.3. It is worth noting that although at that time there was sufficient
precedence in support of the Claisen migration [129-131], there were no reports on
intramolecular Diels-Alder adducts from rearrangements of aryl propargyl ethers.
Along these lines, a retro Diels-Alder fragmentation pathway has been detected in
mass spectrometry studies of several caged *Garcinia* xanthones, providing additional
support to this biosynthesis hypothesis [101, 118].
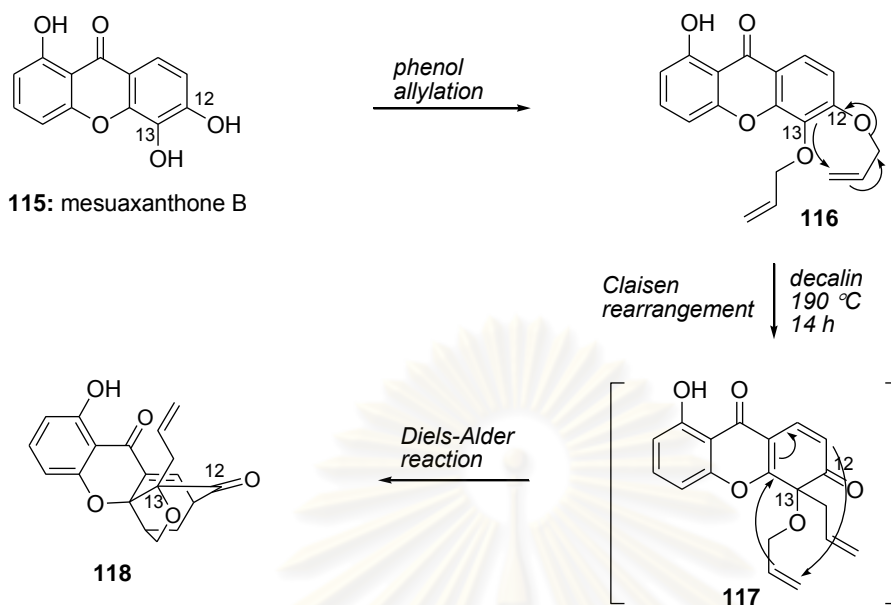
Scheme 3.3 Proposed biosynthesis of the caged xanthone motif *via* a Claisen/Diels-Alder reaction cascade

Quillinan and Scheinmann also provided experimental evidence in support of the Claisen/Diels-Alder reaction cascade. Using mesuaxanthone B (**115**) as the starting material, they successfully prepared and tested their hypothesis on *bis*-allyloxy xanthone **116** (Scheme 3.3). Despite the rather limited experimental details, heating **116** in boiling decalin (190 °C) for 14 h gave rise to the elusive caged structure, assigned as compound **118**, presumably *via* a Diels-Alder cyclization of Claisen intermediate **117**. Compound **118** had similar spectroscopic characteristics with those of morellin (**79**), suggesting that this reaction cascade could account for the biogenesis of the caged xanthones.

The lack of details on the synthesis of caged motif **118**, together with the high temperature and long reaction times required for the Claisen/Diels-Alder reaction, casted some doubts on the synthetic relevance of this reaction cascade. Likely due to these reasons, the Quillinan and Scheinmann hypothesis remained dormant for over 30 years, until Nicolaou and Li masterfully demonstrated its value to a biomimetic synthesis of forbesione (**83**) [132]. Independently, Theodorakis and co-workers explored the site selectivity of the Claisen/Diels-Alder cyclization and further refined

the biosynthesis scenario for all caged *Garcinia* xanthones [133]. These studies will be presented in the following sections.

3.1.3 Literature Review on Biological Activities of the Caged *Garcinia* Xanthones

3.1.3.1 Antimicrobial and Anticancer Activities

Aside from their striking chemical structure and biosynthesis, the caged *Garcinia* natural products exhibit interesting bioactivities and have a documented value in traditional Eastern medicine. In fact, oral and injectable formulations of gamboge have been used in China for the treatment of patients with breast carcinoma and malignant lymphoma [134]. In addition, gamboge has been used topically for treating infected wounds and systemically to alleviate pain and edema. In Thai folk medicine, gamboge has been used as a topical antiinfective agent, and internally as a drastic purgative and a vermifuge to treat tapeworm [14, 135].

Initial biological studies with semipurified gamboge extracts documented its antiprotozoal activities, thus lending support for its indigenous use in the treatment of enteric diseases [136-138]. Morellin (**79**) and gambogic acid (**77**), the major components of semipurified resin extracts of *G. Morella* [139-140], exhibited high *in vitro* specific growth inhibitory effect on Gram-positive bacteria *in vitro* and protective action in experimental staphylococcal infections in mice [141-143]. In particular, gambogic acid (**77**) exhibited high specific inhibitory effect (0.1-1 μg/mL) on the growth of Gram-positive bacteria but had little effect against many Gram-negative bacteria, fungi, yeast and actinomycetes [144-145]. Further experiments in mice indicated that topical applications of gambogic acid (**77**) in experimental septic wounds could offer protection against lethal staphylococcal infections at a dose level of 30 mg/kg/day for 2 days. Interestingly, the susceptibility of a morellin-resistant strain of *Staphylococcus aureus* to penicillin and erythromycin was unaffected, indicating that there is no cross-resistance between the morellin (**79**) and the above antibiotics. Both morellin (**79**) and gambogic acid (**77**) were well tolerated by rats at a dose of 40 mg/kg/day for 40 days. However, a dose of 120 mg/kg/day resulted in side effects including decreased growth and reduced blood cell counts [145]. More

recently, scortechinone B (**95**) showed antibacterial activity on methicillin-resistant *Staphylococcus aureus* with an MIC value of 2.0 μg/mL [108].

In addition, the caged *Garcinia* xanthones have received a great deal of attention for their anti-cancer activity. An ever increasing body of evidence indicates that these compounds are cytotoxic against various cancer cell lines at low μM concentrations [103]. For instance, desoxymorellin (**81**) inhibited the growth of HEL (Human Embryonic Lung fibroblasts) and HeLa (Henrietta Lacks cervical cancer) cells with a MIC of 0.39 μg/mL [105, 146]. The bractatins (**89-91**) were cytotoxic against the KB cell line (human epidermoid carcinoma) with 6-*O*-methylneobractatin (**91**) showing the lowest IC_{50} value of 0.20 μg/mL [10, 106]. The gaudichaudiones have been tested against a panel of cell lines, and found to be broadly cytotoxic with effective dose (ED_{50}) values between 0.50 and 8.0 μg/mL [93]. Selected members of the cantleyanone family displayed significant cytotoxicity against breast cancer (MDA-MB-231 and MCF-7), ovarian cancer (CaOV-3), and HeLa cells with EC_{50} values ranging from 0.22 to 17.17 μg/mL [15]. In addition, lateriflorone (**98**) was cytotoxic against the P388 cancer cell line with ED_{50} value of 5.4 μg/mL [111]. In similar studies, gambogic acid (**77**) inhibited the proliferation of T47D and DLD-1 breast cancer cells with GI_{50} values of 0.04 and 0.03 μM, respectively [19]. Similar observations were reported upon screening gambogic acid and related caged *Garcinia* xanthones against a panel of solid and non-solid tumor cells [147].

Of particular interest are the studies on the activity of gambogic acid (**77**) and related xanthones against various drug-resistant cell lines [14, 91]. For example, gambogic acid (**77**) and its C2 epimer, epigambogic acid, displayed similar cytotoxicity against doxorubicin-sensitive (EC_{50} 1.3 μM) and doxorubicin-resistant (EC_{50} 0.9 μM) human leukemia K562 cells in an MTT assay [118]. More recently, gaudichaudione A (**86**) exhibited strong growth inhibitory activity against both parental murine leukemia P388 and P388/doxorubicin-resistant cell lines at low micromolar concentration [148]. Batova and co-workers [147] confirmed these findings and additionally reported that several caged *Garcinia* xanthones displayed the antiproliferative effects against adriamycin-resistant HL-60 cells and the parental HL-60 cell line. These findings indicate that the caged *Garcinia* xanthones are not

subjects of the multidrug resistance mechanisms, often associated with overexpression of P glycoprotein that is typical of relapsed cancers. Thus these compounds represent a pharmacologically promising chemical scaffold [149-150].

3.1.3.2 Mode-of-Action Studies

The induction of apoptosis has been established as one of the main mechanisms of cytotoxicity exhibited by the caged *Garcinia* xanthones in several tumor cells [19, 147]. Both gambogic acid (**77**) [19] and gaudichaudione A (**86**) [148] have been shown to activate caspase 3, a protein that plays a key role in apoptosis [151]. In MGC-803 cells (human gastric carcinoma), apoptosis was induced by gambogic acid (**77**) after 48 h of treatment with an IC_{50} of 0.96 μg/mL [152]. Immunohistochemical studies indicated that gambogic acid (**77**) regulated the levels of Bax and Bcl-2, a family of proteins that play a crucial role during apoptosis [153-155]. Gambogic acid (**77**) increased the expression of Bax and decreased expression of Bc1-2 genes in a variety of cancer cell lines including human gastric cancer cells MGC-803 [155-156], BGC-82 [157-158] and human malignant melanoma A375 cells [159]. Induction of Bax and suppression of Bc1-2 likely contribute to the apoptosis mechanism in these cell lines. Gambogic acid (**77**) was reported to compete with BH3 peptides for binding to the Bcl-2 family of proteins thereby inhibiting the anti-apoptotic activity of these proteins [160]. Gambogic acid (**77**) inhibited binding of BH3 peptides to 6 members of the Bcl-2 family to various extents with IC_{50} values of up to 2.0 μM, while analogues of gambogic acid (**77**) reduced ability to compete with BH3 peptides. However, gambogic acid (**77**) retained some cytotoxicity in $bax^{-/-}/bak^{-/-}$ cells suggesting that this compound has additional targets that contribute to its cytotoxicity.

In addition to the regulation of genes directly associated with apoptosis, a collection of work has revealed that multiple other genes are regulated by gambogic acid (**77**) which may contribute to its anti-cancer activity. For instance, gambogic acid (**77**) enhanced p53 protein expression but, interestingly, exhibited no influence on p53 mRNA synthesis [161-163]. This result is most likely due to the down-

regulation of mdm2, a negative regulator of p53, at both mRNA and protein levels [161].

Telomerase, an important drug target in cancer therapeutics appears to also be a target for gambogic acid (**77**). Gambogic acid (**77**) suppressed telomerase activity in human gastric carcinoma BGC-823 and SGC-7901 cells by multiple mechanisms including transcriptional down-regulation of hTERT *via* c-Myc and post-translational modification of hTERT protein *via* the deactivation of AKT [16, 164]. Suppression of telomerase was also observed in lung cancer SPCA1 cells upon treatment with gambogic acid (**77**) resulting in inhibition of cell proliferation *in vitro* and *in vivo*.

Steroid receptor coactivator 3 (SRC-3), a member of the p160 family of nuclear receptor coactivators, is an important modulator of cell growth and is often over-expressed in cancer cells. Gambogic acid (**77**) was found to decrease the expression of SRC-3 at both the mRNA and protein levels in human lung adenocarcinoma (A549) cells that over-express this receptor coactivator [165-166].This action presumably accounts for the observed inhibition of proliferation by gambogic acid (**77**) in a time- and dose-dependent manner with IC$_{50}$ of 3.17 ± 0.13 μmol/L after 24 h of treatment.

Gambogic acid (**77**) has been found to also affect microtubules. The treatment of MCF-7 breast cancer cells with 2.5 μM with gambogic acid (**77**) caused microtubule cytoskeleton disruption and microtubule depolymerisation [167]. In addition, gambogic acid (**77**) inhibited the catalytic activity of human topoisomerase IIα by binding to its ATPase domain [168].

Evaluation of the anti-leukemic effect of gambogic acid (**77**) led to the observation that nucleoporin Nup88 expression was downregulated in several leukemia cell lines upon treatment with gambogic acid (**77**) [169-170]. In addition, the distribution of Nup88 was altered from widely dispersed in both nucleus and cytoplasm, to that predominantly localized at the cytoplasmic side of the nuclear membrane. These results suggest that regulation of nucleocytoplasmic transport may be important for the anti-cancer effects of gambogic acid (**77**) in leukemia cells.

In addition to modulating cellular processes directly affecting cancer cells, gambogic acid (**77**) appeared an effect on angiogenesis thereby having the ability to affect tumor cells indirectly. Specifically, gambogic acid (**77**) inhibited angiogenesis by suppressing the activity of vascular endothelial growth factor receptor 2 (VEGFR2) and its downstream protein kinases, c-Src, focal adhesion kinase, and AKT [171-172].

The effect of gambogic acid (**77**) in combination with known anticancer drugs has also been reported. Gambogic acid (**77**) could reverse docetaxel resistance in BGC-823/Doc gastric cancer cells [173].Specifically, treatment of these cells with gambogic acid (**77**) at concentrations up to 0.2 μM led to a dramatic increase in docetaxel-induced apoptosis. Analysis of apoptosis-associated genes revealed that gambogic acid (**77**) singly, or in combination with docetaxel, significantly downregulated the mRNA expression of survivin, a protein associated with resistance to apoptosis [173]. A more recent study showed that the anticancer effect of a simultaneous administration of 5-fluorouridine (5-FU) with gambogic acid (**77**) was much greater than that of 5-FU or gambogic acid (**77**) alone [174]. Furthermore, gambogic acid (**77**) was found to regulate the metabolic enzymes involved in 5-FU metabolism. Specifically, gambogic acid (**77**) decreased mRNA levels of thymidine synthetase (TS) and dihydropyrimidine dehydrogenase (DPD), while it increased the mRNA level of orotate phosphoribosyltransferase (OPRT). These findings suggest that this mechanism account for the observed synergistic effect of gambogic acid (**77**) used in combination with 5-FU [174]. These studies attest to the potential of gambogic acid in combination therapies.

The combination of published reports on the anticancer activity of gambogic acid (**77**) clearly indicates that this compound affects several cellular processes and has multiple targets. Gambogic acid (**77**) could bind to transferrin receptor type 1 (TfR1), a membrane-bound protein involved in iron homeostasis [175-176]. Such binding would then induce a unique signal leading to rapid apoptosis of tumor cells [177]. Furthermore, down-regulation of TfR1 in T47D and 293T cells by RNAi, significantly decreased their sensitivity to gambogic acid-induced apoptosis. Further evidence for a role of the TfR in the induction of apoptosis by gambogic acid (**77**) is

the finding that gambogic acid (**77**) potentiated TNF-induced apoptosis in human leukemia cells through modulation of the NF-κB signalling pathway, and that this was dependent on the expression of TfR [178-179]. Down-regulation of TfR by RNAi reversed the effects of gambogic acid (**77**) on NF-κB signalling and apoptosis. Furthermore, gambogic acid (**77**) enhanced the effect of TNF and chemotherapeutic agents in inhibiting the expression of gene products involved in anti-apoptosis, cell proliferation, invasion, and angiogenesis, all of which are known to be regulated by NF-κB. In addition, gambogic acid (**77**) suppressed NF-κB activation induced by various inflammatory agents and carcinogens. Noteworthy however, gambogic acid (**77**) alone had no effect on NF-κB signalling, in contrast to results of other studies [180-181]. These finding suggested that gambogic acid (**77**) inhibited TNF-induced NF-κB signalling and potentiated apoptosis through its interaction with the TfR-1. Although the results of this study indicate that TfR-1 plays a role in potentiating TNF-induced apoptosis, the direct binding of gambogic acid (**77**) to TfR-1 has not been determined. Hence, it is not clear whether TfR-1 is a primary target of gambogic acid (**77**) in this case. Interestingly, gambogic acid (**77**) was equally cytotoxic against CHO (Chinese Hamster Ovary) cells deficient in endogenous TfR1 (TRVb-neo) and those expressing exogenous human TfR1 (TRVb-hTfR1) suggesting that the cytotoxicity of gambogic acid (**77**) is independent of TfR1 [182]. These results clearly indicated that gambogic acid (**77**) have multiple targets, and that binding to TfR1 may or may not be required for the induction of cytotoxic effects, likely depending on the cell context.

More recently, gambogic acid (**77**) was found to induce production of reactive oxygen species (ROS) in human hepatoma SMMC-7721 cells, resulting in the collapse of the mitochondrial membrane potential. This led to the release of Cytochrome *c* and apoptosis-inducing factor from mitochondria, ultimately leading to apoptosis [183]. Moreover, gambogic acid (**77**) elevated the phosphorylation of c-Jun-N-terminal protein kinase (JNK) and p38, downstream effects of ROS accumulation. N-acetylcysteine, an inhibitor of ROS production, partly reversed the activation of JNK and p38 and the induction of apoptosis in cells treated with gambogic acid (**77**). These results indicated that gambogic acid (**77**) induced apoptosis, in part, by activating the cell stress associated MAPK pathway through the production of ROS.

In summary, gambogic acid (**77**) and related molecules appeared to have multiple targets and mechanisms accounting for their cytotoxicity against cancer cells. Likely, the mechanisms involved would depend on the cellular context. Importantly, further work by independent laboratories will be needed to verify the primary target(s) and most relevant key signalling pathways involved in the action of gambogic acid (**77**).

3.1.3.3 Pharmacology and Animal Model Studies

Several studies with gambogic acid (**77**) in animal models have documented its low toxicity and promising chemotherapeutic value. Using a rat glioma model, gambogic acid (**77**) was taken up by brain microvascular endothelial cells (rBMEC) in a time-dependent fashion, indicating that this compound could pass through the blood brain barrier. Furthermore, intravenous (*iv*) injection of gambogic acid (**77**) once a day for two weeks could significantly reduce tumor volume by inhibiting angiogenesis and inducing apoptosis of glioma cells [184]. As such, this study reveals a possible new therapeutic lead in glioma therapy. Using a rat gastric carcinoma model [152], *iv* injection of gambogic acid (**77**) at 6 mg/kg (4 doses on alternate days) did not affect the body weight or white blood cell count of healthy rats, but induced apoptosis of MGC-803 gastric carcinoma cells. These findings support the notion that gambogic acid (**77**) has little toxicity at therapeutic doses and displays significant tumor selectivity.

Further evidence for the tumor selectivity of gambogic acid (**77**) is provided by multiple studies both *in vitro* and *in vivo* [185-187]. For instance, **77** selectively induced apoptosis of human hepatoma SMMC-7721 cells, while it had relatively less effect on human normal embryonic hepatic L02 cells and primary rat hepatic cells [185]. The treatment of mice bearing SMMC-7721 tumors with gambogic acid (**77**) at dosages of 2, 4, 8 mg/kg resulted in 33.1, 50.3 and 64.2% inhibition of tumor growth, respectively, compared with vehicle control. Moreover, gambogic acid (**77**) was more potent than the standard agent cyclophosphamide (66% inhibition of tumor growth at 30 mg/kg). The tumor selectivity of gambogic acid (**77**) may be partly due to its longer retention time in grafted tumor compared to liver, renal, and other organs.

Additional evidence for the tumor selectivity and efficacy of gambogic acid (**77**) in animal tumor models is the finding that gambogic acid (**77**) activated T lymphocytes to induce cancer cell apoptosis in H22 transplanted mice [187]. Hence, the anti-cancer effects of gambogic acid (**77**) appeared to be at two levels including direct effects on tumor cells as well as activation of immune cells against tumor cells.

In a study examining the acute and chronic toxicity in experimental animals, the LD_{50} of gambogic acid (**77**) in albino mice was in the range of 43.18-48.45 mg/kg [188]. The results from the chronic toxicity studies using beagles demonstrated that the toxicity targets were liver and kidney. The innocuous dose was established to be 4 mg/kg after administration to dogs for a total of 13 weeks at a frequency of one injection every other day. This dose was approximately 9.6 (body weight) or 5.1 (body surface area) times the dosage (25 mg/60 kg, every other day) usually recommended for human trials. Similarly, in a chronic toxicity study using Sprague–Dawley rats, oral administration of gambogic acid (**77**) at 120 mg/kg for 13 weeks resulted in damage of the kidney and liver [189]. An innocuous dose was established to be 60 mg/kg upon oral administration for a total of 13 weeks at a frequency of one administration every other day. This dose was approximately 18.0 (body weight) or 9.6 (body surface area) times higher than that of the dose (200 mg/60 kg, every other day) used for human trials [189]. Additional toxicology studies using beagles revealed that doses of gambogic acid (**77**) up to 4 mg/kg administered *iv* had no effect on blood pressure, heart rate, or rate of respiration [190]. However, higher doses of gambogic acid (**77**) in mice could reduce motor coordination in a dose dependent manner. The most significant toxicity effects of gambogic acid (**77**) in this study were the reduction of maternal and fetal body weight as well as inhibition of fetal skeletal development at doses of 15 mg/kg and above. Also of note was the analgesic activity of gambogic acid (**77**) which was hypothesized to be due to the anti-inflammatory properties of gambogic acid (**77**) [190].

The plasma pharmacokinetics, excretion, and tissue distribution of gambogic acid (**77**) were investigated in several recent studies [191]. Gambogic acid (**77**) was not detected in the urine after *iv* administration and was rapidly eliminated from the blood and transferred to the tissues. The tissue distribution of gambogic acid (**77**) was

limited with the highest concentrations found in the liver. Moreover, the majority of gambogic acid (**77**) appeared to be excreted into the bile within 16 h of *iv* administration. In metabolism studies using rat liver microsomes, gambogic acid (**77**) was rapidly converted to 10-hydroxygambogic acid, 9,10-epoxygambogic acid and their glucuronyl derivatives [192-195]. The formation of 10-hydroxygambogic acid *via* Cytochrome P-450 1A2 was found to be crucial for the elimination of gambogic acid (**77**) in rats. Hence, inhibitors of Cytochrome P-450 1A2 can affect the metabolism of gambogic acid (**77**) and its bioactivity. This finding suggests that possible drug-drug interactions may result in combination therapies if Cytochrome P-450 1A2 activity is affected. Moreover, issues related to the stability and tissue distribution of gambogic acid (**77**) can be addressed by developing appropriate delivery platforms. For instance, gambogic acid (**77**)-loaded micelles based on chitosan derivatives showed increased stability and decreased acute toxicity and vein irritation as compared to non formulated delivery of this compound [196-197].

In summary, potent anti-cancer activity, both *in vitro* and *in vivo,* and relatively low toxicity indicate that gambogic acid (**77**) may be an effective chemotherapeutic agent warranting further study in clinical trials. In fact, this compound has entered clinical trials in cancer patients in China [198]. In turn, this suggests that the caged *Garcinia* xanthones and designed analogues thereof have promising clinical potential.

3.1.4   Literature Review on Synthetic Strategies toward the Caged *Garcinia* Xanthones

Due to the impressive combination of unique chemical architecture, intriguing biological activities and good potential in medicine, the chemical scaffold of the caged *Garcinia* xanthones received significant attention as synthetic targets. The synthesis efforts rely on two general strategies for the construction of the caged motif: a tandem Wessely oxidation/Diels-Alder reaction and a sequence of Claisen rearrangements and Diels-Alder reaction.

3.1.4.1. Tandem Wessely Oxidation/Diels-Alder Reaction

Wessely and co-workers was the first group who reported tetracetate-mediated oxidation of phenols leading to the formation of *o*-benzoquinones in 1950s [199-201]. In the presence of dienophiles and the resulting dienes, it could then conveniently perform *via* Diels-Alder cycloaddition reaction in order to give tricyclic motifs. In 1972, Yates and co-workers applied this reaction for obtention of compounds related to the structures of the caged *Garcinia* xanthones (Scheme 3.4). Therefore, Wessley oxidation of phenol **119** with Pb(OAc)₄ in acetic acid produced 2,4-cyclohexadienone **120**, which followed by heating at 140 °C formed compound **121** (gambogic acid numbering) [202]. Subsequent study of the treatment of xanthene **122** with lead tetraacrylate (formed *in situ* by Pb(OAc)₄ and acrylic acid) produced dienone **123**, and after an intramolecular Diels-Alder reaction of the resulting dienone gave caged compound **124** [203].
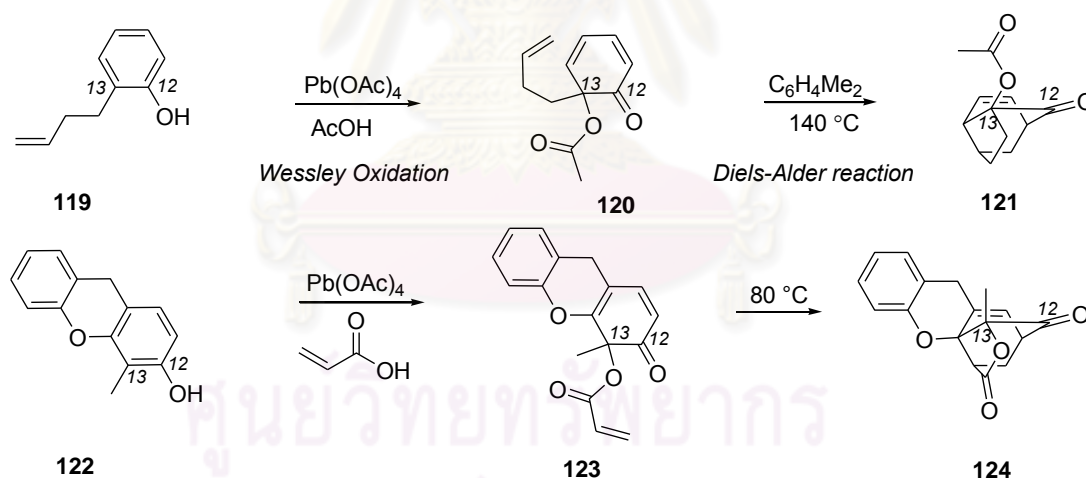
Scheme 3.4 Representative examples of caged structures **121** and **124** formed *via* a Wessely oxidation/Diels-Alder reaction cascade

Theodorakis and co-workers [204] in 2002 applied this strategy to the synthesis of a more hydroxylated caged motif concerned with the synthesis of lateriflorone (**98**) (Scheme 3.5). Treatment of **125** with Pb(OAc)₄ in acrylic acid/CH₂Cl₂ and then heated in refluxing benzene (80 °C) afforded tricyclic lactone **127** in 82% combined yield. Crystallographic studies confirmed that **127** is a

constitutional isomer of desired structure **130** and is defined as the so-called neo caged structure.

The connectivity of compound **127** suggested that upon the Wessely oxidation of phenol **125**, the acrylate unit migrated onto the more electronically rich C11 instead of its migrating onto the desired C13 carbon. This led to the formation of adduct **127** after Diels-Alder cycloaddition of dienone **126** with the pendant acrylate dienophile. However, the desired caged motif **130** could be successfully achieved by installing the acetoxy group at the C13 presented in compound **128**, resulting in the preferential migration of prenyl group took place at C13 to produce intermediate **129**. Along these lines, Claisen rearrangement and Diels-Alder cycloaddition of allyl ether **128** in *m*-xylene (140 °C) gave rise exclusively to caged motif **130**.
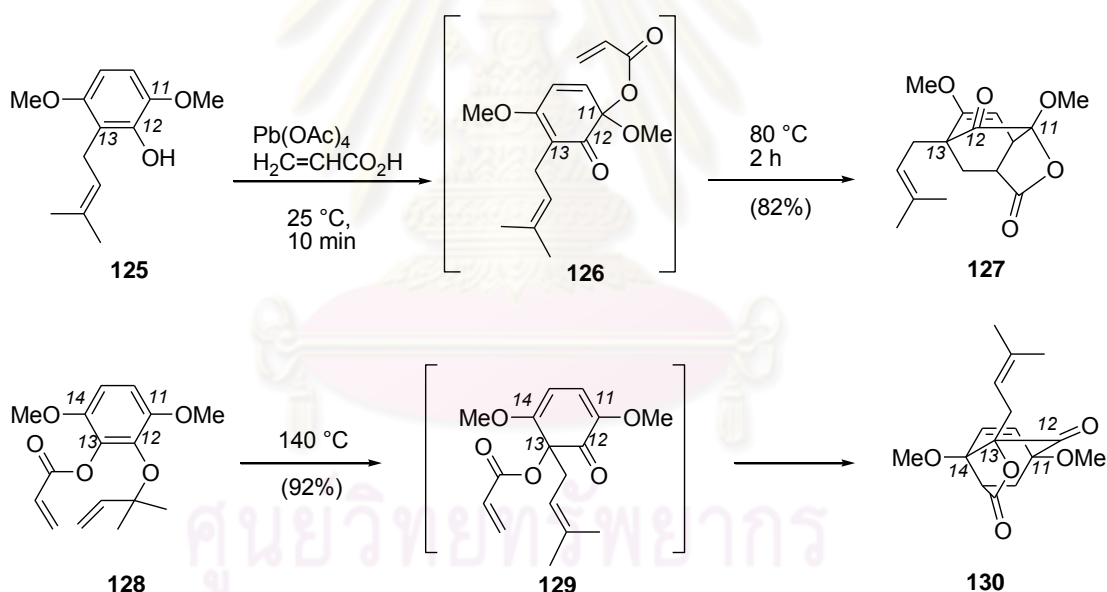
Scheme 3.5 Synthesis of caged structures **127** and **130**

The tandem Wesseley oxidation/Diels-Alder sequence was revived recently by Metha and co-workers (Scheme 3.6) [205].
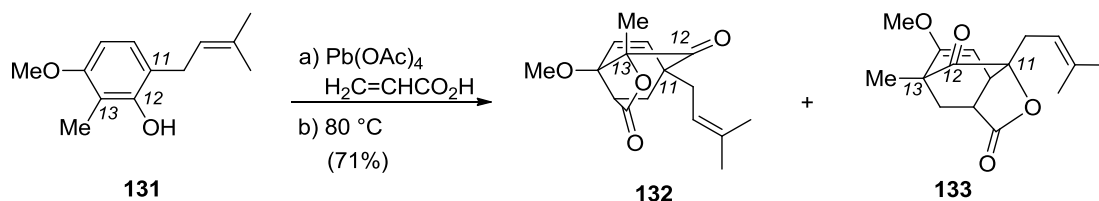
Scheme 3.6 Synthesis of caged structures **132** and **133**

Phenol **131** was subjected to lead tetraacrylate followed by heating in refluxing benzene produced a mixture of two caged structures **132** and **133**, reminiscent of the regular and neo caged motifs respectively, in 1:1 ratio and 71% combined yield. In this case, the acrylate addition proceeds at both C11 and C13 with low selectivity due to their similar electronic density.

3.1.4.2. Tandem Claisen/Diels-Alder Reaction

The Tandem Claisen/Diels-Alder reactions for the preparation of cage scaffolds have been extensively carried out in many research groups. Inspired by the Quillinan and Sheinman proposed biosynthesis, Nicolaou and Li evaluated the tandem Claisen/Diels-Alder sequence for the conversion of *bis*-allylated coumarin **135** to a caged scaffold (Scheme 3.7) [132]. In principle, two competing migrations can occur during the initial Claisen rearrangement of **135** to form intermediates **136** and **137** (path A and path B). Each one of these intermediates can participate in two intramolecular Diels-Alder reactions with the coumarin core producing compounds **138-141** in 91% combined yield after heating of **135** at 125 °C (Scheme 3.7).
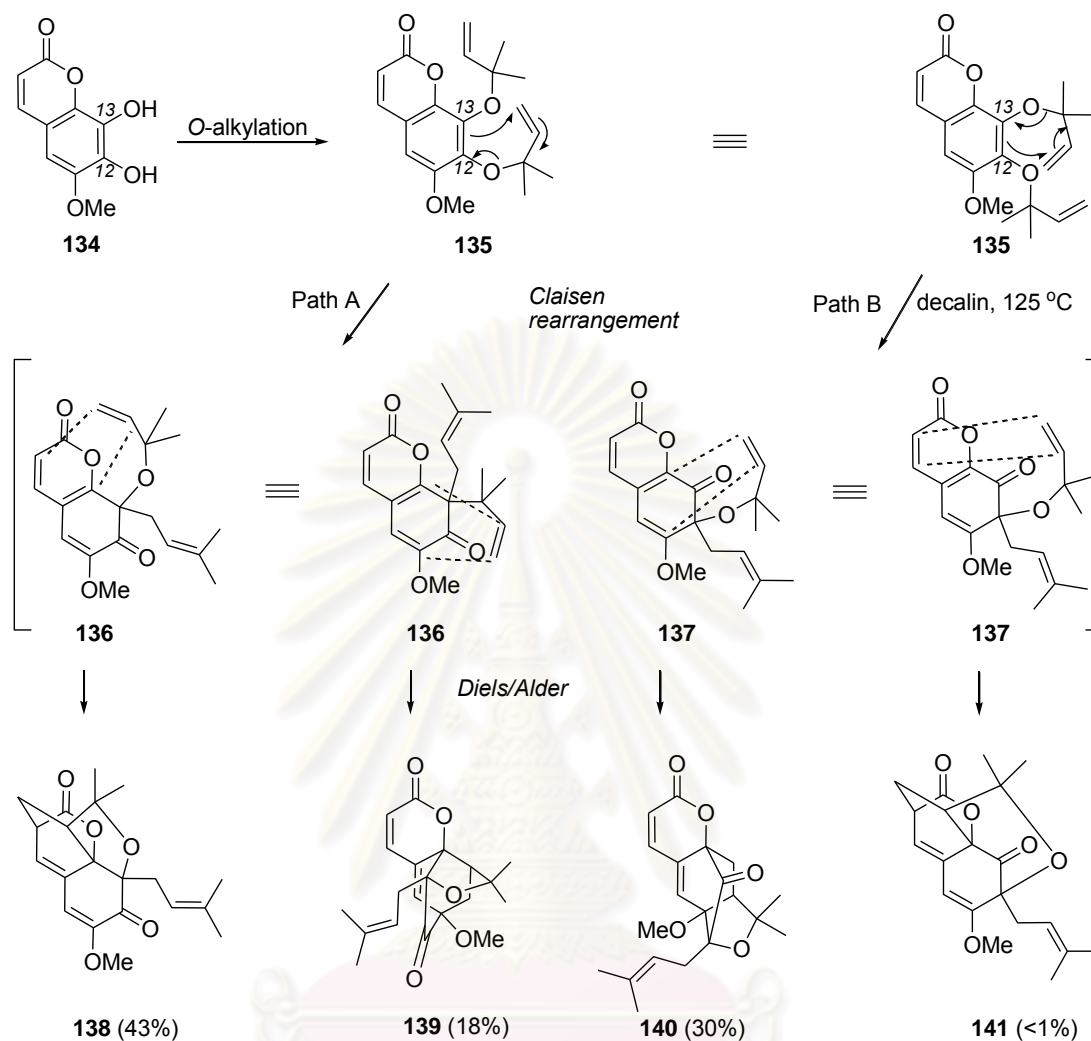
Scheme 3.7 Model studies on the Claisen/Diels-Alder reaction cascade with prenylated coumarin **135**

Application of this approach to the synthesis of forbesione (**83**) [132] and lateriflorone (**98**) [206-207] provided further support for the Quillinan-Scheinmann biosynthetic hypothesis. For example, heating of allyl ether **142** at 120 °C produced a 1:1 mixture of **143** and **144** and in 89% combined yield (Scheme 3.8) [208]. The carbon connectivity of these products corresponded to this of the regular and neo caged scaffolds and indicated that, under these conditions, the Claisen rearrangement proceeds with no significant site selectivity. Interestingly, heating of compound **145** to 110 °C proceeded *via* a selective Claisen rearrangement to form dienone **146** that after the Diels-Alder cycloaddition afforded exclusively the regular caged structure **147** (85% isolated yield) [207]. Comparison of these results suggests that the

selectivity of the opening Claisen rearrangement can be controlled by the electronic density of the C8 carbon. It is reasonable to postulate that the C8 carbonyl group, being para to the C12 allyloxy group, facilitates its Claisen migration at the C13 center.
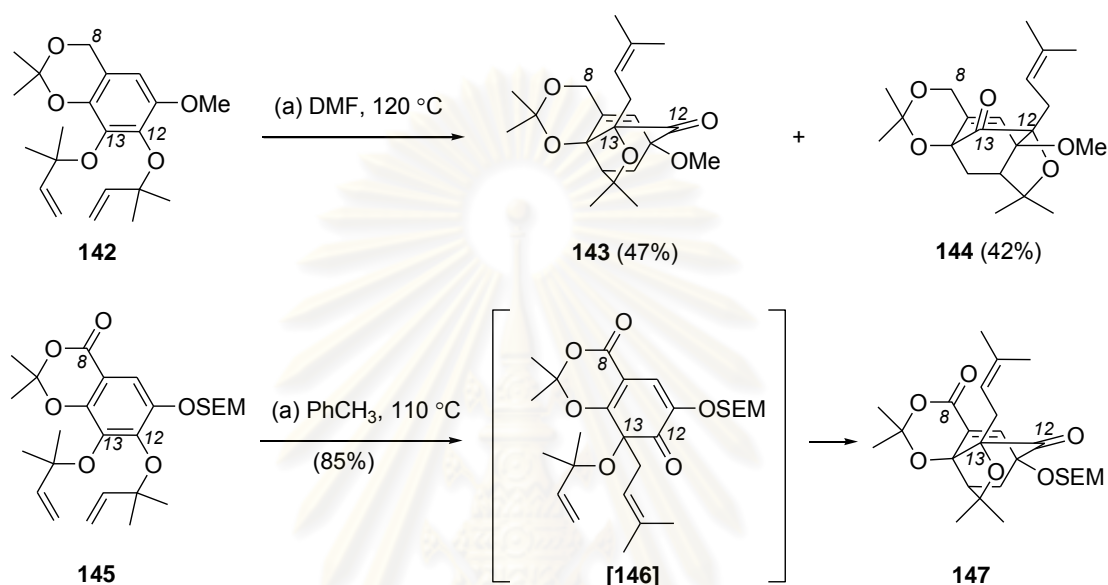
Scheme 3.8 Construction of caged structures **143, 144** and **147** *via* a biomimetic Claisen/Diels-Alder reaction cascade

Parallel studies by the Nicolaou [132] and Theodorakis [209] laboratories evaluated the possibility to synthesize forbesione (**83**) in one pot using *tris*-allylated xanthone **148** as the starting material (Scheme 3.9). In principle, exposure of such motif to heat could produce four products arising from a combination of two competing C-ring Claisen/Diels-Alder reactions (producing regular and neo caged structures) and two competing A-ring Claisen migrations (producing C17 and C5 prenylations). Working with methoxy xanthone **149c** (R= Me), the Nicolaou group was the first to describe its conversion to methyl forbesione (**149c**) and methyl neoforbesione (**150c**) in a 2.4:1 ratio and 89% combined yield [132]. On the other hand, studies by the Theodorakis group showed that heating of xanthone **148a** to 120 °C led only to isolation of forbesione (**83**) and isoforbesione (**151a**) in 84% combined yield. The neo C-ring isomers **150a** and **152a** were not detected in this case. More impressively, the 6-*O*-acetylated xanthone **148b** afforded, upon heating

solely acetyl forbesione (**149b**, 79% isolated yield) [209]. Similar observations have recently been reported by other groups [210].
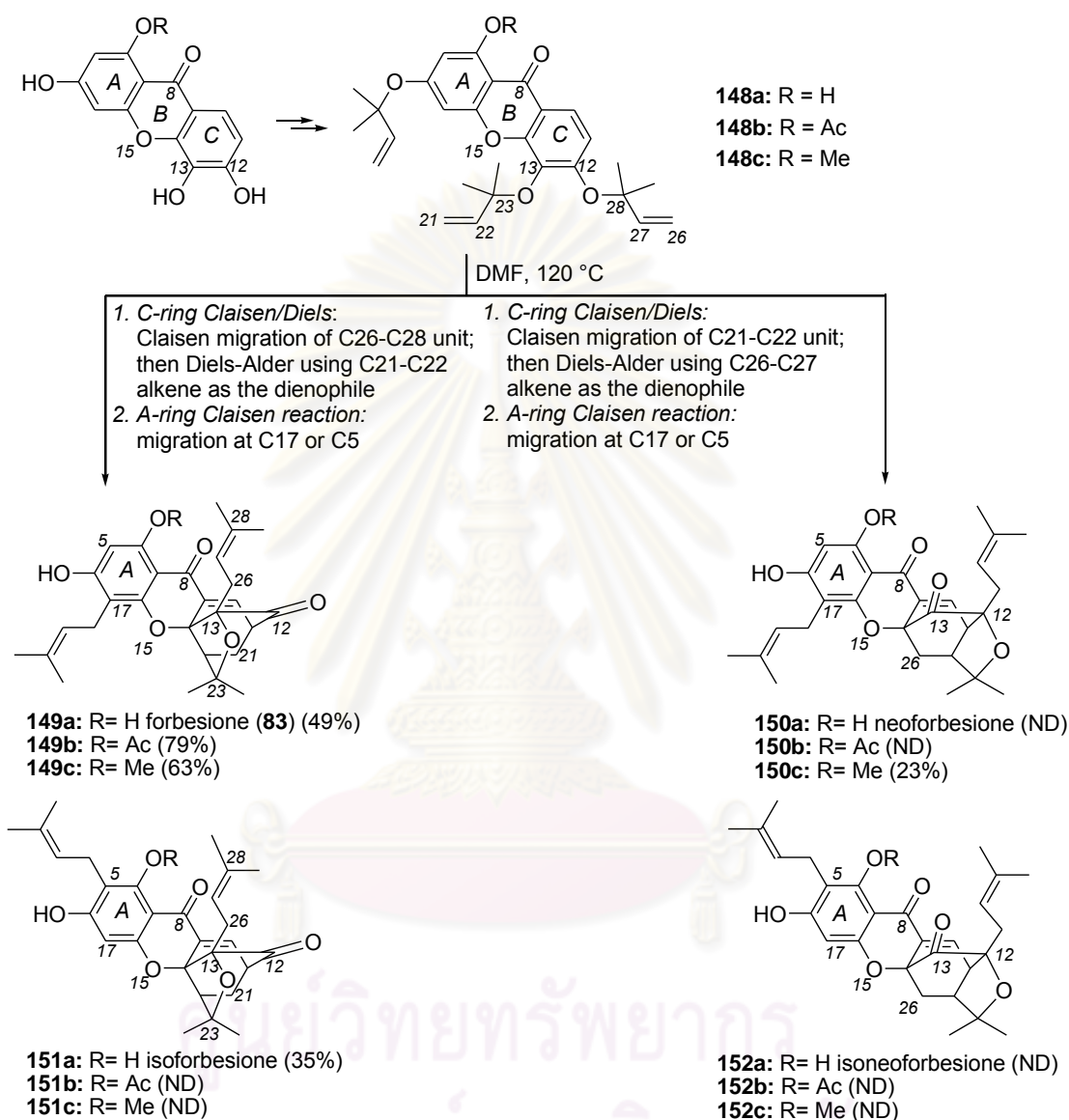
Scheme 3.9 Biomimetic synthesis of forbesione (**83**) and related structures *via* a Claisen/Diels-Alder/Claisen reaction cascade

Several model studies were designed to rationalize these findings [133].The results can be summarized as follows:

i. the C-ring Claisen/Diels-Alder rearrangement proceeds first and is followed by the A-ring Claisen reaction;

ii. the site-selectivity of the A-ring Claisen rearrangement (C5 *vs* C17 prenylation) is controlled by the steric and electronic effects of the C6 phenolic substituent;

iii. the site-selectivity of the C-ring Claisen/Diels-Alder reaction is attributed to and governed by the electronic density of the C8 carbonyl group. Being *para* to the C12 allyloxy unit, the electronically deficient C8 carbonyl carbon polarizes selectively the O-C28 bond and facilitates its rupture. In turn, this leads to a site-selective Claisen rearrangement of the C12 allyloxy unit onto the C13 center, thereby producing exclusively the regular caged motif found in the structure of forbesion (**83**);

iv. the substitution of the C6 phenol can regulate the electronic density of the C8 carbonyl group and thus affect the site selectivity of the C-ring Claisen/Diels Alder reaction.

The experimental findings on the tandem Claisen/Diels-Alder/Claisen reaction cascade provide useful insights regarding the biosynthesis of all known caged *Garcinia* xanthones [133]. As shown in Figure 3.2, all natural products share a common caged motif except 6-*O*-methylneobractatin (**91**) that contains the neo caged motif. The remote electronic effects of the seemingly innocuous 6-*O*-methyl group may explain the concomitant biosynthesis of both 6-*O*-methylbractatin (**90**) and 6-*O*-methylneobractatin (**91**).

Recent studies by the Nicolaou group have shown that the Claisen/Diels-Alder reaction can be accelerated in the presence of polar solvents [211]. For instance, the conversion of allyl ether **153** to caged structure **154a** and its neo isomer **154b** (structure shown in Scheme 3.13) was dramatically accelerated upon changing the solvent from benzene (100 °C, 4 h, 0%) to DMF (100 °C, 2 h, 75%) to a 1/2 mixture of MeOH/water (100 °C, 0.5 h, 100%) (Scheme 3.10).
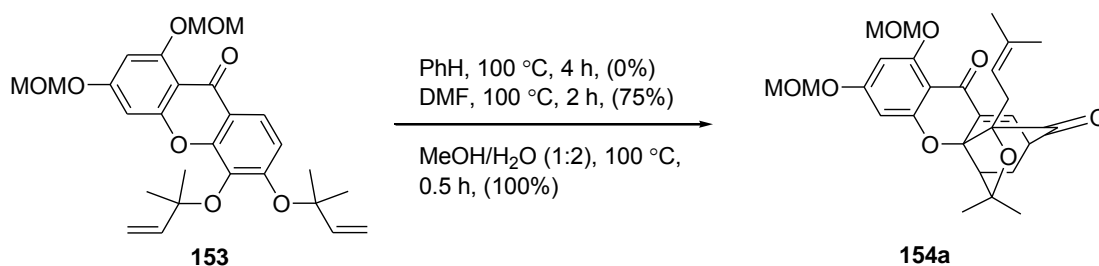
Scheme 3.10 Solvent effect on the rate of the Claisen/Diels-Alder reaction cascade

It has been proposed that polar aprotic solvents, such as DMF, and more impressively protic solvents, such as water, can accelerate the Claisen rearrangement by stabilizing its polar transition state [212-213]. The concurrent acceleration of the Diels-Alder component of this cascade is likely due to the hydrophobic effect of water [214] rather than to a polarity or hydrogen-bonding phenomena [215-217]. Computational studies on the reaction depicted in Scheme 3.10 have also concluded that the Claisen rearrangement is reversible and the energetics of the irreversible Diels-Alder cyclization can determine the product formation [218].

3.1.5. Literature Review on Synthesis of Selected Caged *Garcinia* Xanthones

3.1.5.1 Biomimetic Synthesis of 6-*O*-Methylforbesione (149c)

Developed by Nicolaou and Li [132], the synthetic strategy toward 6-*O*-methylforbesione is highlighted in Scheme 3.11. Construction of xanthone **157** proceeded in 5 steps: (a) coupling of the lithium salt of **155** with aldehyde **156**; (b) deprotection of the C14 silyl ether; (c) oxidation of the C8 alcohol; (d) cyclization of the C14 alkoxy group; and (e) deprotection of the C12 and C13 benzyl ethers (78% combined yield). Treatment of **157** with α-bromoisobutyraldehyde (**158**) and *t*-BuOK followed by Wittig olefination produced a mixture of **159a** and **159b** that, after reiteration of the alkylation/olefination steps, gave rise to *tris*-prenylated xanthone **148c** in 55% combined yield. Heating of **148c** in DMF at 120 °C for 20 min induced the anticipated Claisen/Diels-Alder/Claisen reaction and produced compound **149c** together with its neo isomer **150c** in 89% combined yield.
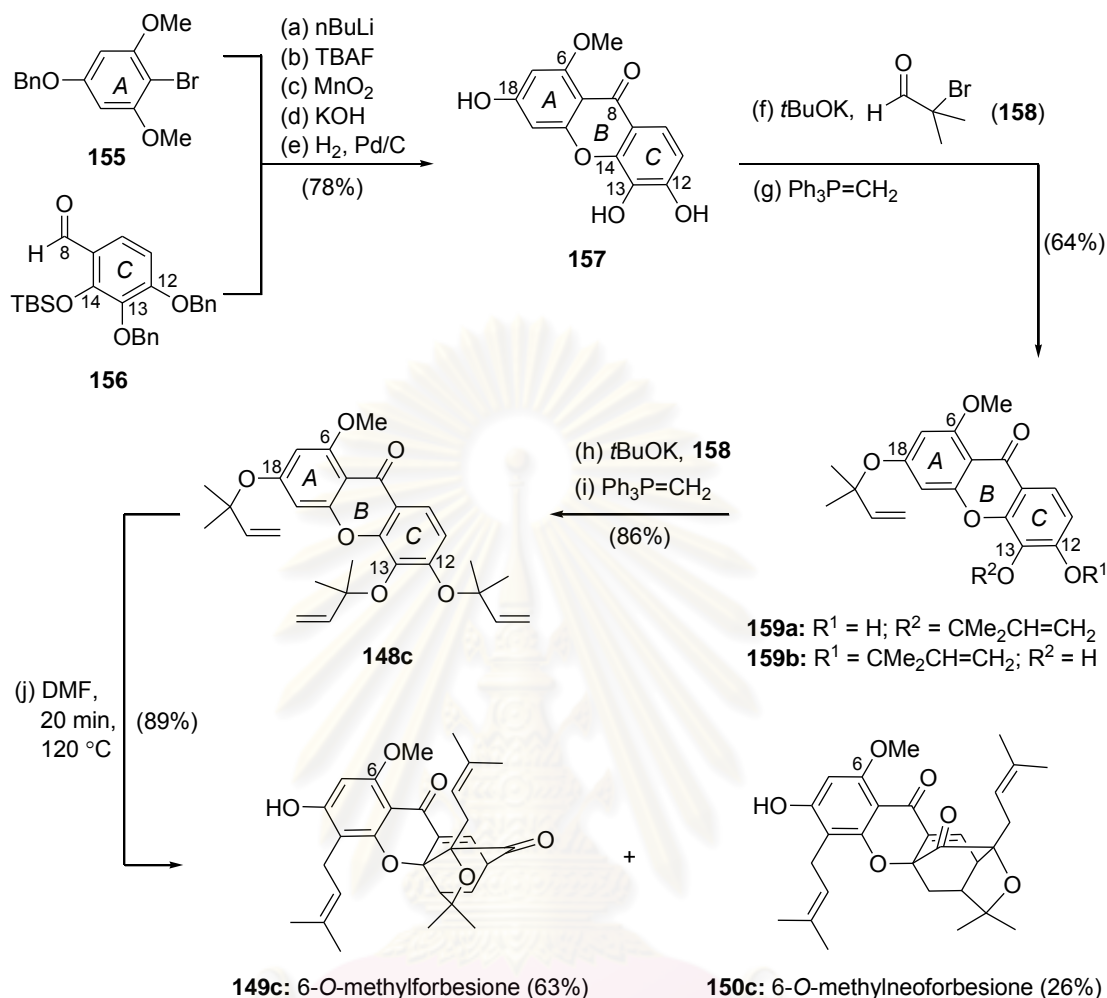
Scheme 3.11 Biomimetic synthesis of 6-*O*-methylforbesione (**149c**)

3.1.5.2 Unified Synthesis of Caged *Garcinia* Xanthones

The common structural features of several caged *Garcinia* natural products (see Figure 3.2) suggest that these compounds can be synthesized by decorating the A ring of forbesione (**83**). Such a strategy, developed by the Theodorakis"s group, uses forbesione (**83**) as a node in a unified synthesis of representative members of the gaudichaudiones, morellins and gambogins [133]. Scheme 3.12 highlights this plan. $ZnCl_2$-mediated condensation of phloroglucinol (**160**) with benzoic acid **161** produced xanthone **157** in 46% yield. Propargylation of **157** with propargyl chloride **162** followed by partial reduction of the alkyne units and acetylation of the C6 phenol formed compound **148b** in 16% combined yield.
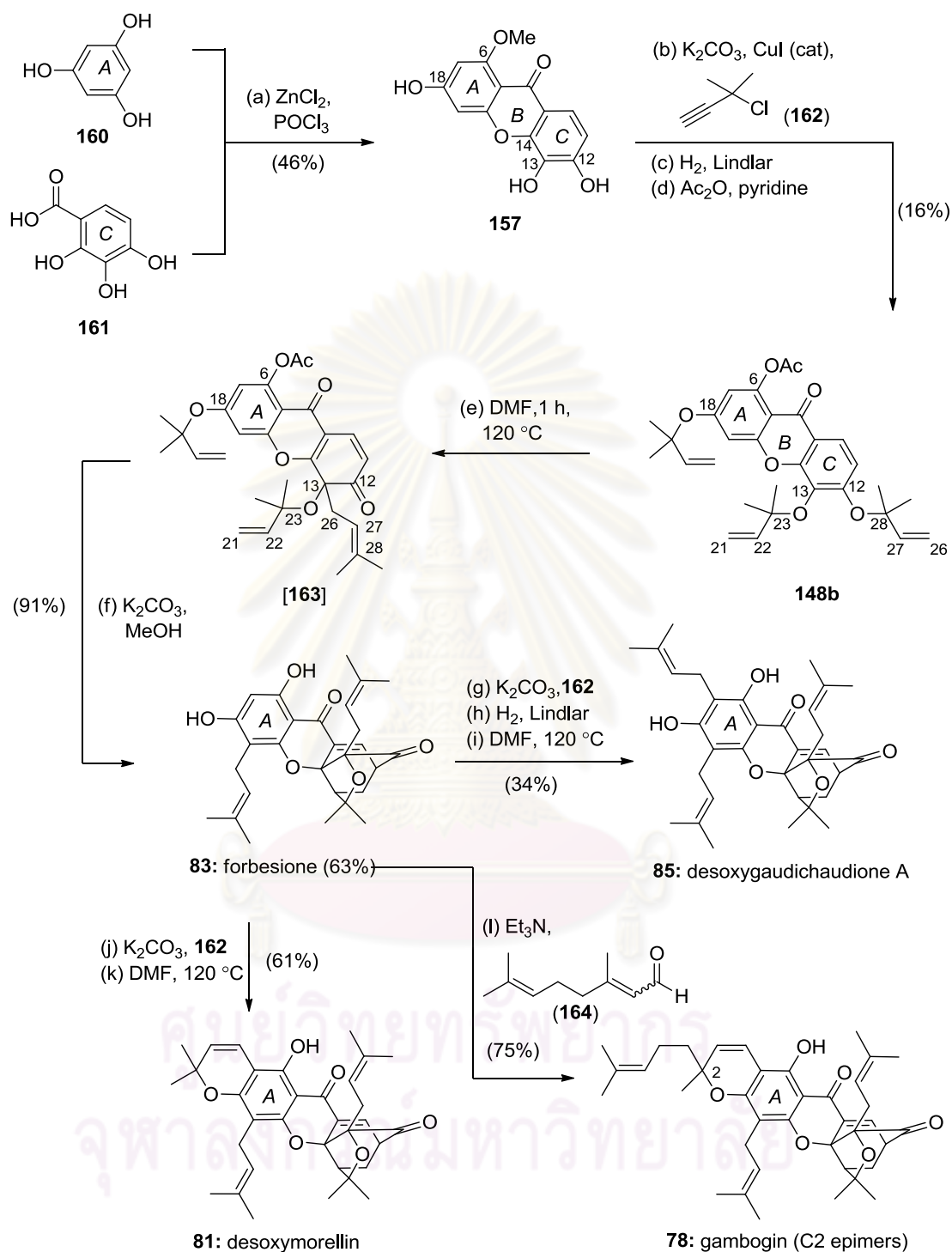
Scheme 3.12 Unified biomimetic synthesis of caged *Garcinia* xanthones

The Claisen/Diels-Alder/Claisen reaction cascade gave rise, after deacetylation, forbesione (**83**) in 72% combined yield. Propargylation of the C18 phenol with chloride **162** afforded, after Lindlar reduction and Claisen rearrangement

desoxygaudichaudione A (**85**) in 34% yield. On the other hand, propargylation and Claisen rearrangement of forbesione formed desoxymorellin (**81**) in 61% combined yield. In a similar manner, condensation of **83** with citral (**164**) in Et$_3$N produced gambogin (**78**) in 75% overall yield.

3.1.5.3 Synthesis of Gambogin (78)

An alternative synthesis of gambogin (**78**) has recently been reported by the Nicolaou group (Scheme 3.13) [211]. The plan involved construction of partially protected xanthone **166**, available in 5 steps from coupling of bromide **165** with aldehyde **156** (44% overall yield). Two rounds of alkylation with α-bromoisobutyraldehyde (**158**) and Wittig olefination produced compound **153** in 42% combined yield. The Claisen/Diels-Alder reaction proceeded in quantitative yield in refluxing MeOH/H$_2$O (1/2) to form regular caged motif **154a** together with the neo isomer **150b** in a 3:1 ratio. MOM deprotection of **154a** followed by propargylation with **168a** at the C18 center and Lindlar reduction afforded compound **169** in 48% combined yield. This compound was then converted to gambogin (**78**) *via* a sequence of steps that involved: acetylation of the C6 phenol, Claisen rearrangement to install the prenyl group at the C17 center, propargylation of the resulting phenol with alkyne **170** and Claisen rearrangement to form the dihydropyran ring of the natural product (12% over 4 steps).
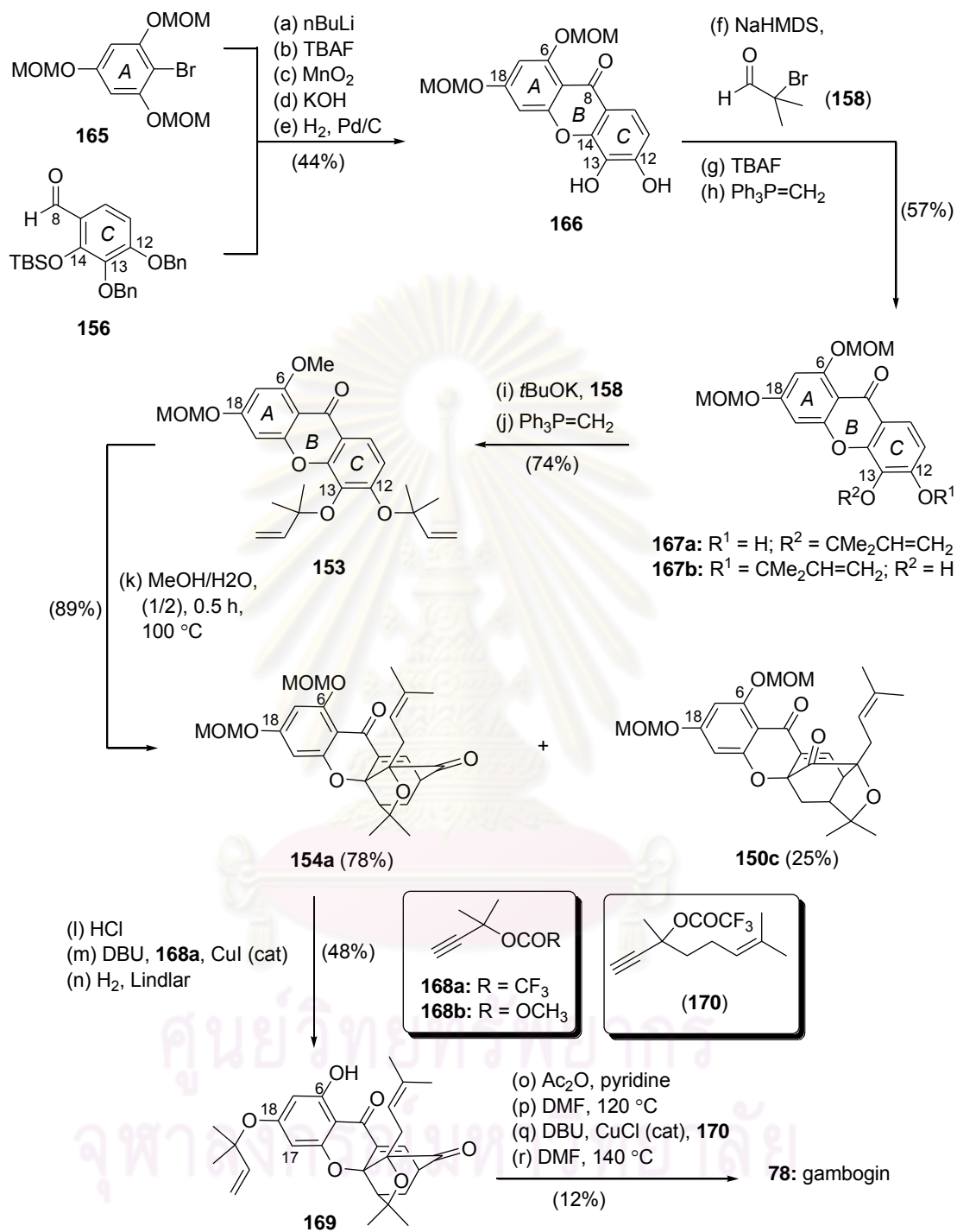
Scheme 3.13 Biomimetic synthesis of gambogin (**78**)

3.1.5.4 Studies toward the Synthesis of Lateriflorone (98)

It has been proposed that the unprecedented spiroxalactone motif of lateriflorone (98) could be formed by condensation of two fully functionalized fragments 171 and 172 (Scheme 3.14). An alternative and likely more biosynthetically relevant hypothesis, could involve conversion of xanthone 173 to dioxepanone 174 that, upon hydrolysis and spirocyclization at the C16, could form the spiroxalactone ring system of lateriflorone.
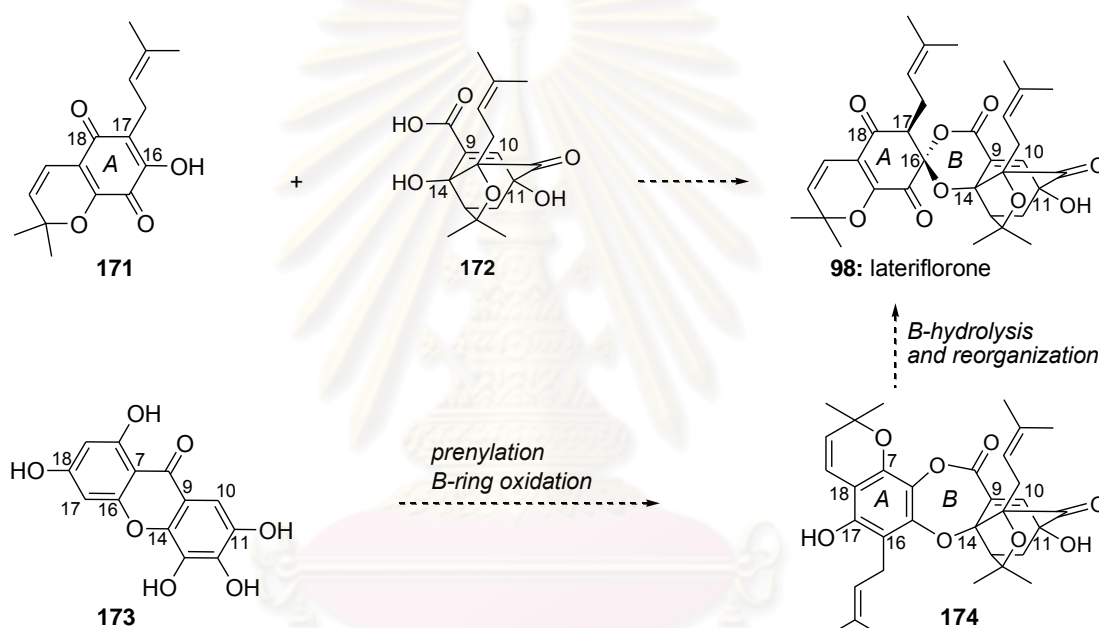
Scheme 3.14 Synthetic plans toward lateriflorone (98) based on biogenetic scenarios

The Theodorakis group has reported an approach toward the synthesis of quinone 171 representing the A ring of lateriflorone (Scheme 3.15) [219]. A sequence of six steps was used to convert phloroglucinol (160) to chromanol 175 that, upon propargylation with 168b, Lindlar reduction and Claisen rearrangement, gave rise to phenol 176 (32% combined yield). Oxidation of 176 at the C7 center using Fremy"s salt and deprotection of the MEM ether then formed chromenequinone 171 in 66% combined yield.
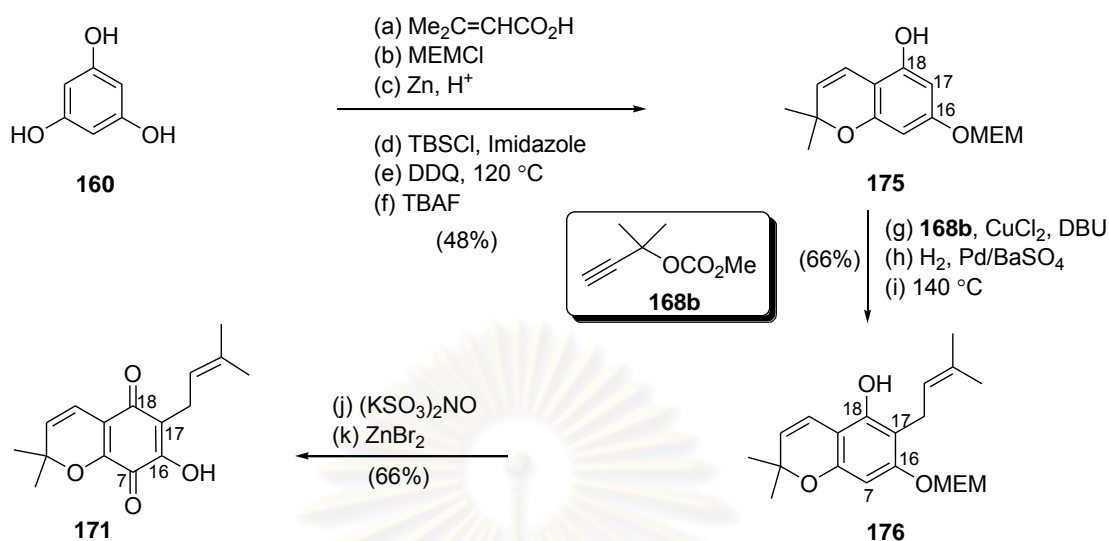
Scheme 3.15 Synthesis of chromenequinone **171**

The synthesis of caged motif **172** and its coupling with quinone **171** are summarized in Scheme 3.16. 4-hydroxysalicylic acid (**177**), containing only two of the four hydroxy groups needed, was selectively brominated at the C11 center and then converted to benzopyran **178** (50% combined yield). Oxygenation at the C11 center *via* the intermediacy of a boronic acid, followed by oxygenation and reverse prenylation at the C13 center, produced compound **145** [207]. A site-selective Claisen/Diels-Alder reaction gave rise, after deprotection, to desired fragment **172** (45% combined yield). Coupling of **171** with **172** then produced secolateriflorone (**180**) that did not undergo the desired spiroxalactonization reaction.
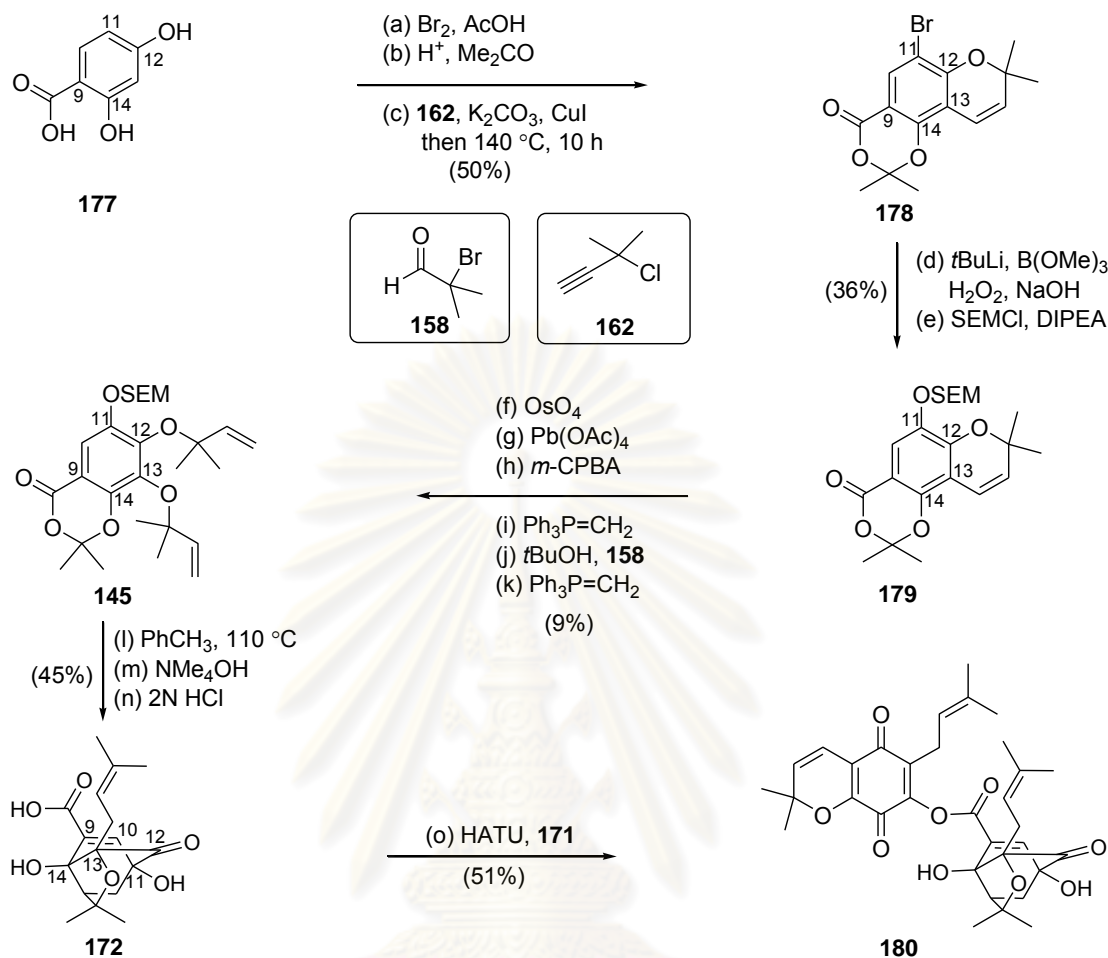
Scheme 3.16 Synthesis of secolateriflorone (**180**)

More recently, the Nicolaou group has reported a synthesis of C11-methyllateriflorone (**186**) (Scheme 3.17) [220]. Key to the strategy was the coupling of orthogonally protected hydroquinone **181** with acid **182** that after selective deprotection of the C7 MOM ether produced compound **183** (61% combined yield). Oxidation of **183** in the presence of iodosobenzene *bis*(trifluoroacetate) in CH_3OH, followed by heating under acidic conditions formed spiroxalactone **185** in 42% combined yield. Acid-catalyzed hydrolysis of **185** gave rise to C11-methyllateriflorone (**186**) in 66% yield.
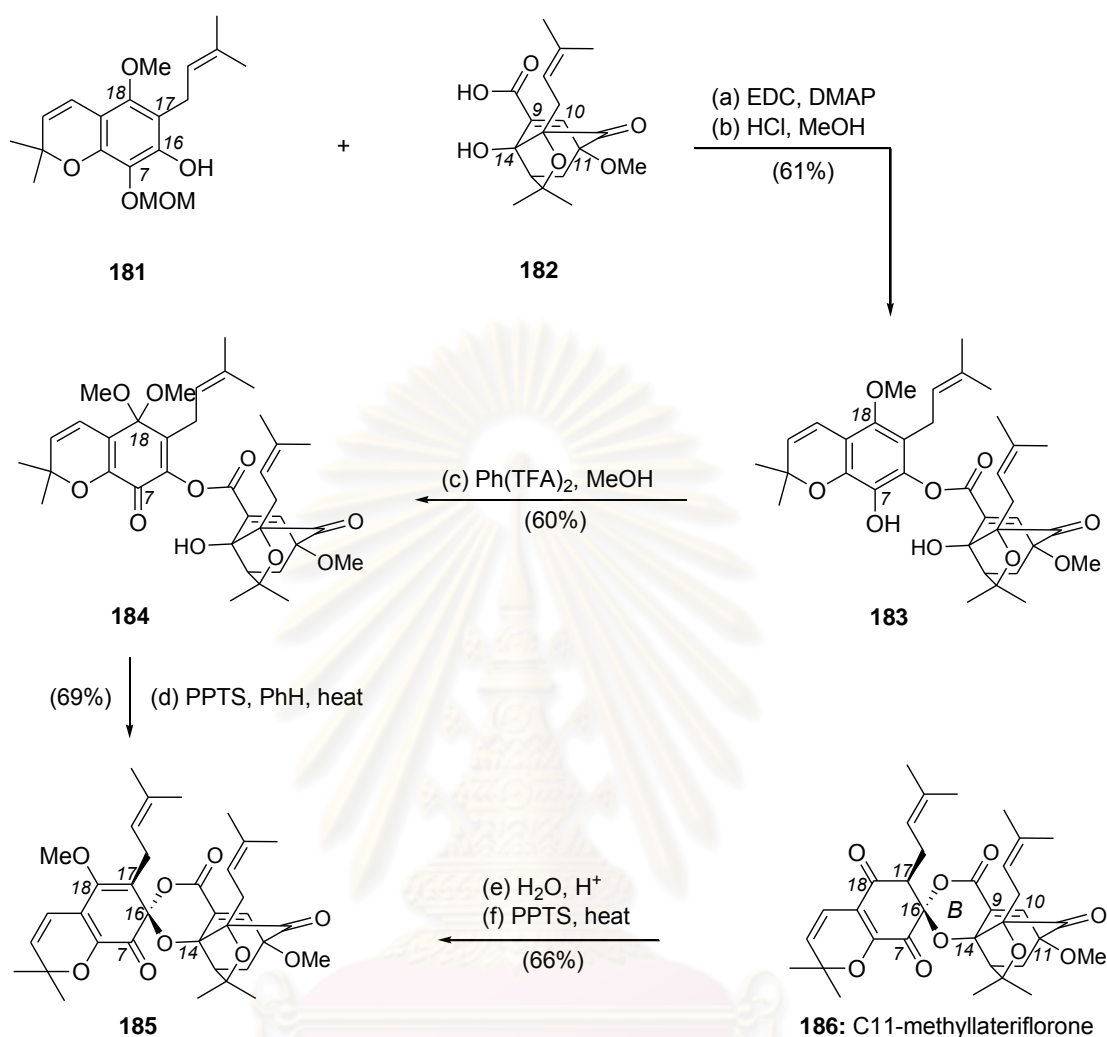
Scheme 3.17 Synthesis of C11-methyllateriflorone (**186**)

3.1.6. Structure-Activity Relationship Studies

The underexplored chemical structures and promising biological activities of the caged *Garcinia* xanthones have fuelled several structure-activity relationship studies. The majority of this effort has been focused on the evaluation of derivatives of gambogic acid (**77**). Early SAR studies showed that the carboxylic acid of gambogic acid (**77**) can be functionalized with groups that modulate the solubility and selectivity properties of the parent molecule without affecting substantially its bioactivity [19]. For example, 2-ethoxyethyl-gambogamide (**187**) [221] and glycine conjugate **188** [222] exhibited comparable antitumor efficacy but improved water solubility as compared to gambogic acid (**77**) (Scheme 3.18). More recently, studies

with neurons showed that gambogic amide **189** can bind to and activate tyrosine kinase A (TrkA) by promoting its dimerization and autophosphorylation. Furthermore, this compound prevented neuronal cell death and provokes prominent neurotrophic activity [223]. Under the same conditions, gambogic acid failed to induce TrkA phosphorylation. The carboxylic acid has also been used for the incorporation of biotin and related probes, such as in compound **190**, in an effort to identify the cellular target of gambogic acid [19].
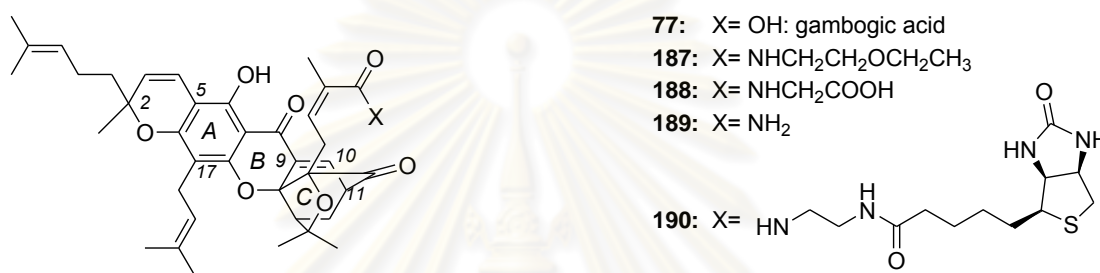
Scheme 3.18 Selected structures of gambogic acid conjugates

The oxidation and/or epoxidation of the prenyl groups of gambogic acid could lead to analogues with improved solubilities and cytotoxicities [224-226]. On the other hand, the caged core of gambogic acid (**77**) was needed for bioactivity since regular xanthones displayed reduced cytotoxicities [227-228]. More importantly, the α,β-unsaturated motif of gambogic acid was critical to its bioactivity and metabolic stability. In fact, conjugate reduction of the C9-C10 double bond, forming compounds **191** and **192**, decreased by more than two orders of magnitude the cytotoxicity of the parent molecule (Scheme 3.19) [19]. A similar decrease in activity has been recorded for compounds **100** (gambogoic acid) and **193** [103, 113]. These compounds have been identified upon prolonged storage (one week at room temperature) of gambogic acid in MeOH and EtOH respectively. Moreover, the C10 hydroxygambogic acid (**194**) was identified as one of the main metabolites of gambogic acid (**77**) formed *in vivo* in rat bile [192].These findings indicate that gambogic acid and related caged *Garcinia* xanthones could exert their bioactivities by reacting in cells as conjugate electrophiles across the C9-C10 enone motif.
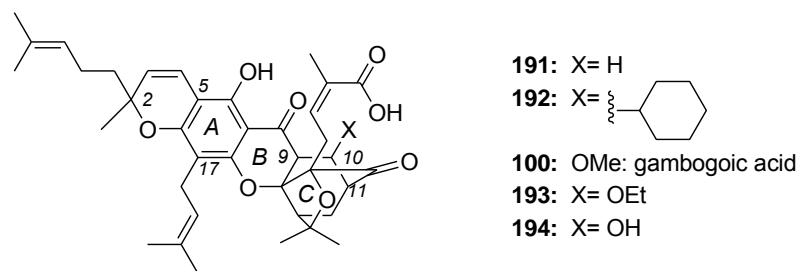
Scheme 3.19 Selected structures of gambogic acid derivatives containing functionalities at the C9-C10

An application of the strategy relies on a biomimetic Claisen/Diels-Alder/Claisen reaction cascade to the synthesis of simplified analogues of gambogic acid and their pharmacological evaluations has been explored in a few manners.

The cytotoxic activities against several cancer cells *in vitro* by MTT method of chromone and xanthone, a simple complex skeleton of gambogic acid, with planar ring were examined. The SAR of synthesized compounds indicated that the prenyl groups and the bridge-core in gambogic acid seemed to be very important for its antitumor activity [227].

Three types of caged 4-oxa-tricyclo[4.3.1.0^{3,7}]dec-8-en-2-one core based on xanthone, 2-phenylchromene-4-one and benzophenone were recently synthesized through a Claisen/Diels-Alder reaction cascade to study SAR of gambogic acid in T47D (human breast cancer cells), HCT116 (human colon cancer cells) and SNU398 (hepatocellular carcinoma cancer cells) cell lines, measured by caspase-based HTS assay (Scheme 20) [229]. Regular caged compound **196** was about three to four times less active than gambogic acid in T47D and HCT116 cells, and about as active as gambogic acid in SNU cells, indicating that compound **196** displayed good apoptosis inducing activity. This result was corresponded to the previous works [147]. The simple structure of **199** was found to be about 10 times less active than gambogic acid (**77**) as an apoptosis inducer in HCT116 and SNU398 cells. This finding was returned to confirm the previous works [147], showing that the appearance of methyl groups at C23 and C28 may be significant

for apoptosis inducing activity. The reduction of **199** at C9-C10 double bond with L-selectride, its activity disappeared with the ED_{50} value up to 20 μM in all three cell lines. This result was similar to the previous reported SAR of gambogic acid (**77**) [19].
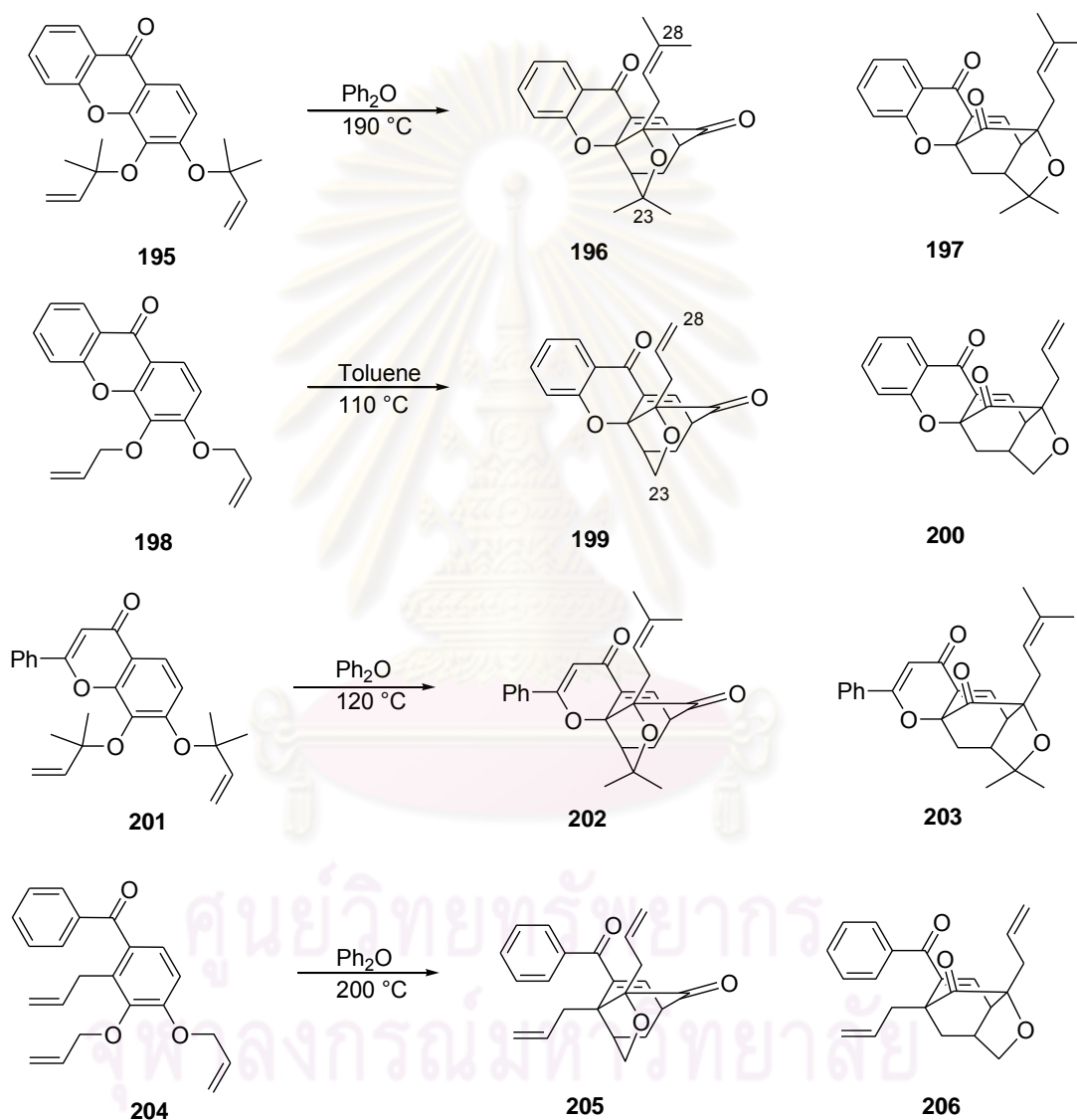
Scheme 3.20 Selected caged structures used to evaluate the minimum pharmacophore of the caged *Garcinia* xanthones

Interestingly, the 4-phenylchromene-2-one based compound **202** was found to be only about 2-fold less active than **196**, indicating that the 6-phenylpyran-4-one ring in **201** can be used to replace the chroman-4-one ring in **196**. Thus the

tetracyclic pyran–xanthone structure of gambogic acid (**77**) can be minimized to a bicyclic chromen-4-one structure and still maintain some of its apoptosis inducing activity. In addition, the neo-isomer **197, 200** and **203** were about as active as their regular caged isomers in inducing apoptosis, suggesting that the regular caged structure may be important for activity, and the positions of the caged structure fused with the bicyclic chroman-4-one may not be critical for activity. On the other hand, the benzophenone-based compound **206** and its neo-isomer **205** were found to be inactive up to 20 μM in all the three cell lines, suggesting that a bicyclic structure such as that in **202** might be the minimum to maintain the apoptosis inducing activity of gambogic acid (**77**). However, those compounds were still active in the growth inhibition assay.

3.2 Experimental

3.2.1 Chemicals, Instruments and Equipment

Gambogic acid (**77**), Pd(PPh$_3$)$_4$, and 2-fluorobenzoic acid (**C17**) were purchased from Gaia Chemical Corporation (Gaylordsville, CT), Strem Chemicals, Inc. (Newburyport, MA), and TCI America (Portland, OR), respectively. Biotin ethylenediamine hydrobromide and BODIPY FL EDA were purchased from Invitrogen (Carlsbad, CA). The rest of the reagents were obtained (Aldrich, Acros) at highest commercial quality and used without further purification except where noted. Air- and moisture-sensitive liquids and solutions were transferred *via* syringe or stainless steel cannula. Organic solutions were concentrated by rotary evaporation below 45 °C at approximately 20 mmHg. All non-aqueous reactions were carried out under anhydrous conditions, *i.e.* using flame-dried glassware, under an argon atmosphere and in dry, freshly distilled solvents, unless otherwise noted. Dimethylformamide (DMF) and quinoline were distilled from calcium hydride under reduced pressure (20 mmHg) and stored over 4 Å molecular sieves until needed. Yields refer to chromatographically and spectroscopically (^{1}H NMR, ^{13}C NMR) homogeneous materials, unless otherwise stated. Reactions were monitored by thin-layer chromatography (TLC) carried out on 0.25 mm E. Merck silica gel plates (60F-254) and visualized under UV light and/or developed by dipping in solutions of 10%

ethanolic phosphomolybdic acid (PMA) or *p*-anisaldehyde and applying heat. E. Merck silica gel (60, particle size 0.040-0.063 mm) was used for flash chromatography. Preparative thin-layer chromatography separations were carried out on 0.25 or 0.50 mm E. Merck silica gel plates (60F-254). NMR spectra were recorded on Varian Mercury 400 and/or Unity 500 MHz instruments and calibrated using the residual undeuterated solvent as an internal reference. The following abbreviations were used to explain the multiplicities: s = singlet, d = doublet, t = triplet, q = quartet, m = multiplet, b = broad. High resolution mass spectra (HRMS) were recorded on a VG 7070 HS mass spectrometer under chemical ionization (CI) conditions or on a VG ZAB-ZSE mass spectrometer under fast atom bombardment (FAB) conditions. X-ray data were recorded on a Bruker SMART APEX 3 kW Sealed Tube X-ray diffraction system.

3.2.2 Procedure for the Synthesis of BC and C Ring Caged Analogues
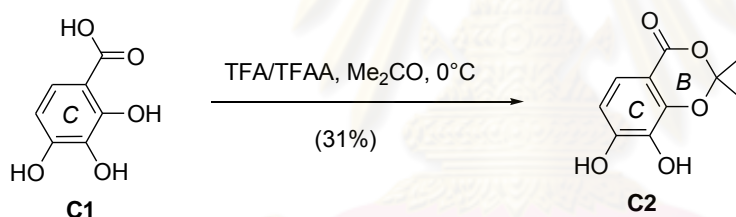
*7,8-Dihydroxy-2,2-dimethyl-4H-benzo[d][1,3]dioxin-4-one (**C02**)*: To a suspension of 2,3,4-trihydroxybenzoic acid **C01** (0.99 g, 6.4 mmol) in TFA (9.5 mL) was added TFAA (10.0 mL, 64.0 mmol) followed by dry acetone (2.8 mL, 38 mmol) at 0 ℃. After 19 h, the homogeneous reaction mixture was concentrated under reduced pressure to half its volume and subsequently stirred with EtOAc (50 mL) and aqueous saturated NaHCO$_3$ (50 mL) in a 500 mL Erlenmeyer flask. The aqueous and EtOAc layers were then separated and the aqueous layer was back-extracted with EtOAc (2 x 25 mL). The combined EtOAc layers were dried over MgSO$_4$, filtered and concentrated by rotary evaporation. The crude material was purified through flash column chromatography (silica, 50% EtOAc-hexane) to give the acetonide **C2** (0.38 g, 31%). **C2**: white solid; R_f = 0.14 (50% EtOAc-hexane); ^{1}H NMR (400 MHz, CDCl$_3$) δ 7.50 (d, J = 8.6 Hz, 1H), 6.72 (d, J = 8.6 Hz, 1H), 6.01 (s, 1H), 5.30 (s, 1H),

1.76 (s, 6H); ^{13}C NMR (100 MHz, CDCl$_3$) δ 161.9, 151.4, 144.4, 131.5, 122.4, 110.7, 107.5, 106.3, 26.0; HRMS calc. for C$_{10}$H$_{10}$O$_5$ (M + H)$^+$ 210.0523, found 210.0524.
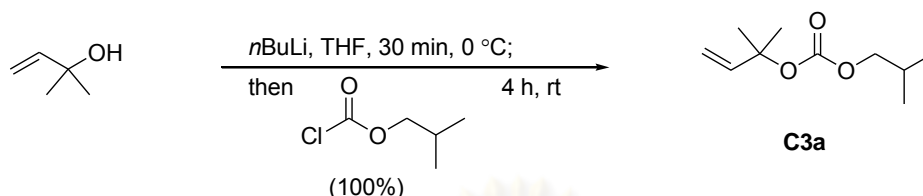
Isobutyl 2-methylbut-3-en-2-yl carbonate (C3a): 2-Methyl-3-buten-2-ol (7.3 mL, 70 mmol) was dissolved in dry THF (125 mL) and stirred under argon at 0 ºC. To the clear solution was added 1.6 M *n*-BuLi in hexane (48.1 mL, 77.0 mmol) dropwise *via* syringe. After 30 min of continued stirring at 0 ºC, isobutyl chloroformate (13.7 mL, 105 mmol) was added dropwise to the reaction mixture. The reaction vessel was then allowed to gradually warm to room temperature and stirred for another 4 h at room temperature. The reaction mixture was acidified by addition of 1M HCl, extracted with Et$_2$O (3 x 50 mL) and washed with water (20 mL). The combined organic layers were dried over MgSO$_4$, filtered, and concentrated by rotary evaporation to give isobutyl 2-methylbut-3-en-2-yl carbonate **C3a** (13.9 mL, 100%). Further purification was not necessary. **C3a**: colorless liquid; R_f = 0.60 (25% EtOAc-hexane); ^{1}H NMR (400 MHz, CDCl$_3$) δ 6.10 (dd, J = 17.5, 10.9 Hz, 1H), 5.22 (d, J = 17.5 Hz, 1H), 5.13 (d, J = 11.0 Hz, 1H), 3.85 (d, J = 6.7 Hz, 1H), 1.99-1.92 (m, 1H), 1.55 (s, 6H), 0.94 (s, 3H), 0.93 (s, 3H); ^{13}C NMR (100 MHz, CDCl$_3$) δ 153.8, 142.0, 113.7, 82.1, 73.5, 28.0, 26.4, 19.2.
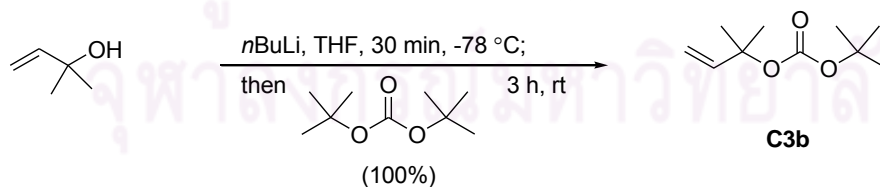
tert-Butyl 2-methylbut-3-en-2-yl carbonate (C3b): To a solution of 2-methyl-3-buten-2-ol (4.0 mL, 38 mmol) in dry THF (80 mL) under argon at -78 ºC was added 1.6 M *n*-BuLi in hexane (26.3 mL, 42.1 mmol) dropwise *via* syringe. After stirring for 30 min, a solution of Boc$_2$O (8.35 g, 38.3 mmol) in THF (5 mL) was added to the reaction mixture. The reaction mixture was allowed to warm to room temperature and

stirred for another 3 h. The reaction mixture was then quenched with saturated aqueous NH_4Cl (20 mL) and extracted with Et_2O (2 x 25 mL). The combined organic layers were washed with water and brine, dried over $MgSO_4$, filtered, and concentrated in vacuo. Purification by flash column chromatography (silica, 100% hexane) gave *tert*-butyl 2-methylbut-3-en-2-yl carbonate **C3b** (7.1 g, 100%). **C3b**: colorless liquid; $R_f = 0.60$ (25% EtOAc-hexane); ^1H NMR (400 MHz, $CDCl_3$) δ 6.11 (dd, $J = 17.5$, 10.9 Hz, 1H), 5.17 (d, $J = 17.5$ Hz, 1H), 5.09 (d, $J = 10.9$ Hz, 1H), 1.51 (s, 6H), 1.45 (s, 6H); 13C NMR (100 MHz, $CDCl_3$) δ 152.1, 142.5, 113.2, 81.6, 81.6, 28.1, 26.6; HRMS calc. for $C_{10}H_{18}O_3$ $(M + Na)^+$ 209.1150, found 209.1148.
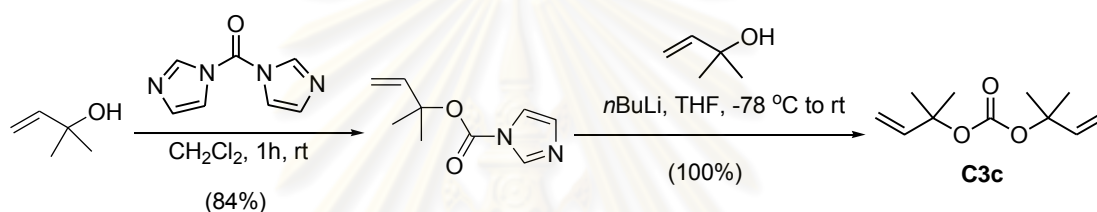
Bis(2-methylbut-3-en-2-yl) carbonate (C3c): Carbonate **C3c** was prepared in two steps: 2-methyl-3-buten-2-ol (2.1 mL, 25 mmol) was dissolved in dry CH_2Cl_2 (20 mL) in a 200 mL round-bottomed flask. To the stirring solution was added carbonyl diimidazole (5.0 g, 31.3 mmol) at room temperature. After 1 h, the reaction mixture was washed with water (2 x 15 mL) and extracted with CH_2Cl_2 (20 mL). The organic layer was dried over $MgSO_4$, filtered, and concentrated by rotary evaporation to yield 2-methylbut-3-en-2-yl $1H$-imidazole-1-carboxylate (3.8 g, 84%) which was used in the next step without further purification. 2-Methylbut-3-en-2-yl $1H$-imidazole-1-carboxylate: colorless liquid; $R_f = 0.48$ (25% EtOAc-hexane); ^1H NMR (400 MHz, $CDCl_3$) δ 8.03 (s, 1H), 7.33 (s, 1H), 6.98 (s, 1H), 6.11 (dd, $J = 17.4$, 10.9 Hz, 1H), 5.27 (d, $J = 17.4$ Hz, 1H), 5.18 (d, $J = 10.9$ Hz, 1H), 1.64 (s, 6H); ^{13}C NMR (100 MHz, $CDCl_3$) δ 147.0, 140.6, 137.2, 130.5, 117.3, 115.0, 85.7, 64.4, 26.4. To a solution of 2-methyl-3-buten-2-ol (4.1 mL, 39 mmol) in dry THF (80 mL) under argon at -78 ^{o}C was added 1.6 M *n*-BuLi in hexane (26.7 mL, 42.7 mmol) dropwise *via* syringe. After stirring for 30 min at -78 ^{o}C, 2-methylbut-3-en-2-yl $1H$-imidazole-1-carboxylate (6.7 mL, 38.8 mmol) was added. The reaction mixture was allowed to warm to room temperature and stirred for another 3 h. The reaction mixture was then quenched with saturated aqueous NH_4Cl (20 mL) and extracted with Et_2O (2 x 25

mL). The combined organic layers were washed with water (2 x 20 mL) and brine (20 mL), dried over MgSO$_4$, and concentrated in vacuo. Purification by flash column chromatography (silica, 100% hexane) gave bis(2-methylbut-3-en-2-yl) carbonate **C3c** (7.7 g, 100%). **C3c**: colorless liquid; R_f = 0.60 (25% EtOAc-hexane); ^{1}H NMR (400 MHz, CDCl$_3$) δ 6.08 (dd, J = 17.5, 10.9 Hz, 2H), 5.15 (d, J = 17.5 Hz, 2H), 5.07 (d, J = 10.9 Hz, 2H), 1.46 (s, 12H); ^{13}C NMR (100 MHz, CDCl$_3$) δ 151.8, 142.2, 113.4, 81.9, 26.5.
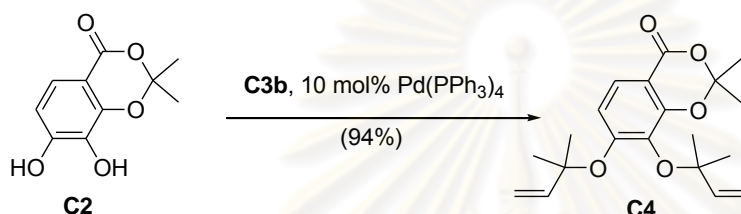
2,2-Dimethyl-7,8-bis(2-methylbut-3-en-2-yloxy)-4H-benzo[d][1,3]dioxin-4-one **(C4)**: To a 25 mL round-bottomed flask was added acetonide **C2** (95 mg, 0.45 mmol) followed by THF (0.65 mL). The reaction vessel was degassed by argon and was placed in an ice bath. To the clear homogeneous solution was added *tert*-butyl 2-methylbut-3-en-2-yl carbonate **C3b** (0.89 mL, 4.50 mmol) *via* syringe, followed by Pd(PPh$_3$)$_4$ (52.0 mg, 45.0 μmol). The reaction vessel was stirred under argon at 5 °C for 20 min. The onset of a blue suspension indicated the formation of the desired product **C4**. The solvent was removed by rotary evaporation and the crude material was purified through flash column chromatography (silica, 10% EtOAc-hexane) to yield the desired product **C4** (146.5 mg, 94%). **C4**: colorless oil; R_f = 0.61 (25% EtOAc-hexane); ^{1}H NMR (400 MHz, CDCl$_3$) δ 7.54 (d, J = 8.8 Hz, 1H), 6.81 (d, J = 8.9 Hz, 1H), 6.16 (m, 2H), 5.20 (m, 3H), 5.02 (d, J = 10.9 Hz, 1H), 1.72 (s, 6H), 1.55 (s, 3H), 1.47 (s, 3H); ^{13}C NMR (100 MHz, CDCl$_3$) δ 161.5, 158.6, 152.1, 143.9, 143.8, 135.6, 124.5, 114.3, 113.7, 113.0, 107.6, 106.4, 106.4, 83.3, 82.1, 27.4, 27.1, 26.1; HRMS calc. for C$_{20}$H$_{26}$O$_5$ (M + H)$^+$ 369.1672, found 369.1674.
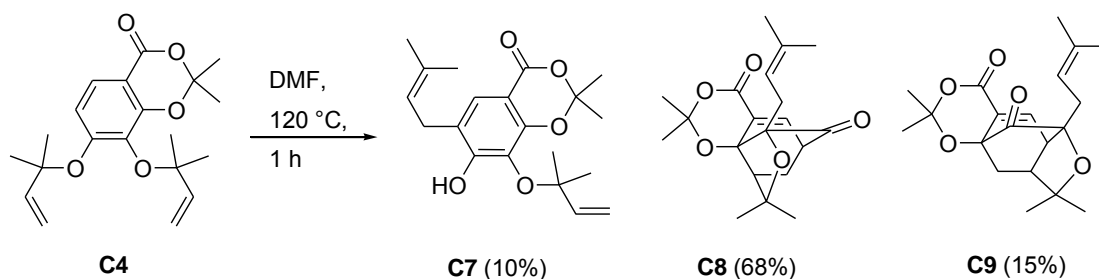
Caged bicycle (C8) and neo-caged bicycle (C9): Alkene **C4** (99 mg, 0.28 mmol) was dissolved in dry DMF (1.8 mL) and the solution was stirred under argon at 120 °C. After 1 h, the reaction mixture was concentrated under reduced pressure. The crude material was purified by flash column chromatography (silica, 10-17% EtOAc-hexane) to yield the caged product **C8** (67 mg, 68%), neo-caged product **C9** (15 mg, 15%), and compound **C7** (10 mg, 10%), respectively. Caged product (**C8**): white solid; R_f = 0.10 (25% EtOAc-hexane); ^{1}H NMR (400 MHz, CDCl$_3$) δ 7.44 (d, J = 6.9 Hz, 1H), 4.41 (m, 1H), 3.42 (t, J = 4.3 Hz, 1H), 2.72 (dd, J = 13.8, 10.4 Hz, 1H), 2.63 (m, 1H), 2.50 (d, J = 9.7 Hz, 1H), 2.31 (dd, J = 13.6, 4.7 Hz, 1H), 1.69 (s, 3H), 1.67 (s, 3H), 1.62 (s, 3H), 1.54 (s, 3H), 1.53 (s, 3H), 1.44 (dd, J = 13.6, 9.3 Hz, 1H), 1.23 (s, 3H); ^{13}C NMR (100 MHz, CDCl$_3$) δ 203.2, 159.9, 139.0, 135.5, 128.1, 118.1, 105.1, 85.0, 84.9, 82.9, 48.6, 46.8, 30.2, 29.1, 28.8, 28.5, 28.0, 26.9, 25.9, 18.4; HRMS calc. for C$_{20}$H$_{26}$O$_5$ (M + Na)$^+$ 369.1672, found 369.1675. Neo-caged product (**C9**): white solid; R_f = 0.30 (25% EtOAc-hexane); ^{1}H NMR (400 MHz, CDCl$_3$) δ 7.41 (d, J = 7.0 Hz, 1H), 4.95 (t, J = 7.0 Hz, 1H), 3.63 (dd, J = 7.0, 4.5 Hz, 1H), 2.36-2.25 (m, 4H), 1.69 (s, 3H), 1.68 (s, 3H), 1.64-1.61 (m, 1H), 1.59 (s, 3H), 1.43 (s, 3H), 1.31 (s, 3H), 1.29 (s, 3H); ^{13}C NMR (100 MHz, CDCl$_3$) δ 205.0, 159.2, 140.1, 136.7, 127.7, 117.2, 106.5, 83.6, 81.2, 80.1, 46.0, 45.5, 34.1, 30.7, 30.2, 28.6, 27.8, 27.0, 26.2, 18.2; HRMS calc. for C$_{20}$H$_{26}$O$_5$ (M + Na)$^+$ 369.1672, found 369.1686. Phenol (**C7**): colorless oil; R_f = 0.52 (25% EtOAc-hexane); ^{1}H NMR (400 MHz, CDCl$_3$) δ 7.50 (s, 1H), 6.27 (s, 1H), 6.15 (dd, J = 17.5, 10.8 Hz, 1H), 5.35-5.25 (m, 2H), 5.17 (d, J = 10.9 Hz, 1H), 3.26 (d, J = 7.1 Hz, 1H), 1.74 (s, 3H), 1.72 (s, 6H), 1.69 (s, 3H) 1.48 (s, 6H); ^{13}C NMR (100 MHz, CDCl$_3$) δ 161.6, 156.0, 149.1, 143.3, 133.9, 130.0, 125.6, 123.1, 121.3, 114.6, 106.4, 105.8, 83.6, 27.9, 26.9, 26.1, 18.0; HRMS calc. for C$_{20}$H$_{26}$O$_5$ (M + Na)$^+$ 369.1672, found 369.1680.
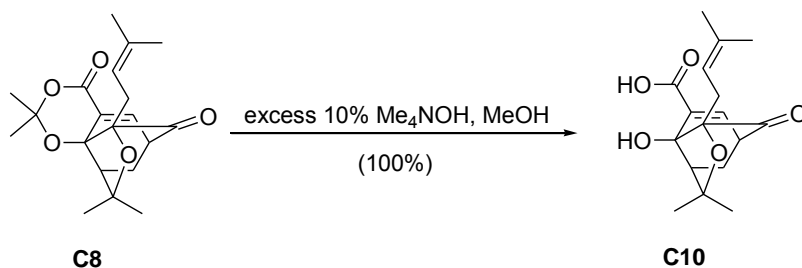
Carboxylic acid (C10): To a 25 mL round-bottomed flask was added caged product **C8** (41 mg, 0.12 mmol) followed by MeOH (1.5 mL). The flask was placed in an ice bath and the solution was stirred at 0 °C. To the stirring solution was then added 10% NMe$_4$OH (aq) (1.7 mL, 159 mmol) dropwise *via* syringe. The light yellow reaction mixture was allowed to warm to room temperature and further stirred at 25 °C for another 24 h. Acetic acid (10 mL) was then added to neutralize the reaction mixture. The reaction mixture was partitioned between EtOAc (2 × 25 mL) and water (25 mL). The combined organic layers were dried over MgSO$_4$, filtered, and concentrated by rotary evaporation. The crude material was purified by recrystallization (CH$_2$Cl$_2$-hexane) to yield the acid **C10** (37 mg, 100%). **C10**: white solid; R_f = 0.11 (67% EtOAc-hexane); ^{1}H NMR (400 MHz, CDCl$_3$) δ 7.45 (d, J = 7.1 Hz, 1H), 4.64 (t, J = 6.4 Hz, 1H), 3.33 (t, J = 5.3 Hz, 1H), 2.69 (dd, J = 13.8, 9.8 Hz, 1H), 2.58 (dd, J = 13.8, 5.3 Hz, 1H), 2.28 (d, J = 4.5 Hz, 1H), 2.24 (d, J = 10.0 Hz, 1H), 1.60 (s, 6H), 1.57 (s, 3H), 1.40 (dd, J = 13.4, 9.6 Hz, 1H), 1.22 (s, 3H); ^{13}C NMR (100 MHz, CDCl$_3$) δ 204.7, 168.4, 142.0, 135.5, 130.7, 118.8, 85.0, 84.0, 83.5, 49.5, 47.1, 30.2, 29.2, 28.7, 27.1, 26.1, 18.0; HRMS calc. for C$_{17}$H$_{22}$O$_5$ (M + Na)$^+$ 329.1359, found 329.1362.
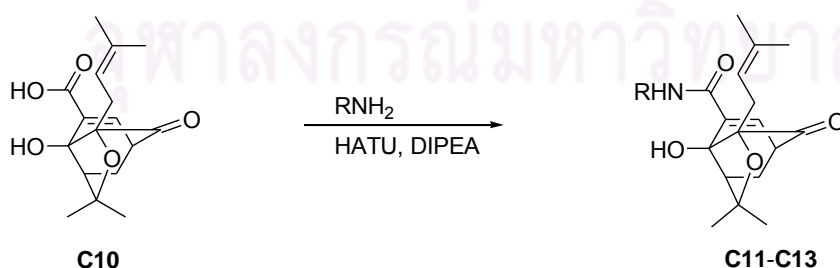
Biotin conjugate (C11): To a solution containing acid **C10** (5.4 mg, 17.6 μmol) and biotin ethylenediamine hydrobromide (7.1 mg, 19.4 μmol) in CH$_2$Cl$_2$ (0.37 mL) was added DIPEA (6.13 μL, 35.2 μmol). Upon adding solid HATU (7.4 mg, 19.4 μmol)

portionwise to the reaction mixture, the reaction mixture turned to pale yellow in color within 5 min. After 24 h, the reaction mixture was partitioned between EtOAc (5 mL) and water (2 mL). The organic layer was washed with water (2 x 1 mL) and brine (2 mL). The combined organic layers were then dried over MgSO$_4$, filtered, and concentrated by rotary evaporation. The crude material was purified by preparative TLC (silica, 9% MeOH-EtOAc) to obtain the amide **C11** (5.5 mg, 9.53 μmol, 54%). **C11**: yellow solid; R_f = 0.28 (20% MeOH-EtOAc); ^{1}H NMR (400 MHz, CDCl$_3$) δ 7.70 (br s, 1H), 7.01 (br s, 1H), 6.89 (d, J = 7.0 Hz, 1H), 6.64 (d, J = 21.9 Hz, 1H), 6.60 (d, J = 8.4 Hz, 1H), 5.49 (d, J = 17.2 Hz, 1H), 4.72 (m, 1H), 4.54 (m, 1H), 4.33 (m, 1H), 3.50-3.33 (m, 4H), 3.23-3.14 (m, 2H), 2.94 (dd, J = 12.9, 4.9 Hz, 1H), 2.74 (d, J = 12.9 Hz, 1H), 2.67-2.18 (m, 6H), 1.80-1.30 (m, 16H), 1.20 (s, 3H); ^{13}C NMR (100 MHz, CDCl$_3$) δ 205.8, 174.5, 167.4, 156.1, 145.0, 135.4, 134.6, 131.9, 128.2, 124.2, 121.1, 118.8, 117.2, 85.3, 84.3, 83.2, 49.7, 46.3, 42.1, 39.4, 35.9, 30.3, 29.3, 28.6, 27.5, 26.2, 25.1, 18.0, 15.3, 11.6; HRMS calc. for C$_{29}$H$_{42}$N$_4$O$_6$S (M + Na)$^+$ 597.2717, found 597.2728.

Coumarin conjugate (C12): To a solution containing acid **C10** (5.40 mg, 17.6 μmol) and coumarin diethyleneamine (5.58 mg, 19.4 μmol) in CH$_2$Cl$_2$ (0.37 mL) was added DIPEA (6.13 μL, 35.2 μmol). Upon adding solid HATU (7.36 mg, 19.4 μmol) portionwise to the reaction mixture, the reaction mixture turned to pale yellow in color within 5 min. After 24 h, the reaction mixture was partitioned between EtOAc (5 mL) and water (2 mL). The organic layer was washed with water (2 x 1 mL) and brine (2 mL). The combined organic layers were then dried over MgSO$_4$, filtered, and concentrated by rotary evaporation. The crude material was purified by preparative TLC (silica, 100% EtOAc) to obtain the amide **C12** (6.0 mg, 59%). **C12**: yellow solid; R_f = 0.17 (100% EtOAc); ^{1}H NMR (400 MHz, CDCl$_3$) δ 7.48 (br s, 1H), 7.45 (br s, 1H), 6.90 (br s, 1H), 6.68 (d, J = 7.0 Hz, 1H), 6.60 (dd, J = 9.1, 2.5 Hz, 1H), 6.46 (d, J = 2.5 Hz, 1H), 6.30 (br s, 1H), 6.00 (br s, 1H), 4.69 (t, J = 7.6 Hz, 1H), 3.64 (s, 2H), 3.52-3.13 (m, 5H), 3.06 (s, 6H), 2.60 (dd, J = 14.0, 9.0 Hz, 1H), 2.47 (dd, J = 13.8, 6.3 Hz, 1H), 2.16 (m, 2H), 1.58 (s, 3H), 1.53 (s, 3H), 1.49 (s, 3H), 1.27 (m, 1H), 1.19 (s, 3H); ^{13}C NMR (100 MHz, CDCl$_3$) δ 205.3, 169.8, 167.0, 165.8, 161.8, 156.1, 153.2, 149.2, 135.3, 134.7, 132.7, 125.4, 118.4, 110.5, 109.2, 108.0, 98.2, 84.7, 84.4,

83.0, 49.4, 46.1, 40.6, 40.5, 40.4, 40.1, 30.1, 29.7, 29.0, 28.2, 27.3, 25.9, 17.8; HRMS calc. for $C_{32}H_{39}N_3O_7$ (M + Na)$^+$ 600.2680, found 600.2688.

BODIPY conjugate (C13): To a solution containing acid **C10** (4.0 mg, 13.1 μmol) and BODIPY FL EDA (4,4-difluoro-5,7-dimethyl-4-bora-3a,4a-diaza-*s*-indacene-3-propionyl ethylenediamine) (5.3 mg, 14.4 μmol) in CH_2Cl_2 (0.27 mL) was added DIPEA (4.56 μL, 26.2 μmol). Upon adding solid HATU (5.9 mg, 15.6 μmol) portionwise to the reaction mixture, the reaction mixture turned to pale yellow in color within 5 min. After 4 h, the reaction mixture was partitioned between EtOAc (5 mL) and water (2 mL). The organic layer was washed with water (2 x 1 mL) and brine (2 mL). The combined organic layers were then dried over $MgSO_4$, filtered, and concentrated by rotary evaporation. The crude material was purified by preparative TLC (silica, 100% EtOAc) to obtain the amide **C13** (5.60 mg, 68%). **C13**: red solid; R_f = 0.62 (100% EtOAc); ^{1}H NMR (400 MHz, CDCl$_3$) δ 7.54 (br s, 1H), 7.11 (s, 1H), 6.92 (s, 1H), 6.87 (d, *J* = 3.8 Hz, 1H), 6.69 (d, *J* = 7.0 Hz, 1H), 6.26 (br s, 1H), 6.24 (d, *J* = 3.8 Hz, 1H), 6.15 (s, 1H), 4.64 (t, *J* = 6.9 Hz, 1H), 3.40-3.10 (m, 7H), 2.71-2.56 (m, 4H), 2.56 (s, 3H), 2.27 (s, 3H), 2.18-2.15 (m, 2H), 1.59 (s, 6H), 1.51 (s, 3H), 1.36-1.27 (m, 1H), 1.19 (s, 3H); ^{13}C NMR (100 MHz, CDCl$_3$) δ 205.8, 174.5, 167.4, 161.4, 156.1, 145.0, 135.4, 134.6, 131.9, 128.2, 124.2, 121.1, 118.8, 117.2, 85.3, 84.3, 83.2, 49.7, 46.3, 42.1, 39.4, 35.9, 30.3, 29.3, 28.6, 27.5, 26.2, 25.1, 18.0, 15.3, 11.6; HRMS calc. for $C_{33}H_{41}BF_2N_4O_5$ (M + Na)$^+$ 645.3030, found 645.3043.
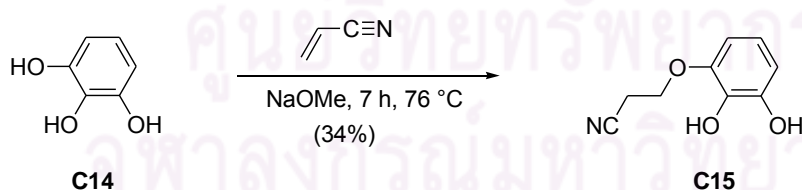
3-(2,3-Dihydroxylphenoxy)propanenitrile (C15): To a 250 mL round-bottomed flask was added pyrogallol **C14** (10.0 g, 79.3 mmol) and acrylonitrile (14.7 g, 278 mmol) followed by NaOMe (4.3 g, 79.3 mmol). The reaction vessel was then equipped with a reflux condenser and stirred under argon at 78 ºC for 7 h. The onset of a dark black color indicated the formation of the 3-(2,3-dihydorxylphenoxy)propanenitrile **C15**. The reaction mixture was then cooled to 25 ºC and the excess acrylonitrile was removed by rotary evaporation. The residue was extracted with EtOAc (5 x 100 mL),

and the combined organic layers were dried over MgSO$_4$, filtered, and concentrated by rotary evaporation. The crude material was purified through flash column chromatography (silica, 40% EtOAc-hexane) to yield the nitrile **C15** (4.5 g, 32%). **C15**: off-white solid; R_f = 0.43 (50% EtOAc-hexane); ^{1}H NMR (400 MHz, DMSO-d$_6$) δ 6.55 (t, J = 8.0 Hz, 1H), 6.44 (m, 2H), 4.11 (t, J = 6.0 Hz, 2H), 2.94 (t, J = 6.0 Hz, 2H); ^{13}C NMR (100 MHz, DMSO-d$_6$) δ 146.8, 146.2, 135.0, 119.0, 118.3, 109.8, 106.0, 64.2, 18.1; HRMS calc. for C$_9$H$_9$NO$_3$ (M + Na)$^+$ 202.0471, found 202.0475.
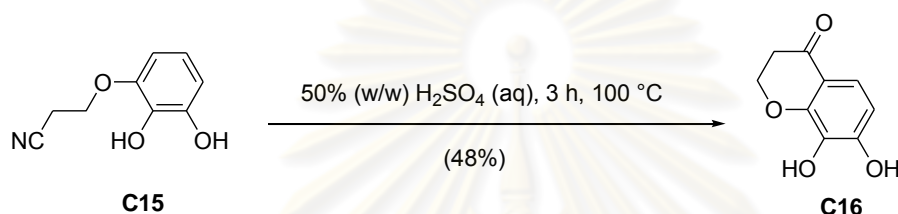
7,8-Dihydroxychroman-4-one (C16): To a 100 mL round-bottomed flask containing 3-(2,3-dihydroxylphenoxy)propanenitrile **C15** (2.05 g, 11.8 mmol) was added slowly dropwise, *via* the addition funnel, aqueous sulfuric acid (50% v/v, 42 mL). The reaction vessel was then equipped with a reflux condenser and stirred under argon at 105 ºC for 3 h. The cooled solution was diluted with water (50 mL) and extracted with EtOAc (4 x 100 mL). The organic layers were washed with water, brine, and dried over MgSO$_4$. The combined organic layers were then filtered and concentrated by rotary evaporation. The crude material was purified through flash column chromatography (silica, 60-70% EtOAc-hexane) to yield 7,8-dihydroxychroman-4-one **C16** (0.98 g, 48%). **C16**: off-white solid; R_f = 0.38 (70% EtOAc-hexane); 1H NMR (400 MHz, DMSO-d$_6$) δ 7.15 (dd, J = 8.7, 1.3 Hz, 1H), 6.49 (dd, J = 8.6, 1.3 Hz, 1H), 4.48 (t, J = 6.3 Hz, 2H), 2.67 (t, J = 6.3 Hz, 2H); 13C NMR (100 MHz, DMSO-d$_6$) δ 190.3, 152.0, 151.3, 132.7, 117.4, 114.5, 109.6, 67.1, 37.1; HRMS calc. for C$_9$H$_8$O$_4$ (M + H)$^+$ 181.0495, found 181.0494.
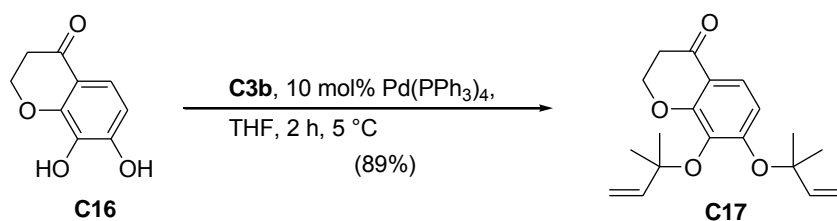
7,8-Bis(2-methylbut-3-en-2-yloxy)chroman-4-one (C17): To a 25 mL round-bottomed flask was added 7,8-dihydroxychroman-4-one **C16** (50 mg, 0.28 mmol) followed by dry THF (1.5 mL). The flask was degassed by argon and was placed in an ice water bath. To the yellow homogeneous solution was added *tert*-butyl 2-methylbut-3-en-2-yl carbonate **C3b** (522 mg, 2.80 mmol), *via* syringe, followed by Pd(PPh₃)₄ (32 mg, 0.028 mmol). The reaction vessel was stirred under argon at 5 °C for 2 h. The onset of a yellow suspension indicated the formation of the alkene **C17**. The solvent was removed by rotary evaporation and the crude material was purified through flash column chromatography (silica, 30-40% EtOAc-hexane) to yield 7,8-*bis*(2-methylbut-3-en-2-yloxy)choman-4-one **C17** (79 mg, 89%). **C17**: yellow oil; R_f = 0.52 (30 % EtOAC-hexane); ^{1}H NMR (400 MHz, CDCl₃) δ 7.49 (d, J = 9.0 Hz, 1H), 6.72 (d, J = 9.0, 1H), 6.19 (dd, J = 17.4, 10.6 Hz, 1H), 6.12 (dd, J = 17.6, 10.9 Hz, 1H), 5.13 (m, 3H), 4.98 (dd, J = 10.9, 1.1 Hz, 1H), 4.47 (t, J = 6.5 Hz, 2H), 2.71 (t, J = 6.6 Hz, 2H), 1.51 (s, 6H), 1.47 (s, 6H); ^{13}C NMR (100 MHz, CDCl₃) δ 191.2, 157.8, 143.7, 135.8, 121.7, 116.7, 113.8, 113.6, 112.5, 82.8, 81.8, 67.1, 37.4, 27.1, 26.7; HRMS calc. for $C_{19}H_{24}O_4$ $(M + Na)^+$ 339.1567, found 339.1569.
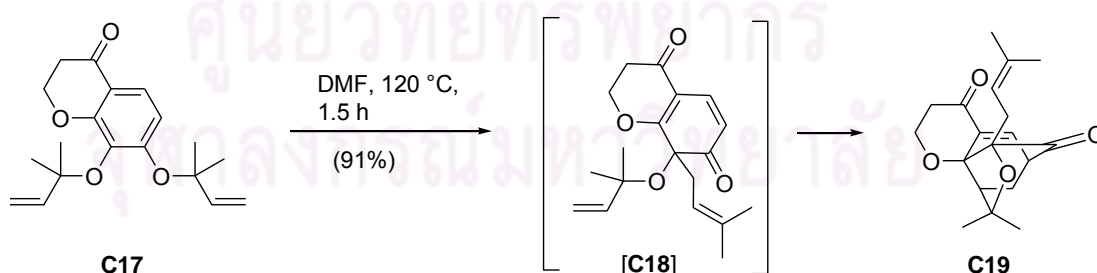
Caged chromanone (C19): A solution of compound **C17** (36 mg, 0.11 mmol) in DMF (1.5 mL) was heated at 120 °C for 1.5 h. The onset of a brown color indicated the formation of the caged xanthone **C19**. The reaction mixture was then cooled to 25 °C and the solvent was removed by rotary evaporation. The crude material was purified through flash column chromatography (silica, 50-55 % EtOAc-hexane) to yield the

caged product **C19** (33 mg, 91%). **C19**: white solid; R_f = 0.21 (30 % EtOAc-hexane); ^{1}H NMR (400 MHz, CDCl$_3$) δ 7.25 (d, J = 6.6 Hz, 1H), 4.41 (m, 1H), 4.17 (ddd, J = 12.1, 6.5, 1.4 Hz, 1H), 3.94 (dt, J = 12.3, 2.9 Hz, 1H), 3.34 (m, 1H), 2.63 (d, J = 8.6 Hz, 2H), 2.50 (dd, J = 12.4, 6.5 Hz, 1H), 2.42 (dd, J = 2.9, 1.4 Hz, 1H), 2.37 (m, 1H), 2.31 (dd, J = 13.6, 4.5 Hz, 1H), 1.59 (s, 3H), 1.53 (s, 3H), 1.48 (s, 3H), 1.32 (m, 1H), 1.23 (s, 3H); ^{13}C NMR (100 MHz, CDCl$_3$) δ 203.9, 192.0, 136.9, 135.4, 133.8, 119.2, 87.4, 84.2, 82.9, 60.0, 46.2, 44.5, 38.1, 30.1, 28.8 (2C), 27.7, 25.5, 17.9; HRMS calc. for C$_{19}$H$_{24}$O$_4$ (M + Na)$^+$ 339.1567, found 339.1571.

3.2.3 Procedure for the Synthesis of ABC Ring Caged Analogues
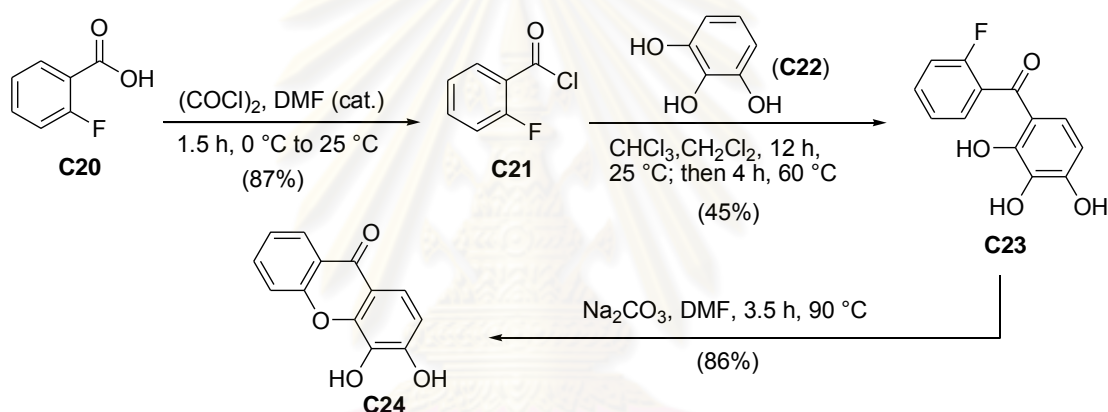
3,4-Dihydroxy-9H-xanthen-9-one (C24): To a clean, dried 250 mL round-bottomed flask was added 2-fluorobenzoic acid **C20** (5.09 g, 36.3 mmol). The flask containing 2-fluorobenzoic acid **C20** and a magnetic stir bar was placed under high vacuum for about 10 min. The flask was carefully sealed and CH$_2$Cl$_2$ (100 mL) was added by using a syringe under argon. The flask was then placed in an ice bath and the reaction mixture was stirred at 0 °C. To the stirring solution of 2-fluorobenzoic acid **20** and CH$_2$Cl$_2$ was added a solution of oxalyl chloride (2.0 M in CH$_2$Cl$_2$, 21.0 mL, 42.0 mmol) dropwise, *via* syringe, followed by a catalytic amount of DMF. The ice bath was removed and the reaction mixture was stirred at room temperature for 1.5 h. The solution was concentrated by rotary evaporation under argon to yield colorless oil, 2-fluorobenzoyl chloride **C21** (5.01 g, 87%). To a mixture of pyrogallol **C22** (6.48 g, 51.3 mmol), aluminium chloride (14.6 g, 110 mmol), chloroform (80 mL), and CH$_2$Cl$_2$ (200 mL) in a 1 L round-bottomed flask was added a solution of 2-

fluorobenzoyl chloride **C21** in CH_2Cl_2 (10 mL) dropwise *via* syringe. The reaction mixture was stirred at room temperature under argon for 12 h. The reaction vessel was then equipped with a reflux condenser and stirred under argon at 80 °C for another 4 h. The cooled, red homogeneous solution was acidified with 1N HCl (300 mL). The reaction mixture was then partitioned between water and EtOAc (3 × 200 mL). The aqueous layer was back-extracted with EtOAc (2 × 200 mL) until the color of the aqueous layer was almost clear. The combined organic layers were dried over $MgSO_4$, filtered, and concentrated to yield (2-fluorophenyl)(2,3,4-trihydroxy-phenyl)methanone **C23** (3.54 g, 45%). To a 500 mL round-bottomed flask containing sodium carbonate (2.27 g, 21.4 mmol) and DMF (100 mL) was added **C23**. The reaction vessel was then equipped with a reflux condenser and stirred under argon at 90 °C for 3.5 h. The dark reaction mixture was cooled to room temperature and acidified with 1N HCl (300 mL). The reaction mixture was then partitioned between water and ethyl acetate (3 × 150 mL). The aqueous layer was back extracted with ethyl acetate (5 × 150 mL). The combined brown organic layers were dried over $MgSO_4$, filtered, and concentrated by rotary evaporation. The crude material was purified through flash column chromatography (silica, 50-60% EtOAc-hexane) to yield 3,4-dihydroxy-9*H*-xanthen-9-one **C24** (2.79 g, 86%). **C24**: pale yellow solid; R_f = 0.42 (90% Et_2O-hexane); ^{1}H NMR (400 MHz, DMSO-d_6) δ 10.49 (s, 1H), 9.43 (s, 1H), 8.15 (dd, J = 7.9, 1.7 Hz, 1H), 7.83 (ddd, J = 8.6, 7.2, 1.7 Hz,1H), 7.63 (d, J = 8.4 Hz, 1H), 7.55 (d, J = 8.7 Hz, 1H), 7.44 (t, J = 7.5 Hz, 1H), 6.94 (d, J = 8.8 Hz, 1H); ^{13}C NMR (100 MHz, DMSO-d_6) δ 175.1, 155.3, 151.4, 146.2, 134.6, 132.5, 125.7, 123.8, 120.7, 117.9, 116.4, 114.6, 113.2; HRMS calc. for $C_{13}H_8O_4$ (M + H)$^+$ 229.0501, found 229.0509.
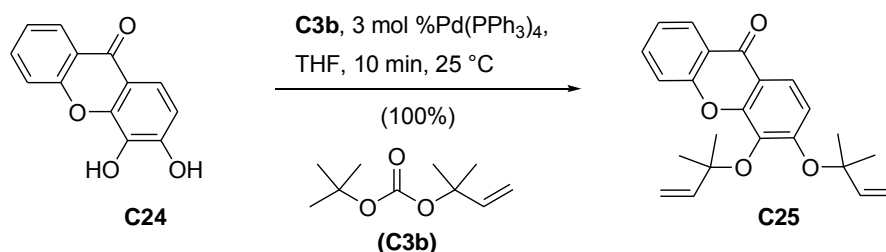
3,4-Bis(2-methylbut-3-en-2-yloxy)-9H-xanthen-9-one (C25): To a 50 mL round-bottomed flask was added 3,4-dihydroxy-9*H*-xanthen-9-one **C24** (1.0 g, 4.39 mmol) followed by dry THF (15 mL). To the yellow homogeneous solution was added *tert*-butyl 2-methylbut-3-en-2-yl carbonate **C3b** (8.18 g, 43.9 mmol), *via* syringe, followed by Pd(PPh₃)₄ (0.15 g, 0.13 mmol). The reaction vessel was stirred under argon at 25 °C for 10 min. The onset of a yellow suspension indicated the formation of the alkene **C25**. The solvent was removed by rotary evaporation and the crude material was purified through flash column chromatography (silica, 10-15% EtOAc-hexane) to yield 3,4-bis(2-methylbut-3-en-2-yloxy)-9*H*-xanthen-9-one **C25** (1.59 g, 100%). **C25**: yellow solid; R_f = 0.67 (30 % EtOAc-hexane); ¹H NMR (400 MHz, CDCl₃) δ 8.30 (dd, J = 8.0, 1.7 Hz, 1H), 7.92 (d, J = 9.1 Hz, 1H), 7.68 (ddd, J = 8.6, 7.1, 1.7 Hz, 1H), 7.49 (d, J = 7.9 Hz, 1H), 7.36 (ddd, J = 8.0, 7.2, 0.9 Hz, 1H), 7.12 (d, J = 8.9 Hz, 1H), 6.28 (dd, J = 17.5, 10.8 Hz, 1H), 6.18 (dd, J = 17.6, 10.9 Hz, 1H), 5.19 (m, 3H), 5.01 (dd, J = 10.9, 1.0 Hz, 1H), 1.58 (s, 6H), 1.56 (s, 6H); ¹³C NMR (100 MHz, CDCl₃) δ 176.8, 156.9, 155.9, 152.4, 143.5, 143.4, 135.7, 134.3, 126.5, 123.7, 121.5, 121.0, 117.8, 117.1, 116.8, 114.1, 113.0, 83.5, 82.1, 27.1, 26.9; HRMS calc. for C₂₃H₂₄O₄ (M + H)⁺ 365.1753, found 365.1740.

C25   **196**: cluvenone (81%)   **C26** (14%)
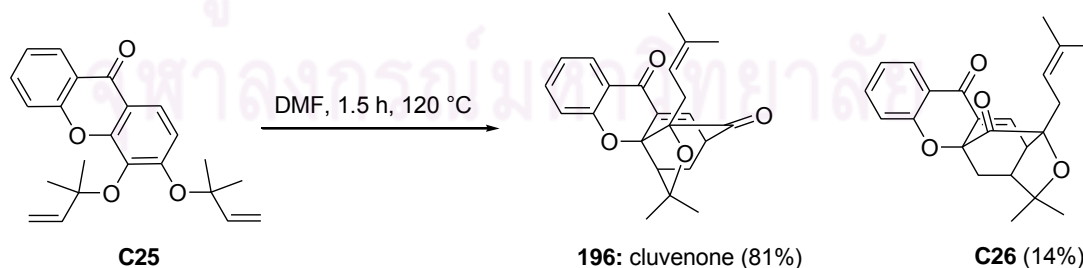
Caged xanthones (196) and (C26): A solution of compound **C25** (350 mg, 0.96 mmol) in DMF (6 mL) was heated at 120 °C for 1.5 h. The onset of a brown color indicated the formation of the xanthones **C26** and **196**. The brown reaction mixture was then cooled to room temperature and the solvent was removed by rotary

evaporation. The crude material was then purified by column chromatography (silica, 20-30% Et_2O-hexane) to yield a mixture of caged products **196** (285 mg, 81%) and **C26** (50 mg, 14%). **196**: white solid; R_f = 0.28 (25% EtOAc-hexane); ^{1}H NMR (400 MHz, $CDCl_3$) δ 7.93 (dd, J = 8.0 Hz, 1.7 Hz, 1H), 7.51 (ddd, J = 8.9, 7.3, 1.7 Hz, 1H), 7.42 (d, J = 6.9 Hz, 1H), 7.05 (m, 2H), 4.39 (m, 1H), 3.48 (dd, J = 6.7 Hz, 4.6 Hz, 1H), 2.64 (m, 2H), 2.45 (d, J = 9.6 Hz, 1H), 2.33 (dd, J = 13.5 Hz, 4.6 Hz, 1H), 1.71 (s, 3H), 1.29 (m, 1H), 1.29 (s, 6H), 0.89 (s, 3H); ^{13}C NMR (100 MHz, $CDCl_3$) δ 203.0, 176.4, 159.5, 136.1, 134.8, 134.7, 133.7, 126.8, 121.8, 118.9, 118.9, 118.0, 90.2, 84.5, 83.4, 48.7, 46.7, 30.2, 29.0, 25.2, 25.0, 16.6; HRMS calc. for $C_{23}H_{24}O_4$ $(M + H)^+$ 365.1753, found 365.1765. **C26**: yellow solid; R_f = 0.34 (25% EtOAc-hexane); ^{1}H NMR (400 MHz, $CDCl_3$) δ 7.91 (dd, J = 7.9, 1.7 Hz, 1H), 7.54 (m, 1H), 7.25 (d, J = 7.1 Hz, 1H), 7.18 (d, J = 8.5 Hz, 1H), 7.05 (ddd, J = 8.0, 7.3, 1.0 Hz, 1H), 5.02 (m, 1H), 3.76 (dd, J = 6.9, 4.6 Hz, 1H), 2.50 (m, 2H), 2.13 (m, 2H), 1.87 (dd, J = 13.2, 10.0 Hz, 1H), 1.71 (s, 3H), 1.59 (s, 3H), 1.38 (s, 3H), 1.34 (s, 3H); ^{13}C NMR (100 MHz, $CDCl_3$) δ 199.7, 175.4, 160.2, 136.5, 136.1, 135.9, 134.9, 127.0, 122.0, 119.2, 118.3, 117.3, 84.1, 83.7, 78.8, 44.8, 42.1, 33.1, 30.2, 29.7, 26.8, 26.0, 18.2; HRMS calc. for $C_{23}H_{24}O_4$ $(M + H)^+$ 365.1753, found 365.1766.

196: cluvenone   **C27** (57%)   **C28** (21%)
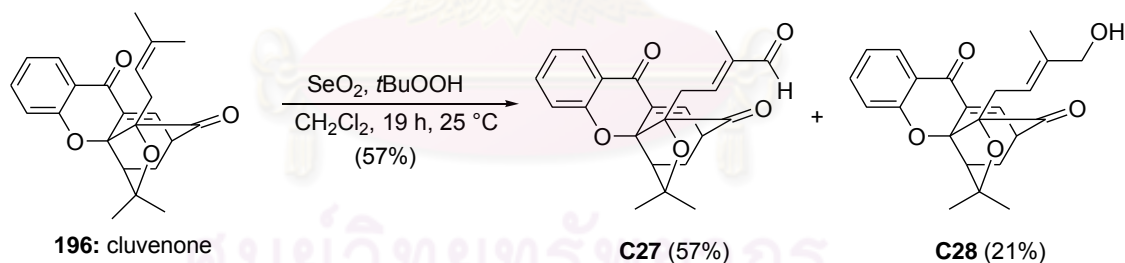
Aldehyde (C27) and Alcohol (C28): A solution of SeO_2 (0.67 mg, 6.00 μmol) and $tBuOOH$ (5.5M in decane, 40.0 μL, 0.22 mmol) in CH_2Cl_2 (1.4 mL) was prepared. To the stirring solution was added a solution of caged xanthone **196** (42.7 mg, 0.12 mmol) in CH_2Cl_2 (0.5 mL) dropwsie, *via* syringe, at room temperature. After stirring for 19 h at room temperature, the reaction mixture was dissolved in diethyl ether (10 mL) and washed with 10% KOH (10 mL), water (10 mL), and brine (10 mL). The ether layer was dried over $MgSO_4$, filtered, and concentrated by rotary evaporation. The crude yellow oil was purified through flash column chromatography to yield the

aldehyde **C28** (26 mg, 57%) and alcohol **C27** (9.6 mg, 21%). **C27**: white solid; Rf = 0.42 (17% EtOAC-hexane); ^{1}H NMR (400 MHz, CDCl$_3$) δ 9.22 (s, 1H), 7.91 (d, J = 7.8 Hz, 1H), 7.59 (d, J = 6.9 Hz, 1H), 7.53 (t, J = 7.5 Hz, 1H), 7.07 (t, J = 7.4 Hz, 1H), 6.94 (d, J = 8.4 Hz, 1H), 6.41 (t, J = 7.2 Hz, 1H), 3.55 (m, 1H), 2.82 (dd, J = 15.9, 7.5 Hz, 1H), 2.65 (dd, J = 15.9, 7.0 Hz, 1H), 2.56 (d, J = 9.5 Hz, 1H), 2.38 (dd, J = 13.6, 4.6 Hz, 1H), 1.76 (s, 3H), 1.42-1.36 (m, 1H), 1.34 (s, 3H), 1.18 (s, 3H); ^{13}C NMR (100 MHz, CDCl$_3$) δ 202.8, 194.8, 176.6, 159.5, 147.3, 140.3, 137.2, 136.6, 134.7, 127.6, 122.7 119.0, 118.2, 91.1, 84.4, 83.4, 48.9, 47.0, 30.3, 29.3, 29.2, 25.1, 8.8; HRMS calc. for C$_{23}$H$_{22}$O$_5$ (M + H)$^+$ 379.1540, found 379.1550. **C28**: white solid; R_f = 0.21 (17% EtOAC-hexane); ^{1}H NMR (400 MHz, CDCl$_3$): δ 7.93 (d, J = 8.2 Hz, 1H), 7.56 (t, J = 8.4 Hz, 1H), 7.54 (d, J = 6.9 Hz, 1H), 7.10-7.07 (m, 2H), 4.75-4.71 (m, 1H), 3.67-3.53 (m, 3H), 2.75-2.67 (m, 2H), 2.49 (d, J = 9.6 Hz, 1H), 2.37 (dd, J = 13.6, 4.7 Hz, 1H), 1.74 (s, 3H), 1.39-1.34 (m, 1H), 1.31(s, 3H), 0.94 (s, 3H); ^{13}C NMR (100 MHz, CDCl$_3$) δ 203.0, 178.8, 159.9, 138.1, 137.0, 135.4, 134.7, 127.4, 122.5, 119.8, 119.4, 118.3, 90.4, 84.7, 84.0, 68.4, 48.9, 47.2, 30.5, 29.3, 29.0, 25.2, 12.7; HRMS calc. for C$_{23}$H$_{24}$O$_5$ (M + Na)$^+$ 403.1516, found 403.1524.
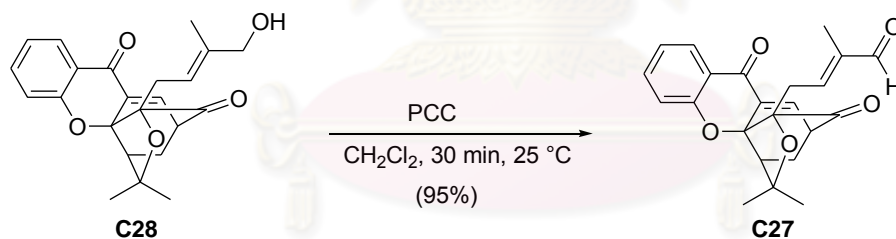
Oxidation of alcohol (C28) to aldehyde (C27): A mixture of alcohol **C28** (20 mg, 52.6 μmol) and PCC (17 mg, 78.9 μmol) in CH$_2$Cl$_2$ (0.2 mL) was stirred at room temperature for 30 min. The reaction mixture was diluted with CH$_2$Cl$_2$ and filtered through a pad of celite. The solvent was removed by rotary evaporation and the crude was purified by preparative TLC (silica, 50% EtOAc-hexane) to yield aldehyde **C27** (19 mg, 95%).
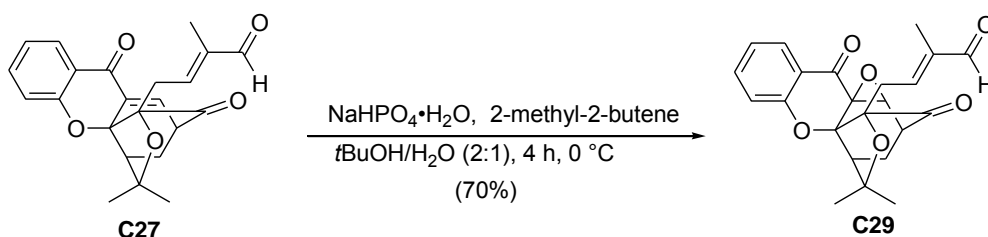
Epoxide (C29): NaH$_2$PO$_4$·H$_2$O (6.8 mg, 49.1 μmol) was added to a solution of **C27** (6.2 mg, 16.4 μmol) in *t*BuOH/H$_2$O (2:1, 0.43 mL). The reaction mixture was stirred at room temperature to fully dissolve the white precipitate and the reaction vessel was placed in an ice bath. To the stirring solution in an ice bath was added 2-methylbut-2-ene (13.9 μL, 131.2 μmol) *via* syringe. After 30 min, NaClO$_2$ (4.4 mg, 49.1 μmol) was added to the reaction mixture. When the reaction was complete 4 h later, the reaction mixture was partitioned between EtOAc (2 x 3 mL) and water (3 mL). The combined organic layers were dried over MgSO4, filtered, and concentrated by rotary evaporation. The crude material was purified through preparative TLC (silica, 50% EtOAc-Hexane) to yield the epoxide **C29** (4.4 mg, 70%). **C29**: white solid; R_f = 0.52 (50% EtOAc-hexane); ^{1}H NMR (400 MHz, CDCl$_3$) δ 9.48 (s, 1H), 7.97 (d, J = 7.9 Hz, 1H), 7.65 (t, J = 7.4 Hz, 1H), 7.20 (t, J = 7.7 Hz, 1H), 7.10 (d, J = 8.3 Hz, 1H), 7.01 (t, J = 8.1 Hz, 1H), 4.29 (d, J = 4.5 Hz, 1H), 3.12 (t, J = 4.6 Hz, 1H), 3.03-3.01 (m, 2H), 2.58 (d, J = 9.2 Hz, 1H), 2.23 (dd, J = 5.1, 14.5 Hz, 1H), 1.81-1.73 (m, 1H), 1.70 (s, 3H), 1.60 (s, 3H), 1.24 (s, 3H); ^{13}C NMR (100 MHz, CDCl$_3$) δ 204.3, 195.6, 184.5, 159.0, 150.3, 139.8, 138.2, 127.8, 123.4, 122.6, 119.4, 89.6, 88.7, 84.0, 59.8, 55.0, 46.9, 42.1, 30.2, 28.3, 27.9, 24.4, 9.5; HRMS calc. for C$_{23}$H$_{22}$O$_6$ (M + Na)$^+$ 417.1309, found 417.1313.
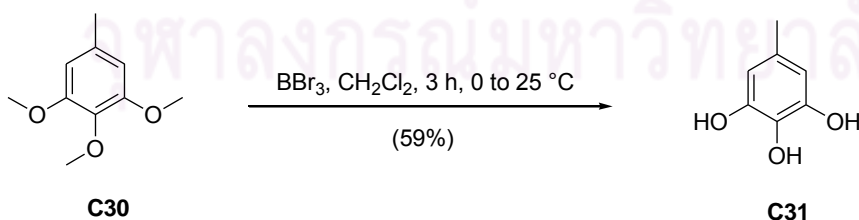
5-Methylbenzene-1,2,3-triol (C31): To a 50 mL round-bottomed flask was added pyrogallol **C30** (372 mg, 2.04 mmol) followed by CH$_2$Cl$_2$ (4.0 mL). The flask was placed on an ice bath and 1.0 M solution of boron tribromide in CH$_2$Cl$_2$ (6.5 mL, 6.52 mmol) was added dropwise, *via* syringe, while stirring over 10 min. The reaction

vessel was then stirred under argon at room temperature for 3.5 h. The reaction was quenched by adding water (10 mL), and the reaction mixture was extracted with EtOAc (3 x 20 mL). The combined organic layers were washed with water, brine, and dried over MgSO$_4$. The solution was then filtered and concentrated by rotary evaporation. The crude material was purified through flash column chromatography (silica, 60-70% EtOAc-hexane) to yield 5-methylbenzene-1,2,3-triol (170 mg, 59%).

C31: off-white solid; R_f = 0.32 (40% EtOAc-hexane); ^{1}H NMR (400 MHz, CDCl$_3$) δ 6.30 (s, 2H), 5.05 (s, 2H), 5.00 (s, 1H), 2.20 (s, 3H); ^{13}C NMR (100 MHz, DMSO-d$_6$) δ 145.9, 130.4, 127.2, 107.6, 20.6; HRMS calc. for C$_7$H$_8$O$_3$ (M) 140.0468, found 140.0470.

C31   **C32**
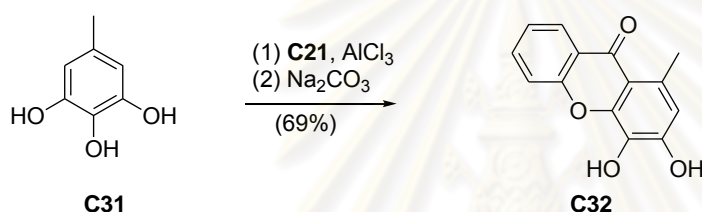
3,4-Dihydroxy-1-methyl-9H-xanthen-9-one (C32): 2-Fluorobenzoyl chloride (**C21**) (170 mg, 1.07 mmol) was added dropwise to a mixture of 5-methylbenzene-1,2,3-triol **C31** (100 mg, 0.71 mmol), aluminum chloride (187 mg, 1.40 mmol), chloroform (2 mL) and CH$_2$Cl$_2$ (6 mL) in a 50 mL round-bottomed flask. The reaction mixture was stirred at room temperature under argon for 1.5 h. The reaction vessel was then equipped with a reflux condenser and stirred under argon at 60 °C for 6 h. The cooled, red homogeneous solution was acidified with 1N HCl (15 mL). The reaction mixture was then partitioned between water and EtOAc (3 x 50 mL). The aqueous layer was back extracted with ethyl acetate (2 x 30 mL) until the color of the aqueous layer was almost clear. The combined organic layers were dried over MgSO$_4$, filtered, and concentrated to yield dark brown oil. The crude oil was then added to a 100 mL round-bottomed flask containing Na$_2$CO$_3$ (98 mg, 0.92 mmol) and DMF (4 mL). The reaction vessel was the equipped with a reflux condenser and stirred under argon at 90 °C for 4 h. The dark reaction mixture was cooled to room temperature and acidified with 1N HCl (15 mL). The reaction mixture was then partitioned between water and EtOAc (3 x 50 mL). The aqueous layer was back extracted with ethyl acetate (2 x 30 mL). The combined brown organic layers were dried over MgSO$_4$,

filtered, and concentrated by rotary evaporation. The crude material was purified through flash column chromatography (silica, 40-50% EtOAc-hexane) to yield the methyl xanthone **C32** (120 mg, 70%). **C32**: off-white solid; R_f = 0.21 (40% EtOAc-hexane); ^{1}H NMR (400 MHz, DMSO-d$_6$) δ 10.15 (br s, 1H), 9.34 (br s, 1H), 8.10 (dd, J = 7.9, 1.6 Hz, 1H), 7.76 (ddd, J = 8.6, 7.3, 1.7 Hz, 1H), 7.56 (d, J = 8.3 Hz, 1H), 7.38 (t, J = 7.5 Hz, 1H), 6.68 (s, 1H), 2.68 (s, 3H); ^{13}C NMR (100 MHz, DMSO-d$_6$) δ 176.8, 154.6, 150.3, 147.4, 134.3, 131.1, 130.7, 126.0, 123.6, 121.8, 117.4, 115.2, 112.8, 22.4; HRMS calc. for $C_{14}H_{10}O_4$ (M + H)$^+$ 243.0652, found 243.0654.
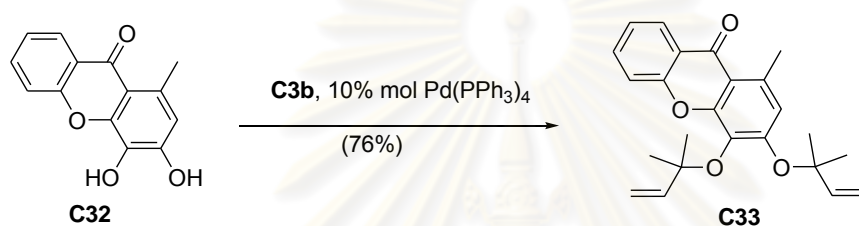
1-Methyl-3,4-bis(2-methylbut-3-en-2-yloxy)-9H-xanthen-9-one (C33): To a 25 mL round-bottomed flask was added methyl xanthone **C32** (46 mg, 0.19 mmol) followed by dry THF (1.5 mL). The flask was degassed by argon and was placed in an ice water bath. To the yellow homogeneous solution was added *tert*-butyl 2-methylbut-3-en-2-yl carbonate **C3b** (354 mg, 1.9 mmol), *via* syringe, followed by Pd(PPh$_3$)$_4$ (22 mg, 0.019 mmol). The reaction vessel was stirred under argon at 5 °C for 2 h. The onset of a yellow suspension indicated the formation of the desired product **C33**. The solvent was removed by rotary evaporation and the crude material was purified through flash column chromatography (silica, 10-15% EtOAc-hexane) to yield 1-methyl-3,4-bis(2-methylbut-3-en-2-yloxy)-9*H*-xanthen-9-one **C33** (55 mg, 76%). **C33**: yellow oil; R_f = 0.66 (30% EtOAc-hexane); ^{1}H NMR (400 MHz, CDCl$_3$) δ 8.24 (dd, J = 7.9, 1.5 Hz, 1H), 7.64 (ddd, J = 8.6, 7.2, 1.7 Hz, 1H), 7.43 (d, J = 8.4 Hz, 1H), 7.31 (t, J = 7.5 Hz, 1H), 6.86 (s, 1H), 6.28 (dd, J = 17.5, 10.9 Hz, 1H), 6.19 (dd, J = 17.6, 10.8 Hz, 1H), 5.18 (m, 3H), 5.01 (dd, J = 10.9, 1.0 Hz, 1H), 2.80 (s, 3H), 1.56 (s, 12H); ^{13}C NMR (100 MHz, CDCl$_3$) δ 178.4, 155.3, 155.0, 153.5, 143.8, 143.6, 136.3, 133.9, 126.5, 123.5, 122.5, 119.1, 117.3, 115.5, 113.9, 112.8, 83.1, 82.0, 27.2, 26.9, 23.5; HRMS calc. for $C_{24}H_{26}O_4$ (M + H)$^+$ 379.1904, found 379.1911.

C33 → **C34**

DMF, 120 °C, 2.5 h
(85%)
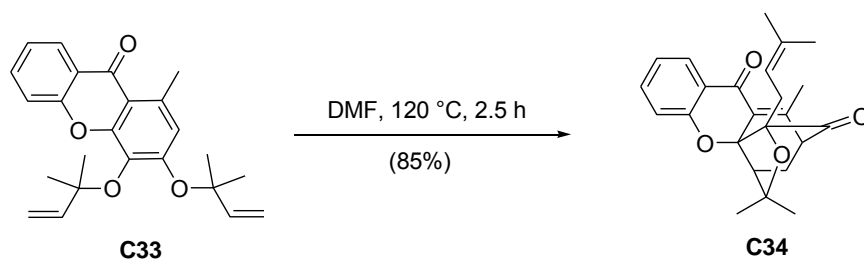
Caged xanthone (C34): A solution of compound **C33** (35 mg, 0.092 mmol) in DMF (1.5 mL) was heated at 120 °C under argon for 2.5 h. The onset of a yellow color indicated the formation of the methyl caged xanthone **C34**. The reaction mixture was then cooled to room temperature and the solvent was removed by rotary evaporation. The crude material was purified through flash column chromatography (silica, 15-20% EtOAc-hexane) to yield the methyl caged xanthone **C34** (30 mg, 85%). **C34**: white solid; R_f = 0.56 (30 % EtOAc-hexane); ^{1}H NMR (400 MHz, CDCl$_3$) δ 7.87 (d, J = 7.7 Hz, 1H), 7.47 (m, 1H), 7.03 (m, 2H), 4.42 (t, J = 7.0 Hz, 1H), 3.18 (d, J = 4.4 Hz, 1H), 2.61 (m, 1H), 2.51 (s, 3H), 2.45 (d, J = 9.5 Hz, 1H), 2.28 (dd, J = 13.5, 4.7 Hz, 1H), 1.70 (s, 3H), 1.35 (s, 3H), 1.34 (m, 1H), 1.27 (s, 3H), 0.96 (s, 3H); ^{13}C NMR (100 MHz, CDCl$_3$) δ 203.6, 179.3, 158.3, 150.7, 135.5, 134.8, 126.8, 121.7, 120.6, 118.3, 117.6, 90.5, 84.8, 83.2, 55.8, 49.2, 30.3, 29.0, 28.6, 25.6, 24.9, 19.7, 16.7; HRMS calc. for C$_{24}$H$_{26}$O$_4$ (M + H)$^+$ 379.1904, found 379.1909.

196 → **C35**

piperidine, CH$_2$Cl$_2$, 6 h, 60 °C
(86%)
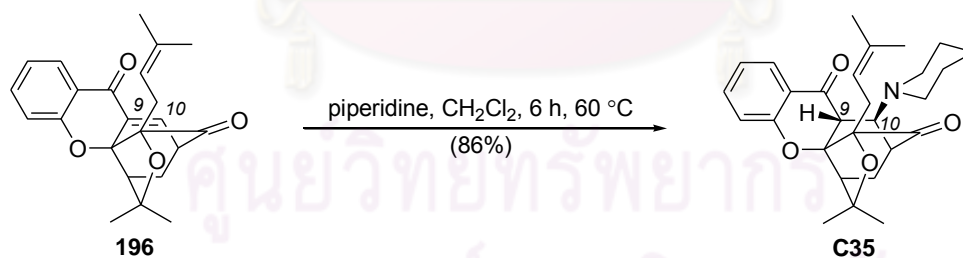
Piperidine addition product (C35): A solution of compound **196** (7.1 mg, 0.019 mmol) in CH$_2$Cl$_2$ (0.5 mL) was treated with piperidine (7 µL, 0.76 mmol) at 60 °C for 6 h. The crude material was purified through flash column chromatography (silica, 20-70% Et$_2$O-hexane) to yield adduct **C35** (7.3 mg, 86%). **C35**: white solid; R_f = 0.71 (70 % Et$_2$O-hexane); ^{1}H NMR (400 MHz, CDCl$_3$) δ 7.90 (d, J = 8 Hz, 1H), 7.56-7.52 (m, 1H), 7.08-7.01 (m, 2H), 5.23-5.50 (m, 1H), 3.36 (s, 1H), 3.26 (s, 1H), 3.15 (b, 1H), 2.91-2.78 (m, 3H), 2.53 (b, 1H), 2.45 (d, J = 8.8 Hz, 1H), 2.34-2.23 (b, 2H), 1.95 (dd, J = 14.8 Hz, 6.4 Hz, 1H), 1.93-1.84 (b, 1H), 1.68 (s, 3H), 1.62 (s, 3H), 1.51-1.40

(m, 6H), 1.37 (s, 3H), 1.13 (s, 3H); 13C NMR (100 MHz, CDCl3) δ 209.1, 191.7, 158.3, 136.4, 132.9, 127.0, 125.4, 121.4, 120.7, 118.3, 118.2, 89.4, 86.7, 81.5, 62.1, 51.3, 48.3, 43.4, 42.0, 30.4, 29.8, 28.0, 27.5, 26.0, 25.7, 24.6, 22.0, 18.1; HRMS calc. for $C_{28}H_{35}NO_4$ $(M + H)^+$ 450.2639, found 450.2620.

196   MeOH, 3 d, 65 °C   (41%)   **C36**
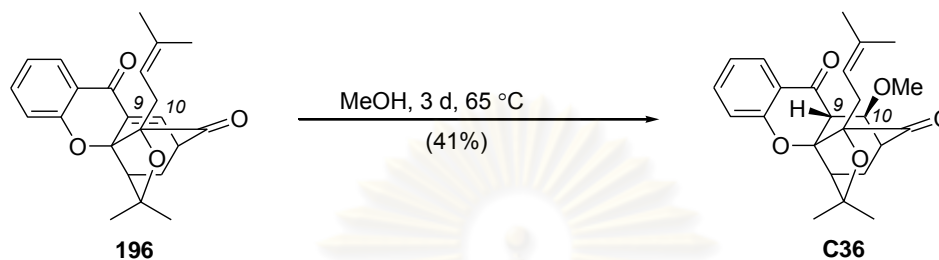
Methanol addition product (C36): A solution of compound **196** (14 mg, 0.038 mmol) in MeOH (0.5 mL) was refluxed at 65 ºC under argon for 3 days. The reaction mixture was then cooled to room temperature and the solvent was removed by rotary evaporation. The crude material was purified through flash column chromatography (silica, 20% EtOAc-hexane) to yield adduct **C36** (6.3 mg, 41%). **C36**: white solid; R_f = 0.39 (25% EtOAc-hexane); ^{1}H NMR (400 MHz, CDCl$_3$): δ 7.92 (d, J = 7.8 Hz, 1H), 7.57 (t, J = 8.5 Hz, 1H), 7.11-7.03 (m, 2H), 5.27-5.23 (m, 1H), 4.38 (d, J = 4.3 Hz, 1H), 3.38 (s, 1H), 3.30 (s, 3H), 2.92-2.78 (m, 3H), 2.42 (d, J = 8.9 Hz, 1H), 1.98 (dd, J = 6.13, 14.7 Hz, 1H), 1.64 (s, 3H), 1.60 (s, 3H), 1.41-1.35 (m, 1H), 1.37 (s, 3H), 1.14 (s, 3H); ^{13}C NMR (100 MHz, CDCl$_3$) δ 208.6, 191.0, 158.8, 137.1, 134.1, 127.5, 122.0, 120.7, 118.7, 118.5, 88.9, 86.9, 81.7, 75.3, 55.8, 49.1, 44.6, 43.6, 29.9, 27.9, 27.7, 26.1, 20.2, 18.1; HRMS calc. for $C_{24}H_{28}O_5$ $(M + H)^+$ 397.2010, found 397.2016.

3.2.4 Procedure for the Isolation and Purification of Gambogic Acid (77)

Gambogic acid (**77**) was isolated from the methanolic extract of gamboge as its pyridine salt **C37**. Then pyridine salt **C37** was acidified with 1N HCl in ether to afford gambogic acid (**77**).

C37
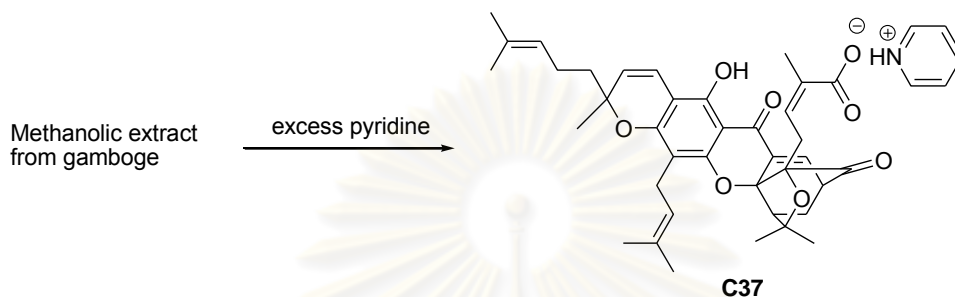
Pyridine salt of gambogic acid (C37): Dry powder of gamboge resin (19.0 g) of *G. hurburyi* tree was extracted with MeOH (80.0 mL) at room temperature for a day. The mixture was filtered and the extraction was repeated two more times with methanol (80.0 mL). The combined filtrate was concentrated under reduced pressure to yield crude extract (13.0 g) as a yellow powder. The crude extract (13.0 g) was dissolved in pyridine (13.0 mL), and then warm water (5.0 mL) was added to the stirred solution. The reaction mixture was cooled to room temperature and some precipitate was observed. Hexane (10.0 mL) was added to the mixture and the mixture was filtered. The solid was collected and washed with hexane and dried to yield pyridine salt of gambogic acid **C37** in 9% (1.8 g). **C37**: yellow solid; ^{1}H NMR (400 MHz, CDCl$_3$) δ 8.58-8.57 (m, 2H), 7.71 (t, J = 7.5 Hz, 1H), 7.53 (d, J = 6.8 Hz, 1H), 7.33-7.30 (m, 2H), 6.55 (d, J = 10.1 Hz, 1H), 6.07 (t, J = 7.1 Hz, 1H), 5.34 (d, J = 10.1 Hz, 1H), 5.02 (br s, 2H), 3.47-3.45 (m, 1H), 3.29-3.26 (m, 1H), 3.14-3.12 (m, 1H), 3.02-2.97 (m, 2H), 2.50 (d, J = 9.2 Hz, 1H), 2.32-2.27 (m, 1H), 2.00-1.98 (m, 2H), 1.73-1.53 (m, 20H), 1.39-1.37 (m, 1H), 1.34 (s, 3H), 1.27 (s, 3H); ^{13}C NMR (100 MHz, CDCl$_3$) δ 203.7, 179.2, 171.1, 161.6, 157.8 (2C), 149.1, 137.1, 136.9 (2C), 135.4, 133.6, 132.0, 131.6, 128.4, 124.6, 124.2 (2C), 124.0, 122.5, 116.1, 107.8, 102.8, 100.7, 91.2, 84.0 (2C), 81.4, 49.2, 47.0, 42.2, 30.1, 29.4, 29.1, 27.9, 25.9 (2C), 25.4, 23.0, 21.8, 21.2, 18.3, 17.8.

C37   1N HCl
ether
(99%)   **77:** gambogic acid
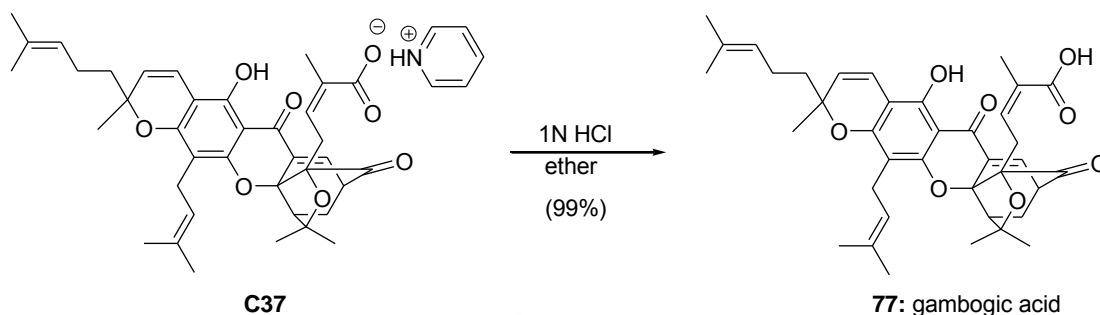
Gambogic acid (77): To a solution of the pyridine salt of gambogic acid **C37** (404.8 mg, 0.57 mmol) in ether (6.0 mL) was added aq. HCl (1N, 4.0 mL) at room temperature. After 1 h, the ether solution was washed with water (3 x 1.0 mL), dried, and evaporated to yield gambogic acid **1** (355.9 mg, 99%). **1:** yellow solid; $R_f = 0.38$ (25% EtOAc-hexane); ^{1}H NMR (400 MHz, CDCl$_3$): δ 7.54 (d, J = 6.9 Hz, 1H), 6.55 (d, J = 10.1 Hz, 1H), 6.12 (t, J = 7.3 Hz, 1H), 5.34 (d, J = 10.2 Hz, 1H), 5.05-5.01 (m, 2H), 3.49-3.46 (m, 1H), 3.31-3.25 (m, 1H), 3.13-3.10 (m, 1H), 2.98 (d, J = 7.3 Hz, 2H), 2.50 (d, J = 9.3 Hz, 1H), 2.30 (dd, J = 13.4, 4.6 Hz, 1H), 2.00-1.98 (m, 2H), 1.72-1.53 (m, 20H), 1.42-1.40 (m, 1H), 1.34 (s, 3H), 1.28 (s, 3H); ^{13}C NMR (100 MHz, CDCl$_3$) δ 203.6, 179.0, 172.1, 161.7, 157.7, 157.5, 138.7, 135.5, 133.5, 132.0, 131.7, 127.7, 124.6, 124.1, 122.4, 116.1, 107.7, 102.9, 100.6, 91.1, 84.1, 84.0, 81.5, 49.2, 47.0, 42.2, 30.1, 29.5, 29.1, 27.9, 25.9 (2C), 25.4, 23.0, 21.8, 21.0, 18.3, 17.9; HRMS calc. for C$_{38}$H$_{44}$O$_8$ $(M + Na)^+$ 651.2928, found 651.2931.

3.2.5 Procedure for the Synthesis of Gambogic Acid Analogues

77   RNH$_2$, HATU,
DIPEA
(67-87%)   **C38-C40**
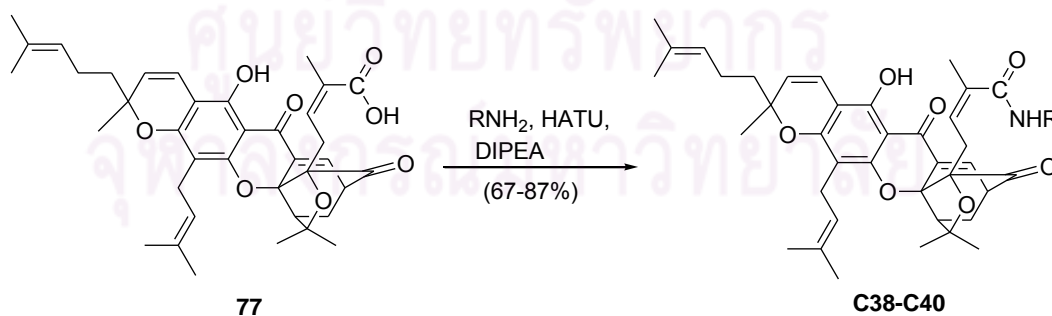
Biotin conjugate (C38): To a solution containing gambogic acid (**77**) (5.0 mg, 7.95 μmol) and biotin ethylenediamine hydrobromide (3.2 mg, 8.75 μmol) in CH$_2$Cl$_2$ (0.34 mL) was added DIPEA (2.77 μL, 15.9 μmol) *via* syringe. Upon adding solid HATU (3.6 mg, 9.46 μmol) portionwise to the reaction mixture, the reaction mixture turned

to pale yellow in color within 5 min. After 24 h, the reaction mixture was diluted with EtOAc (5 mL) and washed with water (2 x 1 mL) and brine (2 mL). The organic layers were dried over MgSO$_4$, filtered and concentrated by rotary evaporation. The crude material was purified through preparative TLC (silica, 17% MeOH-EtOAc) to yield the biotin conjugate **C38** (4.8 mg, 67%). **C38**: yellow solid; R_f = 0.11 (17% MeOH-EtOAc); ^{1}H NMR (400 MHz, CDCl$_3$) δ 7.59 (d, J = 6.9 Hz, 1H), 6.90-7.05 (m, 2H), 6.68 (d, J = 10.2 Hz, 1H), 6.02 (br s, 1H), 5.47 (d, J = 10.3 Hz, 1H), 5.28 (m, 2H), 5.03 (m, 2H), 4.49 (m, 1H), 4.32 (m, 1H), 3.00-3.60 (m, 8H), 2.89 (dd, J = 12.8, 4.8 Hz, 1H), 2.72 (d, J = 13.1 Hz, 2H), 2.54 (d, J = 9.3 Hz, 1H), 2.34 (m, 2H), 2.20 (m, 2H), 2.03 (m, 2H), 1.77-1.25 (m, 33H); ^{13}C NMR (100 MHz, CDCl$_3$) δ 205.1, 179.0, 174.0, 170.2, 163.9, 162.1, 157.9, 157.3, 136.0, 135.6, 133.2, 132.1, 125.2, 123.9, 122.1, 115.9, 108.0, 103.0, 100.6, 91.3, 84.6, 84.0, 81.8, 61.8, 60.4, 55.5, 49.1, 47.0, 42.3, 40.8, 40.0, 39.5, 35.9, 30.1, 29.9, 29.3, 29.1, 28.2, 28.1, 28.0, 25.9, 25.7, 25.4, 22.9, 21.8, 21.3, 18.4, 17.9; HRMS calc. for C$_{50}$H$_{64}$N$_4$O$_9$S (M + Na)$^+$ 919.4286, found 919.4329.

Coumarin conjugate (C39): To a solution containing gambogic acid (**77**) (5.8 mg, 9.22 μmol) and coumarin hexanediamine TFA salt (4.6 mg, 10.1 μmol) in CH$_2$Cl$_2$ (0.30 mL) was added DIPEA (3.21 μL, 18.4 μmol). Upon adding solid HATU (4.2 mg, 10.9 μmol) portionwise to the reaction mixture, the reaction mixture turned to pale yellow in color within 5 min. After 24 h, the reaction mixture was diluted with EtOAc (5 mL) and washed with water (2 x 1 mL) and brine (2 mL). The organic layers were dried over MgSO$_4$, filtered and concentrated by rotary evaporation. The crude material was then purified through preparative TLC (silica, 100% EtOAc) to yield the coumarin conjugate **C39** (7.7 mg, 87%). **C39**: yellow solid; R_f = 0.29 (100% EtOAc); ^{1}H NMR (400 MHz, CDCl$_3$) δ 7.49 (d, J = 9.1 Hz, 2H), 6.66 (d, J = 10.1 Hz, 1H), 6.60 (dd, J = 9.0, 2.4 Hz, 1H), 6.47 (s, 2H), 6.04 (s, 2H), 5.46 (d, J = 10.0 Hz, 1H), 5.30 (t, J = 8.2 Hz, 1H), 5.07-5.02 (m, 2H), 3.63 (s, 2 H), 3.46 (t, J = 6.1 Hz, 1H), 3.33-3.19 (m, 6H), 3.03 (s, 6H), 2.55 (d, J = 9.2 Hz, 2H), 2.38-2.29 (m, 2H), 2.08-2.01 (m, 2H), 1.77-1.25 (m, 35H); ^{13}C NMR (100 MHz, CDCl$_3$) δ 204.4, 178.9, 169.5, 168.1, 162.0, 157.9, 156.3, 153.3, 150.1, 135.9, 132.2, 132.1, 126.0, 125.1, 124.1, 123.9, 122.2, 115.9, 110.6, 109.4, 108.6, 108.1, 103.0, 100.5, 98.3, 91.3, 84.3, 83.7,

81.8, 49.2, 47.2, 42.3, 41.0, 40.3, 39.6, 38.9, 30.2, 29.9, 29.5, 29.3, 29.2, 29.0, 28.1, 26.1, 26.0, 25.9, 25.4, 22.9, 21.8, 21.5, 18.4, 17.9; HRMS calc. for $C_{57}H_{69}N_3O_{10}$ (M + H)$^+$ 956.5056, found 956.5069.

BODIPY conjugate (C40): To a solution containing gambogic acid (**77**) (6.1 mg, 9.70 µmol) and BODIPY FL EDA (3.95 mg, 10.7 *µmol*) in CH_2Cl_2 (0.24 mL) was added DIPEA (3.38 *µL*, 19.4 *µmol*). Upon adding solid HATU (4.37 mg, 11.5 µmol) portionwise to the reaction mixture, the reaction mixture turned to pale yellow in color within 5 min. After 24 h, the reaction mixture was diluted with EtOAc (5 mL) and washed with water (2 x 1 mL) and brine (2 mL). The organic layers were dried over $MgSO_4$, filtered and concentrated by rotary evaporation. The crude material was purified by preparative TLC (silica, 100% EtOAc) to yield the amide **C40** (7.05 mg, 77%). **C40**: red solid; R_f = 0.38 (100% EtOAc); ^{1}H NMR (400 MHz, CDCl$_3$) δ 7.51 (d, J = 6.9 Hz, 1H), 7.03 (s, 1H), 6.92-6.90 (m, 1H), 6.85 (d, J = 4.1 Hz, 1H), 6.68 (d, J = 10.2 Hz, 1H), 6.62 (m, 1H), 6.27 (d, J = 3.9 Hz, 1H), 6.09 (s, 1H), 5.46 (d, J = 10.2 Hz, 1H), 5.22-5.16 (m, 1H), 5.09-4.99 (m, 2H), 3.49-3.15 (m, 9H), 2.64 (m, 3H), 2.53 (s, 3H), 2.31-2.27 (m, 3H), 2.21 (s, 3H), 2.06-2.02 (m, 2H), 1.75-1.24 (m, 27 H); ^{13}C NMR (100 MHz, CDCl3) δ 204.8, 178.9, 172.4, 169.5, 162.0, 157.9, 157.3, 135.8, 133.3, 132.1, 128.8, 125.2, 124.9, 124.0, 123.9, 122.2, 120.4, 117.9, 115.9, 108.0, 103.0, 100.5, 91.3, 84.5, 84.0, 81.8, 49.1, 46.9, 42.3, 39.9, 39.8, 35.8, 30.1, 29.9, 29.2, 29.0, 28.1, 25.9, 25.4, 24.9, 22.9, 21.8, 21.4, 18.4, 17.9, 15.1, 11.5; HRMS calc. for $C_{54}H_{63}BF_2N_4O_8S$ (M + H)$^+$ 944.4816, found 944.4860.

3.2.6 Biological Assay

3.2.6.1 ^{3}H-Thymidine Incorporation Assay

Cells were plated in a 96-well plate at 10-20 x 10^3 cells/well in RPMI supplemented with 10% fetal bovine serum, 2 mM glutamine, 1% penicillin/streptomycin (complete medium). The caged *Garcinia* xanthones were added to the cells at increasing concentrations and 0.1% DMSO was added to control cells. Cells were incubated for 48 h and then pulsed with ^{3}H-thymidine for 6 h. Incorporation of ^{3}H-thymidine was determined in a scintillation counter (Beckman

Coulter Inc., Fullerton, CA) after cells were washed and deposited onto glass microfiber filters using a cell harvester M-24 (Brandel, Gaithersbur, MD).

3.2.6.2 Apoptosis Assays

3.2.6.2.1 ELISA Assay

The compounds were dissolved in DMSO and further diluted in complete medium to obtain final concentrations as indicated. HL-60 and HL-60/ADR cells were seeded into each well of a 96-well cell culture plate at 10,000 cells per well and incubated at 37 °C for 7 h with the indicated concentrations of each compound. Control samples were incubated in 0.1% DMSO. Each condition was in triplicate. The proapoptotic effect was detected by using the Cell Death Detection ELISA^{PLUS} kit (Roche Applied Science, Indianapolis, IN) according to the manufacturer instructions. This kit constitutes a photometric enzyme-immunoassay for the qualitative and quantitative *in vitro* determination of cytoplasmic histone-associated-DNA-fragments (mono- and oligo-nucleosomes) after induced cell death. The absorption values A (A_{405nm} − A_{490nm}) measured give a quantitative indication of the induced amount of apoptosis.

3.2.6.2.2 Fluorescence Microscopy of Annexin V/PI Stained Cells

HL-60/ADR cells were plated in a 6-well plate at 1 x 10^6 cell/ml (4 mL) and treated with 0.5 μM of cluvenone (**196**) while control cells received 0.1% DMSO. Cells were incubated overnight and then stained with Alexa Fluor 488 annexin V and propidium iodide using the Vybrant Apoptosis Assay Kit (Molecular Probes, Eugene, OR) according to manufacturer's recommendations. Cells were then viewed on an E800 Nikon (New York City, NY) research microscope equipped with an EXFO (Vanier, Canada) X-cite fluorescent 120 W metal halide illuminator and imaged with a DMX 1200F Nikon fluorescence sensitive digital camera.

3.3   Results & Discussion

3.3.1   Synthesis of BC and C ring Caged Analogues

The observation that lateriflorone (**98**) maintains the desired bioactivity profile despite the modification of structure at the AB rings creating an interesting question: Is the xanthone backbone (ABC scaffold) necessary for bioactivity or can the A-ring and even the B-ring be eliminated without significant loss of function? In other words, do compounds **C8**, **C9** and **C19** maintain the desired bioactivity? The BC and C ring caged analogues were thus synthesized and evaluated to test these hypotheses.

The initial studies aimed to manipulate analogues of the caged *Garcinia* xanthones lacking the A ring: caged compounds **C8** and **C9**. The preparation of **C8** and **C9** could be achieved in three steps as shown in Scheme 3.21. Using commercially available 2,3,4-trihydroxybenzoic acid (**C1**) as a starting material, **C2** was obtained by protection of **C1** with acetone in the presence of TFA/TFAA. Attempts to decrease the amount of di-protected products by performing the reaction at 0 °C proved to be fruitless, resulting in dioxanone **C2** in 31% yield with 60% of recovered starting material **C1**.
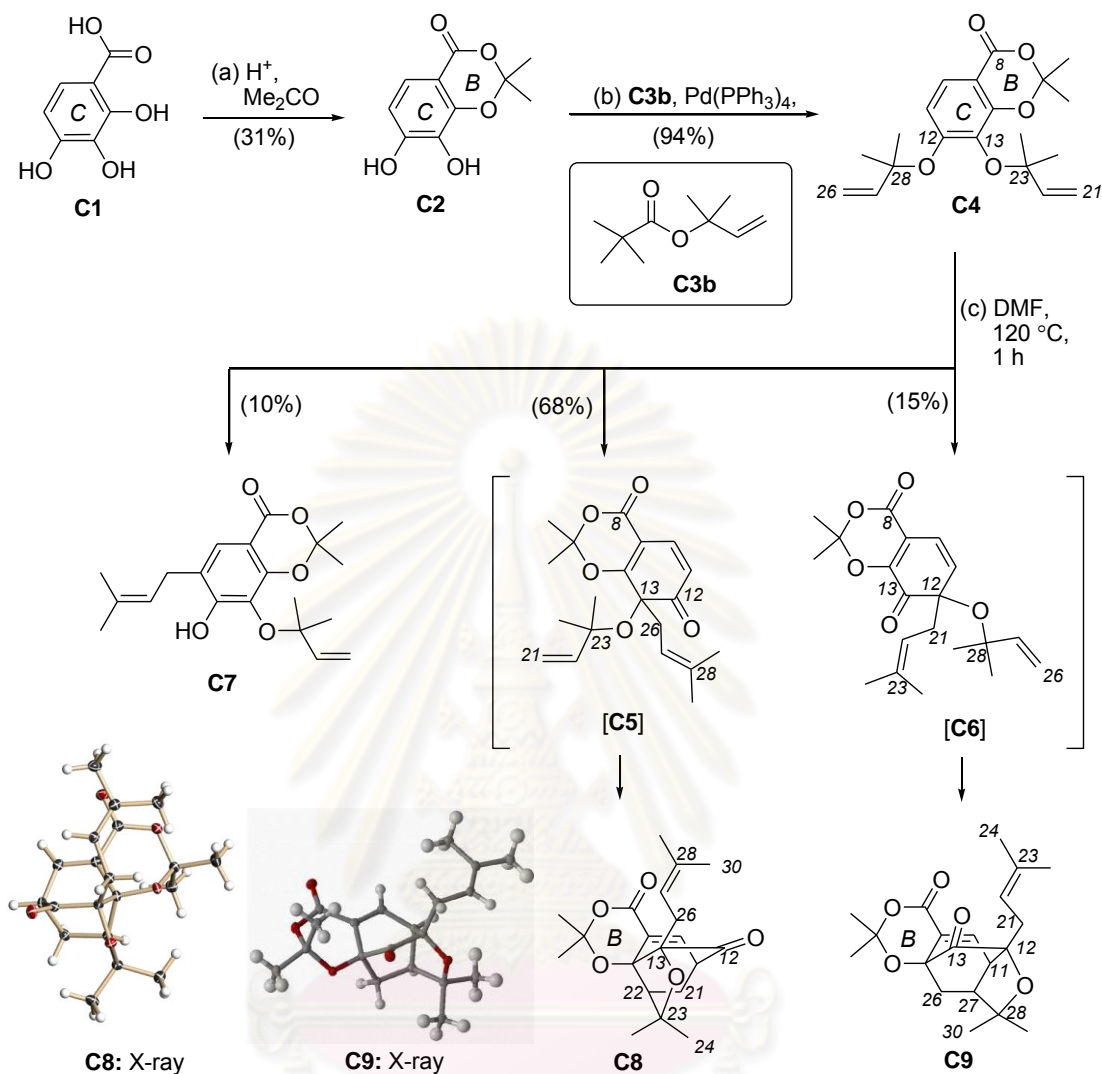
Scheme 3.21 Reagents and conditions: (a) 6.0 equiv. $(CH_3)_2CO$, 20 equiv. TFA, 10 equiv. TFAA, 19 h, 0 °C, 31% of **C2**, 60% RSM; (b) 10 equiv. 1,1-dimethylpropenyl *t*-butyl carbonate (**C3b**), 10 mol% $Pd(PPh_3)_4$, THF, 20 min, 5 °C, 94%; (c) DMF, 1 h, 120 °C, **C7:** 10%, **C8:** 68%, **C9:** 15%.

To generate di-allyloxy units in **C4**, an alternative method for the one-step introduction of the 1,1-dimethyl-2-propenyl unit (reverse prenyl group) to a catechol motif was developed and the results are illustrated in Table 3.1.

Table 3.1 Effect of carbonate (**C3**) on Pd-catalyzed reverse prenylation of **C2**
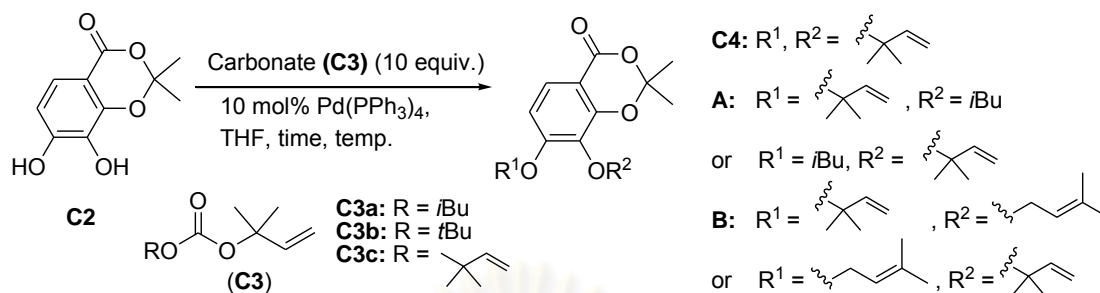
Entry	Carbonate (**C3**)	Conditions		%Yield		
		Time (h)	Temp (°C)	**C4**	**A**	**B**
1	**C3a**	4	RT (25-30)	69	10	15
2			5	62	5	-
3[a]		48	5	no reaction		
4	**C3b**	20 min	5	94	-	-
5	**C3c**	20 min	5	92	-	-

[a] 0.1 equiv. RhCl(PPh$_3$)$_3$ was used.

Support for this reaction came from a report on the reverse prenylation of a substituted phenol using 1,1-dimethylpropenyl isobutyl carbonate (**C3a**) under Pd(0) catalysis [230]. Using **C3a**, the desired compound **C4** (62-69% yield, entries 1 and 2) was obtained together with significant amounts of side products which seemed to be isobutyl addition product **A** (5-10%) and rearranged prenyl product **B** (15%). To minimize the formation of side product **A**, the allylation with 1,1-dimethylpropenyl *t*-butyl carbonate (**C3b**) was tested and to decrease the side product **B**, the reaction was also carried out at 5 °C. Fortunately, the formation of **C4** was observed as the only product in near quantitative yield (94% isolated yield, entry 4) without any formation of side products. Similar yields (90-92%) were obtained using the unexplored *bis*(1,1-dimethylpropenyl)carbonate (**C3c**) (entry 5) [231]. This reaction was in addition evaluated under Rh(I) catalysis, but did not observe the formation of any reverse prenyl product (entry 3) [232]. This might be suggested that the reactivity on the reverse prenylation of di-hydroxy compounds depended on the electronic and steric effects of the metals and ligands.

There are many advantages of the one-step installation of reverse prenyl units onto di-hydroxy phenols using Pd(PPh$_3$)$_4$ as a catalyst and either carbonate **C3b** or

C3c as a prenylating agent over the previous procedure concerning with the two-step process: (a) *O*-alkylation; (b) reduction of alkyne to alkene [209] or Witting reaction [132]. This developed method was successfully utilized to prepare di-allyloxy units in excellent yields with short reaction time under mild conditions. In addition, this is the first time to exploit carbonate **C3b** as a prenylating agent on the reverse prenylating reaction.

To attain the caged motif, heating of **C4** in DMF (120 °C, 1 h) could engage in two possible Claisen rearrangement pathways (Scheme 3.22) to furnish the two intermediates **C5** and **C6**. These two intermediates could then undergo the intramolecular Diels/Alder reactions which would lead to two caged compounds **C8** and **C9** in 68% and 15% yields, respectively (Scheme 3.21). The caged structures **C8** and **C9** were truly confirmed by NMR, and relative stereochemistry of these caged compounds was unambiguously confirmed *via* a single-crystal X-ray analysis.

The ^{1}H NMR spectrum of **C8** (Figure 3.4) revealed the presence of the characteristic olefinic proton signal of C9-C10 double bond at δ_H 7.44 (d, J = 6.9 Hz, 1H, H-10). There were resonances for an olefinic proton at δ_H 4.41 (m, 1H, H-27), the proton on the carbon connecting to C12 carbonyl group at δ_H 3.42 (t, J = 4.3 Hz, 1H, H-11). The signals of two methylene groups belonged to H-26 and H-21 were observed at δ_H 2.72 (dd, J = 13.8, 10.4 Hz, 1H, H-26) and 2.63 (m, 1H, H-26), and 2.31 (dd, J = 13.6, 4.7 Hz, 1H, H-21) and 1.44 (dd, J = 13.6, 9.3 Hz, 1H, H-21), respectively. The appearance of doublet signal at δ_H 2.50 (d, J = 9.7 Hz, 1H) was assigned to H-22.The two singlet signals of acetonide unit at δ_H 1.69 (s, 3H) and 1.67 (s, 3H), and four singlet signals of four methyl groups at δ_H 1.62 (s, 3H, H-24), 1.54 (s, 3H, H-29), 1.53 (s, 3H, H-25) and 1.23 (s, 3H, H-30) were also shown.

The ^{13}C NMR spectrum (Figure 3.5) revealed resonances for two carbonyl carbons of ketone and ester at δ_C 203.2 (C-12) and 159.9 (C-8), respectively, and two carbons of C9-C10 double bond at δ_C 139.0 (C-10) and 135.5 (C-9). The signals of four oxygenated quaternary carbons at δ_C 105.1 (C-16), 85.0 (C-13), 84.9 (C-23) and 82.9 (C-14), and two olefinic carbons at δ_C 128.1 (C-28) and 118.1 (C-27) were detected. The signals of two methylene carbons at δ_C 29.1 (C-26) and 26.9 (C-21), sp3

carbon at δ_C 48.6 (C-22) and 46.8 (C-11), and six methyl carbons at δ_C 30.2 (C-24), 28.8 (C-25), 28.5 (C-16a), 28.0 (C-16a′), 25.9 (C-29) and 18.4 (C-30) were also presented.

The ^{1}H NMR spectrum of **C9** (Figure 3.6) disclosed an olefinic proton at δ_H 7.41 (d, $J = 7.0$ Hz, 1H, H-10) and 4.95 (t, $J = 7.0$ Hz, 1H, H-22), belonging to enone bond and reversed prenyl unit, respectively. The signal at δ_H 3.63 (dd, $J = 7.0$, 4.5 Hz, 1H) was assigned to H11, and 2.36-2.25 were ascribed to protons H21 (m, 2H), H26 (m, 1H), and H27 (m, 1H). A multiplet signal belonging to H26 was also detected at δ_H 1.64-1.61 (m, 1H). Two singlet signals at δ_H1.69 (s, 3H, H-16a′) and 1.68 (s, 3H, H-16a) were ascribed to six methyl protons of acetonide group. The remaining methyl proton signals were observed at δ_H 1.59 (s, 3H, H-29), 1.43 (s, 3H, H-24), 1.31 (s, 3H, H-30), and 1.29 (s, 3H, H-25). The ^{13}C NMR spectrum (Figure 3.7) signified two carbonyl carbons at δ_C 205.0 (C-12) and 159.2 (C-8), two carbons of C9-C10 double bond at δ_C 139.0 (C-10) and 135.5 (C-9), methine carbon at δ_C 117.2 (C-22), and four oxygenated quaternary carbons at δ_C 106.5 (C-16), 83.6 (C-28), 81.2 (C-13) and 80.1 (C-14). The quaternary carbon signal at δ_C 127.7 (C-23) and two methylene carbon signals at δ_C 30.7 (C-21) and 27.0 (C-26) were detected. The signals at δ_C 46.0 and 45.0 were ascribed to C27 and C11, respectively. The signals at δ_C 34.1 (C-30), 30.2 (C-29), 28.6 (C-16a′), 27.8 (C-16a), 26.2 (C-24), and 18.2 (C-25) could be designated for six methyl carbons.

Under these conditions, the formation of phenol **C7** arising from a Claisen rearrangement of **C4** was detected in 10% yield. However, upon additional heating at 120 °C, the prenyl group of phenol **C7** could migrate back to give the stating material **C4** and after Claisen rearrangement/Diels-Alder cycloaddition produced caged compounds **C8** and **C9**, supporting the reversibility of the Claisen rearrangement [218, 233-235].

Figure 3.4 The ^{1}H NMR spectrum (CDCl$_3$, 400 MHz) of compound **C8**

Figure 3.5 The ^{13}C NMR spectrum (CDCl$_3$, 100 MHz) of compound **C8**

Figure 3.6 The ^{1}H NMR spectrum (CDCl$_3$, 400 MHz) of compound **C9**

Figure 3.7 The ^{13}C NMR spectrum (CDCl$_3$, 100 MHz) of compound **C9**

To accomplish the C-ring caged analogues, the acetonide unit of compound **C8** was deprotected to open the B ring (Scheme 3.22). The protection did not proceed well under acidic condition in the presence of 1N or 2N HCl in MeOH while the exposure of **C8** to 10% aqueous Me$_4$NOH in MeOH provided the optimum saponification conditions, producing the desired β-hydroxy acid **C10** in quantitative yield. The ^{1}H NMR spectrum of **C10** (Figures 3.8) was compared to those of **C8**. It was similar to that of **C8** except the disappearance of two singlet signals belonging to acetonide group at δ_H 1.69-1.67. To consider ^{13}C NMR spectrum (Figure 3.9) of this compound, the chemical shifts of carbon signals were similar to those of **C8**; nonetheless, the characteristic carbonyl signal of carboxylic group was downfield shifted to δ_C 168.4. In addition, the signals of C16 oxygenated quaternary carbon at δ_C 105.1 and two methyl carbons at δ_C 28.5 (C-16a′) and 28.0 (C-16a), all of which attributed for an acetonide group were disappeared.
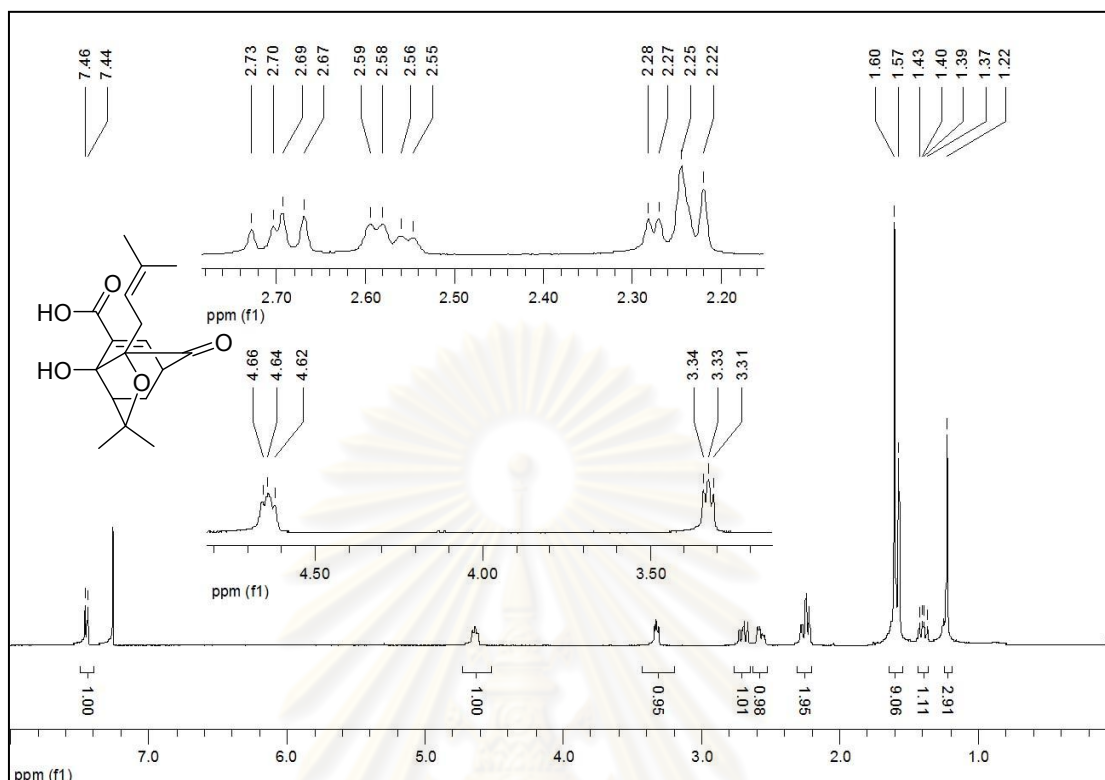
Figure 3.8 The ^{1}H NMR spectrum (CDCl$_3$, 400 MHz) of compound **C10**
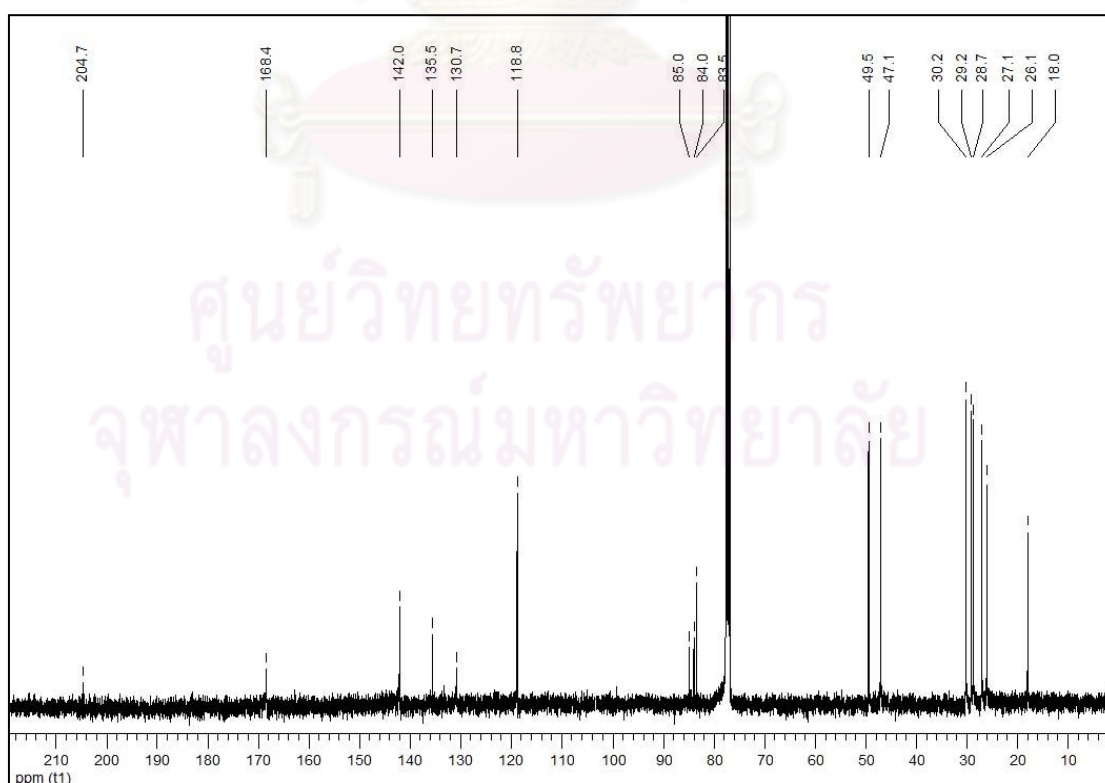
Figure 3.9 The ^{13}C NMR spectrum (CDCl$_3$, 100 MHz) of compound **C10**

Carboxylic acid **C10** was then used to react with the diverse amines containing the fluorescence probes such as biotin, coumarin and BODIPY. The reactions were smoothly performed using HATU as a coupling reagent to convert the carboxyl groups to amides **C11-C13** in good yields (54-68%) [100].
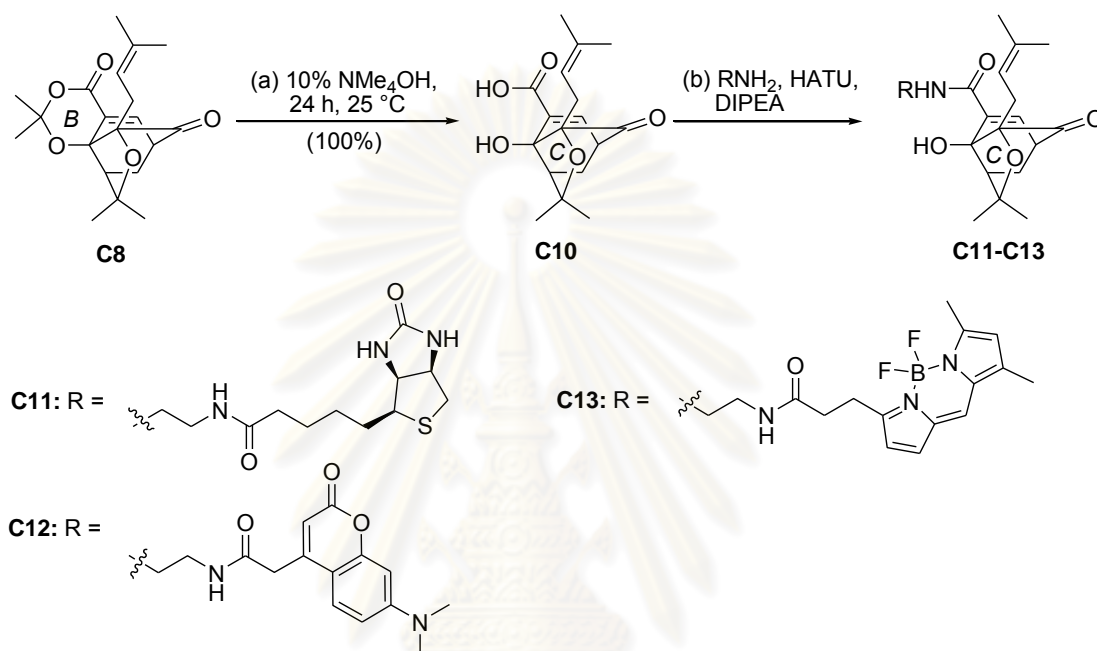
Scheme 3.22 Reagents and conditions: (a) excess 10% NMe$_4$OH (aq), MeOH, 24 h, 25 °C, 100%; (b) 2.0 equiv. DIPEA, 1.2 equiv. HATU, CH$_2$Cl$_2$, 24 h, 25 °C, **C11: 54%, C12: 59%, C13: 68%.**

The structures of fluorescent amides **C11-C13** were fully confirmed by ^{1}H, ^{13}C NMR and MS techniques. The ^{1}H NMR spectrum of biotin conjugate (**C11**) (Figure 3.10) showed five signals of four NH protons and a hydroxyl proton at δ_H 8.00-5.00. A doublet signal at δ_H 6.60 (J = 8.4 Hz) and a multiplet signal at δ_H 4.72 were due to an enone proton H10 and an olefinic proton H27, respectively. The two multiplet signals at δ_H 4.54 and 4.33 were ascribed to two protons on a carbon connecting with urea group.The multiplet signal at δ_H 3.50-3.33 was assigned for four protons on a carbon connecting with an amino group of amide bond. The signals at δ_H 3.23 (m), 2.94 (dd, J = 12.9, 4.9 Hz) and 2.74 (d, J = 12.9 Hz) were detected as the presence of three protons on a carbon connecting to a sulfur atom. Six proton signals of caged core were observed at δ_H 3.14 (H-11), 2.67-2.18 (H-21, H-22, H-26) and 1.40 (H-21). The chemical shifts at 2.30-1.60 indicated the presence of eight

methylene protons between a biotin unit and an amide bond. The signals belonging to twelve methyl protons were observed at δ_H 1.80-1.60 and 1.20. The ^{13}C NMR spectrum (Figure 3.11) displayed four peaks at δ_C 205.8, 175.4, 167.6, and 164.2 of four carbonyl carbons for ketone, amide, α,β-unsaturated amide and urea, respectively. Four sp2 carbons were observed at δ_C 134.5, 133.2, 132.6, and 118.7. The signals at δ_C 85.2, 84.3, and 83.2 could be designated for three oxygenated quaternary carbons. The chemical shifts of two aliphatic carbons connecting to a urea bond and two carbons bearing to a sulfur atom were observed at 61.9 and 60.4, and 55.8 and 41.1, respectively. Three signals at δ_C 40.8-35.9 could be assigned for three methylene carbons connected to amide bond. The nine peaks at δ_C 49.7, 46.4, and 30.4-18.1 were assigned to eleven aliphatic carbons.

The ^{1}H NMR spectrum of coumarin conjugate (**C12**) (Figure 3.12) exhibited seven signals of a hydroxyl proton, three aromatic protons, an olefinic proton connected to an ester bond and two NH protons at δ_H 7.60-6.00. The signals belonging to caged motif were detected as follows: doublet at δ_H 6.68 ($J = 7.0$ Hz , H-10); triplet at δ_H 4.69 ($J = 7.6$ Hz, H-27); two sets of doublet of doublet at δ_H 2.60 ($J = 14.0, 9.0$ Hz, H-26) and 2.47 ($J = 13.8, 6.3$ Hz, H-26); three multiplet signals at δ_H 3.10-3.20 (H-11), 2.16 (H-21 and H-22) and 1.27 (H-21); four singlet signals at δ_H 1.58-1.19 (each 3H, C-24, C-25, C-29 and C-30). The presence of two singlet signals at δ_H 3.64 and 3.06 was referred to two methylene protons on a carbon connected to a carbonyl group of amide bond and six methyl protons substituted on a nitrogen atom, respectively. The multiplet signal at δ_H 3.52-3.20 was ascribed to four methyl protons connected to a nitrogen atom of amide group. The ^{13}C NMR spectrum (Figure 3.13) revealed four peaks at δ_C 205.3, 169.8, 170.0, and 161.8 referred to four carbonyl carbons for ketone, amide, α,β-unsaturated amide and ester groups, respectively. Twelve peaks at δ_C 156.1-98.2 were assigned to twelve sp2 carbons. The three signals at δ_C 84.7, 84.4, and 83.0 could be assigned for three oxygenated quaternary carbons. The four peaks at δ_C 40.6, 40.1 and 30.1 were belonged to three methylene carbons connected to an amide bond. Two signals were observed at δ_C 40.5 and 40.4, pointing out the presence of two nitrogen-attached methyl carbons. The eight peaks at δ_C 49.1, 46.1, and 29.7-17.8 were ascribed to eight aliphatic carbons of caged motif.

The ^{1}H NMR spectrum of BODIPY conjugate (**C13**) (Figure 3.14) contained the signals of four olefinic protons at δ_H 7.11-6.24 and two methyl protons at δ_H 2.56 and 2.27, belonged to BODIPY core. The presences of two NH amide protons at δ_H 6.26 and 6.15, four methylene protons connecting to nitrogen atom around δ_H 3.40-3.10 was detected. Four methylene protons being between the BODIPY and amide groups were observed at δ_H 3.40-3.10 and 2.18-2.15. The H10 enone and hydroxyl protons of caged motif were observed as a doublet at δ_H 6.69 (J = 7.0 Hz) and broad singlet at δ_H 7.54, respectively. The chemical shifts assigned for caged core at 4.64 (t, J = 6.9 Hz, 1H, H-27), 3.20 (m, 1H, H-11), 2.71-2.56 (m, H-21 (1H), H-22 (1H), H-26 (2H)), and 1.36-1.27 (m, 1H, H-21) were detected. The remaining signals at δ_H 1.59 (6H), 1.51 (3H), and 1.19 (3H) were due to twelve methyl protons. The ^{13}C NMR spectrum (Figure 3.15) exhibited three peaks at δ_C 205.8, 174.5 and 167.3, belonging to the carbonyl carbons of ketone, amide and α,β-unsaturated amide, respectively. The twelve peaks at δ_C 161.4-117.2 were assigned to thirteen sp2 carbons. The signals at δ_C 85.3, 84.3, and 83.2 could be designated for three oxygenated quaternary carbons. The chemical shifts of three methylene carbons adjacent to an amide bond were detected at δ_C 42.1-35.9. The eight aliphatic carbons of caged motif were observed at δ_C 49.7, 46.3 and 29.3-18.0. The signals of methylene carbon connecting to a BODIPY unit at δ_C 30.3 and two methyl carbons substituted on a C=C bond at δ_C 15.3 and 11.6 were detected.
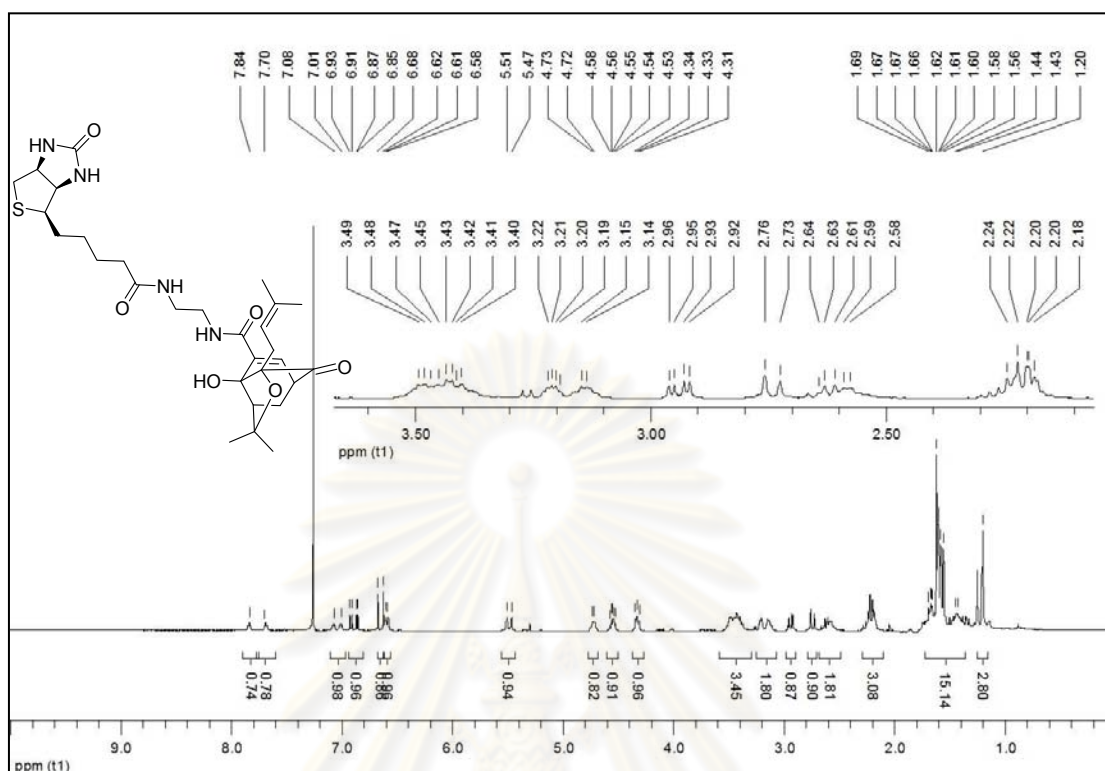
Figure 3.10 The ^{1}H NMR spectrum (CDCl$_3$, 400 MHz) of compound **C11**
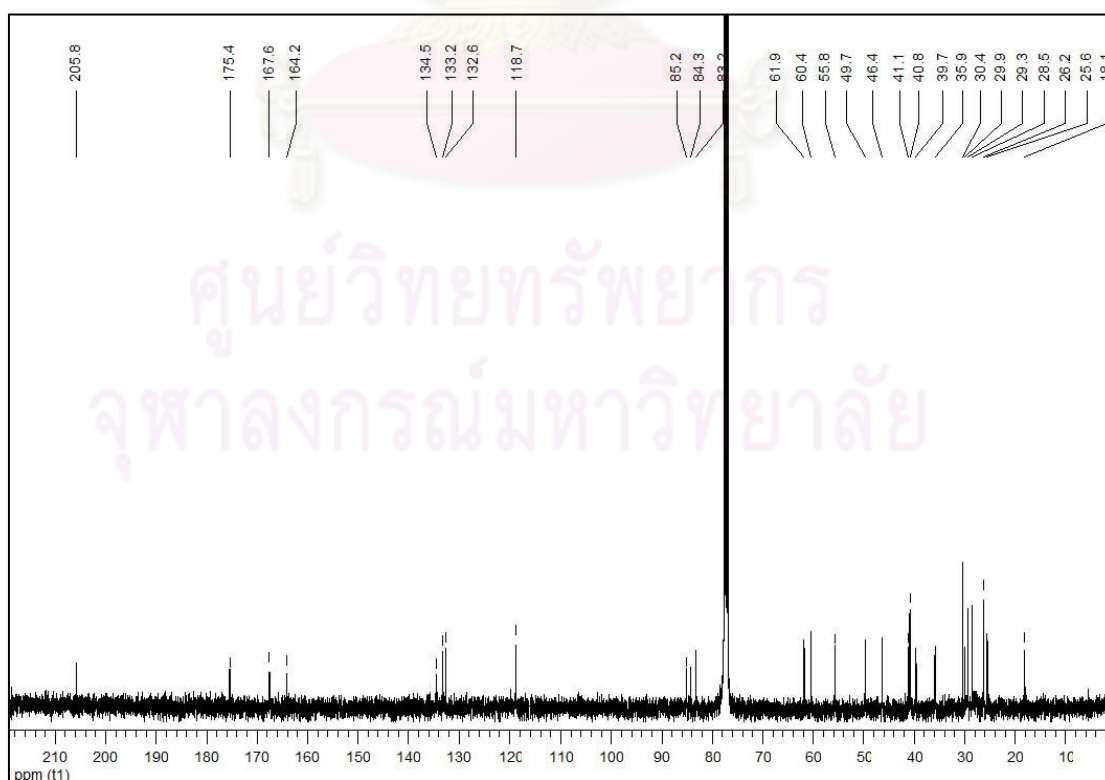
Figure 3.11 The ^{13}C NMR spectrum (CDCl$_3$, 100 MHz) of compound **C11**
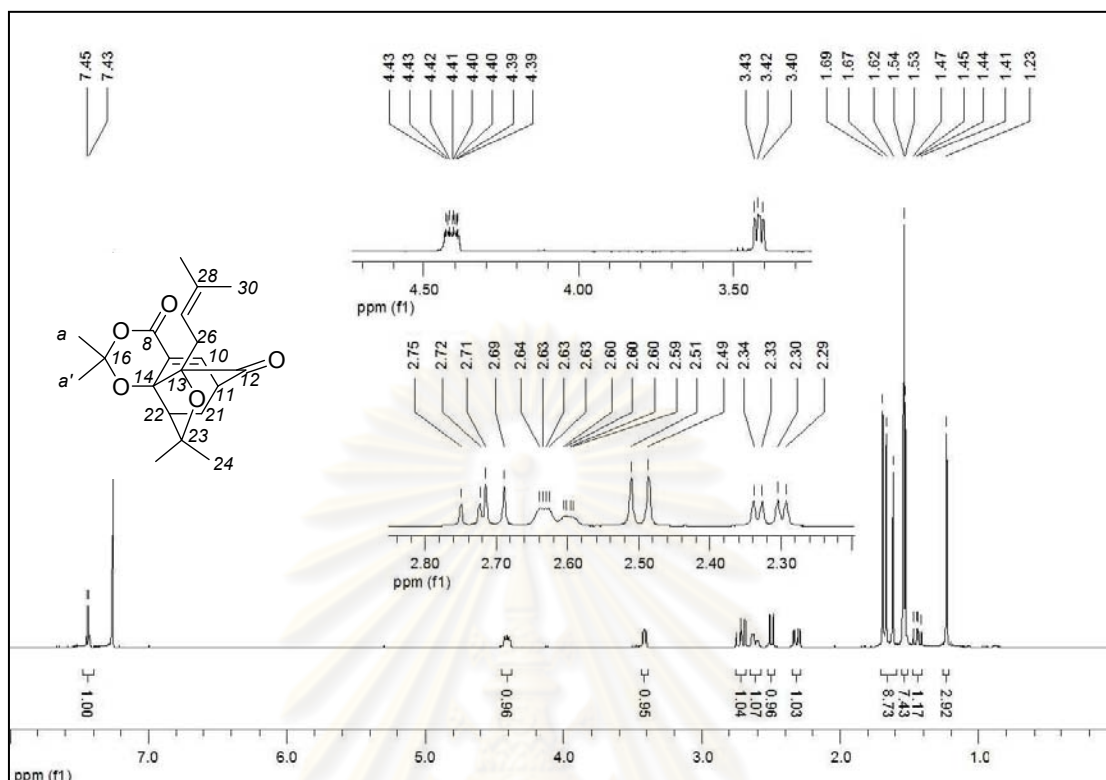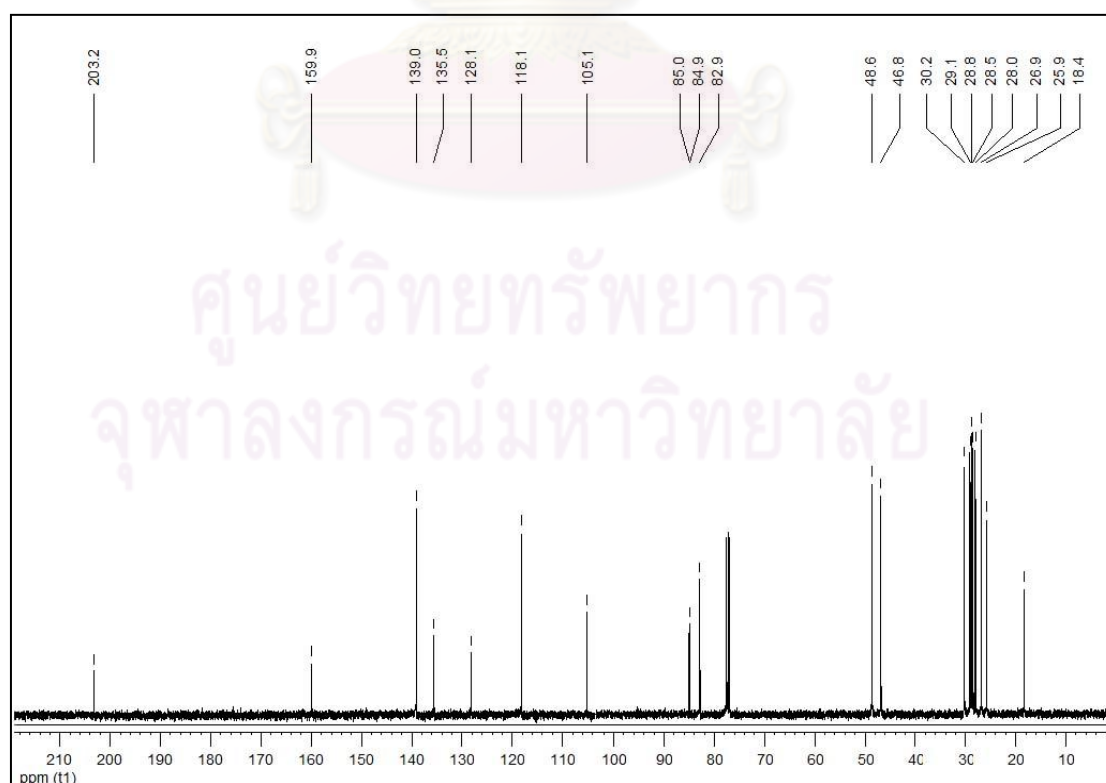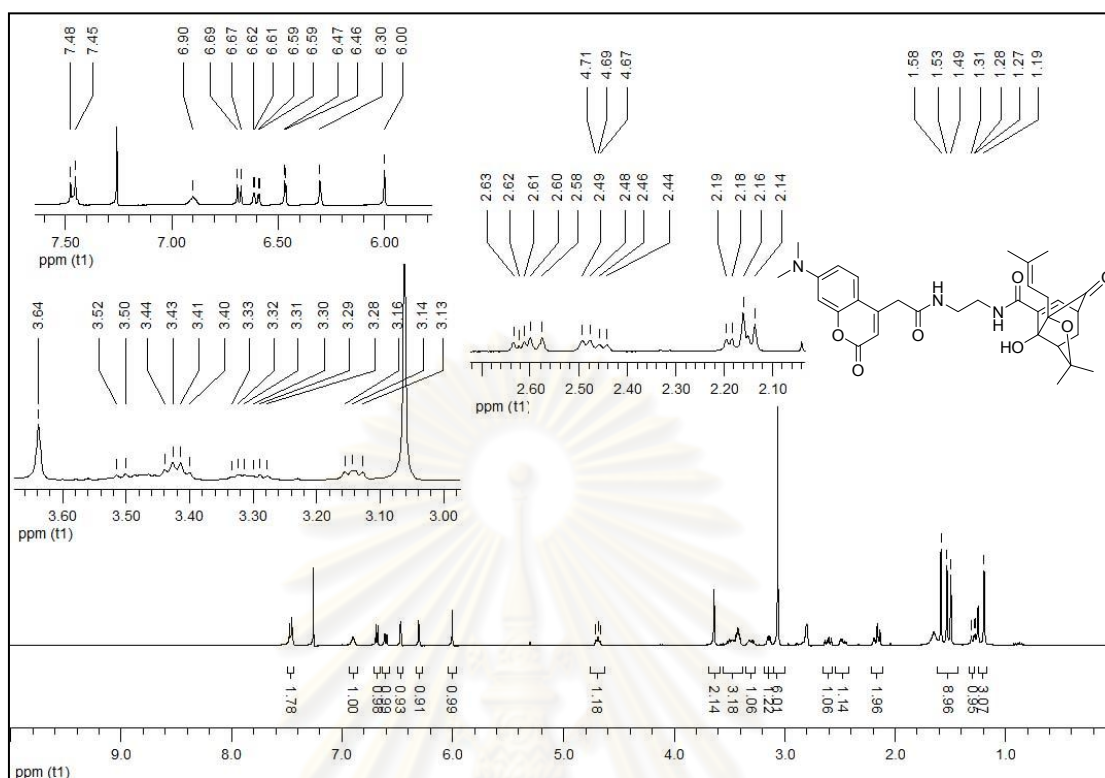
Figure 3.12 The ^{1}H NMR spectrum (CDCl$_3$, 400 MHz) of compound **C12**

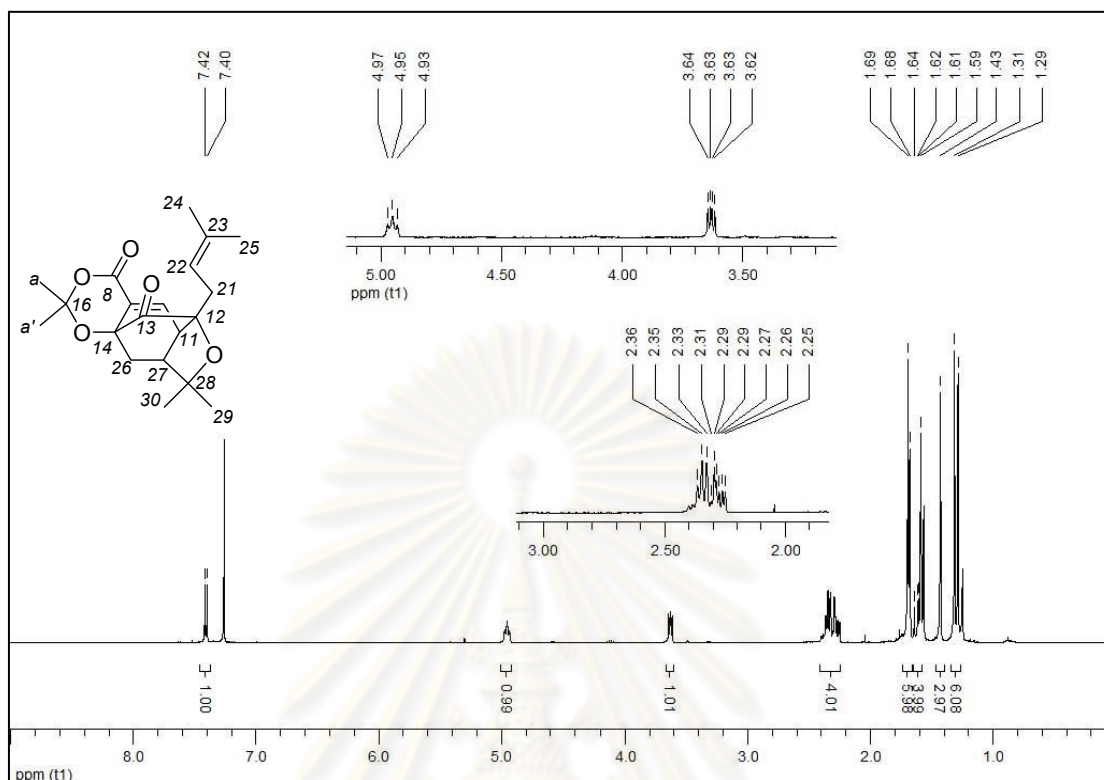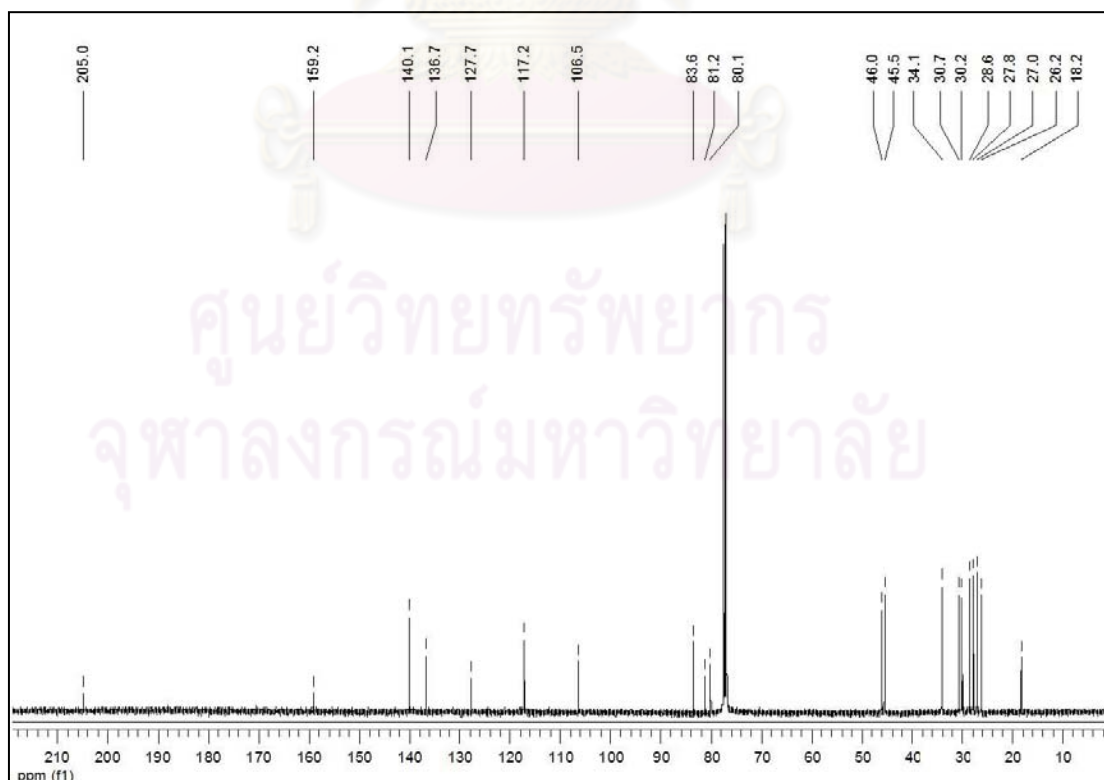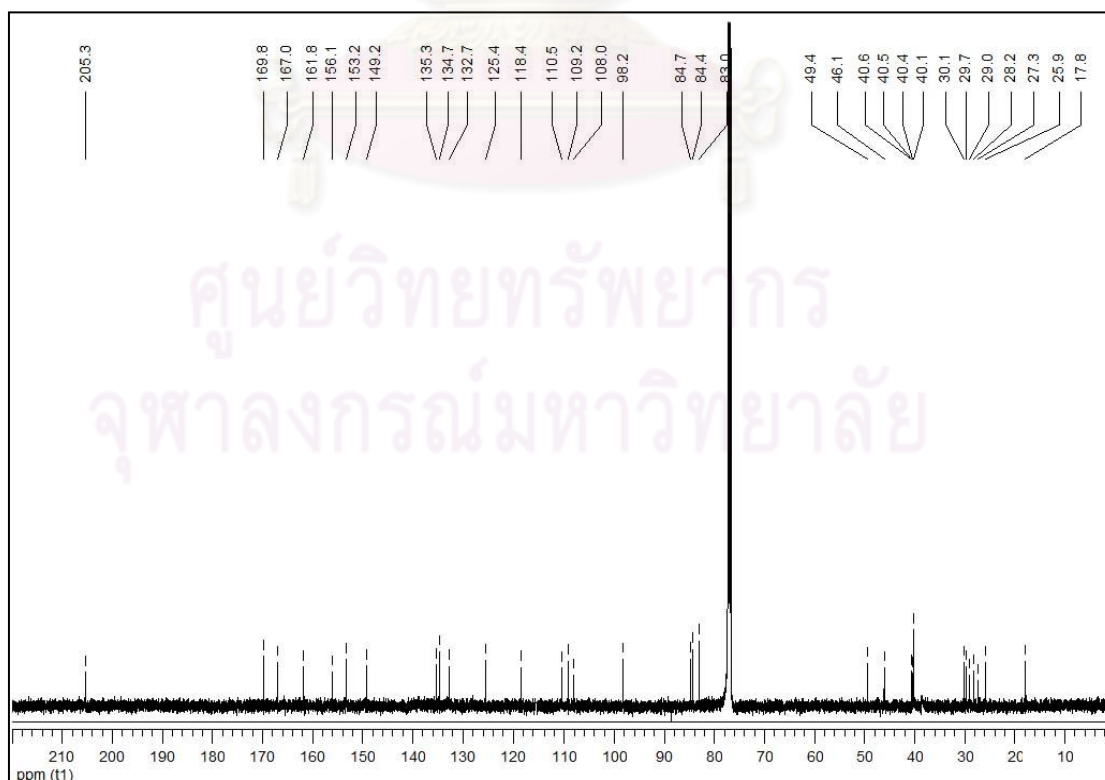**Figure 3.13** The ^{13}C NMR spectrum (CDCl$_3$, 100 MHz) of compound **C12**
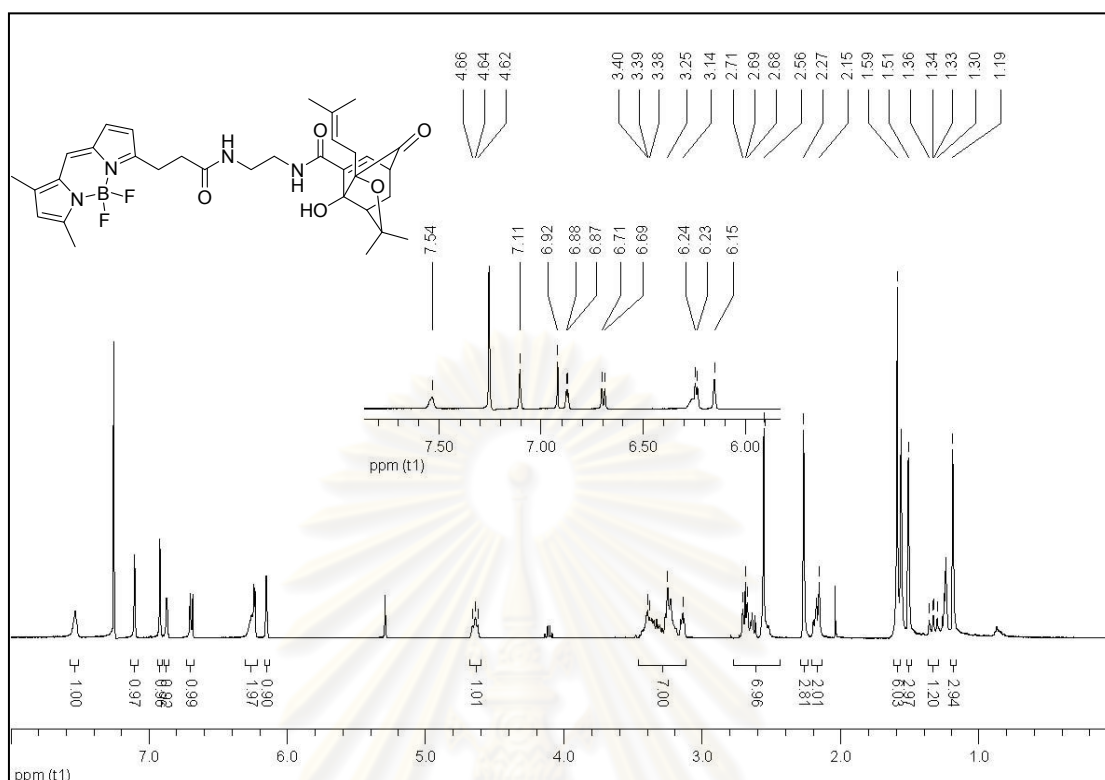
Figure 3.14 The ^{1}H NMR spectrum (CDCl$_3$, 400 MHz) of compound **C13**
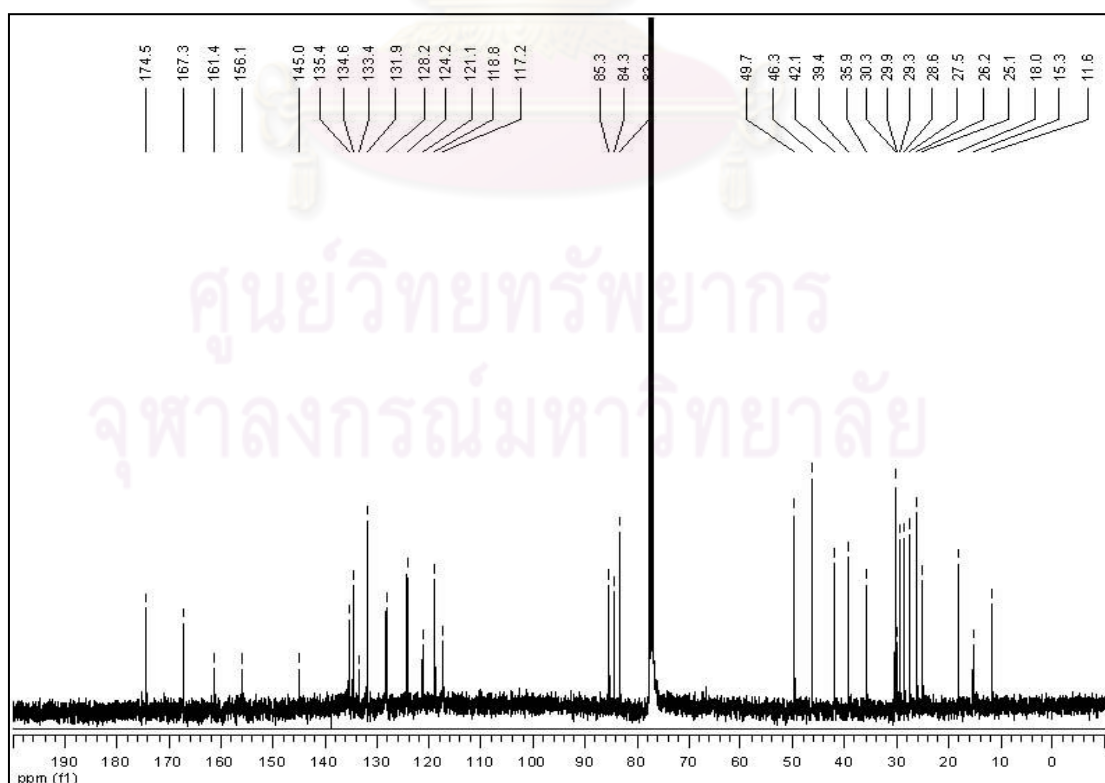
Figure 3.15 The ^{13}C NMR spectrum (CDCl$_3$, 100 MHz) of compound **C13**

In a similar manner, dihydroxychromanone **C16** can be synthesized in 16% combined yield by the two steps of the reaction of pyrogallol (**C14**) with acrylonitrile in the presence of sodium methoxide, followed by cyclization with aqueous sulfuric acid (50% aq.) (Scheme 3.23) [236]. The Pd(0)-catalyzed reverse prenylation of **C16** with carbonate **C3b** formed compound **C17** in 89% yield. With alkene **C17** in hand, the stage was set for the implementation of a tandem Claisen/Diels-Alder reaction. Along these lines, heating of **C17** in DMF at 120 °C gave rise selectively to a single caged product **C19** in 91% yield *via* intermediate **C18**. Spectroscopic techniques and single crystal X-ray analysis of **C19** confirmed its chemical structure. In this case, the formation of the neo caged structure was not detected.
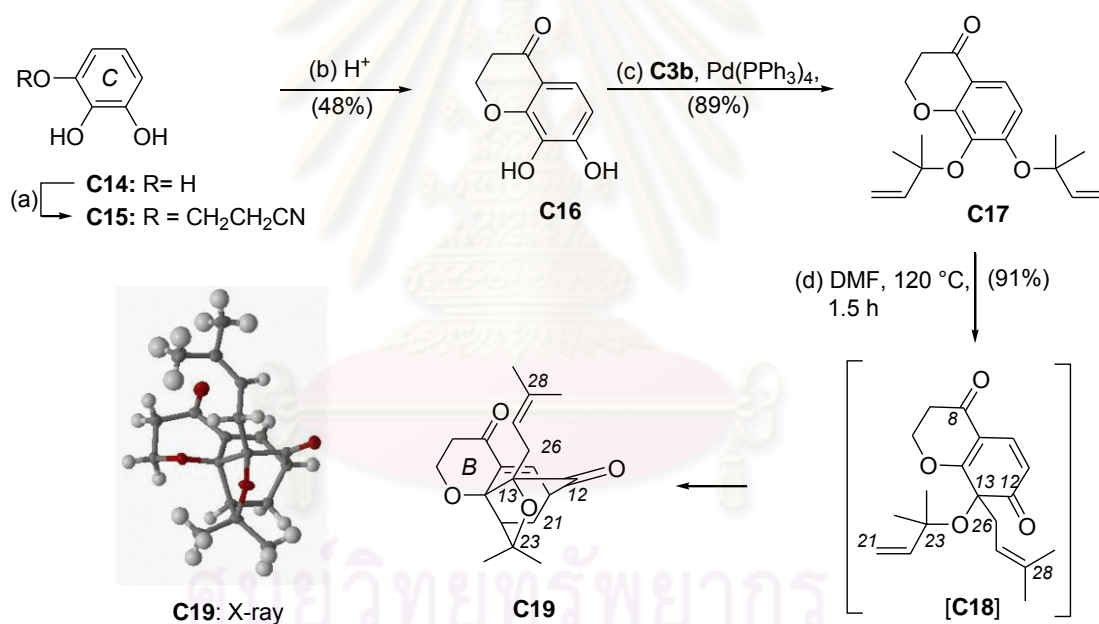
Scheme 3.23 Reagents and conditions: (a) 3.4 equiv. acrylonitrile, 0.3 equiv. NaOMe, 7 h, 76 °C, 34%; (b) excess 50% (w/w) H_2SO_4 (aq), 3 h, 100 °C, 48%; (c) 10 equiv. 1,1-dimethylpropenyl *t*-butyl carbonate (**C3b**), 10 mol% Pd(PPh$_3$)$_4$, THF, 2 h, 5 °C, 89%; (d) DMF, 1.5 h, 120 °C, 91%.

The ^{1}H NMR spectrum of **C19** (Figure 3.16) revealed the presence of characteristic signals of caged motif at δ_H 7.25 (d, J = 6.6 Hz, 1H, H-10), 3.34 (m, 1H, H-11), 2.37 (m, 1H, H-22), and 2.31 (dd, J = 13.6, 4.5 Hz, 1H, H-21). The chemical shifts of olefinic and methylene protons belonging to the reverse prenyl unit on C ring were observed at δ_H 4.41 (m, 1H, H-27), 2.50 (dd, J = 12.4, 6.5 Hz, 1H, H-26), and

2.42 (dd, J = 2.9, 1.4 Hz, 1H, H-26). The presence of four singlet signals at δ_H 1.59 (s, 3H, H-24), 1.53 (s, 3H, H-29), 1.48 (s, 3H, H-25), and 1.23 (s, 3H, H-30) were detected. The signals at δ_H 4.17 (ddd, J = 12.1, 6.5, 1.4 Hz, 1H, H-16), 3.94 (dt, J = 12.3, 2.9 Hz, 1H, H-16), and 2.63 (d, J = 8.6 Hz, 2H, H-16) were also assigned to four methylene groups on B ring. The ^{13}C NMR spectrum (Figure 3.17) displayed two carbonyl signals at δ_C 203.9 (C-12) and 192.0 (C-8). The signals of two methine carbons were observed at δ_C 135.4 (C-10) and 119.2 (C-27). Three signals of oxygenated quaternary carbon were shown at δ_C 87.4 (C-13), 84.2 (C-23), and 82.9 (C-14). The quaternary carbon signals at δ_C 136.9 and 133.8 were assigned to carbons C9 and C28, respectively. Four signals of methylene carbons were exhibited at δ_C 60.0 (C-16), 38.1 (C-7), 28.8 (C-26) and 27.7 (C-21). The chemical shifts at 46.2 and 44.5 were ascribed to carbons C22 and C11, respectively. The signals of methyl group were observed at δ_C 30.1 (C-24), 28.8 (C-25), 25.5 (C-29), and 17.9 (C-30).
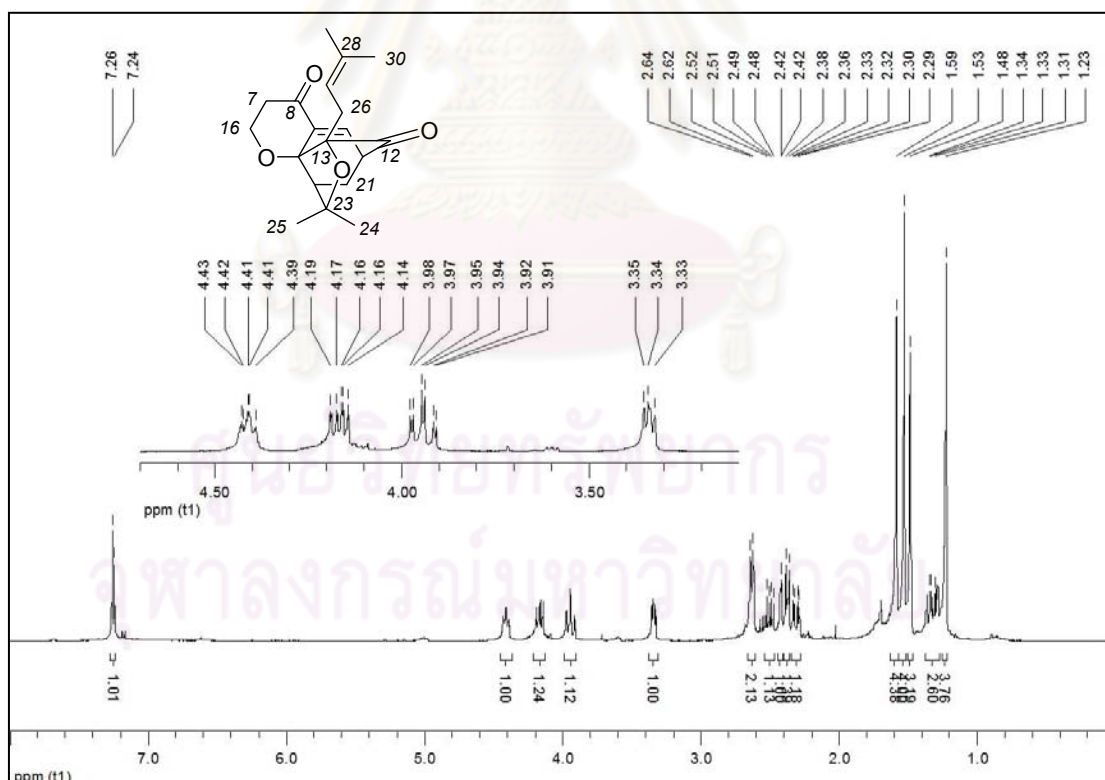
Figure 3.16 The ^{1}H NMR spectrum (CDCl$_3$, 400 MHz) of compound **C19**
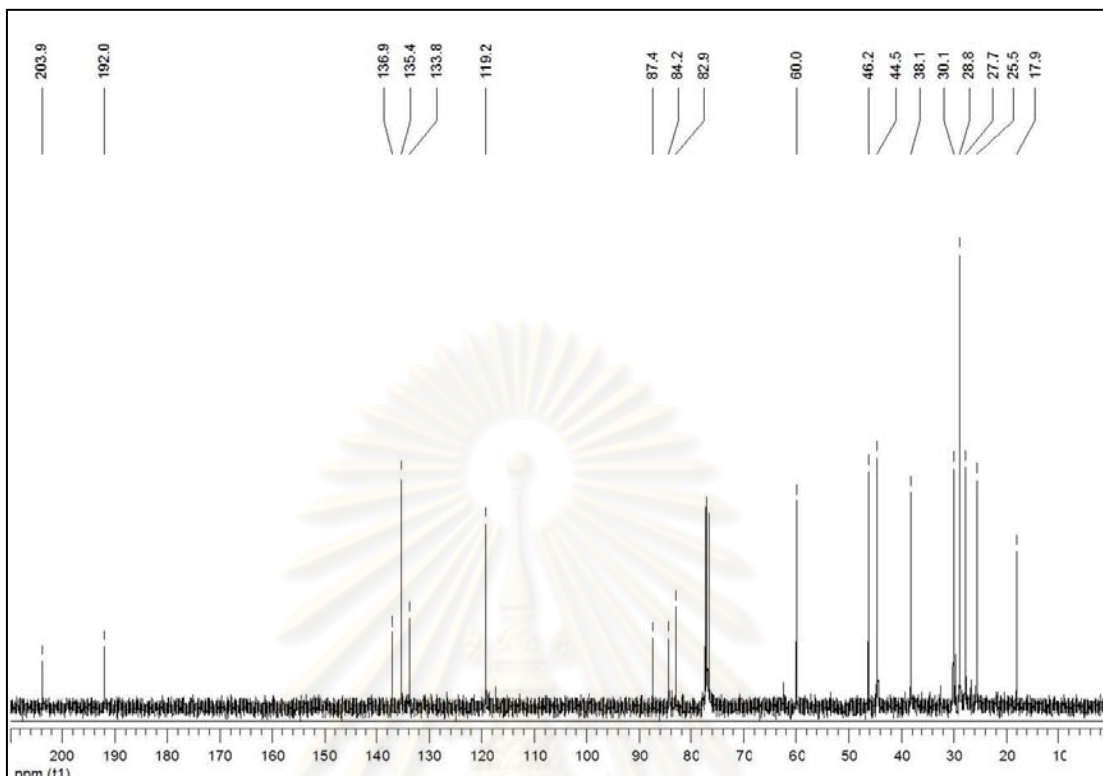
Figure 3.17 The ^{13}C NMR spectrum (CDCl$_3$, 100 MHz) of compound **C19**

3.3.2 Improved Synthesis of Cluvenone (ABC Caged Analogues)

Cluvenone (**196**) was selected as a model ABC caged compound to prepare in this study because it has been addressed as a potential anti-cancer agent against adriamycin resistant promyelocytic leukemia cells (HL-60/ADR) with the IC$_{50}$ of 1.4 μM [147]. According to the previous study, the synthesis of cluvenone (**196**) was concerned with a two-step sequence: (a) propargylation of xanthone using 2-chloro-2-methyl butyne and (b) Lindlar reduction of the resulting alkynes. This two-step process proved to be very tedious because of the lower yield obtained (45% yield over two steps) and significant amounts of side product formation [147]. In addition, during the reduction step, it was difficult to control over-reduction of alkenes to alkanes. Therefore, the Pd(0)-catalyzed reverse prenylation reaction was utilized to apply to the preparation of di-allyloxy xanthone (**C25**) for the formation of cluvenone (**196**) as shown in Scheme 3.24. Stating material 2-fluorabenzoic acid was first converted to its acid chloride using oxalyl chloride and catalytic amounts of DMF. Then, the Friedel-Crafts acylation of pyrrogallol (**C22**) with 2-fluorobenzoyl chloride

(**C21**) in the presence of AlCl$_3$ was employed to produce benzophenone adduct **C23**, that underwent a base-induced cyclization to form xanthone **C24** (2 steps, 34% combined yield).
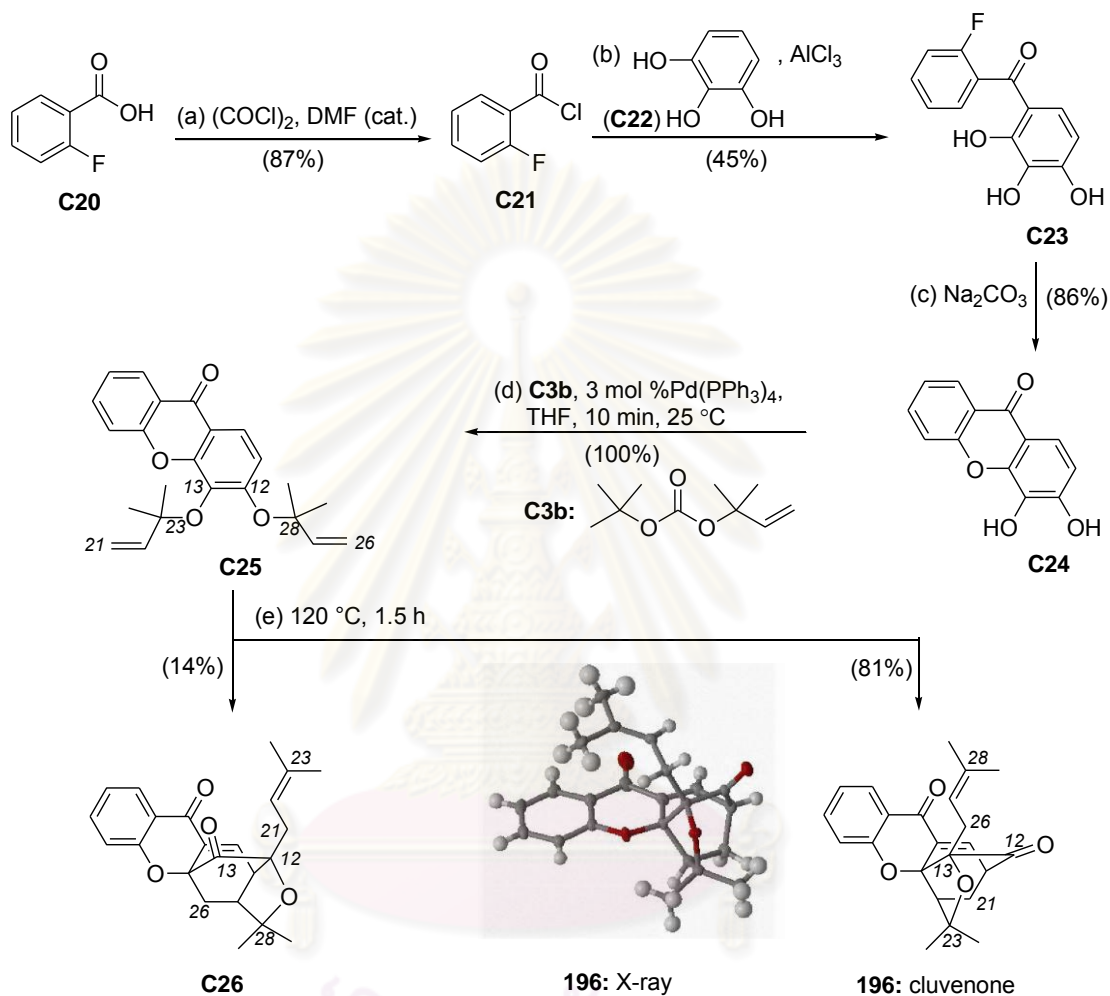
Scheme 3.24 Reagents and conditions: (a) 1.2 equiv. (COCl)$_2$ (2.0 M in CH$_2$Cl$_2$), CH$_2$Cl$_2$, DMF (cat.), 1.5 h, 0 °C to 25 °C, 87%; (b) 2.0 equiv. **C22**, 2.9 equiv. AlCl$_3$, CHCl$_3$, CH$_2$Cl$_2$, 12 h, 25 °C; then 4 h, 60 °C, 45%; (c) 1.5 equiv. Na$_2$CO$_3$, DMF, 3.5 h, 90 °C, 86%; (d) 10 equiv. 1,1-dimethylpropenyl *t*-butyl carbonate (**C3b**), 3 mol% Pd(PPh$_3$)$_4$, THF, 10 min, 25 °C, 100%; (e) DMF, 1.5 h, 120 °C, **196**: 81%, **C26**: 14%.

To generate di-allyloxy xanthone **C25**, it was easily accomplished by the reverse prenylation of xanthone **C24** using 10 mol% Pd(0) catalyst and 1,1-dimethylpropenyl *t*-butyl carbonate (**C3b**) as a prenylating agent. This reaction proceeded well to obtain compound **C25** in quantitative yield within 10 mins at 5 °C. Importantly, the scale-up of synthesis of compound **C25** to gram amounts was

carefully performed. Under scaling up the process, the amount of the Pd(0) could be successfully decreased from 10 to 3 mol% and the reaction time could be reduced to 10 mins at 25 °C furnishing the desired compound **C25** in excellent yield.

The heat-induced Claisen/Diels–Alder reaction cascade gave cluvenone (**196**) in 81% yield, along with small amounts of the neo caged xanthone **C26** (14% yield). The structures of **196** and **C26** were characterized by spectroscopic methods. In addition, the absolute stereochemistry of **196** was confirmed by X-ray analysis. **196** and **C26** were synthetically-known compounds, and their ^{1}H and ^{13}C NMR spectral data were corresponded to those of Batova and co-workers [147].

3.3.3 Selectivity of the C-ring Claisen/Diels-Alder Rearrangement

During the synthesis of BC, C and ABC ring caged analogues by heating each di-hydroxyl compound (**C4**, **C17** and **C25**) in DMF at 120 °C *via* Claisen/Diels-Alder reaction cascade, the site-selectivity of this reaction cascade was observed. That was the heating of **C4** and **C25** gave rise to both regular and neo caged compounds in 68% and 15%, and 81% and 14%, respectively. On the other hand, the reaction of chromanone **C17** gave only regular caged motif in 91% yield (Table 3.2).

Table 3.2 Selectivity of the C-ring Claisen/Diels-Alder rearrangement on **C4**, **C17** and **C25**
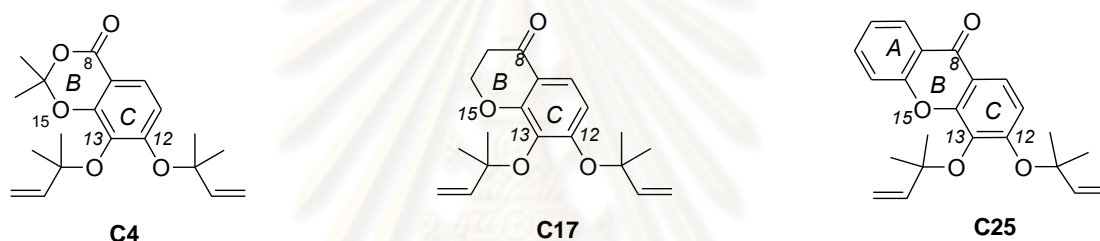
Entry	Compound	% yield of caged compound	
		Regular	Neo
1	**C4**	68	15
2	**C17**	91	0
3	**C25**	81	14

It was interesting to figure out that why Claisen/Diels-Alder reaction cascade favor the formation of regular caged motif over the neo isomer, and why the corresponding neo caged motif was not produced by heating of **C17**. The observed site-selectivity of Claisen rearrangements on C ring (C12 *vs* C13 allylation) could be rationalized by the electronic effect of C8 carbonyl carbon and O15 xanthone oxygen as presented in Scheme 3.25.
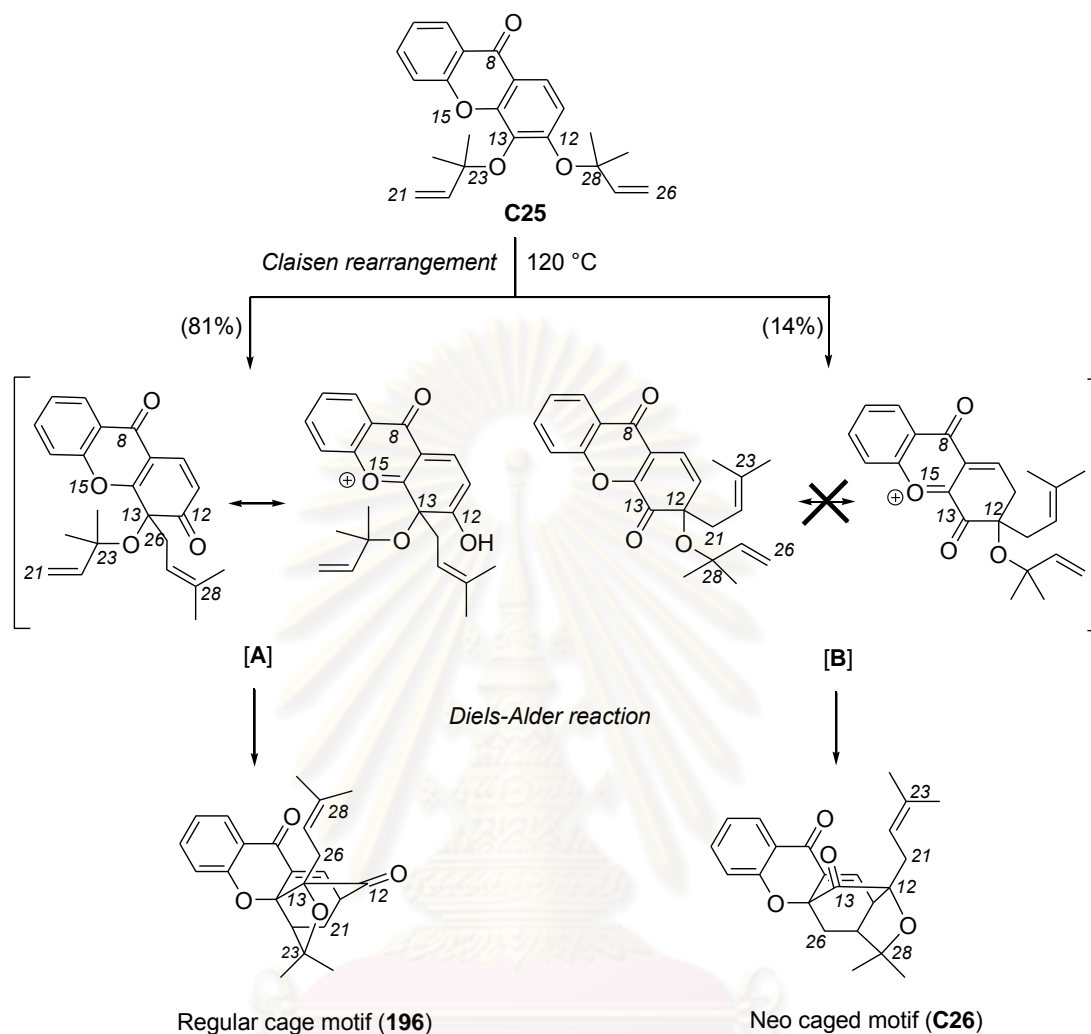
Scheme 3.25 Site-selectivity of Claisen/Diels-Alder rearrangement on the conversion of **C25** to **196** and **C26**

Being *para* to the C12 allyl ether, the electronically deficient C8 carbonyl group polarized selectively the O-C28 bond, which made this bond easier to break. Another important reason may come from the resonance stabilization of C12 carbonyl group of intermediate **A** by O15 xanthone oxygen performed in the intermediate **A**, but C13 carbonyl group of intermediate **B** could not be stabilized by O15 xanthone oxygen. The aforementioned effects could further explain the site-selectivity of the Claisen/Diels-Alder rearrangement on the compounds **C4**, **C17** and **C25**. Considering the electronic deficiency of C8 carbonyl carbon of each compound tested. The C8 carbonyl group of compound **C17** showed the most electronic deficiency among all the compounds utilized. This led to a high selectivity of migration of C12 allyloxy

ether on the C13 center, and after Diels-Alder rearrangement of the resulting diene with the more reactive C21-C22 dienophile gave only regular caged scaffold in 91% yield. A partial loss of the site selectivity was observed with the compounds **C4** and **C25**, producing both the regular caged scaffold and the isomeric neo caged motif in an approximate ratio of 4.5:1 and 5.8:1, respectively. This may be because either the oxygen atom or the phenyl moiety connecting to C8 carbonyl carbon decreased the withdrawing effect of the C8 of those compounds, resulting to cut down the preference for cleavage of the O-C28 bond and allowed the competitive migration of C13 allyloxy ether on the C12 center to proceed. This phenomenon paralleled the previous observations [133, 147] and could be used to explain why natural caged *Garcinia* xanthones have been prominently found as a regular caged motif in a nature.

3.3.4 Synthesis of Allylic Oxidation Products of Cluvenone (ABC Caged Analogues) and Related Compound

The compound cluvenone (**196**) was used as a lead structure to make its ABC caged analogues **C27**, **C28** and **C29** to investigate the significance of prenyl chain for bioactivity.

Allylic oxidation of **196** using SeO_2 and *t*BuOOH gave the corresponding aldehyde **C27** in 57% isolated yield as a major product together with 21% yield of alcohol **C28** (Scheme 3.26). PCC oxidation of the latter compound was carried out to give aldehyde **C27** back in 95% yield. The structures of aldehyde **C27** and alcohol **C28** were characterized by ^1H, ^{13}C NMR and HRMS techniques.
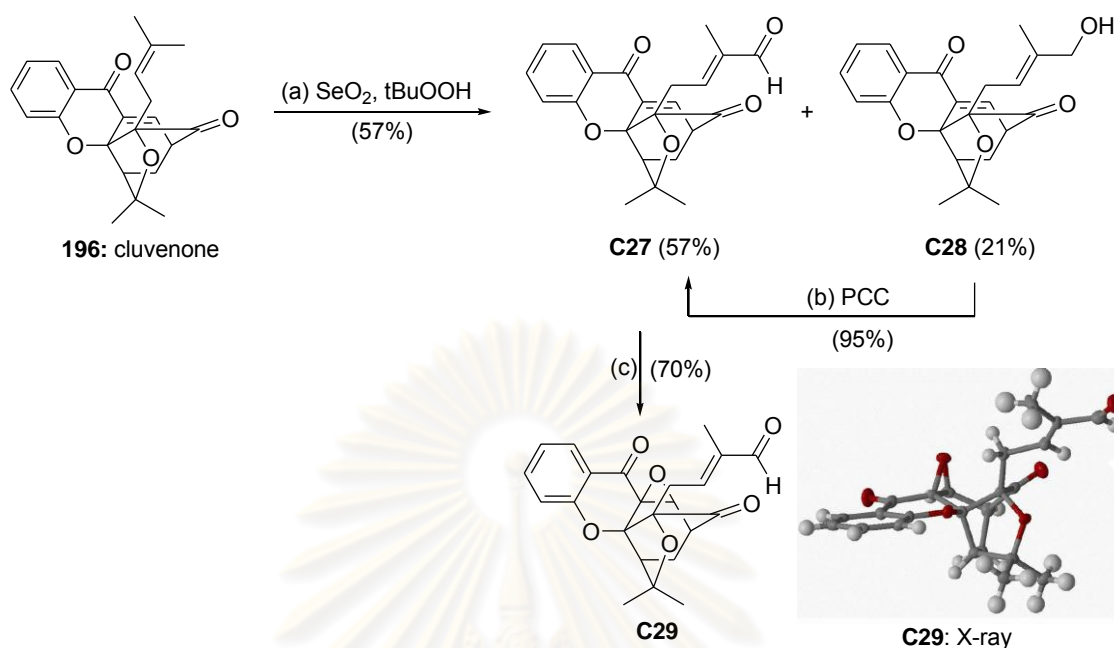
Scheme 3.26 Reagents and conditions: (a) 5 mol% SeO$_2$, 1.8 equiv. tBuOOH, CH$_2$Cl$_2$, 19 h, 25 °C, **C27:** 57%, **C28:** 21%; (b) 1.5 equiv. PCC, CH$_2$Cl$_2$, 30 min, 25 °C, 95%; (c) 3.0 equiv. NaClO$_2$, 3.0 equiv. NaHPO4·H$_2$O, 8.0 equiv. 2-methyl-2-butene, tBuOH/H$_2$O (2:1), 4 h, 0 °C, 70%

The ^{1}H NMR spectrum of **C27** (Figure 3.18) showed the characteristic signals of caged motif at δ_H 7.59 (d, J = 6.9 Hz, 1H, H-10), 3.55 (m, 1H, H-11), 2.56 (d, J = 9.5 Hz, 1H, H-22), 2.38 (dd, J = 13.6, 4.6 Hz, 1H, H-21), and 1.42-1.36 (m, 1H, H-21), together with a signal of aldehyde proton at δ_H 9.22 (s, 1H). The signals of four aromatic protons at δ_H 7.91 (d, J = 7.8 Hz, 1H, H-6), 7.53 (t, J = 6.9 Hz, 1H, H-5), 7.07 (t, J = 7.4 Hz, 1H, H-18), and 6.94 (d, J = 8.4 Hz, 1H, H-17) were displayed. An olefinic signal at δ_H 6.41 (t, J = 7.2 Hz, 1H, H-27), two methylene signals at δ_H 2.82 (dd, J = 15.9, 7.5 Hz, 1H, H-26) and 2.65 (dd, J = 15.9, 7.0 Hz, 1H, H-26), and three methyl signals at δ_H 1.76 (s, 3H, H-24), 1.34 (s, 3H, H-25), and 1.18 (s, 3H, H-30) were detected. The ^{13}C NMR spectrum (Figure 3.19) displayed three signals at δ_C 202.8 (C-12), 194.8 (C-29), and 176.6 (C-8), indicating for a carbonyl carbon of ketone, aldehyde, and xanthone, respectively. The signals of four aromatic carbons at δ_C 136.6 (C-18), 127.6 (C-6), 119.0 (C-5), and 118.2 (C-17), four olefinic carbons at δ_C 147.3 (C-27), 140.3 (C-28), 137.2 (C-10), and 134.7 (C-9), three oxygenated

quaternary carbons at δ_C 91.1 (C-14), 84.4 (C-13), and 83.4 (C-23), and seven aliphatic carbons at δ_C 48.9 (C-22), 47.0 (C-11), 30.3 (C-26), 29.3 (C-24), 29.2 (C-25), 25.1 (C-21), and 8.8 (C-30) were observed.

The ^{1}H NMR spectrum of **C28** (Figure 3.20) exhibited the characteristic signals of caged motif at δ_H 7.54 (d, J = 6.9 Hz, 1H, H-10), 3.67-3.55 (m, 1H, H-11), 2.549 (d, J = 9.6 Hz, 1H, H-22), 2.37 (dd, J = 13.6, 4.7 Hz, 1H, H-21), and 1.39-1.34 (m, 1H, H-21). The signals at δ_H 7.93 (d, J = 8.2 Hz, 1H, H-6), 7.56 (t, J = 8.4 Hz, 1H, H-5), and 7.10-7.07 (m, 2H, H-17 and H-18) were ascribed to four aromatic protons. A multiplet signal at δ_H 3.67-3.53 (C-27) and a doublet signal at δ_H 7.54 (J = 6.9 Hz, 1H, H-10) were ascribed to an olefinic proton. The signals at δ_H 2.75-2.67 (m, 2H, H-26) and 2.65 (dd, J = 15.9, 7.0 Hz, 1H, H-26), and 3.67-3.53 (m, 2H, H-29) were assigned to four methylene protons. Three singlet signals at δ_H 1.74 (s, 3H, H-24), 1.31 (s, 3H, H-25), and 0.94 (s, 3H, H-30) were belonged to a methyl proton. The ^{13}C NMR spectrum (Figure 3.21) presented two signals at δ_C 203.2 and 178.8 which could be assigned to C12 and C8, respectively. The four signals of aromatic carbons were observed at δ_C 137.0 (C-18), 127.4 (C-6), 119.4 (C-5), and 118.3 (C-17). The peaks of olefinic carbon were observed at δ_C 138.1 (C-10), 135.4 (C-28), 134.7 (C-9), and 122.5 (C-27). The presence of three oxygenated quaternary carbons was inferred from the presence of four peaks at δ_C 90.4 (C-14), 84.7 (C-13), and 84.0 (C-23). The peak of methylene carbon connected to hydroxyl group was detected at δ_C 68.4 (C-29). The peaks displayed at δ_C 48.9 (C-22), 47.2 (C-11), 30.5 (C-26), 29.3 (C-24), 29.0 (C-25), 25.2 (C-21), and 12.7 (C-30), indicating the presence of seven aliphatic carbons.

To attach a carboxylic functionality on a prenyl unit of culvenone (**196**), a variety of conditions staring from different material were tried as follows: (a) oxidation of aldehyde **C27** using NaClO$_2$ [237] or MnO$_4$ in acetic acid; (b) oxidation of alcohol **C28** using IBX/NHS [238]; (c) olefin cross-metathesis of **196** and methyl acrylic methyl ester using 2nd generation Grubbs' catalyst followed by hydrolysis of the resulting methyl ester; (d) oxidative cleavage of **196** using OsO$_4$/NMO [239] or AD mix-β followed by Witting reaction [240]. Unfortunately, all attempts to generate carboxylic acid met with failure. In all these cases the characteristic doublet signal corresponding to the proton of α,β-unsaturated ketone disappeared, indicating a

conjugate addition reaction of the enone bond. Under relatively mild oxidation conditions (NaClO$_2$) for oxidizing aldehyde **C27**, the unexpected epoxide **C29** was isolated in 70% yield. The mass analysis result of this compound showed a molecular ion peak (M+Na)$^+$ at m/z 417.1313, corresponding with the elemental formular C$_{23}$H$_{22}$O$_6$. This pointed out that it has an extra oxygen atom. In addition, the structure of this compound was characterized by NMR analysis and its absolute stereochemistry was confirmed *via* a single-crystal X-ray analysis.

The ^{1}H NMR spectrum of **C29** (Figure 3.22) showed the characteristic signals of caged motif at δ_H 3.12 (t, J = 4.6 Hz, 1H, H-11), 2.58 (d, J = 9.2 Hz, 1H, H-22), 2.23 (dd, J = 14.5, 5.1 Hz, 1H, H-21), and 1.81-1.73 (m, 1H, H-21) as well as aldehyde proton at δ_H 9.48 (s, 1H). A doublet signal at δ_H 4.29 (J = 4.5 Hz) was assigned to H10 of epoxide ring. The presence of four aromatic protons were inferred from the detection of four signals at δ_H 7.97 (d, J = 7.9 Hz, 1H, H-6), 7.65 (t, J = 7.4 Hz, 1H, H-5), 7.20 (t, J = 7.7 Hz, 1H, H-18), and 7.10 (d, J = 8.3 Hz, 1H, H-17). The chemical shift of H27 olefinic proton was shifted to 7.01 (t, J = 8.1 Hz). A multiplet signal at δ_H 3.03-3.01 indicated to H26 methylene proton and singlet signals of three methyl groups at δ_H 1.70 (s, 3H, H-24), 1.60 (s, 3H, H-25), and 1.24 (s, 3H, H-30) were observed. The ^{13}C NMR spectrum (Figure 3.23) of this compound was similar to that of **C27**, except the signals of C9 and C10 were shifted from δ_C 134.7 and 137.2 to 59.8 and 55.0, respectively, indicating that those carbons connected to an oxygen atom.

All the aforementioned data suggested that the structure of **C29** was epoxide-contained caged compound at C9-C10 center. The formation of this epoxide ring was found to be in the opposite direction from caged core. This observation supports the expected reactivity of the enone motif as a conjugate electrophile.

Figure 3.18 The ^{1}H NMR spectrum (CDCl$_3$, 400 MHz) of compound **C27**
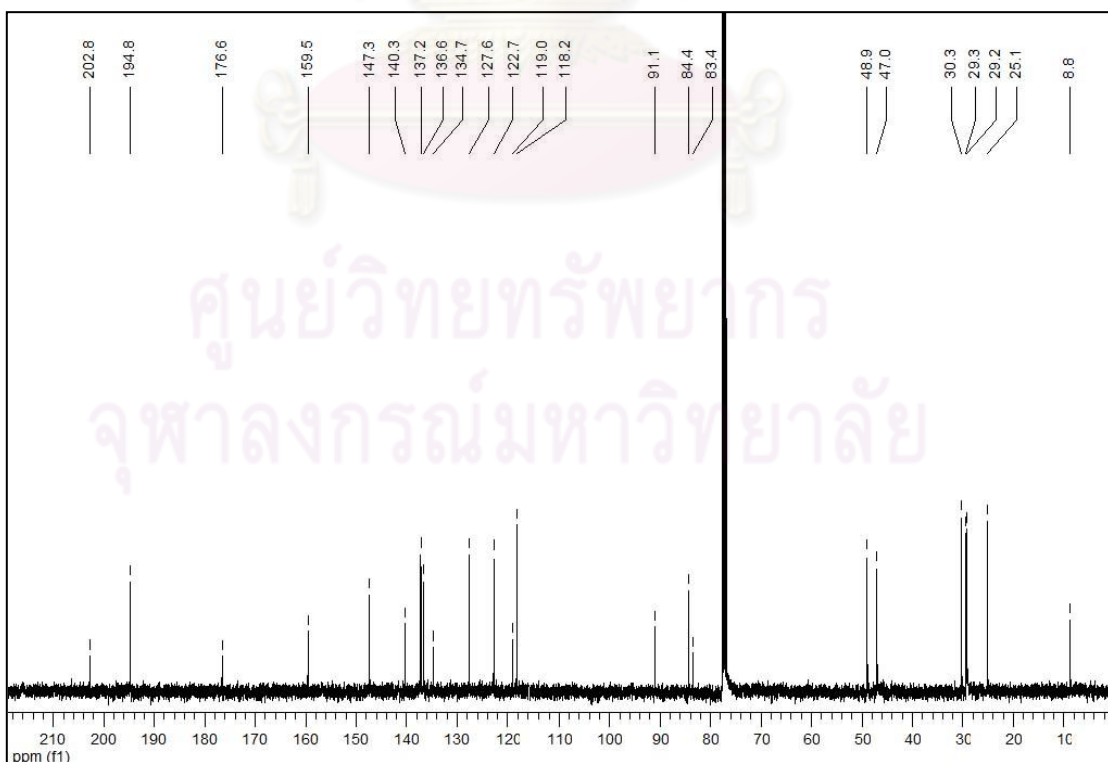
Figure 3.19 The ^{13}C NMR spectrum (CDCl$_3$, 100 MHz) of compound **C27**

Figure 3.20 The ^{1}H NMR spectrum (CDCl$_3$, 400 MHz) of compound **C28**
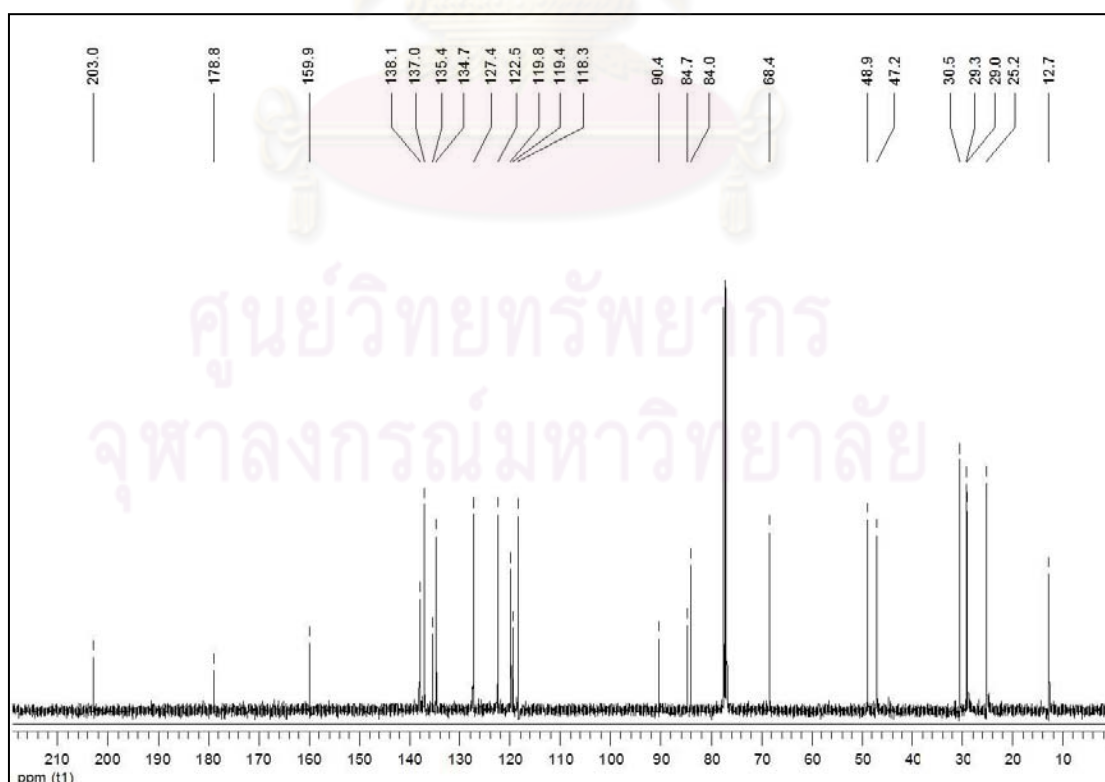
Figure 3.21 The ^{13}C NMR spectrum (CDCl$_3$, 100 MHz) of compound **C28**

Figure 3.22 The ^{1}H NMR spectrum (CDCl$_3$, 400 MHz) of compound **C29**
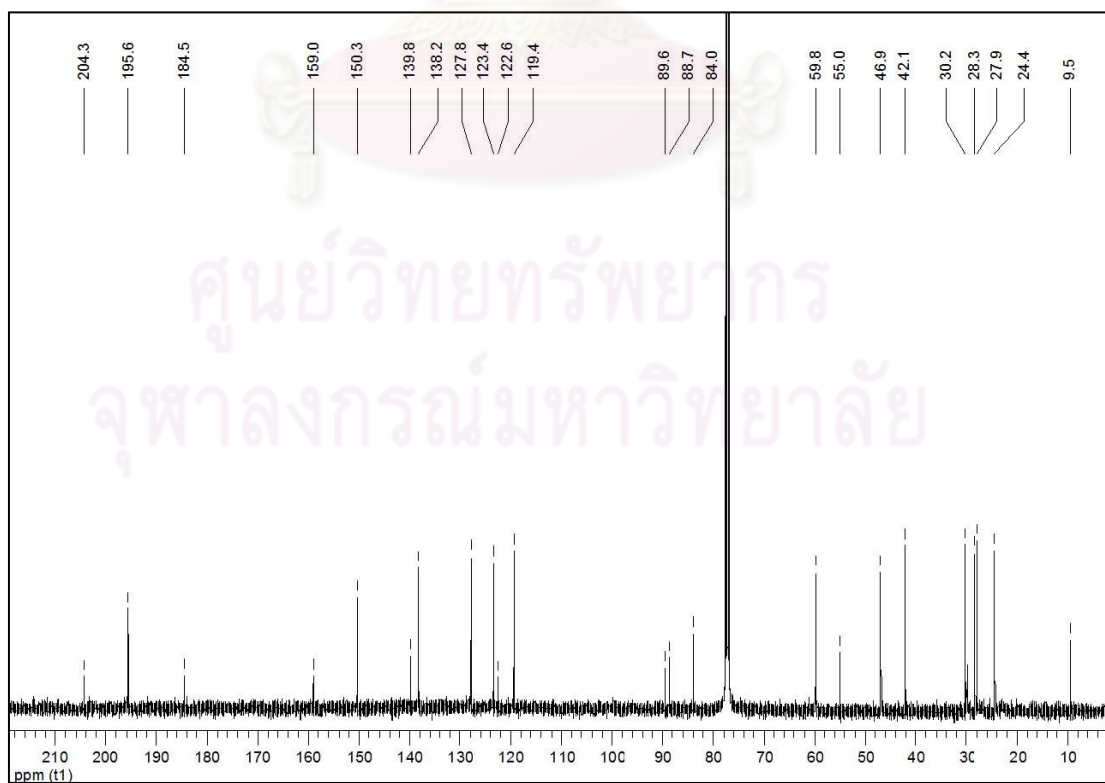
Figure 3.23 The ^{13}C NMR spectrum (CDCl$_3$, 100 MHz) of compound **C29**

3.3.5 Synthesis of Caged *Garcinia* Xanthone Analogues Modified at the C9-C10 Enone Bond

According to the literature reviews, the bioactivity was found to disappear when the C9-C10 double bond of the caged *Garcinia* xanthones was destroyed. This could be suggested that the enone bond play an essential role in bioactivities of these molecules [19]. It has been hypothesized that such enone bonds, act as a Michael acceptor (conjugate electrophile), could be attracted by some bio-nucleophiles during being in the cells. Therefore, the bioactivity of those compounds should disappear in case that enone bonds are substituted or reduced. To test this hypothesis, the C10 methylated analogue **C34**, addition products **C35** and **C36** were prepared and their bioactivity were evaluated. The synthesis of **C34** was prepared as shown in Scheme 3.27.
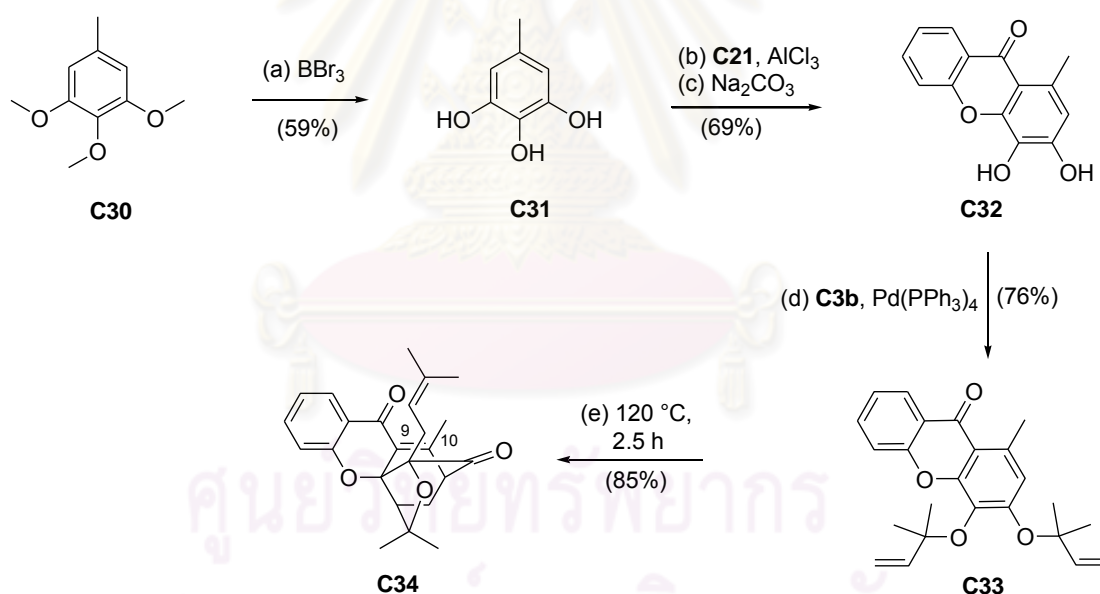
Scheme 3.27 Reagents and conditions: (a) excess BBr₃, CH₂Cl₂, 3 h, 0 to 25 °C, 59%; (b) 1.5 equiv. 2-fluorobenzoyl chloride (**C21**), 2.0 equiv. AlCl₃, CHCl₃, CH₂Cl₂, 1.5 h, 25 °C; then 6 h, reflux, 60 °C; (c) 1.5 equiv. Na₂CO₃, DMF, 69% (over two steps); (d) 10.0 equiv. 1,1-dimethylpropenyl *t*-butyl carbonate (**C3b**),10 mol% Pd(PPh₃)₄, THF, 2 h, 5 °C, 76%; (e) DMF, 2.5 h, 120 °C, 85%

Commercially available 1,2,3-trimethoxy-5-methylbenzene (**C30**) was demethylated with excess BBr₃ to form polyphenol **C31** in 59% yield [241]. Friedel-Crafts acylation of **C31** with 2-fluorobenzoyl chloride (**C21**) in the presence of AlCl₃

followed by Na₂CO₃-induced cyclization of the resulting benzophenone produced xanthone **C32** in 69% combined yield. The Pd(0)-catalyzed reverse prenylation with carbonate **C3b** gave rise to compound **C33** in good yield (76%). The Claisen/Diels-Alder reaction cascade of **C33** in DMF furnished caged xanthone **C34** in 85% yield (Scheme 3.27). The structure of this compound was characterized by ¹H and ¹³C NMR techniques. The ¹H and ¹³C NMR spectra of this compound (Figure 3.24 and 3.25) were similar to those of cluvenone (**196**). In addition, the signal of methyl group substituted on enone bond was observed at δ_H 2.52 in ¹H NMR spectrum and δ_C 16.7 in ¹³C NMR spectrum.
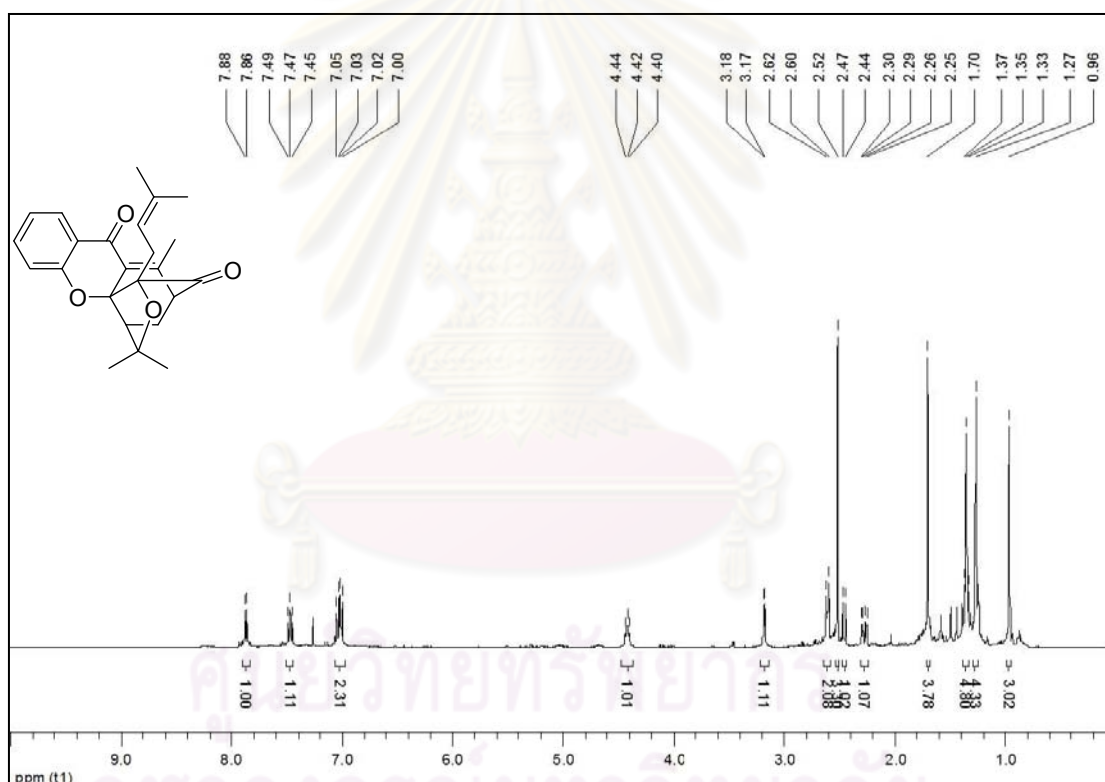
Figure 3.24 The ¹H NMR spectrum (CDCl₃, 400 MHz) of compound **C34**
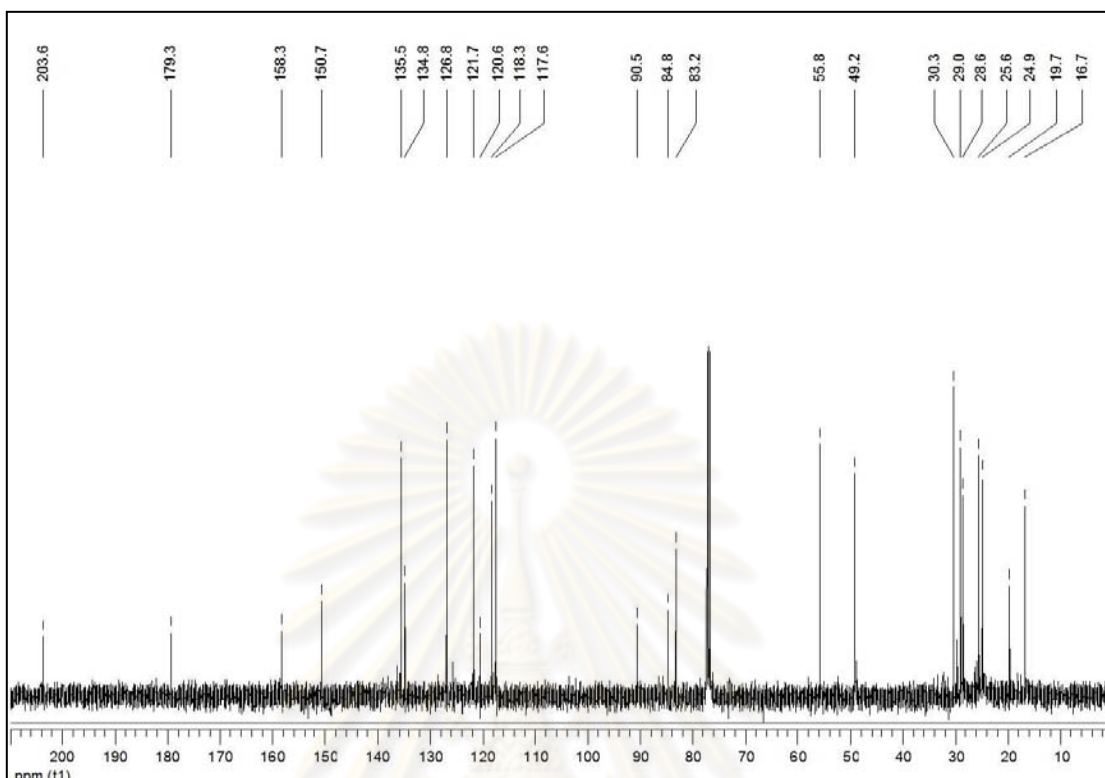
Figure 3.25 The ^{13}C NMR spectrum (CDCl$_3$, 100 MHz) of compound **C34**

The treatments of cluvenone (**196**) with piperidine and MeOH under basic conditions were also performed to form the conjugate addition products **C35** and **C36** in 86% and 41% isolated yield, respectively (Scheme 3.28). The structures of these compounds were determined *via* a single crystal X-ray analysis [18]. From X-ray studies, it pointed out that the conjugate addition took place in a *syn* fashion across the C9-C10 enone bond because the steric hindrance at the top faces was much more than that of the bottom ones. In addition, the structures of **C35** and **C36** were characterized by ^{1}H and ^{13}C NMR spectroscopic analyses.
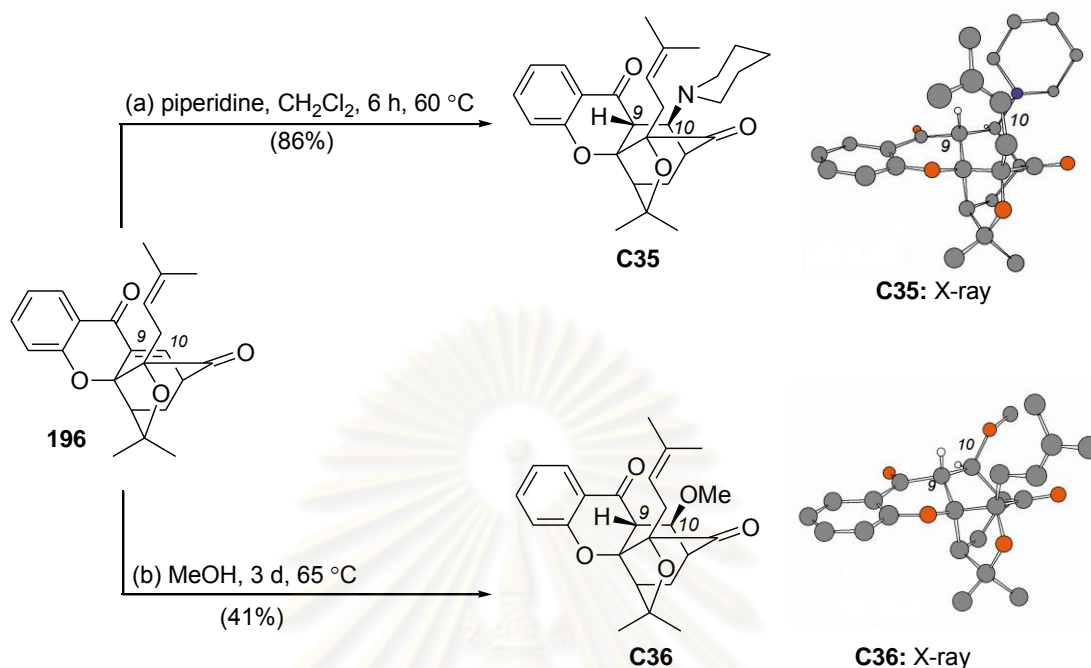
Scheme 3.28 Reagents and conditions: (a) 4.0 equiv. piperidine, CH_2Cl_2, 6 h, 60 °C, 86%; (b) MeOH, 3 d, 65 °C, 41%

Comparison of the ^1H NMR spectrum of **C35** (Figure 3.26) with that of cluvenone (**196**), a doublet signal of H10 olefinic proton disappeared, and two singlet signals assigned to protons H9 (3.36 ppm) and H10 (3.26 ppm) were observed. In addition, three broad singlets of four protons (CH_2NCH_2) were detected at δ_H 3.15 (1H), 2.53 (1H), and 2.34-2.23 (2H), together with a multiplet signal at δ_H 1.51-1.40 inferred to six protons of piperidine ring. The ^{13}C NMR spectrum (Figure 3.27) was compared to that of cluvenone (**196**). It indicated that the carbon signals of C9 and C10 were shifted at δ_C 43.3 and 30.4, respectively. Four peaks at δ_C 62.1, 51.3, 25.7, and 24.6 could be designated for six carbons of piperidine ring.

The ^1H NMR spectrum of **C36** (Figure 3.28) was similar to that of cluvenone (**196**) except the disappearance of olefinic proton at C10. In addition, three new signals: a doublet at δ_H 4.38 (J = 4.3 Hz) referred to H9; a singlet at δ_H 3.38 assigned to H10; and the singlet signal of methoxy proton at δ_H 3.30 (3H) were detected. The ^{13}C NMR spectrum (Figure 3.29) presented a new peak of methoxy carbon at δ_C 55.8 and the shift of C9 and C10 signals to 44.6 and 75.3, respectively compared to cluvenone (**196**).
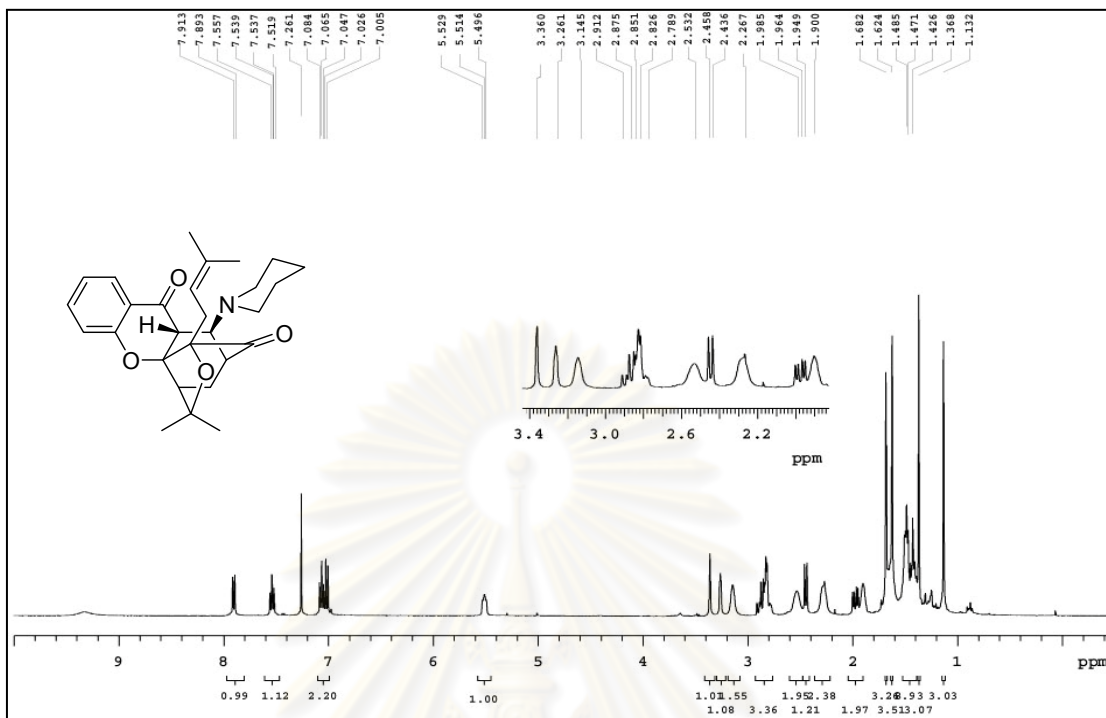
Figure 3.26 The ^{1}H NMR spectrum (CDCl$_3$, 400 MHz) of compound **C35**
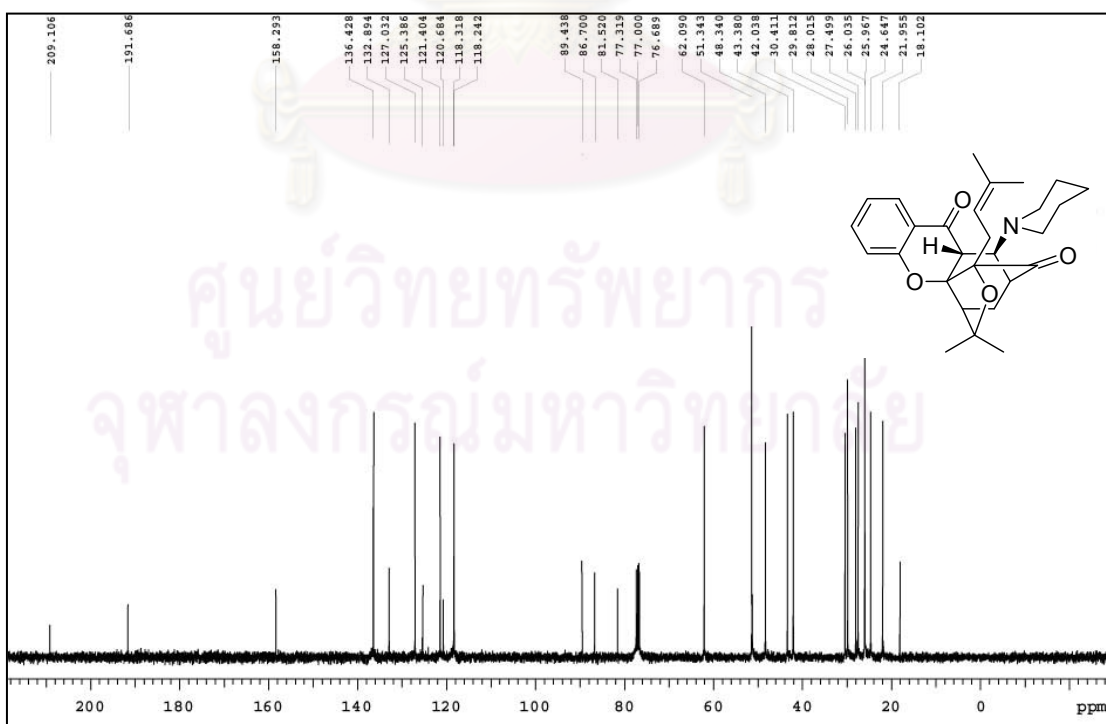
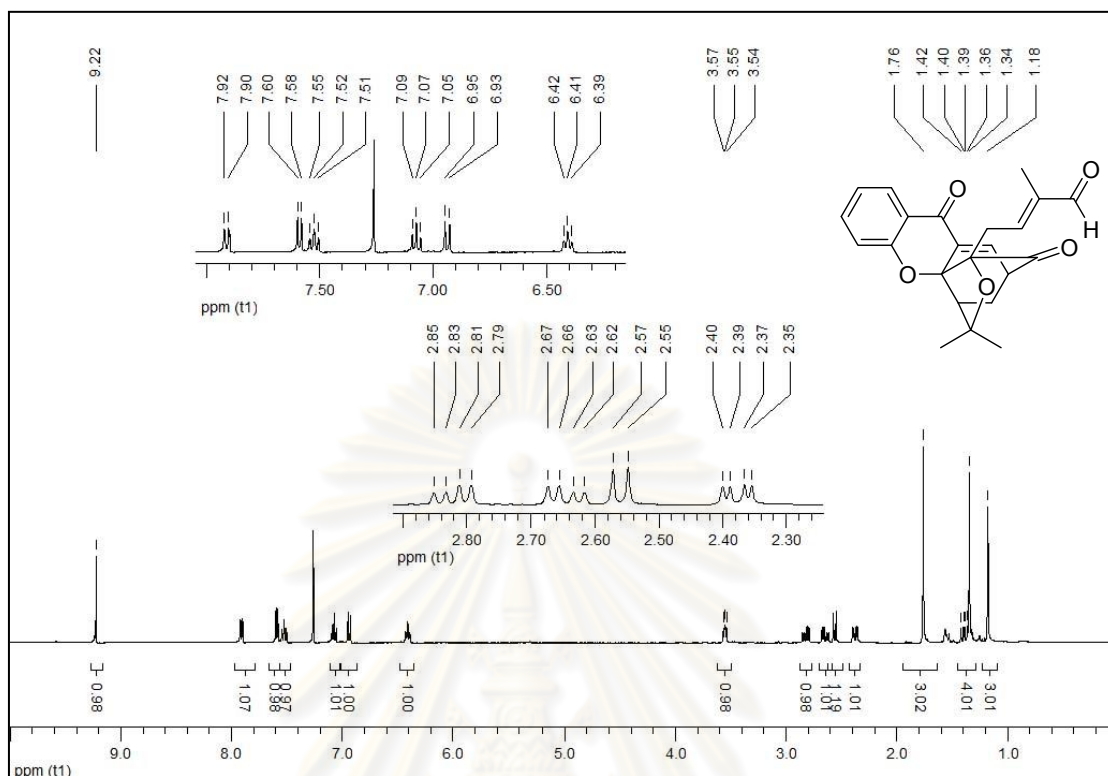**Figure 3.27** The ^{13}C NMR spectrum (CDCl$_3$, 100 MHz) of compound **C35**
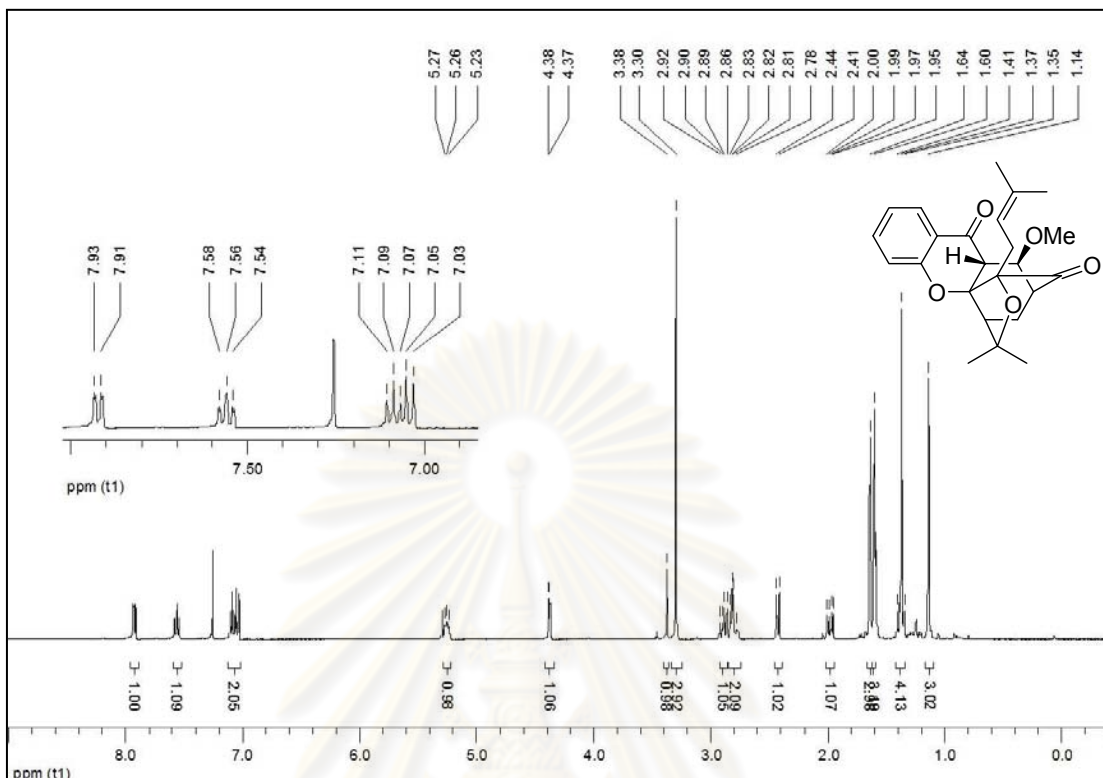
Figure 3.28 The ^{1}H NMR spectrum (CDCl$_3$, 400 MHz) of compound **C36**

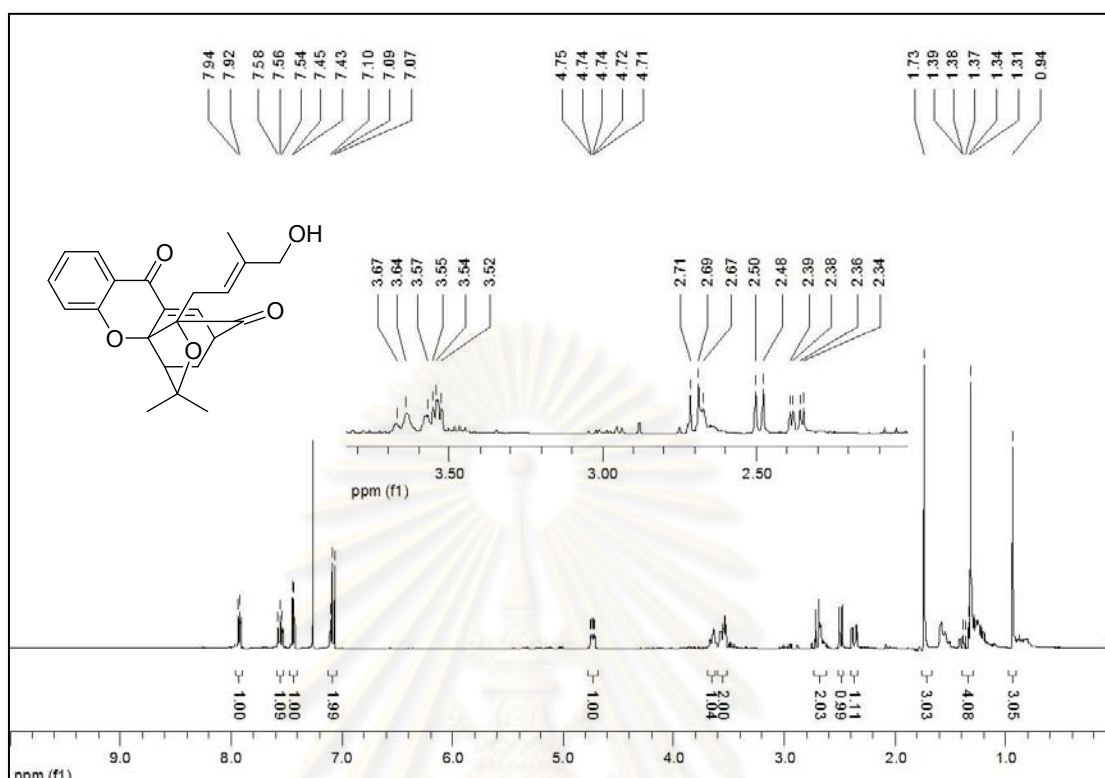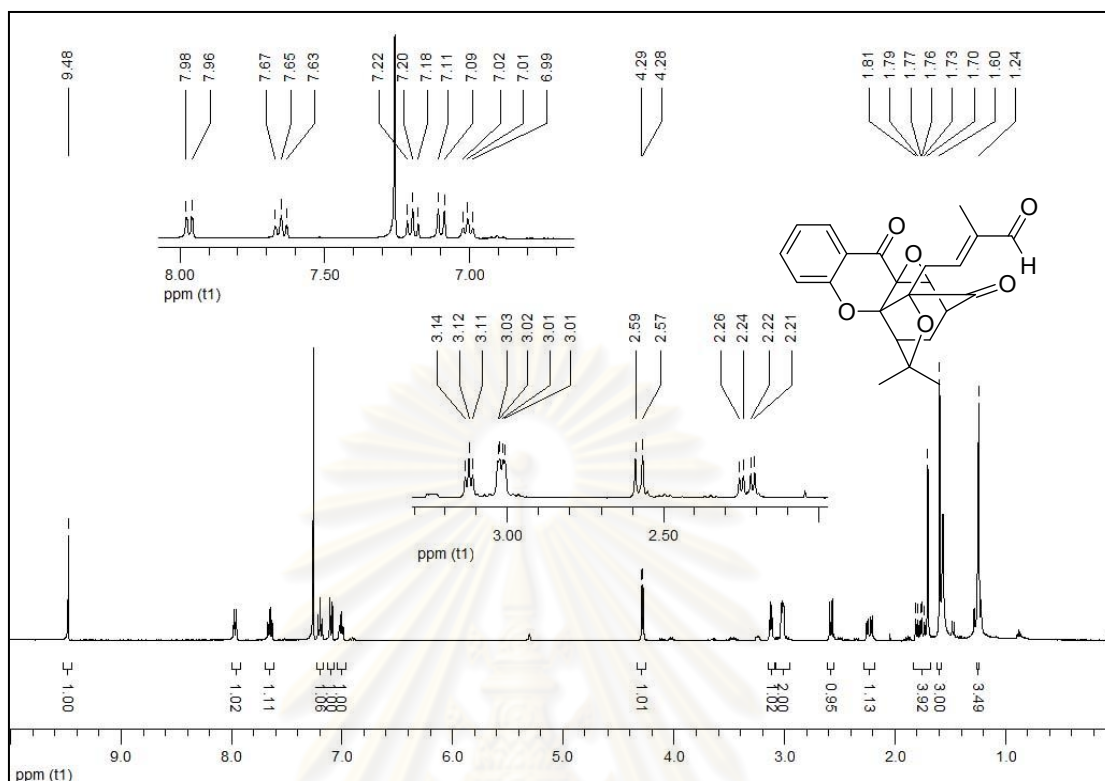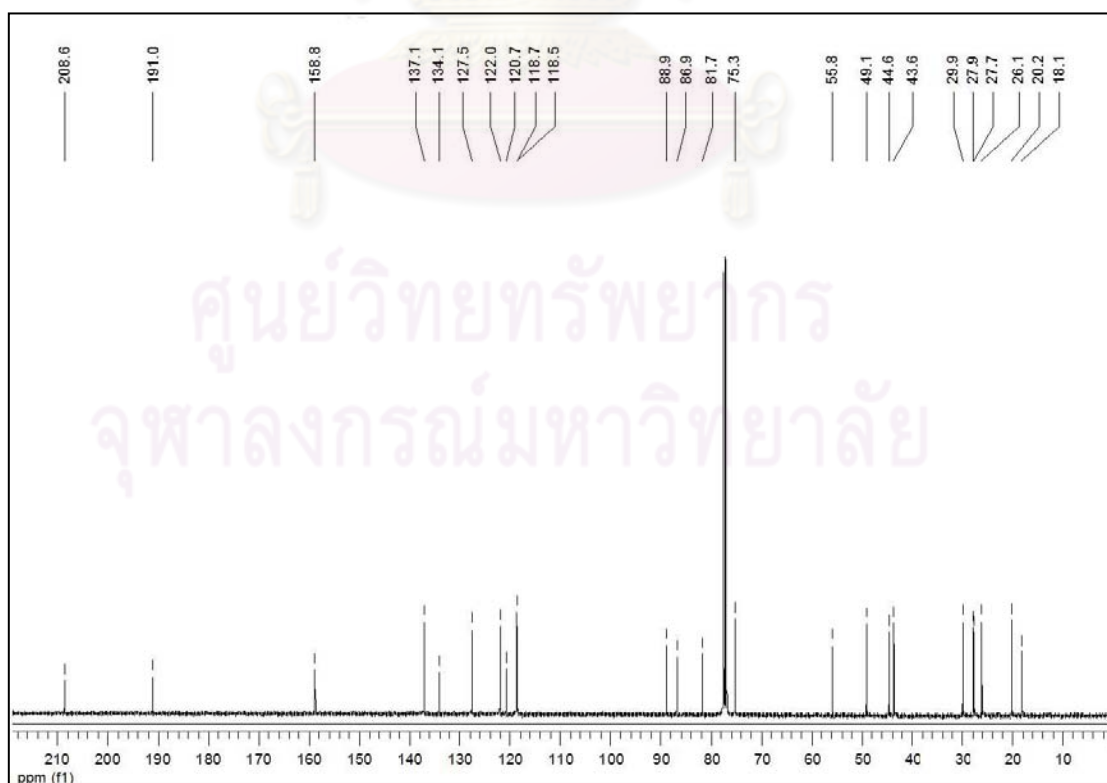**Figure 3.29** The ^{13}C NMR spectrum (CDCl$_3$, 100 MHz) of compound **C38**

3.3.6 Isolation of Gambogic Acid from Gamboge

In order to evaluate the minimum pharmacophore of caged *Garcinia* natural xanthones, gambogic acid (**77**) was decided to evaluate the bioactivity as a standard compound because it has been shown to be active against a variety of cancer cell lines [19, 225, 242]. Gambogic acid (**77**) was isolated from gamboge resin of *G. hanburyi* as its pyridine salt [19, 87] as shown below.

Gamboge

MeOH (3 times)

MeOH crude extract   Marc
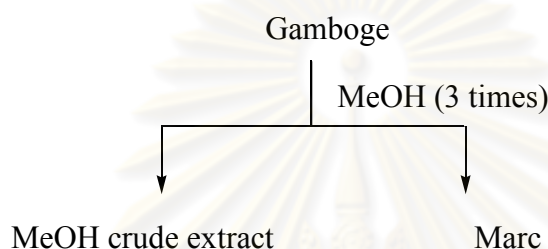
A commercially available gamboge was exacted with MeOH, and the resulting MeOH extract was subsequently dissolved in excess pyridine to obtain the corresponding gambogic pyridine salt **C37** as a yellow solid in 9% yield. The structure of **C37** was characterized by ^{1}H and ^{13}C NMR techniques. The ^{1}H NMR spectrum of **C37** (Figure 3.30) displayed three signals for five aromatic protons of pyridine ring at δ_H 8.58-8.57 (m, 2H), 7.71 (t, J = 7.5 Hz, 1H) and 7.33-7.30 (m, 2H). Three doublet signals at δ_H 7.53 (J = 6.8 Hz, 1H), 6.55 (J = 10.1 Hz, 1H) and 5.34 (J = 10.1 Hz, 1H), triplet signal at δ_H 6.07 (J = 7.1 Hz, 1H), and multiplet signal at δ_H 5.02 (br s, 2H) were referred to six olefinic protons. The signals of four methylene protons on a carbon connected to C=C bond unit of prenyl group, two methylene protons on a carbon connected to α,β-unsaturated carboxylate and three protons (H-11, H-21 and H-22) of caged core were detected at δ_H 3.47-1.98. The presence of twenty-four methyl protons, H11 and two methylene protons on a carbon connected to an oxygenated quaternary carbon C2 were observed at δ_H 1.73-1.27. The ^{13}C NMR spectrum (Figure 3.31) showed three signals at δ_C 203.7, 179.2 and 171.1, indicative of three carbonyl carbons of ketone (C-12), and α,β-unsaturated ketone (C-8), and α,β-unsaturated carboxylate (C-30), respectively. The presence of three oxygenated aromatic carbons was inferred from the presence of peaks at δ_C 161.6-157.8. The signals at δ_C 149.1, 136.9 and 124.2 were belonged to five aromatic carbons of

pyridine ring. The thirteen signals at δ_C 137.1-100.7, four signals at δ_C 91.2-81.4 and fifteen signals at δ_C 49.2-17.8 could be assigned for another thirteen sp2, four oxygenated quaternary and fifteen sp3 carbons, respectively.
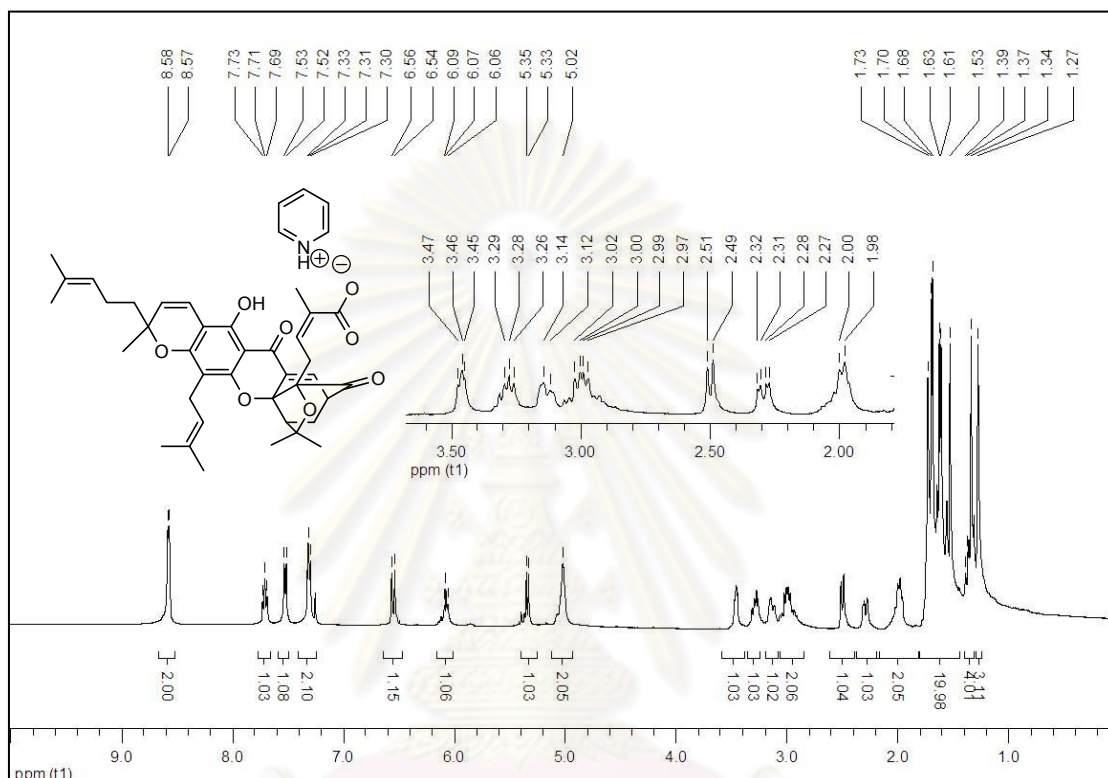
Figure 3.30 The ^{1}H NMR spectrum (CDCl$_3$, 400 MHz) of **C37**
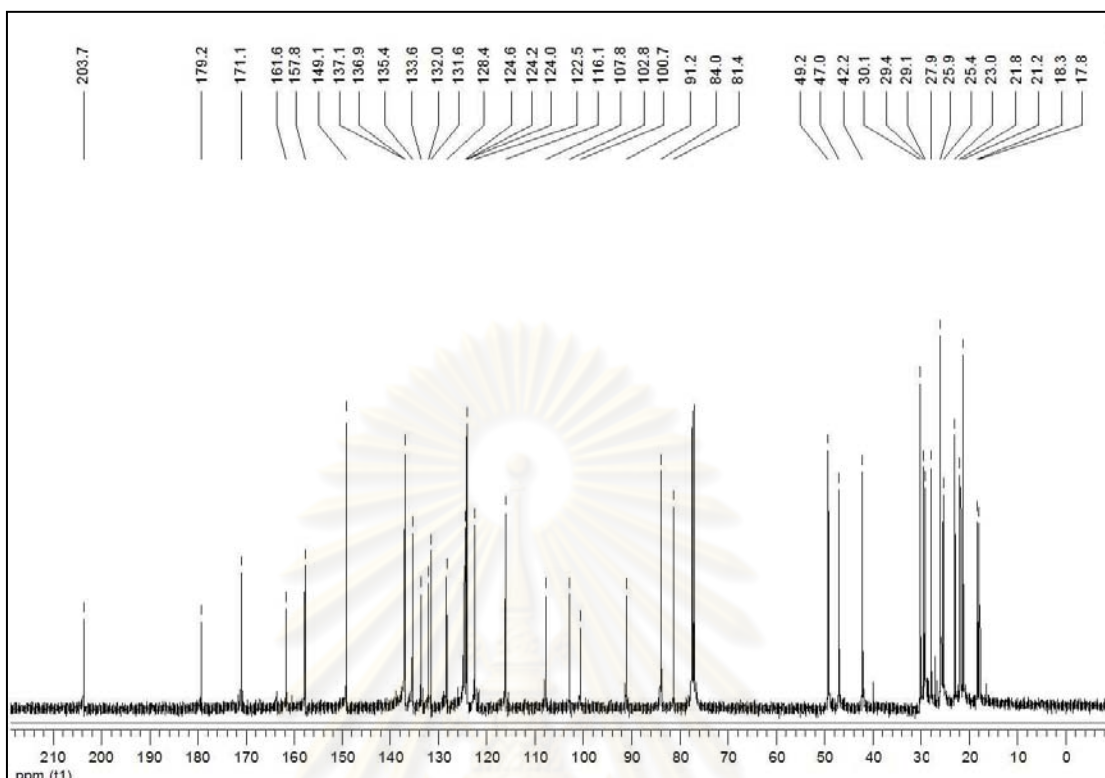
Figure 3.31 The ^{13}C NMR spectrum (CDCl$_3$, 100 MHz) of **C37**

The pyridine salt of gambogic acid **C37** was then acidified with 1N HCl at room temperature for 1 h to give gambogic acid (**77**) in 99% yield (Scheme 3.29), which can be further used without employing any chromatographic methods.
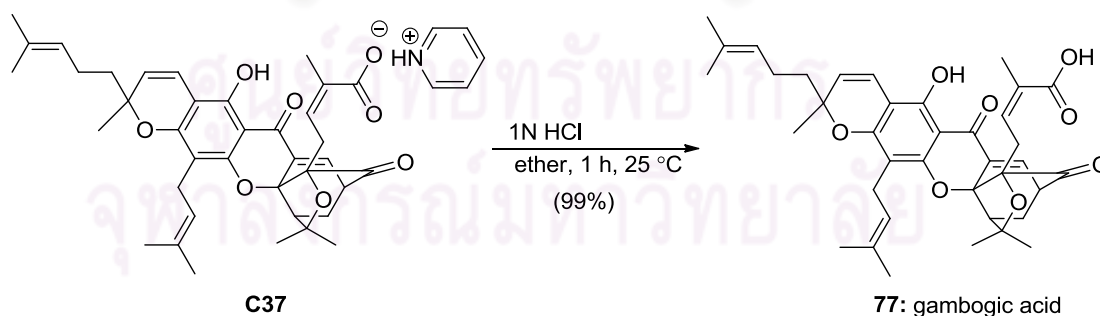
Scheme 3.29 Acidification of **C37** to gambogic acid (**77**)

The molecular composition of gambogic acid (**77**) was defined as C$_{38}$H$_{44}$O$_8$ by the HR-MS analysis. In addition, the identity of this compound was characterized by ^{1}H and ^{13}C NMR techniques. The ^{1}H NMR spectrum of gambogic acid (**77**) (Figure 3.32) exhibited three doublet signals at δ_H 7.54 (J = 6.9 Hz, 1H), 6.55 (J = 10.1 Hz,

1H), 5.34 (*J* = 10.2 Hz, 1H), triplet signal at δ_H 6.12 (t, *J* = 7.3 Hz, 1H), and board signal at δ_H 5.05-5.01 (2H) were suggested to the presence of six olefinic protons. This spectrum further presented the signals of four methylene protons on a carbon connected to C=C bond unit of prenyl group, two methylene protons on a carbon connected to *α,β*-unsaturated carboxylate and three protons (H-11, H-21 and H-22) of caged core at δ_H 3.49-1.98. It also showed the chemical shifts at 1.72-1.28, indicating to twenty-four methyl protons, H11 and two methylene protons on a carbon connected to an oxygenated quaternary carbon C2. Comparison of ^{13}C NMR data (Figure 3.33) of this compound with that of pyridine salt **C37** indicated that the peaks of pyridine ring disappeared, and carbonyl carbon signal of carboxylic acid was revealed at δ_C 172.1. The signals of three oxygenated aromatic carbons at δ_C 161.7-157.5, thirteen sp2 carbons at δ_C 138.7-100.6 and fifteen sp3 carbons δ_C 49.2-17.0 were also detected.
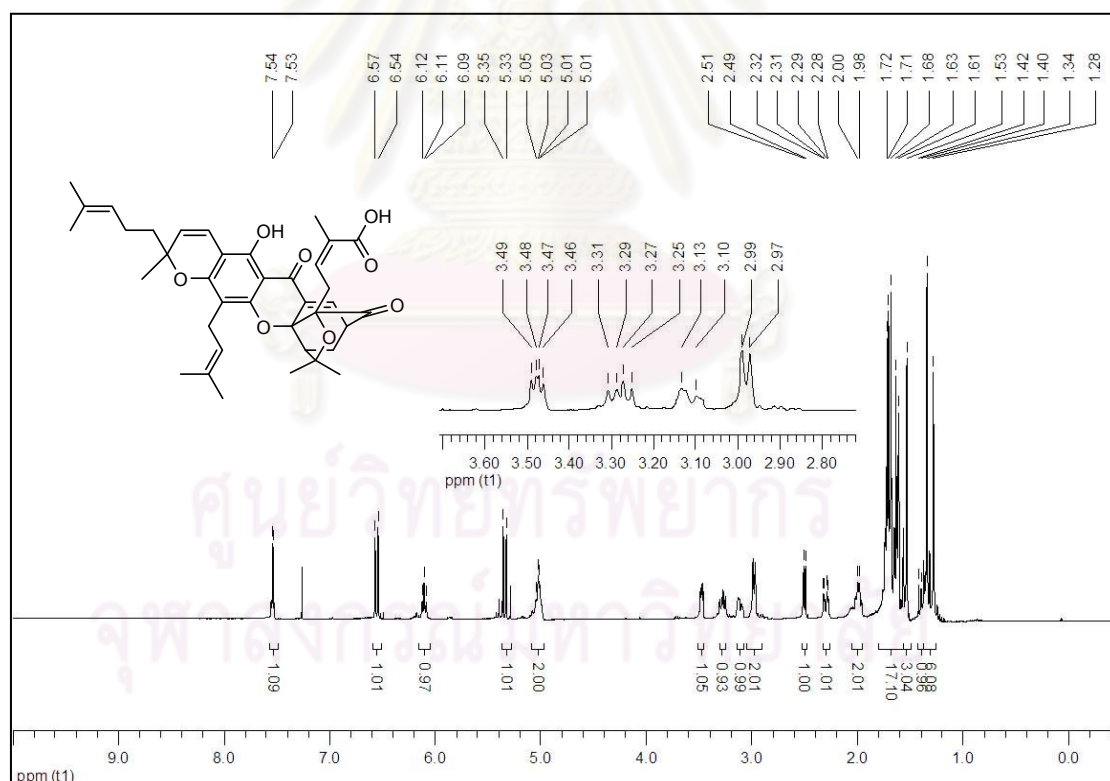
Figure 3.32 The ^{1}H NMR spectrum (CDCl$_3$, 400 MHz) of gambogic acid (**77**)
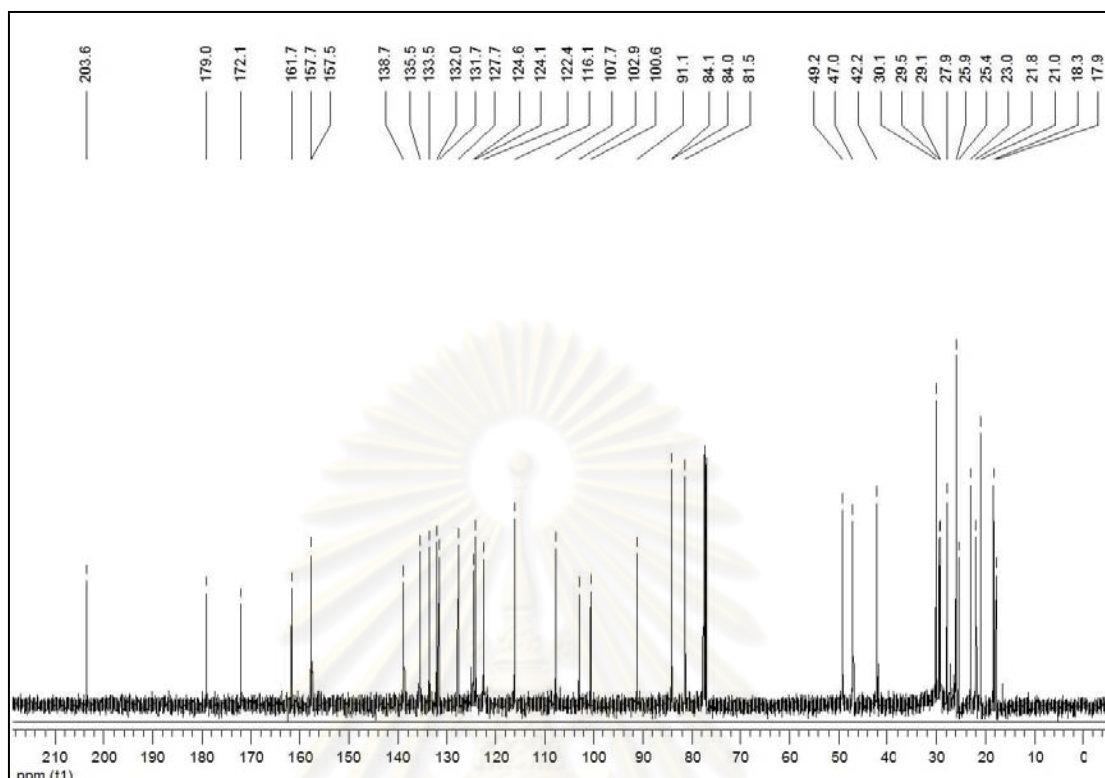
Figure 3.33 ^{13}C NMR spectrum (CDCl$_3$, 100 MHz) of gambogic acid (**77**)

3.3.7 Synthesis of Amide Analogues of Gambogic Acid

To evaluate the significance of carboxylic acid functionality of gambogic acid (**77**) for the bioactivity, its amide derivatives were prepared. Amines contained affinity and fluorescent probes such as biotin, coumarin and BODIPY were selected to couple with the carboxyl group of gambogic acid (**77**) since their desired amides could be also used for studies related to receptor binding assays and subcellular localization of the caged *Garcinia* xanthones. The synthesis of amide analogues of gambogic acid was similar to that of C-ring caged compounds **C11-C13**, which concerned with the amide coupling reaction using the DIPEA and HATU. This reaction was smoothly proceeded to afford the desired amides **C38-C40** in high yields (67-87%) (Scheme 3.30).
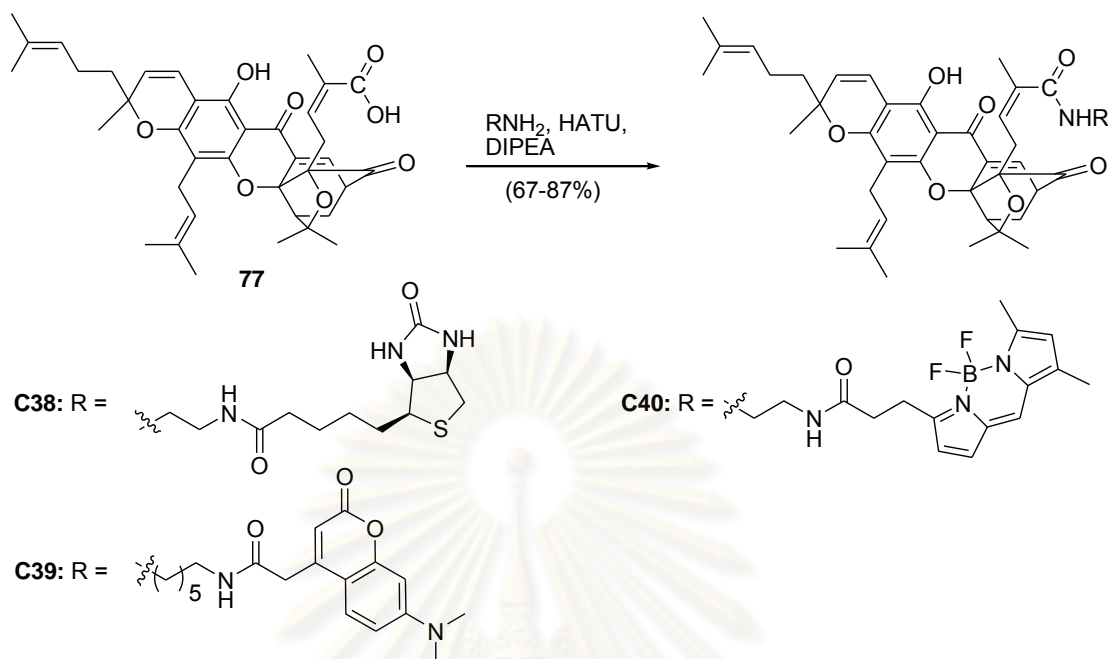
Scheme 3.30 Reagents and conditions: 2.0 equiv. DIPEA, 1.2 equiv. HATU, CH$_2$Cl$_2$, 24 h, 25 °C, **C38:** 67%, **C39:** 87%, **C40:** 77%

The structures of amides **C38-C40** were fully characterized by HR-MS, ^{1}H and ^{13}C NMR techniques. The ^{1}H NMR spectrum of biotin conjugate **C38** (Figure 3.34) was similar to that of gambogic acid (**77**). In addition, it showed the signals of biotin as follows: the signals of four NH protons at δ_H 8.00-5.00; two multiplet signals of two protons on a carbon connecting to a urea group at δ_H 4.49 and 4.32; the multiplet signals of four protons on a carbon connecting to an amino group of amide bond and one proton on a carbon connecting to a sulfur atom at δ_H 3.60-3.00; multiplet signal for two methylene protons on a carbon connecting to a sulfur atom at δ_H 3.23 and 2.89 (dd, J = 12.8, 4.8 Hz, 1H) and 2.72 (d, J = 13.1 Hz, 2H; two multiplet signals for eight methylene protons being between a biotin unit and an amide bond at δ_H 2.20 and 1.80-1.60. The ^{13}C NMR spectrum (Figure 3.35) showed the five characteristic carbonyl signals of ketone, α,β-unsaturated ketone, amide, α,β-unsaturated amide and urea at δ_C 205.1-163.9 and three oxygenated aromatic signals at δ_C 162.1-157.3. The signals indicative of sp2 carbons at δ_C 136.0-100.6, sp3 aliphatic carbons connected with nitrogen or sulfur atom at δ_C 61.8-35.9 and sp3 aliphatic carbons at δ_C 30.1-17.8 were also observed.

The ^{1}H NMR spectrum of coumarin conjugate **C39** (Figure 3.36) was compared with that of gambogic acid (**77**). It exhibited the additional signals of four aromatic protons of coumarin core and two amide protons at δ_H 7.60-5.30, two methylene protons on a carbon being between amide bond and coumarin motif at δ_H 3.63, four methylene protons on a carbon connecting with a nitrogen atom at δ_H 3.40-3.20, and eight methylene protons of diaminohexyl chain at δ_H 1.80-1.60. The ^{13}C NMR spectrum (Figure 3.37) showed the new characteristic carbonyl signal of α,β-unsaturated amide (C-30) at δ_C 168.1.

Comparison of the ^{1}H NMR spectrum of BODIPY conjugate **C40** (Figure 3.38) with that of gambogic acid (**77**) indicated that it contained more six protons at δ_H 7.00-5.20, referring to two NH protons of amide bond and four aromatic protons of BODIPY. In addition, the new signals were observed at δ_H 4.00-3.00 assigned for four protons on a carbon connecting with an amino group and two methane protons on a carbon connecting to BODIPY core and at δ_H 2.80-2.00 referred to six methyl protons on a carbon substituted on BODIPY ring and two methylene protons on a carbon bearing to carbonyl unit of amide bond. The ^{13}C NMR spectrum (Figure 3.39) contained the new characteristic signal of α,β-unsaturated amide (C-30) at δ_C 169.5.

Figure 3.34 The ^{1}H NMR spectrum (CDCl$_3$, 400 MHz) of compound **C38**

Figure 3.35 The ^{13}C NMR spectrum (CDCl$_3$, 100 MHz) of compound **C38**
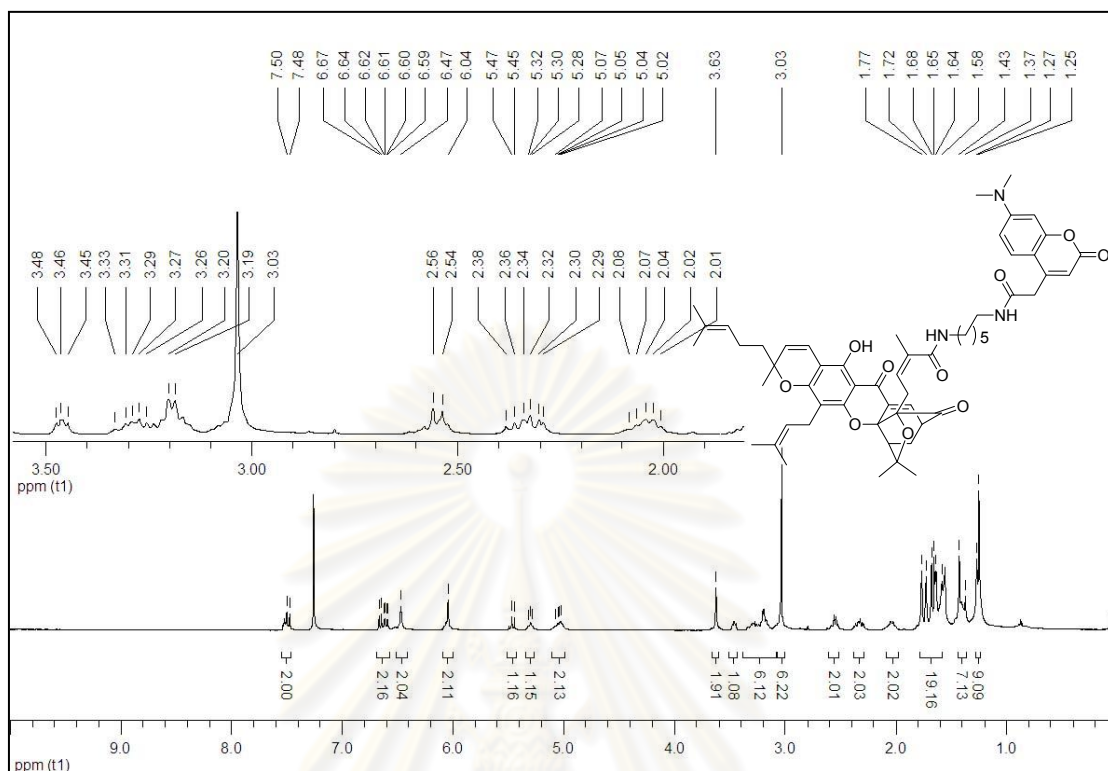
Figure 3.36 The ^{1}H NMR spectrum (CDCl$_3$, 400 MHz) of compound **C39**
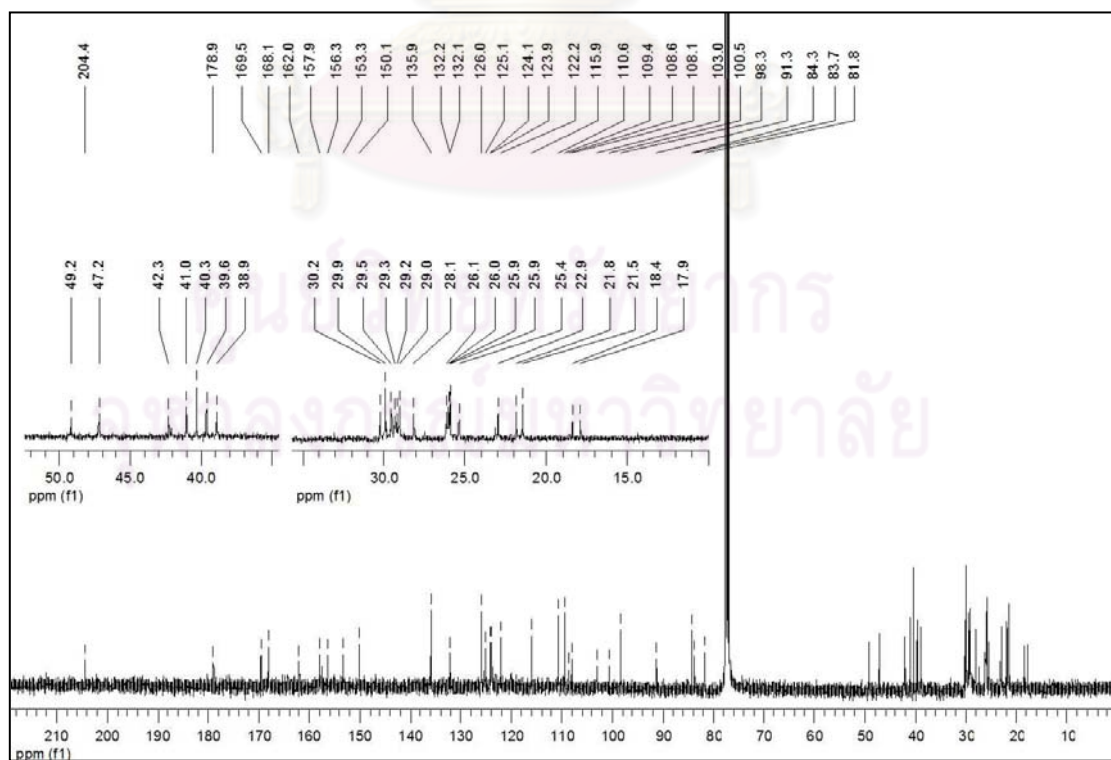
Figure 3.37 The ^{13}C NMR spectrum (CDCl$_3$, 100 MHz) of compound **C39**
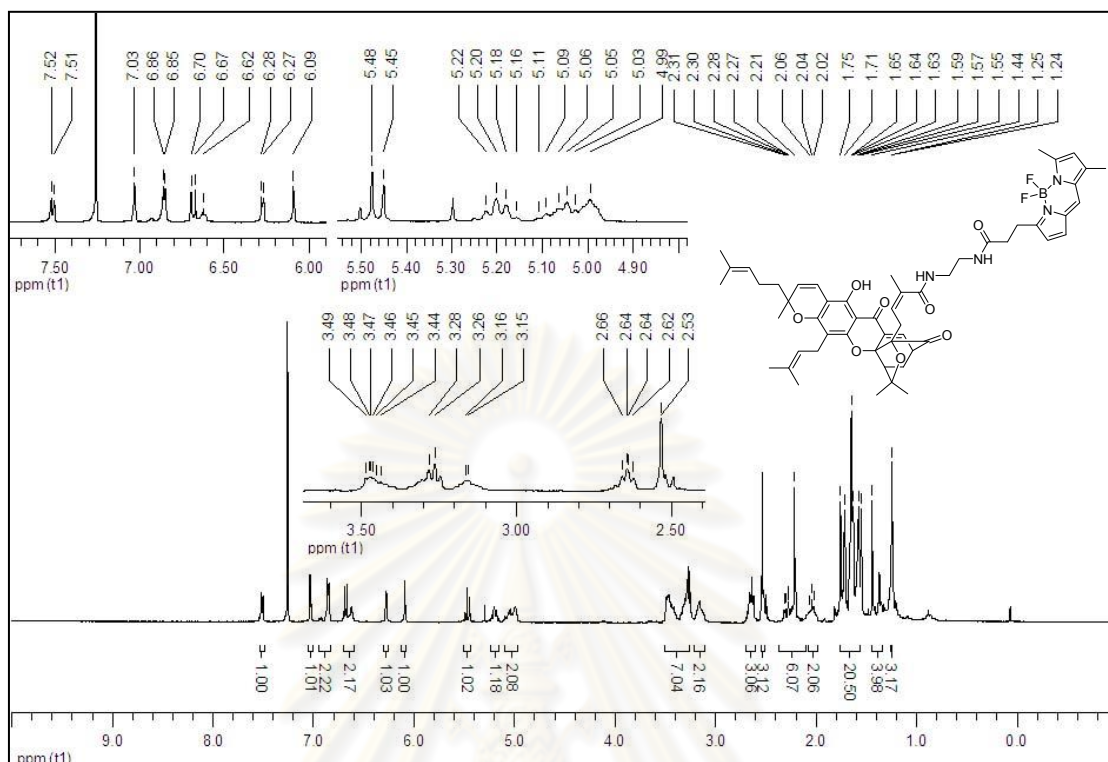
Figure 3.38 The ^{1}H NMR spectrum (CDCl$_3$, 400 MHz) of compound **C40**
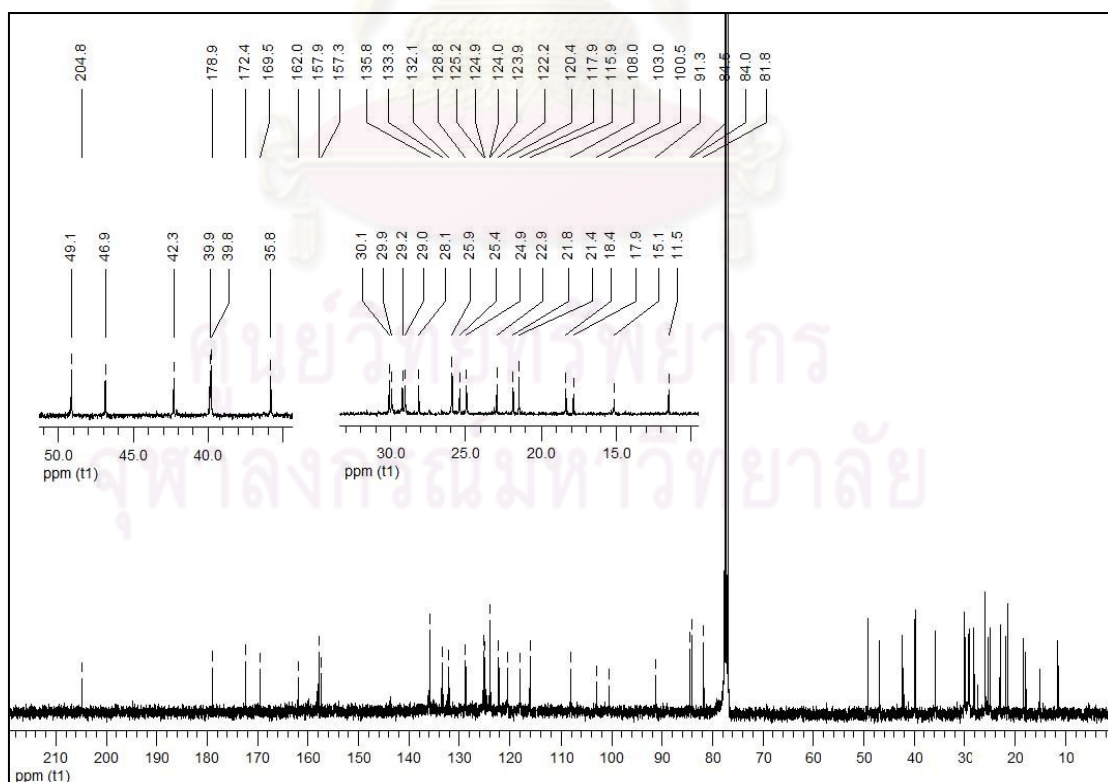
Figure 3.39 The ^{13}C NMR spectrum (CDCl$_3$, 100 MHz) of compound **C40**

3.3.8   Cell Proliferation Studies

The ability of two caged *Garcinia* natural products, gambogic acid (**77**) and gambogin (**78**) and   seventeen synthetic caged compounds to inhibit cancer cell growth was evaluated in a multidrug-resistant promyelocytic leukemia cell line, HL-60, using a ^{3}H-thymidine incorporation assay. This study was kindly tested by Dr. A. Batova, University of California at San Diego, and the results are displayed in Table 3.3. Cells were incubated with increasing concentrations of the compounds for 48 h, and then pulsed with ^{3}H-thymidine for 6 h.

Gambogic acid (**77**) and cluvenone (**196**) were found to be the most active among all the compounds tested and exhibited IC$_{50}$ values of 0.5 and 0.4 μM, respectively (entries 1 and 3). Gambogin (**78**) also exhibited the potent activity at a low μM concentration (entry 2). These findings indicated that the A-ring functionalities, dihydropyran unit, of gambogic acid (**77**) and gambogin (**78**) were not crucial to the bioactivity. The structural modification of carboxyl group of gambogic acid (**77**) to the corresponding amide moieties (compounds **C38**, **C39** and **C40**, entries 1 *vs* 18-20) did not affect the bioactivity. These compounds still showed the good activity in the cell lines tested as well as for the oxidized analogues of cluvenone (compounds **C27** and **C28**, entries 12 and 13). These results suggested that the carboxylic acid of gambogic acid (**77**) can be functionalized without loss of activity and oxidation and derivatization of the prenyl group of those compounds were well tolerated during binding to the putative receptor.

On the other hand, compounds **C8**, **C9** and **C10**, lacking both A and B rings, were inactive. They induced less than 10% growth inhibition at up to 10 μM concentrations (entries 4-6). The similar activity was observed with the C-ring amide analogues **C11-C13**, having IC$_{50}$ values greater than 20 μM (entries 7-9). In addition, compound **C19**, which lacks the A ring, showed no good activity with an IC$_{50}$ value of 10 μM (entry 10). These results pointed out that the completion of ABC-ring caged compound was significantly needed for the bioactivity.

Table 3.3 Inhibition of cell proliferation by caged *Garcinia* xanthones and analogues in multi-drug resistant promyelocytic leukemia cells (HL-60/ADR)

Entry	Compound	IC$_{50}$ (μM)
1	gambogic acid (**77**)	0.5
2	gambogin (**78**)	1.1
3	cluvenone (**196**)	0.4
4	**C8**	ND^a
5	**C9**	ND^a
6	**C10**	ND^a
7	**C11**	20.1
8	**C12**	20.7
9	**C13**	27.3
10	**C19**	10.4
11	**C26**	1.3
12	**C27**	0.7
13	**C28**	0.8
14	**C29**	2.5
15	**C34**	5.1
16	**C35**	2.8
17	**C36**	2.5
18	**C38**	1.1
19	**C39**	0.3
20	**C40**	0.6

^{a} Less than 10% inhibition at 10.0 μM.

Moreover, neo caged structure **C26** has a low micromolar activity (IC$_{50}$ value of 1.3 μM) but was about 3 times less potent than cluvenone (**196**) and related compounds with the regular caged motif (entries 11 *vs* 3). It suggested that the structural changes at the caged motif affected dramatically the biological properties.

C29 and **C34-C36** in HL-60/ADR cell lines were also examined to confirm the importance of C9-C10 enone functionalities of caged compounds for the bioactivity. It was clearly found that substitution of the C9-C10 enone functionality decreased substantially the bioactivity. For instance, compounds **C29**, **C35**, and **C36** were about 5 times less active than cluvenone (**196**), while compound **C34** was almost 10 times less active than cluvenone (**196**) (entries 14-17 *vs* entry 3). These results corresponded to the previous study related to the decreased cytotoxicity of gambogoic acid, the conjugate addition product of gambogic acid (**77**) with MeOH [113]. The significance of enone functionalities may come from their reactivities as a conjugate electrophile.

3.3.9   Apoptosis Studies

Studies from several laboratories have shown that the caged *Garcinia* xanthones induce apoptotic cell death in a variety of cancer cell lines [161, 163, 187, 226, 243]. Apoptosis, or programmed cell death, is a highly regulated process that allows a cell to self-degrade in order for the body to eliminate unwanted or dysfunctional cells. As such, it is essential to embryonic development and the maintenance of homeostasis in multicellular organisms. In humans, for example, the rate of cell growth and cell death is balanced to maintain the weight of the body. It has been estimated that each day between 50-70 billion cells in the human body perish due to apoptosis [244]. This event is necessary to make room for the billions of new cells produced daily. In fact, within one year this flux of cells corresponds to a production and eradication of a mass equal to almost our entire body weight. Once triggered, the apoptotic event leads to cell deletion *via* a process that includes chromatin condensation, nuclear fragmentation, cell shrinkage, plasma membrane blebbing and other ultrastructural changes [245]. These changes lead ultimately to phagocytosis by the neighboring cells without inciting unnecessary inflammatory reactions or tissue scaring.

In general, apoptosis can be induced in two different ways, referred to as the intrinsic and extrinsic pathways (Figure 3.40) [246]. The intrinsic pathway is activated by stress signals resulting from cellular damage sensors (e.g. p53) or

developmental cues. Upon receiving the stress signal, pro-apoptotic members of the Bcl-2 family of proteins, such as Bax and Bid, bind to the outer membrane of the mitochondria to signal the release of cytochrome C [247]. Cytochrome C binds to ATP and Apaf-1 to form a large ternary protein complex, known as the apoptosome that recruits and activates caspase-9 [248].
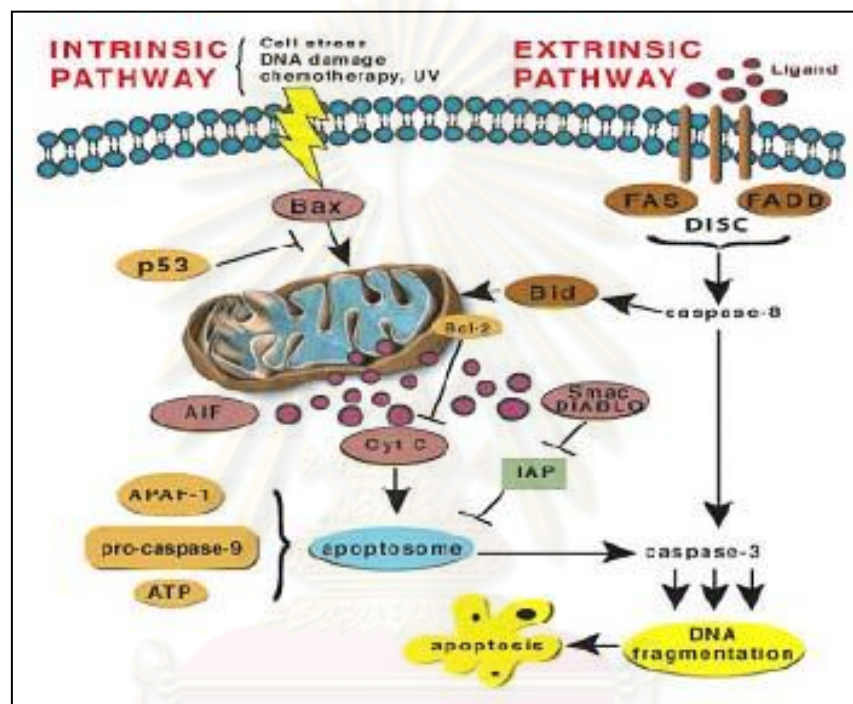
Figure 3.40 Intrinsic and extrinsic pathways of apoptosis

In turn, this activates caspase-3, the executioner of apoptosis that initiates DNA fragmentation. Besides the release of cytochrome C from the intramembrane space, the intramembrane content released also contains apoptosis inducing factor (AIF) to facilitate DNA fragmentation, and Smac/Diablo proteins to inhibit the inhibitor of apoptosis (IAP). On the other hand, the extrinsic pathway is initiated by binding of a small molecule to a death receptor, such as TNF-R1, Fas or DR4, which leads to receptor aggregation (usually homo-trimerization). The activated receptor then recruits the cytoplasmic proteins FADD (Fas-associated death domain protein) and procaspase-8 to form a complex known as death-inducing signaling complex (DISC). In certain cells, such as lymphocytes, DISC formation leads directly to activation of caspase-3, to trigger apoptosis without involving mitochondria. In other

cells, the formation of DISC can activate the mitochondrial apoptotic pathway through cleavage and activation of the Bid protein [249].

There is compelling evidence that insufficient apoptosis can result in cancer or autoimmunity while accelerated cell death is evident in degenerative diseases, immunodeficiency and infertility. In fact, tumorigenesis is a multi-step process based on genetic alterations that drive the progressive transformation of normal cells into highly malignant derivatives. It has been suggested that the large diversity of human cancer cell genotypes is a manifestation of six essential alterations in cell physiology that collectively dictate malignant growth [151]. These alterations, also referred to as the hallmarks of cancer, involve: (a) self-sufficiency in growth signals; (b) insensitivity to growth inhibitory signals; (c) evasion of apoptosis; (d) limitless replicating ability; (e) sustained angiogenesis; and (f) tissue invasion and metastasis. These physiologic changes are shared by most, if not all, types of human cancer and represent points for therapeutic intervention. The third alteration from the above list refers to the ability of cancer cells to circumvent normal pathways leading to apoptosis, thus expanding their population in a non-controlled manner. Downregulation of pro-apoptotic proteins, such as Bax, overexpression of the anti-apoptotic protein Bcl-2, and/or mutations that destroy their function (e.g. p53 mutations), decrease the ability of the cell to undergo apoptosis leading ultimately to tumorigenesis [250-251]. It has also been shown that effectively all traditional anticancer drugs use apoptosis pathways to exert their cytotoxic actions [245]. Consequently, defects in the regulation of apoptosis can render cells intrinsically resistant to chemotherapy, not because the drugs or irradiation fails to induce damage to DNA, microtubules and other structures, but because tumor cells remain viable after suffering the damage and hence have opportunities to undergo repair and resume their proliferative activities [252].

To determine whether the mechanism of cytotoxicity of these compounds involved the induction of apoptosis, a cell death detection ELISA which measured histone-associated DNA fragments was performed by Dr. Asyse Batova, University of California at San Diego. This study was performed with cluvenone (**196**) and is shown in Figure 3.41. Compound **196** induced apoptosis, after 7 h of treatment of HL-

60 and HL-60/ADR cells, in a dose-dependent manner with EC_{50} values of 0.25 and 0.32 μM respectively. These results were comparable to the apoptotic effect of gambogic acid and related caged *Garcinia* natural products. Specifically, the EC_{50} values of gambogic acid (**77**) in human breast cancer cells T47D, human colon cancer cells HCT116, and hepatocellular carcinoma cancer cells SNU398 were reported to be about 0.7 μM [229]. More importantly, the similar EC_{50} values observed for cluvenone (**196**) in the HL-60 and HL-60/ADR cells parallels the previous observations [147] and confirm that its cytotoxicity was not affected by the expression of P-glycoprotein which renders the HL-60/ADR cell lines multidrug-resistant [149, 253-254].
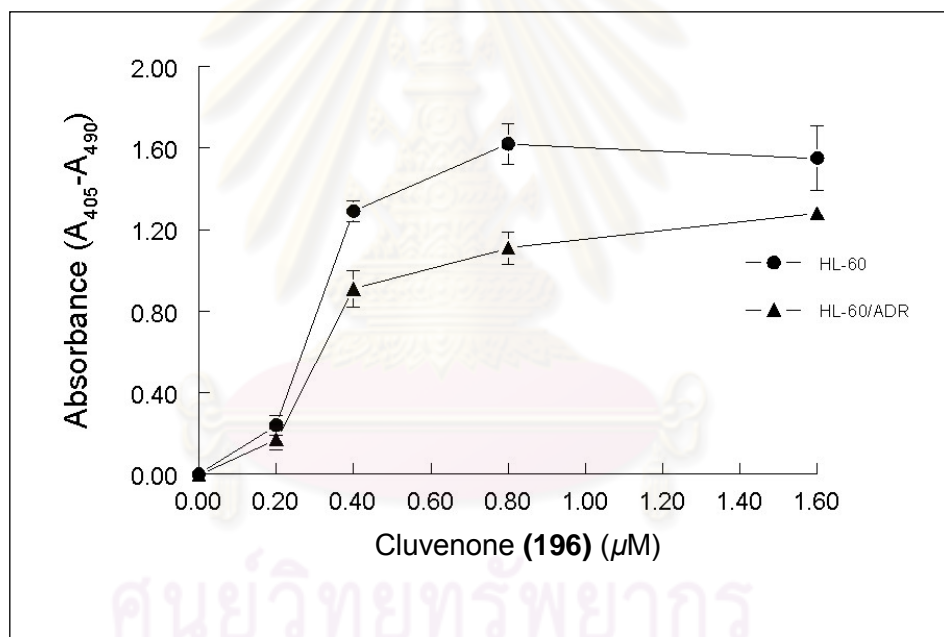
Figure 3.41 Induction of apoptosis by cluvenone (**196**) in promyelocytic leukemia
cells

Apoptosis induced in HL60/ADR cells by cluvenone (**196**) was also visualized by fluorescence microscopy after staining with Alexa Fluor® 488 annexin V and propidium iodide (PI) (Figure 3.42).
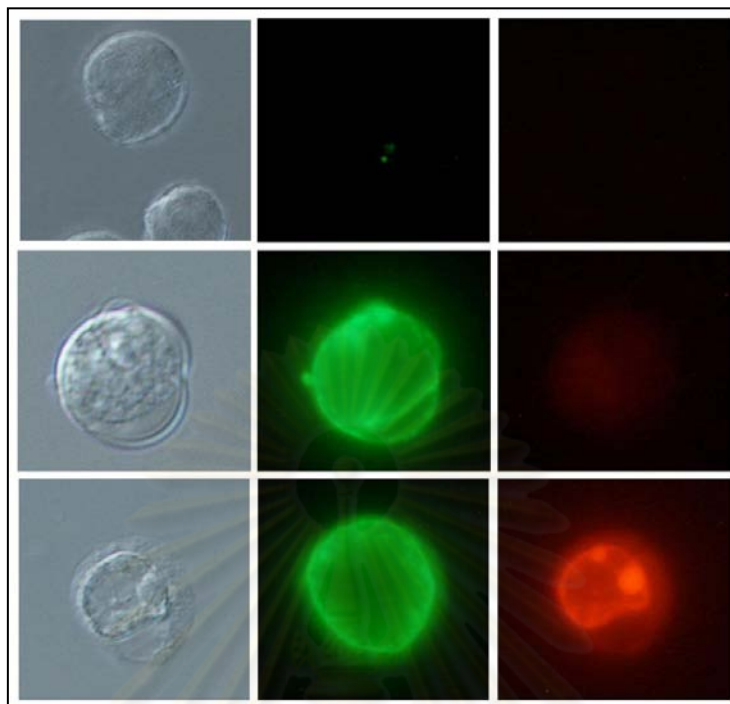
Figure 3.42 Induction of apoptosis in HL-60/ADR cells by cluvenone (**196**) visualized by differential interference contrast microscopy (left column) and fluorescence microscopy (middle and right column). Control unreated cells are shown in the top row. Treated cells undergoing early and late stage apoptosis are shown in the middle and bottom row respectively.

The green-fluorescent Alexa Fluor® 488 annexin V detected the externalization of phosphatidylserine, a hallmark of apoptosis (Figure 3.42, middle column) [151, 244, 255]. The red-fluorescent propidium iodide stained DNA during advanced stages of apoptosis and necrosis (Figure 3.42, right column). Cells in the left column of Figure 3.42 were visualized by differential interference contrast (DIC) microscopy. While untreated live cells showed little or no fluorescence (Figure 3.5, top row), cluvenone-treated cells undergoing early stage apoptosis showed only green fluorescence after staining with both probes (Figure 3.42, middle row). In the middle row was also evident the membrane blebbing, which is the characteristic of apoptosis [151, 244, 255]. Cluvenone-treated cells undergoing late stage apoptosis, at which point DNA becames accessible to staining by PI, displayed both green and red fluorescence (Figure 3.42, bottom row). In this row the chromatin fragmentation was also evident.

3.3.10 Selectivity of Gambogic acid (77) and Cluvenone (196) for Cancer Cells over Normal Cells

To determine whether cluvenone (196) has any selectivity for cancer cells over normal cells, the effect of cluvenone in a primary human leukemia and peripheral blood mononuclear cells (PBMC) obtained from a normal donor was examined. This study was kindly tested by Dr. A. Batova, University of California at San Diego. Primary cells were exposed to increasing concentrations of cluvenone (196) for 48 h and then viable cell numbers were determined. Cluvenone (196) was almost 5-fold (4.7) more toxic to leukemia cells (IC_{50} 1.1 μM) than PBMC from normal donors (IC_{50} 5.2 μM). Interestingly, in the same experiment, gambogic acid (77) was 3.9-fold more toxic to acute lymphoblastic leukemia cells than PBMC suggesting that it may have greater toxicity to normal cells compared to cluvenone (196). The observed differential cytotoxicity of cluvenone (196) against leukemia cells *vs* PBMC from normal individuals is extremely encouraging as standard chemotherapeutic agents are generally similarly toxic to PBMC and tumor cells. Based on the observed tumor selectivity, it is anticipated that cluvenone (196) will be well tolerated at the low doses which are therapeutically effective.

3.3.11 Antibacterial Activity of Caged Compounds and SAR Study

Caged compounds were tested against the community-associated MRSA strain TCH1516 (USA300 strain of CA-MRSA), performed by Dr. M. Hensler at Nizet Laboratory, Department of Pediatrics, UCSD School of Medicine. All of the results are shown in Table 3.4.

Table 3.4 Antibacterial activity of caged compounds against the community-associated MRSA strain TCH1516

Entry	Compound	MIC (μM)
1	gambogic acid (**77**)	12.5
2	Cluvenone (**196**)	50
3	**C8**	>100
4	**C10**	>100
5	**C19**	>100
6	**C34**	>100

Gambogic acid (**77**) exhibited good activity with the MIC value of 12.5 μM (entry 1). Cluvanone (**196**) was moderately active with the MIC value of 50 μM (entry 2). **C8**, **C10** and **C19**, which lack the A or B ring, were inactive with the MIC values up to 100 μM (entries 3-5). These findings indicated that the intact ABC ring containing the C-ring caged structure presented the minimum bioactive motif of such compounds. Similarly, **C34**, the enone bond was substituted, did not show any activity with the MIC value up to 100 μM (entry 6). This observation suggested that the C9=C10 enone bond was also important for bioactivity. These findings were corresponded to the SAR studies on cell proliferation.

CHAPTER IV
CONCLUSION

α-Mangostin (**1**) was isolated from the pericarps of mangosteen in 1% w/w and was then utilized to prepare three 3-mono, fourteen 6-mono and ten 3,6-di-*O*-substituted *α*-mangostins, along with 3-isomangostin (**7**), BR-xanthone A (**30**) and five 6-*O*-acylated 3-isomangostins.

α-Mangostin (**1**) exhibited the same potent activity against both *S. aureus* ATCC 25923 and *S. aureus* ATCC 43300 (MRSA) with the MIC and MBC values of 0.78 and 1.56 μg/mL, respectively. The replacement of hydroxyl groups at C3 and C6 and cyclization of prenyl units at C2 and C8 markedly decreased the activities. The SAR studies indicated that the polar hydroxyl groups on C3 and C6 and nonpolar prenyl chains substituted on C2 and C8 of *α*-mangostin (**1**) displayed an essential role for bioactivity. In addition, all tested compounds were inactive against *C. albicans* with the MIC value up to 2,000 μg/mL.

For the termite antifeedant activity, *α*-mangostin (**1**) completely inhibited termite feeding with the %FI of 97.8 at a dose of 100 μg/disk, and still showed good termicidal activity with the %FI value of 85.0 at a dose of 50 μg/disk. In contrast, the derivatization of hydroxyl groups at C3 and C6 decreased antifeedant activities. The SAR study indicated that the hydrophilic hydroxyl groups at C3 and C6 may be necessary for bioactivity.

Based on an unusual architecture of caged *Garcinia* natural xanthones and their fascinating bioactivities, especially gambogic acid (**77**), the synthesis of its simplified analogues and their pharmacological evaluations have been explored.

A novel method for the reverse prenylation of catechols was successfully explored. This reaction proceeded in excellent yield under Pd(0)-catalysis using 1,1-dimethylpropenyl *t*-butyl carbonate (**C3b**) or *bis*(1,1-dimethylpropenyl)carbonate (**C3c**) as the prenylation reagents in short reaction time. The resulting di-allylloxy

materials were then used as a precursor for the Claisen/Diels–Alder reaction cascade to produce various caged analogues.

The SAR studies of gambogic acid (**77**), gambogin (**78**) and synthetic caged analogues were evaluated in a multi-drug resistant promyelocytic leukemia cell line, HL-60/ADR (Adriamycin). The minimum bioactive motif of such compounds was represented by the intact ABC ring containing the C-ring caged structure. Structural changes to this motif resulted in substantial loss of activity. The C9=C10 enone functionality was also important to the activity, while the C5 prenyl group could be oxidized and functionalized without loss of bioactivity. In fact, this site could be used for modifications that will improve the solubility and pharmacology of these compounds.

From the cell proliferation and apoptosis studies, cluvenone (**196**) had significant cytotoxicity in multidrug-resistant and sensitive leukemia cells by inducing apoptosis comparable to the reported natural products such as gambogic acid (**77**). Furthermore, the observed differential cytotoxicity between leukemia cells and peripheral blood mononuclear cells (PBMC) from normal donors, suggesting that cluvenone (**196**) has tumor selectivity. These results reinforced the concept of finding new and potent pharmacophores which will increase the understanding of the SAR and eventually ring to the success of the preparation of therapeutically relevant agents.

The SAR studies on gambogic acid (**77**) and simplified caged analogues **196**, **C8**, **C10**, **C19** and **C34** for antibacterial activity against the community-associated methicillin-resistant *S. aureus* (MRSA) strain TCH1516 found that the intact ABC ring containing the C-ring caged structure presented the minimum bioactive motif of such compounds. The C9=C10 enone bond was also important for bioactivity. These findings were corresponded to the SAR studies on cell proliferation.

In addition, the Pd(0)-catalyzed reverse prenylation was applied to an improved synthesis of a lead analogue cluvenone (**196**) in a gram scale. The amount

of Pd(PPh$_3$)$_4$ could be successfully reduced to 3mol%, producing *bis*-allyloxy xanthone **C25** in quantitative yield within 10 mins at room temperature.

Proposed for the Further Work

This research relates to the Pd(0)-catalyzed installation of 1,1-dimethyl-2-propenyl units to dihydroxy compounds. The investigation of scope and limitation of the developed method should be extended. From the SAR studies of gambogic acid, its fluorescent amide analogues could be used to investigate on the mechanism of cytotoxicity.

REFERENCES

[1]   Ollis, W. D.; Redman, B. T.; Sutherland, I. O.; Jewers, K. Constitution of ronianone. J. Chem. Soc. D 15 (1969) : 879-880.

[2]   Moongkarndi, P.; Kosem, N.; Kaslungka, S.; Luanratana, O.; Pongpan, N.; Neungton, N. Antiproliferation, antioxidation and induction of apoptosis by *Garcinia mangostana* (mangosteen) on SKBR3 human breast cancer cell line. J Ethnopharmacol. 90 (2004) : 161-166.

[3]   Chomnawang, M. T.; Surassmo, S.; Nukoolkarn V. S.; Gritsanapan, W. Effect of *Garcinia mangostana* on inflammation caused by Propionibacterium acnes. Fitoterapia 78 (2007) : 401-408.

[4]   Kosem, N.; Han, Y. -H.; Moongkarndi, P. Antioxidant and cytoprotective activities of methanolic extract from *Garcinia mangostana* hulls. ScienceAsia 33 (2007) : 283-292.

[5]   Martin, F. W. Durian and mangosteen. Westport CT: AVI; 1980.

[6]   Harbborn, J. B.; Baxter, H. Phytochemical Dictionary: A Handbook of Bioactive Compounds from Plants. 2 ed.: CRC Press; 1999.

[7]   Ji, X.; Avula, B.; Khan, I. A. Quantitative and qualitative determination of six xanthones in *Garcinia mangostana* L. by LC-PDA and LC-ESI-MS. J. Pharm. Biomed. Anal. 43 (2007) : 1270-1276.

[8]   Chen, L. -G.; Yang, L. -L.; Wang, C. -C. Anti-inflammatory activity of mangostins from *Garcinia mangostana*. Food Chem. Toxicol. 46 (2008) : 688-693.

[9]   Mahabusarakam, W.; Wiriyachitra, P.; Phongpaichit, S. Antimicrobial activities of chemical constituents from *Garcinia mangostana* Linn. J. Sci. Soc. Thailand 12 (1986) : 239-243.

[10]   Thoison, O.; Fahy, J.; Dumontet, V.; Chiaroni, A.; Riche, C.; Tri, M. V.; Sevenet, T. Cytotoxic Prenylxanthones from *Garcinia bracteata*. J. Nat. Prod. 63 (2000) : 441-446.

[11]   Wu, J.; Xu, Y. J.; Cheng, X. F.; Harrison, L. J.; Sim, K. Y.; Goh, S. H. A highly rearranged tetraprenylxanthonoid from *Garcinia gaudichaudii* (Guttiferae). Tetrahedron Lett. 42 (2001) : 727-729.

[12]   Karanjgaonkar, C. G.; Nair, P. M.; Venkataraman, K. The coloring matters of *Garcinia morella*. VI. Morellic, isomorellic, and gambogic acids. Tetrahedron Lett. (1966) : 687-691.

[13]   Rukachaisirikul, V.; Kaewnok, W.; Koysomboon, S.; Phongpaichit, S.; Taylor, W. C. Caged-tetraprenylated xanthones from *Garcinia scortechinii*. Tetrahedron 56 (2000) : 8539-8543.

[14]   Lin, L. J.; Lin, L. Z.; Pezzuto, J. M.; Cordell, G. A.; Ruangrungsi, N. Isogambogic acid and isomorellinol from *Garcinia hanburyi*. Magn. Reson. Chem. 31 (1993) : 340-347.

[15]   Shadid, K. A.; Shaari, K.; Abas, F.; Israf, D. A.; Hamzah, A. S.; Syakroni, N.; Saha, K.; Lajis, N. H. Cytotoxic caged-polyprenylated xanthonoids and a xanthone from *Garcinia cantleyana*. Phytochemistry. 68 (2007) : 2537-2544.

[16]   Wu, Z. -Q.; Guo, Q. -L.; You, Q. -D.; Zhao, L.; Gu, H. -Y. Gambogic acid inhibits proliferation of human lung carcinoma SPC-A1 cells *in vivo* and *in vitro* and represses telomerase activity and telomerase reverse transcriptase mRNA expression in the cells. Biol. Pharm. Bull. 27 (2004) : 1769-1774.

[17]   Reutrakul, V.; Anantachoke, N.; Pohmakotr, M.; Jaipetch, T.; Sophasan, S.; Yoosook, C.; Kasisit, J.; Napaswat, C.; Santisuk, T.; Tuchinda, P. Cytotoxic and anti-HIV-1 caged xanthones from the resin and fruits of *Garcinia hanburyi*. Planta Med. 73 (2007) : 33-40.

[18]   Sukpondma, Y.; Rukachaisirikul, V.; Phongpaichit, S. Antibacterial caged-tetraprenylated xanthones from the fruits of *Garcinia hanburyi*. Chem. Pharm. Bull. 53 (2005): 850-852.

[19]   Zhang, H. -Z.; Kasibhatla, S.; Wang, Y.; Herich, J.; Guastella, J.; Tseng, B.; Drewe, J.; Cai, S. X. Discovery, characterization and SAR of gambogic acid as a potent apoptosis inducer by a HTS assay. Bioorg. Med. Chem. 12 (2004) : 309-317.

[20]   Hu, J.; Chen, J.; Zhao, Y.; Wang, R.; Zheng, Y.; Zhou, J. Chemical constituents from fruit hulls of *Garcinia mangostana* (Cuttiferae). Yunnan Zhiwu Yanjiu 28 (2006) : 319-322.

[21] Tadtong, S.; Viriyaroj, A.; Vorarat, S.; Nimkulrat, S.; Suksamrarn, S. Antityrosinase and antibacterial activities of mangosteen pericarp extract. J. Health Res. 23 (2009) : 99-102.

[22] Moffett, A.; Shah, P. Pharmaceutical, therapeutic, nutritional, cosmetic, and dermatological compositions derived from *Garcinia mangostana* L plant. (Renaissance Herbs, Inc., USA). City, 2006, pp. 39

[23] Chairungsrilerd, N.; Furukawa, K. I.; Ohta, T.; Nozoe, S.; Ohizumi, Y. Histaminergic and serotonergic receptor blocking substances from the medical plant *Garcinia mangostana*. Planta Med. 62 (1996) : 471-472.

[24] Williams, P.; Ongsakul, M.; Proudfoot, J.; Croft, K.; Beilin, L. Mangostin inhibits the oxidative modification of human low density lipoprotein. Free Radical Res. 23 (1995) : 175-184.

[25] Abbiw, D. K. The Useful Plants of Ghana. Practical Action 1989.

[26] Gritsanapan, W.; Chulasiri, M. A preliminary study of antidiarrheal plants and antibacterial activity. Mahidol Univ. J. Pharm. Sci. 10 (1983) : 119-122.

[27] Voravuthikunchai, S. P.; Kitpipit, L. Activity of medicinal plant extracts against hospital isolates of methicillin-resistant *Staphylococcus aureus*. Clin. Microbiol. Infect. 11 (2005) : 510-512.

[28] Puripattanavong, J.; Khajorndetkun, W.; Chansathirapanich, W. Improved isolation of α-mangostin from the fruit hull of *Garcinia mangostana* and its antioxidant and antifungal activity. Planta Med. (2006) : 1078.

[29] Bullangpoti, V.; Visetson, S.; Milne, M.; Milne, J.; Pornbanlualap, S.; Sudthongkong, C.; Tayapat, S. The novel botanical insecticide for the control brown planthopper (*Nilaparvata lugens* Stal.). Commun. Agric. Appl. Biol. Sci. 71 (2006) : 475-481.

[30] Nakatani, K.; Atsumi, M.; Arakawa, T.; Oosawa, K.; Shimura, S.; Nakahata, N.; Ohizumi, Y. Inhibitions of histamine release and prostaglandin E2 synthesis by mangosteen, a Thai medicinal plant. Biol. Pharm. Bull. 25 (2002) : 1137-1141.

[31] Schmid, W. Ann. Chem. Pharm. 93 (1855) : 83.

[32] Dragendorff, O. Ibid 482 (1930) : 280.

[33] Yates, P.; Stout, G. H. The structure of mangostin. J. Am. Chem. Soc. 80 (1958) : 1691-1700.

[34] Peres, V.; Nagem, T. J.; de Oliveira, F. F. Tetraoxygenated naturally occurring xanthones. Phytochemistry 55 (2000) : 683-710.

[35] Mahabusarakam, W.; Wiriyachitra, P.; Taylor, W. C. Chemical constituents of *Garcinia mangostana*. J. Nat. Prod. 50 (1987) : 474-478.

[36] Malathi, R.; Kabaleeswaran, V.; Rajan, S. S. Structure of mangostin. J. Chem. Crystallogr. 30 (2000) : 203-205.

[37] Gales, L.; Damas, A. M. Xanthones-a structural perspective. Curr. Med. Chem. 12 (2005) : 2499-2515.

[38] Zhao, J.; Qi, Q.; Yang, Y.; Gu, H.-Y.; Lu, N.; Liu, W.; Wang, W.; Qiang, L.; Zhang, L. -B.; You, Q. -D.; Guo, Q. -L. Inhibition of $\alpha 4$ integrin mediated adhesion was involved in the reduction of B16-F10 melanoma cells lung colonization in C57BL/6 mice treated with Gambogic acid. Eur. J. Pharmacol. 589 (2008) : 127-131.

[39] Chairungsrilerd, N.; Takeuchi, K.; Ohizumi, Y.; Nozoe, S.; Ohta, T. Mangostanol, a prenyl xanthone from *Garcinia mangostana*. Phytochemistry 43 (1996) : 1099-1102.

[40] Yu, L.; Zhao, M.; Yang, B.; Zhao, Q.; Jiang, Y. Phenolics from hull of *Garcinia mangostana* fruit and their antioxidant activities. Food Chem. 104 (2007) : 176-181.

[41] Suksamrarn, S.; Komutiban, O.; Ratananukul, P.; Chimnoi, N.; Lartpornmatulee, N.; Suksamrarn, A. Cytotoxic prenylated xanthones om the young fruit of *Garcinia mangostana*. Chem. Pharm. Bull. 54 (2006) : 301-305.

[42] Suksamrarn, S.; Suwannapoch, N.; Ratananukul, P.; Aroonlerk, N.; Suksamrarn, A. Xanthones from the green fruit hulls of Garcinia mangostana. J. Nat. Prod. 65 (2002) : 761-763.

[43] Ee, G. C. L.; Daud, S.; Taufiq-Yap, Y. H.; Ismail, N. H.; Rahmani, M. Xanthones from *Garcinia mangostana* (Guttiferae). Nat. Prod. Res., Part A 20 (2006) : 1067-1073.

[44]   Ee, G. C. L.; Izzaddin, S. A.; Rahmani, M.; Sukari, M. A.; Lee, H. L. *γ*-mangostin and rubraxanthone, two potential lead compounds for anti-cancer activity against CEM-SS cell line. Nat. Prod. Sci. 12 (2006) : 138-143.

[45]   Ee, G. C. L.; Daud, S.; Izzaddin, S. A.; Rahmani, M. *Garcinia mangostana*: a source of potential anti-cancer lead compounds against CEM-SS cell line. J. Asian Nat. Prod. Res. 10 (2008) : 481-485.

[46]   Chin, Y. -W.; Jung, H. -A.; Chai, H.; Keller, W. J.; Kinghorn, A. D. Xanthones with quinone reductase-inducing activity from the fruits of *Garcinia mangostana* (Mangosteen). Phytochemistry 69 (2008) : 754-758.

[47]   Parveen, M.; Ud-din Khan, N. Two xanthones from *Garcinia mangostana*. Phytochemistry 27 (1988) : 3694-3696.

[48]   Sen, A. K.; Sarkar, K. K.; Mazumder, P. C.; Banerji, N.; Uusvuori, R.; Hase, T. A. A xanthone from *Garcinia mangostana*. Phytochemistry 19 (1980): 2223-2225.

[49]   Sen, A. K.; Sarkar, K. K.; Majumder, P. C.; Banerji, N. Minor xanthones of *Garcinia mangostana*. Phytochemistry 20 (1981) : 183-185.

[50]   Sen, A. K.; Sarkar, K. K.; Mazumder, P. C.; Banerji, N.; Uusuori, R.; Hase, T. A. The structures of garcinones A, B, and C: three new xanthones from *Garcinia mangostana*. Phytochemistry 21 (1982) : 1747-1750.

[51]   Huang, Y. -L.; Chen, C. -C.; Chen, Y. -J.; Huang, R. -L.; Shieh, B. -J. Three xanthones and a benzophenone from *Garcinia mangostana*. J. Nat. Prod. 64 (2001) : 903-906.

[52]   Vieira, L. M. M.; Kijjoa, A. Naturally-occurring xanthones: Recent developments. Curr. Med. Chem. 12 (2005) : 2413-2446.

[53]   Jung, H. -A.; Su, B. -N.; Keller, W. J.; Mehta, R. G.; Kinghorn, A. D. Antioxidant Xanthones from the Pericarp of *Garcinia mangostana* (Mangosteen). J. Agric. Food Chem. 54 (2006) : 2077-2082.

[54]   Nilar; Harrison, L. J. Xanthones from the heartwood of *Garcinia mangostana*. Phytochemistry 60 (2002) : 541-548.

[55]   Zhang, Y.; Song, Z.; Hao, J.; Qiu, S.; Xu, Z. Two new prenylated xanthones and a new prenylated tetrahydroxanthone from the pericarp of *Garcinia mangostana*. Fitoterapia 81 (2010) : 595-599.

[56]   Balasubramanian, K.; Rajagopalan, K. Studies of indigenous medicinal plants. Part 1. Novel xanthones from *Garcinia mangostana*, structures of BR-xanthone-A and BR-xanthone-B. Phytochemistry 27 (1988) : 1552-1554.

[57]   Nilar; Nguyen, L. -H. D.; Venkatraman, G.; Sim, K. -Y.; Harrison, L. J. Xanthones and benzophenones from *Garcinia griffithii* and *Garcinia mangostana*. Phytochemistry 66 (2005) : 1718-1723.

[58]   Farnsworth, R. N.; Bunyapraphatsara, N. Garcinia mangostana Linn. In Thai Medicinal Plants. Bangkok: Prachachon Co., Ltd.; 1992.

[59]   Asai, F.; Tosa, H.; Tanaka, T.; Iinuma, M. A xanthone from pericarps of *Garcinia mangostana*. Phytochemistry 39 (1995) : 943-944.

[60]   Matsumoto, K.; Akao, Y.; Kobayashi, E.; Ohguchi, K.; Ito, T.; Tanaka, T.; Iinuma, M.; Nozawa, Y. Induction of apoptosis by xanthones from mangosteen in human leukemia cell Lines. J. Nat. Prod. 66 (2003) : 1124-1127.

[61]   Suksamrarn, S.; Suwannapoch, N.; Phakhodee, W.; Thanuhiranlert, J.; Ratananukul, P.; Chimnoi, N.; Suksamrarn, A. Antimycobacterial activity of prenylated xanthones from the fruits of *Garcinia mangostana*. Chem. Pharm. Bull. 51 (2003) : 857-859.

[62]   Gopalakrishnan, G.; Balaganesan, B. Two novel xanthones from *Garcinia mangostana*. Fitoterapia 71 (2000) : 607-609.

[63]   Iinuma, M.; Tosa, H.; Tanaka, T.; Asai, F.; Kobayashi, Y.; Shimano, R.; Miyauchi, K. -I. Antibacterial activity of xanthones from guttiferaeous plants against methicillin-resistant *Staphylococcus aureus*. J. Pharm. Pharmacol. 48 (1996) : 861-865.

[64]   Sakagami, Y.; Iinuma, M.; Piyasena, K. G. N. P.; Dharmaratne, H. R. W. Antibacterial activity of α-mangostin against vancomycin resistant *Enterococci* (VRE) and synergism with antibiotics. Phytomedicine 12 (2005) : 203-208.

[65]   Azebaze, A. G. B.; Meyer, M.; Valentin, A.; Nguemfo, E. L.; Fomum, Z. T.;
       Nkengfack, A. E. Prenylated xanthone derivatives with antiplasmodial
       activity from *Allanblackia monticola* STANER L.C. Chem. Pharm. Bull.
       54 (2006) : 111-113.

[66]   Gopalakrishnan, G.; Banumathi, B.; Suresh, G. Evaluation of the antifungal
       activity of natural xanthones from *Garcinia mangostana* and their
       synthetic derivatives. J. Nat. Prod. 60 (1997) : 519-524.

[67]   Kaomongkolgit, R.; Jamdee, K.; Chaisomboon, N. Antifungal activity of
       alpha-mangostin against *Candida albicans*. J Oral Sci. 51 (2009) : 401-
       406.

[68]   Sato, A.; Fujiwara, H.; Oku, H.; Ishiguro, K.; Ohizumi, Y. *α*-Mangostin
       induces Ca2+-ATPase-dependent apoptosis via mitochondrial pathway
       in PC12 cells. J. Pharmacol. Sci. 95 (2004) : 33-40.

[69]   Nakagawa, Y.; Iinuma, M.; Naoe, T.; Nozawa, Y.; Akao, Y. Characterized
       mechanism of *α*-mangostin-induced cell death: Caspase-independent
       apoptosis with release of endonuclease-G from mitochondria and
       increased miR-143 expression in human colorectal cancer DLD-1 cells.
       Bioorg. Med. Chem. 15 (2007) : 5620-5628.

[70]   Matsumoto, K.; Akao, Y.; Ohguchi, K.; Ito, T.; Tanaka, T.; Iinuma, M.;
       Nozawa, Y. Xanthones induce cell-cycle arrest and apoptosis in human
       colon cancer DLD-1 cells. Bioorg. Med. Chem. 13 (2005) : 6064-6069.

[71]   Larson, R. T.; Lorch, J. M.; Pridgeon, J. W.; Becnel, J. J.; Clark, G. G.; Lan, Q.
       The biological activity of *α*-magostin, a larvicidal botanic mosquito
       sterol carrier protein-2 inhibitor. J. Med. Entomol. 47 (2010) : 249-257.

[72]   Lu, Z. X.; Hasmeda, M.; Mahabusarakam, W.; Ternai, B.; Ternai, P. C.; Polya,
       G. M. Inhibition of eukaryote protein kinases and of a cyclic nucleotide-
       binding phosphatase by prenylated xanthones. Chem.-Biol. Interact. 114
       (1998) : 121-140.

[73]   Mahabusarakam, W.; Proudfoot, J.; Taylor, W.; Croft, K. Inhibition of
       lipoprotein oxidation by prenylated xanthones derived from mangostin.
       Free Radical Res. 33 (2000) : 643-659.

[74] Mahabusarakam, W.; Kuaha, K.; Wilairat, P.; Taylor, W. C. Prenylated xanthones as potential antiplasmodial substances. <u>Planta Med</u>. 72 (2006) : 912-916.

[75] Ha, L. D.; Hansen, P. E.; Vang, O.; Duus, F.; Pham, H. D.; Nguyen, L. -H. D. Cytotoxic geranylated xanthones and O-alkylated derivatives of *α*-mangostin. <u>Chem. Pharm. Bull</u>. 57 (2009) : 830-834.

[76] Chantarasriwong, O.; Jang, D. O.; Chavasiri, W. Cl$_3$CCONH$_2$/PPh$_3$. A versatile reagent for synthesis of esters. <u>Synth. Commun</u>. 38 (2008) : 2845-2856.

[77] Samanta, D.; Sawoo, S.; Patra, S.; Ray, M.; Salmain, M.; Sarkar, A. Synthesis of hydrophilic Fischer carbene complexes as organometallic marker and PEGylating agent for proteins. <u>J. Organomet. Chem</u>. 690 (2005) : 5581-5590.

[78] National Committeefor Clinical Laboratory Standards. <u>Performance standards for antimicrobial disk susceptibility tests</u>. 6th ed. Approved standard M2-A6 ed. Wayne, Pa:1997.

[79] Clinical and Laboratory Standards Institute. <u>Performance standards for antimicrobial susceptibility testing</u>. Wayne, Pa.; 2007.

[80] Morimoto, M.; Ohta, Y.; Ihara, T.; Arima, K.; Fukumoto, H.; Chavasir, W.; Komai, K. Insect antifeedants in Thailand plant extracts against the commom cutworm, *Spodaptea litura*, and a subterranean termite, *Reticulitermes speratus* <u>J. Environ. Entomol. Zool</u>. 17 (2006) : 1-7.

[81] Kubo, I.; Xiao, P.; Fujita, K. Anti-MRSA activity of alkyl gallates. <u>Bioorg. Med. Chem. Lett</u>. 12 (2002) : 113-116.

[82] Kubo, I.; Muroi, H.; Kubo, A. Structural functions of antimicrobial long-chain alcohols and phenols. <u>Bioorg. Med. Chem</u>. 3 (1995) : 873-880.

[83] Ollis, W. D.; Ramsay, M. V. J.; Sutherland, I. O.; Mongkolsuk, S. Constitution of gambogic acid. <u>Tetrahedron</u> 21 (1965) : 1453-1470.

[84] Ahmad, S. A.; Rigby, W.; Taylor, R. B. Gamboge. II. <u>J. Chem. Soc. C</u> (1966) : 772-779.

[85] Yates, P.; Karmarkar, S. S.; Rosenthal, D.; Stout, G. H.; Stout, V. F. Acetyl-*a*-gambogic acid. <u>Tetrahedron Lett</u>. 4 (1963) : 1623-1629.

[86] Anthony, A.; Desiraju, G. R. Crystallization of pseudopolymorphs of some gamboge pigments. Pyridine, dimethylformamide and dimethylsulfoxide solvates of morellic acid, gambogic acid and guttiferic acid. Supramol. Chem. 13 (2001) : 11-23.

[87] Weakley, T. J. R.; Cai, S. X.; Zhang, H. -Z.; Keana, J. F. W. Crystal structure of the pyridine salt of gambogic acid. J. Chem. Crystallogr. 31 (2002) : 501-505.

[88] Rao, B. S. Morellin, a constituent of the seeds of Garcinia morella. J. Chem. Soc. (1937): 853-855.

[89] Rao, P. L. N.; Murthy, D. V. K.; Verma, S. C. L. Antibiotic principles of *Garcinia morella*. Constitution of morellin. Naturwissenschaften 41 (1954) : 66-67.

[90] Leong, Y. -W.; harrison, L. J.; Bennett, G. J.; Tan, H. T. W. Forbesione, a modified xanthone from *Garcinia forbesii*. J. Chem. Res., Synop. (1996) : 392-393.

[91] Wang, L. L.; Li, Z. L.; Xu, Y. P.; Liu, X. Q.; Pei, Y. H.; Jing, Y. K.; Hua, H. M. A new cytotoxic caged polyprenylated xanthone from the resin of *Garcinia hanburyi*. Chin. Chem. Lett. 19 (2008) : 1221-1223.

[92] Li, S. -L.; Song, J. -Z.; Han, Q. -B.; Qiao, C. -F.; Xu, H. -X. Improved high-performance liquid chromatographic method for simultaneous determination of 12 cytotoxic caged xanthones in gamboges, a potential anticancer resin from *Garcinia hanburyi*. Biomed. Chromatogr. 22 (2008) : 637-644.

[93] Cao, S. -G.; Sng, V. H. L.; Wu, X. -H.; Sim, K. -Y.; Tan, B. H. K.; Pereira, J. T.; Goh, S. H. Novel cytotoxic polyprenylated xanthonoids from *Garcinia gaudichaudii* (Guttiferae). Tetrahedron 54 (1998) : 10915-10924.

[94] Cao, S. -G.; Wu, X. -H.; Sim, K. -Y.; Tan, B. K. H.; Pereira, J. T.; Wong, W. H.; Hew, N. F.; Goh, S. H. Cytotoxic caged tetraprenylated xanthonoids from *Garcinia gaudichaudii* (Guttiferae). Tetrahedron Lett. 39 (1998) : 3353-3356.

[95]   Xu, Y. J.; Yip, S. C.; Kosela, S.; Fitri, E.; Hana, M.; Goh, S. H.; Sim, K. Y. Novel cytotoxic, polyprenylated heptacyclic xanthonoids from Indonesian *Garcinia gaudichaudii* (Guttiferae). <u>Org. Lett</u>. 2 (2000) : 3945-3948.

[96]   Wu, X. -H.; Tan, B. K. H.; Cao, S. -G.; Sim, K. Y.; Goh, S. H. Two minor, cytotoxic caged xanthonoids from *Garcinia gaudichaudii*. <u>Nat. Prod. Lett</u>. 14 (2000) : 453-458.

[97]   Han, Q. -B.; Wang, Y. -L.; Yang, L.; Tso, T. -F.; Qiao, C. -F.; Song, J. -Z.; Xu, L. -J.; Chen, S. -L.; Yang, D. -J.; Xu, H. -X. Cytotoxic polyprenylated xanthones from the resin of *Garcinia hanburyi*. <u>Chem. Pharm. Bull</u>. 54 (2006) : 265-267.

[98]   Venkataraman, K. Pigments of Garcinia species. <u>Proc. Indian Natl. Sci. Acad., Part A</u> 39 (1974) : 365-381.

[99]   Adawadkar, P. D.; Srinivasan, R.; Yemul, S. S. Coloring matters of *Garcinia morella*: Part VIII. Morellinol, dihydromorelloflavone and morelloflavone-7"-*β*-glucoside. <u>Indian J. Chem., Sect. B</u> 14B (1976) : 19-21.

[100]   Feng, F.; Liu, W. -Y.; Chen, Y. -S.; Guo, Q. -L.; You, Q. -D. Five novel prenylated xanthones from *Resina Garciniae*. <u>J. Asian Nat. Prod. Res</u>. 9 (2007) : 735-741.

[101]   Yemul, S. S.; Rao, A. V. R. Electron-impact-induced fragmentation of morellin and related compounds. <u>Org. Mass Spectrom</u>. 9 (1974) : 1063-1072.

[102]   Bhat, H. B.; Nair, P. M.; Venkataraman, K. The coloring matters of *Garcinia morella*. V. Isolation of deoxymorellin and dihydroisomorellin. <u>Indian J. Chem</u>. 2 (1964) : 405-410.

[103]   Tao, S. -J.; Guan, S. -H.; Wang, W.; Lu, Z. -Q.; Chen, G. -T.; Sha, N.; Yue, Q. -X.; Liu, X.; Guo, D. -A. Cytotoxic polyprenylated xanthones from the resin of *Garcinia hanburyi*. <u>J. Nat. Prod</u>. 72 (2009) : 117-124.

[104]   Nair, P. M.; Venkataraman, K. The coloring matters of *Garcinia morella*. IV. Isomorellin. <u>Indian J. Chem</u>. 2 (1964) : 402-404.

[105]   Asano, J.; Chiba, K.; Tada, M.; Yoshii, T. Cytotoxic xanthones from *Garcinia hanburyi*. Phytochemistry 41 (1996) : 815-820.

[106]   Thoison, O.; Cuong, D. D.; Gramain, A.; Chiaroni, A.; Hung, N. V.; Sevenet, T. Further rearranged prenylxanthones and benzophenones from *Garcinia bracteata*. Tetrahedron 61 (2005) : 8529-8535.

[107]   Sukpondma, Y.; Rukachaisirikul, V.; Phongpaichit, S. Xanthone and sesquiterpene derivatives from the fruits of *Garcinia scortechinii*. J. Nat. Prod. 68 (2005) : 1010-1017.

[108]   Rukachaisirikul, V.; Phainuphong, P.; Sukpondma, Y.; Phongpaichit, S.; Taylor, W. C. Antibacterial caged-tetraprenylated xanthones from the stem bark of *Garcinia scortechinii*. Planta Med. 71 (2005) : 165-170.

[109]   Rukachaisirikul, V.; Painuphong, P.; Sukpondma, Y.; Koysomboon, S.; Sawangchote, P.; Taylor, W. C. Caged-Triprenylated and -tetraprenylated xanthones from the latex of *Garcinia scortechinii*. J. Nat. Prod. 66 (2003) : 933-938.

[110]   Mahabusarakam, W.; Nuangnaowarat, W.; Taylor, W. C. Xanthone derivatives from *Cratoxylum cochinchinense* roots. Phytochemistry 67 (2006) : 470-474.

[111]   Kosela, S.; Cao, S. -G.; Wu, X. -H.; Vittal, J. J.; Sukri, T.; Masdianto; Goh, S. -H.; Sim, K. -Y. Lateriflorone, a cytotoxic spiroxalactone with a novel skeleton, from *Garcinia lateriflora* Bl. Tetrahedron Lett. 40 (1999) : 157-160.

[112]   Rao, D. R.; Gurudutt, K. N.; Mamatha, S.; Rao, L. J. M. Guttiferic acid, a novel rearrangement product from minor chromenoxanthone pigments of *Garcinia morella* Desr. Magn. Reson. Chem. 45 (2007) : 578-582.

[113]   Han, Q. -B.; Cheung, S.; Tai, J.; Qiao, C. -F.; Song, J. -Z.; Xu, H. -X. Stability and cytotoxicity of gambogic acid and its derivative, gambogoic acid. Biol. Pharm. Bull. 28 (2005) : 2335-2337.

[114]   Rao, G. S. R. S.; Rathnamala, S.; Sivaramakrishnan, R. Structure of moreollin, a pigment isolated from G*arcinia morella* Desser. Proc. Indian Acad. Sci., Sect. A 87 (1978) : 75-86.

[115] Subba Rao, G. S. R.; Ratna Mala, S.; Surendranath, V.; Gupta, V. S.; Narasimha, R. P. L. Structure of moreollin. Tetrahedron Lett. (1974) : 1259-1262.

[116] Han, Q. B.; Song, J. Z.; Qiao, C. F.; Wong, L.; Xu, H. X. Preparative separation of gambogic acid and its C-2 epimer using recycling high-speed counter-current chromatography. J. Chromatogr. A 1127 (2006) : 298-301.

[117] Cardillo, G.; Merlini, L. Absolute configuration of C-2 in the chromene ring of gambogic acid. Tetrahedron Lett. (1967) : 2529-2530.

[118] Han, Q.; Yang, L.; Liu, Y.; Wang, Y.; Qiao, C.; Song, J.; Xu, L.; Yang, D.; Chen, S.; Xu, H. Gambogic acid and epigambogic acid, C-2 epimers with novel anticancer effects from *Garcinia hanburyi*. Planta Med. 72 (2006) : 281-284.

[119] Zhou, Y.; Liu, X.; Yang, J.; Han, Q. -B.; Song, J. -Z.; Li, S. -L.; Qiao, C. -F.; Ding, L. -S.; Xu, H. -X. Analysis of caged xanthones from the resin of *Garcinia hanburyi* using ultra-performance liquid chromatography/electrospray ionization quadrupole time-of-flight tandem mass spectrometry. Anal. Chim. Acta 629 (2008) : 104-118.

[120] Han, Q. -B.; Zhou, Y.; Feng, C.; Xu, G.; Huang, S. -X.; Li, S. -L.; Qiao, C. -F.; Song, J. -Z.; Chang, D. C.; Luo, K. Q.; Xu, H. -X. Bioassay guided discovery of apoptosis inducers from gamboge by high-speed counter-current chromatography and high-pressure liquid chromatography/electrospray ionization quadrupole time-of-flight mass spectrometry. J. Chromatogr. B 877 (2009) : 401-407.

[121] Dewick, P. M. The biosynthesis of shikimate metabolites. Nat. Prod. Rep. 15 (1998) : 17-58.

[122] Knaggs, A. R. The biosynthesis of shikimate metabolites. Nat. Prod. Rep. 20 (2003) : 119-136.

[123] Birch, A. J.; Baldas, J.; Hlubucek, J. R.; Simpson, T. J.; Westerman, P. W. Biosynthesis of the fungal xanthone ravenelin. J. Chem. Soc. Perkin Trans. 1 (1976) : 898-904.

[124] Locksley, H. D.; Moore, I.; Scheinmann, F. Extractives from guttiferae-VI: The significance of maclurin in xanthone biosynthesis. Tetrahedron 23 (1967) : 2229-2234.

[125] Bennett, G. J.; Lee, H. -H. The biosynthesis of mangostin: the origin of the xanthone skeleton. J. Chem. Soc. Chem. Commun. (1988): 619-620.

[126] Bennett, G. J.; Lee, H. -H.; Das, N. P. Biosynthesis of mangostin. Part 1. The origin of the xanthone skeleton. J. Chem. Soc. Perkin Trans 1 (1990) : 2671-2676.

[127] Kartha, G. Unit cell and space group of morellin. Curr. Sci. 23 (1954) : 8.

[128] Quillinan, A. J.; Scheinmann, F. Application of the Claisen rearrangement to the synthesis of heterocyclic bicyclo[2,2,2]octenones: an approach to the morellins based on new biogenetic suggestions. J. Chem. Soc. Chem. Commun. (1971) : 966-967.

[129] Jackson, B.; Locksley, H. D.; Scheinmann, F. Extractives from Guttiferae. Part V. Scriblitifolic acid, a new xanthone from *Calophyllum scriblitifolium* Henderson and Wyatt-Smith. J. Chem. Soc. C (1967) : 785-796.

[130] Jefferson, A.; Scheinmann, F. Molecular rearrangements related to the Claisen rearrangement. Q. Rev. Chem. Soc. 22 (1968) : 391-421.

[131] Locksley, H. D.; Quillinan, A. J.; Scheinmann, F. Extractives from Guttiferae. Part XXIII. An unambiguous synthesis of 6-deoxyjacareubin and related 3,3- and 1,1-dimethylallyl and annulated xanthones. J. Chem. Soc. C (1971) : 3804-3814.

[132] Nicolaou, K. C.; Li, J. "Biomimetic" cascade reactions in organic synthesis: construction of 4-oxatricyclo[4.3.1.0]decan-2-one systems and total synthesis of 1-*O*-methylforbesione *via* tandem Claisen rearrangement/Diels-Alder reactions. Angew. Chem. Int. Ed. 40 (2001) : 4264-4268.

[133] Tisdale, E. J.; Slobodov, I.; Theodorakis, E. A. Unified synthesis of caged Garcinia natural products based on a site-selective Claisen/Diels-Alder/Claisen rearrangement. Proc. Natl. Acad. Sci. USA 101 (2004) : 12030-12035.

[134] Jiangsu New Medical College. <u>Dictionary of Chinese Traditional Medicines</u>. Shanghai: Shanghai Scientific and Technical Publishers; 1977, pp. 3805-3807.

[135] Panthong, A.; Norkaew, P.; Kanjanapothi, D.; Taesotikul, T.; Anantachoke, N.; Reutrakul, V. Anti-inflammatory, analgesic and antipyretic activities of the extract of gamboge from *Garcinia hanburyi* Hook f. <u>J Ethnopharmacol</u>. 111 (2007) : 335-340.

[136] Sani, B. P.; Narasimha Rao, P. L. Antibiotic principles of *Garcinia morella*. VII. Antiprotozoal activity of morellin, neomorellin and other insoluble neutral phenols of the seed coat of Garcinia morella. <u>Indian J. Exp. Biol</u>. 4 (1966) : 27-28.

[137] Santhanam, K.; Rao, P. L. N. Antibiotic principles of *Garcinia morella*. XII. Characterization of *β*- and *α*-guttiferins as cathartic principles of gamboge and seed coat of *G. morella*. <u>Indian J. Exp. Biol</u>. 6 (1968) : 158-159.

[138] Puttanna, C. R.; Rao, P. L. N. Antibiotic principles of *Garcinia morella*. XI. Mode of action of *β*- and *α*-2-guttiferins on *Spirostomum ambiguum* and *Paramecium caudatum*. <u>Indian J. Exp. Biol</u>. 6 (1968) : 150-152.

[139] Rao, K. V. N.; Rao, P. N. *α*- and *β*-Guttiferrins. <u>Experientia</u> 17 (1961) : 213-214.

[140] Gupta, V. S.; Rao, P. L. N.; Vaidya, S. N.; Ramaseshan, R. Molecular formula and indentity of *β*-guttiferin and *α*-gambogic acid. <u>Chem. Ind</u>. (1962) : 1469-1470

[141] Santhanam, K.; Rao, P. L. N. Antibiotic principles of *Garcinia morella*. XIII. Antimicrobial activity and toxicity of *α*- and *γ*-guttiferins and their derivatives. <u>Indian J. Exp. Biol</u>. 7 (1969) : 34-36.

[142] Sani, B. P.; Rao, P. L. N. Antibiotic principles of *Garcinia morella*. XIV. Neomorellin and X-guttiferin. <u>Indian J. Chem</u>. 7 (1969) : 680-684.

[143] Verma, S. C. L.; Rao, P. L. N. Antibiotic principles of *Garcinia morella*. X. Quantitative estimation of morellin. <u>Indian J. Exp. Biol</u>. 5 (1967) : 106-109.

[144] Rao, K. V. N.; Rao, P. L. N. Antibiotic principles of *Garcinia morella*. IX. Antimicrobial activity of *α*- and *β*-guttierins and their derivatives. <u>Indian J. Exp. Biol</u>. 5 (1967) : 101-105.

[145] Rao, K. V. N.; Rao, P. L. N. Antibiotic principles of *Garcinia morella*. VIII. Toxicity and pharmacodynamic effects of *α*-guttiferin. <u>Indian J. Exp. Biol</u>. 5 (1967) : 96-100.

[146] Khalid, R. M.; Jabit, M. L.; Abas, F.; Stanslas, J.; Shaari, K.; Lajis, N. H. Cytotoxic Xanthones from the Leaves of *Garcinia urophylla*. <u>Nat.Prod. Commun</u>. 2 (2007) : 271-276.

[147] Batova, A.; Lam, T.; Wascholowski, V.; Yu, A. L.; Giannis, A.; Theodorakis, E. A. Synthesis and evaluation of caged *Garcinia* xanthones. <u>Org. Biomol. Chem</u>. 5 (2007) : 494-500.

[148] Wu, X.; Cao, S.; Goh, S.; Hsu, A.; Tan, B. K. H. Mitochondrial destabilisation and caspase-3 activation are involved in the apoptosis of Jurkat cells induced by gaudichaudione A, a cytotoxic xanthone. <u>Planta Med</u>. 68 (2002) : 198-203.

[149] Larsen, A. K.; Escargueil, A. E.; Skladanowski, A. Resistance mechanisms associated with altered intracellular distribution of anticancer agents. <u>Pharmacol. Ther</u>. 85 (2000) : 217-229.

[150] La Porta, C. A. Drug resistance in melanoma: new perspectives. <u>Curr. Med. Chem</u>. 14 (2007) : 387-391.

[151] Hanahan, D.; Weinberg, R. A. The hallmarks of cancer. <u>Cell</u> 100 (2000) : 57-70.

[152] Zhao, L.; Guo, Q.-L.; You, Q.-D.; Wu, Z.-Q.; Gu, H.-Y. Gambogic acid induces apoptosis and regulates expressions of bax and Bcl-2 protein in human gastric carcinoma MGC-803 cells. <u>Biol. Pharm. Bull</u>. 27 (2004) : 998-1003.

[153] Reed, J. C.; Pellecchia, M. Apoptosis-based therapies for hematologic malignancies. <u>Blood</u> 106 (2005) : 408-418.

[154] Reed, J. C. Apoptosis-targeted therapies for cancer. <u>Cancer Cell</u> 3 (2003) : 17-22.

[155] Zhai, D.; Jin, C.; Satterthwait, A. C.; Reed, J. C. Comparison of chemical inhibitors of antiapoptotic Bcl-2-family proteins. <u>Cell Death Differ</u>. 13 (2006) : 1419-1421.

[156] Vogler, M.; Dinsdale, D.; Dyer, M. J.; Cohen, G. M. Bcl-2 inhibitors: small molecules with a big impact on cancer therapy. <u>Cell Death Differ</u>. 16 (2009) : 360-367.

[157] Liu, W.; Guo, Q. -L.; You, Q. -D.; Zhao, L.; Gu, H. -Y.; Yuan, S. -T. Anticancer effect and apoptosis induction of gambogic acid in human gastric cancer line BGC-823. <u>World J. Gastroenterol</u>. 11 (2005) : 3655-3659.

[158] Gu, H.; Rao, S.; Zhao, J.; Wang, J.; Mu, R.; Rong, J.; Tao, L.; Qi, Q.; You, Q.; Guo, Q. Gambogic acid reduced bcl-2 expression *via* p53 in human breast MCF-7 cancer cells. <u>J. Cancer Res. Clin. Oncol</u>. 135 (2009) : 1777-1782.

[159] Xu, X.; Liu, Y.; Wang, L.; He, J.; Zhang, H.; Chen, X.; Li, Y.; Yang, J.; Tao, J. Gambogic acid induces apoptosis by regulating the expression of Bax and Bcl-2 and enhancing caspase-3 activity in human malignant melanoma A375 cells. <u>Int. J. Dermatol</u>. 48 (2009) : 186-192.

[160] Zhai, D.; Jin, C.; Shiau, C. -w.; Kitada, S.; Satterthwait, A. C.; Reed, J. C. Gambogic acid is an antagonist of antiapoptotic Bcl-2 family proteins. <u>Mol. Cancer Ther</u>. 7 (2008) : 1639-1646.

[161] Gu, H.; Wang, X.; Rao, S.; Wang, J.; Zhao, J.; Ren, F. L.; Mu, R.; Yang, Y.; Qi, Q.; Liu, W.; Lu, N.; Ling, H.; You, Q.; Guo, Q. Gambogic acid mediates apoptosis as a p53 inducer through down-regulation of mdm2 in wild-type p53-expressing cancer cells. <u>Mol. Cancer Ther</u>. 7 (2008) : 3298-3305.

[162] Rong, J. -J.; Hu, R.; Qi, Q.; Gu, H. -Y.; Zhao, Q.; Wang, J.; Mu, R.; You, Q. -D.; Guo, Q. -L. Gambogic acid down-regulates MDM2 oncogene and induces p21Waf1/CIP1 expression independent of p53. <u>Cancer Lett</u>. 284 (2009) : 102-112.

[163] Gu, H. -Y.; Guo, Q. -L.; You, Q. -D.; Liu, W.; Qi, Q.; Zhao, L.; Yuan, S. -T.; Zhang, K. Gambogic acid induced apoptosis in human hepatoma

SMMC-7721 cells with p53 and bax up-regulated. <u>Chin. J. Nat. Med</u>. 3 (2005): 168-172.

[164] Yu, J.; Guo, Q. -L.; You, Q. -D.; Lin, S. -S.; Li, Z.; Gu, H. -Y.; Zhang, H. -W.; Tan, Z.; Wang, X. Repression of telomerase reverse transcriptase mRNA and hTERT promoter by gambogic acid in human gastric carcinoma cells. <u>Cancer Chemother. Pharmacol</u>. 58 (2006): 434-443.

[165] Li, R.; Chen, Y.; Shu, W. -x.; Zhao, F.; Liu, Y.; Wen, L. Effects of gambogic acid on regulation of steroid receptor coactivator-3 in lung adenocarcinoma A549 cells. <u>Chin. J. Cancer Res</u>. 21 (2009) : 68-73.

[166] Li, R.; Chen, Y.; Zeng, L. -l.; Shu, W. -x.; Zhao, F.; Wen, L.; Liu, Y. Gambogic acid induces G0/G1 arrest and apoptosis involving inhibition of SRC-3 and inactivation of Akt pathway in K562 leukemia cells. <u>Toxicology</u> 262 (2009) : 98-105.

[167] Chen, J.; Gu, H. -Y.; Lu, N.; Yang, Y.; Liu, W.; Qi, Q.; Rong, J. -J.; Wang, X. -T.; You, Q. -D.; Guo, Q. -L. Microtubule depolymerization and phosphorylation of c-Jun N-terminal kinase-1 and p38 were involved in gambogic acid induced cell cycle arrest and apoptosis in human breast carcinoma MCF-7 cells. <u>Life Sci</u>. 83 (2008) : 103-109.

[168] Qin, Y.; Meng, L.; Hu, C.; Duan, W.; Zuo, Z.; Lin, L.; Zhang, X.; Ding, J. Gambogic acid inhibits the catalytic activity of human topoisomerase IIα by binding to its ATPase domain. <u>Mol. Cancer Ther</u>. 6 (2007): 2429-2440.

[169] Shu, W.; Chen, Y.; Li, R.; Wu, Q.; Cui, G.; Ke, W.; Chen, Z. Involvement of regulations of nucleophosmin and nucleoporins in gambogic acid-induced apoptosis in Jurkat cells. <u>Basic Clin. Pharmacol. Toxicol</u>. 103 (2008) : 530-537.

[170] Shu, W. X.; Chen, Y.; He, J. Effects of gambogic acid on the regulation of nucleoporin Nup88 in HL-60 cells. <u>Chin. J. Oncol</u>. 30 (2008) : 484-489.

[171] Yi, T.; Yi, Z.; Cho, S. -G.; Luo, J.; Pandey, M. K.; Aggarwal, B. B.; Liu, M. Gambogic Acid Inhibits Angiogenesis and Prostate Tumor Growth by Suppressing Vascular Endothelial Growth Factor Receptor 2 Signaling. <u>Cancer Res</u>. 68 (2008) : 1843-1850.

[172] Lu, N.; Yang, Y.; You, Q. -D.; Ling, Y.; Gao, Y.; Gu, H. -Y.; Zhao, L.; Wang, X. -T.; Guo, Q. -L. Gambogic acid inhibits angiogenesis through suppressing vascular endothelial growth factor-induced tyrosine phosphorylation of KDR/Flk-1. Cancer Lett. 258 (2007) : 80-89.

[173] Wang, T.; Wei, J.; Qian, X.; Ding, Y.; Yu, L.; Liu, B. Gambogic acid, a potent inhibitor of survivin, reverses docetaxel resistance in gastric cancer cells. Cancer Lett. 262 (2008) : 214-222.

[174] Wang, J.; Liu, W.; Zhao, Q.; Qi, Q.; Lu, N.; Yang, Y.; Nei, F. -F.; Rong, J. -J.; You, Q. -D.; Guo, Q. -L. Synergistic effect of 5-fluorouracil with gambogic acid on BGC-823 human gastric carcinoma. Toxicology 256 (2009) : 135-140.

[175] Prutki, M.; Poljak-Blazi, M.; Jakopovic, M.; Tomas, D.; Stipancic, I.; Zarkovic, N. Altered iron metabolism, transferrin receptor 1 and ferritin in patients with colon cancer. Cancer Lett. 238 (2006) : 188-196.

[176] Aisen, P. Transferrin receptor 1. Int. J. Biochem. Cell Biol. 36 (2004) : 2137-2143.

[177] Kasibhatla, S.; Jessen, K. A.; Maliartchouk, S.; Wang, J. Y.; English, N. M.; Drewe, J.; Qiu, L.; Archer, S. P.; Ponce, A. E.; Sirisoma, N.; Jiang, S.; Zhang, H.-Z.; Gehlsen, K. R.; Cai, S. X.; Green, D. R.; Tseng, B. A role for transferrin receptor in triggering apoptosis when targeted with gambogic acid. Proc. Natl. Acad. Sci. USA 102 (2005) : 12095-12100.

[178] Pandey, M. K.; Sung, B.; Ahn, K. S.; Kunnumakkara, A. B.; Chaturvedi, M. M.; Aggarwal, B. B. Gambogic acid, a novel ligand for transferrin receptor, potentiates TNF-induced apoptosis through modulation of the nuclear factor-κB signaling pathway. Blood 110 (2007) : 3517-3525.

[179] Zhu, X.; Zhang, H.; Lin, Y.; Chen, P.; Min, J.; Wang, Z.; Xiao, W.; Chen, B. a. Mechanisms of gambogic acid-induced apoptosis in non-small cell lung cancer cells in relation to transferrin receptors. J. Chemother. 21 (2009) : 666-672.

[180] Wang, Y.; Chen, Y.; Chen, Z.; Wu, Q.; Ke, W.-j.; Wu, Q.-l. Gambogic acid induces death inducer-obliterator 1-mediated apoptosis in Jurkat T cells. Acta Pharmacol. Sin. 29 (2008) : 349-354.

[181] Palempalli, U. D.; Gandhi, U.; Kalantari, P.; Vunta, H.; Arner, R. J.; Narayan, V.; Ravindran, A.; Prabhu, K. S. Gambogic acid covalently modifies IκB kinase-β subunit to mediate suppression of lipopolysaccharide-induced activation of NF-κB in macrophages. Biochem. J. 419 (2009) : 401-409.

[182] Ortiz-Sanchez, E.; Daniels, T. R.; Helguera, G.; Martinez-Maza, O.; Bonavida, B.; Penichet, M. L. Enhanced cytotoxicity of an anti-transferrin receptor IgG3-avidin fusion protein in combination with gambogic acid against human malignant hematopoietic cells: functional relevance of iron, the receptor, and reactive oxygen species. Leukemia 23 (2009) : 59-70.

[183] Nie, F.; Zhang, X.; Qi, Q.; Yang, L.; Yang, Y.; Liu, W.; Lu, N.; Wu, Z.; You, Q.; Guo, Q. Reactive oxygen species accumulation contributes to gambogic acid-induced apoptosis in human hepatoma SMMC-7721 cells. Toxicology 260 (2009) : 60-67.

[184] Qiang, L.; Yang, Y.; You, Q. -D.; Ma, Y. -J.; Yang, L.; Nie, F. -F.; Gu, H. -Y.; Zhao, L.; Lu, N.; Qi, Q.; Liu, W.; Wang, X. -T.; Guo, Q. -L. Inhibition of glioblastoma growth and angiogenesis by gambogic acid: An in vitro and in vivo study. Biochem. Pharmacol. 75 (2008) : 1083-1092.

[185] Yang, Y.; Yang, L.; You, Q. -D.; Nie, F. -F.; Gu, H. -Y.; Zhao, L.; Wang, X. -T.; Guo, Q. -L. Differential apoptotic induction of gambogic acid, a novel anticancer natural product, on hepatoma cells and normal hepatocytes. Cancer Lett. 256 (2007) : 259-266.

[186] Guo, Q. -l.; You, Q. -d.; Wu, Z. -q.; Yuan, S. -t.; Zhao, L. General gambogic acids inhibited growth of human hepatoma SMMC-7721 cells in vitro and in nude mice. Acta Pharmacol. Sin. 25 (2004) : 769-774.

[187] Gu, H.; You, Q.; Liu, W.; Yang, Y.; Zhao, L.; Qi, Q.; Zhao, J.; Wang, J.; Lu, N.; Ling, H.; Guo, Q.; Wang, X. Gambogic acid induced tumor cell apoptosis by T lymphocyte activation in H22 transplanted mice. Int. Immunopharmacol. 8 (2008) : 1493-1502.

[188] Guo, Q.; Qi, Q.; You, Q.; Gu, H.; Zhao, L.; Wu, Z. Toxicological studies of gambogic acid and its potential targets in experimental animals. Basic Clin. Pharmacol. Toxicol. 99 (2006) : 178-184.

[189] Qi, Q.; You, Q.; Gu, H.; Zhao, L.; Liu, W.; Lu, N.; Guo, Q. Studies on the toxicity of gambogic acid in rats. J. Ethnopharmacol. 117 (2008) : 433-438.

[190] Zhao, L.; Zhen, C.; Wu, Z.; Hu, R.; Zhou, C.; Guo, Q. General pharmacological properties, developmental toxicity, and analgesic activity of gambogic acid, a novel natural anticancer agent. Drug Chem. Toxicol. 33 (2010) : 88-96.

[191] Hao, K.; Liu, X. -Q.; Wang, G. -J.; Zhao, X. -P. Pharmacokinetics, tissue distribution and excretion of gambogic acid in rats. Eur. J. Drug Metab. Pharmacokinet. 32 (2007) : 63-68.

[192] Liu, Y.-t.; Hao, K.; Liu, X. -q.; Wang, G. -j. Metabolism and metabolic inhibition of gambogic acid in rat liver microsomes. Acta Pharmacol. Sin. 27 (2006) : 1253-1258.

[193] Feng, F.; Liu, W.; Wang, Y.; Guo, Q.; You, Q. Structure elucidation of metabolites of gambogic acid in vivo in rat bile by high-performance liquid chromatography-mass spectrometry and high-performance liquid chromatography-nuclear magnetic resonance. J. Chromatogr. B 860 (2007) : 218-226.

[194]   Ding, L.; Huang, D.; Wang, J.; Li, S. Determination of gambogic acid in human plasma by liquid chromatography-atmospheric pressure chemical ionization-mass spectrometry. J. Chromatogr. B 846 (2007) : 112-118.

[195] Yang, J.; Ding, L.; Jin, S.; Liu, X.; Liu, W.; Wang, Z. Identification and quantitative determination of a major circulating metabolite of gambogic acid in human. J. Chromatogr. B 878 (2010) : 659-666.

[196] Qu, G.; Zhu, X.; Zhang, C.; Ping, Q. Modified chitosan derivative micelle system for natural anti-tumor product gambogic acid delivery. Drug Delivery 16 (2009) : 363-370.

[197] Zhu, X.; Zhang, C.; Wu, X.; Tang, X.; Ping, Q. Preparation, physical properties, and stability of gambogic acid-loaded micelles based on chitosan derivatives. Drug Dev. Ind. Pharm. 34 (2008) : 2-9.

[198] Zhou, Z. T.; Wang, J. W. Phase I human tolerability trial of gambogic acid. Chin. J. New Drugs 16 (2007) : 79-82.

[199] Wessely, F.; Sinwel, F. Action of lead tetraacetate on phenols. II. *o*-Quinols. Monatsh. Chem. 81 (1950) : 1055-1070.

[200] Wessely, F.; Lauterbach-Keil, G.; Sinwel, F. Monatsh. Chem. 81 (1950): 811-818.

[201] Wessely, F.; Kotlan, J.; Sinwel, F. Monatsh. Chem. 83 (1952) : 902-914-914.

[202] Bhamare, N. K.; Granger, T.; John, C. R.; Yates, P. The synthesis of homoisotwistanes by the tandem Wessely oxidation-Diels-Alder reaction sequence. Tetrahedron Lett. 32 (1991) : 4439-4442.

[203] Bichan, D. J.; Yates, P. Two syntheses of the 2,4a-ethano-2,3,4,4a-tetrahydroxanthene system. J. Amer. Chem. Soc. 94 (1972) : 4773-4774.

[204] Tisdale, E. J.; Chowdhury, C.; Vong, B. G.; Li, H.; Theodorakis, E. A. Regioselective synthesis of the bridged tricyclic core of *Garcinia* natural products *via* intramolecular aryl acrylate cycloadditions. Org. Lett. 4 (2002) : 909-912.

[205] Mehta, G.; Maity, P. Construction of the 3-prenyl-4-oxa-tricyclo[4.3.1.03,7]dec-8-en-2-one core of caged xanthonoid natural products *via* tandem Wessely oxidation-intramolecular [4+2] cycloaddition. Tetrahedron Lett. 49 (2008) : 318-322.

[206] Nicolaou, K. C.; Sasmal, P. K.; Xu, H.; Namoto, K.; Ritzen, A. Total synthesis of 1-*O*-methyllateriflorone. Angew. Chem. Int. Ed. 42 (2003) : 4225-4229.

[207] Tisdale, E. J.; Li, H.; Vong, B. G.; Kim, S. H.; Theodorakis, E. A. Regioselective synthesis of the tricyclic core of lateriflorone. Org. Lett. 5 (2003) : 1491-1494.

[208] Nicolaou, K. C.; Sasmal Pradip, K.; Xu, H.; Namoto, K.; Ritzen, A. Total synthesis of 1-*O*-methyllateriflorone. Angew. Chem. Int. Ed. 42 (2003) : 4225-4229.

[209] Tisdale, E. J.; Slobodov, I.; Theodorakis, E. A. Biomimetic total synthesis of forbesione and desoxymorellin utilizing a tandem Claisen/Diels-Alder/Claisen rearrangement. Org. Biomol. Chem. 1 (2003) : 4418-4422.

[210] Li, N. -G.; Wang, J. -X.; Liu, X. -R.; Lin, C. -J.; You, Q. -D.; Guo, Q. -L. A novel and efficient route to the construction of the 4-oxa-

tricyclo[4.3.1.0]decan-2-one scaffold. Tetrahedron Lett. 48 (2007) : 6586-6589.

[211] Nicolaou, K. C.; Xu, H.; Wartmann, M. Biomimetic total synthesis of gambogin and rate acceleration of pericyclic reactions in aqueous media. Angew. Chem. Int. Ed. 44 (2005) : 756-761.

[212] Gajewski, J. J. The Claisen rearrangement. Response to solvents and substituents: The case for both hydrophobic and hydrogen bond acceleration in water and for a variable transition state. Acc. Chem. Res. 30 (1997) : 219-225.

[213] Ganem, B. The mechanism of the Claisen rearrangement: deja vu all over again. Angew. Chem., Int. Ed. 35 (1996) : 936-945.

[214] Tanford, C. The Hydrophobic Effect: Formation of Micelles and Biological Membranes. 2nd edition. New York: John Wiley & Sons 1980.

[215] Grieco, P. A.; Kaufman, M. D. Construction of carbocyclic arrays containing nitrogen via Iintramolecular imino Diels-Alder reactions in polar media. A comparative study: 5.0 M Lithium perchlorate-diethyl ether *versus* water. J. Org. Chem. 64 (1999) : 6041-6048.

[216] Lindström, U. M. Stereoselective organic reactions in water. Chem. Rev. 102 (2002) : 2751-2772.

[217] Breslow, R. Determining the geometries of transition states by use of antihydrophobic additives in water. Acc. Chem. Res. 37 (2004) : 471-478.

[218] Hayden, A. E.; Xu, H.; Nicolaou, K. C.; Houk, K. N. Origins of selectivity in pericyclic reaction cascades for the synthesis of gambogin and lateriflorone. Org. Lett. 8 (2006) : 2989-2992.

[219] Tisdale, E. J.; Vong, B. G.; Li, H.; Kim, S. H.; Chowdhury, C.; Theodorakis, E. A. Total synthesis of seco-lateriflorone. Tetrahedron 59 (2003) : 6873-6887.

[220] Nicolaou, K. C.; Sasmal, P. K.; Xu, H. Biomimetically inspired total synthesis and structure activity relationships of 1-*O*-methyllateriflorone. 6π Electrocyclizations in organic synthesis. J. Am. Chem. Soc. 126 (2004) : 5493-5501.

[221] Tao, Z.; Zhou, Y.; Lu, J.; Duan, W.; Qin, Y.; He, X.; Lin, L.; Ding, J. Caspase-8 preferentially senses the apoptosis-inducing action of NG-18, a gambogic acid derivative, in human leukemia HL-60 cells. Cancer Biol. Ther. 6 (2007) : 691-696.

[222] Xie, H.; Qin, Y. -x.; Zhou, Y. -l.; Tong, L. -j.; Lin, L. -p.; Geng, M. -y.; Duan, W. -h.; Ding, J. GA3, a new gambogic acid derivative, exhibits potent antitumor activities in vitro via apoptosis-involved mechanisms. Acta Pharmacol. Sin. 30 (2009) : 346-354.

[223] Jang, S. -W.; Okada, M.; Sayeed, I.; Xiao, G.; Stein, D.; Jin, P.; Ye, K. Gambogic amide, a selective agonist for TrkA receptor that possesses robust neurotrophic activity, prevents neuronal cell death. Proc. Natl. Acad. Sci. USA 104 (2007) : 16329-16334.

[224] Wang, J.; Zhao, L.; Hu, Y.; Guo, Q.; Zhang, L.; Wang, X.; Li, N.; You, Q. Studies on chemical structure modification and biology of a natural product, Gambogic acid (I): Synthesis and biological evaluation of oxidized analogues of gambogic acid. Eur. J. Med. Chem. 44 (2009) : 2611-2620.

[225] Mu, R.; Lu, N.; Wang, J.; Yin, Y.; Ding, Y.; Zhang, X.; Gui, H.; Sun, Q.; Duan, H.; Zhang, L.; Zhang, Y.; Ke, X.; Guo, Q. An oxidative analogue of gambogic acid-induced apoptosis of human hepatocellular carcinoma cell line HepG2 is involved in its anticancer activity in vitro. Eur. J. Cancer Prev. 19 (2010) : 61-67.

[226] Li, Q.; Cheng, H.; Zhu, G.; Yang, L.; Zhou, A.; Wang, X.; Fang, N.; Xia, L.; Su, J.; Wang, M.; Peng, D.; Xu, Q. Gambogenic acid inhibits proliferation of A549 cells through apoptosis-inducing and cell cycle arresting. Biol. Pharm. Bull. 33 (2010) : 415-420.

[227] Li, N. G.; You, Q. D.; Huang, X. F.; Wang, J. X.; Guo, Q. L.; Chen, X. G.; Li, Y.; Li, H. Y. Synthesis and antitumor activity of small compounds structurally related to gambogic acid. Chin. Chem. Lett. 18 (2007) : 659-662.

[228] Han, Q. -B.; Yang, N. -Y.; Tian, H. -L.; Qiao, C. -F.; Song, J. -Z.; Chang, D. C.; Chen, S. -L.; Luo, K. Q.; Xu, H. -X. Xanthones with growth

inhibition against HeLa cells from Garcinia xipshuanbannaensis. Phytochemistry 69 (2008) : 2187-2192.

[229] Kuemmerle, J.; Jiang, S.; Tseng, B.; Kasibhatla, S.; Drewe, J.; Cai, S. X. Synthesis of caged 2,3,3a,7a-tetrahydro-3,6-methanobenzofuran-7(6*H*)-ones: Evaluating the minimum structure for apoptosis induction by gambogic acid. Bioorg. Med. Chem. 16 (2008) : 4233-4241.

[230] Kamei, T.; Shindo, M.; Shishido, K. First enantioselective total synthesis of (-)-heliannuol C. Tetrahedron Lett. 44 (2003) : 8505-8507.

[231] Le Gall, N.; Luart, D.; Salauen, J. -Y.; Talarmin, J.; des Abbayes, H.; Toupet, L.; Menendez, N.; Varret, F. Synthesis and characterization of high-spin [(CO)₃FeII(CO₂R)₃]₂FeII complexes formed by thermolysis of *cis*-(CO)₄Fe(CO₂R)₂ (R = Me, *t*-Bu, allyl, 1,1'-dimethylallyl). X-ray crystal structure of the allyl derivative. Organometallics 21 (2002) : 1775-1781.

[232] Evans, P. A.; Nelson, J. D. Regioselective rhodium-catalyzed allylic alkylation with a modified Wilkinson's catalyst. Tetrahedron Lett. 39 (1998) : 1725-1728.

[233] Gozzo, F. C.; Fernandes, S. A.; Rodrigues, D. C.; Eberlin, M. N.; Marsaioli, A. J. Regioselectivity in aromatic Claisen rearrangements. J. Org. Chem. 68 (2003) : 5493-5499.

[234] Pettus, T. R. R.; Chen, X. -T.; Danishefsky, S. J. A fully synthetic route to the neurotrophic illicinones by sequential aromatic claisen rearrangements. J. Am. Chem. Soc. 120 (1998) : 12684-12685.

[235] Pettus, T. R. R.; Inoue, M.; Chen, X. -T.; Danishefsky, S. J. A fully synthetic route to the neurotrophic illicinones: syntheses of tricycloillicinone and bicycloillicinone aldehyde. J. Am. Chem. Soc. 122 (2000) : 6160-6168.

[236] Siddaiah, V.; Maheswara, M.; Rao, C. V.; Venkateswarlu, S.; Subbaraju, G. V. Synthesis, structural revision, and antioxidant activities of antimutagenic homoisoflavonoids from Hoffmanosseggia intricata. Bioorg. Med. Chem. Lett. 17 (2007) : 1288-1290.

[237] Kogen, H.; Tago, K.; Kaneko, S.; Hamano, K.; Onodera, K.; Haruyama, H.; Minagawa, K.; Kinoshita, T.; Ishikawa, T.; *et al.* Schizostatin, a novel squalene synthase inhibitor produced by the mushroom, Schizophyllum

commune. II. Structure elucidation and total synthesis. J. Antibiot. 49 (1996) : 624-630.

[238] Satam, V.; Harad, A.; Pati, H. 2-Iodoxybenzoic acid (IBX): an efficient hypervalent iodine reagent. Tetrahedron In Press, Corrected Proof.

[239] Piccialli, V.; Borbone, N.; Oliviero, G. Ruthenium-catalyzed oxidative cyclization of 1,7-dienes. A novel diasteroselective synthesis of 2,7-disubstituted trans-oxepane diols. Tetrahedron Lett. 48 (2007) : 5131-5135.

[240] Khripach, V. A.; Zhabinskii, V. N.; Konstantinova, O. V.; Khripach, N. B.; Antonchick, A. P. Synthesis of 24-Functionalized Oxysterols. Russ. J. Bioorg. Chem. 28 (2002) : 257-261.

[241] Paizs, C.; Bartlewski-Hof, U.; Retey, J. Investigation of the mechanism of action of pyrogallol-phloroglucinol transhydroxylase by using putative intermediates. Chem. Eur. J. 13 (2007) : 2805-2811.

[242] Yu, J.; Guo, Q. -L.; You, Q. -D.; Zhao, L.; Gu, H. -Y.; Yang, Y.; Zhang, H. -w.; Tan, Z.; Wang, X. Gambogic acid-induced G2/M phase cell-cycle arrest via disturbing CDK7-mediated phosphorylation of CDC2/p34 in human gastric carcinoma BGC-823 cells. Carcinogenesis 28 (2007) : 632-638.

[243] Guo, Q. -L.; Zhao, L.; You, Q. -D.; Wu, Z. -Q.; Gu, H. -Y. Gambogic acid inducing apoptosis in human gastric adenocarcinoma SGC-7901 cells. Chin. J. Nat. Med. 2 (2004) : 106-110.

[244] Reed, J. C.; Tomaselli, K. J. Drug discovery opportunities from apoptosis research. Curr. Opin. Biotechnol. 11 (2000) : 586-592.

[245] Reed, J. C. Dysregulation of apoptosis in cancer. J. Clin. Oncol. 17 (1999) : 2941-2953.

[246] Wesche-Soldato, D. E.; Swan, R. Z.; Chung, C. -S.; Ayala, A. The apoptotic pathway as a therapeutic target in sepsis. Current Drug Targets 8 (2007) : 493-500.

[247] van Gurp, M.; Festjens, N.; van Loo, G.; Saelens, X.; Vandenabeele, P. Mitochondrial intermembrane proteins in cell death. Biochem. Biophys. Res. Commun. 304 (2003): 487-497.

[248] Acehan, D.; Jiang, X.; Morgan, D. G.; Heuser, J. E.; Wang, X.; Akey, C. W. Three-dimensional structure of the apoptosome: implications for assembly, procaspase-9 binding, and activation. Mol. Cell 9 (2002) : 423-432.

[249] Beurel, E.; Jope, R. S. The paradoxical pro- and anti-apoptotic actions of GSK3 in the intrinsic and extrinsic apoptosis signaling pathways. Prog. Neurobiol. 79 (2006) : 173-189.

[250] Rapp, U. R.; Rennefahrt, U.; Troppmair, J. Bcl-2 proteins: master switches at the intersection of death signaling and the survival control by Raf kinases. Mol. Cell Res. 1644 (2004) : 149-158.

[251] Catz, S. D.; Johnson, J. L. BCL-2 in prostate cancer: a minireview. Apoptosis 8 (2003) : 29-37.

[252] Kim, R.; Tanabe, K.; Uchida, Y.; Emi, M.; Inoue, H.; Toge, T. Current status of the molecular mechanisms of anticancer drug-induced apoptosis. The contribution of molecular-level analysis to cancer chemotherapy. Cancer Chemother. Pharmacol. 50 (2002) : 343-352.

[253] Gottesman, M. M.; Pastan, I. Biochemistry of multidrug resistance mediated by the multidrug transporter. Annu. Rev. Biochem. 62 (1993) : 385-427.

[254] Simon, S.; Roy, D.; Schindler, M. Intracellular pH and the control of multidrug resistance. Proc. Natl. Acad. Sci. USA 91 (1994) : 1128-1132.

[255] McKenna, S. L.; Cotter, T. G. Apoptosis in leukemia. Apoptosis Cancer (1997) : 192-221.

APPENDICES

Table A1 Crystal data and structure refinement for Compound **196**

Identification code	CCDC-737621
Empirical formula	C23 H24 O4
Formula weight	364.42
Temperature	100(2) K
Wavelength	1.54178 Å
Crystal system	Monoclinic
Space group	P2(1)/c
Unit cell dimensions	a = 10.2829(5) Å α= 90°.
	b = 13.7839(7) Å β= 109.118(2)°.
	c = 13.8591(8) Å γ = 90°.
Volume	1856.02(17) Å^3
Z	4
Density (calculated)	1.304 Mg/m^3
Absorption coefficient	0.711 mm^{-1}
F(000)	776
Crystal size	0.33 x 0.22 x 0.08 mm^3
Crystal color, habit	Colorless Plate
Theta range for data collection	4.55 to 68.30°.
Index ranges	-12<=h<=12, -16<=k<=16, -15<=l<=16
Reflections collected	10317
Independent reflections	3330 [R(int) = 0.0251]
Completeness to theta = 65.00°	98.4 %
Absorption correction	Semi-empirical from equivalents
Max. and min. transmission	0.914 and 0.789
Refinement method	Full-matrix least-squares on F^2
Data / restraints / parameters	3330 / 0 / 249
Goodness-of-fit on F2	1.087
Final R indices [I>2sigma(I)]	R1 = 0.0380, wR2 = 0.1066
R indices (all data)	R1 = 0.0414, wR2 = 0.1092
Extinction coefficient	0.0019(3)
Largest diff. peak and hole	0.314 and -0.219 e.Å^{-3}

Table A2 Crystal data and structure refinement for Compound **C8**

Identification code	CCDC-737622
Empirical formula	C20 H26 O5
Formula weight	346.41
Temperature	100(2) K
Wavelength	1.54178 Å
Crystal system	Monoclinic
Space group	P2(1)/n
Unit cell dimensions	a = 10.9193(4) Å α= 90°.
	b = 12.8300(5) Å β= 105.650(2)°.
	c = 13.3814(5) Å γ = 90°.
Volume	1805.16(12) Å^3
Z	4
Density (calculated)	1.275 Mg/m^3
Absorption coefficient	0.739 mm^{-1}
F(000)	744
Crystal size	0.30 x 0.20 x 0.08 mm^3
Crystal color, habit	Colorless Rod
Theta range for data collection	4.66 to 68.40°.
Index ranges	-13<=h<=13, -15<=k<=15, -15<=l<=11
Reflections collected	11208
Independent reflections	3199 [R(int) = 0.0345]
Completeness to theta = 60.00°	98.2 %
Absorption correction	Semi-empirical from equivalents
Max. and min. transmission	0.9432 and 0.8087
Refinement method	Full-matrix least-squares on F^2
Data / restraints / parameters	3199 / 0 / 233
Goodness-of-fit on F2	1.003
Final R indices [I>2sigma(I)]	R1 = 0.0343, wR2 = 0.0864
R indices (all data)	R1 = 0.0422, wR2 = 0.0916
Extinction coefficient	0.00144(19)
Largest diff. peak and hole	0.267 and -0.173 e.Å^{-3}

Table A3 Crystal data and structure refinement for Compound **C9**

Identification code	CCDC-737623
Empirical formula	C20 H26 O5
Formula weight	346.41
Temperature	100(2) K
Wavelength	1.54178 Å
Crystal system	Monoclinic
Space group	P2(1)/n
Unit cell dimensions	a = 8.0045(2) Å α = 90°.
	b = 13.2751(4) Å β = 92.4170(10)°.
	c = 16.4708(5) Å γ = 90°.
Volume	1748.64(9) Å^3
Z	4
Density (calculated)	1.316 Mg/m^3
Absorption coefficient	0.763 mm^{-1}
F(000)	744
Crystal size	0.33 x 0.30 x 0.27 mm^3
Crystal color, habit	Colorless Block
Theta range for data collection	4.28 to 68.15°.
Index ranges	-9<=h<=9, -15<=k<=15, -19<=l<=15
Reflections collected	13879
Independent reflections	3087 [R(int) = 0.0209]
Completeness to theta = 60.00°	97.3 %
Absorption correction	Semi-empirical from equivalents
Max. and min. transmission	0.919 and 0.791
Refinement method	Full-matrix least-squares on F^2
Data / restraints / parameters	3087 / 0 / 233
Goodness-of-fit on F2	1.043
Final R indices [I>2sigma(I)]	R1 = 0.0315, wR2 = 0.0739
R indices (all data)	R1 = 0.0322, wR2 = 0.0744
Extinction coefficient	0.0044(2)
Largest diff. peak and hole	0.293 and -0.185 e.Å^{-3}

Table A4 Crystal data and structure refinement for Compound **C19**

Identification code	737624
Empirical formula	C19 H24 O4
Formula weight	316.38
Temperature	100(2) K
Wavelength	1.54178 Å
Crystal system	Orthorhombic
Space group	Pbca
Unit cell dimensions	a = 7.6777(4) Å $\quad$ α= 90°.
	b = 12.8146(8) Å $\quad$ β= 90°.
	c = 33.0175(18) Å $\quad$ γ = 90°.
Volume	3248.5(3) Å^3
Z	8
Density (calculated)	1.294 Mg/m^3
Absorption coefficient	0.724 mm^{-1}
F(000)	1360
Crystal size	0.42 x 0.38 x 0.08 mm^3
Crystal color, habit	Colorlesss Plate
Theta range for data collection	6.36 to 68.23°.
Index ranges	-9<=h<=7, -15<=k<=13, -39<=l<=39
Reflections collected	14719
Independent reflections	2918 [R(int) = 0.0579]
Completeness to theta = 55.00°	98.9 %
Absorption correction	Semi-empirical from equivalents
Max. and min. transmission	0.9444 and 0.7508
Refinement method	Full-matrix least-squares on F^2
Data / restraints / parameters	2918 / 0 / 213
Goodness-of-fit on F2	1.014
Final R indices [I>2sigma(I)]	R1 = 0.0396, wR2 = 0.0951
R indices (all data)	R1 = 0.0593, wR2 = 0.1051
Extinction coefficient	0.00068(13)
Largest diff. peak and hole	0.303 and -0.164 e.Å-3

Table A5 Crystal data and structure refinement for Compound **C29**

Identification code	CCDC-737625
Empirical formula	C23 H22 O6
Formula weight	394.41
Temperature	100(2) K
Wavelength	1.54178 Å
Crystal system	Triclinic
Space group	P-1
Unit cell dimensions	a = 9.8298(5) Å α= 89.130(3)°.
	b = 9.8418(4) Å β= 89.002(4)°.
	c = 20.5815(9) Å γ = 67.618(3)°.
Volume	1840.76(14) Å^3
Z	4
Density (calculated)	1.423 Mg/m^3
Absorption coefficient	0.849 mm^{-1}
F(000)	832
Crystal size	0.25 x 0.18 x 0.12 mm^3
Crystal color, habit	Colorless Block
Theta range for data collection	4.30 to 65.15°.
Index ranges	-10<=h<=11, -10<=k<=10, -16<=l<=21
Reflections collected	13913
Independent reflections	4995 [R(int) = 0.0559]
Completeness to theta = 60.00°	95.9 %
Absorption correction	Semi-empirical from equivalents
Max. and min. transmission	0.9050 and 0.8158
Refinement method	Full-matrix least-squares on F^2
Data / restraints / parameters	4995 / 0 / 530
Goodness-of-fit on F2	1.083
Final R indices [I>2sigma(I)]	R1 = 0.0640, wR2 = 0.1547
R indices (all data)	R1 = 0.0783, wR2 = 0.1654
Largest diff. peak and hole	0.619 and -0.309 e.Å^{-3}

Table A6 Crystal data and structure refinement for Compound **C35**

Identification code	CCDC-737626
Empirical formula	C28 H35 N O4
Formula weight	449.57
Temperature	100(2) K
Wavelength	0.71073 Å
Crystal system	Triclinic
Space group	P-1
Unit cell dimensions	a = 9.8106(7) Å α= 106.4770(10)°.
	b = 10.1395(8) Å β= 93.9620(10)°.
	c = 12.1918(9) Å γ = 92.8280(10)°.
Volume	1157.17(15) Å3
Z	2
Density (calculated)	1.290 Mg/m^3
Absorption coefficient	0.085 mm^{-1}
F(000)	484
Crystal size	0.40 x 0.40 x 0.30 mm^3
Crystal color, habit	Colorless Plate
Theta range for data collection	1.75 to 27.50°.
Index ranges	-12<=h<=12, -13<=k<=13, -15<=l<=15
Reflections collected	9915
Independent reflections	5073 [R(int) = 0.0157]
Completeness to theta = 27.50°	95.2 %
Absorption correction Semi-empirical from equivalents	
Max. and min. transmission	0.9749 and 0.9667
Refinement method	Full-matrix least-squares on F^2
Data / restraints / parameters	5073 / 0 / 298
Goodness-of-fit on F2	1.095
Final R indices [I>2sigma(I)]	R1 = 0.0468, wR2 = 0.1261
R indices (all data)	R1 = 0.0530, wR2 = 0.1308
Largest diff. peak and hole	0.422 and -0.351 e.Å^{-3}

Table A7 Crystal data and structure refinement for Compound **C36**

Identification code	CCDC-614936
Empirical formula	C24 H28 O5
Formula weight	396.46
Temperature	100(2) K
Wavelength	0.71073 Å
Crystal system	Triclinic
Space group	P-1
Unit cell dimensions	a = 10.5010(10) Å α= 112.0840(10)°.
	b = 14.3480(14) Å β= 90.4770(10)°.
	c = 14.6990(14) Å γ = 104.1960(10)°.
Volume	1977.0(3) Å^3
Z	4
Density (calculated)	1.332 Mg/m^3
Absorption coefficient	0.092 mm^{-1}
F(000)	848
Crystal size	0.20 x 0.20 x 0.10 mm^3
Crystal color, habit	Colorless Block
Theta range for data collection	2.21 to 28.22°.
Index ranges	-13<=h<=13, -18<=k<=18, -19<=l<=19
Reflections collected	20632
Independent reflections	8823 [R(int) = 0.0209]
Completeness to theta = 25.00°	99.3 %
Absorption correction	Semi-empirical from equivalents
Max. and min. transmission	0.9908 and 0.9818
Refinement method	Full-matrix least-squares on F^2
Data / restraints / parameters	8823 / 0 / 533
Goodness-of-fit on F2	1.021
Final R indices [I>2sigma(I)]	R1 = 0.0502, wR2 = 0.1287
R indices (all data)	R1 = 0.0583, wR2 = 0.1345
Largest diff. peak and hole	0.749 and -0.301 e.Å^{-3}
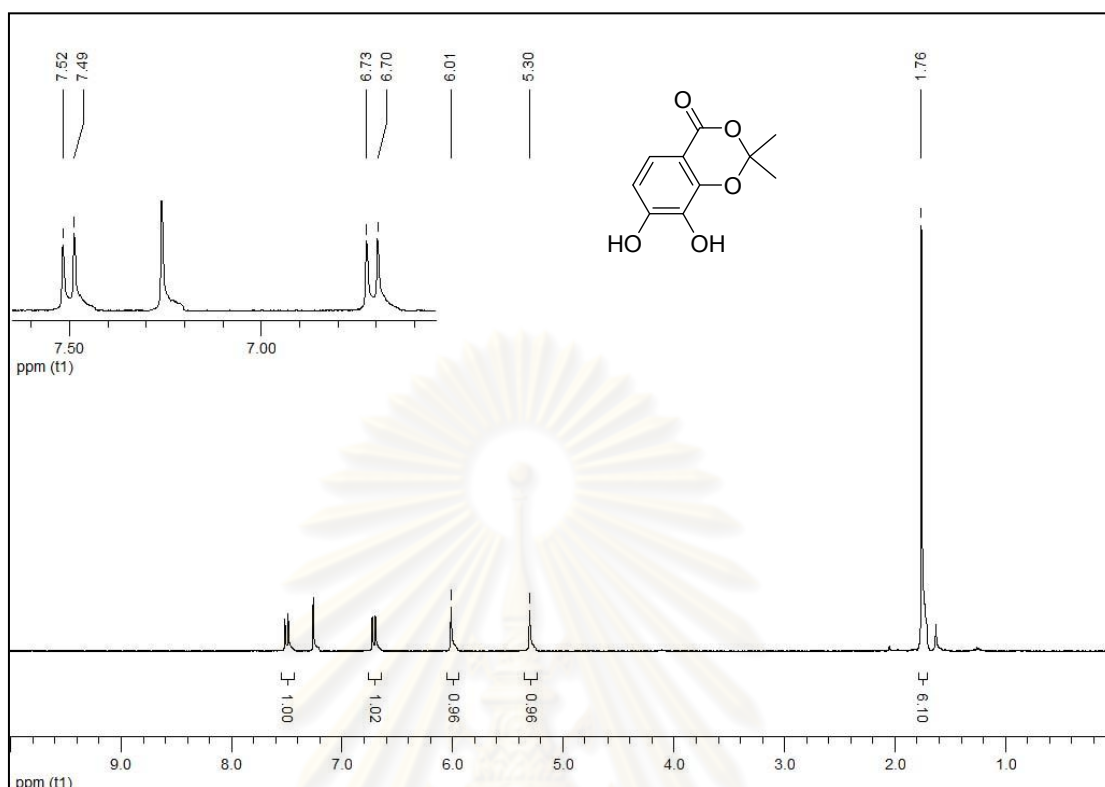
Figure A1 The ^{1}H NMR spectrum (CDCl$_3$, 400 MHz) of compound **C2**
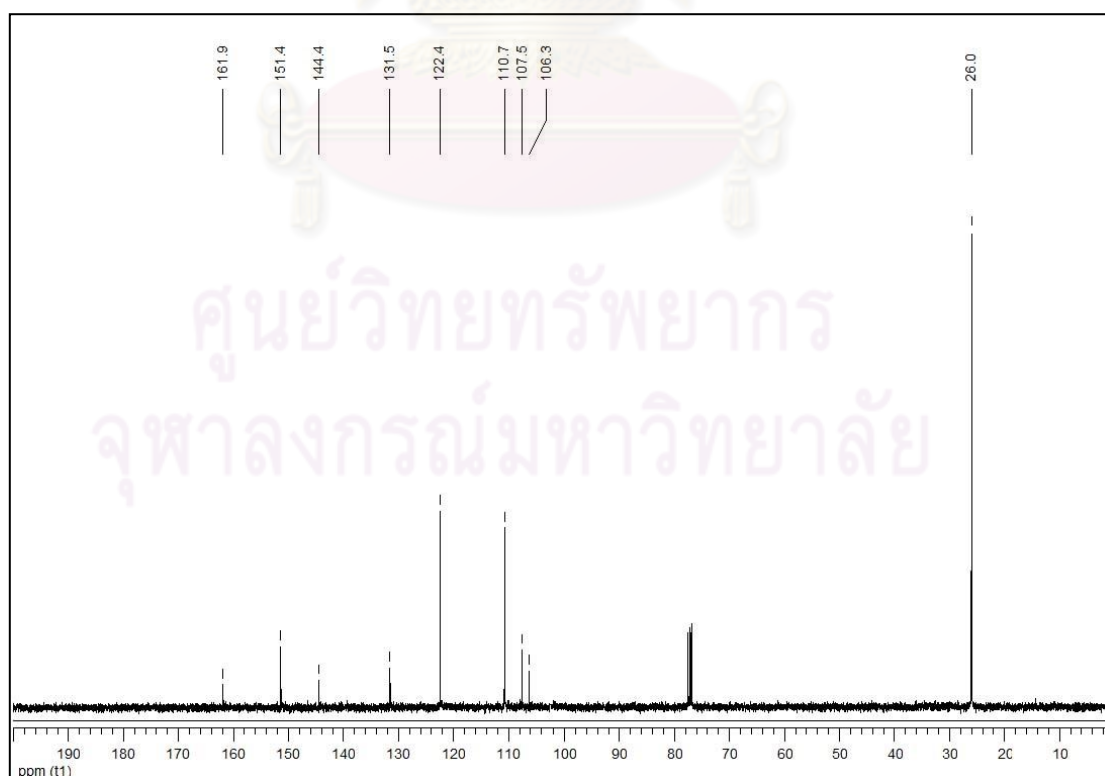
Figure A2 The ^{13}C NMR spectrum (CDCl$_3$, 100 MHz) of compound **C2**
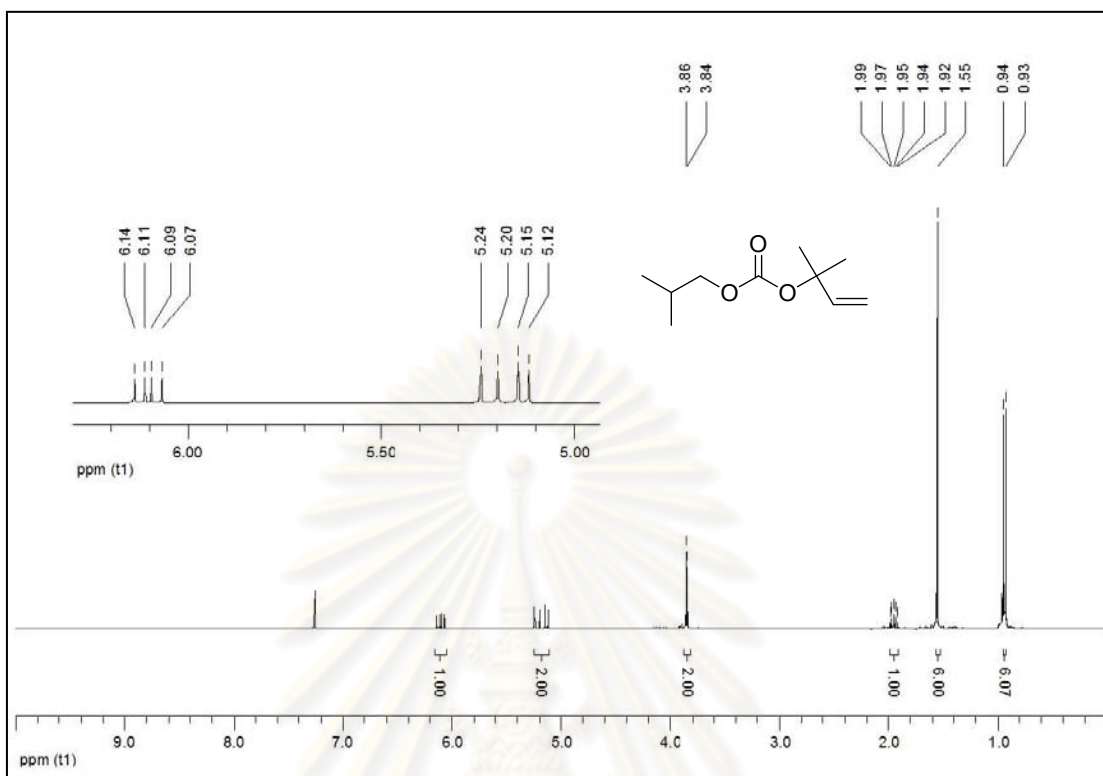
Figure A3 The ^{1}H NMR spectrum (CDCl$_3$, 400 MHz) of compound **C3a**
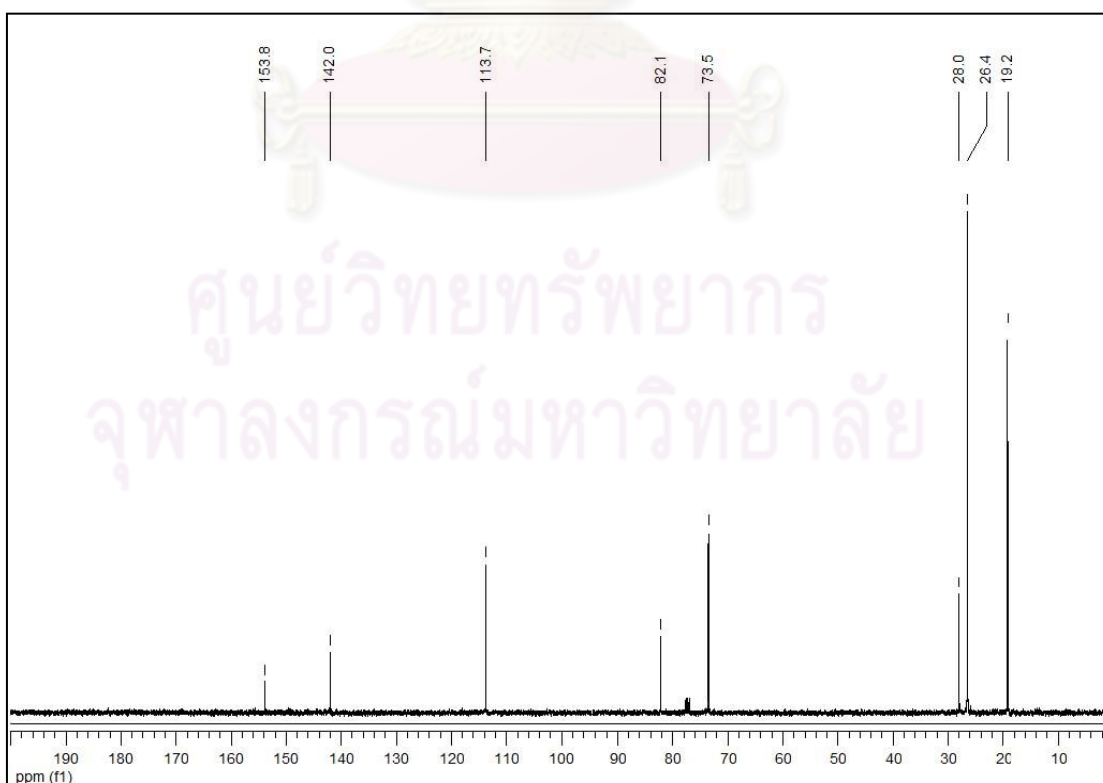
Figure A4 The ^{13}C NMR spectrum (CDCl$_3$, 100 MHz) of compound **C3a**
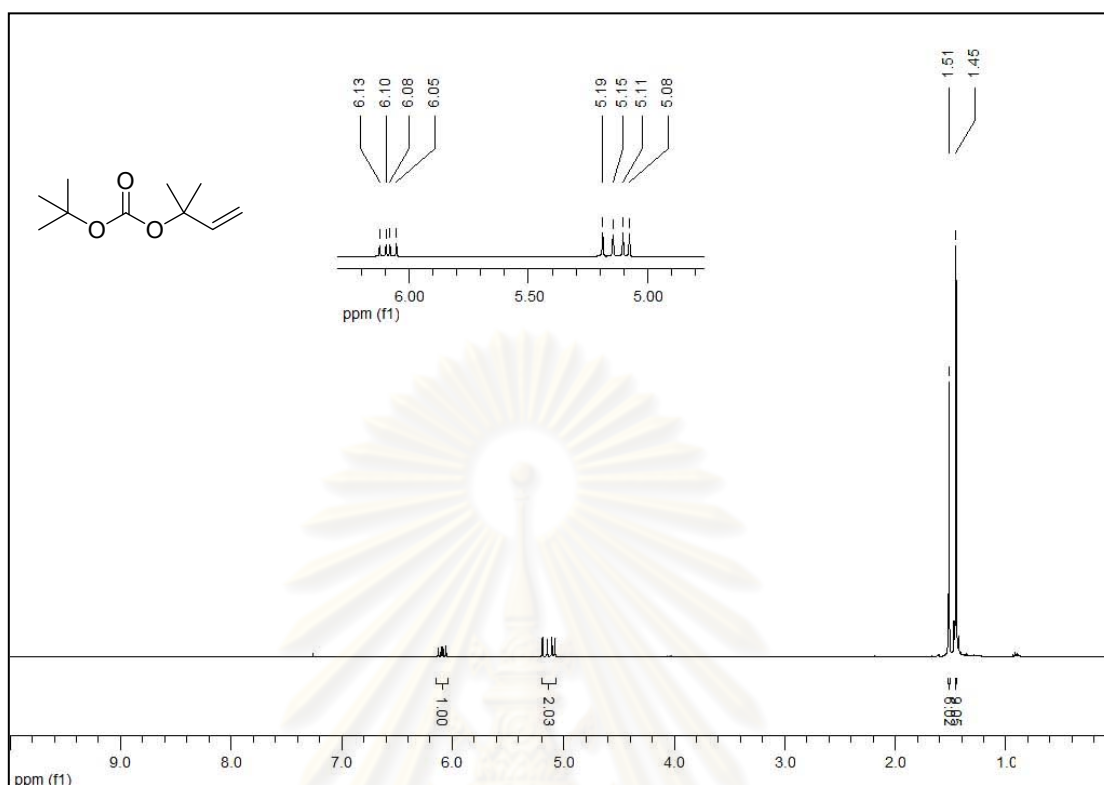
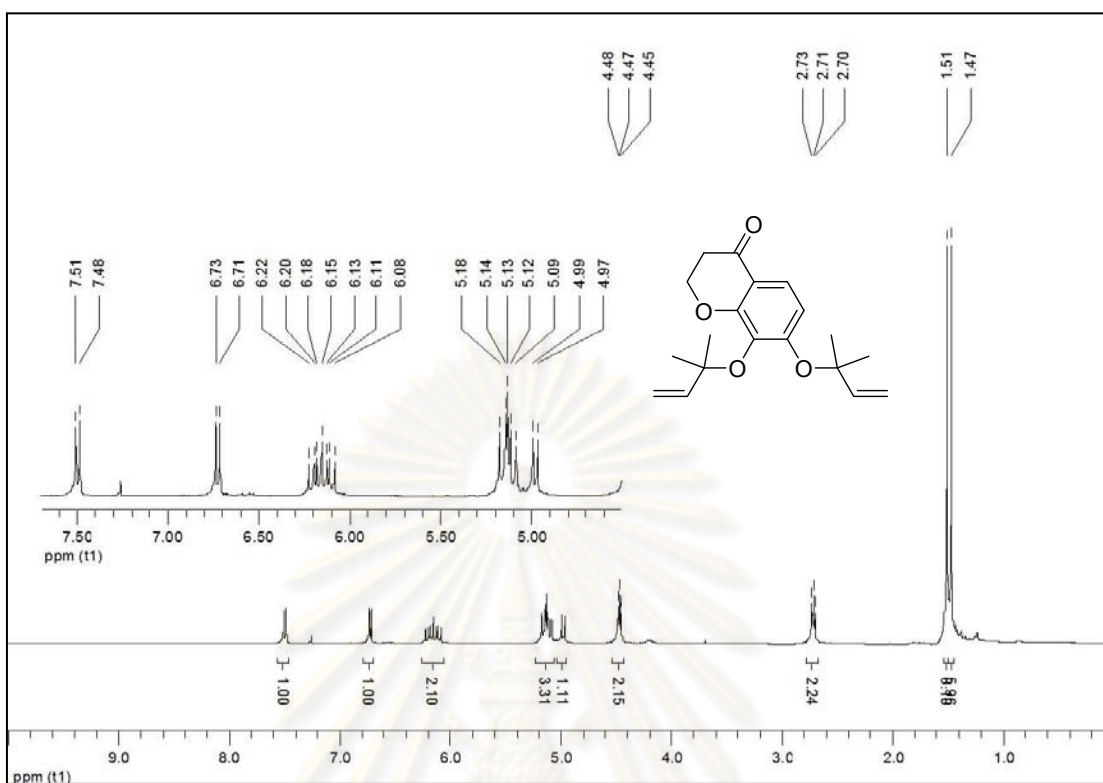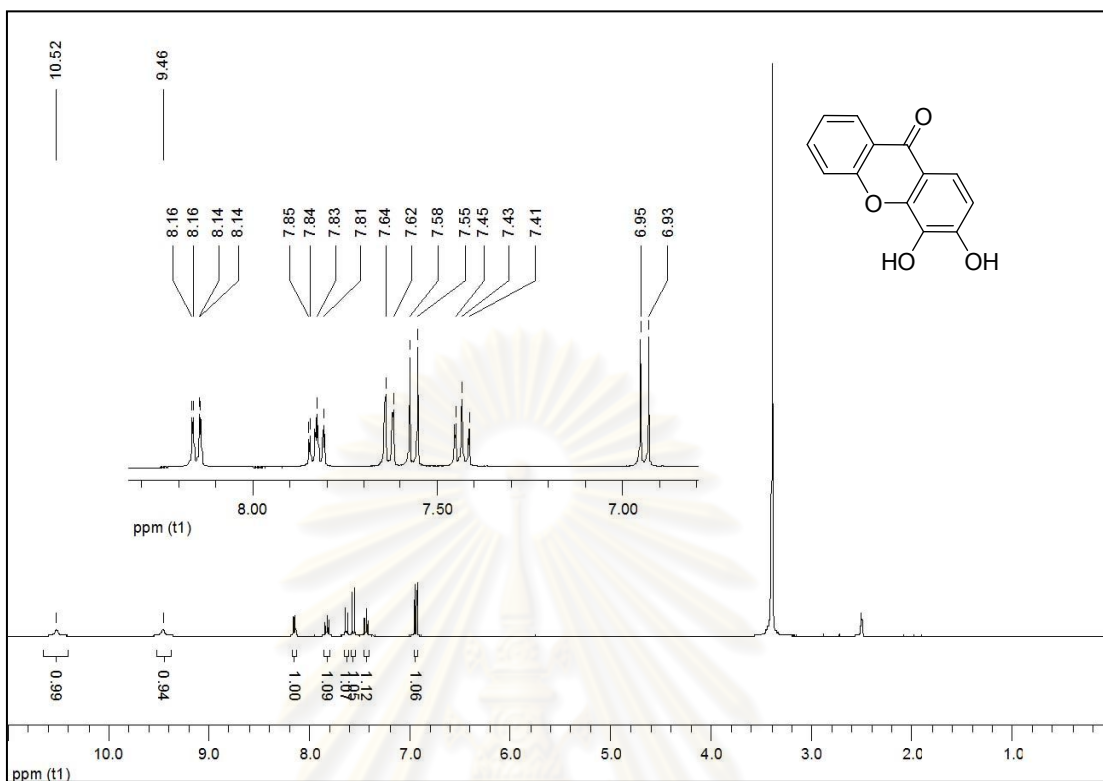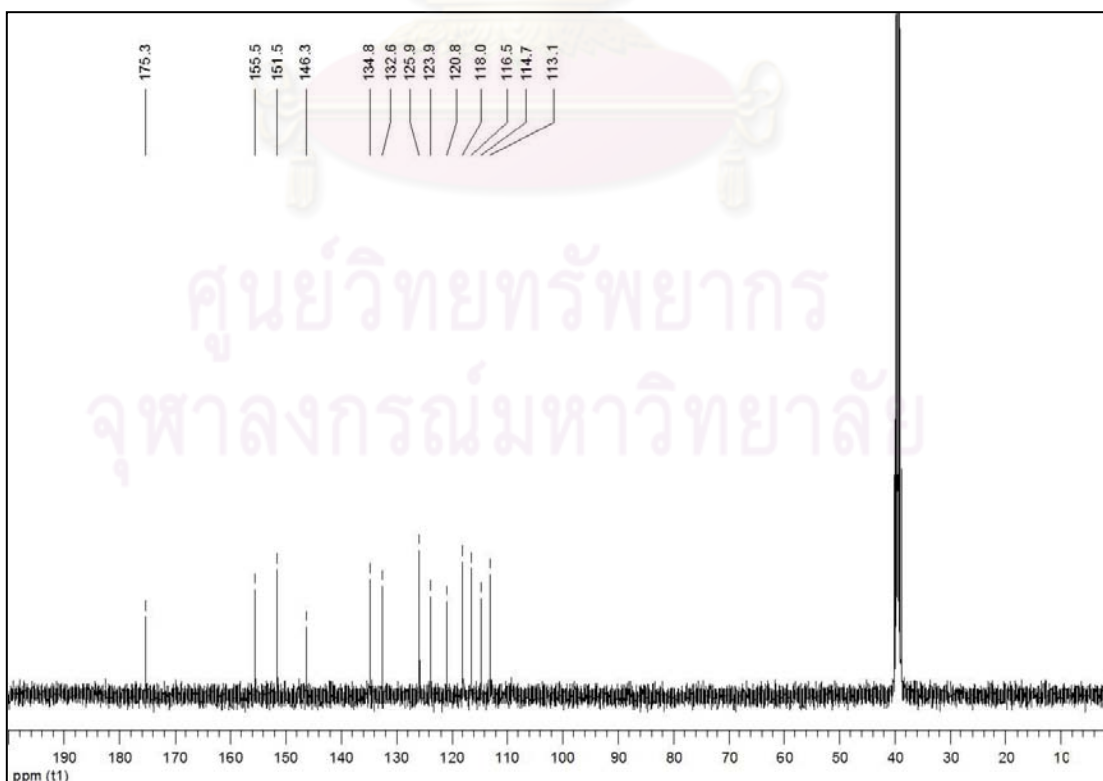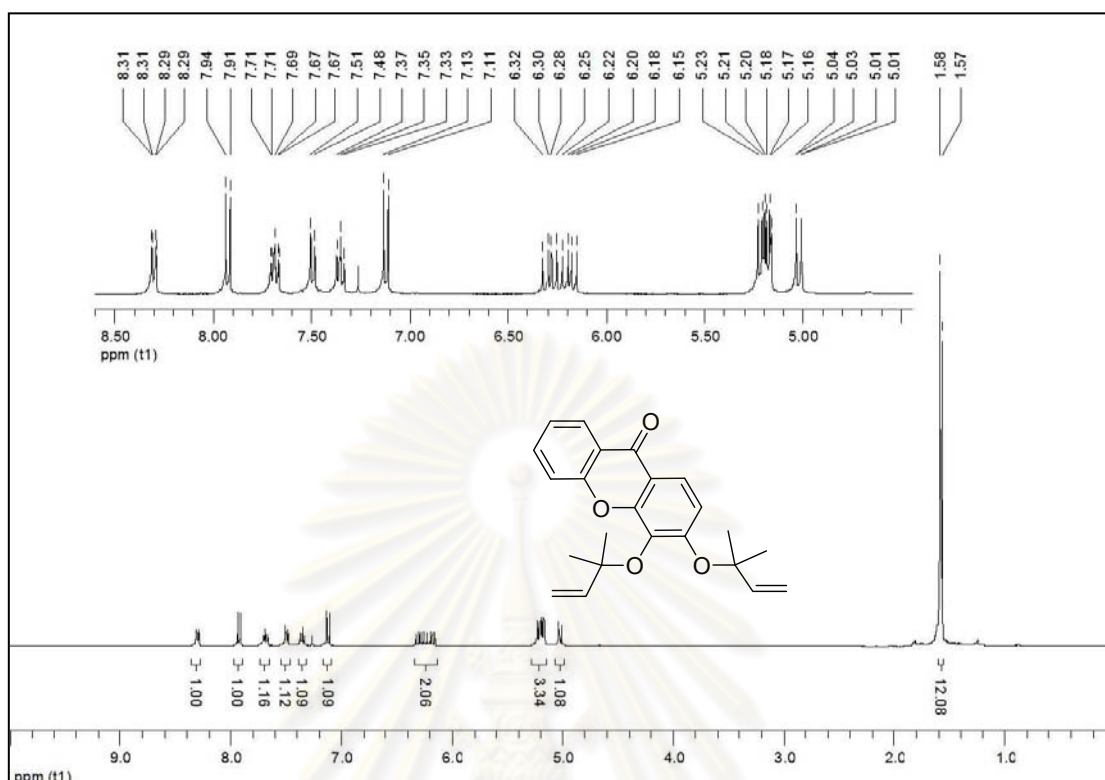**Figure A5** The ^{1}H NMR spectrum (CDCl$_3$, 400 MHz) of compound **C3b**
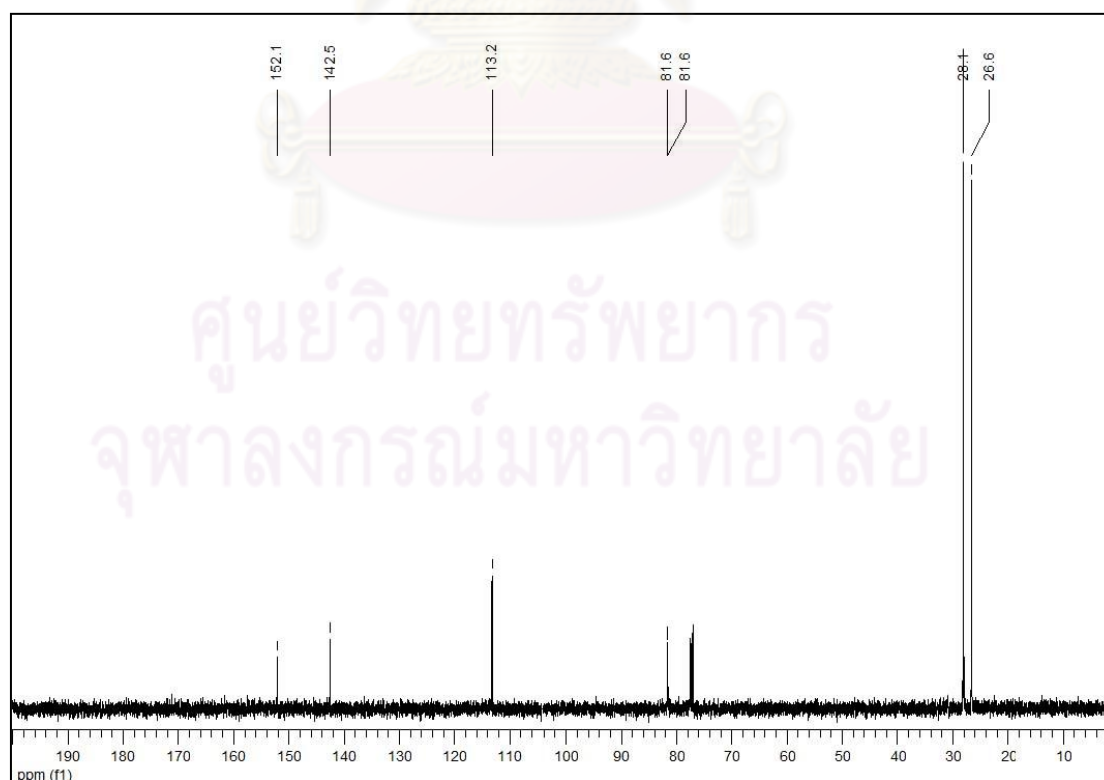
Figure A6 The ^{13}C NMR spectrum (CDCl$_3$, 100 MHz) of compound **C3b**
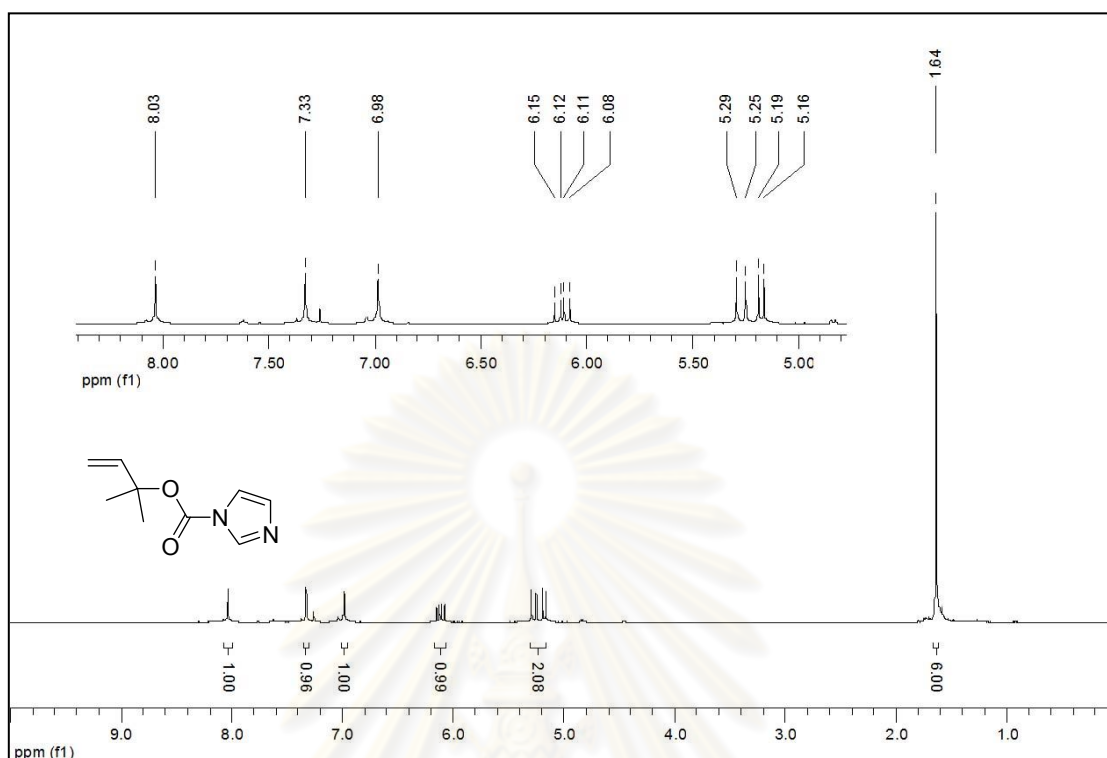
Figure A7 The ^{1}H NMR spectrum (CDCl$_3$, 400 MHz) of 2-methylbut-3-en-2-yl 1*H*-imidazole-1-carboxylate
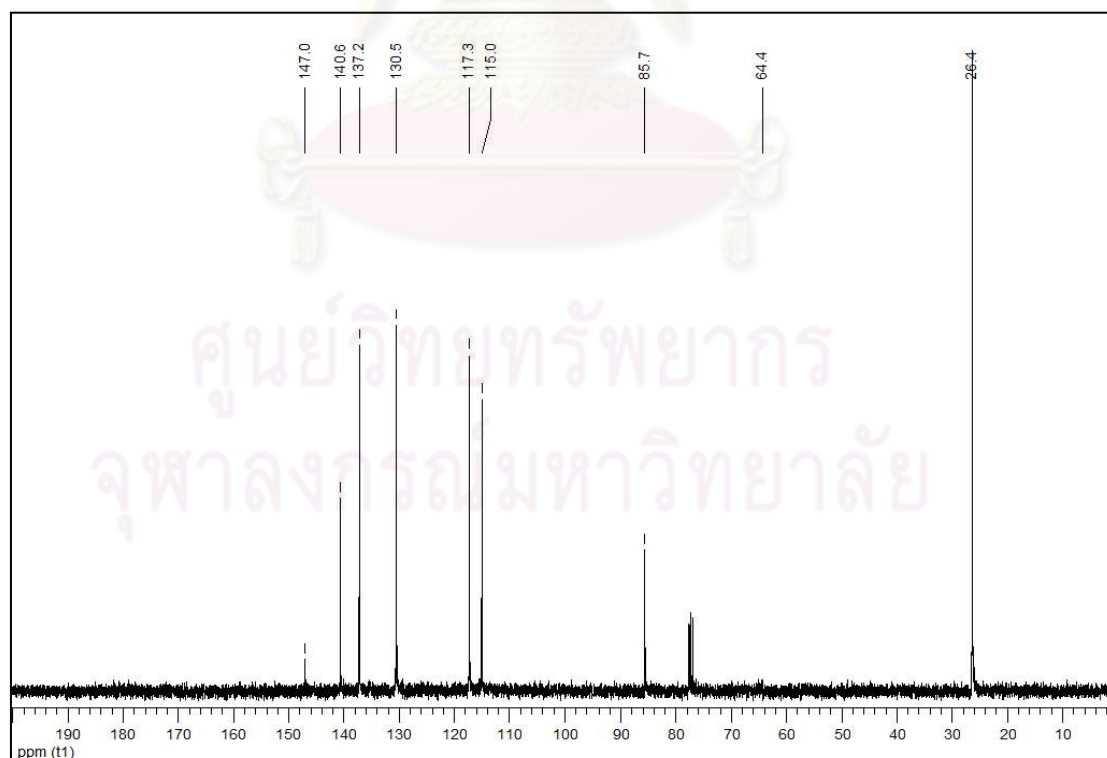
Figure A8 The ^{13}C NMR spectrum (CDCl$_3$, 100 MHz) of 2-methylbut-3-en-2-yl 1*H*-imidazole-1-carboxylate
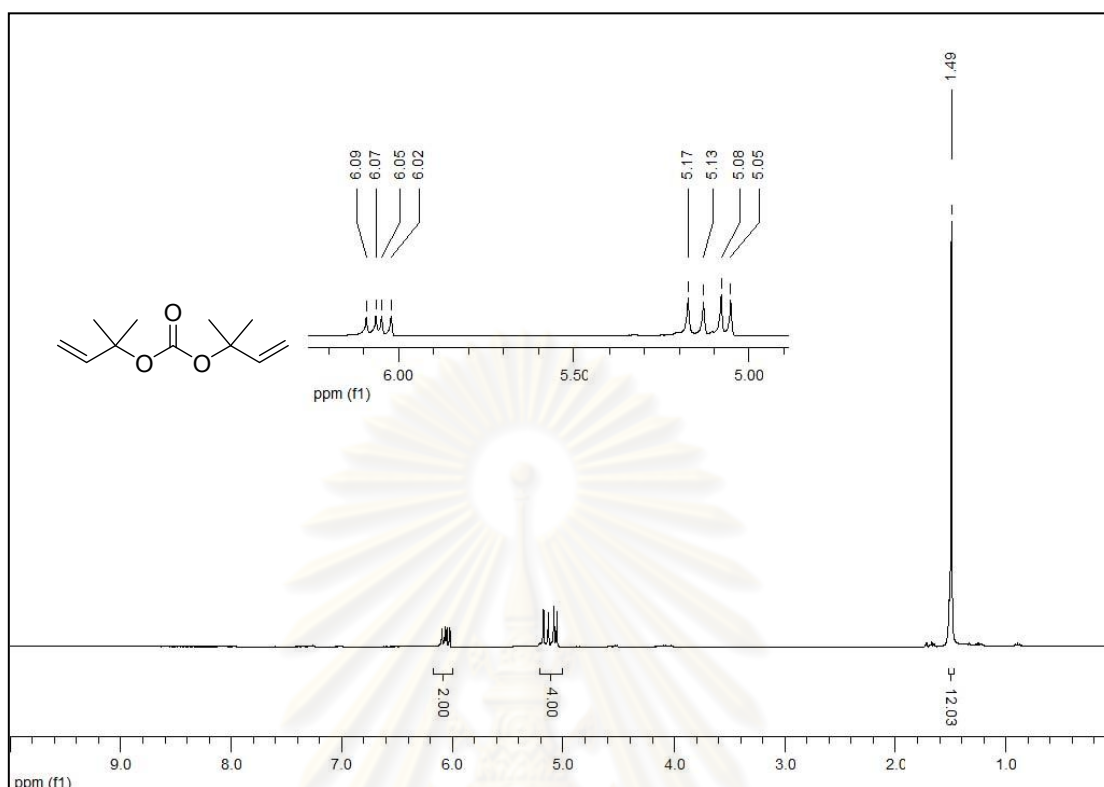
Figure A9 The ^{1}H NMR spectrum (CDCl$_3$, 400 MHz) of compound **C3c**
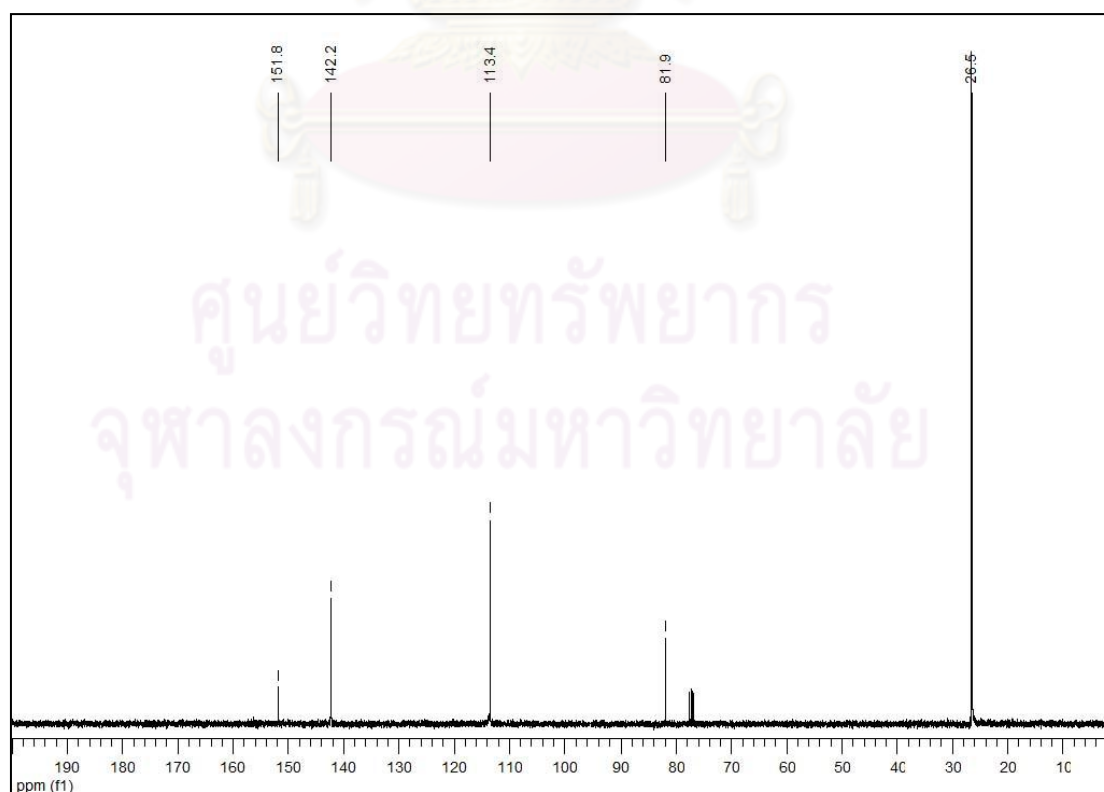
Figure A10 The ^{13}C NMR spectrum (CDCl$_3$, 100 MHz) of compound **C3c**
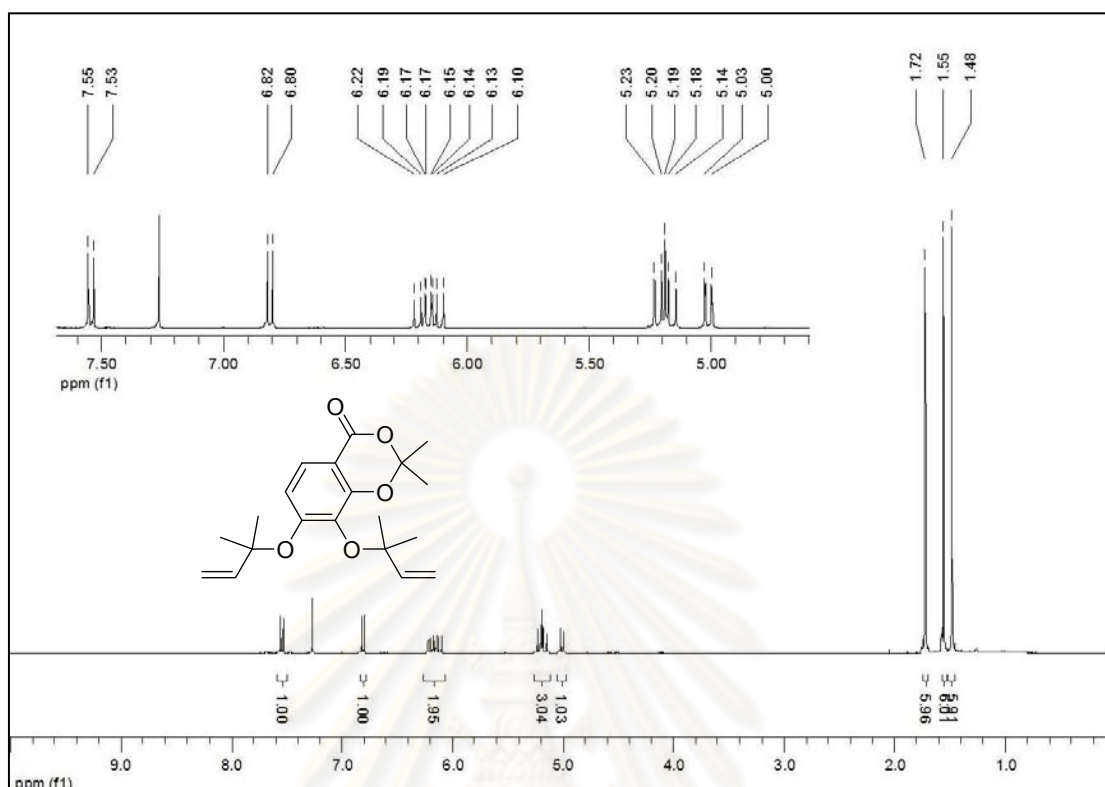
Figure A11 The ^{1}H NMR spectrum (CDCl$_3$, 400 MHz) of compound **C4**
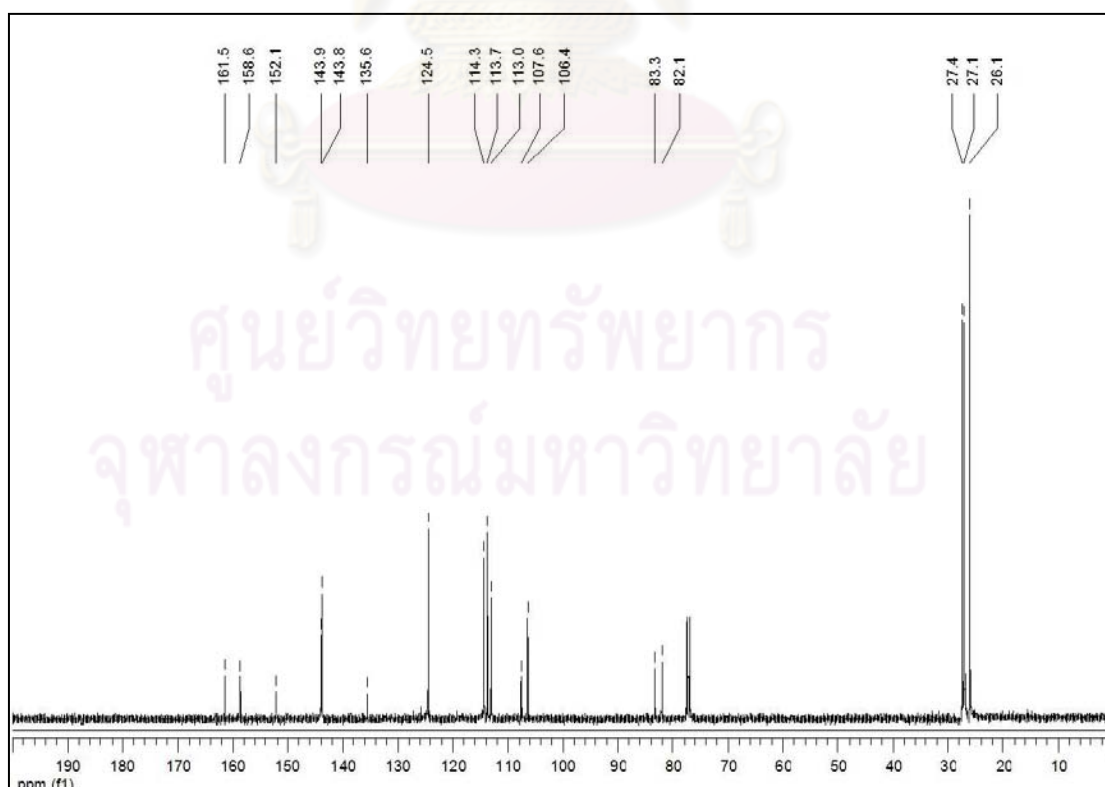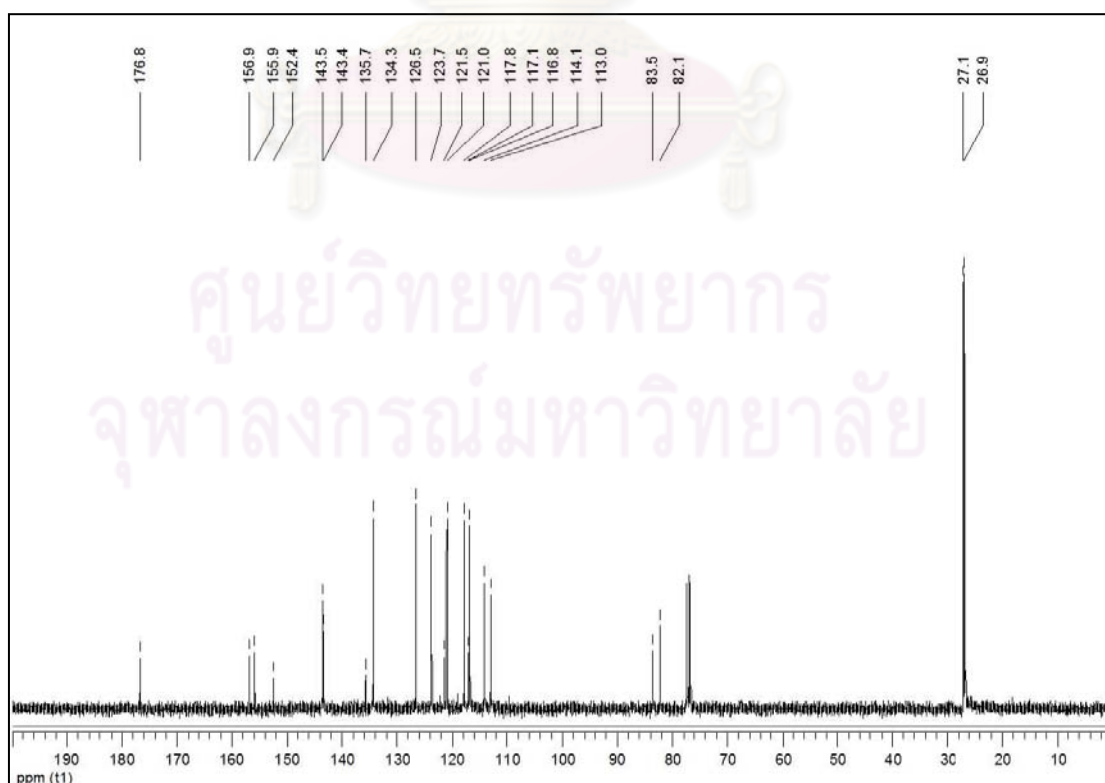

Figure A12 The ^{13}C NMR spectrum (CDCl$_3$, 100 MHz) of compound **C4**
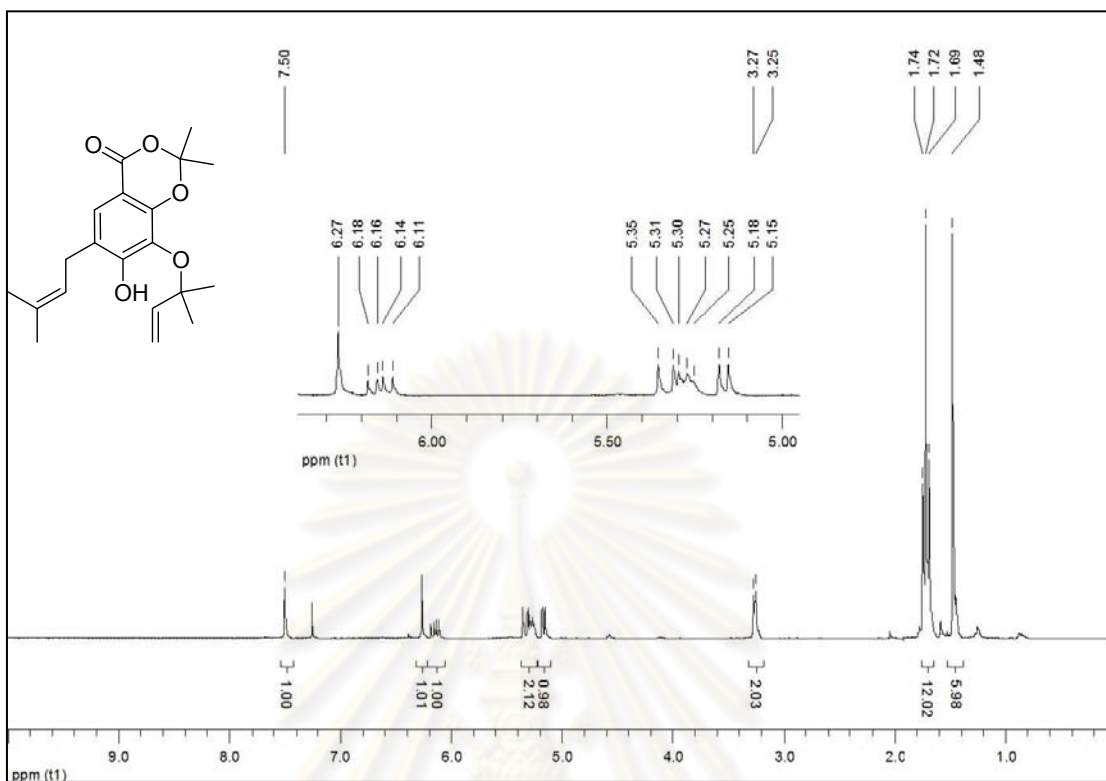
Figure A13 The ^{1}H NMR spectrum (CDCl$_3$, 400 MHz) of compound **C7**
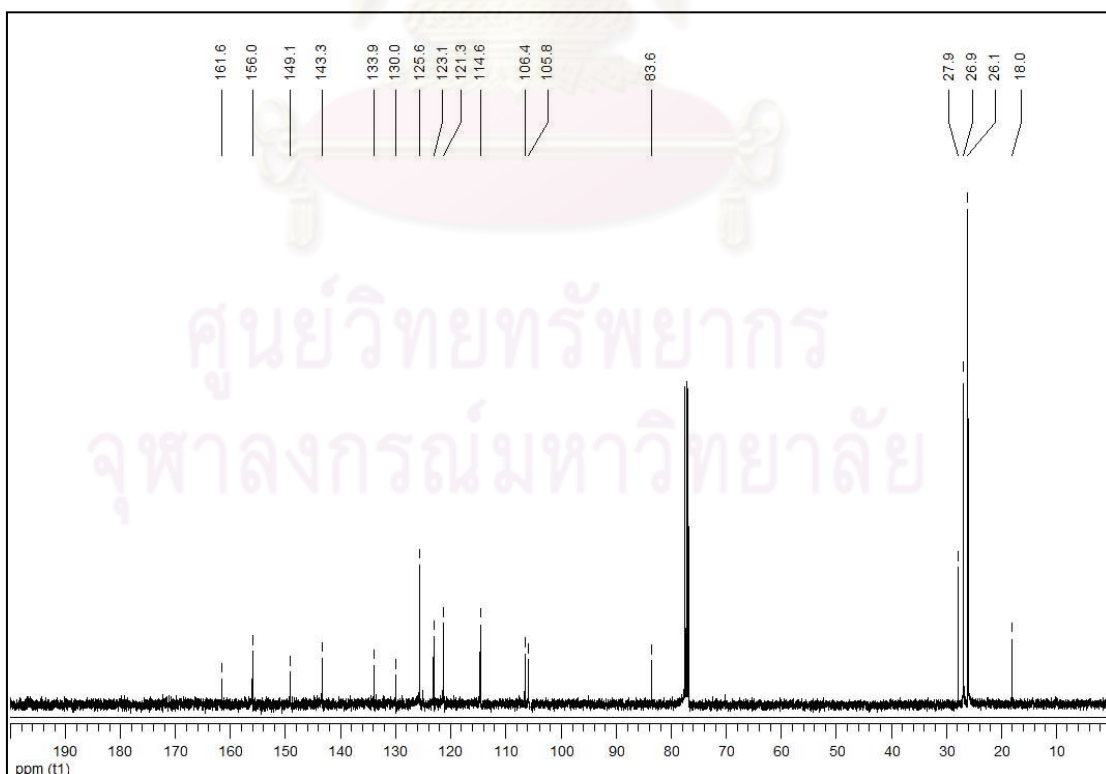
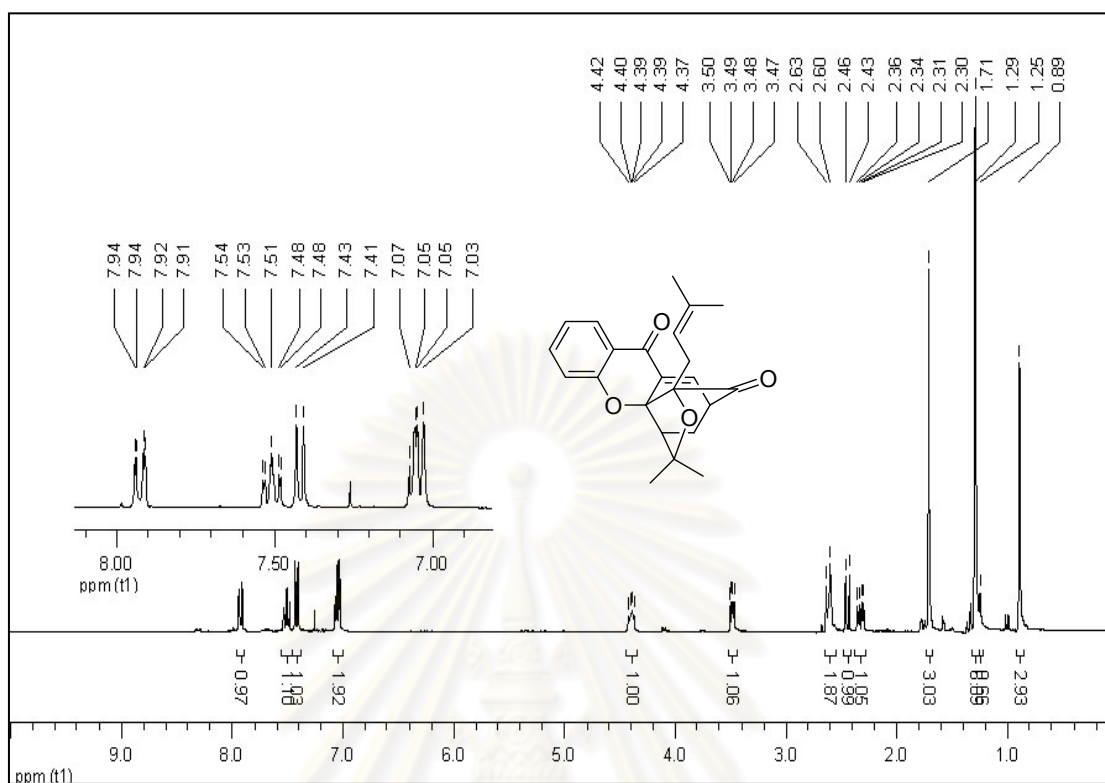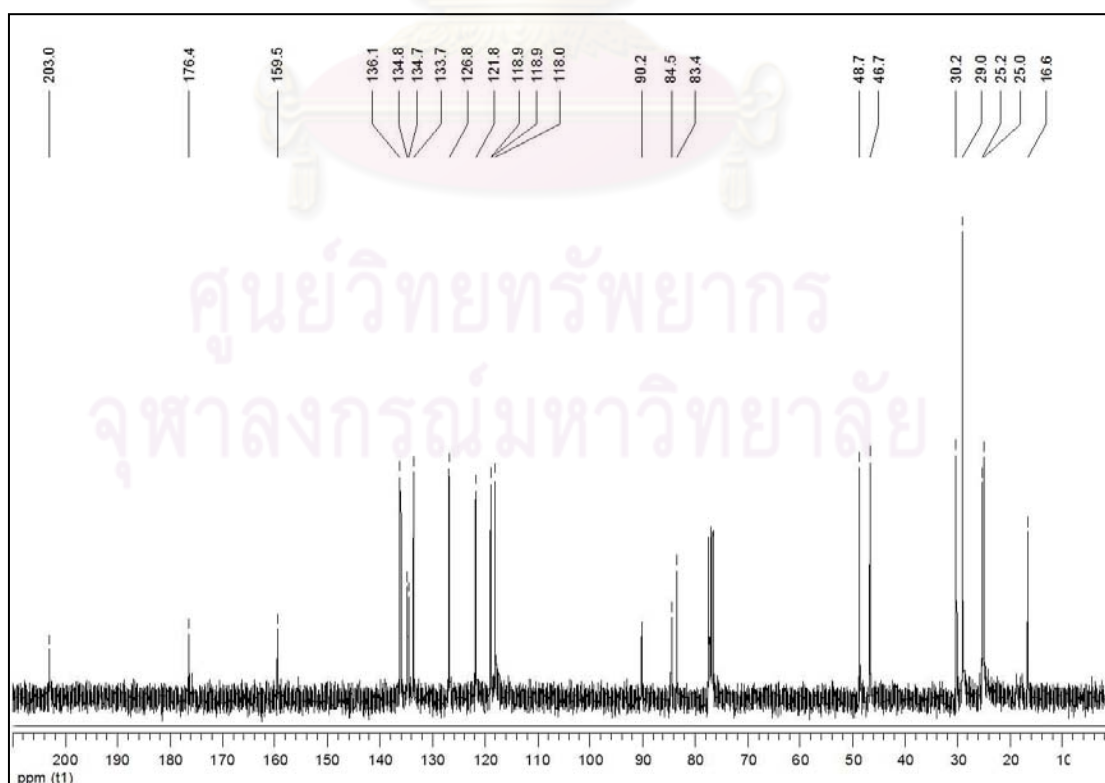**Figure A14** The ^{13}C NMR spectrum (CDCl$_3$, 100 MHz) of compound **C7**
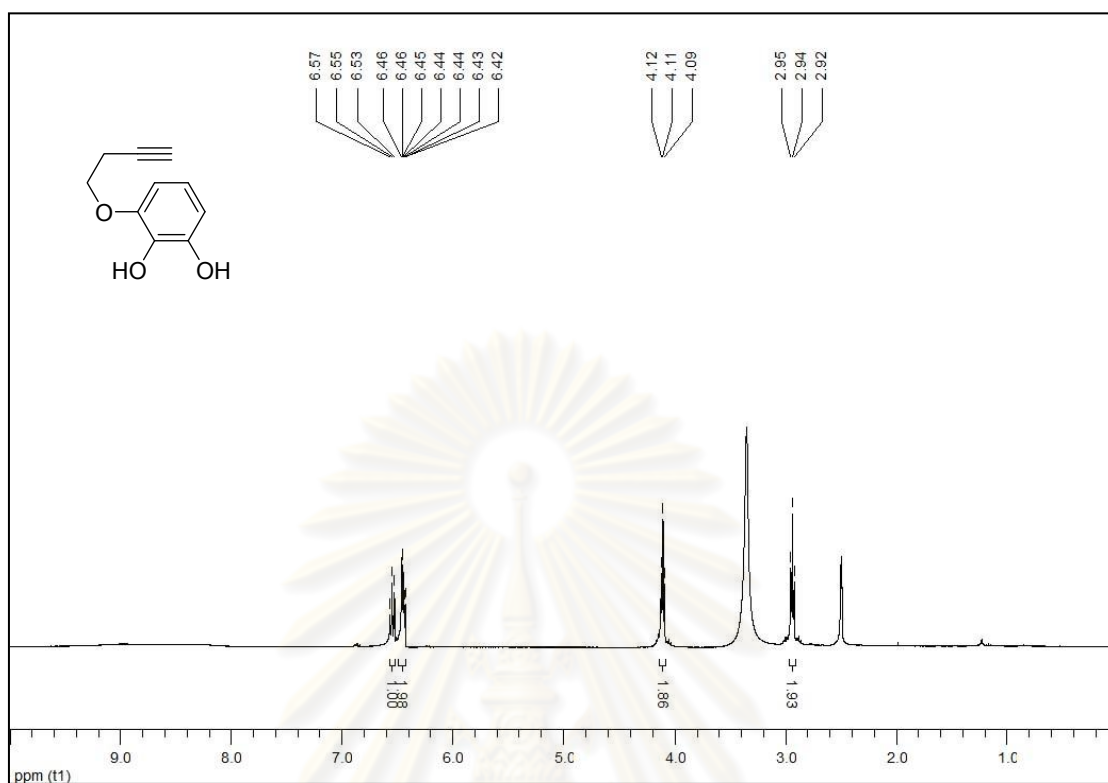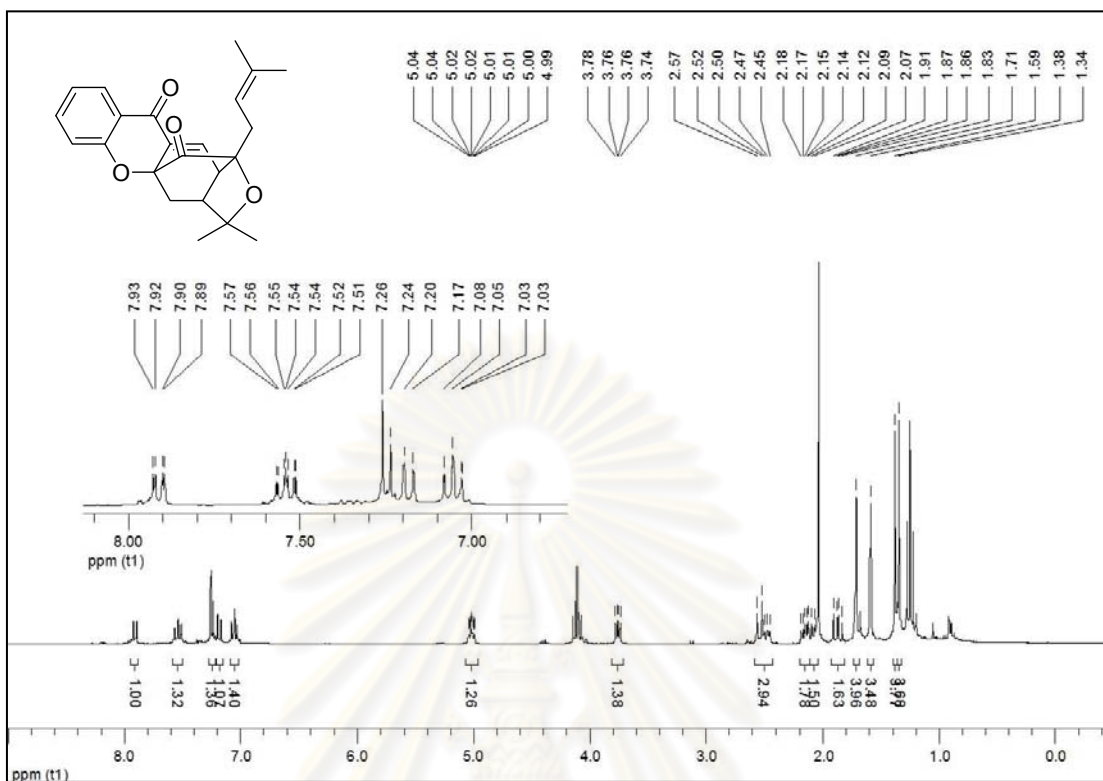
Figure A15 The ^{1}H NMR spectrum (DMSO-d_6, 400 MHz) of compound **C15**
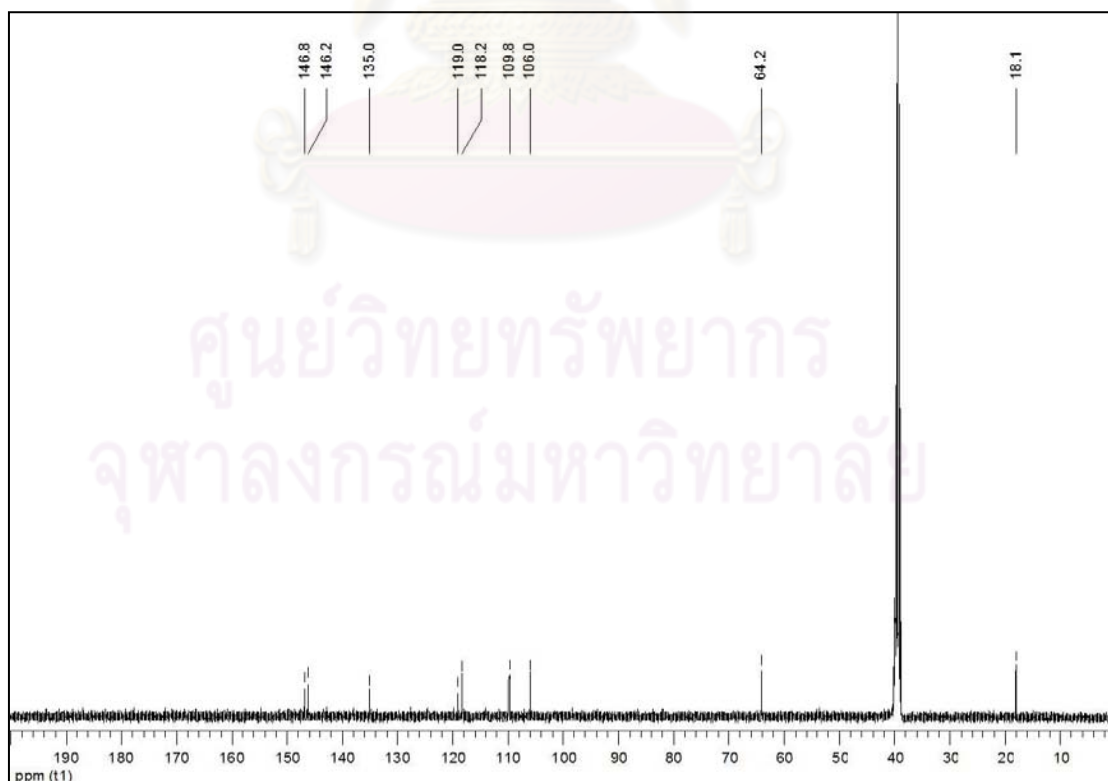
Figure A16 The ^{13}C NMR spectrum (DMSO-d_6, 100 MHz) of compound **C15**
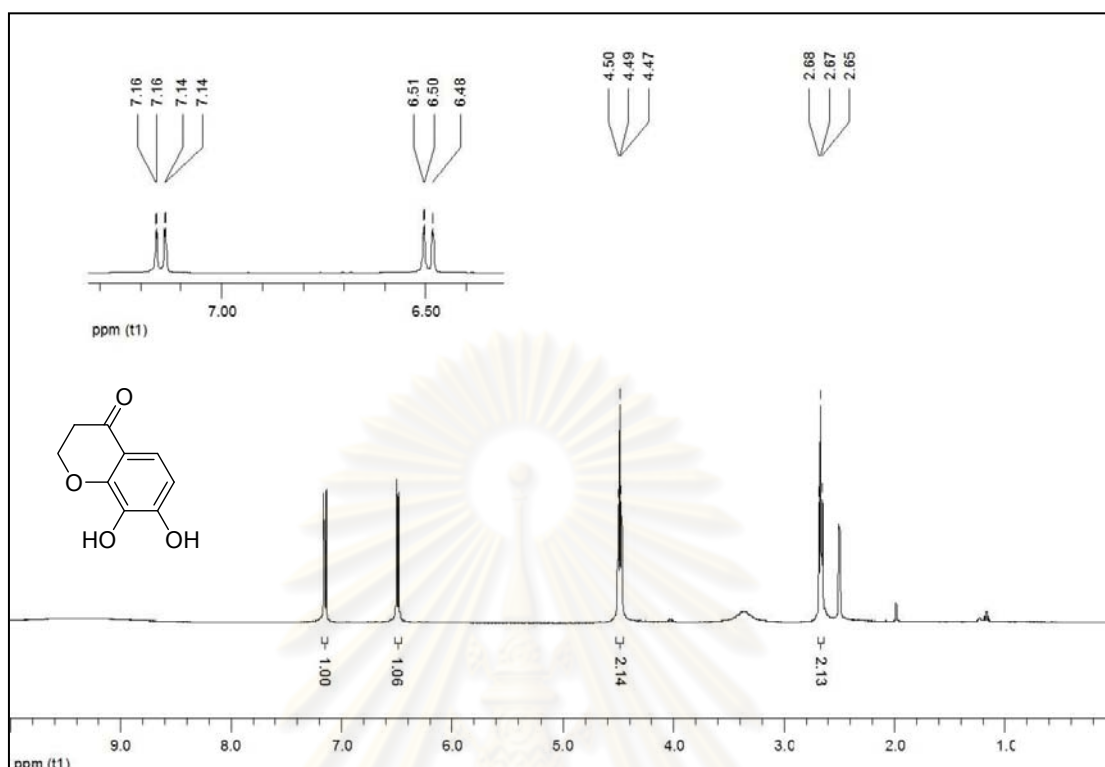
Figure A17 The ^{1}H NMR spectrum (DMSO-d$_6$, 400 MHz) of compound **C16**
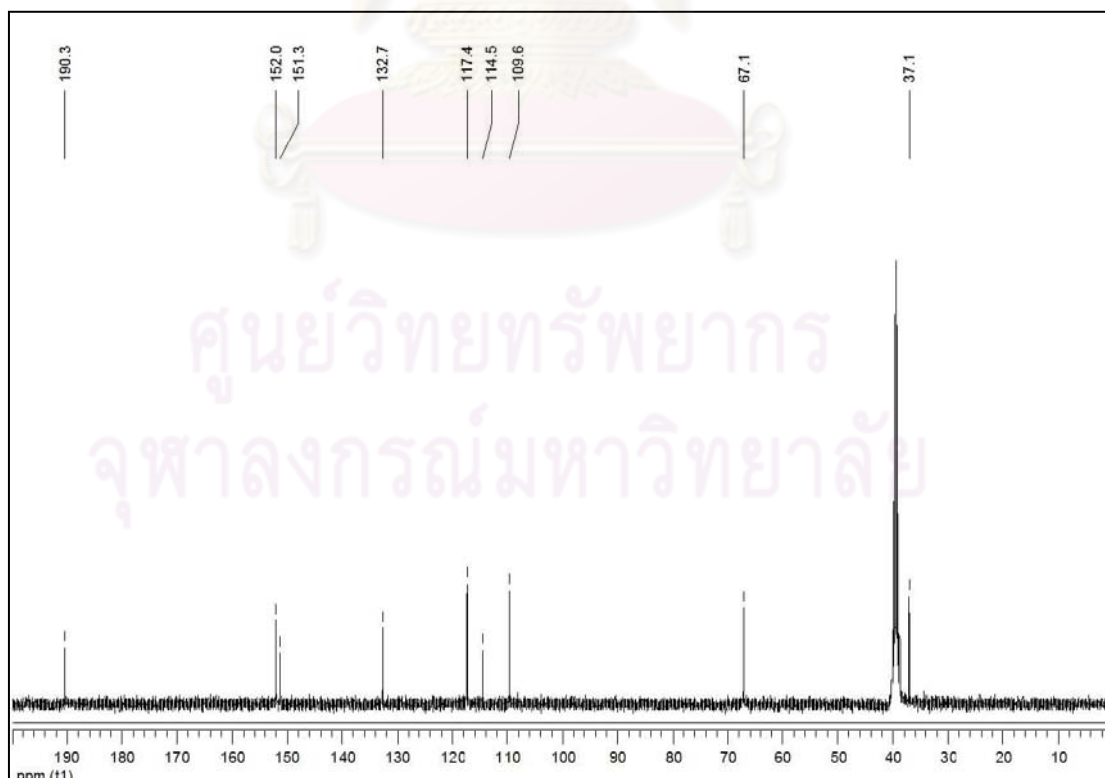
Figure A18 The ^{13}C NMR spectrum (DMSO-d$_6$, 100 MHz) of compound **C16**

Figure A19 The ^{1}H NMR spectrum (CDCl$_3$, 400 MHz) of compound **C17**
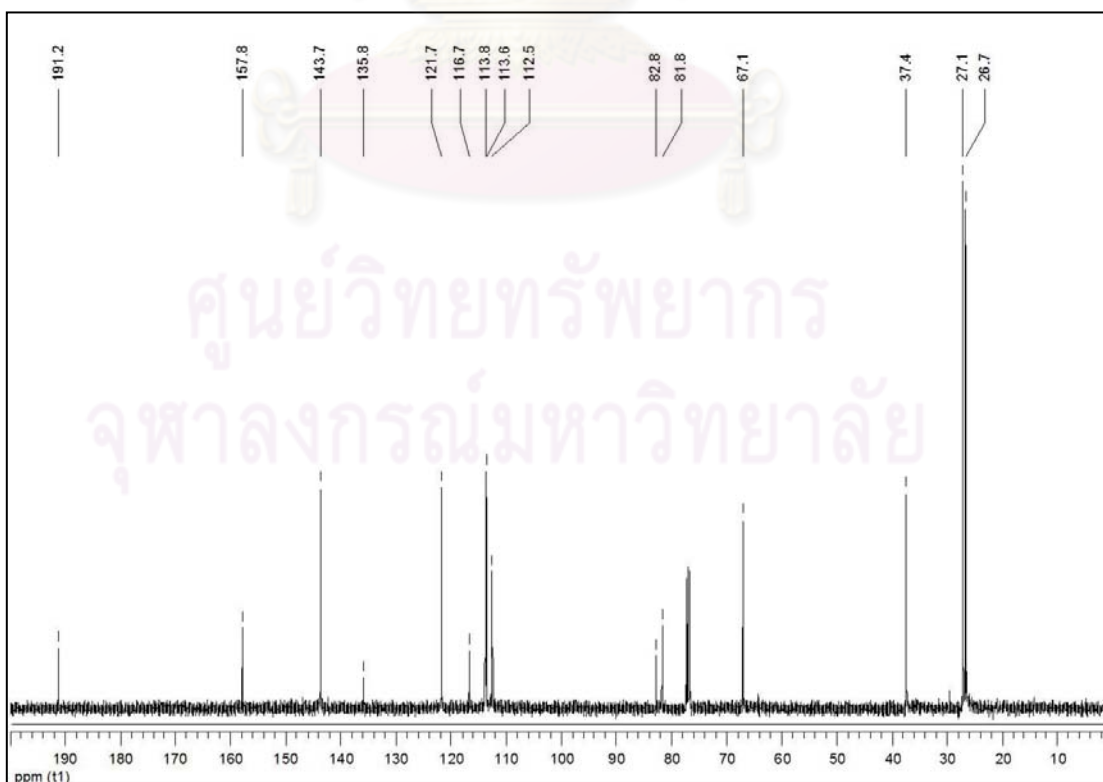
Figure A20 The ^{13}C NMR spectrum (CDCl$_3$, 100 MHz) of compound **C17**

Figure A21 The ^{1}H NMR spectrum (DMSO-d$_6$, 400 MHz) of compound **C24**

Figure A22 The ^{13}C NMR spectrum (DMSO-d$_6$, 100 MHz) of compound **C24**

Figure A23 The ^{1}H NMR spectrum (CDCl$_3$, 400 MHz) of compound **C25**

Figure A24 The ^{13}C NMR spectrum (CDCl$_3$, 100 MHz) of compound **C25**

Figure A25 The ^{1}H NMR spectrum (CDCl$_3$, 400 MHz) of compound **196**

Figure A26 The ^{13}C NMR spectrum (CDCl$_3$, 100 MHz) of compound **196**

Figure A27 The ^{1}H NMR spectrum (CDCl$_3$, 400 MHz) of compound **C26**
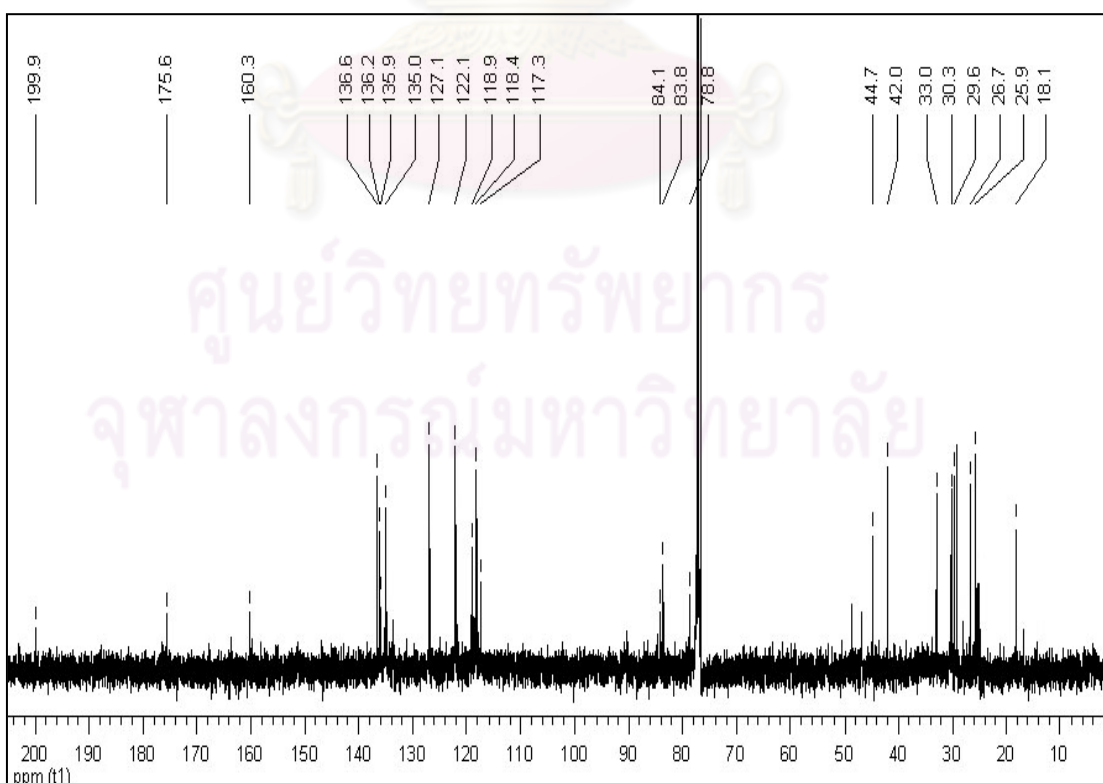
Figure A28 The ^{13}C NMR spectrum (CDCl$_3$, 100 MHz) of compound **C26**
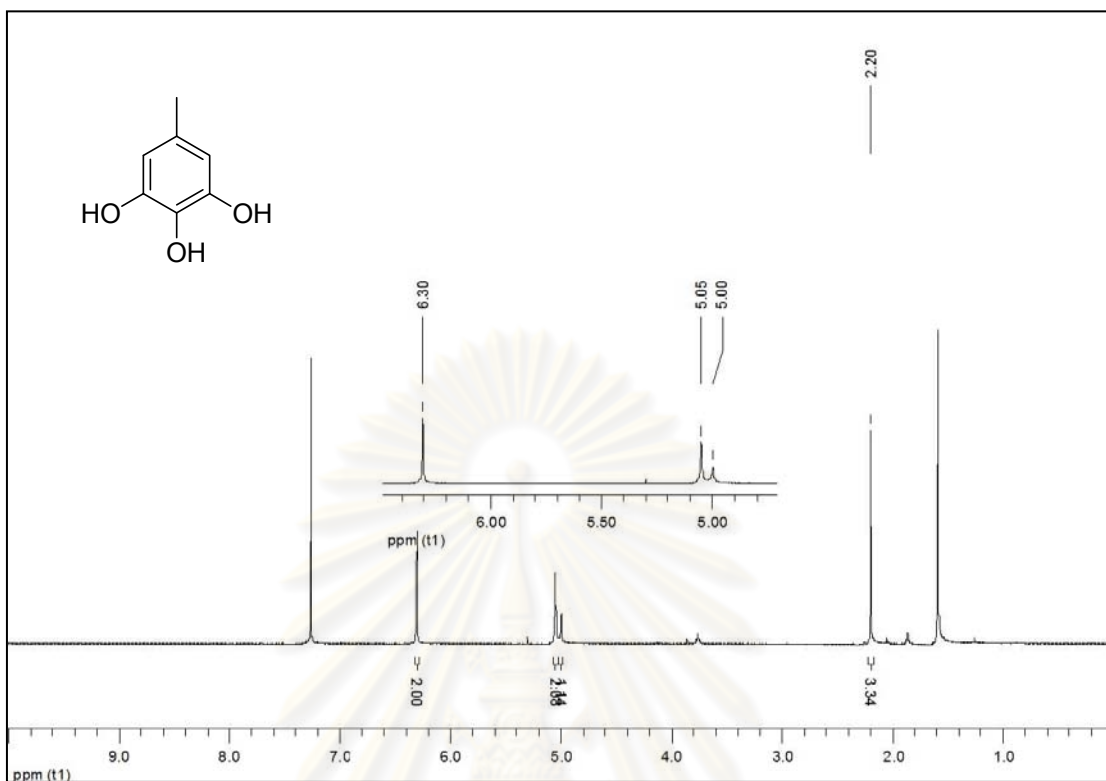
Figure A29 The ^{1}H NMR spectrum (CDCl$_3$, 400 MHz) of compound **C31**
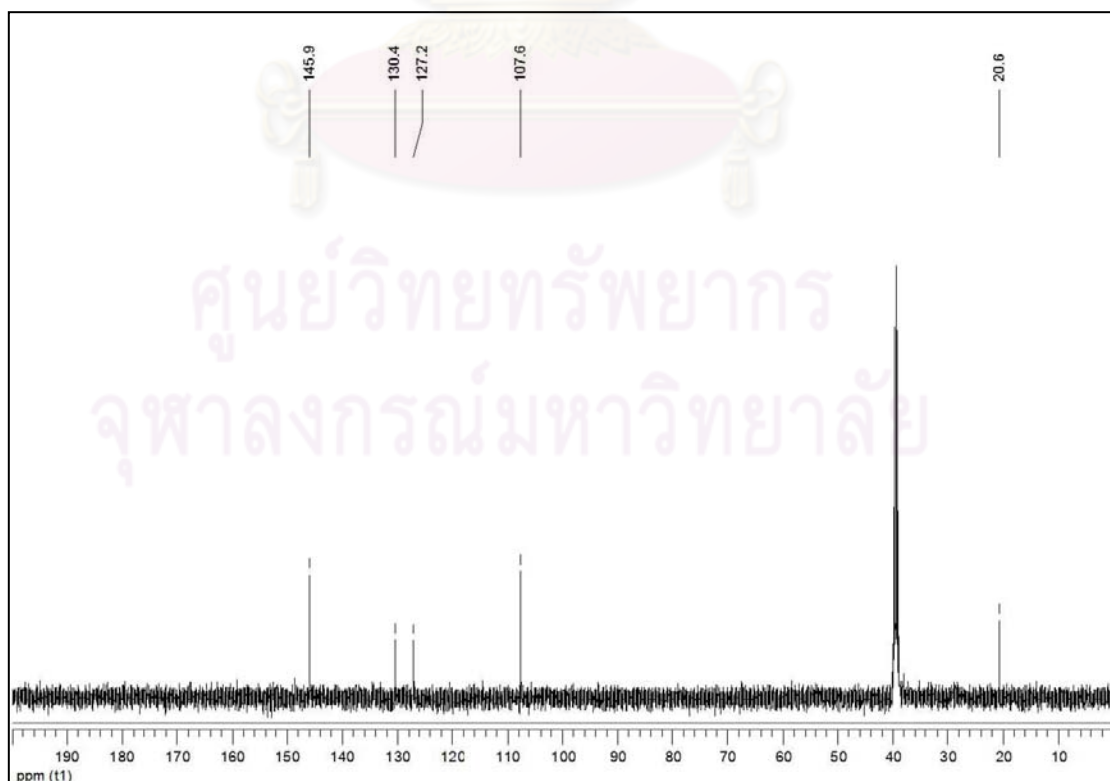
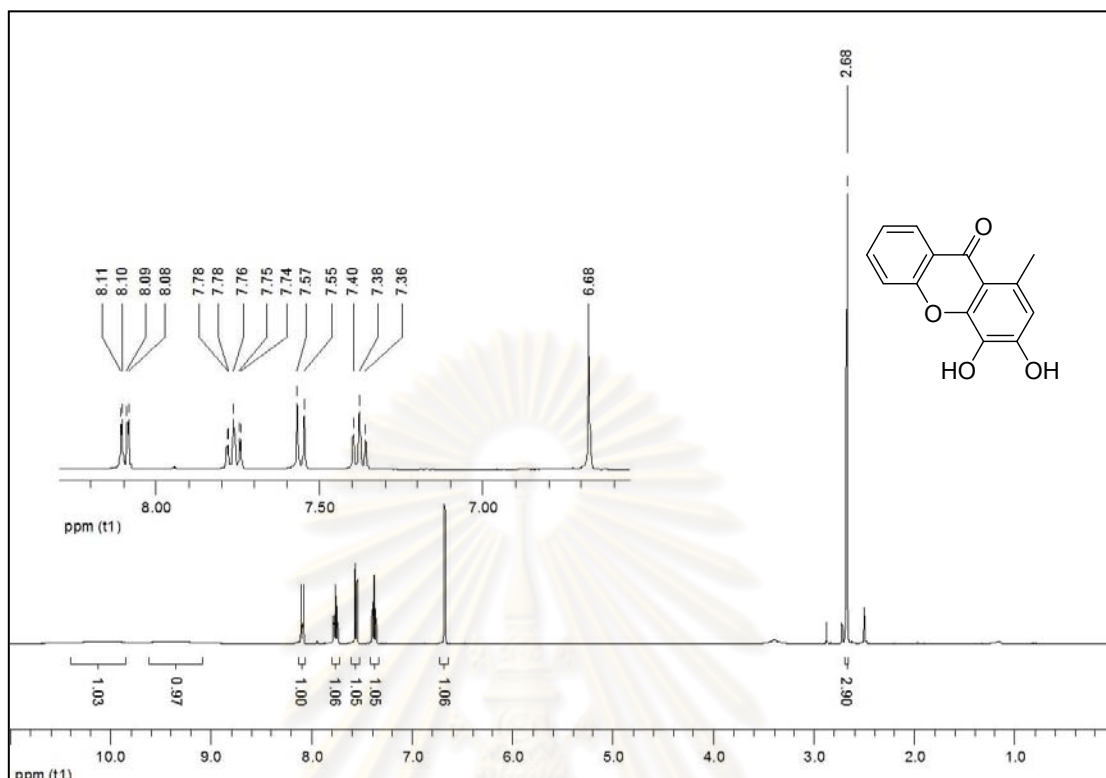**Figure A30** The ^{13}C NMR spectrum (DMSO-d$_6$, 100 MHz) of compound **C31**

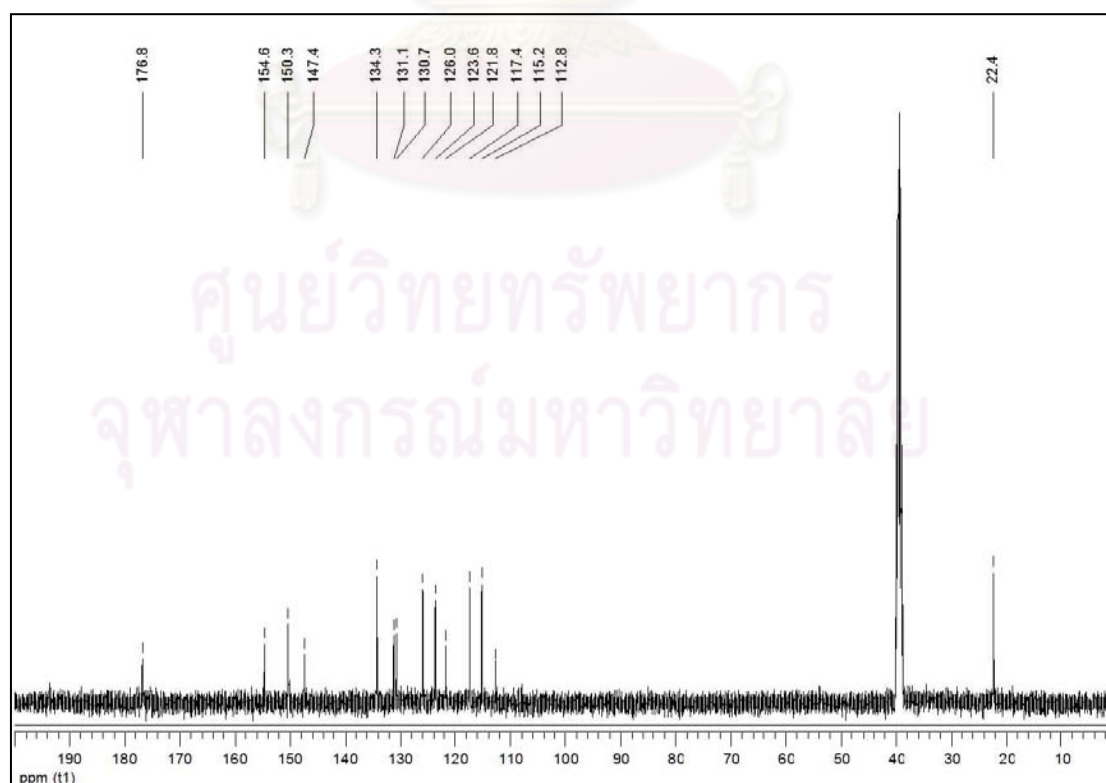**Figure A31** The ^{1}H NMR spectrum (DMSO-d[6], 400 MHz) of compound **C32**

Figure A32 The ^{13}C NMR spectrum (DMSO-d[6], 100 MHz) of compound **C32**
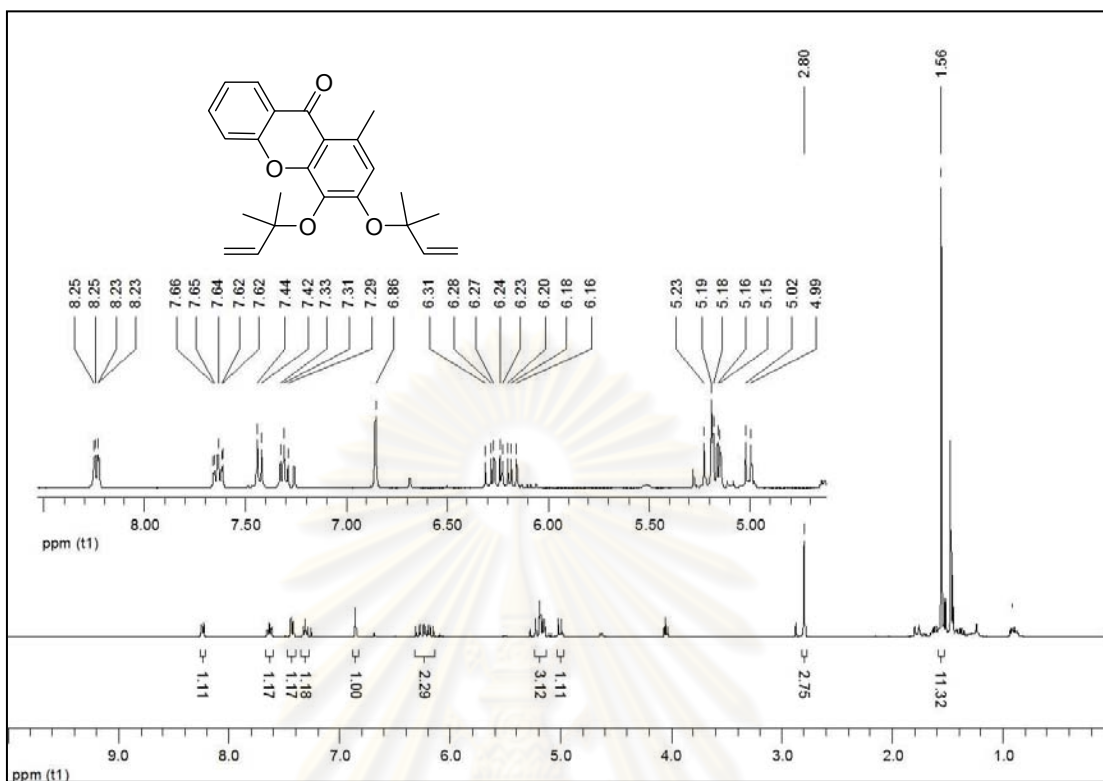
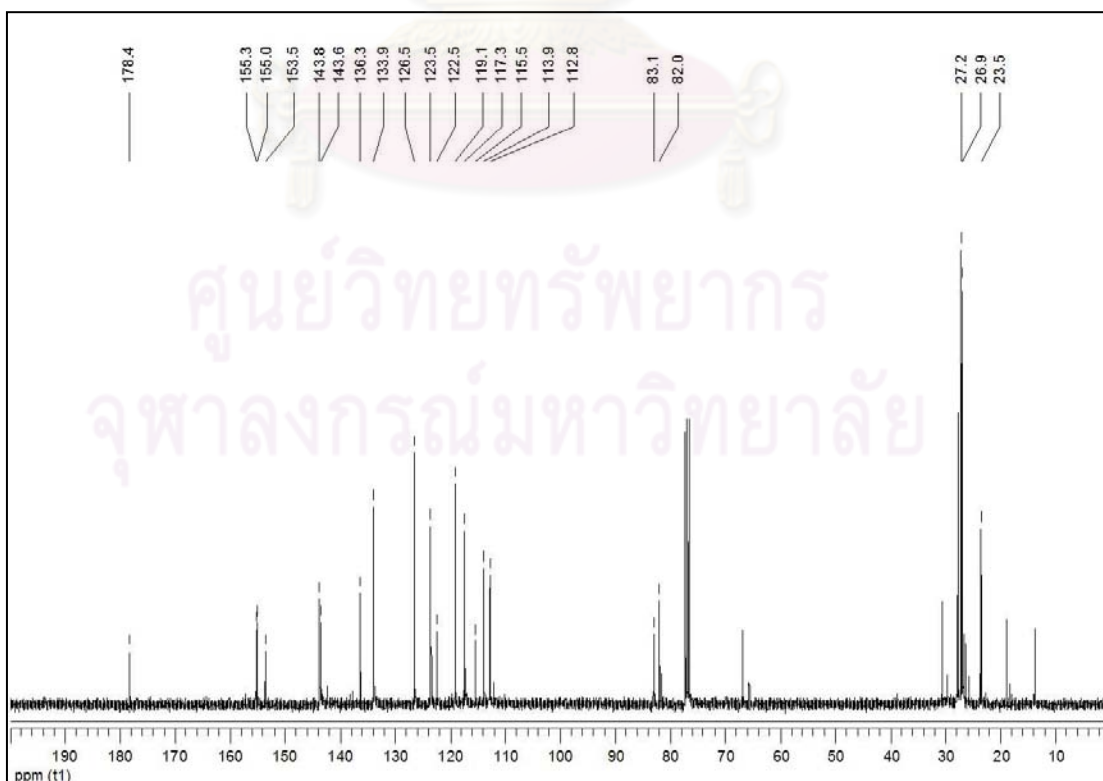**Figure A33** The ^{1}H NMR spectrum (CDCl$_3$, 400 MHz) of compound **C33**

Figure A34 The ^{13}C NMR spectrum (CDCl$_3$, 100 MHz) of compound **C33**

VITA

Miss Oraphin Chantarasriwong was born on November 11, 1982 in Phitsanulok, Thailand. She received a Bachelor and Master Degree of Science in Chemistry from Chulalongkorn University in 2004 and 2006. Since then, she has been a graduate student studying Organic Chemistry at Chulalongkorn University. During the study, she was supported by research grant for the Degree of Doctor of Philosophy Program in Chemistry from the Thailand Research Fund for a Royal Golden Jubilee Ph.D. fellowship and Center for Petroleum, Petrochemicals, and Advanced Materials.

Her present address is 1154 Soi 40 (Sriburapa Soi. 6) Sriburapa Rd., Klongchan, Bangkapi, Bangkok 10240, Thailand.